frontiers | Research Topics

Mars analogs: Environment, habitability and biodiversity

Edited by
André Antunes, Maggie Cy Lau Vetter, Yiliang Li and David Flannery

Published in
Frontiers in Astronomy and Space Sciences
Frontiers in Microbiology

ISSN 1664-8714
ISBN 978-2-83251-882-3
DOI 10.3389/978-2-83251-882-3

About Frontiers

Frontiers is more than just an open access publisher of scholarly articles: it is a pioneering approach to the world of academia, radically improving the way scholarly research is managed. The grand vision of Frontiers is a world where all people have an equal opportunity to seek, share and generate knowledge. Frontiers provides immediate and permanent online open access to all its publications, but this alone is not enough to realize our grand goals.

Frontiers journal series

The Frontiers journal series is a multi-tier and interdisciplinary set of open-access, online journals, promising a paradigm shift from the current review, selection and dissemination processes in academic publishing. All Frontiers journals are driven by researchers for researchers; therefore, they constitute a service to the scholarly community. At the same time, the *Frontiers journal series* operates on a revolutionary invention, the tiered publishing system, initially addressing specific communities of scholars, and gradually climbing up to broader public understanding, thus serving the interests of the lay society, too.

Dedication to quality

Each Frontiers article is a landmark of the highest quality, thanks to genuinely collaborative interactions between authors and review editors, who include some of the world's best academicians. Research must be certified by peers before entering a stream of knowledge that may eventually reach the public - and shape society; therefore, Frontiers only applies the most rigorous and unbiased reviews. Frontiers revolutionizes research publishing by freely delivering the most outstanding research, evaluated with no bias from both the academic and social point of view. By applying the most advanced information technologies, Frontiers is catapulting scholarly publishing into a new generation.

What are Frontiers Research Topics?

Frontiers Research Topics are very popular trademarks of the *Frontiers journals series*: they are collections of at least ten articles, all centered on a particular subject. With their unique mix of varied contributions from Original Research to Review Articles, Frontiers Research Topics unify the most influential researchers, the latest key findings and historical advances in a hot research area.

Find out more on how to host your own Frontiers Research Topic or contribute to one as an author by contacting the Frontiers editorial office: frontiersin.org/about/contact

Mars analogs: Environment, habitability and biodiversity

Topic editors

Yiliang Li — The University of Hong Kong, SAR China
André Antunes — Macau University of Science and Technology, China
Maggie Cy Lau Vetter — Institute of Deep-Sea Science and Engineering, Chinese Academy of Sciences (CAS), China
David Flannery — Queensland University of Technology, Australia

Citation

Li, Y., Antunes, A., Vetter, M. C. L., Flannery, D., eds. (2023). *Mars analogs: Environment, habitability and biodiversity*. Lausanne: Frontiers Media SA. doi: 10.3389/978-2-83251-882-3

Table of contents

frontiers in Astronomy and Space Sciences

ORIGINAL RESEARCH
published: 14 December 2021
doi: 10.3389/fspas.2021.741053

The Capability of Utilizing Abiotic Enantiomers of Amino Acids by *Halomonas* sp. LMO_D1 Derived From the Mariana Trench

Xiangyu Wang[1,2], *Yi Yang*[1,2], *Yongxin Lv*[1,2], *Xiang Xiao*[1,2,3] *and Weishu Zhao*[1,2]*

[1]State Key Laboratory of Microbial Metabolism, School of Life Sciences and Biotechnology, Shanghai Jiao Tong University, Shanghai, China, [2]International Center for Deep Life Investigation (IC-DLI), Shanghai Jiao Tong University, Shanghai, China, [3]Southern Marine Science and Engineering Guangdong Laboratory (Zhuhai), Zhuhai, China

D-amino acids (D-AAs) have been produced both in organisms and in environments *via* biotic or abiotic processes. However, the existence of these organic materials and associated microbial degradation activity has not been previously investigated in subduction zones where tectonic activities result in the release of hydrothermal organic matter. Here, we isolated the bacterium *Halomonas* sp. LMO_D1 from a sample obtained from the Mariana trench, and we determined that this isolate utilized 13 different D-AAs (D-Ala, D-Glu, D-Asp, D-Ser, D-Leu, D-Val, D-Tyr, D-Gln, D-Asn, D-Pro, D-Arg, D-Phe, and D-Ile) in the laboratory and could grow on D-AAs under high hydrostatic pressure (HHP). Moreover, the metabolism of L-AAs was more severely impaired under HHP conditions compared with that of their enantiomers. The essential function gene (Chr_2344) required for D-AA catabolism in strain LMO_D1 was identified and confirmed according to the fosmid library method used on the D-AAs plate. The encoded enzyme of this gene (DAADH_2344) was identified as D-amino acid dehydrogenase (DAADH), and this gene product supports the catabolism of a broad range of D-AAs. The ubiquitous distribution of DAADHs within the Mariana Trench sediments suggests that microorganisms that utilize D-AAs are common within these sediments. Our findings provide novel insights into the microbial potential for utilizing abiotic enantiomers of amino acids within the subduction zone of the Mariana trench under HHP, and our results provide an instructive significance for understanding these abiotic enantiomers and allow for insights regarding how organisms within extraterrestrial HHP environments can potentially cope with toxic D-AAs.

Keywords: D-amino acids, Mariana trench, high hydrostatic pressure, D-amino acids dehydrogenase, abiotic enantiomers

OPEN ACCESS

Edited by:
Yiliang Li,
The University of Hong Kong, Hong Kong SAR, China

Reviewed by:
Henry Sun,
Desert Research Institute (DRI), United States
Zhiyong Huang,
Tianjin Institute of Industrial Biotechnology (CAS), China

***Correspondence:**
Weishu Zhao
zwsh88@sjtu.edu.cn

Specialty section:
This article was submitted to Astrobiology, a section of the journal Frontiers in Astronomy and Space Sciences

Received: *14 July 2021*
Accepted: *29 October 2021*
Published: *14 December 2021*

Citation:
Wang X, Yang Y, Lv Y, Xiao X and Zhao W (2021) The Capability of Utilizing Abiotic Enantiomers of Amino Acids by Halomonas *sp. LMO_D1 Derived From the Mariana Trench. Front. Astron. Space Sci. 8:741053. doi: 10.3389/fspas.2021.741053*

INTRODUCTION

Among all three domains of life, proteins are composed of 19 L-form amino acids (along with the achiral glycine), and these are known as the 20 proteinogenic amino acids (Burton and Berger, 2018). The use of one type of enantiomers instead of enantiomers mixtures is considered to be the foundation for the stability of biomolecules (Hein and Blackmond, 2012). Although single handedness has been selected for use in proteins, both of the mirror-image forms of amino

acids can be generated *via* abiotic or biotic processes. The simulated scenarios in the context of laboratory abiotic synthesis of these chiral molecules, including spark discharge experiments (Miller, 1953), the Strecker reaction (Peltzer et al., 1984), and other hydrothermal reactions (Kebukawa et al., 2017) have demonstrated that racemic mixtures are always yielded. Racemization is another non-negligible process that can generate enantiomer mixtures. The estimated racemization half-lives of amino acids are 0.1–1 million years at temperatures comparable with that of the surface of the Earth (Bada and Miller, 1987). Natural abiotic synthesis products are primarily identified in meteorites, where the vast majority of chiral molecules are racemic (Pizzarello, 2006). To date, 14 of the 20 proteinogenic amino acids (Ala, Asp, Glu, Gly, Ile, Leu, Pro, Ser, Thr, Val, Tyr, Phe, Met, and Trp) have been detected in meteorites or identified in abiotic synthesis (Menez et al., 2018; Glavin et al., 2020). The amounts of amino acids can reach the order of ppm (parts per million) and can vary according to the types of amino acids or meteorites (Pizzarello et al., 2012; Glavin et al., 2020). In addition to their generation *via* biotic processes, certain D-AAs have also been discovered in some functional structures present in prokaryotes, eukaryotes, and viruses. For example, D-AAs (usually D-Ala, D-Glu, D-Ser, and D-Asp) are components of the cell walls of bacteria (Vollmer et al., 2008). D-Ser acts as a neurotransmitter in the brain (Snyder and Kim, 2000). These D-AAs are generated from L-AAs by enzymatic racemization that occurs *via* racemases (Zhang and Sun, 2014) and are released into the environment by direct secretion or through cell lysis (Zhang et al., 2015).

As enantiomers of proteinogenic amino acids, D-AAs present within various environments are toxic to organisms due to their ability to interfere with translation by binding to tRNA (Soutourina et al., 2004) and to interfere with the formation of peptidoglycans (Caparros et al., 1992). Therefore, the catabolism of D-AAs is a significant component of the detoxification process, and this process can be summarized into two aspects that include the direct oxidization of D-AAs to α-keto acids and the transformation of D-AAs into L-enantiomers in a manner that is coupled with L-AA catabolism (Zhang et al., 2021). Related enzymes involved in D-AA catabolism can be divided into broad-spectrum oxidase/dehydrogenases, substrate-specific oxidases, and racemases. DAADHs are the most commonly used broad-spectrum oxidases for D-AA direct oxidation to the corresponding α-keto acids and ammonia in prokaryotes, and have been identified in various species such as *Pseudomonas aeruginosa* (Marshall and Sokatch, 1968), *Escherichia coli* (Olsiewski et al., 1980), and *Helicobacter pylori* (Tanigawa et al., 2010). D-AA oxidases catalyze the oxidative deamination of uncharged aliphatic, aromatic, and polar D-AAs to produce α-keto acids, ammonia, and hydrogen peroxide that have been observed in most eukaryotic organisms and in some bacteria (Pollegioni et al., 2008). The substrate-specific oxidases include D-aspartate oxidase, D-Ser dehydratase, D-Cys desulfhydrase, and D-proline dehydrogenase. Conversely, amino acid racemases that function to mediate the interconversion of amino acid enantiomers are ubiquitous in bacteria and are consequently considered to play an important role in preventing the toxicity of D-AAs (Zhang and Sun, 2014). In archaea, a PLP-dependent racemase enables *Pyrococcus horikoshii* OT-3 to offset the essential L-amino acid requirement by adding D-type enantiomers (Kawakami et al., 2015). These enzymes are related to either D-AA oxidation or to D-AA transformation to the L-enantiomers and can also enable the utilization of D-AAs as carbon or nitrogen sources. The bioavailability of D-AAs has been verified in a number of microbes that have been isolated from a number of sources including soils, the rhizosphere (Radkov et al., 2016), seawater, and sediments (Fu et al., 2016; Kubota et al., 2016; Yu et al., 2019). As the formation of D-AAs by biotic racemization is a ubiquitous process, the utilization of D-AAs may not be limited to the above ecosystems. In this study, we primarily aim to extend the knowledge of the catabolic processes of D-AAs to the deepest area on Earth (the hadal trench).

The hadal trench possesses a water depth of greater than 6,000 m and contains complex processes that occur at different scales, such as geology, physical dynamics, geochemistry, and biology, and this is currently the least studied area within the ocean (Jamieson, 2011). The subduction zones in the hadal trench was formed as a result of oceanic plate converging with continental plate in combination with multiple extreme characteristics, such as extremely deep water depth, high pressure, cold, and geological activity. Organic matter arrived in the hadal trench through deposition from upper water or due to migration from steep slopes that benefit from the unique funnel-like shape of the trench and frequent seismic activity (Jamieson, 2011; Luo et al., 2017). During the descent of the oceanic plate, materials within the subduction slab and the seawater are transported to the overlying mantle (Plumper et al., 2017) or reach the oceanic mantle through cracks generated by slab flexing (Zhou et al., 2015). The slab hydration and serpentinization processes liberated mantle carbon and, by reducing power, generated alkaline fluids that erupted through slab faults and fueled the ecosystem (Ohara et al., 2012). Evidence of abiotically formatted amino acids beneath the Atlantis Massif during the alteration of serpentinites indicate the potential for fluid–rock interactions that may allow for abiotic formation of amino acids in the oceanic lithosphere (Menez et al., 2018). No available data have indicated the existence of D-AAs within the Mariana trench; however, it is still reasonable to assume that both abiotic and biotic racemization from L-AAs and also the abiotic formation of amino acids can generate D-AAs within the hadal environment.

Here, we report a bacterial strain (*Halomonas* sp. LMO_D1) that possesses the ability to utilize D-AAs, and this bacterial strain was enriched and isolated from subduction zones within the Mariana trench. Cultivation experiments demonstrated that the LMO_D1 strain could grow on D-AAs even under HHP conditions. One of the essential enzymes for D-AA utilization (DAADH) has been confirmed to function well both *in vivo* and *in vitro*. Our results revealed the capability of one microbe to utilize D-AAs under HHP conditions within the subduction zone, and these results extended our knowledge of the microbes within

the hadal trench and provided a valuable microbiological material for abiotic enantiomer utilization.

MATERIALS AND METHODS

Sample collection

The sediment sample MT086 from the Mariana rench was used in this study for enrichment and strain isolation. MT086 was collected in the Challenger Deep (11°11.6988′N, 141°48.7008′E) at a depth of 8,636 m during cruise TS01 using a submersible manipulator in August of 2016. The collected samples were stored in sterile pressurized vessels at 45 MPa and 4°C for further processing.

Enrichment, isolation, and cultivation using defined medium

The medium used in this study was based on an artificial seawater (ASW) and composed of the following components per liter: 26.0 g of NaCl, 5.0 g of MgCl2·6H_2O, 1.06 g of $CaCl_2$, 4.0 g of $NaSO_4$, 0.3 g of NH_4Cl, 0.1 g of KH_2PO_4, 0.5 of g KCl, and 2.52 g of $NaHCO_3$. Additionally, ASW was supplemented with 1 ml of a trace element mixture, a vitamin mixture, a vitamin B12 solution, and a thiamine solution as described previously (Widdel et al., 2006). The pH of the medium was adjusted to 7.0 using 1 M HCl solution. A mixture of 19 D-AAs (0.01% w/v for each) was supplemented as the sole carbon source for enrichment and isolation of microbes with corresponding metabolic potential. The cultures were incubated at 8°C, and this was designed based on the optimal growth temperature of the majority of obligate piezophiles (2°C–10°C). To test the bioavailability of different amino acids, the cells were harvested, washed three times with PBS buffer, and then inoculated into ASW medium that was supplemented with 6 mM amino acids. When amino acids served as the sole nitrogen source, NH_4Cl was removed, and 6 mM glucose was added.

Enrichment and cultivation under various pressures were both performed as previously described (Wang et al., 2021). Sediments (0.15% w/v) or pure-cultured cells (initial OD600 = 0.01) were inoculated into the defined medium. The cultures were transferred into sterile plastic syringes and sealed with a rubber cover. The syringes were placed into a stainless pressure vessel (Feiyu Science and Technology Exploitation Co. Ltd., Nantong, China) and compressed as described in a previous study (Wang et al., 2021). Each culture was repeated in triplicate.

DNA extraction and PCR/qPCR amplification of 16S rRNA genes

Total DNA from sediments and enrichment samples was extracted and purified using the FastDNA™ Spin Kit for Soil (MP Biomedicals, USA) following the manual protocol. Genomic DNA from strain LMO_D1 was extracted using the phenol–chloroform method. The full-length bacterial 16S rRNA genes were amplified using primers 27F (5-AGAGTT TGATCCTGGCTCAG-3) and 1492R (5-GGTTACCTTGTT ACGACTT-3). The amplified products were ligated into the pMD18-T vector (TaKaRa, Tokyo, Japan) for sequencing. To determine the cell density of the sediment samples and enrichment culture, 16S rRNA genes from bacteria and archaea were quantified by qPCR using primers 341F/519R (5-CCTACGGGWGGCWGCA-3/5-TTACCGCGGCKGCTG-3) and 519F/908R (5-CAGCMGCCGCGGTAA-3/5-CCCGCCAAT TCCTTTAAGTT-3), respectively. Plasmids possessing archaea and bacterial 16S rRNA genes were used for standard curve construction. The quantification standard consisted of a dilution series of 1×10^3 and 1×10^9 copies/μl. To analyze the microbial composition, the V4 and V4–V5 regions of the 16S rRNA genes were amplified with primers 515F (5-GTGCCAGCMGCCGCGGTAA-3) and 806R (5-GGACTACHVGGGTWTCTAAT-3) for bacteria and 516F (5-TGYCAGCCGCCGCGGTAAHACCVGC-3) and 855R (5-TCC CCCGCCAATTCCTTTAA-3) for archaea.

Genome and 16S rRNA gene amplicon sequencing and data analysis

Genomic DNA was sequenced using an Illumina HiSeq (400 bp pair-end library; Illumina, USA) and PacBio (20-kb insert library; Pacific Biosciences, USA) platform at Shanghai Personal Biotechnology Co., Ltd. (Shanghai, China). The raw sequence reads were trimmed with SOAPec v2.0 based on the k-mer length at 17 (Luo et al., 2012). The trimmed sequences from the Illumina HiSeq platform were assembled using A5-miseq version 20160825 (Tritt et al., 2012) and SPAdes genome assembler v3.11.1 (Bankevich et al., 2012). Sequences from the PacBio platform were assembled using HGAP4 (Chin et al., 2016) and CANU V1.6 (Koren et al., 2017). Misassemblies were detected using MUMmer v3 (Delcher et al., 1999) and corrected using Pilon version 1.22 (Walker et al., 2014). Open reading frames (ORFs) were predicted using GeneMarkS version 4.32 (Besemer et al., 2001). The annotation and alignment of ORFs were both performed using Diamond v0.9.10.111 (Buchfink et al., 2015) against the NCBI NR database using an E-value cutoff of less than 10^{-6}.

The 16S rRNA gene amplicons with different barcodes were mixed together at the same amounts and sequenced on an Illumina MiSeq platform using 2×250-bp cycles. For raw sequence data, low-quality reads (average quality value <20) and lengths <150 bp and also any ambiguities were excluded from the analysis. Further analysis was performed using the QIIME2 version 2020.11 software pipeline (Bolyen et al., 2019). Taxonomic assignment was conducted using the SILVA database release 138 (Quast et al., 2013).

Fosmid library construction, screening, and identification

The genomic library of the LMO_D1 strain was constructed using the CopyControl™ HTP Fosmid Library Production Kit (Cat. No. CCFOS059) according to the instructions of the manufacturer. High-molecular-weight genomic DNA was sheared randomly, ligated into the fosmid vector pCC2FOS™,

and transfected into *E. coli* strain EPI300™-T1^{R}. Then clones were inoculated onto M9 minimal agar that was supplemented with a D-AAs mixture (0.01% w/v for each), 12.5 μg ml^{-1} of chloramphenicol, and 0.1% CopyControl™ induction solution to induce clones with high copy numbers. Fosmid DNA from positive clones was extracted using the E. Z.N.A.™ plasmid mini kit (Omega Bio-Tek, USA). The flanking sequences of the cloned insert DNA were sequenced using pCC2FOS forward and reverse sequencing primers (5′-GTACAACGA CACCTAGAC-3′ and 5′-CAGGAAACAGCCTAGGAA-3′) and blasted with the genome of strain LMO_D1 to identify the position of the insert DNA within the genome.

Protein expression, purification, and enzyme assay

The DAADH gene (Chr_2344) was cloned into the pET-28a vector between the NdeI and HindIII sites and expressed heterologously in *E. coli* BL21 (DE3). The recombinant *E. coli* strain was induced with isopropyl-β-D-thiogalactoside (0.1 mM) at 16°C for 20 h. Cells were harvested by centrifugation at 3,000 × *g* for 3 min and suspended in Buffer A containing 20 mM Tris-HCl (pH 8.0), 0.3 M NaCl, and 10% glycerol. Cells were lysed by sonication, and cell debris was removed by centrifugation at 8,000 × *g* for 40 min. The soluble and membrane fractions were separated by ultra-speed centrifugation at 160,000 × *g* for 60 min. The membrane fraction was suspended in buffer A that was supplemented with 0.03% Triton X-100. Sonication and ultra-speed centrifugation were repeated to obtain solubilized membrane proteins. The target protein was purified using Ni^{2+}-NTA resin and eluted with Buffer B containing 20 mM Tris-HCl (pH 8.0), 0.3 M NaCl, 0.3 M imidazole, and 10% glycerol.

Enzyme activity was detected using a modified method as described previously (Tanigawa et al., 2010). The reaction mixture was composed of 50 mM Tris-HCl (pH 8.0), 20 mM D-AA, 10 μM flavin adenine dinucleotide (FAD), 1.8 μM phenazine methosulfate (PMS), 0.5 mM 2,6-dichlorophenolindophenol (DCIP), and an appropriate amount of enzyme. The reaction was initiated by the addition of substrate, subsequently performed at 37°C, and ultimately terminated by the addition of 0.25% SDS. Enzyme activity was quantified by measuring the reduction of DCIP at 600 nm. As PMS could be reduced nonenzymatically by Cys, the substrate specificity for Cys was detected using the 3-methyl-2-benzothiazolinone hydrazine (MBTH) method as described previously (Yu et al., 2019).

RESULTS

Enriching and screening of a microorganism possessing D-amino acid metabolic potential

We conducted two sets of enrichment experiments that were supplemented with D-AAs as the sole carbon source. Each set of enrichment experiments was performed using two independent groups that differed in regard to cultivation pressure, and these groups were denoted as GA (at 0.1 MPa) and GH (at 70 MPa). As low temperature and HHP resulted in a reduced growth rate, the enrichment was continued for 69 days. After enrichment, the biomass yields of the GA and GH groups were estimated by quantification of 16S rRNA that was increased to 4.87×10^{8} and 2.61×10^{5} cells/ml, respectively, from an initial biomass of 1.0×10^{3} cells/ml. The structures of the microbial communities for these two enrichments were analyzed and compared with that of the original sediment *via* 16S rRNA amplicon analysis (*Materials and methods* section). The enrichment samples were dominated by *Halomonas*, and the abundances of this species were increased to 95.5% and 73.9% in the GA and GH groups from 1.9% in the sediment sample MT086. The abundance of *Macellibacteroides* was also increased to 0.9% and 11.7% in the GA and GH groups, and this value was less than 0.001% in MT086 (**Figure 1**).

Strain isolation was performed by spreading sediment or enrichment samples onto the plates. The growth was

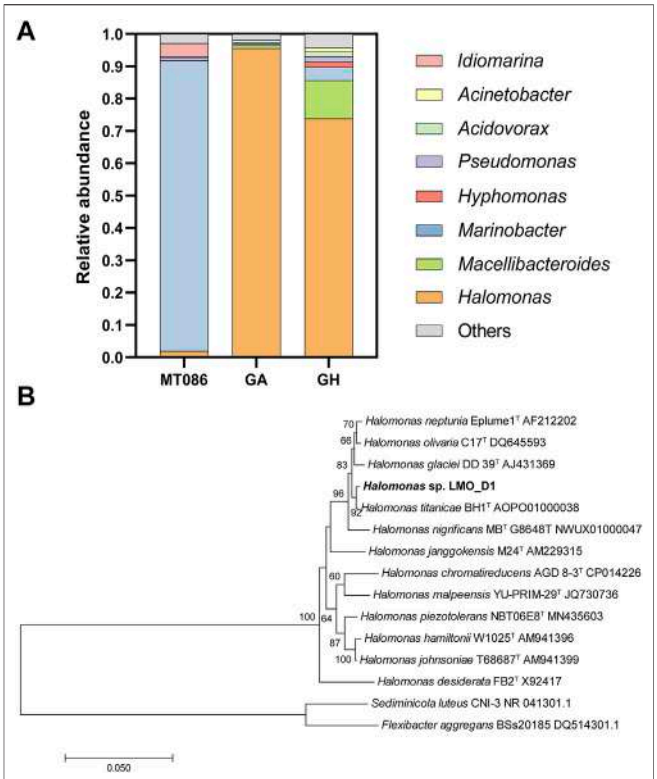

FIGURE 1 | Enrichments and isolations of microorganisms with the D-amino acid (D-AA) utilization capability. **(A)** Microbial community composition of MT086 sediment sample, enrichment sample with D-AAs as sole carbon source under 0.1 MPa (GA) and 70 MPa (GH) at genus level. **(B)** Neighbor-joining phylogenetic tree based on 16S rRNA gene sequences showing the phylogenetic position of strain LMO_D1 and other closely related species. Percentage bootstrap values above 60% (1,000 replicates) are shown at branch nodes. *Sediminicola luteus* CNI-3 and *Flexibacter aggregans* BSs20185 were used as an outgroup. Bar, 0.05 substitutions per nucleotide position.

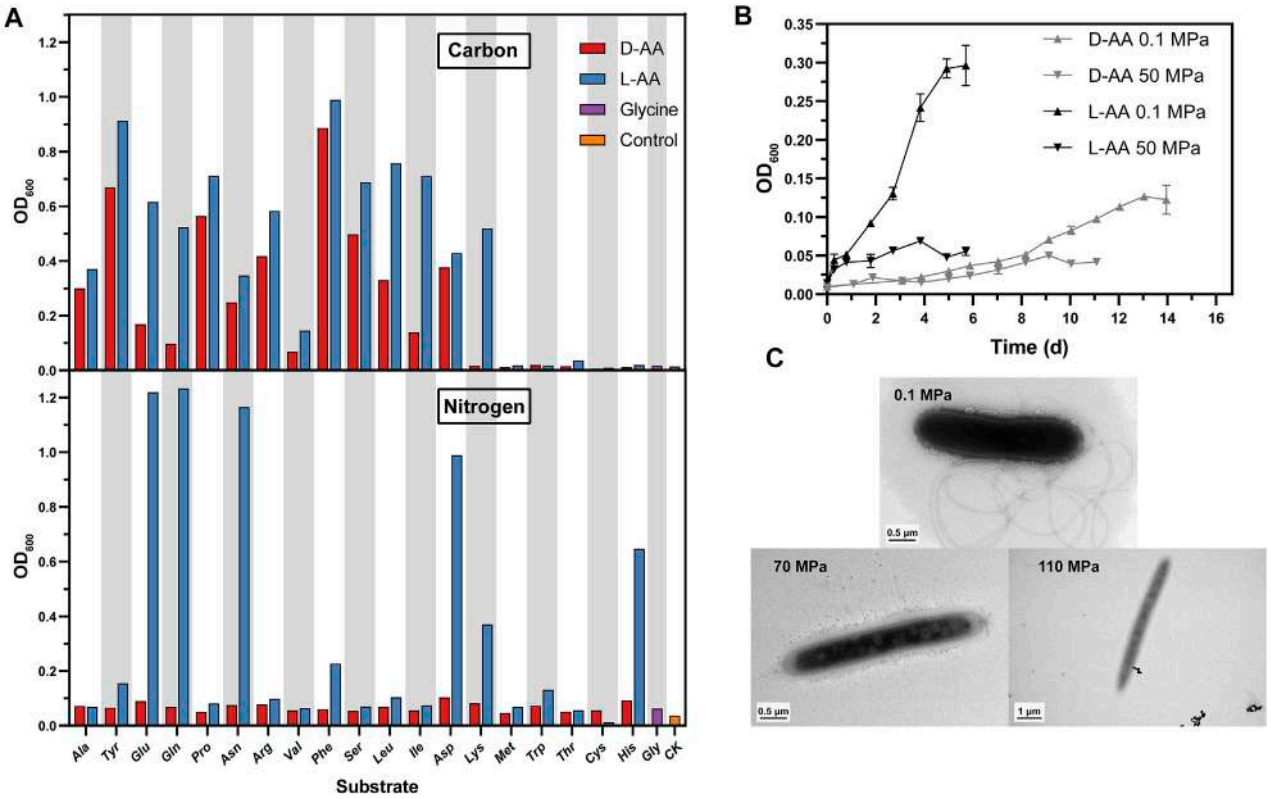

FIGURE 2 | Physiology and morphology of strain LMO_D1. **(A)** Amino acids as sole carbon or nitrogen source. CK, negative control without adding any carbon or nitrogen source. **(B)** Growth curve of strain LMO_D1 supplemented with the mixture of 19 D-AAs or 19 L-AAs as sole carbon source under 0.1 MPa or 50 MPa. Error bars represent the standard deviations among triplicates. **(C)** Transmission electron microscopic image of strain LMO_D1 cultivated under various pressure conditions (i.e., 0.1, 70, and 110 MPa).

monitored, and visible clones were present after a 2-week incubation at 8°C. When the screening plates were supplemented with all 19 D-AAs as the sole carbon source, strain LMO_D1 derived from the sediment sample MT086 was identified as *Halomonas* (**Figure 1B**). Strains were also isolated from D-AA-enriched samples of the GA and GH groups, and these were all identified as the same species as strain LMO_D1.

D-amino acid utilization by strain LMO_D1 under atmospheric pressure

When supplied as nutrients, D-AAs can be utilized as carbon or nitrogen sources, and these were separately tested in this study. The capacity of strain LMO_D1 to utilize each individual D-AA as a sole carbon and/or sole nitrogen source was investigated by cultivation under atmospheric pressure (0.1 MPa) (**Figure 2A**). For comparison, 20 proteinogenic amino acids (L-type) were also used as the sole carbon/nitrogen sources to measure the growth of the LMO_D1 strain. Each individual amino acid at a concentration of 6 mM was tested as the sole nitrogen source (6 mM D-glucose supplemented as a carbon source). Modified ASW medium (NH_4Cl removed) without the addition of any nitrogen source was used as a negative control. Individually, all 19 D-AAs were able to independently support the growth of strain LMO_D1, as indicated by an obviously increasing biomass compared with that of the negative control. Similarly, 18L-AAs and Gly could also be utilized as a nitrogen source by strain LMO_D1, with the exception of L-Cys. L-Cys cannot support the growth of strain LMO_D1, while D-Cys does support the growth of this strain. For the other 18 amino acids where both the L and D-types can be used as sole nitrogen sources, an overall improved growth was observed in response to supplementation with L-AAs as the sole nitrogen source compared with that observed in response to supplementation with D-AAs, and this was particularly true for Phe, His, Lys, Glu, Asp, Gln, and Asn (**Figure 2**).

When each individual amino acid at a concentration of 6 mM was tested as a sole carbon source (5.6 mM NH_4Cl was used as the nitrogen source), ASW medium without the addition of any carbon source was used as a negative control. Strain LMO_D1 exhibited broad utilization capability for these D-AAs (13 individuals in total), including four common D-AAs (D-Ala, D-Glu, D-Asp, and D-Ser) that are components of peptidoglycans in most bacteria and have been widely reported to be present in marine systems (McCarthy et al., 1998) and nine uncommon D-AAs (D-Leu, D-Val, D-Tyr, D-Gln, D-Asn, D-Pro, D-Arg, D-Phe, D-Ile) that are rarely detected in environments

(McCarthy et al., 1998; Kaiser and Benner, 2008) (**Figure 2A**). A similar trend was also observed for L-AA utilization in strain LMO_D1. Individual L-types of 13 AAs (Ala, Glu, Asp, Ser, Leu, Val, Tyr, Gln, Asn, Pro, Arg, Phe, and Ile) can support the growth in a manner similar to that of their D-types, thus indicating the existence of consistent catabolic pathways for amino acid enantiomers. Another L-AA (L-Lys) can support the growth of strain LMO_D1, while D-Lys cannot, thus, indicating the presence of an L-Lys utilization pathway in LMO_D1 and a lack of transfer enzymes between L-Lys and D-Lys in this strain.

Overall, better growth was observed when the medium was supplemented with L-type AA as the sole carbon or nitrogen source compared with growth in response to supplementation with the D-type. Strain LMO_D1 can utilize a greater number of D-AAs as a nitrogen source than they can as a carbon source, thus, indicating that D-AAs are more easily used as nitrogen sources. This is consistent with the results of a previous study (Wang et al., 2020).

Utilization of D-amino acids by strain LMO_D1 under high hydrostatic pressure

Considering that strain LMO_D1 was isolated from the hadal zone with a water depth of 8,636 m (equal to ~86 MPa) where the HHP caused by *in situ* water depth typically affects the metabolism of microorganisms, we also conducted D-AA utilization experiments under HHP to test if D-AA utilization can occur in the *in situ* environment (**Figure 2B**). The enrichment results indicated that the utilization of D-AAs occurred under 70 MPa conditions. However, the pre-experiments revealed that it is difficult to monitor and quantify the growth in a relatively short time under 70 and 110 MPa conditions, despite the integral cells being observed under these two pressures (**Figure 2C**). Thus, we chose a moderate pressure of 50 MPa that represents an upper limit that inhibits the growth of most piezosensitive microorganisms (Bartlett, 2002) to perform physiological experiments under HHP.

Strain LMO_D1 was then cultivated by supplementing individual L- or D-AAs as sole carbon sources under 50 MPa, and these were compared with cultivations performed under 0.1 MPa (**Figure 2B**). In general, the growth yields under HHP were lower than those under 0.1 MPa, and this was consistent with the enrichment results. When supplemented with D-AAs, growth under two different pressures exhibited a similar trend during the early stage. Subsequently, the maximum biomass yields were observed after approximately 9 and 13 days of incubation under 50 and 0.1 MPa, respectively, with a 2.52-fold higher biomass yield under 0.1 MPa. However, when cultivated with L-AAs, strain LMO_D1 exhibited a significantly higher growth rate and biomass yield under 0.1 MPa compared with these values in response to cultivation under 50 MPa. The maximum biomass under 0.1 MPa was 4.29-fold higher than that under 50 MPa. When comparing the cultivation results in response to supplementation with L-AAs and D-AAs, better growth was observed under both 0.1 and 50 MPa when L-AAs were supplemented. The growth variances under two different pressures were more significant when L-AAs were supplemented, and this indicated that the influence of HHP was different for the utilization of different amino acid enantiomers. In our experimental conditions, L-AA metabolism was more severely impaired under HHP compared with this value using their enantiomers.

TABLE 1 | Annotated genes involved in D-AAs metabolism.

Classification	Gene ID	Annotation
Racemase	Chr_1049	Glutamate racemase
	Chr_1066	Proline racemase
	Chr_1375	Asp/Glu racemase
	Chr_1541	Glutamate racemase
	Chr_3379	Proline racemase
	Chr_3588	Alanine racemase
	Chr_3707	Asp/Glu/hydantoin racemase
	Chr_4336	Asp/Glu racemase
Dehydrogenase	Chr_1066	D-amino-acid dehydrogenase (Phenylalanine)
	Chr_3502	D-amino-acid dehydrogenase (Phenylalanine)
	Chr_4236	D-amino-acid dehydrogenase (Phenylalanine)
	Chr_3902	D-amino acid dehydrogenase, small subunit
Dehydratase	Chr_1770	D-serine dehydratase
Desulfhydrase	Chr_4292	D-cysteine desulfhydrase

Genomic evidence of D-amino acid catabolism

To investigate the catabolism of D-AAs, the complete genome of *Halomonas* sp. LMO_D1 was acquired using Illumina Hiseq and Pacbio platforms and subsequently analyzed (*Materials and methods* section). The complete genome of strain LMO_D1 contained a circular chromosome possessing a sequence length of 5.41 Mb and GC content of 54.77%. The genome possessed the highest identity with *Halomonas* sp. KHS3 (average nucleotide identity = 99.12% with 91.57% sequence alignment) that was isolated from the seawater of Mar del Plata. This bacterial strain harbors a strong ability to degrade different types of aromatic compounds (Corti Monzon et al., 2018), and no reports have been published on the capacity of this strain to utilize D-AAs.

According to the genomic information, strain LMO_D1 contained a complete glycolysis/glycogenesis pathway and TCA cycle that enabled the catabolism of the carbon skeleton of D-AAs. Four types of D-AA catabolism genes were identified in the strain LMO_D1 genome, including eight amino acid racemases, four DAADHs, one D-Ser dehydratase, and one D-Cys desulfhydrase (**Table 1**). Racemase mediates the interconversion of enantiomers. The annotated amino acid racemases present in strain LMO_D1 included alanine racemase, glutamate racemase, Asp/Glu racemase, and proline racemase. DAADHs are FAD-dependent oxidases that catalyze the deamination of D-AAs to the corresponding α-keto acids and ammonia. Four genes (Chr_2344, Chr_3502, Chr_3902, and Chr_4236) were annotated as DAADH within the genome of strain LMO_D1 based on the KEGG and COG databases (Galperin et al., 2021; Kanehisa et al., 2021). However, the proteins encoded by these genes shared very low identity

TABLE 2 | Substrate specificity of DAADH_2344.

Substrate	Enzyme activity (μmol min^{-1} mg^{-1})	(%)
D-Methionine	2.20 ± 0.02	100
D-Phenylalanine	2.18 ± 0.07	99.2
D-Histidine	1.23 ± 0.03	56.2
D-Valine	1.22 ± 0.08	55.7
D-Leucine	1.14 ± 0.02	52.1
D-Tyrosine	1.13 ± 0.02	51.2
D-Tryptophan	0.74 ± 0.10	33.8
D-Threonine	0.69 ± 0.01	31.3
D-Isoleucine	0.57 ± 0.01	26.2
D-Alanine	0.33 ± 0.01	14.8
D-Asparagine	0.31 ± 0.01	14.1
D-Serine	0.23 ± 0.01	10.5
D-Arginine	0.17 ± 0.01	7.6
D-Glutamine	0.12 ± 0.01	5.6
D-Aspartic acid	0.10	4.7
D-Lysine	0.03 ± 0.02	1.4
D-Glutamic acid	--	--
D-Proline	--	--
D-Cysteine	--	--

(22.07–28.77%), thus, suggesting potentially different functions. D-Ser dehydratase transforms D-Ser into pyruvate, and ammonia D-Cys desulfhydrase transforms D-Cys into hydrogen sulfide, ammonia, and pyruvate. The abundant genes involved in D-AA catabolism may be attributed to the broad utilization of D-AAs in strain LMO_D1. Although the genome annotation revealed a small number of candidates for D-AA utilization in strain LMO_D1, it remains unclear as to which gene(s) are essential.

Functional gene screening for D-amino acid catabolism *via* fosmid library

To further identify key enzymes functioning in D-AA metabolism, a genomic DNA fosmid library of strain LMO_D1 in the heterologous host *E. coli* EPI300™–$T1^R$ was screened based on functions, where target clones grew on a mixture of 19 D-AAs as the sole carbon source with NH_4Cl as the nitrogen source. The host cells were confirmed to be unable to subsist on D-AAs. The titer of the constructed library was estimated to be 50,000 colony-forming units (cfu) per milliliter. The number of clones required to ensure a 99% probability of a given DNA sequence for strain LMO_D1 (genome = 5.4 Mb) contained within a fosmid library composed of 30-kb inserts was calculated as $N = \ln(1–0.99)/\ln[1—(30 \times 10^3 \text{ bases}/5.4 \times 10^6 \text{ bases})] = 827$ clones. A total of 3,168 clones (containing ~95.0 Mb sequence) from the library were inoculated on the D-AA screening plate, and 13 clones grew on the plate after 72-h incubation (**Supplementary Figure S1**).

The sequencing results revealed that there is a 9,203-bp sequence (the location in the genome is 2,544,984–2,554,187) containing seven coding sequences (**Supplementary Figure S2**) that are mutual for the 13 positive clones. Among them, five coding sequences were annotated with a definite function, and only one of them (Chr_2344) was annotated as a D-AA dehydrogenase (DAADH _2344) that may be related to D-AA utilization. The fosmid DNA of all 13 positive clones covered an overall 64.4-kb sequence (the location in the genome is 2,515,951–2,579,915) containing the coding sequences from Chr_2310 to Chr_2371. With the exception of the encoding gene for DAADH_2344 (Chr_2344), none of the other genes were annotated as related genes for D-AA metabolism. Specifically, the clones containing DAADH_2344 were able to grow on the D-AAs plate; other genes involved in D-AA catabolism were not included in the insert DNA of the positive clones. Our findings revealed a key role for DAADH _2344 in D-AA utilization in strain LMO_D1.

DAADH_2344 exhibited low identity (<28.34%) with all reviewed DAADHs according to the Swiss-Prot database (UniProt, 2021) (**Supplementary Figure S3**). Among the DAADHs whose functions have been identified, DAADH_2344 possessed the highest identity (26.00%) with DAADH from *Pseudomonas aeruginosa* PAO1 (NCBI accession NP_253,991.1). These low identities compared with the known DAADH indicate that the function of DAADH_2344 should be further confirmed.

Purification and identification of key enzyme D-amino acid dehydrogenase_2344 for D-amino acid metabolism

To further identify the function of DAADH_2344, we expressed its encoding gene (Chr_2344) in recombinant *E. coli*. Although DAADH has been reported as a membrane-bond protein in previous studies (Olsiewski et al., 1980; Tanigawa et al., 2010), we observed that DAADH_2344 was primarily distributed in the soluble fraction, thus, indicating that DAADH_2344 is a novel type DAADH compared with the previously reported enzyme (**Supplementary Figure S4**). The apparent molecular mass of the purified enzyme possessing two copies of the His6-tag was approximately 47 kDa according to SDS-PAGE, and this was consistent with the calculated value of 47.27 kDa for DAADH_2344 (**Supplementary Figure S4**).

The purified DAADH_2344 exhibited the specific activity of this enzyme in the presence of cofactor FAD and possessed a broad substrate scope according to the results of substrate specificity measurements using 19 D-AAs. In total, DAADH_2344 exhibited enzymatic activity against 16 D-AAs. By measuring the reduction of DCIP, the highest specific activity was observed for D-Met and D-Phe with specific activities of 2.20 and 2.18 μmol min^{-1} mg^{-1}, respectively, and this was followed by D-His, D-Val, and D-Leu with ~50% specific activity compared with that against D-Met. D-Trp, D-Thr, and D-Ile with ~30% specific activity compared with that against D-Met. Relatively low activities were observed for D-Ala, D-Asn, D-Ser, D-Arg, D-Gln, D-Asp, and D-Lys (<15% compared with D-Met). In contrast, no activity was observed for D-Pro, D-Glu, and D-Cys (**Table 2**). Additionally, DAADH_2344 exhibited strict stereospecificity, and none of the L-AAs could be used as a substrate.

Interestingly, despite the ability of the enzyme DAADH_2344 to function well against D-Met, D-Trp, D-Thr, and D-His *in vitro*, the strain LMO_D1 can only utilize D-Met, D-Trp, D-Thr, and D-His physiologically (the same as their L-type) as a nitrogen

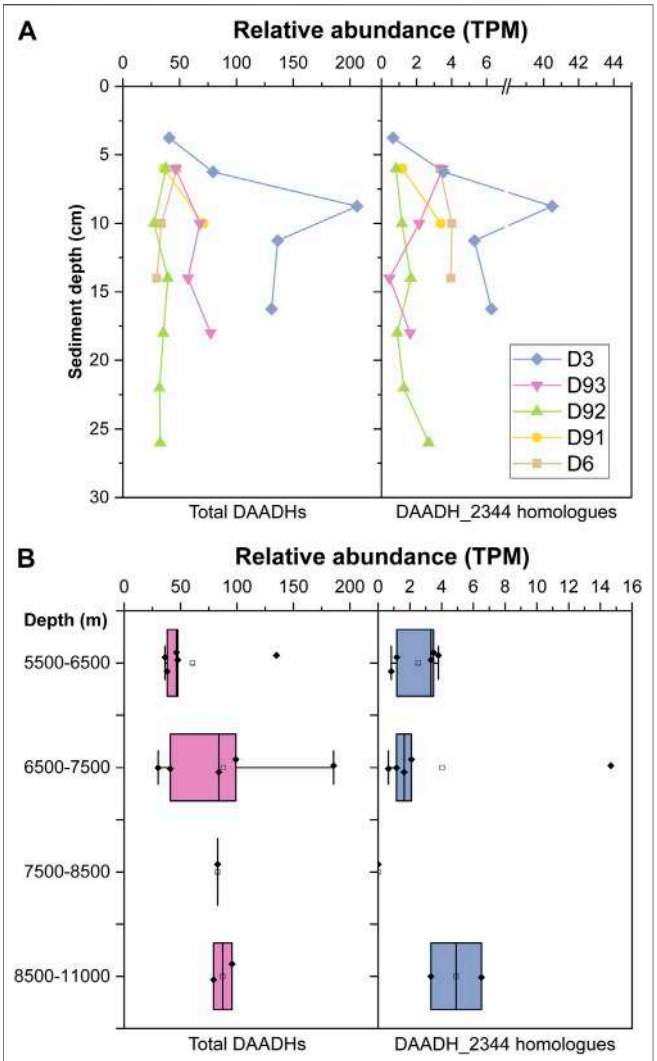

FIGURE 3 | Relative abundance [transcripts per million (TPM)] of total D-amino acid dehydrogenase (DAADHs) and DAADH_2344 homologs (identity >30%) in Mariana trench sediment samples from different sediment layers **(A)** and water depth **(B)**. Boxplots represent the statistical analysis among metagenome data of sediment samples from a certain range of water layers. Solid squares represent TPM value of an individual sample; Hollow squares represent the means; bars inside the boxes represent the medians; the hinges out of the boxes represent the lower and upper quartiles; the whiskers extend to the most extreme values (no more than 1.5 times the interquartile range from the box).

source and not as a carbon source. The failure to utilize these amino acids was assumed to be restricted by the catabolism of corresponding α-keto acids (4-methylthio-2-oxobutanoic acid, indolepyruvate, 2-oxobutanoate, urocanate), and the pathways for these compounds to enter the TCA cycle were incomplete in the genome of strain LMO_D1. Thus, neither the D nor the L-type of these amino acids was bioavailable as a carbon source. In contrast, strain LMO_D1 could utilize D-Pro, D-Glu, and D-Cys as carbon or nitrogen sources for which DAADH exhibited no activity. Hence, the catabolism of D-Pro, D-Glu, and D-Cys may be conducted by other D-AA catabolic enzymes, such as racemase, desulfhydrase, or other DAADHs encoded by the LMO_D1 strain (**Table 1**). The other 11 D-AAs (D-Ala, D-Asp, D-Ser, D-Leu, D-Val, D-Tyr, D-Gln, D-Asn, D-Arg, D-Phe, and D-Ile) that can support the growth of strain LMO_D1 could be deaminated by DAADH_2344. Based on the genomic evidence, the deaminization product of 3 D-AAs [pyruvate (D-Ala and D-Ser) and oxaloacetate (D-Asp)] could enter the TCA cycle directly. Among the α-keto acids of other D-AAs, phenylpyruvate (D-Phe), 4-methyl-2-oxopentanoate (D-Leu), and (S)-3-Methyl-2-oxopentanoic acid (D-Ile) could be transformed into acetyl-CoA, 4-hydroxyphenylpyruvate (D-Tyr) could be transformed to fumarate, and 3-methyl-2-oxobutanoic acid (D-Val) could be transformed to succinate. The 5-guanidino-2-oxopentanoate (D-Arg) could be transformed to L-Arg *via* L-arginine:pyruvate aminotransferase, and this could later be catabolized to succinate. The 2-oxoglutarate (D-Gln) and 2-oxosuccinamate could be transformed to 2-oxoglutarate and oxaloacetate, respectively, *via* the function of omega-amidase.

D-amino acid dehydrogenase distribution in Mariana trench sediment samples

DAADH_2344 was observed to strongly facilitate D-AA catabolism in strain LMO_D1 and enabled *E. coli* to grow with D-AAs as a carbon source. In regard to the essential function, the abundance of DAADH can represent the abundance of the microorganisms possessing a relatively strong adaptation to the toxic D-AAs environment. To explore the potential D-AA utilization activity in the hadal trench, we further investigated the abundance of DAADHs in sediment samples collected at a water depth of 5,481–10,893 m and those were distributed in different layers of the push cores (**Figure 3**) based on the metagenomic data of the sediment samples in the Mariana trench (unpublished data from our lab and public database). To compare the relative abundance of DAADHs in the different samples, the read counts for DAADHs (KO number K00285) were normalized to transcripts per million (TPM) counts. The relative abundance of homologous sequences of DAADH_2344 (identity >30%, e-value $<10^{-5}$) was also investigated. Overall, DAADHs were widespread within the sediment samples in the Mariana trench, and their abundance ranged from 27.60 to 206.20 TPM. Similarly, homologs (identity >30%) of DAADH_2344 were also common in the majority of the investigated samples, with the exception of one sample (Mariana_7939) that exhibited an abundance ranging from 0 to 40.47 TPM. An increase in the abundance of DAADH in conjunction with sediment depth was evident, particularly in samples D3 and D93 (**Figure 3A**). A similar trend was observed for the distribution of proteins that are closely related to DAADH_2344. However, there was no clear tendency for sediment samples at deeper water depths to harbor higher abundances of DAADHs. (**Figure 3B**).

DISCUSSION

In this study, we isolated *Halomonas* sp. LMO_D1 that possesses a broad range of D-AA utilization capability from the sample

collected from subduction zones in the Mariana trench. In previous studies, the catabolism of D-AAs was primarily examined in soils, surface marine zones, or sediments within a 1,500-m water depth (Kubota et al., 2016). Our study extends the current knowledge base to the deep trench, where both racemization and abiotic synthesis of amino acids are expected to occur in this rarely explored environment. The occurrence of D-AA catabolism is prompted by the adaptation of organisms to toxic D-AA environment. D-AA utilizers are typically discovered in environments where a high abundance of D-AAs is detected (Kawasaki and Benner, 2006; Vranova et al., 2011). Therefore, the capability of D-AA catabolism by *Halomonas* sp. LMO_D1 indicated a potentially high abundance of D-AAs in the hadal trench. Additionally, the hadal trench is an oligotrophic environment in which the catabolism of D-AAs is a strategy for better use of limited nutrients.

The isolate in this study, *Halomonas* sp. LMO_D1 is the reported microorganism that can utilize the broadest range of D-AAs. When comparing the bioavailability of D-AAs and L-AAs, the usable D-AAs for strain LMO_D1 are less abundant than are L-AAs as carbon sources, and this indicates that the carbon skeleton degradation of D-AAs shared a similar pathway to that of their L-enantiomer. However, when D-AAs are utilized as a nitrogen source, one more D-AA (D-Cys) can support cell growth, while their L-enantiomers cannot. In the genome of strain LMO_D1, the existence of D-Cys desulfhydrase that converts D-Cys into hydrogen sulfide, ammonia, and pyruvate can explain the utilization of D-Cys. However, it is difficult to determine why L-Cys cannot be utilized in the context of a general Cys desulfhydrase. This is likely correlated with the transcription level of genes or the tolerance upper limit of the substrates. A similar phenomenon in which D-AAs supported higher biomass yield than L-enantiomers has also been reported previously in experiments examining *Raoultella ornithinolytica* A25; however, the mechanism remains unclear (Naganuma et al., 2018). Further investigation may be required to fill the knowledge gap in regard to the metabolism of amino acid enantiomers.

In the genome of strain LMO_D1, the enzymes involved in D-AA catabolism covered all three types of enzymes, including racemases, substrate-specific oxidases, and broad-spectrum oxidase/dehydrogenases. Amino acid racemases participate in both the synthetic and catabolic processes of D-AAs (Zhang et al., 2021). Biosynthesis racemases are universal in bacteria that contain Ala, Glu, Asp, Ser, Lys, Pro, and broad-spectrum racemase (Hernandez and Cava, 2016), while catabolic racemases are only reported to function on Ala and are inducible by L-AAs (Walsh, 1989). For substrate-specific oxidase in the LMO_D1 genome, D-Ser dehydratase and D-Cys desulfhydrase only act on D-Ser and D-Cys, respectively. Therefore, the broad D-AA catabolism in LMO_D1 relies on the broad-spectrum oxidase/dehydrogenase DAADH. We confirmed the essential function of DAADH_2344 according to the ability of *E. coli* clones containing DAADH_2344 to grow on the D-AAs plate. The enhanced ability to subsist on D-AAs supported by DAADH_2344 and not by the other enzymes can be explained by the broad substrate specificity of the enzyme and a possible D-AA-induced transcriptional mechanism. The relative activity of DAADH_2344 against the primary components of peptidoglycans (D-Ala, D-Glu, D-Ser, and D-Asp) was much lower (<15%) than that of the optimal substrate D-Met. A similar low activity against D-Glu and D-Asp was also observed in DAADH_PA (highest identity to DAADH_2344 among all identified DAADHs) from *Pseudomonas aeruginosa* PAO1 (He et al., 2011). However, DAADH_PA exhibited higher relative activity against D-Ala and D-Ser. These results revealed that with the exception of the D-AAs from peptidoglycans, DAADH_2344 exhibits a greater preference for D-AAs that are less common in peptidoglycans and instead are likely generated through abiotic processes or other biotic processes such as secretions by microorganisms for physiological regulation (Lam et al., 2009).

Based on the various production mechanisms of D-AAs within the environment, we believe that D-AAs exert an impact on the hadal trench ecosystem. However, we only obtained *Halomonas* in the enrichment and isolation experiments. The substrate concentration supplied in this study (100 mg/L of each D-AA) was much higher than the concentration of free D-AAs in the environment (Lomstein et al., 2006), and this may have resulted in a selective growth advantage for the dominant group and the inhibition of the growth of microbes possessing lower tolerances to D-AAs. As two catabolic strategies for coping with D-AAs, racemases are universal in bacteria and represent a common adaptation to the toxic D-AA environment. Moreover, oxidase/dehydrogenases allow microorganisms to possess an enhanced ability to utilize D-AAs. We attempted to fully understand these microorganisms based on metagenomic data. DAADHs are widespread in all samples examined in this study, and this indicates that D-AA utilizers are common in the environment. D-AA-utilizing species are likely far more diverse than the limited species that we isolated in our current study. In addition to the limitations of our isolation methods, some amino acid auxotrophs may be able to utilize D-AAs as a carbon/nitrogen source but not as their sole source. Additionally, we can search for more D-AA utilizers based on metagenome data. The discovery of an increasing abundance of DAADH in conjunction with sediment depth is consistent with the increasing proportion of D-AAs with sediment depth that was reported in a previous study (Pedersen et al., 2001), likely due to the observation that D-AAs were retained for a longer period compared with L-AAs and also likely due to the racemization process. As the generation of D-AAs is mediated by both biotic and abiotic processes, more sample sites are required to clarify the connection between the abundance of DAADH and the water depth of samples and the contribution of hydrothermal activities in regard to D-AA input in the subduction zone.

In this study, the cultivation experiments under HHP demonstrated that the strain was able to perform D-AA utilization in the original environment. The enrichment experiment was performed at 70 MPa, and the increased biomass suggested that D-AA utilization can occur at least at a water depth of 7,000 m. Under these conditions, the growth of most mesophilic microorganisms, such as *E. coli*, from the surface is completely inhibited (Bartlett, 2002). The strain LMO_D1

continued to grow at such a high hydrostatic pressure, and this indicated that it performed as a piezotolerant bacterium that should not originate from surface water. We observed that HHP exerted different degrees of impact on the metabolism of amino acid enantiomers. Under HHP, the metabolism of L-AAs was impaired more severely than that of D-AAs. A likely reason for this is that DAADH mediated the catabolic reaction using quinone rather than oxygen as an electron acceptor, thus, avoiding the production of H_2O_2 that would diminish cellular oxidative stress and benefit growth under HHP (Xiao et al., 2021). Whether the phenomenon of HHP in reducing the difference between L-AAs and D-AAs in regard to supporting growth is common or exclusive in strain LMO_D1 required further investigation in other deep-sea inhabitants. The study of how pizeotolerant or piezophilic life copes with toxic D-AAs here on Earth will inspire speculation regarding how extraterrestrial life may be sustained in the icy moons of Jupiter or Saturn and the subsurface environment in Mars, where HHP would also exert a large impact on the potential life. The expanded knowledge regarding the different physiological characteristics required in response to L-AAs and D-AAs will aid in refining life detection experiments (Navarro-Gonzalez et al., 2003; Zhang et al., 2021).

DATA AVAILABILITY STATEMENT

The datasets presented in this study can be found in online repositories. The names of the repository/repositories and accession number(s) can be found below: https://www.ncbi.nlm.nih.gov/, PRJNA744311 and https://www.ncbi.nlm.nih.gov/, SRX5177670 and https://www.ncbi.nlm.nih.gov/, SRR15098654 and https://www.ncbi.nlm.nih.gov/, SRR15098655.

AUTHOR CONTRIBUTIONS

XW, XX, and WZ designed this study. XW and YY performed the experiments. XW and YL contributed to data analysis. XW and WZ wrote the article. XX revised the article.

FUNDING

This study was financially supported by the following funding: the Natural Science Foundation of China (grant numbers 41921006, 41530967, and 41776173). the National Key R and D project of China (grant number 2018YFC0309800).

ACKNOWLEDGMENTS

We are grateful to all the team members on the R/V Tansuo01 for their invaluable efforts in the sampling cruise.

SUPPLEMENTARY MATERIAL

The Supplementary Material for this article can be found online at: https://www.frontiersin.org/articles/10.3389/fspas.2021.741053/full#supplementary-material

REFERENCES

Bada, J. L., and Miller, S. L. (1987). Racemization and the Origin of Optically Active Organic Compounds in Living Organisms. *Biosystems* 20 (1), 21–26. doi:10.1016/0303-2647(87)90016-5

Bankevich, A., Nurk, S., Antipov, D., Gurevich, A. A., Dvorkin, M., Kulikov, A. S., et al. (2012). SPAdes: a New Genome Assembly Algorithm and its Applications to Single-Cell Sequencing. *J. Comput. Biol.* 19 (5), 455–477. doi:10.1089/cmb.2012.0021

Bartlett, D. H. (2002). Pressure Effects on *In Vivo* Microbial Processes. *Biochim. Biophys. Acta* 1595 (1), 367–381. doi:10.1016/S0167-4838(01)00357-0

Besemer, J., Lomsadze, A., and Borodovsky, M. (2001). GeneMarkS: a Self-Training Method for Prediction of Gene Starts in Microbial Genomes. Implications for Finding Sequence Motifs in Regulatory Regions. *Nucleic Acids Res.* 29 (12), 2607–2618. doi:10.1093/nar/29.12.2607

Bolyen, E., Rideout, J. R., Dillon, M. R., Bokulich, N. A., Abnet, C. C., Al-Ghalith, G. A., et al. (2019). Reproducible, Interactive, Scalable and Extensible Microbiome Data Science Using QIIME 2. *Nat. Biotechnol.* 37 (8), 852–857. doi:10.1038/s41587-019-0209-9

Buchfink, B., Xie, C., and Huson, D. H. (2015). Fast and Sensitive Protein Alignment Using DIAMOND. *Nat. Methods* 12 (1), 59–60. doi:10.1038/nmeth.3176

Burton, A., and Berger, E. (2018). Insights into Abiotically-Generated Amino Acid Enantiomeric Excesses Found in Meteorites. *Life* 8 (2), 14. doi:10.3390/life8020014

Caparrós, M., Pisabarro, A. G., and de Pedro, M. A. (1992). Effect of D-Amino Acids on Structure and Synthesis of Peptidoglycan in *Escherichia coli*. *J. Bacteriol.* 174 (17), 5549–5559. doi:10.1128/jb.174.17.5549-5559.1992

Chin, C.-S., Peluso, P., Sedlazeck, F. J., Nattestad, M., Concepcion, G. T., Clum, A., et al. (2016). Phased Diploid Genome Assembly with Single-Molecule Real-Time Sequencing. *Nat. Methods* 13 (12), 1050–1054. doi:10.1038/nmeth.4035

Corti Monzón, G., Nisenbaum, M., Herrera Seitz, M. K., and Murialdo, S. E. (2018). New Findings on Aromatic Compounds' Degradation and Their Metabolic Pathways, the Biosurfactant Production and Motility of the Halophilic Bacterium Halomonas Sp. KHS3. *Curr. Microbiol.* 75 (8), 1108–1118. doi:10.1007/s00284-018-1497-x

Delcher, A. L., Kasif, S., Fleischmann, R. D., Peterson, J., White, O., and Salzberg, S. L. (1999). Alignment of Whole Genomes. *Nucleic Acids Res.* 27 (11), 2369–2376. doi:10.1093/nar/27.11.2369

Fu, Y., Wang, R., Zhang, Z., and Jiao, N. (2016). Complete Genome Sequence of the D -Amino Acid Catabolism Bacterium Phaeobacter Sp. Strain JL2886, Isolated from Deep Seawater of the South China Sea. *Genome Announc* 4 (5). doi:10.1128/genomeA.00913-16

Galperin, M. Y., Wolf, Y. I., Makarova, K. S., Vera Alvarez, R., Landsman, D., and Koonin, E. V. (2021). COG Database Update: Focus on Microbial Diversity, Model Organisms, and Widespread Pathogens. *Nucleic Acids Res.* 49 (D1), D274–D281. doi:10.1093/nar/gkaa1018

Glavin, D. P., Burton, A. S., Elsila, J. E., Aponte, J. C., and Dworkin, J. P. (2020). The Search for Chiral Asymmetry as a Potential Biosignature in Our Solar System. *Chem. Rev.* 120 (11), 4660–4689. doi:10.1021/acs.chemrev.9b00474

He, W., Li, C., and Lu, C.-D. (2011). Regulation and Characterization of the dadRAX Locus for D -Amino Acid Catabolism in Pseudomonas aeruginosa PAO1. *J. Bacteriol.* 193 (9), 2107–2115. doi:10.1128/JB.00036-11

Hein, J. E., and Blackmond, D. G. (2012). On the Origin of Single Chirality of Amino Acids and Sugars in Biogenesis. *Acc. Chem. Res.* 45 (12), 2045–2054. doi:10.1021/ar200316n

Hernández, S. B., and Cava, F. (2016). Environmental Roles of Microbial Amino Acid Racemases. *Environ. Microbiol.* 18 (6), 1673–1685. doi:10.1111/1462-2920.13072

Jamieson, A. J. (2011). "Ecology of Deep Oceans: Hadal Trenches," in *eLS*. (Chichester: John Wiley and Sons, Ltd). doi:10.1002/9780470015902.a0023606

Kaiser, K., and Benner, R. (2008). Major Bacterial Contribution to the Ocean Reservoir of Detrital Organic Carbon and Nitrogen. *Limnol. Oceanogr.* 53 (1), 99–112. doi:10.4319/lo.2008.53.1.0099

Kanehisa, M., Furumichi, M., Sato, Y., Ishiguro-Watanabe, M., and Tanabe, M. (2021). KEGG: Integrating Viruses and Cellular Organisms. *Nucleic Acids Res.* 49 (D1), D545–D551. doi:10.1093/nar/gkaa970

Kawakami, R., Ohmori, T., Sakuraba, H., and Ohshima, T. (2015). Identification of a Novel Amino Acid Racemase from a Hyperthermophilic Archaeon Pyrococcus Horikoshii OT-3 Induced by D-Amino Acids. *Amino Acids* 47 (8), 1579–1587. doi:10.1007/s00726-015-2001-6

Kawasaki, N., and Benner, R. (2006). Bacterial Release of Dissolved Organic Matter during Cell Growth and Decline: Molecular Origin and Composition. *Limnol. Oceanogr.* 51 (5), 2170–2180. doi:10.4319/lo.2006.51.5.2170

Kebukawa, Y., Chan, Q. H. S., Tachibana, S., Kobayashi, K., and Zolensky, M. E. (2017). One-pot Synthesis of Amino Acid Precursors with Insoluble Organic Matter in Planetesimals with Aqueous Activity. *Sci. Adv.* 3 (3), e1602093. doi:10.1126/sciadv.1602093

Koren, S., Walenz, B. P., Berlin, K., Miller, J. R., Bergman, N. H., and Phillippy, A. M. (2017). Canu: Scalable and Accurate Long-Read Assembly via Adaptivek-Mer Weighting and Repeat Separation. *Genome Res.* 27 (5), 722–736. doi:10.1101/gr.215087.116

Kubota, T., Kobayashi, T., Nunoura, T., Maruyama, F., and Deguchi, S. (2016). Enantioselective Utilization of D-Amino Acids by Deep-Sea Microorganisms. *Front. Microbiol.* 7, 511. doi:10.3389/fmicb.2016.00511

Lam, H., Oh, D.-C., Cava, F., Takacs, C. N., Clardy, J., de Pedro, M. A., et al. (2009). D-amino Acids Govern Stationary Phase Cell wall Remodeling in Bacteria. *Science* 325 (5947), 1552–1555. doi:10.1126/science.1178123

Lomstein, B. A., Jørgensen, B. B., Schubert, C. J., and Niggemann, J. (2006). Amino Acid Biogeo- and Stereochemistry in Coastal Chilean Sediments. *Geochimica Et Cosmochimica Acta* 70 (12), 2970–2989. doi:10.1016/j.gca.2006.03.015

Luo, M., Gieskes, J., Chen, L., Shi, X., and Chen, D. (2017). Provenances, Distribution, and Accumulation of Organic Matter in the Southern Mariana Trench Rim and Slope: Implication for Carbon Cycle and Burial in Hadal Trenches. *Mar. Geology.* 386, 98–106. doi:10.1016/j.margeo.2017.02.012

Luo, R., Liu, B., Xie, Y., Li, Z., Huang, W., Yuan, J., et al. (2012). SOAPdenovo2: an Empirically Improved Memory-Efficient Short-Read De Novo Assembler. *GigaSci* 1 (1), 18. doi:10.1186/2047-217X-1-18

Marshall, V. P., and Sokatch, J. R. (1968). Oxidation of D -Amino Acids by a Particulate Enzyme from Pseudomonas aeruginosa. *J. Bacteriol.* 95 (4), 1419–1424. doi:10.1128/jb.95.4.1419-1424.1968

McCarthy, M. D., Hedges, J. I., and Benner, R. (1998). Major Bacterial Contribution to marine Dissolved Organic Nitrogen. *Science* 281 (5374), 231–234. doi:10.1126/science.281.5374.231

Ménez, B., Pisapia, C., Andreani, M., Jamme, F., Vanbellingen, Q. P., Brunelle, A., et al. (2018). Abiotic Synthesis of Amino Acids in the Recesses of the Oceanic Lithosphere. *Nature* 564 (7734), 59–63. doi:10.1038/s41586-018-0684-z

Miller, S. L. (1953). A Production of Amino Acids under Possible Primitive Earth Conditions. *Science* 117 (3046), 528–529. doi:10.1126/science.117.3046.528

Naganuma, T., Iinuma, Y., Nishiwaki, H., Murase, R., Masaki, K., and Nakai, R. (2018). Enhanced Bacterial Growth and Gene Expression of D-Amino Acid Dehydrogenase with D-Glutamate as the Sole Carbon Source. *Front. Microbiol.* 9, 2097. doi:10.3389/fmicb.2018.02097

Navarro-Gonza´lez, R., Rainey, F. A., Molina, P., Bagaley, D. R., Hollen, B. J., de la Rosa, J., et al. (2003). Mars-like Soils in the Atacama Desert, Chile, and the Dry Limit of Microbial Life. *Science* 302 (5647), 1018–1021. doi:10.1126/science.1089143

Ohara, Y., Reagan, M. K., Fujikura, K., Watanabe, H., Michibayashi, K., Ishii, T., et al. (2012). A Serpentinite-Hosted Ecosystem in the Southern Mariana Forearc. *Proc. Natl. Acad. Sci.* 109 (8), 2831–2835. doi:10.1073/pnas.1112005109

Olsiewski, P. J., Kaczorowski, G. J., and Walsh, C. (1980). Purification and Properties of D-Amino Acid Dehydrogenase, an Inducible Membrane-Bound Iron-Sulfur Flavoenzyme from *Escherichia coli* B. *J. Biol. Chem.* 255 (10), 4487–4494. doi:10.1016/S0021-9258(19)85517-5

Pedersen, A.-G. U., Thomsen, T. R., Lomstein, B. A., and Jørgensen, N. O. G. (2001). Bacterial Influence on Amino Acid Enantiomerization in a Coastal marine Sediment. *Limnol. Oceanogr.* 46 (6), 1358–1369. doi:10.4319/lo.2001.46.6.1358

Peltzer, E. T., Bada, J. L., Schlesinger, G., and Miller, S. L. (1984). The Chemical Conditions on the Parent Body of the Murchison Meteorite: Some Conclusions Based on Amino, Hydroxy and Dicarboxylic Acids. *Adv. Space Res.* 4 (12), 69–74. doi:10.1016/0273-1177(84)90546-5

Pizzarello, S., Schrader, D. L., Monroe, A. A., and Lauretta, D. S. (2012). Large Enantiomeric Excesses in Primitive Meteorites and the Diverse Effects of Water in Cosmochemical Evolution. *Proc. Natl. Acad. Sci. USA* 109 (30), 11949–11954. doi:10.1073/pnas.1204865109

Pizzarello, S. (2006). The Chemistry of Life's Origin: a Carbonaceous Meteorite Perspective. *Acc. Chem. Res.* 39 (4), 231–237. doi:10.1021/ar050049f

Plümper, O., King, H. E., Geisler, T., Liu, Y., Pabst, S., Savov, I. P., et al. (2017). Subduction Zone Forearc Serpentinites as Incubators for Deep Microbial Life. *Proc. Natl. Acad. Sci. USA* 114 (17), 4324–4329. doi:10.1073/pnas.1612147114

Pollegioni, L., Molla, G., Sacchi, S., Rosini, E., Verga, R., and Pilone, M. S. (2008). Properties and Applications of Microbial D-Amino Acid Oxidases: Current State and Perspectives. *Appl. Microbiol. Biotechnol.* 78 (1), 1–16. doi:10.1007/s00253-007-1282-4

Quast, C., Pruesse, E., Yilmaz, P., Gerken, J., Schweer, T., Yarza, P., et al. (2013). The SILVA Ribosomal RNA Gene Database Project: Improved Data Processing and Web-Based Tools. *Nucleic Acids Res.* 41 (Database issue), D590–D596. doi:10.1093/nar/gks1219

Radkov, A. D., McNeill, K., Uda, K., and Moe, L. A. (2016). D-amino Acid Catabolism Is Common Among Soil-Dwelling Bacteria. *Microb. Environ.* 31 (2), 165–168. doi:10.1264/jsme2.ME15126

Snyder, S. H., and Kim, P. M. (2000). D-amino Acids as Putative Neurotransmitters: Focus on D-Serine. *Neurochem. Res.* 25 (5), 553–560. doi:10.1023/A:1007586314648

Soutourina, O., Soutourina, J., Blanquet, S., and Plateau, P. (2004). Formation of D-Tyrosyl-tRNATyr Accounts for the Toxicity of D-Tyrosine toward *Escherichia coli*. *J. Biol. Chem.* 279 (41), 42560–42565. doi:10.1074/jbc.M402931200

Tanigawa, M., Shinohara, T., Saito, M., Nishimura, K., Hasegawa, Y., Wakabayashi, S., et al. (2010). D-amino Acid Dehydrogenase from Helicobacter pylori NCTC 11637. *Amino Acids* 38 (1), 247–255. doi:10.1007/s00726-009-0240-0

Tritt, A., Eisen, J. A., Facciotti, M. T., and Darling, A. E. (2012). An Integrated Pipeline for De Novo Assembly of Microbial Genomes. *PLoS One* 7 (9), e42304. doi:10.1371/journal.pone.0042304

UniProt, C. (2021). UniProt: the Universal Protein Knowledgebase in 2021. *Nucleic Acids Res.* 49 (D1), D480–D489. doi:10.1093/nar/gkaa1100

Vollmer, W., Blanot, D., and de Pedro, M. A. (2008). Peptidoglycan Structure and Architecture. *FEMS Microbiol. Rev.* 32 (2), 149–167. doi:10.1111/j.1574-6976.2007.00094.x

Vranova, V., Zahradnickova, H., Janous, D., Skene, K. R., Matharu, A. S., Rejsek, K., et al. (2011). The Significance of D-Amino Acids in Soil, Fate and Utilization by Microbes and Plants: Review and Identification of Knowledge Gaps. *Plant Soil* 354 (1-2), 21–39. doi:10.1007/s11104-011-1059-5

Walker, B. J., Abeel, T., Shea, T., Priest, M., Abouelliel, A., Sakthikumar, S., et al. (2014). Pilon: an Integrated Tool for Comprehensive Microbial Variant Detection and Genome Assembly Improvement. *PLoS One* 9 (11), e112963. doi:10.1371/journal.pone.0112963

Walsh, C. T. (1989). Enzymes in the D-Alanine branch of Bacterial Cell wall Peptidoglycan Assembly. *J. Biol. Chem.* 264 (5), 2393–2396. doi:10.1016/s0021-9258(19)81624-1

Wang, H., Zhang, Y., Bartlett, D. H., and Xiao, X. (2021). Transcriptomic Analysis Reveals Common Adaptation Mechanisms under Different Stresses for Moderately Piezophilic Bacteria. *Microb. Ecol.* 81 (3), 617–629. doi:10.1007/s00248-020-01609-3

Wang, R., Zhang, Z., Sun, J., and Jiao, N. (2020). Differences in Bioavailability of Canonical and Non-canonical D-Amino Acids for marine Microbes. *Sci. Total Environ.* 733, 139216. doi:10.1016/j.scitotenv.2020.139216

Widdel, F., Boetius, A., and Rabus, R. (2006). Anaerobic Biodegradation of Hydrocarbons Including Methane. *The prokaryotes* 2, 1028–1049. doi:10.1007/0-387-30742-7_33

Xiao, X., Zhang, Y., and Wang, F. (2021). Hydrostatic Pressure Is the Universal Key Driver of Microbial Evolution in the Deep Ocean and beyond. *Environ. Microbiol. Rep.* 13 (1), 68–72. doi:10.1111/1758-2229.12915

Yu, Y., Yang, J., Zheng, L.-Y., Sheng, Q., Li, C.-Y., Wang, M., et al. (2019). Diversity of D-Amino Acid Utilizing Bacteria from Kongsfjorden, Arctic and the Metabolic Pathways for Seven D-Amino Acids. *Front. Microbiol.* 10, 2983. doi:10.3389/fmicb.2019.02983

Zhang, G., and Sun, H. J. (2014). Racemization in Reverse: Evidence that D-Amino Acid Toxicity on Earth Is Controlled by Bacteria with Racemases. *PLoS One* 9 (3), e92101. doi:10.1371/journal.pone.0092101

Zhang, L., Zeng, F., McKay, C. P., Navarro-González, R., and Sun, H. J. (2021). Optimizing Chiral Selectivity in Practical Life-Detection Instruments. *Astrobiology* 21 (5), 505–510. doi:10.1089/ast.2020.2381

Zhang, Z., Zheng, Q., and Jiao, N. (2015). Microbial D-Amino Acids and marine Carbon Storage. *Sci. China Earth Sci.* 59 (1), 17–24. doi:10.1007/s11430-015-5155-x

Zhou, Z., Lin, J., Behn, M. D., and Olive, J. A. (2015). Mechanism for normal Faulting in the Subducting Plate at the Mariana Trench. *Geophys. Res. Lett.* 42 (11), 4309–4317. doi:10.1002/2015gl063917

Conflict of Interest: The authors declare that the research was conducted in the absence of any commercial or financial relationships that could be construed as a potential conflict of interest.

Publisher's Note: All claims expressed in this article are solely those of the authors and do not necessarily represent those of their affiliated organizations, or those of the publisher, the editors, and the reviewers. Any product that may be evaluated in this article, or claim that may be made by its manufacturer, is not guaranteed or endorsed by the publisher.

frontiers in Astronomy and Space Sciences

REVIEW
published: 12 January 2022
doi: 10.3389/fspas.2021.810426

The Atacama Desert in Northern Chile as an Analog Model of Mars

Armando Azua-Bustos[1,2]*, *Carlos González-Silva*[3] and *Alberto G. Fairén*[1,4]

[1]Centro de Astrobiología (CSIC-INTA), Madrid, Spain, [2]Instituto de Ciencias Biomédicas, Facultad de Ciencias de la Salud, Universidad Autónoma de Chile, Santiago, Chile, [3]Facultad de Ciencias, Universidad de Tarapacá, Arica, Chile, [4]Department of Astronomy, Cornell University, Ithaca, NY, United States

The Atacama Desert is by far the driest and oldest desert on Earth, showing a unique combination of environmental extremes (extreme dryness, the highest UV radiation levels on Earth, and highly saline and oxidizing soils), explaining why the Atacama has been largely investigated as a Mars analog model for almost 20 years. Based on the source and the amount of water available for life and its analogy with Mars, two ecosystems are of interest in the Atacama: its Coastal Range and the much drier hyperarid core, which we here review in detail. Members of the three domains of life have been found across these ecosystems living at the limit of habitability, suggesting the potential dry limits for each domain and also unveiling the highly patchy distribution of microbial life in its most extreme regions. The thorough study of the Atacama has allowed us to understand how life has adapted to its extreme conditions, the specific habitats that life occupies in each case (thus suggesting the most likely places in which to search for evidence for life on Mars), and the number of biosignatures detected across this desert. Also, the characterization of west-to-east transects across this desert has shown to be of significant value to understand the potential adaptations that Martian microorganisms may have followed in an ever-drying planet. All of this explains why the Atacama is actively used as the testing ground of the technologies (detection instruments, rovers, etc.) that were sent and will be sent to Mars. We also highlight the need to better inform the exact locations of the sites studied to understand general trends, the need to identify the true native microbial species of the Atacama, and the impact of climate change on the most arid and most Martian desert of Earth.

Keywords: Atacama, desert, astrobiology, hyperarid, Mars analog

OPEN ACCESS

Edited by:
André Antunes,
Macau University of Science and Technology, China

Reviewed by:
Don A. Cowan,
University of Pretoria, South Africa
Daniela Billi,
University of Rome Tor Vergata, Italy

***Correspondence:**
Armando Azua-Bustos
aazua@cab.inta-csic.es

Specialty section:
This article was submitted to Astrobiology, a section of the journal Frontiers in Astronomy and Space Sciences

Received: *06 November 2021*
Accepted: *06 December 2021*
Published: *12 January 2022*

Citation:
Azua-Bustos A, González-Silva C and Fairén AG (2022) The Atacama Desert in Northern Chile as an Analog Model of Mars. Front. Astron. Space Sci. 8:810426. doi: 10.3389/fspas.2021.810426

INTRODUCTION

The Atacama Desert is located in northern Chile, framed by the Andes Mountains on the east and by the Pacific Ocean on the west (**Figures 1A,B**). The Atacama is well known as the driest place on Earth (Houston and Hartley, 2003; Hartley et al., 2005; Rech et al., 2006; Sun et al., 2018). The extreme aridity of the Atacama is explained by three main factors (**Figure 2**); its location within the southern hemisphere dry subtropical climate belt, the pronounced rain shadow effect of the Andean Mountains that prevent the incoming of humid masses of air coming from the Amazon Basin, and the presence of the upwelling, north-flowing, cold Humboldt Current, which significantly reduces sea water evaporation and cloud formation (which when they form, are stopped by the Coastal Range) (Somoza and Tomlinson, 2002; Houston and Hartley, 2003; Hartley et al., 2005; Azua-Bustos et al., 2015). In addition, since the South American plate has maintained

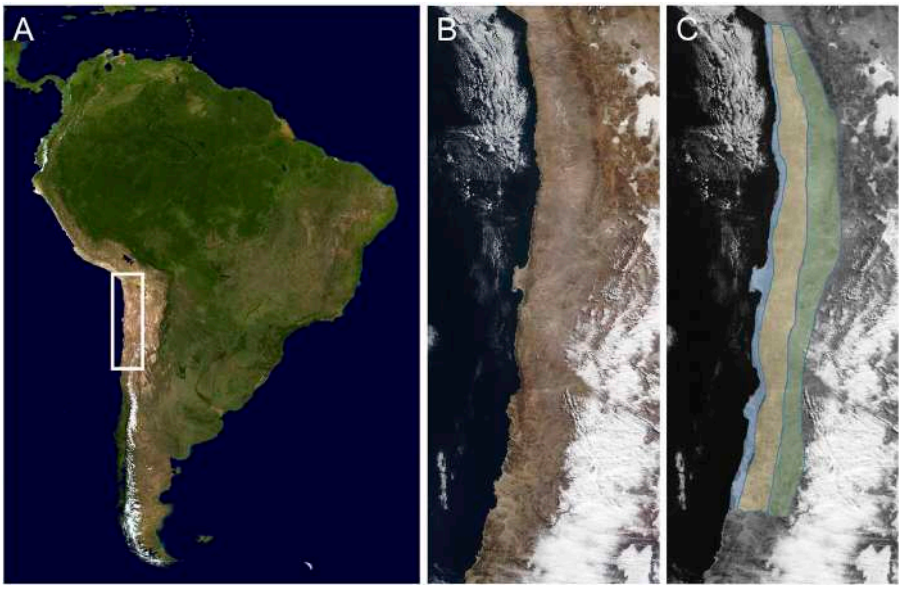

FIGURE 1 | Location of the Atacama Desert. **(A)** Location of the Atacama in South America. **(B)** Zoom of the white frame shown in A. Note the masses of clouds at the eastern side of the Andes over Argentina and Bolivia. **(C)** General location of the Coastal Range (light blue), the hyperarid core (Yellow), and the Andes Mountains and its foothills (green).

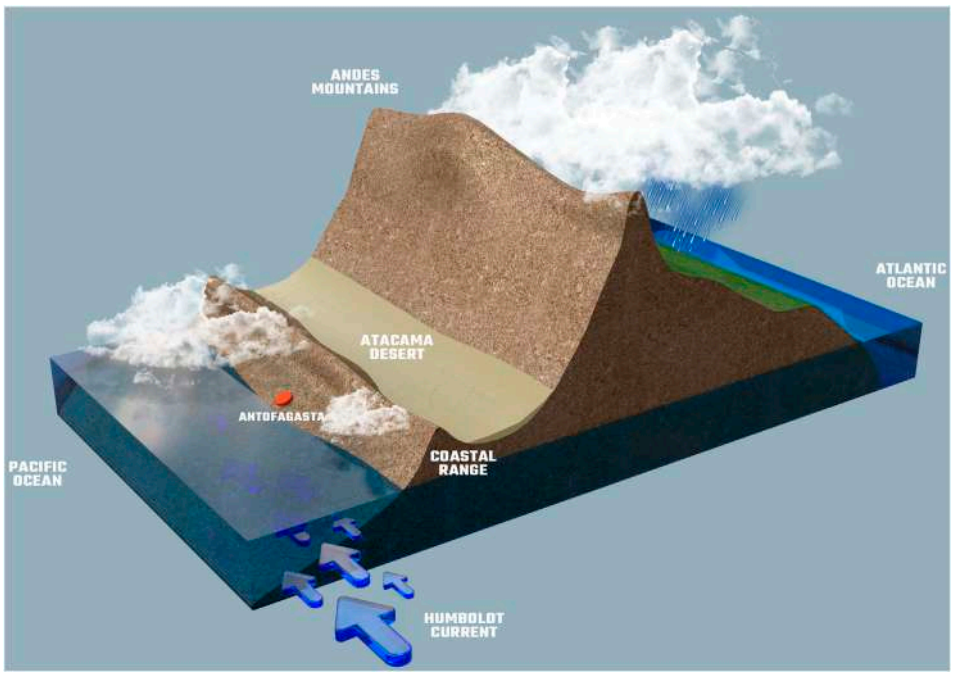

FIGURE 2 | Climatic and geographic factors that explain the extreme aridity of the Atacama.

its latitudinal position relatively in the same place for the past 150 million years, the Atacama is also the oldest desert on Earth, due to its zonal position relative to the Hadley circulation (Hartley et al., 2005). As a consequence, rains in some regions of the Atacama are as infrequent as once every 20 years (Lettau and Lettau 1978; McKay et al., 2003), with places with mean annual precipitations of only 0.15 mm (Houston 2006).

FIGURE 3 | Low-altitude clouds that originate in the Pacific Ocean (locally known as camanchaca) as they encounter the Coastal Range of the Atacama.

FIGURE 4 | Salar Grande, located at the eastern margin of the Coastal Range near the coastal city of Iquique.

FIGURE 5 | SOLID, the Signs of Life Detector, developed a the Centro de Astrobiology (Center of Astrobiology) in Spain. Photo credit: Victor Robles.

Since the times of Darwin the Atacama was considered a "sterile wasteland" (Darwin, 1845; James, 1927); however, this view dramatically changed in 2003, when Yungay, a site located in the hyperarid core of the Atacama, was suggested to be a good analog model of Mars (Navarro-González et al., 2013) (details on this report commented later in the Hyperarid Core section). In addition, the Atacama is known for having the highest UV radiation on Earth, with annual UVB doses ranging from 3.5 to 5 kWh/m^2 on the Coastal Range of the Atacama and UVA doses ranging from 130 to 160 kWh/m^2 on the Andes Mountains (Cordero et al., 2018).

This assemblage of extreme environmental conditions explains why since 2003, many reports have described the meteorological, geophysical, and microbiological characteristics of the Atacama in order to study it as a Mars analog model (Azua-Bustos et al., 2012). To aid the organization of the findings covered in this review, we summarize them into two main ecosystems from the point of view of the analogy with Mars (**Figure 1C**); the Coastal Range and the hyperarid core, a selection also based on the source and critically, the amount of water available for life in each region.

THE TWO MOST MARTIAN-LIKE ECOSYSTEMS OF THE ATACAMA DESERT

The Coastal Range

The Coastal Range is a 3,000-km-long mountain that runs from north to south along the Pacific coast at the west margin of Chile. With a maximum altitude of 3,100 m in front of the Atacama, it is much lower than the Andes Mountains (Morata et al., 2008). With a mean width of approximately 50 km, it still causes a very effective rain shadow effect, impeding the entrance of the few clouds that form due to the low temperatures of the Pacific Ocean. Even so, the main source of water for life in the Coastal Range is these low clouds that regularly cover and moist this area typically during the night and the early hours of the morning (**Figure 3**) (Cereceda et al., 2008; Azua-Bustos et al., 2010; Azua-Bustos et al., 2011).

It is at the eastern face of the Coastal Range that the studies with a focus of the Atacama as a Mars analog model were first undertaken, when in advance of the Viking missions, a team from the Jet Propulsion Laboratory inspected soil samples from deserts around the world, reporting in this case a number of microorganisms (*Streptomyces*, *Bacillus*, and *Micrococcus*) in soils samples of Uribe, a now abandoned train station (Cameron and Gensel, 1966; Bollen, 1967).

More than forty years later, Zöe (an autonomous rover) was also tested in the Coastal Range (Weinstein et al., 2008), using a daylight fluorescence imager to detect surface biosignatures near the Salar Grande (**Figure 4**), a small salt pan flanking the eastern side of the Coastal Range. Using this imager, autofluorescent biomolecules such as chlorophyll were readily detected, along other molecules such as DNA, proteins, carbohydrates, and lipids, when previously sprayed with specific fluorescent probes.

This salt pan was further investigated as a Mars analog model by drilling, in which subsurface samples were analyzed with the LDChip300 (Parro et al., 2011), a chip containing an array of

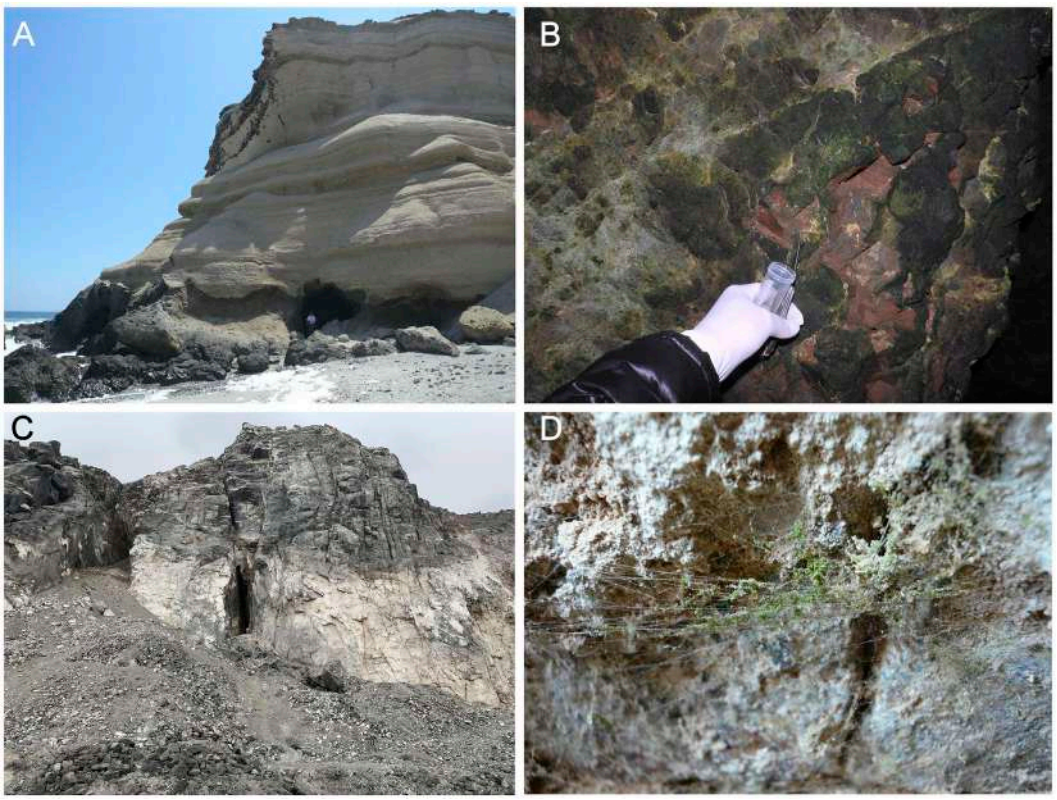

FIGURE 6 | Caves of astrobiological interest in the Coastal Range of the Atacama. **(A)** La Portada cave near the coastal city of Antofagasta. **(B)** *Cyanidium* sp. Atacama epilithic biofilms covering the rocks at the bottom of La Portada Cave. **(C)** Huanillos cave entrance (center of image shown). **(D)** A spider web colonized with *Dunaliella atacamensis* cells at Huanillos cave entrance walls.

antibodies part of the SOLID Instrument (Signs of Life Detector), planned as one of the payloads of the proposed IceBreaker Life mission to Mars (Davé et al., 2013). Using this instrument (**Figure 5**), these authors detected the biosignatures of bacteria and archaea associated with halite, nitrate, and perchlorate salts at a depth of 2 m. Phylogenetic analyses of 16 S rRNA gene sequences suggested the presence of species such as *Vibrio* and *Pseudomonas*. This same group of authors later analyzed samples from a pit 100 m of depth in this salt pan as an analog of Martian halite deposits (Sánchez-García et al., 2018). Using a number of techniques, including the LDChip, biosignatures from Haloarchaea and Cyanobacteria were found in near surface halite-rich samples, while deeper samples, composed by albite and quartz, contained biosignatures from methanogenic archaea and sulfur-oxidizing bacteria. Altogether, the analyses undertaken at Salar Grande suggested that similar subsurface environments could shelter Martian microorganisms, based on the deliquescence of hygroscopic salts such as halite, perchlorates, nitrates, and sulfates, with some of these which could also be used as potential electron acceptors by Martian microorganisms.

Other interesting biosignatures have also been found in the Coastal Range; a miniaturized Raman system was tested with samples of the Coastal Range, along other samples collected further inland (Vitek et al., 2014). Gypsum crusts from a site south of the Salar Grande and from the Salar de Llamara saline ponds (both located at the eastern margin of the Coastal Range) were analyzed, reporting the evaporites (sulfates, carbonates, and halites) characteristic of this region. These authors found that only carotenoids were detected as biosignatures in these samples, while carotenoids and chlorophyll were detected in the hyperarid core samples.

Caves of the Coastal Range have also been studied as analogs of Martian caves, of which several have been detected up to date (Cushing et al., 2007; Cushing, 2017; Titus et al., 2021). In order to test whether phototrophic microorganisms (or its remnants) could be found inside caves on Mars, well protected from the outside radiation environment, but still close enough to nearby entrances in order to perform photosynthesis, one of such caves (**Figure 6A**) was inspected north of the city of Antofagasta (Azua-Bustos et al., 2009). In support of this hypothesis, a biofilm composed by the red microalgae *Cyanidium* was found at the bottom of this cave (**Figure 6B**), surviving with only 0.06% (1 μE) of the outside photosynthetic active radiation. Transmission electron microscopy micrographs showed that cells of these microalgae had a single chloroplast using more than 50% of the cell interior, unveiling a unique adaptation to the extremely low-light conditions of the cave. Another cave, about 250 km north (**Figure 6C**), was also inspected by this team of researchers,

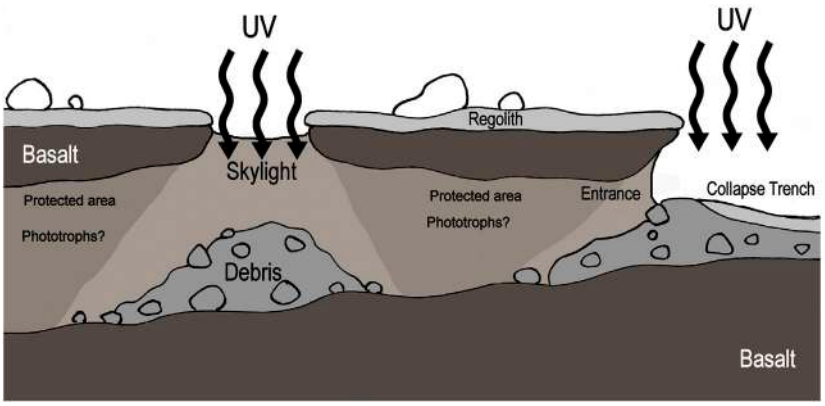

FIGURE 7 | Hypothetic location of phototrophic microorganisms in Martian caves. Modified from image of Melissa Ausburn.

FIGURE 8 | Hypolithic biofilms under quartz stones of the Coastal Range south of the city of Antofagasta.

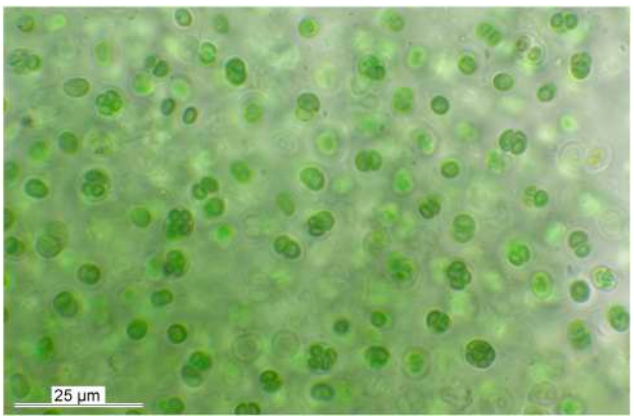

FIGURE 9 | *Gloeocapsopsis dulcis*, a cyanobacterium isolated from quartz hypolithic biofilms. Photo credit: Patrick Jung.

where the only known subaerial member of the *Dunaliella* genus of microalgae was reported growing on top of the spider webs that cover the cave wall entrance (**Figure 6D**) (Azua-Bustos et al., 2010). Such adaptation suggested that this microalgae is able to use the water condensing on the hydrophilic spider webs for photosynthesis.

The unique adaptations to alternative sources of water and low-light conditions inside these caves suggest that microbial life on Mars may have used similar strategies and similar hygroscopic materials in order to photosynthesize in a protected cave environment (**Figure 7**), where different types of chlorophyll-like molecules may be used for this end (Behrendt et al., 2020), in one of the last refuge potentially used by life in an ever-drying planet.

Hypolithic habitats have also been discovered and studied in the Coastal Range. Azua-Bustos et al. (2011) reported a community containing members of the three domains of life inhabiting the underside of translucent quartz stones (**Figure 8**) southeast of the city of Antofagasta. These authors reported that these hypolithic communities depended on fog as a source of water, and that the interaction of fog and the higher thermal conductivity of the quartz rocks (which keep them cooler than the surrounding soil environment during the day time hours), allowed for water condensation and colonization under them. Later, this team of researchers better described the diversity of microbial species under these quartzes (Azua-Bustos et al., 2014) reporting the finding of at least 70 new species from the three domains of life, among others, cyanobacteria (*Cyanothece*, *Gloeocapsopsis*, and *Nostoc*) microalgae (*Oocystis* and *Chlorella*), archaea (*Haloferax* and *Halococcus*), and a number of heterotrophic bacteria (*Bacillus*, *Deinococcus*, *Geobacillus*, *Halomonas*, and *Streptococcus*). From this hypolithic community, these authors isolated the cyanobacterium *Gloeocapsopsis dulcis* (**Figure 9**) (Azua-Bustos et al., 2014; Jung et al., 2021), a species phylogenetically close to *Chroococcidiopsis* which was used to study the molecular mechanisms explaining the tolerance of such species to extremely low water activity. These authors found that *G. dulcis* chlorophyll *a* conserved its structural integrity and autofluorescence at a water activity (a_w) as low as 0.4 for several months and that cells desiccated at a_w 0.4 synthesized increasing amounts of sucrose and trehalose, both sugars known

FIGURE 10 | Plant (*Tillandsia* sp.) banding growth patterns on top of Coastal Range hills. The inset shows how these plants look from space.

for their role as compatible solutes involved in extreme desiccation tolerance (Azua-Bustos et al., 2014).

G. dulcis cells were also used in a study aimed to detect biosignatures in distant exoplanets using polarimetry (Sterzik et al., 2010). Considering that homochirality, common in amino acids and sugars used by life on Earth, is known to induce circular polarization in the diffuse reflectance spectra, these authors used the EFOSC2 (the European Southern Observatory Faint Object Spectrograph and Camera) to analyze samples of *G. dulcis* cells, in which chiral signatures were indeed detected coming from chlorophyll *a*. The studies on the hypolithic communities unveiled the role of such ecosystems as islands of biodiversity in an extremely dry environment (as originally proposed by Warren-Rhodes et al., 2006) of critical importance when searching for evidences of life on Mars.

Even plants of the Coastal Range of the Atacama have been of use for how to detect evidences of life on Mars (Azua-Bustos and Vega-Martínez 2013). These authors argued that any lifeform in the Universe should decrease their internal entropy at the expense of free energy obtained from its surroundings. Thus, among other study models used, by using satellite images of plant growth patterns on the Coastal Range (**Figure 10**) and software based on fractal mathematics, these authors found that plants could be readily differentiated from morphologically similar surrounding abiotic patterns, which along with the analysis of sedimentary patterns on both Earth and Mars, showed that similar entropy differences could be used to detect environments altered by life on Mars.

The Coastal Range has also been searched for UV-tolerant microorganisms, with a number of *Bacillus* and *Pseudomonas* species isolated from its soils (Paulino-Lima et al., 2013). One of these *Bacillus* isolates showed a tolerance somewhat lower than that of *Deinococcus radiodurans*, suggesting that high UV tolerance was common in the Atacama. UV radiation reaches the surface of Mars unimpeded, and the finding of species extremely tolerant to UV radiation on deserts such as the Atacama suggests that microbial life in Mars may have developed similar adaptations in time.

The Hyperarid Core

With the analysis of samples of this region, the Atacama was first proposed as a pertinent model for the extremely dry conditions of Mars (Dose et al., 2001), which explains why this region of the Atacama was by far the most studied since then. These authors reported the environmental parameters (relative humidity and temperature) of two sites, Chacabuco and Yungay (**Figure 11**), in order to assess the survivability of a number of desiccation-tolerant microorganisms under the extremely dry conditions of the hyperarid core. By using the cells and spores of two bacteria and three fungi (*Bacillus subtilis spores*, *Deinococcus radiodurans*, *Aspergillus niger*, *A. ochraceus*, and *A. versicolor*), these authors found that the cells of *D. radiodurans* barely tolerated the direct daily solar radiation and extreme dryness of Yungay, although *B. subtilis* spores and *A. niger* conidia survived for more than a year in shaded areas, when exposed to direct sunlight, they survived only for a few hours.

A similar experiment was performed a few years later by Cockell *et al.* (2008), which tested whether UV radiation could prevent epilithic colonization in Yungay. With maximal UV radiation fluxes of 0.58 W/m^2 taking place at 13:00 h, two "biological dosimeters" were tested: *Chroococcidiopsis* cells from the Negev Desert and *Bacillus subtilis* spores. These authors found that the viability of *Chroococcidiopsis* cells was relatively stable until noon, with a sharp reduction in the afternoon. In the case of *B. subitilis*, its spores were completely killed within 1 day of exposure, with maximum inactivation rates taking place between 14:00 and 15:00 h. When the cells of these species were protected by 1 mm of either gypsum or quartz in order to simulate the hypolithic and cryptoendolithic environment, there was no measurable loss of viability, suggesting that the hyperarid core represented a critical threshold where extreme desiccation and UV radiation completely inhibited epilithic colonization. These results suggested that although the UV radiation fluxes are much

FIGURE 11 | Yungay, located in the hyperarid core of the Atacama. This site, reported by NASA in 2003, although not the driest, is one of the best studied on the Atacama as analog of Mars.

higher on Mars, micro-habitats within minerals may similarly attenuate UV fluxes and allow for photosynthesis to take place. However, when Yungay soil Bacteria were tested in a Mars simulation chamber (Thomas et al., 2007), including heterotrophic isolates such as *Klebsiella oxytoca*, and *Bacillus licheniformis*, these authors reported that these bacteria survived for 2 weeks in the Mars simulation chamber, with survival rates between 35% (*Bacillus licheniformis*) and 100% (*Bacillus* sp.).

The most important study that fully established the Atacama as an analog model of Mars was reported 2 years later, also using samples of Yungay (Navarro-González et al., 2013). By using surface samples collected along a north to south precipitation gradient and pyrolysis–gas chromatography–mass spectrometry (pyr-GC-MS), these authors reported that Yungay samples were almost depleted of organics, with almost undetectable amounts of formic acid and benzene, which ratio suggested that Yungay organics were highly oxidized. When these analyses were repeated at the highest temperatures (500°C) used by the Viking landers, the amount of formic acid was greatly diminished, while benzene was undetectable. This suggested that metastable organics such as the salts of aromatic and aliphatic mono and polycarboxylic acids may have been indeed present in the Martian regolith, but would not have been detected by the Viking instruments. These authors also performed a modified version of the Viking labeled release experiment (Levin and Straat, 1979) by incubating Yungay samples in an 13C-labeled sodium formate aqueous solution, observing that a fraction of the added formate was decomposed even when no cultivable microorganisms were detected, suggesting the presence of strong oxidant soil species. Yungay samples had extremely low levels of heterotrophic bacteria (1×10^3), and in many cases, no bacterial colonies were observed at any dilutions of the growing media used. In addition, no DNA was recoverable from the samples analyzed. Altogether, the collection of results allowed us to propose Yungay to be a good analog model of Martian soils, thus providing an invaluable testing ground for instruments and experiments designed for future Mars missions.

This team of researchers later continued their analysis of samples of the hyperarid core to better understand the results obtained by the Viking mission (Navarro-González et al., 2010). As the Phoenix Lander found perchlorates in the Martian regolith, these researchers reported that when Yungay samples containing small amounts (32 ppm) of organic carbon were mixed with 1% of magnesium perchlorate and then heated, most of the organics present were decomposed to water and carbon dioxide, with a small amount getting chlorinated. This result suggested that the Viking landing sites may have contained small amounts of perchlorate (0.1%) and as much as 6.5 ppm of organic carbon.

The potential effects that perchlorates would have in the detection of organics on Mars were examined using soil samples from the hyperarid core (Yungay and Lomas Bayas, among others) (Montgomery et al., 2019). These authors reported that perchlorates were highly soluble and easily leached with water. Thus, when organics were searched for (by pyrolysis–GC-MS) in unleached samples, no organics were detected, but when dried samples after leaching were analyzed, organics were easily detected. This approach unveiled that leaching prevented the complete destruction of organic compounds mediated by highly oxidant species (such as perchlorates) in detection methods where pyrolysis is used, of particular importance for the case of Mars, where perchlorates are present almost three orders of magnitude higher than those of hyperarid core soil samples. These authors suggested that on Mars, ancient surface or near-surface water flows may have concentrated organic compounds downslope, leaching away highly oxidant species at the same time, thus making the detection of organics easier in such regions.

In order to better understand the pH changes that took place with Viking Martian surface samples were wetted during the Labeled release experiment, Yungay samples among other samples from the hyperarid core were studied on the magnitude and kinetics of pH shifts upon wetting (Quinn R. et al., 2005). After wetting, both the Martian and Yungay surface samples pH underwent a rapid shift from acidic to slightly basic, shift that was not observed in the samples collected from the wetter regions of the Atacama or in the Yungay subsurface samples. The response of Yungay surface samples was consistent with a dry deposition and accumulation of atmospheric acid aerosols and acid precursors on the soil surface. These findings suggested that the sites of the hyperarid core such as Yungay are so dry that acids accumulate on its surface, and that the addition of water (mostly coming from fog) causes its dissolution and neutralization. To test such a hypothesis, this group of authors then characterized the chemical reactivity of surface and near-surface atmosphere samples by using the Mars oxidation instrument (MOI, an array of sensors that measures the reaction rates of chemical films sensitive to oxidants or that mimics chemical characteristics of prebiotic and biotic materials) which allowed the *in situ* characterization of oxidation mechanisms and kinetics (Quinn R. C. et al., 2005).

On the one hand, MOI confirmed that RH at Yungay typically reached below 10% in the afternoon hours and that each day shortly after sunset, the fog that typically covers this area caused a rapid increase up to 90% of RH in some days. In parallel, MOI recorded a chemical response immediately following the rapid increase in RH, suggesting that during the day, dry acids were created photochemically in the atmosphere from SO_2 and NO_x precursors, which then adsorbed onto dust and regolith surfaces, with oxidative acid reactions taking place at night during periods of high RH. Altogether, these responses suggested that these types of acids play an important role in the oxidizing nature and the modification of organics of Yungay surface soils, unveiling the hyperarid core photochemical environment as a pertinent model to understand the photochemical origin of Martian oxidants.

An additional approach to understand the results of the Viking labeled release experiment was focused on the analysis of the decomposition of organic compounds in aqueous solutions of Yungay soil samples by this same group of authors (Quinn et al., 2007). In the LR experiment, the addition of a ^{14}C-labeled aqueous organic substrate to a sealed test cell that contained a Martian regolith sample resulted in the evolution of ^{14}CO2. Thus, these authors added ^{13}C-labeled formate to Yungay surface soil

samples, using similar volumetric ratios used by Vikings, along a peroxide-modified titanium dioxide to simulate a nonbiological LR response. The initial pattern of CO_2 released caused by decomposition of formate was found to match those of Martian surface samples. When the D and L enantiomers of glucose and alanine were used, both decomposed at approximately equal linear rates during the first days, suggesting a nonbiological decomposition. However, an increase in $^{13}CO_2$ production in the D-glucose and L-Alanine samples compared to the L-glucose and D-Alanine samples was observed after 5 days. This lagged response followed by an increase in CO_2 production was deemed to be an indicator of biological activity. Heating the soil samples significantly attenuated the release of CO_2, suggesting the death of the microorganisms present in these samples. Although a number of alternative explanations that do not involve biology have been suggested for the Viking LR results, Quinn et al.'s (2007) results were consistent with the decomposition of formate by OH radicals as the primary mechanism for the decomposition of organics. Thus, considering the results first reported by this group of authors on the magnitude and kinetics of pH shifts of these samples upon wetting (Quinn R. et al., 2005), it seems that the three criteria established for a positive detection of life in an LR experiment were indeed met: the decomposition of organics until the added organic substrate is completely used, additional CO_2 release after additional nutrient is added, and an attenuated response of the heated control, again showing the value of analog studies with samples of the hyperarid core.

As commented before, Yungay soils have extremely low organic carbon contents, but oddly, PLFA (phospholipid fatty acids) surface concentrations were found to be five times higher than that of subsurface samples by Lester et al. (2007) (although Wilhelm et al. (2017) reported an increased presence in depth of a number of fatty acids with a high degree of structural conservancy in Yungay soils). In both cases PLFA composition was dominated by monoenoic PLFA, suggesting the presence of Gram-negative Proteobacteria. In turn, monoenoic PLFA were lower in subsurface samples, suggesting a Firmicutes community, while Mid-branched saturated PLFAs represented a small percentage of the total content, suggesting the presence of Actinobacteria. R2A and TSA growth media plate counts revealed up to 4.6×10^3 CFU per gram of soil. In order to reveal endospore-forming bacteria, a heat shock was applied to these samples, resulting in up to 300 CFU per gram of soil (for comparison, other desert soils range significantly higher, starting at 10^4 CFU/g, Kieft, 2002). 16S rRNA gene sequencing analysis of the heat-treated samples unveiled bacteria such as *Bradyrhizobium*, *Rhodopseudomonas palustris*, and *Bacillus pumilus*. Thus, given the high variations in the cultivable biomass at Yungay, these authors first unveiled the patchy distribution of microbial life in soils of the hyperarid core, suggesting that a similar, and significant spatial and possibly temporal heterogeneities in microbial distribution may also be the case on Mars.

A number of biosignatures have also been found in the soils of the hyperarid core (Wilhelm et al., 2018). In a continuation of their report of 2017, these authors reported on the diversity and abundance of lipids and other biomolecules in surface soil samples, using among other techniques, the LDChip. By inspecting a number of sites, including Yungay and Maria Elena South (details on the discovery of this site later), these authors reported that the abundance and diversity of free and membrane-bound fatty acids decreased with increasing aridity. Similarly, the LDChip also unveiled a decrease in total fluorescence by a factor of 24 in the driest sites compared to wetter sites further south, again suggesting that the surface soils of the hyperarid core were a good analog model for developing new instruments to search for evidences of life in the Martian surface.

Yungay samples were also studied using a method able to estimate bacterial cell counts based on the sublimation of adenine from *E. coli* (Glavin et al., 2004), with only traces of nucleobases identified in subsurface soils samples and no adenine detected in surface samples. DAPI staining unveiled bacterial counts of 0.7×10^6 cells/g in surface samples and 9.6×10^6 cells/g in subsurface samples, values coherent with sublimation cell count estimates. DAPI counts were higher than total counts of viable cultivable heterotrophic bacteria measured by Navarro-González et al. (2013), suggesting that the Yungay soil samples contained mostly noncultivable bacteria or again, a patchy distribution of microorganisms due to abiotic causes such as perchlorates. These authors also suggested that the Yungay soil samples were a valuable analog for life-detecting instruments on Mars, as bacterial cells should be detectable in the Martian regolith with the reported sublimation technique. These results later helped this group of authors to develop the first steps conducive to SAM, the Sample Analysis at Mars instrument now onboard the Curiosity rover (Glavin et al., 2006). By coupling their previously reported sublimation/chemical derivatization technique (Glavin et al., 2004) to GCMS (gas chromatography mass spectrometry), hyperarid core samples were analyzed in order to detect nucleobases and other volatile organic compounds derived from soil bacteria. Yungay soil surface samples showed adenine concentrations of 0.04 nmol/g, value at least two orders of magnitude higher than total viable counts previously reported in Yungay samples by Navarro-González et al. (2013), again suggesting that these samples contained mostly noncultivable bacteria.

Similarly, MOA, the Mars Organic Analyzer, a microfabricated capillary electrophoresis instrument for the detection of amino acids as biosignatures originally developed for the ExoMars mission, was also tested with Yungay samples (Skelley et al., 2005). These authors found low levels (up to 70 ppb) of alanine, aspartic acid, glycine, glutamic acid, and serine on northern and mid-latitude samples of the Atacama, while southern samples showed several amino acids, including alanine, aspartic acid, glycine, glutamic acid, serine, and valine, with values up to 500 ppb. Continuing their studies, this same group of authors then tested two instruments using Yungay samples (Skelley et al., 2007). The first was Urey, an *in situ* organics analyzer containing a subcritical water extractor. The second was MOA, already tested in 2005. Samples were collected from the top soil surface centimeter, shielded from the Sun either by rocks or from the Sun-exposed surface. These authors found that shielded samples contained low monoamine and neutral amino acid signals (i.e., valine, alanine/serine, glycine), while the exposed samples showed no signals. To improve the sensitivity limits, homogenized samples were extracted using a portable

FIGURE 12 | Colonized halites in Yungay. Note the gray/greenish layer a few mm below the artificially fractured halite surface.

subcritical water extractor (Amashukeli et al., 2007), which also showed that shielded samples contained higher levels of amino acids than exposed samples. These results showed that the exposure context significantly influenced the amount of biosignatures, an important finding to consider for the search for life on Mars. In addition, a chiral analysis used to examine the potential biotic/abiotic source of the amino acids showed similar D/L ratios of alanine/serine in shielded samples compared to gypsum-rich surface samples, unveiling the presence of viable microorganisms. The findings in gypsum-rich samples also unveiled that surface moisture is an important factor for biosignature synthesis and preservation in soils of the hyperarid core. The site containing the gypsum-rich samples is located in an ancient and now dry water flow channel, similar to those observed on Mars (Malin and Edgett, 2003). As gypsum is an evaporite of watery origin, it is interesting that samples containing it showed the presence of amines and amino acids, as it validated the capability of Urey to find potential biosignatures on similar samples on Mars.

Among other interesting discoveries in Yungay, microbial communities were then found living inside surface halites (Wierzchos et al., 2006), a finding that then gave rise to one of the best studied models on how life is still able to persist under the extreme conditions of the hyperarid core. Halite rocks in this site are composed of almost pure sodium chloride, with minor amounts of gypsum and traces of potassium chloride and quartz. Following the initial observation that many of these halites had a thin gray/greenish layer a few mm below the rock surface (**Figure 12**), samples were collected and further inspected. Light microscopy examination of this layer revealed cells similar to the cyanobacterium *Chroococcidiopsis*, with low temperature scanning electron microscopy (LTSEM) unveiling abundant cells in the spaces between salt crystals along the condensation of water in the pores among halite crystals where these cells were located. In a follow-up, these authors reported the microclimate inside and around colonized halites, to test whether the hygroscopicity of halite was involved in the survivability of its endolithic microorganisms (Davila et al., 2008). These authors found that depending on the season, air temperatures close to the soil were similar to those inside the halites, reaching up to around 50°C during the day, and as low −3°C during the night. However, during the day, RH inside the halites remained relatively high and constant for one to 3 days, while the outside RH showed the normal daily variations. These events took place when the RH inside the halites reached higher than 75% (value that matched the deliquescence RH of this mineral) and interpreted as water condensing within its internal porous spaces. This was caused by humid masses of air coming from the Pacific Ocean which with some periodicity are able to reach Yungay resulting in dew and fog, thus providing a source of water for the endolithic communities living inside halites. These findings are relevant for the case of Mars, as large regions such as Meridiani Planum or Gale Crater once hosted evaporitic environments that resulted in the precipitation of salt-rich deposits (Nachon et al., 1991; Vaniman et al., 2018). Thus, if life ever arose on Mars, biosignatures left behind by similar microorganisms may still be found inside halites. Later it was confirmed that halites were also able to condense and retain liquid water inside them due to the presence of a nano-porous phase with a smooth surface that covered large crystals and filled the larger pore spaces inside these halites (Wierzchos et al., 2012). This nano-porous phase contained pores smaller than 100 nm, allowing for capillary water condensation at RH lower than the deliquescence RH of halites, which in turn allowed for this water to be used by the endolithic microorganisms.

Continuing the characterization of hyperarid core halites, de los Ríos et al. (2010) compared the endolithic communities inside halites from three different sites (Yungay, Salar Grande, and Salar de Llamara), finding by Denaturing Gradient Gel Electrophoresis analysis (DGGE), that all these communities were composed by a single cyanobacterial species (*Chroococcidiopsis*), along a few diverging heterotrophic bacteria and archaea. An additional study of Yungay halites using Raman spectroscopy (along halites of Salar Grande and an additional unmanned site) reported the presence of chlorophyll and UV-protective biomolecules such as scytonemin, b-carotene, zeaxanthine, and lutein, all indicators of the photosynthetic activity being undertaken by these cyanobacteria (Vitek et al., 2010), deemed to be potential biosignatures to be searched for on Mars. This study was later complemented by the use of two miniaturized Raman spectrometers that searched for such biosignatures inside Yungay halites (Vítek et al., 2012). By directly analyzing halites or homogenized powdered samples (in order to simulate the sampling of Mars rovers), these authors found that carotenoids were readily detected in both samples. This suggested that carotenoids are an interesting biosignature to be searched for, as it was detectable down to 100 ppb.

These findings made possible to model what may happen with the water activity of the deliquescent solutions of chloride salts as a function of temperature in the regions of Mars containing chloride-bearing evaporites (Davila et al., 2010). According to the model proposed, RH in these regions often reached the deliquescence points of different chloride salts, and

temperatures reached levels above their eutectic points in the course of a Martian year. Considering the limits of water activity which define the so-called Mars special regions, these authors found that the deliquescence of Martian calcium chloride deposits would allow the colonization of terrestrial microorganisms at temperatures between −8 and −20°C, and metabolic activity (but not growth) at temperatures between −20 and −40°C. Altogether, the findings on halites added to the concept that hygroscopic salts may have been one of the last refuges for life on Mars (Fairén et al., 2010).

The key processes involved in the formation of the soils of the hyperarid core have also been studied (Ewing et al., 2006). These authors showed that soil formation may be explained by a shift in the balance of pedogenic processes as a function of extreme aridity. By taking soil samples across the hyperarid core, including Yungay, these authors found that along decreasing rainfall and biotic activity, soil formation crossed a threshold from net long-term mass loss (due to biogeochemical alteration of the geologic substrate), to increasing soil volume with retention of atmospheric inputs. These authors suggested that the hyperarid core pedogenic processes could be of use to understand the accumulation of atmospheric dust and solutes in the ancient Martian landscapes, as the Martian regolith contains sulfates and chlorides comparable to those of hyperarid core.

These authors also studied the still enigmatic origin of the extensive nitrate deposits only present in the hyperarid core of the Atacama have also been investigated (Ewing et al., 2007). By analyzing soil samples up to 2 m deep in a decreasing rainfall gradient from Yungay to Copiapó, these authors reported that while organic carbon decreased to 0.3 kg Cm^{-2} with decreasing rainfall, biological activity became insignificant, and nitrates and organic nitrogen increased to 4 kg Nm^{-2} and 1.4 kg Nm^{-2}. As rainfall decreased, isotopic analyses showed that atmospheric NO_3 increased from 39 to 80% of total soil NO_3. The type of soil nitrogen also changed, from 88% of organic origin at the less arid sites to 28% at the driest sites of the hyperarid core. These results suggested that the origin of the atmospheric nitrates in hyperarid core could be caused by the photochemical mobilization of upwelling marine NO_2/NO_3, as a marine origin was also consistent with observations of soil sulfates in sites of the coasts in front of the studied sites (Rech et al., 2003). This observation added an additional factor of analogy with Mars, as this report unveiled that extreme aridity stalls the nitrogen cycle by limiting the biotic component, resulting in the accumulation of oxidized N. Thus, nitrates (Stern et al., 2015) and the relatively low N_2 content of the Martian atmosphere may be reflecting the storage of nitrates in its regolith similar to the Atacama case.

The response of the direct addition of water to Yungay soils has also been studied (Davis et al., 2010). These authors performed a series of simulated rain experiments in the early evening hours south of Yungay, observing that the addition of the equivalent of less than 1 mm of rain did not saturate the surface soil. Davis and colleagues also found that the crust that covered the soil surface acted as a strong barrier to diffusion of subsurface moisture and subsequent evaporation. In turn, simulated rain events of two or more mm generated free water in the pore space of the soil surface, which could be used by microbial life, with larger amounts of water resulting in moisture retention at depth that during subsequent nights, which then diffused upward as water vapor, mobilizing salts and rewetting the dry surface. These results were deemed of value for modeling how water vapor in the upper portion of the surface of Mars could get moisture from the environment.

As oxalates in the Martian surface might account for the CO_2 release from Martian regolith observed by Viking missions (Benner et al., 2000; Applin et al., 2015), it was proposed that its detection in soils of the hyperarid core may be taken as a mineral marker that could help to understand the sources of organic carbon on Mars (Cheng et al., 2016). Thus, by reporting the presence of two oxalates at the Salar Grande, weddellite and whewellite, these authors found that weddellite was associated with surface biota, and that its presence in subsurface detrital rocks also suggested a potential biological origin, supporting the idea that life is uniquely capable of concentrating oxalates at detectable levels.

A related report focused on the hyperarid core as a model to understand the evolution of the Martian atmosphere, as the anomalous ^{17}O enrichment found in the nitrate ore fields only known in this region was proposed to be evidence of the atmospheric deposition of particles accumulated in a period of 200,000–2.0 Myears (Michalski et al., 2004). These authors suggested that ^{17}O values were a preserved isotopic signature of atmospheric processes that took place over long periods of time, and that ^{17}O measurements could be used to identify products of nitrification by potential biologic processes in Martian samples.

Similar to the case of the Coastal Range, hypolithic cyanobacteria have also been reported in Yungay (Warren-Rhodes et al., 2006). These authors reported a decrease in cyanobacterial colonization between much wetter sites such as Copiapó to nearly zero at Yungay, with a decreasing loss of diversity along the aridity gradient. Among the cyanobacteria found in Copiapó were species of *Chroococcidiopsis*, *Nostoc*, and *Phormidium* (along heterotrophic bacteria such as *Acidobacteria*, *Bradyrhizobium*, and *Caulobacter*), while below quartz stones at Yungay, only two species were found; *Chroococcidiopsis* and an unidentified γ-proteobacterium. Radiocarbon analysis of these cyanobacterial communities unveiled that microbial activity declined abruptly along the aridity gradient, with steady-state residence time values of about a year at the wettest end of the transect, and 3,000 years at Yungay. These authors also found that total organics were five times less in the surface soils than in the soils under the quartz stones where the hypolithic communities were located, first suggesting that quartz stones acted as islands of fertility and biodiversity in the extreme environment of the Atacama. Radiocarbon values showed an important difference between carbon cycling rates of the hypolithic soils and the surrounding surface soils; at wetter sites mean turnover times of hypolithic soils were the same as those of surface soils. In contrast, Yungay surface soils showed a turnover time of 13,000 years, four times greater than that of the hypolithic soils (3,200 years), suggesting that as colonization rates exponentially decline in the hyperarid core, the photosynthetic communities drove a carbon cycle in an extremely confined scale.

FIGURE 13 | María Elena South. Located in the middle of the hyperarid core and the driest site of the Atacama.

These results suggested that at Yungay, the biological threshold for photosynthetic life was mainly defined by water availability, contributing to the question of where to specifically search for photosynthetic life on Mars.

The metabolic state of the microbial species found in the hyperarid core has also been inspected (Schulze-Makuch et al., 2018). By revisiting a number of sites, including those reported by Azua-Bustos et al. (2015) (Maria Elena South and Lomas Bayas), as well as Yungay, these authors reported that surface soils were dominated by species already reported such as *Geodermatophilus* and *Rubrobacter*, while subsurface soils contained species such as Betaproteobacteria, Firmicutes (Bacillaceae, Alicyclobacillaceae), and halophilic archaea (*Halobacterium*). These authors confirmed what was previously known that although microbial biomass and microbial diversity in the Atacama Desert decrease with increasing aridity, extremely low inputs of water in this regions can sustain microbial activity, again, of interest for the case of Mars.

Although Yungay was considered the paradigm of the extreme dryness of the Atacama, the original exploration and characterization of this site was not the result of a systematic search for the driest sites of the hyperarid core, but chosen for logistical reasons (Christopher McKay, per. comm). Thus, by setting atmospheric temperature/relative humidity loggers during a 4-year interval, three sites were later reported as being much drier than Yungay; Moctezuma, Cerritos Bayos, and María Elena South (MES) with MES (**Figure 13**) being the driest of all (Azua-Bustos et al., 2015). These authors reported that while mean atmospheric RH at MES was 17.3%, at the same time period, RH at Yungay was 28.8%, with previous works reporting even higher mean atmospheric RH (36.9%) at Yungay (de los Ríos et al., 2010). Although minimum atmospheric RH was extremely low at both MES and Yungay (0 and 1%, respectively), maximum atmospheric RH was much lower at MES (54.7%) that that at Yungay (86.8%). These authors then set RH/temperature loggers in the soil profile up to a depth of 1 m at MES, finding that at 80 cm down RH was only 14.2% (equivalent to a water activity of 0.142), with little variations in time (between 12.7 and 17%). In this way, these authors reported the driest site of Atacama and of Earth, as in comparison, other hyperarid sites such as the Dry Valleys of Antarctica showed mean atmospheric RH values in the range of 55–74% (Doran et al., 2002). Extraordinarily, soil RH in depth at MES matched the lowest RH values recorded by the Remote Environmental Monitoring Station (REMS) recorded at the same time by NASA's Curiosity rover (Haberle et al. 2014), making MES one of the best analog models of Mars in terms of the extreme aridity. MES soil samples had extremely low levels of organics (up to 1.1%) and although these authors were aiming to find the dry limit of life on Earth, even soils of this site contained a number of different microorganisms, such as *Aciditerrimonas*, *Geodermatophilus*, *Caulobacter*, and *Sphingomonas*, as detected by DGGE. Culturing also allowed the isolation of a number of bacteria (*Bacillus*, *Streptomyces*, and *Geodermatophilus*). Interestingly, no archaea or any type of phototrophs were found with the culture dependent or independent methods used, suggesting that although the dry limit for life on Earth has not yet been found, at least MES was too dry for archaea and photosynthetic microorganisms such as cyanobacteria and microalgae.

Zöe also investigated the spatial distribution of microbial life in subsurface soils of the hyperarid core (including Yungay) (Warren-Rhodes et al., 2019). By analyzing a number of samples up to a depth of 80 cm, these authors found that surface sediments and subsurface horizons showed the known patchy distribution of life at the hyperarid core, with extremely low yields of DNA (0.067–6.5 ng/g), unveiling the extremely low habitability of soils of the hyperarid core, with some sites where again no DNA could be recovered at any depth, findings again in line with the first reports on the hyperarid core (Navarro-Gonzalez et al., 2013). Bacterial diversity was found to decrease in depth, with mid-depth soils showing the highest bacterial diversity dominated by Chloroflexi, Actinobacteria, and Alphaproteobacteria, a finding adding to previous reports where the Firmicutes was shown as one of the most prevalent phyla on hyperarid core samples, most likely explained by the type of sites inspected (desert pavement and desert playa only) and the amount of subsurface salts present in the sites inspected that decreased water activity.

UV-tolerant microorganisms have also been isolated from soils of the hyperarid core (Paulino Lima et al., 2016). These authors reported a number of species encompassing 28 genera of bacteria (*Bacillus*, *Hymenobacter*, *Arthrobacter*, and *Hydrogenophaga*, among others) from UVC-irradiated samples, with one of these isolates, *Hymenobacter* sp. AT01-02, found to be more tolerant to UVC than *Radiococcus radiodurans*. Intracellular Mn/Fe ratios in these isolates were found to be correlated with the level of tolerance; however, these authors found no correlation between the presence of the isolates and the contents of manganese in the soil in which they were found, suggesting that these species were able to uptake and accumulate manganese even in soils with low manganese concentrations.

The small lagoons of the Salar de Llamara (**Figure 14**) have also been investigated (Rasuk et al., 2014). This salt pan is unique as it contains a number of highly saline shallow lagoons with partially submerged fungus-shaped structures composed of calcium sulfate (Azua-Bustos et al., 2009), highly reminiscent

FIGURE 14 | Salar de Llamara salt pan, showing submerged gypsum stromatolite-like structures.

FIGURE 15 | Lagoons that formed in Yungay due to the very rare rain event that took place in 2017.

of stromatolites. Rasuk et al. (2014) analyzed the microbial communities associated with these structures by 16S rDNA gene sequencing, finding a number of bacteria (Bacteroidetes, Proteobacteria, and Planctomycetes) as the main phylogenetic groups, a diversity that increased in winter time. Although the presence of bacteria was found in these stromatolite-like structures, it is still unclear whether these are made by these microorganisms or are simply used as support, nevertheless still important as a model for similar structures that may be found on Mars (Rhawn et al., 2020).

The highly unexpected effects on the massive rain event that affected the hyperarid core in 2017 were also reported (Azua-Bustos et al., 2018). It must be noted that rains are common at the western edge of the Atacama (at the foothills of the Andes Mountains), caused by the masses of moist air coming from the Amazon basin that sometimes are able to go over the Andes during the southern hemisphere summer, thus the cause of a completely different ecosystem in this region. However, in 2015 (and also 2017 and 2019), extensive mass of rain clouds entered the hyperarid core from the Pacific Ocean, meteorological events never recorded in this region. These resulted in a number of lagoons in sites such as Yungay in 2017, which again were never recorded before in the middle of the hyperarid core of the Atacama (**Figure 15**). Strikingly, these authors found only four types of bacteria inhabiting these lagoons (*Halomonas*, Marinimicrobia, *Marinobacter*, and *Acinetobacter*), which compared with the microorganisms reported in the soils of Yungay where these lagoons formed, unveiled that the rains caused a reduction of up to 87% in the soil microbial diversity. These authors suggested that the microbial species that inhabit the hyperarid core are extremely adapted to survive with almost no water, thus when confronted with the sudden input of abundant water, they quickly perished from osmotic burst. Thus, as the Martian transition to hyperaridity is suggested to have been punctuated by episodes of vast aqueous discharges (Baker, 2004), these authors suggested that similar decimated local microbial ecosystems may have not adapted to a fast changing environment, resulting in a patchy distribution of life across the Martian surface.

The potential sources of origin of the species that have been found in the hyperarid core have been inspected too (Azua-Bustos et al., 2019). By setting plates with a number of growth media in west-to-east transects across the Coastal Range and the hyperarid core, these authors showed that wind-driven particles were a highly efficient mode of transport for microbial life across the Atacama, a process that took place in a matter of hours. As winds in this region first come over the Pacific Ocean from the south and then go east inland into the Atacama, these authors found the potential origin of the species that colonize the driest regions of the Atacama on the beaches and hills of the Coastal Range. These authors also found that, as the speed of these winds are higher in the late afternoon and nighttime hours, the transport of viable microorganisms was favored by the relatively higher RH and the lower or complete absence of UV radiation during the night. Altogether, these findings suggested that due to global wind storms on Mars, potential Martian microorganisms (both past or extant) may similarly use wind to colonize the entire planet, an observation of particular importance for planetary protection and the advent of future human colonies.

Finally, other caves have also been investigated at the eastern edge of the hyperarid core (Wynne et al., 2008), a region much wetter due to its proximity to the foothills of the Andes. Here, infrared thermal imaging was confirmed as a tool to detect caves entrances on Mars (Cushing et al., 2007). As temperatures inside a cave differ from the environment where they are located, these researchers, by studying two caves in the Cordillera de la Sal (a highly saline mountainous range at the foothills of the Andes), found that indeed cave entrances could be detected due to the thermal differences with their surroundings, particularly during midday hours.

What Has Been Learned, and Some Advisories

Due to its extreme aridity, high UV radiation, and highly saline soils, the Atacama Desert is well known in the scientific

TABLE 1 | Selected main findings covered in this review.

Main finding	Location	References
First report of microorganisms with the focus of the future Viking missions	Coastal Range	Cameron and Gensel (1966)
The Atacama Desert first proposed as a Mars analog	Yungay and Chacabuco	Dose et al. (2001)
The Atacama Desert widely accepted as an analog model of Mars	Yungay	Navarro-Gonzalez et al. (2013)
170 as potential signature of biological nitrification	Various sites hyperarid core	Michalski et al. (2004)
Dry accumulation of atmospheric aerosols on soil surfaces	Yungay	Quinn et al. (2005a)
MOI testing suggested the photochemical origin of Martian oxidants	Yungay	Quinn et al. (2005b)
Testing of MOA, the Mars Organic Analyzer	Yungay	Skelley et al. (2005)
Discovery of endolithic communities inside halites of the hyperarid core	Yungay	Wierzchos et al. (2006)
Preliminary testing conducive to SAM, Sample Analysis at Mars instrument	Yungay	Glavin et al. (2006)
Atacama soil sulfates and chlorides comparable to those of Mars	Yungay and other sites	Ewing et al. (2006)
Potential decomposition of organics by OH radicals in Viking LR experiment	Yungay	Quinn et al. (2007)
Significant spatial distribution of microbial life in Atacama soils	Yungay	Lester et al. (2007)
Extreme aridity stalls the nitrogen cycle by limiting the biotic component	Yungay and other sites	Ewing et al. (2007)
Detection of biosignatures by Zoe, an autonomous rover	Salar Grande	Weinstein et al. (2008)
Atacama hyperarid core as threshold for epilithic life	Yungay	Cockell et al. (2008)
Cave-adapted epilithic phototrophic biofilms	Coastal Range cave	Azua-Bustos et al. (2009)
Cave-adapted microalgae	Coastal Range cave	Azua-Bustos et al. (2010)
Chiral biosignatures from quartz cyanobacteria	Coastal Range	Sterzik et al. (2010)
Perchlorates as potential decomposers of organics on Mars	Yungay	Navarro-Gonzalez et al. (2010)
Hygroscopic salts as one of the last refuges for life on Mars	Yungay	Vitek et al. (2010)
Detection of biosignatures with the SOLID instrument	Salar Grande	Parro et al. (2011)
Hypolithic biofilms under quartz	Coastal Range	Azua-Bustos et al. (2011)
Fractal mathematics to detect entropy of life	Coastal Range	Azua-Bustos and Vega-Martinez (2013)
Extreme UV-tolerant microorganisms	Coastal Range	Paulino-Lima et al. (2013)
Detection of carotenoids in evaporites	Salar Grande, Salar de Llamara	Vitek et al. (2014)
Discovery of the driest site of the Atacama, still inhabited	Maria Elena South	Azua-Bustos et al. (2015)
Report of UVC tolerant bacteria	Various sites hyperarid core	Paulino-Lima et al. (2016)
Oxalates a mineral marker or organic carbon	Salar Grande	Cheng et al. (2016)
Toxic effect of rains on Atacama xerotolerant microorganisms	Yungay	Azua-Bustos et al. (2018)
Surface water flows may concentrate organics downslope	Yungay, Lomas Bayas	Montgomery et al. (2019)
Wind-transported dust, efficient transport for microbial life across the Atacama	Various sites hyperarid core	Azua-Bustos et al. (2019)

community as a good analog model of Mars (**Table 1**). Its environmental and geological characteristics have been well studied, which along the description and diversity of microorganisms and the habitats colonized by life have helped to better suggest where to look for evidences of life on Mars. Epilithic, hypolithic, endolithic, chasmoendolithic, and subsurface habitats have been reported all across the Atacama, suggesting that extreme aridity, nor high UV radiation or highly saline/oxidizing soil species, would completely hinder the presence of life on Mars. Water is available for life even in the most extreme habitats of the Atacama through different mechanisms that are still being uncovered, such as thermal differences, capillarity, hygroscopicity, or deliquescence, which explain the existence of microhabitats as true "islands of biodiversity" in an extremely harsh environment, and thus, the most interesting analog targets for the search of evidences of life on Mars. Microbial members of the three domains of life have been reported across the Atacama, with only heterotrophic bacteria reported in its driest regions, thus suggesting a potential "dry limit" for photosynthetic bacteria, eukaryotes, and archaea in such sites. For these reasons, the Atacama has turned into a leading location to test the technologies (detection instruments, rovers, etc.) to be sent to Mars (**Table 2**), and from the point of view of extreme desiccation and extremely high UV radiation, the site "Maria Elena South," located in the middle of the hyperarid core of the Atacama, is, up to now, one of the closest analogs of Mars on Earth. Also, contradictory reports on the presence and diversity of microbial life in Atacama soils have unveiled the uneven, extremely "patchy" distribution in regions in which life is at the limit of detectability, as well as the advantages and drawbacks of a number of techniques used for detecting microorganisms that are at extremely low population numbers.

TABLE 2 | Field-tested Robotic missions in the Atacama Desert.

Mission	Rover
ARADS—NASA's Atacama Rover Astrobiology Drilling Studies	KREX-2
Chameleon	SOLO
SAFER—Sample Acquisition Field Experiment with a Rover	BRIDGET
StarTiger	SEEKER
LITA—Life in the Atacama	Zoe, Hyperion
Nomad Rover Field Experiment	NOMAD

In general terms, west-to-east transects from the relatively wetter Coastal Range inland into the hyperarid core of the Atacama may in fact be considered one of the best analogs to retrace and study the potential adaptations to different habitats for life on Mars from a wetter to a dryer planet. Thus, Martian microorganisms, if ever existed, may have evolved from being able to thrive on its surface (as they do in some sites of the Coastal Range), then step-wise colonized more protected habitats as Mars got progressively drier and colder in order to survive, with

epilithic habitats in the Noachian, hypolithic in the Noachian/Hesperian transition, endolithic during the Hesperian, and then into the subsurface during the Amazonian, as is the case of the hyperarid core of the Atacama.

There are a number of key research areas and subjects to be pursued in the coming years. Currently, there are but a few reports focused on the molecular mechanisms that explain how such microorganisms are able to tolerate the extreme conditions of the Atacama, their levels of metabolic activity in different extreme environmental conditions (including Mars simulation chambers), and the potential origin and age of these species. Although wind-transported dust particles have been reported as an efficient transport mechanism to disperse microbial life across the Atacama, we still do not understand how these species are able to adapt to its new environment, and thus understand which of these can be considered distinctly "native." Also, there is a need to search for more evidences of xerophilic species unique to the Atacama, analogous to polar or saline environments elsewhere. The tools provided by the "omics" will undoubtedly help to solve these interesting questions. Similarly, few reports have studied the transition between the eastern edge of the hyperarid core of the Atacama and the much wetter foothills of the Andes Mountains. It is also important to understand the general impact of the unusual precipitations that have recently affected the Atacama, which, thought to be caused by global warming, have randomly affected different regions of this desert with yet unpredictable long-term consequences on the geology and diversity of the xerotolerant microbial species of the Atacama.

Finally, we recommend that future reports should all inform the precise location of their study sites as most give incomplete coordinates and/or the exact depths from where samples were taken, critical for understanding general trends. Care must also be taken to properly inform the general geographical frame of the study sites as there are a number of reports that comment on the well-known characteristics of the hyperarid core but with the actual study sites located in the Andes Mountains or its foothills, quite different ecosystems, and not precisely analogs of Mars. These considerations are particularly important given the highly patchy distribution of life in the Atacama, which, in addition, takes place at the limit of habitability in the most Martian place on Earth.

AUTHOR CONTRIBUTIONS

AA-B wrote the manuscript. All authors contributed to the manuscript revision, read, and approved the submitted version.

FUNDING

AAB was supported by the project UVEnergy RGY0066/2018 funded by the Human Frontiers Science Program. AAB and AGF were supported by the Project "MarsFirstWater", funded by the European Research Council, ERC Consolidator Grant No. 818602 to AGF.

REFERENCES

Amashukeli, X., Pelletier, C. C., Kirby, J. P., and Grunthaner, F. J. (2007). Subcritical Water Extraction of Amino Acids from Atacama Desert Soils. *J. Geophys. Res. Biogeosci* 11, 1–10. doi:10.1029/2006jg000308

Applin, D. M., Izawa, M. R. M., Cloutis, E. A., Goltz, D., and Johnson, J. R. (2015). Oxalate Minerals on Mars? *Earth Planet. Sci. Lett.* 420, 127–139. doi:10.1016/j.epsl.2015.03.034

Azua-Bustos, A., González-Silva, C., Fernández-MartínezArenas-Fajardo, M. Á. C., Arenas-Fajardo, C., Fonseca, R., Martín-Torres, F. J., et al. (2019). Aeolian Transport of Viable Microbial Life across the Atacama Desert, Chile: Implications for Mars. *Sci. Rep.* 9, 11024. doi:10.1038/s41598-019-47394-z

Azua-Bustos, A., Caro-Lara, L., and Caro-Lara, L. (2015). Discovery and Microbial Content of the Driest Site of the Hyperarid Atacama Desert, Chile. *Environ. Microbiol. Rep.* 7, 388–394. doi:10.1111/1758-2229.12261

Azua-Bustos, A., Fairén, A. G., González-Silva, C., Ascaso, C., Carrizo, D., Fernández-Martínez, M. Á., et al. (2018). Unprecedented rains Decimate Surface Microbial Communities in the Hyperarid Core of the Atacama Desert. *Sci. Rep.* 8, 16706. doi:10.1038/s41598-018-35051-w

Azúa-Bustos, A., González-Silva, C., Mancilla, R. A., Salas, L., Gómez-Silva, B., McKay, C. P., et al. (2011). Hypolithic Cyanobacteria Supported Mainly by Fog in the Coastal Range of the Atacama Desert. *Microb. Ecol.* 61, 568–581. doi:10.1007/s00248-010-9784-5

Azúa-Bustos, A., González-Silva, C., Mancilla, R. A., Salas, L., Palma, R. E., Wynne, J. J., et al. (2009). Ancient Photosynthetic Eukaryote Biofilms in an Atacama Desert Coastal Cave. *Microb. Ecol.* 58, 485–496. doi:10.1007/s00248-009-9500-5

Azúa-Bustos, A., González-Silva, C., Salas, L., Palma, R. E., and Vicuña, R. (2010). A Novel Subaerial Dunaliella Species Growing on Cave Spiderwebs in the Atacama Desert. *Extremophiles* 14, 443–452. doi:10.1007/s00792-010-0322-7

Azua-Bustos, A. (2009). Living Stromatolites in the Midst of the Atacama Desert: A Paradigm for the Origin of Life. *Astrobiology* 9, 518–519.

Azua-Bustos, A., Urrejola, C., and Vicuña, R. (2012). Life at the Dry Edge: Microorganisms of the Atacama Desert. *FEBS Lett.* 586, 2939–2945. doi:10.1016/j.febslet.2012.07.025

Azua-Bustos, A., and Vega-Martínez, C. (2013). The Potential for Detecting 'life as We Don't Know it' by Fractal Complexity Analysis. *Int. J. Astrobiology* 12, 314–320. doi:10.1017/s1473550413000177

Azua-Bustos, A., Zúñiga, J., Arenas-Fajardo, C., Orellana, M., Salas, L., and Rafael, V. (2014). Gloeocapsopsis AAB1, an Extremely Desiccation-Tolerant Cyanobacterium Isolated from the Atacama Desert. *Extremophiles* 18, 61–74. doi:10.1007/s00792-013-0592-y

Baker, V. R. (2004). "A Brief Geological History of Water on Mars," in *Origins. Cellular Origin, Life in Extreme Habitats and Astrobiology*. Editor J. Seckbach (Dordrecht: Springer), Vol. 6.

Behrendt, L., Trampe, E. L., Nord, N. B., Nguyen, J., Kühl, M., Lonco, D., et al. (2020). Life in the Dark: Far-red Absorbing Cyanobacteria Extend Photic Zones Deep into Terrestrial Caves. *Environ. Microbiol.* 22, 952–963. doi:10.1111/1462-2920.14774

Benner, S. A., Devine, K. G., Matveeva, L. N., and Powell, D. H. (2000). The Missing Organic Molecules on MarsMolecules on Mars. *Proc. Natl. Acad. Sci.* 97, 2425–2430. doi:10.1073/pnas.040539497

Bollen, W. B. (1967). "Identification of Chile Atacama Desert Soil Isolants," in *Progress Report Microorganisms Study. JPL Contract No 9500783.*

Cameron, R. E., and Gensel, D. R. (1966). Soil Studies—Desert Microflora. XII. Abundance of Microflora in Soil Samples from the Chile Atacama Desert. *JPL Space Programs Summ. No* IV, 37–38.

Cereceda, P., Larrain, H., Osses, P., Farías, M., and Egaña, I. (2008). The Spatial and Temporal Variability of Fog and its Relation to Fog Oases in the Atacama Desert, Chile. *Atmos. Res.* 87, 3–4. doi:10.1016/j.atmosres.2007.11.012

Cheng, Z. Y., Fernández-Remolar, D. C., Izawa, M. R. M., Applin, D. M., Chong Díaz, M., Fernandez-Sampedro, M. T., et al. (2016). Oxalate Formation under the Hyperarid Conditions of the Atacama Desert as a mineral Marker to Provide Clues to the Source of Organic Carbon on Mars. *J. Geophys. Res. Biogeosci.* 121, 1593–1604. doi:10.1002/2016jg003439

Cockell, C. S., McKay, C. P., Warren-Rhodes, K., and Horneck, G. (2008). Ultraviolet Radiation-Induced Limitation to Epilithic Microbial Growth in Arid Deserts - Dosimetric Experiments in the Hyperarid Core of the Atacama Desert. *J. Photochem. Photobiol. B: Biol.* 90, 79–87. doi:10.1016/j.jphotobiol.2007.11.009

Cordero, R. R., Damiani, A., Jorquera, J., Sepúlveda, E., Caballero, M., Fernandez, S., et al. (2018). Ultraviolet Radiation in the Atacama Desert. *Antonie Van Leeuwenhoek* 111, 1301–1313. doi:10.1007/s10482-018-1075-z

Cushing, G. E. (2017). *Mars Global Cave Candidate Catalog Archive Bundle*. Reston, Va: U.S. Geological Survey. Available at: astrogeology.usgs.gov/search/map/Mars/MarsCaveCatalog/mars_cave_catalog.zip.

Cushing, G. E., Titus, T. N., Wynne, J. J., and Christensen, P. R. (2007). THEMIS Observes Possible Cave Skylights on Mars. *Geophys. Res. Lett.* 34, L17201. doi:10.1029/2007gl030709

Darwin, C. (1845). *The Voyage of the Beagle. Excerpts from Charles Darwin, Journal of Researches into the Natural History and Geology of the Countries Visited during the Voyage of HMS Beagle Round the World: Under the Command of Capt*. Patagonia: Fitz Roy.

Davé, A., Thompson, S. J., McKay, C. P., Stoker, C. R., Zacny, K., Paulsen, G., et al. (2013). The Sample Handling System for the Mars Icebreaker Life Mission: From Dirt to Data. *Astrobiology* 13, 354–369. doi:10.1089/ast.2012.0911

Davila, A. F., Duport, L. G., Melchiorri, R., Jänchen, J., Valea, S., de los Rios, A., et al. (2010). Hygroscopic Salts and the Potential for Life on Mars. *Astrobiology* 10, 617–628. doi:10.1089/ast.2009.0421

Davila, A. F., Gómez-Silva, B., de los Rios, A., Ascaso, C., Olivares, H., McKay, C. P., et al. (2008). Facilitation of Endolithic Microbial Survival in the Hyperarid Core of the Atacama Desert by mineral Deliquescence. *J. Geophys. Res.* 113, 01028. doi:10.1029/2007jg000561

Davis, W. L., de Pater, I., and McKay, C. P. (2010). Rain Infiltration and Crust Formation in the Extreme Arid Zone of the Atacama Desert, Chile. *Planet. Space Sci.* 58, 616–622. doi:10.1016/j.pss.2009.08.011

de Los Ríos, A., Valea, S., Ascaso, C., Davila, A., Kastovsky, J., McKay, C. P., et al. (2010). Comparative Analysis of the Microbial Communities Inhabiting Halite Evaporites of the Atacama Desert. *Int. Microbiol.* 13, 79–89. doi:10.2436/20.1501.01.113

Doran, P. T., McKay, C. P., Clow, G. D., Dana, G. L., Fountain, A. G., Nylen, T., et al. (2002). Valley Floor Climate Observations from the McMurdo Dry Valleys, Antarctica, 1986–2000. *J. Geophys. Res.* 107, 1–12. doi:10.1029/2001jd002045

Dose, K., Bieger-Dose, A., Ernst, B., Feister, U., Gómez-Silva, B., Klein, A., et al. (2001). Survival of Microorganisms under the Extreme Conditions of the Atacama Desert. *Orig. Life Evol. Biosph.* 31, 287–303. doi:10.1023/a:1010788829265

Ewing, S. A., Michalski, G., Thiemens, M., Quinn, R. C., Macalady, J. L., Kohl, S., et al. (2007). Rainfall Limit of the N Cycle on Earth. *Glob. Biogeochem. Cycles* 21, GB3009. doi:10.1029/2006gb002838

Ewing, S. A., Sutter, B., Owen, J., Nishiizumi, K., Sharp, W., Cliff, S. S., et al. (2006). A Threshold in Soil Formation at Earth's Arid-Hyperarid Transition. *Geochimica et Cosmochimica Acta* 70, 5293–5322. doi:10.1016/j.gca.2006.08.020

Fairén, A. G., Davila, A. F., Lim, D., Bramall, N., Bonaccorsi, R., Zavaleta, J., et al. (2010). Astrobiology through the Ages of Mars: the Study of Terrestrial Analogues to Understand the Habitability of Mars. *Astrobiology* 10, 821–843. doi:10.1089/ast.2009.0440

Glavin, D. P., Cleaves, H. J., Buch, A., Schubert, M., Aubrey, A., Bada, J. L., et al. (2006). Sublimation Extraction Coupled with Gas Chromatography-Mass Spectrometry: A New Technique for Future *In Situ* Analyses of Purines and Pyrimidines on Mars. *Planet. Space Sci.* 54, 1584–1591. doi:10.1016/j.pss.2005.12.023

Glavin, D. P., Cleaves, H. J., Schubert, M., Aubrey, A., and Bada, J. L. (2004). New Method for Estimating Bacterial Cell Abundances in Natural Samples by Use of Sublimation. *Appl. Environ. Microbiol.* 70, 5923–5928. doi:10.1128/aem.70.10.5923-5928.2004

Haberle, R. M., Gómez-Elvira, J., de la Torre Juárez, M., Harri, A.-M., Hollingsworth, J. L., Kahanpää, H., et al. (2014). Preliminary Interpretation of the REMS Pressure Data from the First 100 Sols of the MSL mission. *J. Geophys. Res. Planets* 119, 440–453. doi:10.1002/2013je004488

Hartley, A. J., Chong, G., Houston, J., and Mather, A. E. (2005). 150 Million Years of Climatic Stability: Evidence from the Atacama Desert, Northern Chile. *J. Geol. Soc.* 162, 421–424. doi:10.1144/0016-764904-071

Houston, J. (2006). Evaporation in the Atacama Desert: An Empirical Study of Spatio-Temporal Variations and Their Causes. *J. Hydrol.* 330, 402–412. doi:10.1016/j.jhydrol.2006.03.036

Houston, J., and Hartley, A. J. (2003). The central Andean West-Slope Rainshadow and its Potential Contribution to the Origin of Hyper-Aridity in the Atacama Desert. *Int. J. Climatol.* 23, 1453–1464. doi:10.1002/joc.938

James, P. E. (1927). Iquique and the Atacama Desert. *Scottish Geographical Mag.* 43, 203–215. doi:10.1080/00369222708734550

Jung, P., Azua-Bustos, A., Gonzalez-Silva, C., Mikhailyuk, T., Zabicki, D., Holzinger, A., et al. (2021). Emendation of the Coccoid Cyanobacterial Genus Gloeocapsopsis and Description of the New Species Gloeocapsopsis Diffluens Sp. Nov. And Gloeocapsopsis Dulcis Sp. Nov. Isolated from the Coastal Range of the Atacama Desert (Chile). *Front. Microbiol.* 12, 671742. doi:10.3389/fmicb.2021.671742

Kieft, T. L. (2002). "Hot Desert Soil Communities," in *Encyclopedia of Environmental Microbiology*. Editor G. S. Bitton (New York: John Wiley), 1576–1586.

Lester, E. D., Satomi, M., and Ponce, A. (2007). Microflora of Extreme Arid Atacama Desert Soils. *Soil Biol. Biochem.* 39, 704–708. doi:10.1016/j.soilbio.2006.09.020

Lettau, H., and Lettau, K. (1978). *Exploring the World's Driest Climate*. Madison, Wisconsin: Center for Climatic Research, Institute for Environmental Studies, University of Wisconsin-Madison.

Levin, G. V., and Straat, P. A. (1979). Completion of the Viking Labeled Release experiment on Mars. *J. Mol. Evol.* 14, 167–183. doi:10.1007/bf01732376

Malin, M. C., and Edgett, K. S. (2003). Evidence for Persistent Flow and Aqueous Sedimentation on Early Mars. *Science* 302, 1931–1934. doi:10.1126/science.1090544

McKay, C. P., Friedmann, E. I., Gómez-Silva, B., Cáceres-Villanueva, L., Andersen, D. T., and Landheim, R. (2003). Temperature and Moisture Conditions for Life in the Extreme Arid Region of the Atacama Desert: Four Years of Observations Including the El Niño of 1997-1998. *Astrobiology* 3, 393–406. doi:10.1089/153110703769016460

Michalski, G., Böhlke, J. K., and Thiemens, M. (2004). Long Term Atmospheric Deposition as the Source of Nitrate and Other Salts in the Atacama Desert, Chile: New Evidence from Mass-independent Oxygen Isotopic Compositions. *Geochimica et Cosmochimica Acta* 68, 4023–4038. doi:10.1016/j.gca.2004.04.009

Montgomery, W., Jaramillo, E. A., Royle, S. H., Kounaves, S. P., Schulze-Makuch, D., and Sephton, M. A. (2019). Effects of Oxygen-Containing Salts on the Detection of Organic Biomarkers on Mars and in Terrestrial Analog Soils. *Astrobiology* 19, 711–721. doi:10.1089/ast.2018.1888

Morata, D., Féraud, G., Aguirre, L., Arancibia, G., Belmar, M., Morales, S., et al. (2008). Geochronology of the Lower Cretaceous Volcanism from the Coastal Range at the 29°20-30°s, Chile. *Revista Geológica De Chile* 35, 123–145. doi:10.4067/s0716-02082008000100006

Nachon, M., Clegg, S. M., Mangold, N., Schröder, S., Kah, L. C., Dromart, G., et al. (1991). Calcium Sulfate Veins Characterized by ChemCam/Curiosity at Gale Crater, Mars. *J. Geophys. Res. Planets* 119, 1991–2016. doi:10.1002/2013JE004588

Navarro-González, R., Vargas, E., de La Rosa, J., Raga, A. C., and McKay, C. P. (2010). Reanalysis of the Viking Results Suggests Perchlorate and Organics at Mid Latitudes on Mars. *J. Geophys. Res. Planets* 115, E12.

Navarro-González, R., Rainey, F. A., Molina, P., Bagaley, D. R., Hollen, B. J., de la Rosa, J., et al. (2013). Mars-like Soils in the Atacama Desert, Chile, and the Dry Limit of Microbial Life. *Science* 302, 1018–1021. doi:10.1126/science.1089143

Parro, V., de Diego-Castilla, G., Moreno-Paz, M., Blanco, Y., Cruz-Gil, P., Rodríguez-Manfredi, J. A., et al. (2011). A Microbial Oasis in the Hypersaline Atacama Subsurface Discovered by a Life Detector Chip: Implications for the Search for Life on Mars. *Astrobiology* 11, 969–996. doi:10.1089/ast.2011.0654

Paulino-Lima, I. G., Azua-Bustos, A., Vicuña, R., González-Silva, C., Salas, L., Teixeira, L., et al. (2013). Isolation of UVC-Tolerant Bacteria from the Hyperarid Atacama Desert, Chile. *Microb. Ecol.* 65, 325–335. doi:10.1007/s00248-012-0121-z

Paulino-Lima, I. G., Fujishima, K., Navarrete, J. U., Galante, D., Rodrigues, F., Azua-Bustos, A., et al. (2016). Extremely High UV-C Radiation Resistant Microorganisms from Desert Environments with Different Manganese

Concentrations. *J. Photochem. Photobiol. B: Biol.* 163, 327–336. doi:10.1016/j.jphotobiol.2016.08.017

Quinn, R. C., Ehrenfreund, P., Grunthaner, F. J., Taylor, C. L., and Zent, A. P. (2007). Decomposition of Aqueous Organic Compounds in the Atacama Desert and in Martian Soils. *J. Geophys. Res.* 112, 04–18. doi:10.1029/2006jg000312

Quinn, R. C., Zent, A. P., Ehrenfreund, P., Taylor, C. L., McKay, C. P., Garry, J. R. C., et al. (2005a). Dry Acid Deposition and Accumulation on the Surface of Mars and in the Atacama Desert, Chile. *36th Annu. Lunar Planet. Sci. Conf.* 36, 2282.

Quinn, R. C., Zent, A. P., Grunthaner, F. J., Ehrenfreund, P., Taylor, C. L., and Garry, J. R. C. (2005b). Detection and Characterization of Oxidizing Acids in the Atacama Desert Using the Mars Oxidation Instrument. *Planet. Space Sci.* 53, 1376–1388. doi:10.1016/j.pss.2005.07.004

Rasuk, M. C., Kurth, D., Flores, M. R., Contreras, M., Novoa, F., Poire, D., et al. (2014). Microbial Characterization of Microbial Ecosystems Associated to Evaporites Domes of Gypsum in Salar de Llamara in Atacama Desert. *Microb. Ecol.* 68, 483–494. doi:10.1007/s00248-014-0431-4

Rech, J. A., Currie, B. S., Michalski, G., and Cowan, A. M. (2006). Neogene Climate Change and Uplift in the Atacama Desert, Chile. *Geol* 34, 761–764. doi:10.1130/g22444.1

Rech, J. A., Quade, J., and Hart, W. S. (2003). Isotopic Evidence for the Source of Ca and S in Soil gypsum, Anhydrite and Calcite in the Atacama Desert, Chile. *Geochimica et Cosmochimica Acta* 67, 575–586. doi:10.1016/s0016-7037(02)01175-4

Rhawn, G. J., Planchon, O., Duxbury, N. S., Latif, K., Kidron, G. J., Consorti, L., et al. (2020). Oceans, Lakes, and Stromatolites on Mars. *Adv. Astron.* 2020, 6959532. doi:10.1155/2020/6959532

Sánchez-García, L., Aeppli, C., Parro, V., Fernandez-Remolar, D., Chong-Díaz, M. G., Blanco, Y., et al. (2018). Molecular Biomarkers in the Subsurface of the Salar Grande (Atacama, Chile) Evaporitic Deposits. *Biogeochemistry* 140, 31–52.

Schulze-Makuch, D., Wagner, D., Kounaves, S. P., Mangelsdorf, K., Devine, K. G., de Vera, J. P., et al. (2018). Transitory Microbial Habitat in the Hyperarid Atacama Desert. *Proc. Natl. Acad. Sci. U S A.* 115, 2670–2675. doi:10.1073/pnas.1714341115

Skelley, A. M., Aubrey, A. D., Willis, P. A., Amashukeli, X., Ehrenfreund, P., Bada, J. L., et al. (2007). Organic Amine Biomarker Detection in the Yungay Region of the Atacama Desert with the Urey Instrument. *J. Geophys. Res. Biogeo.* 112, 04–11. doi:10.1029/2006jg000329

Skelley, A. M., Scherer, J. R., Aubrey, A. D., Grover, W. H., Ivester, R. H. C., Ehrenfreund, P., et al. (2005). Development and Evaluation of a Microdevice for Amino Acid Biomarker Detection and Analysis on Mars. *Proc. Natl. Acad. Sci.* 102, 1041–1046. doi:10.1073/pnas.0406798102

Somoza, R., and Tomlinson, A. (2002). Paleomagnetism in the Precordillera of Northern Chile (22°30'S): Implications for the History of Tectonic Rotations in the Central Andes. *Earth Planet. Sci. Lett.* 194, 369–381. doi:10.1016/s0012-821x(01)00548-9

Stern, J. C., Sutter, B., Freissinet, C., Navarro-González, R., McKay, C. P., Archer, P. D., et al. (2015). Evidence for Indigenous Nitrogen in Sedimentary and Aeolian Deposits from the Curiosity Rover Investigations at Gale Crater, Mars. *Proc. Natl. Acad. Sci. USA* 112, 4245–4250. doi:10.1073/pnas.1420932112

Sterzik, M., Bagnulo, S., Azua, A., Salina, F., Alfaro, J., and Vicuna, R. (2010). Astronomy Meets Biology: EFOC2 and the Chirality of Life. *ESO, The Messenger* 142, 25–27.

Sun, T., Bao, H., Reich, M., and Hemming, S. R. (2018). More Than Ten Million Years of Hyper-Aridity Recorded in the Atacama Gravels. *Geochimica et Cosmochimica Acta* 227, 123–132. doi:10.1016/j.gca.2018.02.021

Thomas, D. J., Boling, J., Boston, P. J., Campbell, K. A., McSpadden, T., McWilliams, L., et al. (2007). Extremophiles for Ecopoiesis: Desirable Traits for and Survivability of pioneer Martian Organisms. *Gravit. Space Biol.* 19, 91–103.

Titus, T. N., Wynne, J. J., Malaska, M. J., Agha-Mohammadi, A-A., Buhler, P. B., Alexander, E. C., et al. (2021). A Roadmap for Planetary Caves Science and Exploration. *Nat. Astron.* 5, 524–525. doi:10.1038/s41550-021-01385-1

Vaniman, D. T., Martínez, G. M., Rampe, E. B., Bristow, T. F., Blake, D. F., Yen, A. S., et al. (2018). Gypsum, Bassanite, and Anhydrite at Gale Crater, Mars. *Am. Mineral. J. Earth Planet. Mater.* 103, 1011–1020. doi:10.2138/am-2018-6346

Vítek, P., Edwards, H. G. M., Jehlička, J., Ascaso, C., Ríos, A. D. L., Valea, S., et al. (2010). Microbial Colonization of Halite from the Hyper-Arid Atacama Desert Studied by Raman Spectroscopy. *Phil. Trans. R. Soc. A.* 368, 3205–3221.

Vítek, P., Jehlička, J., Edwards, H. G. M., Hutchinson, I., Ascaso, C., and Wierzchos, J. (2014). Miniaturized Raman Instrumentation Detects Carotenoids in Mars-analogue Rocks from the Mojave and Atacama Desert. *Phil. Trans. R. Soc. A.* 372, 20140196.

Vítek, P., Jehlička, J., Edwards, H. G. M., Hutchinson, I., Ascaso, C., and Wierzchos, J. (2012). The Miniaturized Raman System and Detection of Traces of Life in Halite from the Atacama Desert: Some Considerations for the Search for Life Signatures on Mars. *Astrobiology* 12, 1095–1099.

Warren-Rhodes, K. A., Archer, S. D. J., Cabrol, N., Ng-Boyle, L., Wettergreen, D., Zacny, K., et al. (2019). Subsurface Microbial Habitats in an Extreme Desert Mars-Analog Environment. *Front. Microbiol.* 10, 69. doi:10.3389/fmicb.2019.00069

Warren-Rhodes, K. A., Rhodes, K. L., Pointing, S. B., Ewing, S. A., Lacap, D. C., Gómez-Silva, B., et al. (2006). Hypolithic Cyanobacteria, Dry Limit of Photosynthesis, and Microbial Ecology in the Hyperarid Atacama Desert. *Microb. Ecol.* 52, 389–398. doi:10.1007/s00248-006-9055-7

Weinstein, S., Pane, D., Ernst, L. A., Warren-Rhodes, K., Dohm, J. M., Hock, A. N., et al. (2008). Application of Pulsed-Excitation Fluorescence Imager for Daylight Detection of Sparse Life in Tests in the Atacama Desert. *J. Geophys. Res. Biogeosci.* 113, 01–90. doi:10.1029/2006jg000319

Wierzchos, J., Ascaso, C., and McKay, C. P. (2006). Endolithic Cyanobacteria in Halite Rocks from the Hyperarid Core of the Atacama Desert. *Astrobiology* 6, 415–422. doi:10.1089/ast.2006.6.415

Wierzchos, J., Davila, A. D., Sánchez-Almazo, I. M., Hajnos, M., Swieboda, R., and Ascaso, C. (2012). Novel Water Source for Endolithic Life in the Hyperarid Core of the Atacama Desert. *Biogeosciences* 9, 3071–3098. doi:10.5194/bg-9-2275-2012

Wilhelm, M. B., Davila, A. F., Eigenbrode, J. L., Parenteau, M. N., Jahnke, L. L., Liu, X.-L., et al. (2017). Xeropreservation of Functionalized Lipid Biomarkers in Hyperarid Soils in the Atacama Desert. *Org. Geochem.* 103, 97–104. doi:10.1016/j.orggeochem.2016.10.015

Wilhelm, M. B., Davila, A. F., Parenteau, M. N., Jahnke, L. L., Abate, M., Cooper, G., et al. (2018). Constraints on the Metabolic Activity of Microorganisms in Atacama Surface Soils Inferred from Refractory Biomarkers: Implications for Martian Habitability and Biomarker Detection. *Astrobiology* 18, 955–966. doi:10.1089/ast.2017.1705

Wynne, J. J., Titus, T. N., and Chong Diaz, G. (2008). On Developing thermal Cave Detection Techniques for Earth, the Moon and mars. *Earth Planet. Sci. Lett.* 272, 240–250. doi:10.1016/j.epsl.2008.04.037

Conflict of Interest: The authors declare that the research was conducted in the absence of any commercial or financial relationships that could be construed as a potential conflict of interest.

frontiers in Astronomy and Space Sciences

REVIEW
published: 17 January 2022
doi: 10.3389/fspas.2021.796943

How to Live on Mars With a Proper Circadian Clock?

*Rujia Luo, Yutao Huang, Huan Ma and Jinhu Guo**

Key Laboratory of Gene Engineering of the Ministry of Education, State Key Laboratory of Biocontrol, School of Life Sciences, Sun Yat-sen University, Guangzhou, China

Intrinsic circadian clocks generate circadian rhythms of physiology and behavior, which provide the capabilities to adapt to cycling environmental cues that result from the self-rotation of the Earth. Circadian misalignment leads to deleterious impacts on adaptation and health in different organisms. The environmental cues on the interplanetary journey to and on Mars dramatically differ from those on Earth. These differences impose numerous adaptive challenges, including challenges for humans' circadian clock. Thus, adaptation of circadian rhythms to the Martian environment is a prerequisite for future landing and dwelling on Mars. Here, we review the progress of studies associated with the influence of the Martian environment on circadian rhythms and propose directions for further study and potential strategies to improve the adaptation of the circadian clock for future Mars missions.

Keywords: Mars, circadian clock, gravity, radiation, magnetic field, isolation, confinement, countermeasure

OPEN ACCESS

Edited by:
Yiliang Li,
University of Hong Kong, Hong Kong SAR, China

Reviewed by:
Zhongchen Wu,
Shandong University, Weihai, China
Xinli Wei,
Institute of Microbiology (CAS), China

****Correspondence:***
Jinhu Guo
guojinhu@mail.sysu.edu.cn

Specialty section:
This article was submitted to Astrobiology, a section of the journal Frontiers in Astronomy and Space Sciences

Received: *18 October 2021*
Accepted: *01 December 2021*
Published: *17 January 2022*

Citation:
Luo R, Huang Y, Ma H and Guo J (2022) How to Live on Mars With a Proper Circadian Clock? Front. Astron. Space Sci. 8:796943. doi: 10.3389/fspas.2021.796943

INTRODUCTION

Human factors determine the success or failure of a space mission (Oluwafemi et al., 2021). Manned space exploration creates many physiological challenges for astronauts (Kandarpa et al., 2019; Garrett-Bakelman et al., 2019). Astronauts encounter a variety of environmental factors that are dramatically different from the Earth's surface during the journey to and from and after dwelling on the Moon or Mars.

After humans landed on the Moon more than half a century ago, the next objective is to land on Mars. Mars is a red planet with a mean radius of 0.53 that of Earth and possesses the most similar environment to Earth among the solar planets. Mars is also the most likely planet to find extraterrestrial life and is the most habitable for humans (Levchenko et al., 2018). The average distance between Earth and Mars is 54.6 million kilometers, and a to and from journey between Earth and Mars would last more than 500 days (Tafforin, 2015). To date, the space agencies of the US and China have proposed plans for manned Mars exploration (Parihar et al., 2015; China Global Television Network, 2021). To live on Mars, artificial ecosystems must be established, and other organisms must be transported from Earth, including crops and animals, as food sources. For instance, in the Controlled Ecological Life Support System (CELSS) experiment, volunteers in a simulated cabin cultured crops such as zophobas, spirulina, maize, potato, sweet potato, other vegetables, and fruits (Tong, 2018). After landing on Mars, the survival and adaptation of these species will be critical issues.

Altered circadian rhythms in many other species have also been observed in space conditions (Mergenhagen and Mergenhagen, 1989; Hoban-Higgins et al., 2003; Sulzman et al., 1984; Wang et al., 2014; Guo et al., 2014). The circadian rhythms of Earthly organisms will be subject to change to a number of environmental cues on Mars and during the journey, including light, radiation, gravity, magnetic field, isolation, and confinement. As noted by Barger et al., "Clearly, without appropriate

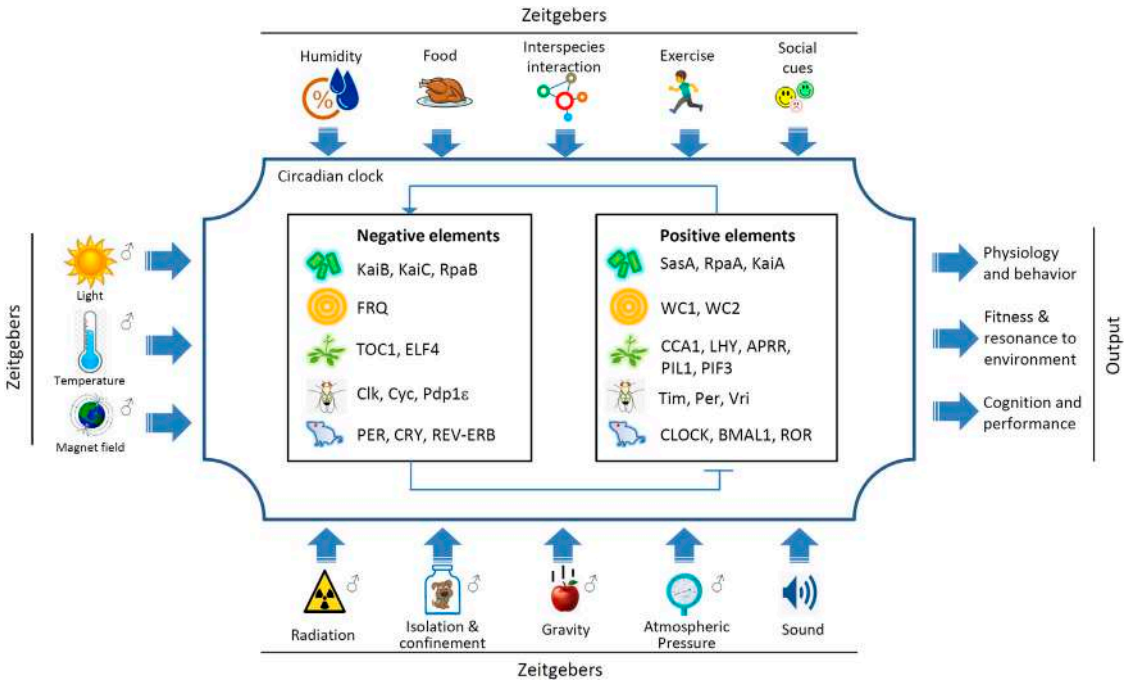

FIGURE 1 | The molecular control of circadian clock systems. The negative and positive elements of circadian clock factors in representative models are depicted, and bacteria (*S. elongatus*), fungi (*N. crassa*), plants (*A. thaliana*), insects (*D. melanogaster*), and mammals (*Mus musculus*) are depicted (Bell-Pedersen et al., 2005; Doherty and Kay, 2010; Zhang et al., 2011). Environmental cues that dramatically differ from those on Earth are presented. Note that in this figure, cognition refers to animals only and performance refers to humans only. Isolation and confinement apply to animals and humans.

circadian rhythm and fatigue management countermeasures, maintaining daily life on the Mars day presents a significant challenge" (Barger et al., 2012).

CIRCADIAN RHYTHMS AND ENTRAINMENT

Circadian rhythms of numerous physiological and behavioral variables, e.g., locomotor activity, growth, body temperature, photosynthesis, hormone secretion, and oxygen consumption, have been documented across kingdoms. Circadian rhythms are generated and controlled by endogenous circadian clocks. In higher animals, circadian clocks constitute pacemakers as central oscillators and peripheral oscillators (Bliss and Heppner, 1976). In humans, suprachiasmatic nuclei (SCN) are the pacemakers that orchestrate circadian rhythms of the remaining peripheral tissues (Welsh et al., 2010).

At the molecular level, eukaryotic circadian clock systems consist of positive and negative elements that form the transcription-translational feedback loop (TTFL). Basically, in TTFL the positive elements function as transcription factors (TFs) binding to the promoter regions of the negative elements to trigger the transcription of the latter; the transcribed and translated proteins act as negative elements to repress the capability of the positive elements as TFs (Bell-Pedersen et al., 2005; Zhang et al., 2011) (**Figure 1**). The circadian clock genes between animals, such as fruit flies and mammals, have certain homology. In contrast, there is no significant conservation between the clock counterparts in bacteria, fungi, plants, and animals (**Figure 1**). However, the regulatory mechanisms are highly conserved across kingdoms. In addition to TTFL, multiple regulatory layers are involved in the regulation of circadian clock gene expression and function, including at epigenetic, post-transcriptional and post-translational levels (Gallego and Virshup, 2007; Doherty and Kay, 2010; Hirano et al., 2016; Proietto et al., 2015; Hurley et al., 2016).

In prokaryotes, Cyanobacteria *Synechococcus elongatus* is one of the few species that have been found to possess an endogenous circadian clock. In *S. elongatus*, the core circadian clock protein KaiABC can dynamically interact and generate oscillations of phosphorylation changes in the KaiC protein. In addition, transcriptional regulation and KaiABC oscillation promote the circadian robustness of each other reciprocally under different growth conditions (Zwicker et al., 2010).

Circadian clocks endow the capabilities (also called fitness) to adapt to cycling environments. Consequently, circadian misalignment leads to comprehensive negative effects on physiology, psychology and behavior. Organisms show the highest adaptability to the environment when the periods of their endogenous circadian clocks are the closest to the environmental cycling periods (Ouyang et al., 1998; Woelfle et al., 2004; Johnson 2005; Sharma 2003). The free running period (FRP) of humans is approximately 24.9 h (Miles et al., 1977). Forced desynchronization under short light-dark (LD) cycles has also been used to measure the length of FRP, and the

result is approximately 24.2 h (Czeisler et al., 1999; Duffy et al., 2011). However, short LD cycles may add superimposed impacts on the endogenous circadian system. In the entrainment range, a circadian rhythm can be aligned with the period of the cycling environmental cue. Environmental cues, including natural factors (e.g., light, temperature, gravity, magnetic field, sound, atmospheric pressure) and social factors (e.g., exercise, social interaction, interspecies interaction), are termed zeitgeber (German) or time givers (**Figure 1**) (Honma and Honma, 2001). The entrainment ranges differ for different organisms and different physiological or behavioral variables may exist in the same species (Guo et al., 2020).

Desynchronization of circadian rhythms in ambient environments with periods beyond the entrainment ranges causes decreased adaptation, competence, fitness, growth rate, fertility, and shortened lifespan (López-Otín and Kroemer, 2021; Allada and Bass, 2021; Sharma, 2003; Pittendrigh and Minis, 1972; Mormont et al., 2000). Circadian rhythm is a hallmark of human health (López-Otín and Kroemer, 2021), and circadian misalignment accounts for a variety of diseases, impaired mood (e.g., depression), decreased cognition and performance (Woller and Gonze, 2021; Ma et al., 2019; Guo et al., 2020; Bechtold et al., 2010; Mallis and DeRoshia, 2005). A circadian rhythm with less robust rhythmicity usually possesses a wider entrainment range. The locomotor rhythmicity of *Clock* mutant mice could be aligned with LD28 and LD32 compared to wild type, which only adapts to the LD24 regimen (Udo et al., 2004; Erzberger et al., 2013). However, a more robust circadian rhythm shows higher adaptability under LD24 (Solovev et al., 2019).

DIFFERENT ENVIRONMENTAL CUES ON MARS AND THEIR EFFECTS ON CIRCADIAN RHYTHMS

Light Conditions and Day Length

Light is the strongest zeitgeber to entrain circadian rhythms in most species. However, Mars and Earth have dramatically different light conditions, e.g., light intensity, light spectrum, and solar day-night cycling period (Mcphee and Charles, 2009). These factors make circadian adaptation more complex to achieve and results in negative effects on humans and other Earthly organisms to visit and live on Mars.

Light Intensity and Spectrum on Mars

Blue light at approximately 460 nm is the most effective at entraining circadian rhythms in many organisms, e.g., *Cyanobacteria*, *Neurospora crassa*, *Arabidopsis thaliana*, *Drosophila melanogaster*, and mammals, including humans. In addition, red light modulates cyanobacteria and the plant circadian clock (Cashmore et al., 1999; McClung, 2006; Linden 2002; Mullineaux, 2001). Regarding light intensity, only bright white light (over 2,500 lux) appears to be a sufficiently effective circadian zeitgeber in humans (Broadway et al., 1987). However, the sky radiant energy density on Mars is about 43% (1.5 in $W\,m^{-2}\mu m^{-1}\ sr^{-1}$–10.2 in $W\,m^{-2}\mu m^{-1}\ sr^{-1}$) of that on Earth, which is due to the distance from the sun, dust in the air, season, and weather (Moores et al., 2007; Whiteway et al., 2008; National Aeronautics and Space Administration (NASA), 2020). Although the intrinsic period of the human circadian clock is ~25 h, under weak lighting conditions, the rhythms of the activity–rest cycle and melatonin could only be entrained to a period of 24 h but not 23.5 h or 24.6 h (Wright et al., 2001).

The light spectrum on Mars is also dramatically different. With an atmosphere rich in dust particles, blue light is preferentially absorbed, and as a result, the sky looks redder (chromaticity of $x = 0.35$, $y = 0.34$ standard deviations of $\sigma x = 0.01$ and $\sigma y = 0.02$) than that on Earth by $\delta x = 0.04$ and $\delta y = 0.01$ (Maki et al., 1999; Maki et al., 2021; Selsis et al., 2008), which is adverse for maintaining circadian rhythms in many Earth organisms. In addition to the circadian system, light parameters are crucial for many other physiological processes, and light intensity, light-dark ratio, and dark length are determinants for growth, development and reproduction (Saunders, 1982; Bennie et al., 2016; Irwin, 2018).

Martian Day Length

The solar day length of Mars is 24 h 39 min and 35 s (~24.65 h), which is the closest to that of Earth among the solar planets or satellites. Repeated failure to enter this period will result in circadian desynchrony and survival for Earthly organisms and, consequently, disrupted sleep, impaired cognition and decision-making, and poor performance for animals and humans. During the Mars Pathfinder and Mars MER missions, ground mission control personnel were required to work on a Mars day schedule to interact with the spacecraft. They found it challenging to continuously stay on the 24.65 h period which led to increased fatigue, sleepiness, and irritability, and decreased concentration and energy. During the nearly 3-months Mars Pathfinder Mission, the Sojourner Rover supporting personnel abandoned the Mars day work schedule 1 month after the initiation (Barger et al., 2012). These data suggest that the Martian daily cycling period is outside the entrainment range of the human circadian system and that the circadian rhythms and performance of the personnel living on the Martian schedule will be impaired.

The 180-days CELSS experiment commenced in June 2016 to explore physiological, psychological, and behavioral changes during long-term isolation and exposure to Mars solar days (Shi et al., 2018; Yang et al., 2021). In the four volunteers of this experiment, the levels of total protein and globulin decreased and the bilirubin level increased under the isolation environment; the levels of total protein and globulin increased on Day 75 in the Mars solar day period (Chen et al., 2020). CELSS lasted for 180 days during which the volunteers lived under a Mars day (24.65 h) during the period from 71 to 107 days. One of the four volunteers wrote a diary every day and had it published (Tong, 2018). Yang et al. (2021) analyzed the published diary using a natural language processing tool and found a decrease in positive emotion during the Mars day period and an increased ratio of diaries with lower positive scores than average, although these changes were not significant. This single case report suggests that psychological changes may occur due to misalignment with the Mars day schedule. Comprehensive evaluation of the changes in physiological and behavioral rhythms under a simulated Martian daily period is necessary,

as desynchronization between different rhythms may occur under a non-24 h environmental period.

Microgravity and Low Gravity

Gravity is almost zero during orbital flight or on the journey to and from Mars. The gravity on Mars is 3.711 m/s^2, which is approximately 38% of the gravity on Earth (9.807 m/s^2) (Heer et al., 2000). Microgravity has been shown to induce changes in circadian rhythms in many tested organisms (Sulzman et al., 1984; Hoban-Higgins et al., 2003; Wang et al., 2014; Guo et al., 2014; Holley et al., 2003). *Chlamydomonas reinhardii* displayed an increased amplitude of photoaccumulation rhythm under microgravity (Mergenhagen and Mergenhagen, 1989). Desert beetles showed differential locomotor periods and activity patterns in constant light and constant dark under microgravity or hypergravity (Hoban-Higgins et al., 2003).

For humans and animals, exposure to low gravity causes shifts in body fluids, space motion sickness, atrophy, bone demineralization and mass loss, immune system deregulation and disruption of senses (Bettiol et al., 2018). Circadian rhythms, including body temperature, sleep-wake cycle, cardiovascular variables, locomotor activity, affected cognition and performance of astronauts, are prone to change under microgravity (Pavy Le-Traon and Roussel, 1993; Flynn-Evans et al., 2016; Mallis and DeRoshia, 2005; Guo et al., 2014; Ma et al., 2015; Garrett-Bakelman et al., 2019; Zhang et al., 2021). RNA-sequencing data from the NASA GeneLab space mission revealed that clock gene expression in spaceflight mice revealed an expression pattern different from the ground control, and spaceflight promoted asynchrony of gene expression of circadian clock genes between peripheral tissues. Genes showing altered circadian expression are associated with jet lag, sleep disorder, cancer, lifestyle-related diseases, and mental disorders (Fujita et al., 2020).

Microorganisms in space are prone to changes in their metabolism, antibiotic efficacy, pathogenicity and virulence and exhibit increased virulence, enhanced formation of biofilms, or development of resistance to specific antibiotics (Green et al., 2021; Gilbert et al., 2020; Huang et al., 2018; Klaus and Howard et al., 2006; Bijlani et al., 2021). Immune cell stimulation, Toll-like receptors and pathogen-associated molecular patterns can be altered in microgravity, which affects immunological crosstalk and response. As a consequence, immune dysfunction caused by exposure to microgravity may increase the chance of bacterial infection (Krieger et al., 2021; Gertz et al., 2020; ElGindi et al., 2021; Wilson et al., 2007). As the circadian clock extensively regulates immunity, it is likely to be implicated or relayed in the alteration of immunity in space (Scheiermann et al., 2013).

Low Magnetic Field

Organisms living on Earth are under the influence of Earth's magnetic field, which affects development, metabolism, and information processing in their daily lives (Lindauer and Martin, 1985). The magnetic field has been linked to the circadian system, although the effects and mechanisms remain largely vague (Lewczuk et al., 2014). Small changes in Earth's magnetic field result in modified circadian rhythms in fiddler crabs and other organisms (Brown et al., 1964; Bliss and Heppner, 1976). The orientation and navigation of many organisms is closely associated with the circadian clock, and the orientation may differentially rely on celestial bodies, meteorological variables, geomagnetism and intrinsic factors (Borgioli et al., 1999). Circadian clock-dependent orientation was altered in sparrows (*Passer domesticus*) under a zero magnetic field (Bliss and Heppner, 1976). The orientation of *Dugesia* and *Nassarius* showed circalunar rhythmicity, which could be modified by changing the direction or strength of the magnetic field (Brown et al., 1970; Bitz and Sargent, 1974). The magnetoreceptor is located in the abdomen of honey bees. Inconsistent results were reported regarding the effects of a magnetic field on the circadian rhythm of honey bees; one found no influence, and the other found that a strong magnetic field led to changes in the circadian rhythms (Gould et al., 1978; Neumann, 1988). The effects of magnetic fields on circadian rhythms are not aligned for all organisms; for instance, no significant effects were found in the filamentous fungus *Neurospora* (Bitz and Sargent, 1974).

Melatonin is a hormone synthesized in a circadian fashion in the pineal glands of vertebrates, including humans, that regulates sleep, circadian rhythm, and antioxidation (Turek and Gillette, 2004). In the pied flycatcher, melatonin synthesis was significantly repressed in a changed magnetic field (Schneider et al., 1994). The spiking of guinea pig pineal cells was changed by altering the magnetic field at the Earth-strength level (Semm et al., 1980), suggesting that the magnetic field affects circadian rhythms at physiological and tissue levels. The melatonin of a migratory bird, the pied flycatcher, exhibits a circadian rhythm that can be modified by an artificial magnetic field (Schneider et al., 1994).

At the molecular level, CRY1 determines magnetosensitivity, which is dependent on light but independent of the circadian clock (Gegear et al., 2008). A near null magnetic field (NNMF) caused changes in circadian clock genes (*LHY*, *PRR7*, and *GI*) in *Arabidopsis* (Agliassa and Maffei, 2019). CRY1 shows promoted phosphorylation, which may be associated with *Arabidopsis* seedling growth in a 500 μT magnetic field under pulsed light (Hammad et al., 2020). In *Drosophila*, putative magnetoreceptor (MagR)/CG8198, which is a homolog of the bacterial iron-sulfur cluster assembly IscA1, binds with the CRY1 protein, a highly conserved blue light-absorbing flavoprotein involved in the positive elements of circadian circuits. This Cry/MagR complex displays an intrinsic magnetic moment, suggesting that it is a *Drosophila* putative magnetosensor (Qin et al., 2016; Wan et al., 2021). On the other hand, an altered magnetic field elicits changed expression of circadian clock genes. Mouse SCN slices expressing PERIOD2:LUCIFERASE were exposed to MS consisting of a 50-mT field, and the amplitude and period of the luciferase rhythms were differentially affected at different circadian time points (Kassahun et al., 2020). These data demonstrate that magnetic fields exert influences on circadian rhythms.

Mars has a crustal magnetic field magnetized by an ancient global dynamo field ~4 Ga ago; however, it does not have a global dipole magnetic field like Earth. The dipole core field at the surface is weaker than the present core field at the surface of the Earth (Mittelholz et al., 2018; Stevenson, 2001). These differences

in the Mars magnetic field will exert influences on the circadian rhythms of Earth emigrants.

Exposure to Exceptional Radiation

Regarding the surface radiation of Earth, species are primarily exposed to low linear energy transfer (LET) photon radiation (i.e., X-rays and γ-rays with LET values of <10 keV/μm). In contrast, space radiation comprises electrons, protons (hydrogen nuclei), neutrons, alpha particles (helium nuclei) and heavy nuclei with very high energies (high charge and energy particles) and LET values of >10 keV/μm (Mishra and Luderer, 2019). In interplanetary space, the primary components of the radiation field comprise galactic cosmic rays (GCRs) and solar cosmic radiation. The journey to Mars is beyond the protective magnetosphere of the Earth, and the long period increases the exposure of astronauts to the spectrum of galactic cosmic rays (GCRs), which are low fluence but highly energetic and fully ionized nuclei (Hellweg and Baumstark-Khan, 2007; Parihar et al., 2015). During interplanetary travel, astronauts will be exposed to radiation belts containing charged particles trapped by the planet magnetic field. The estimated cumulative dose of radiation from a 3-years-long Mars mission is 0.4 Gy (Cucinotta and Durante, 2006). Owing to the lack of protection by the magnetosphere and the loss of atmosphere, the radiation is much higher on the surface of Mars than on Earth, which imposes many hazards on human health. Radiation on Mars and on the journey has been considered the most critical issue for long-term space missions (Hellweg and Baumstark-Khan, 2007; McPhee and Charles, 2009).

One essential hypothesis of circadian adaptive advantage is "escape from light" (Ditty et al., 2009), suggesting that circadian rhythms are protective against radiation damage. Gamma radiation has been demonstrated to affect the circadian patterns of mouse activity and potato O_2 consumption (Brown et al., 1970). In addition to dictating circadian rhythm, circadian clock genes play a role in regulating cell division and tumorigenesis. Multiple circadian components have been implicated in the defense against radiation hazards. PER2 regulates the expression of a series of genes associated with the cell cycle and tumor suppression. Fu et al. found that after gamma radiation, *Per2* mutation resulted in a marked increase in tumor development and reduced apoptosis in thymocytes compared to control mice (Fu et al., 2002). PER1 modulates the expression of key cell cycle regulators that sensitize human cancer cells to DNA damage-induced apoptosis. PER1 interacts with the checkpoint proteins ATM and checkpoint kinase 2 (CHK2). Abnormal expression of Per1 resulted in disturbed apoptosis induced by DNA damage or radiation (Gery et al., 2006; Zhu et al., 2019). CHK2 is a key component of the DNA damage response that links DNA damage–activated kinases with checkpoint effectors in the cell cycle and DNA repair machinery, and its expression is under circadian control. *Neurospora* PRD4, the homolog of CHK2, consistently interacts with FRQ, the counterpart of the negative element circadian clock in *Neurospora*. DNA damage induced by radiation resets the circadian clock in a CHK2-dependent fashion (Pregueiro et al., 2006). Based on these findings, maintenance of circadian rhythms may help alleviate radiation hazards.

Isolation and Confinement

During the long-distance interplanetary journey between Mars and Earth, astronauts will encounter long-term isolation and confinement (Oluwafemi et al., 2021). After the astronauts reach Mars and live there, they will spend most of their time in a closed ecological facility. The negative consequences of isolation comprise decrements in mood, sleep deprivation, problems in concentration, and interpersonal tensions (Tafforin, 2015).

Isolation and confinement impose effects on circadian rhythms and sleep. Wrist actigraph records indicated that weightlessness simulated by head-down bed rest led to decreased activity, which was immediately recovered after bed rest (Liang et al., 2014). During the Mars500 project, which is a simulation of manned flight to Mars, the volunteers displayed increased sleep and rest times across the mission until the last 2 months (Basner et al., 2013), reflecting the effects of simulated isolation on sleep-wake dynamics.

Similar experiments or trainings include the Isolation Study for European Manned Space Infrastructure (ISEMSI), Experimental campaign for European Manned Space Infrastructure (EXEMSI), Human Behavior in Extended Space flight (HUBES), Simulation of Flight International Crew on Space Station (SFINCSS) and programs conducted at the Flashline Mars Arctic Research Station (Tafforin 2015).

Social and Interspecies Interaction

Psychological challenges, including crew interaction, must also be considered (Oluwafemi et al., 2021; Dietrich 2004; Kanas et al., 2000). Social interaction has been shown to affect circadian rhythms in a variety of species, including rodents, roosters, *Drosophila*, and cave glowworms (Levine et al., 2002; Shimmura et al., 2015; Maynard and Merritt 2013; Oluwafemi et al., 2021). Interspecies interactions also contribute to circadian modification. Reciprocal influences exist extensively between some symbiotic species, and the circadian rhythms of the hosts are modulated by symbionts, such as the bobtail squid *Euprymna scolopes* and its luminous symbiont *Vibrio fischeri* (Heath-Heckman et al., 2013) and *Convoluta roscoffensis* and its symbiont green alga living inside the worm (Palmer, 2002). Here, we refer to social interaction as not only the interaction between human individuals but also the interaction between humans and other species.

Abundant microorganisms colonize the human body, including mucosal and skin environments, which is closely associated with human physiology and health. A prevalent proportion of the human microbiota displays a diurnal oscillatory pattern in its abundance (Ma et al., 2019; Collado et al., 2018; Thaiss et al., 2014). Furthermore, the symbiosis between the host and gut microbiota plays a critical role in maintaining the homeostasis of the host and dysbiosis of microbiota, which accounts for immune dysregulation and an impaired digestive system and metabolism (Knight and Girling, 2003; Thaiss et al., 2014). Symbiotic microbiota functions to bridge circadian rhythms with diverse effects, including development immunity and metabolism (Brooks et al., 2021; Kuang et al., 2019; Thaiss et al., 2014; Ma et al., 2019; Collado et al., 2018). Much evidence has revealed that space environment factors or analog conditions (e.g., microgravity, radiation, low

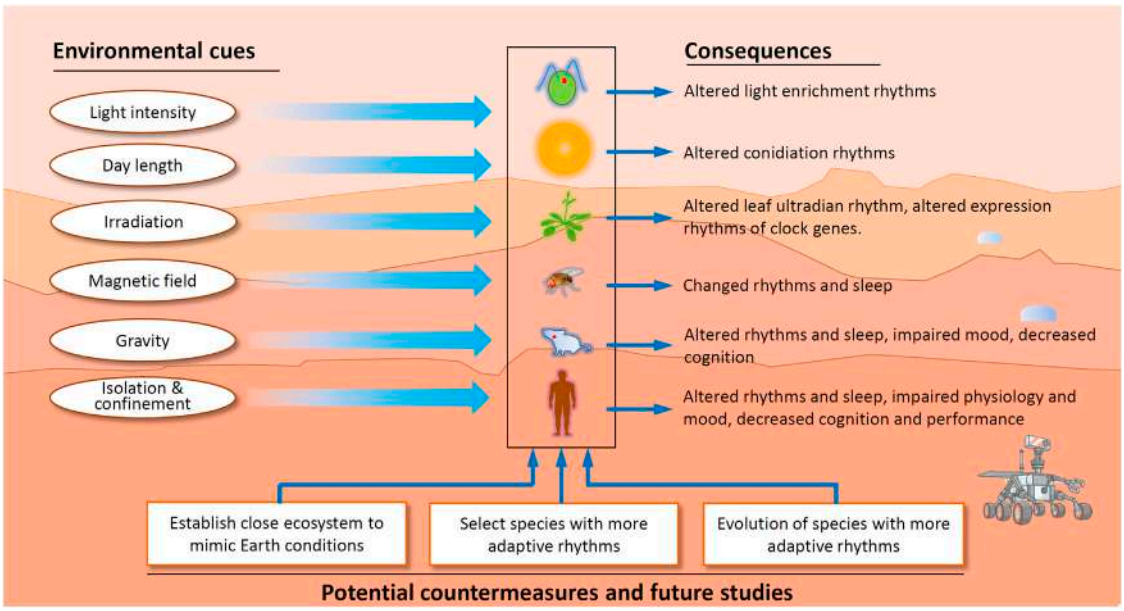

FIGURE 2 | Martian factors with effects on the circadian clock and strategies for future investigation and improvement of circadian rhythms in representative species. *C. rheinhardi*, *N. crassa*, Arabidopsis, mouse and human are depicted in the central column (Sulzman et al., 1984; Mergenhagen and Mergenhagen, 1989; Mallis and DeRoshia, 2005; Guo et al., 2014; Ma et al., 2015; Agliassa and Maffei, 2019; Kandarpa et al., 2019; Zhang et al., 2021).

fluid shear, and diet) cause altered composition of gut microbiota (Siddiqui et al., 2021; Acres et al., 2021; Cervantes and Hong, 2016; Saei and Barzegari et al., 2012; Li et al., 2015; Jiang et al., 2019). Improving the balance of symbiotic microbiota and the association between the circadian clock and microbiota in space remain areas to be further investigated.

Temperature is also a critical circadian zeitgeber as periodic temperature change can reset the phase and amplitude of circadian rhythm in many species (Rensing and Ruoff, 2002). However, to survive on Mars we have to maintain a similar ambient temperature region in the habitats to that on Earth. Atmospheric pressure, has also been demonstrated to affect circadian rhythms, for instance, the phosphorylation rhythms of KaiC protein in Cyanobateria (Kitahara et al., 2019), however, the study on this issue is very limited. Therefore, the potential effects of these two factors are not discussed in this review.

COUNTERMEASURES TO IMPROVE CIRCADIAN RHYTHMS UNDER MARTIAN CONDITIONS

Regardless of whether we are still living on Earth, some pilot studies have been carried out to assess potential countermeasures against circadian misalignment on Mars. To date, light is the only approach used as a countermeasure in almost all of the available reports. In the Phoenix Mars Lander (PML) mission, the personnel worked on a Mars day (24.65 h) for 78 days with additional manual illumination (0–4,000 lux) when at work as a countermeasure. However, the daily sleep durations were 5.98 ± 0.94 h for those who showed a synchronized sleep-wake cycle to the Mars day and 4.91 ± 1.22 h for those who failed to synchronize their sleep-wake cycles (Barger et al., 2012). As 7–8 h sleep is critical for sleep duration (Chen et al., 2020), this data suggests that all of the personnel may have insufficient sleep (Sgobba and Schlacht, 2018; Flynn-Evans et al., 2016). Certain human rhythms can be entrained to the Martian period; for instance, under moderately bright light (~450 lux) or with bright light pulses, the sleep-wake cycles of the volunteers were synchronized with LD24.65 h (Scheer et al., 2007; Gronfier et al., 2007). However, assessment of the potential desynchronization between tissues and its physiological and behavioral consequences is critical since the adaptation of the sleep-wake cycle does not equal sychronization at other levels.

Candidate organisms to send to Mars could be screened. Nonhuman species (especially crops) with less robust rhythms and organisms with longer intrinsic periods might be more likely to adapt to the Martian environment (**Figure 2**). For instance, hydrodictyon shows high plasticity in its circadian period compared to other organisms (Bünning, 1964), suggesting that entrainment plasticity is adjustable. It is noteworthy to mention that despite the entrainment range of the locomotor rhythms, at the molecular and metabolic levels, they may have much narrower windows. Altered expression of circadian clock genes, such as Clock, also extends the entrainment range or accelerates adaptation to shifted environmental cues (Udo et al., 2004).

Food and exercise may also be used as countermeasures. Food is effective in entraining peripheral circadian clocks (Mendoza, 2007). Exercise also acts as a countermeasure to adjust circadian rhythm, but its effects are roughly opposite to those of melatonin according to the PRCs, which has been validated in a long-term space mission (Mendt et al., 2021). It will be interesting to assess

whether atrophy and osteoporosis can be alleviated by exercise and whether timing has an influence on exercise effects, as the physiology and function of muscle and bone metabolism are under circadian control (Lefta et al., 2011; Zhang et al., 2020; Mayeuf-Louchart et al., 2015; Song et al., 2018; Swanson et al., 2018). Exercise affects circadian phase and amplitude with a roughly reversed PRC pattern to light entrainment (Lewis et al., 2018; Juhl et al., 2021; Moosavi et al., 2021; Refinetti 2016). However, the effects of these factors also require further assessment. In addition, other environmental factors may also affect circadian rhythms and sleep-wake cycles, for instance, the continuous and inevitable noise in the spacecraft during extended interplanetary travel. To this end, the reduction of noise through technology updates will be the solution.

CONCLUSION AND PROSPECTS

Astronauts and other Earth organisms will encounter many threats to their circadian rhythms during their travel to or from Mars and dwelling on Mars. Among the different cues from Earth, compared to light conditions, the conditions of low gravity, low magnetic field and stronger radiation are very challenging to change or overcome. These facts raise the following question: living on Mars with an Earth circadian clock or adapting the circadian clock to the Mars environment, which is more effective? This is not a black-or-white question; instead, it is a multidimensional question. For crops, plants, lower animals, and microorganisms, it is possible to screen those showing better adaptation to the Mars environment. Nevertheless, this does not apply to humans, at least at the beginning of Mars exploration, in light of ethics.

Establish an Enclosed Ecosystem to Mimic Earth Conditions

For humans, in the long future, the practicable strategy is to establish Earth-like closed ecosystems to shield hazardous cues and simulate Earth conditions, where most of the time living and working is spent (Bamsey et al., 2009). For crops, in the short-term future, people will cultivate crops in greenhouses in which the conditions are controlled to be similar to those on Earth. This process consumes a considerable amount of energy while artificial selection requires a large amount of time.

Select Emigrant Organisms With More Adaptive Rhythms

For organisms such as crops, farm animals or poultry, those with periods slightly longer than 24 h, adaptability to low light intensity and red light, a wide entrainment range or less robust rhythmicity might be considered prior candidates to transport to Mars. For the former, it might be easier for them to adapt to the Mars period; for the latter, arrhythmic organisms or organisms with less robust rhythms may be more competent than rhythmic organisms under a cycling environment with a period far beyond the entrainment range of rhythmic organisms (Ouyang et al., 1998; Erzberger et al., 2013).

Evolution of Circadian Clock on Mars

In an even longer-term future, the organisms on Mars may not always live in a closed ecosystem similar to Earth's environment. More or less, fast or slow, circadian clocks and other aspects will start to evolve. We have limited knowledge about the evolutionary processes of the circadian clock, but further understanding of the circadian rhythms in caverns or other special environments may help. Moreover, we may impose artificial selection pressure to accelerate evolution in crops (Cavallari et al., 2011; Müller et al., 2016; Arnold et al., 2018; Lu et al., 2010).

In this article, there is little discussion on circalunar and circannual rhythms. Organisms on Earth are more or less modulated by the Moon (Raible et al., 2017). Mars has two satellites, Phobos and Deimos, suggesting a more complex influence. In addition, the Mars year is approximately 687 days, nearly double the year length of Earth, which also challenges Earthly organisms. As the regulation and underlying mechanisms of circalunar and circannual rhythms of Earth lives remain less investigated than circadian rhythms, there is even more research necessary on this topic in regards to live on Mars.

AUTHOR CONTRIBUTIONS

RL, YH, and JG wrote the first draft of the manuscript and all authors contributed to manuscript revision, read, and approved the submitted version.

FUNDING

This work was supported by the Experiments for Space Exploration Program and the Qian Xuesen Laboratory, China Academy of Space Technology (TKTSPY-2020-04-21), the National Natural Science Foundation of China (Grants 31871188 and 3217090153), the Space Medical Experiment Program (HYZHXM03007) and the Open Fund of the National Key Laboratory of Human Factors Engineering in the Astronaut Center of China (SYFD062008K).

ACKNOWLEDGMENTS

We apologize for not citing all relevant important references due to the space limit.

REFERENCES

Acres, J. M., Youngapelian, M. J., and Nadeau, J. (2021). The Influence of Spaceflight and Simulated Microgravity on Bacterial Motility and Chemotaxis. *NPJ Microgravity* 7 (1), 7. doi:10.1038/s41526-021-00135-x

Agliassa, C., and Maffei, M. E. (2019). Reduction of Geomagnetic Field (GMF) to Near Null Magnetic Field (NNMF) Affects Some *Arabidopsis thaliana* Clock Genes Amplitude in a Light Independent Manner. *J. Plant Physiol.* 232, 23–26. doi:10.1016/j.jplph.2018.11.008

Allada, R., and Bass, J. (2021). Circadian Mechanisms in Medicine. *N. Engl. J. Med.* 384 (6), 550–561. doi:10.1056/NEJMra1802337

Arnold, W., Ruf, T., Loe, L. E., Irvine, R. J., Ropstad, E., Veiberg, V., et al. (2018). Circadian Rhythmicity Persists through the Polar Night and Midnight Sun in Svalbard Reindeer. *Sci. Rep.* 8, 14466. doi:10.1038/s41598-018-32778-4

Bamsey, M., Berinstain, A., Graham, T., Neron, P., Giroux, R., Braham, S., et al. (2009). Developing Strategies for Automated Remote Plant Production Systems: Environmental Control and Monitoring of the Arthur Clarke Mars Greenhouse in the Canadian High Arctic. *Adv. Space Res.* 44, 1367–1381. doi:10.1016/j.asr.2009.08.012

Barger, L. K., Sullivan, J. P., Vincent, A. S., Fiedler, E. R., McKenna, L. M., Flynn-Evans, E. E., et al. (2012). Learning to Live on a Mars Day: Fatigue Countermeasures during the Phoenix Mars Lander mission. *Sleep* 35, 1423–1435. doi:10.5665/sleep.2128

Basner, M., Dinges, D. F., Mollicone, D., Ecker, A., Jones, C. W., Hyder, E. C., et al. (2013). Mars 520-d mission Simulation Reveals Protracted Crew Hypokinesis and Alterations of Sleep Duration and Timing. *Proc. Natl. Acad. Sci. U S A.* 110, 2635–2640. doi:10.1073/pnas.1212646110

Bechtold, D. A., Gibbs, J. E., and Loudon, A. S. (2010). Circadian Dysfunction in Disease. *Trends Pharmacol. Sci.* 31, 191–198. doi:10.1016/j.tips.2010.01.002

Bell-Pedersen, D., Cassone, V. M., Earnest, D. J., Golden, S. S., Hardin, P. E., Thomas, T. L., et al. (2005). Circadian Rhythms from Multiple Oscillators: Lessons from Diverse Organisms. *Nat. Rev. Genet.* 6, 544–556. doi:10.1038/nrg1633

Bennie, J., Davies, T. W., Cruse, D., and Gaston, K. J. (2016). Ecological Effects of Artificial Light at Night on Wild Plants. *J. Ecol.* 104, 611–620. doi:10.1111/1365-2745.12551

Bettiol, L., Kamaletdinova, G., Patel, D., Lakmal, Y., Oluwafemi, F., De La Torre, A., et al. (2018). "Manned Mars mission Risks Evaluation [Conference Presentation]," in IAC-18- B3.9.5. Proceedings of the 69th International Astronautical Congress, Bremen, Germany, October 1-5, 2018.

Bijlani, S., Stephens, E., Singh, N. K., Venkateswaran, K., and Wang, C. C. C. (2021). Advances in Space Microbiology. *iScience* 24, 102395. doi:10.1016/j.isci.2021.102395

Bitz, D. M., and Sargent, M. L. (1974). A Failure to Detect an Influence of Magnetic Fields on the Growth Rate and Circadian Rhythm of Neurospora Crassa. *Plant Physiol.* 53, 154–157. doi:10.1104/pp.53.2.154

Bliss, V. L., and Heppner, F. H. (1976). Circadian Activity Rhythm Influenced by Near Zero Magnetic Field. *Nature* 261, 411–412. doi:10.1038/261411a0

Borgioli, C., Martelli, L., Porri, F., D'Elia, A., Marchetti, G. M., and Scapini, F. (1999). Orientation in Talitrus Saltator (Montagu): Trends in Intrapopulation Variability Related to Environmental and Intrinsic Factors. *J. Exp. Mar. Biol. Ecol.* 238, 29–47. doi:10.1016/S0022-0981(99)00012-X

Broadway, J., Arendt, J., and Folkard, S. (1987). Bright Light Phase Shifts the Human Melatonin Rhythm during the Antarctic winter. *Neurosci. Lett.* 79, 185–189. doi:10.1016/0304-3940(87)90694-x

Brooks, J. F., 2nd, Behrendt, C. L., Ruhn, K. A., Lee, S., Raj, P., Takahashi, J. S., et al. (2021). The Microbiota Coordinates Diurnal Rhythms in Innate Immunity with the Circadian Clock. *Cell* 184 (16), 4154–4167.e12. doi:10.1016/j.cell.2021.07.001

Brown, F. A., Jr., Barnwell, F. H., and Webb, H. M. (1964). Adaptation of the Magnetoreceptive Mechanism of Mud-Snails to Geomagnetic Strength. *Biol. Bull.* 127, 221–231. doi:10.2307/1539221

Brown, F. A., Jr., Hastings, J. W., and Palmer, J. D. (1970). *The Biological Clock: Two Views*. New York: Academic Press.

Bünning, E. (1964). *The Physiological Clock*. Berlin: Springer-Verlag Berlin Heidelberg.

Cashmore, A. R., Jarillo, J. A., Wu, Y. J., and Liu, D. (1999). Cryptochromes: Blue Light Receptors for Plants and Animals. *Science* 284, 760–765. doi:10.1126/science.284.5415.760

Cavallari, N., Frigato, E., Vallone, D., Fröhlich, N., Lopez-Olmeda, J. F., Foà, A., et al. (2011). A Blind Circadian Clock in Cavefish Reveals that Opsins Mediate Peripheral Clock Photoreception. *Plos Biol.* 9, e1001142. doi:10.1371/journal.pbio.1001142

Cervantes, J. L., and Hong, B. Y. (2016). Dysbiosis and Immune Dysregulation in Outer Space. *Int. Rev. Immunol.* 35, 67–82. doi:10.3109/0883018510.3109/08830185.2015.1027821

Chen, H., Lv, K., Ji, G., Yuan, Y., Lu, L., Liang, F., et al. (2020). Physiological Acclimatization of the Liver to 180-Day Isolation and the Mars Solar Day. *Biomed. Res. Int.* 2020, 2796510. doi:10.1155/2020/2796510

China Global Television Network (2021). China Global Television Network. Available at: https://news.cgtn.com/news/2021-06-26/China-plans-to-launch-first-crewed-mission-to-Mars-in-2033-11oS5qxFp0k/index.html (Accessed June 26, 2021).

Collado, M. C., Engen, P. A., Bandín, C., Cabrera-Rubio, R., Voigt, R. M., Green, S. J., et al. (2018). Timing of Food Intake Impacts Daily Rhythms of Human Salivary Microbiota: a Randomized, Crossover Study. *FASEB J.* 32, 2060–2072. doi:10.1096/fj.201700697RR

Cucinotta, F. A., and Durante, M. (2006). Cancer Risk from Exposure to Galactic Cosmic Rays: Implications for Space Exploration by Human Beings. *Lancet Oncol.* 7, 431–435. doi:10.1016/S1470-2045(06)70695-7

Czeisler, C. A., Duffy, J. F., Shanahan, T. L., Brown, E. N., Mitchell, J. F., Rimmer, D. W., et al. (1999). Stability, Precision, and Near-24-Hour Period of the Human Circadian Pacemaker. *Science* 284, 2177–2181. doi:10.1126/science.284.5423.2177

Dietrich, M. (2004). Human Missions to Mars: New Psychological Challenges and Research Issues. *Acta Astronautica* 55, 781–790. doi:10.1016/j.actaastro.2004.05.013

Ditty, J. L., Mackey, S. R., and Johnson, C. H. (2009). *Bacterial Circadian Programs*. Berlin: Springer-Verlag Berlin Heidelberg, 212–219.

Doherty, C. J., and Kay, S. A. (2010). Circadian Control of Global Gene Expression Patterns. *Annu. Rev. Genet.* 44, 419–444. doi:10.1146/annurev-genet-102209-163432

Duffy, J. F., Cain, S. W., Chang, A. M., Phillips, A. J. K., Münch, M. Y., Gronfier, C., et al. (2011). Sex Difference in the Near-24-Hour Intrinsic Period of the Human Circadian Timing System. *Proc. Nat. Acad. Sci. U S A.* 108, 15602–15608. doi:10.1073/pnas.1010666108

ElGindi, M., Sapudom, J., Ibrahim, I. H., Al-Sayegh, M., Chen, W., Garcia-Sabaté, A., et al. (2021). May the Force Be with You (Or Not): The Immune System under Microgravity. *Cells* 10, 1941. doi:10.3390/cells10081941

Erzberger, A., Hampp, G., Granada, A. E., Albrecht, U., and Herzel, H. (2013). Genetic Redundancy Strengthens the Circadian Clock Leading to a Narrow Entrainment Range. *J. R. Soc. Interf.* 10, 20130221. doi:10.1098/rsif.2013.0221

Flynn-Evans, E. E., Barger, L. K., Kubey, A. A., Sullivan, J. P., and Czeisler, C. A. (2016). Circadian Misalignment Affects Sleep and Medication Use before and during Spaceflight. *NPJ Microgravity* 2, 15019. doi:10.1038/npjmgrav.2015.19

Fu, L., Pelicano, H., Liu, J., Huang, P., and Lee, C. (2002). The Circadian Gene Period2 Plays an Important Role in Tumor Suppression and DNA Damage Response *In Vivo*. *Cell* 111, 41–50. doi:10.1016/s0092-8674(02)00961-3

Fujita, S. I., Rutter, L., Ong, Q., and Muratani, M. (2020). Integrated RNA-Seq Analysis Indicates Asynchrony in Clock Genes between Tissues under Spaceflight. *Life* 10, 196. doi:10.3390/life10090196

Gallego, M., and Virshup, D. M. (2007). Post-translational Modifications Regulate the Ticking of the Circadian Clock. *Nat. Rev. Mol. Cel. Biol.* 8, 139–148. doi:10.1038/nrm2106

Garrett-Bakelman, F. E., Darshi, M., Green, S. J., Gur, R. C., Lin, L., Macias, B. R., et al. (2019). The NASA Twins Study: A Multidimensional Analysis of a Year-Long Human Spaceflight. *Science* 364, eaau8650. doi:10.1126/science.aau8650

Gegear, R. J., Casselman, A., Waddell, S., and Reppert, S. M. (2008). Cryptochrome Mediates Light-dependent Magnetosensitivity in Drosophila. *Nature* 454, 1014–1018. doi:10.1038/nature07183

Gertz, M. L., Chin, C. R., Tomoiaga, D., MacKay, M., Chang, C., Butler, D., et al. (2020). Multi-omic, Single-Cell, and Biochemical Profiles of Astronauts Guide Pharmacological Strategies for Returning to Gravity. *Cell Rep* 33, 108429. doi:10.1016/j.celrep.2020.108429

Gery, S., Komatsu, N., Baldjyan, L., Yu, A., Koo, D., and Koeffler, H. P. (2006). The Circadian Gene Per1 Plays an Important Role in Cell Growth and DNA Damage Control in Human Cancer Cells. *Mol. Cel* 22 (3), 375–382. doi:10.1016/j.molcel.2006.03.038

Gilbert, R., Torres, M., Clemens, R., Hateley, S., Hosamani, R., Wade, W., et al. (2020). Spaceflight and Simulated Microgravity Conditions Increase Virulence of *Serratia marcescens* in the *Drosophila melanogaster* Infection Model. *NPJ Microgravity* 6, 4. doi:10.1038/s41526-019-0091-2

Gould, J. L., Kirschvink, J. L., and Deffeyes, K. S. (1978). Bees Have Magnetic Remanence. *Science* 201, 1026–1028. doi:10.1126/science.201.4360.1026

Green, M. J., Aylott, J. W., Williams, P., Ghaemmaghami, A. M., and Williams, P. M. (2021). Immunity in Space: Prokaryote Adaptations and Immune Response in Microgravity. *Life* 11, 112. doi:10.3390/life11020112

Gronfier, C., Wright, K. P., Jr., Kronauer, R. E., and Czeisler, C. A. (2007). Entrainment of the Human Circadian Pacemaker to longer-Than-24-h Days. *Proc. Natl. Acad. Sci. U S A.* 104, 9081–9086. doi:10.1073/pnas.0702835104

Guo, J. H., Ma, X. H., Ma, H., Zhang, Y., Tian, Z. Q., Wang, X., et al. (2020). Circadian Misalignment in Submarine and Other Non-24 Hour Conditions – from Research to Application. *Mil. Med. Res.* 7, 39. doi:10.1186/s40779-020-00268-2

Guo, J. H., Qu, W. M., Chen, S. G., Chen, X. Y., Lv, K., Huang, Z. L., et al. (2014). Keeping the Right Time in Space: Importance of Circadian Clock and Sleep for Physiology and Performance of Astronauts. *Mil. Med. Res.* 1, 23. doi:10.1186/2054-9369-1-23

Hammad, M., Albaqami, M., Pooam, M., Kernevez, E., Witczak, J., Ritz, T., et al. (2020). Cryptochrome Mediated Magnetic Sensitivity in Arabidopsis Occurs Independently of Light-Induced Electron Transfer to the Flavin. *Photochem. Photobiol. Sci.* 19, 341–352. doi:10.1039/c9pp00469f

Heath-Heckman, E. A., Peyer, S. M., Whistler, C. A., Apicella, M. A., Goldman, W. E., and McFall-Ngai, M. J. (2013). Bacterial Bioluminescence Regulates Expression of a Host Cryptochrome Gene in the Squid-Vibrio Symbiosis. *mBio* 4, e00167–13. doi:10.1128/mBio.00167-13

Heer, M., Boerger, A., Kamps, N., Mika, C., Korr, C., and Drummer, C. (2000). Nutrient Supply during Recent European Missions. *Pflugers Arch.* 441 (2-3 Suppl. l), R8–R14. doi:10.1007/s004240000334

Hellweg, C. E., and Baumstark-Khan, C. (2007). Getting Ready for the Manned mission to Mars: the Astronauts' Risk from Space Radiation. *Naturwissenschaften* 94, 517–526. doi:10.1007/s00114-006-0204-0

Hirano, A., Fu, Y. H., and Ptáček, L. J. (2016). The Intricate Dance of post-translational Modifications in the Rhythm of Life. *Nat. Struct. Mol. Biol.* 23, 1053–1060. doi:10.1038/nsmb.3326

Hoban-Higgins, T. M., Alpatov, A. M., Wassmer, G. T., Rietveld, W. J., and Fuller, C. A. (2003). Gravity and Light Effects on the Circadian Clock of a Desert Beetle, Trigonoscelis Gigas. *J. Insect Physiol.* 49, 671–675. doi:10.1016/s0022-1910(03)00068-4

Holley, D. C., DeRoshia, C. W., Moran, M. M., and Wade, C. E. (2003). Chronic Centrifugation (Hypergravity) Disrupts the Circadian System of the Rat. *J. Appl. Physiol.* 95, 1266–1278. doi:10.1152/japplphysiol.00707.2002

Honma, K. I., and Honma, S. (2001). *Zeitgebers, Entrainment and Masking of the Circadian System*. Sapporo. Japan: Hokkaido University Press.

Huang, B., Li, D. G., Huang, Y., and Liu, C. T. (2018). Effects of Spaceflight and Simulated Microgravity on Microbial Growth and Secondary Metabolism. *Mil. Med. Res.* 5, 18. doi:10.1186/s40779-018-0162-9

Hurley, J. M., Loros, J. J., and Dunlap, J. C. (2016). Circadian Oscillators: Around the Transcription-Translation Feedback Loop and on to Output. *Trends Biochem. Sci.* 41, 834–846. doi:10.1016/j.tibs.2016.07.009

Irwin, A. (2018). The Dark Side of Light: How Artificial Lighting Is Harming the Natural World. *Nature* 553, 268–270. doi:10.1038/d41586-018-00665-7

Jiang, P., Green, S. J., Chlipala, G. E., Turek, F. W., and Vitaterna, M. H. (2019). Reproducible Changes in the Gut Microbiome Suggest a Shift in Microbial and Host Metabolism during Spaceflight. *Microbiome* 7, 113. doi:10.1186/s40168-019-0724-4

Johnson, C. H. (2005). Testing the Adaptive Value of Circadian Systems. *Methods Enzymol.* 393, 818–837. doi:10.1016/S0076-6879(05)93043-7

Juhl, O. J., 4th, Buettmann, E. G., Friedman, M. A., DeNapoli, R. C., Hoppock, G. A., and Donahue, H. J. (2021). Update on the Effects of Microgravity on the Musculoskeletal System. *NPJ Microgravity* 7, 28. doi:10.1038/s41526-021-00158-4

Kanas, N., Salnitskiy, V., Grund, E. M., Gushin, V., Weiss, D. S., Kozerenko, O., et al. (2000). Social and Cultural Issues during Shuttle/Mir Space Missions. *Acta Astronaut* 47, 647–655. doi:10.1016/s0094-5765(00)00102-8

Kandarpa, K., Schneider, V., and Ganapathy, K. (2019). Human Health during Space Travel: An Overview. *Neurol. India* 67 (Suppl.), S176–S181. doi:10.4103/0028-3886.259123

Kassahun, B. T., Bier, M., and Ding, J. (2020). Perturbing Circadian Oscillations in an *In Vitro* Suprachiasmatic Nucleus with Magnetic Stimulation. *Bioelectromagnetics* 41, 63–72. doi:10.1002/bem.22235

Kitahara, R., Oyama, K., Kawamura, T., Mitsuhashi, K., Kitazawa, S., Yasunaga, K., et al. (2019). Pressure Accelerates the Circadian Clock of Cyanobacteria. *Sci. Rep.* 9, 12395. doi:10.1038/s41598-019-48693-1

Klaus, D. M., and Howard, H. N. (2006). Antibiotic Efficacy and Microbial Virulence during Space Flight. *Trends Biotechnol.* 24, 131–136. doi:10.1016/j.tibtech.2006.01.008

Knight, D. J., and Girling, K. J. (2003). Gut flora in Health and Disease. *Lancet* 361, 1831. doi:10.1016/s0140-6736(03)13438-1

Krieger, S. S., Zwart, S. R., Mehta, S., Wu, H., Simpson, R. J., Smith, S. M., et al. (2021). Alterations in Saliva and Plasma Cytokine Concentrations during Long-Duration Spaceflight. *Front. Immunol.* 12, 725748. doi:10.3389/fimmu10.3389/fimmu.2021.725748

Kuang, Z., Wang, Y., Li, Y., Ye, C., Ruhn, K. A., Behrendt, C. L., et al. (2019). The Intestinal Microbiota Programs Diurnal Rhythms in Host Metabolism through Histone Deacetylase 3. *Science* 365, 1428–1434. doi:10.1126/science.aaw3134

Lefta, M., Wolff, G., and Esser, K. A. (2011). Circadian Rhythms, the Molecular Clock, and Skeletal Muscle. *Curr. Top. Dev. Biol.* 96, 231–271. doi:10.1016/B978-0-12-385940-2.00009-7

Levchenko, I., Xu, S., Mazouffre, S., Keidar, M., and Bazaka, K. (2018). Mars Colonization: Beyond Getting There. *Glob. Chall.* 3, 1800062. doi:10.1002/gch2.201800062

Levine, J. D., Funes, P., Dowse, H. B., and Hall, J. C. (2002). Resetting the Circadian Clock by Social Experience in *Drosophila melanogaster*. *Science* 298, 2010–2012. doi:10.1126/science.1076008

Lewczuk, B., Redlarski, G., Zak, A., Ziółkowska, N., Przybylska-Gornowicz, B., and Krawczuk, M. (2014). Influence of Electric, Magnetic, and Electromagnetic fields on the Circadian System: Current Stage of Knowledge. *Biomed. Res. Int.* 2014, 169459. doi:10.1155/2014/169459

Lewis, P., Korf, H. W., Kuffer, L., Groß, J. V., and Erren, T. C. (2018). Exercise Time Cues (Zeitgebers) for Human Circadian Systems Can foster Health and Improve Performance: a Systematic Review. *BMJ Open Sport Exerc. Med.* 4, e000443. doi:10.1136/bmjsem-2018-000443

Li, P., Shi, J., Zhang, P., Wang, K., Li, J., Liu, H., et al. (2015). Simulated Microgravity Disrupts Intestinal Homeostasis and Increases Colitis Susceptibility. *FASEB J.* 29, 3263–3273. doi:10.1096/fj.15-271700

Liang, X., Zhang, L., Shen, H., Chen, X., Wan, Y., Li, L., et al. (2014). Effects of a 45-day Head-Down Bed Rest on the Diurnal Rhythms of Activity, Sleep and Heart Rate. *Biol. Rhythm Res.* 45, 596–601. doi:10.1080/09291016.2014.882093

Lindauer, M., and Martin, H. (1985). "The Biological Significance of the Earth's Magnetic Field," in *Progress in Sensory Physiology*. Editors H. Autrum, D. Ottoson, E. R. Perl, R. F. Schmidt, H. Shimazu, and W. D. Willis (Berlin, Heidelberg: Springer), Vol. 5. doi:10.1007/978-3-642-70408-6_3

Linden, H. (2002). Circadian Rhythms. A white Collar Protein Senses Blue Light. *Science* 297, 777–778. doi:10.1126/science.1075485

López-Otín, C., and Kroemer, G. (2021). Hallmarks of Health. *Cell* 184, 33–63. doi:10.1016/j.cell.2020.11.034

Lu, W., Meng, Q. J., Tyler, N. J., Stokkan, K. A., and Loudon, A. S. (2010). A Circadian Clock Is Not Required in an Arctic Mammal. *Curr. Biol.* 20, 533–537. doi:10.1016/j.cub.2010.01.042

Ma, H., Li, Y., Liang, H., Chen, S., Pan, S., Chang, L., et al. (2019). Sleep Deprivation and a Non-24 H Working Schedule lead to Extensive Alterations in Physiology and Behavior. *FASEB J.* 33, 6969–6979. doi:10.1096/fj.201802727R

Ma, L., Ma, J., and Xu, K. (2015). Effect of Spaceflight on the Circadian Rhythm, Lifespan and Gene Expression of *Drosophila melanogaster*. *PLoS One* 10, e0121600. doi:10.1371/journal.pone.0121600

Maki, J. N., Golombek, M., Banerdt, W., Smrekar, S., Deen, R., Abarca, H., et al. (2021). Color Properties at the Mars InSight landing Site. *Earth Space Sci.* 8, e2020EA001336. doi:10.1029/2020EA001336

Maki, J. N., Lorre, J. J., Sith, P. H., Brandt, R. D., and Steinwand, D. J. (1999). The Color of Mars: Spectrophotometric Measurements at the Pathfinder landing Site. *Geophys. Res.* 104 (E4), 8781–8794. doi:10.1029/98JE01767

Mallis, M. M., and DeRoshia, C. W. (2005). Circadian Rhythms, Sleep, and Performance in Space. *Aviat. Space Environ. Med.* 76 (6 Suppl. l), B94–B107.

Mayeuf-Louchart, A., Staels, B., and Duez, H. (2015). Skeletal Muscle Functions Around the Clock. *Diabetes Obes. Metab.* 17 (Suppl. 1), 39–46. doi:10.1111/dom.12517

Maynard, A. J., and Merritt, D. J. (2013). Synchronization of Circadian Bioluminescence as a Group-Foraging Strategy in Cave Glowworms. *Integr. Comp. Biol.* 53, 154–164. doi:10.1093/icb/ict011

McClung, C. R. (2006). Plant Circadian Rhythms. *Plant Cell* 18, 792–803. doi:10.1105/tpc.106.040980

Mcphee, J. C., and Charles, J. B. (2009). *Human Health and Performance Risks of Space Exploration Missions*. Washington, D.C., USA: National Aeronautics and Space Administration. Lyndon B. Johnson Space Center. NASA SP-2009-3405, 106.

Mendoza, J. (2007). Circadian Clocks: Setting Time by Food. *J. Neuroendocrinol.* 19, 127–137. doi:10.1111/j.1365-2826.2006.01510.x

Mendt, S., Gunga, H. C., Felsenberg, D., Belavy, D. L., Steinach, M., and Stahn, A. C. (2021). Regular Exercise Counteracts Circadian Shifts in Core Body Temperature during Long-Duration Bed Rest. *NPJ Microgravity* 7, 1. doi:10.1038/s41526-020-00129-1

Mergenhagen, D., and Mergenhagen, E. (1989). The Expression of a Circadian Rhythm in Two Strains of Chlamydomonas Reinhardii in Space. *Adv. Space Res.* 9, 261–270. doi:10.1016/0273-1177(89)90082-3

Miles, L. E. M., Raynal, D. M., and Wilson, M. A. (1977). Blind Man Living in normal Society Has Circadian Rhythms of 24.9 Hours (Letter). *Science* 198, 421–423. doi:10.1126/science.910139

Mishra, B., and Luderer, U. (2019). Reproductive Hazards of Space Travel in Women and Men. *Nat. Rev. Endocrinol.* 15, 713–730. doi:10.1038/s41574-019-0267-6

Mittelholz, A., Morschhauser, A., Johnson, C. L., Langlais, B., Lillis, R. J., Vervelidou, F., et al. (2018). The Mars 2020 Candidate Landing Sites: A Magnetic Field Perspective. *Earth Space Sci.* 5, 410–424. doi:10.1029/2018EA000420

Moores, J. E., Smith, P. H., Tanner, R., Schuerger, A. C., and Venkateswaran, K. J. (2007). The Shielding Effect of Small Scale Martian Surface Geometry on Ultraviolet Flux. *Icarus* 192, 417–433. doi:10.1016/j.icarus.2007.07.003

Moosavi, D., Wolovsky, D., Depompeis, A., Uher, D., Lennington, D., Bodden, R., et al. (2021). The Effects of Spaceflight Microgravity on the Musculoskeletal System of Humans and Animals, with an Emphasis on Exercise as a Countermeasure: a Systematic Scoping Review. *Physiol. Res.* 70, 119–151. doi:10.33549/physiolres.934550

Mormont, M. C., Waterhouse, J., Bleuzen, P., Giacchetti, S., Jami, A., Bogdan, A., et al. (2000). Marked 24-h Rest/activity Rhythms Are Associated with Better Quality of Life, Better Response, and Longer Survival in Patients with Metastatic Colorectal Cancer and Good Performance Status. *Clin. Cancer Res.* 6, 3038–3045. PMID: 10955782.

Müller, N. A., Wijnen, C. L., Srinivasan, A., Ryngajllo, M., Ofner, I., Lin, T., et al. (2016). Domestication Selected for Deceleration of the Circadian Clock in Cultivated Tomato. *Nat. Genet.* 48, 89–93. doi:10.1038/ng.3447

Mullineaux, C. W. (2001). How Do Cyanobacteria Sense and Respond to Light? *Mol. Microbiol.* 41, 965–971. doi:10.1046/j.1365-2958.2001.02569.x

NASA (2020). NASA. https://nssdc.gsfc.nasa.gov/planetary/factsheet/marsfact.html (Accessed November 27, 2021).

Neumann, M. F. (1988). Is There Any Influence of Magnetic or Astrophysical fields on the Circadian Rhythm of Honeybees? *Behav. Ecol. Sociobiol.* 23, 389–393. doi:10.1007/BF00303713

Oluwafemi, F. A., Abdelbaki, R., Lai, J. C., Mora-Almanza, J. G., and Afolayan, E. M. (2021). A Review of Astronaut Mental Health in Manned Missions: Potential Interventions for Cognitive and Mental Health Challenges. *Life Sci. Space Res.* 28, 26–31. doi:10.1016/j.lssr.2020.12.002

Ouyang, Y., Andersson, C. R., Kondo, T., Golden, S. S., and Johnson, C. H. (1998). Resonating Circadian Clocks Enhance Fitness in Cyanobacteria. *Proc. Natl. Acad. Sci. U S A.* 95, 8660–8664. doi:10.1073/pnas.95.15.8660

Palmer, J. D. (2002). *The Living Clok: The Orchestrator of Biological Rhythms*. Oxord: Oxord University Press, Inc.

Parihar, V. K., Allen, B., Tran, K. K., Macaraeg, T. G., Chu, E. M., Kwok, S. F., et al. (2015). What Happens to Your Brain on the Way to Mars. *Sci. Adv.* 1, e1400256. doi:10.1126/sciadv.1400256

Pavy Le-Traon, A., and Roussel, B. (1993). Sleep in Space. *Acta Astronaut* 29, 945–950. doi:10.1016/0094-5765(93)90014-n

Pittendrigh, C. S., and Minis, D. H. (1972). Circadian Systems: Longevity as a Function of Circadian Resonance in *Drosophila melanogaster*. *Proc. Natl. Acad. Sci. U S A.* 69, 1537–1539. doi:10.1073/pnas.69.6.1537

Pregueiro, A. M., Liu, Q., Baker, C. L., Dunlap, J. C., and Loros, J. J. (2006). The Neurospora Checkpoint Kinase 2: a Regulatory Link between the Circadian and Cell Cycles. *Science* 313, 644–649. doi:10.1126/science.1121716

Proietto, M., Bianchi, M. M., Ballario, P., and Brenna, A. (2015). Epigenetic and Posttranslational Modifications in Light Signal Transduction and the Circadian Clock in Neurospora Crassa. *Int. J. Mol. Sci.* 16, 15347–15383. doi:10.3390/ijms160715347

Qin, S., Yin, H., Yang, C., Dou, Y., Liu, Z., Zhang, P., et al. (2016). A Magnetic Protein Biocompass. *Nat. Mater.* 15, 217–226. doi:10.1038/nmat4484

Raible, F., Takekata, H., and Tessmar-Raible, K. (2017). An Overview of Monthly Rhythms and Clocks. *Front. Neurol.* 8, 189. doi:10.3389/fneur.2017.00189

Refinetti, R. (2016). *Circadian Physiology*. Boca Raton, Florida, USA: CRC Press, 328–330. doi:10.3389/fneur.2017.00189

Rensing, L., and Ruoff, P. (2002). Temperature Effect on Entrainment, Phase Shifting, and Amplitude of Circadian Clocks and its Molecular Bases. *Chronobiol. Int.* 19, 807–864. doi:10.1081/cbi-120014569

Saei, A. A., and Barzegari, A. (2012). The Microbiome: the Forgotten Organ of the Astronaut's Body-Pprobiotics beyond Terrestrial Limits. *Future Microbiol.* 7, 1037–1046. doi:10.2217/fmb.12.82

Saunders, D. S. (1982). *Insect Clock*. Oxford: Pergamon Press.

Scheer, F. A., Wright, K. P., Jr., Kronauer, R. E., and Czeisler, C. A. (2007). Plasticity of the Intrinsic Period of the Human Circadian Timing System. *PLoS ONE* 2, e721. doi:10.1371/journal.pone.0000721

Scheiermann, C., Kunisaki, Y., and Frenette, P. S. (2013). Circadian Control of the Immune System. *Nat. Rev. Immunol.* 13, 190–198. doi:10.1038/nri3386

Schneider, T., Thalau, H. P., and Semm, P. (1994). Effects of Light or Different Earth-Strength Magnetic fields on the Nocturnal Melatonin Concentration in a Migratory Bird. *Neurosci. Lett.* 168, 73–75. doi:10.1016/0304-3940(94)90419-7

Selsis, F., Kaltenegger, L., and Paillet, J. (2008). Terrestrial Exoplanets: Diversity,habitability and Characterization. *Phys. Scr.* T130, 014032. doi:10.1088/0031-8949/2008/T130/014032

Semm, P., Schneider, T., and Vollrath, L. (1980). Effects of an Earth-Strength Magnetic Field on Electrical Activity of Pineal Cells. *Nature* 288, 607–608. doi:10.1038/288607a0

Sgobba, T., and Schlacht, I. L. (2018). *Chapter 15 - Habitability and Habitat Design in Space Safety and Human Performance*. Amsterdam: Elsevier. doi:10.1016/B978-0-08-101869-9.00015-7

Sharma, V. K. (2003). Adaptive Significance of Circadian Clocks. *Chronobiol. Int.* 20, 901–919. doi:10.1081/cbi-120026099

Shi, Y. S., Jing, X. L., Tong, F. Z., Hu, Y., Sun, H. Y., Tian, L. P., et al. (2018). Research on Adaptive Process of Crew's Affect and Cognition during 4-person 180-day CELSS Integrated Experiment. *Space Med. Med. Eng.* 31, 414–419. doi:10.16289/j.cnki.1002-0837.2018.04.004

Shimmura, T., Ohashi, S., and Yoshimura, T. (2015). The Highest-Ranking Rooster Has Priority to Announce the Break of Dawn. *Sci. Rep.* 5, 11683. doi:10.1038/srep11683

Siddiqui, R., Akbar, N., and Khan, N. A. (2021). Gut Microbiome and Human Health under the Space Environment. *J. Appl. Microbiol.* 130, 14–24. doi:10.1111/jam.14789

Solovev, I., Dobrovolskaya, E., Shaposhnikov, M., Sheptyakov, M., and Moskalev, A. (2019). Neuron-specific Overexpression of Core Clock Genes Improves Stress-Resistance and Extends Lifespan of *Drosophila melanogaster*. *Exp. Gerontol.* 117, 61–71. doi:10.1016/j.exger.2018.11.005

Song, C., Wang, J., Kim, B., Lu, C., Zhang, Z., Liu, H., et al. (2018). Insights into the Role of Circadian Rhythms in Bone Metabolism: A Promising Intervention Target? *Biomed. Res. Int.* 2018, 9156478. doi:10.1155/2018/9156478

Stevenson, D. J. (2001). Mars' Core and Magnetism. *Nature* 412, 214–219. doi:10.1038/35084155

Sulzman, F. M., Ellman, D., Fuller, C. A., Moore-Ede, M. C., and Wassmer, G. (1984). Neurospora Circadian Rhythms in Space: a Reexamination of the Endogenous-Exogenous Question. *Science* 225, 232–234. doi:10.1126/science.11540800

Swanson, C. M., Kohrt, W. M., Buxton, O. M., Everson, C. A., Wright, K. P., Jr., Orwoll, E. S., et al. (2018). The Importance of the Circadian System & Sleep for Bone Health. *Metabolism* 84, 28–43. doi:10.1016/j.metabol.2017.12.002

Tafforin, C. (2015). Confinement vs. Isolation as Analogue Environments for Mars Missions from a Human Ethology Viewpoint. *Aerosp. Med. Hum. Perform.* 86, 131–135. doi:10.3357/AMHP.4100.2015

Thaiss, C. A., Zeevi, D., Levy, M., Zilberman-Schapira, G., Suez, J., Tengeler, A. C., et al. (2014). Transkingdom Control of Microbiota Diurnal Oscillations Promotes Metabolic Homeostasis. *Cell* 159, 514–529. doi:10.1016/j.cell.2014.09.048

Tong, F. Z. (2018). *Feizhou's Diary - Space 180-d Experiment*. Beijing: Higher Education Press.

Turek, F. W., and Gillette, M. U. (2004). Melatonin, Sleep, and Circadian Rhythms: Rationale for Development of Specific Melatonin Agonists. *Sleep Med.* 5, 523–532. doi:10.1016/j.sleep.2004.07.009

Udo, R., Hamada, T., Horikawa, K., Iwahana, E., Miyakawa, K., Otsuka, K., et al. (2004). The Role of Clock in the Plasticity of Circadian Entrainment. *Biochem. Biophys. Res. Commun.* 318, 893–898. doi:10.1016/j.bbrc.2004.04.113

Wan, G., Hayden, A. N., Iiams, S. E., and Merlin, C. (2021). Cryptochrome 1 Mediates Light-dependent Inclination Magnetosensing in Monarch Butterflies. *Nat. Commun.* 12, 771. doi:10.1038/s41467-021-21002-z

Wang, D., Zhang, L., Liang, X., Shen, H., Chen, X., Wan, Y., et al. (2014). "Space Meets Time: Impact of Gravity on Circadian/Diurnal Rhythms," in *A Sponsored Supplement to Science: Human Performance in Space - Advancing Astronautics Research in China*, 15–17.

Welsh, D. K., Takahashi, J. S., and Kay, S. A. (2010). Suprachiasmatic Nucleus: Cell Autonomy and Network Properties. *Annu. Rev. Physiol.* 72, 551–577. doi:10.1146/annurev-physiol-021909-135919

Whiteway, J., Daly, M., Carswell, A., Duck, T., Dickinson, C., Komguem, L., et al. (2008). Lidar on the Phoenix mission to Mars. *J. Geophys. Res.* 113, E00A08. doi:10.1029/2007JE003002

Wilson, J. W., Ott, C. M., Höner zu Bentrup, K., Ramamurthy, R., Quick, L., Porwollik, S., et al. (2007). Space Flight Alters Bacterial Gene Expression and Virulence and Reveals a Role for Global Regulator Hfq. *Proc. Natl. Acad. Sci. U S A.* 104, 16299–16304. doi:10.1073/pnas.0707155104

Woelfle, M. A., Ouyang, Y., Phanvijhitsiri, K., and Johnson, C. H. (2004). The Adaptive Value of Circadian Clocks: an Experimental Assessment in Cyanobacteria. *Curr. Biol.* 14, 1481–1486. doi:10.1016/j.cub.2004.08.023

Woller, A., and Gonze, D. (2021). Circadian Misalignment and Metabolic Disorders: A Story of Twisted Clocks. *Biology* 10, 207. doi:10.3390/biology10030207

Wright, K. P., Jr., Hughes, R., Kronauer, R. E., Dijk, D. J., and Czeisler, C. A. (2001). Intrinsic Near-24-H Pacemaker Period Determines Limits of Circadian Entrain-Ment to a Wea Synchronizer in Humans. *Proc. Natl. Acad. Sci. U S A.* 98, 14027–14032. doi:10.1073/pnas.201530198

Yang, H., Tong, F., Ma, X., Huang, T., Gan, X., Zhang, Y., et al. (2021). A Case Study of Emotional Changes of One Volunteer under the 180-day Combinational Environment Using Natural Language Processing Tool. *Space Med. Med. Eng.* 34, 222–228. doi:10.16289/j.cnki.1002-0837.2021.03.006

Zhang, H., Liang, J., and Chen, N. (2020). Do Not Neglect the Role of Circadian Rhythm in Muscle Atrophy. *Ageing Res. Rev.* 63, 101155. doi:10.1016/j.arr.2020.101155

Zhang, H., Wang, Y., Zhang, Z., Zhang, L., Tang, C., Sun, B., et al. (2021). Alterations in the Activity and Sleep of *Drosophila melanogaster* under Simulated Microgravity. *NPJ Microgravity* 7, 27. doi:10.1038/s41526-021-00157-5

Zhang, L., Weng, W., and Guo, J. (2011). Posttranscriptional Mechanisms in Controlling Eukaryotic Circadian Rhythms. *FEBS Lett.* 585, 1400–1405. doi:10.1016/j.febslet.2011.03.018

Zhu, L., Wang, Q., Hu, Y., and Wang, F. (2019). The Circadian Gene Per1 Plays an Important Role in Radiation-Induced Apoptosis and DNA Damage in Glioma. *Asian Pac. J. Cancer Prev.* 20, 2195–2201. doi:10.31557/APJCP.2019.20.7.2195

Zwicker, D., Lubensky, D. K., and ten Wolde, P. R. (2010). Robust Circadian Clocks from Coupled Protein-Modification and Transcription-Translation Cycles. *Proc. Natl. Acad. Sci. U S A.* 107, 22540–22545. doi:10.1073/pnas.1007613107

Conflict of Interest: The authors declare that the research was conducted in the absence of any commercial or financial relationships that could be construed as a potential conflict of interest.

Publisher's Note: All claims expressed in this article are solely those of the authors and do not necessarily represent those of their affiliated organizations, or those of the publisher, the editors and the reviewers. Any product that may be evaluated in this article, or claim that may be made by its manufacturer, is not guaranteed or endorsed by the publisher.

frontiers in Astronomy and Space Sciences

ORIGINAL RESEARCH
published: 28 January 2022
doi: 10.3389/fspas.2022.817900

Microbial Survival in an Extreme Martian Analog Ecosystem: Poás Volcano, Costa Rica

Justin L. Wang[1]*, *Nicholas B. Dragone*[2], *Geoffroy Avard*[3] and *Brian M. Hynek*[1,4]

[1]Laboratory for Atmospheric and Space Physics, University of Colorado, Boulder, CO, United States, [2]Department of Ecology and Evolutionary Biology, University of Colorado, Boulder, CO, United States, [3]OVISCORI, National University of Costa Rica, Heredia, Costa Rica, [4]Department of Geological Sciences, University of Colorado, Boulder, CO, United States

Past acid-sulfate hydrothermal systems on Mars have promise in their ability to have hosted life for billions of years. One method for analyzing these systems is to study analog environments on Earth. To assess the astrobiological potential of Martian acid-sulfate hydrothermal systems, the crater lake of the active Poás Volcano, Laguna Caliente, was sampled in 2013 and 2017. Laguna Caliente presents an extremely dynamic terrestrial environment with near-ambient to boiling temperatures, pH fluctuations from –0.87 to 1.5, a wide range of chemistries and redox potential, and frequent phreatic-to-phreatomagmatic eruptions. Samples of lake fluid, sulfur clumps, and lake bottom sediment underwent 16S rRNA gene sequencing and metagenomic "shotgun" sequencing, which revealed this lake hosts an extremely low biodiversity of microorganisms dominated by *Acidiphilium* spp. Shotgun metagenomics of the samples suggests this community has numerous genetic adaptations that confer survival, including functional pathways to reduce the effects of toxic metals and numerous metabolic pathways utilizing a variety of simple and complex sugar molecules. The identification of these various metabolic pathways suggests adaptations related to carbon limited environments, fulfillment of high energy requirements, and survival in a hostile volcanic setting. The perseverance of life in Laguna Caliente indicates life on Mars could have thrived in analogous environments, stressing the need for the search for life in relict Martian acid-sulfate hydrothermal systems.

Keywords: mars, astrobiology, acid-sulfate hydrothermal systems, extremophiles, metagenomic sequencing, acidiphilium bacteria

OPEN ACCESS

Edited by:
Maggie C. Y. Lau Vetter, Institute of Deep-Sea Science and Engineering (CAS), China

Reviewed by:
Rachel Lee Harris, Harvard University, United States
Akos Kereszturi, Hungarian Academy of Sciences (MTA), Hungary

***Correspondence:**
Justin L. Wang
justin.wang@colorado.edu

Specialty section:
This article was submitted to Astrobiology, a section of the journal Frontiers in Astronomy and Space Sciences

Received: *18 November 2021*
Accepted: *03 January 2022*
Published: *28 January 2022*

Citation:
Wang JL, Dragone NB, Avard G and Hynek BM (2022) Microbial Survival in an Extreme Martian Analog Ecosystem: Poás Volcano, Costa Rica. Front. Astron. Space Sci. 9:817900. doi: 10.3389/fspas.2022.817900

INTRODUCTION

The science discipline of Astrobiology is rather broad and leads to research ranging from studying the origins of life on Earth to searching for extraterrestrial life on alien worlds (Domagal-Goldman et al., 2016; Davila, 2021). To prepare for space missions with key goals to find signs of life on these extraterrestrial planets and moons, we must better understand how life in these environments may look like (Ehrenfreund et al., 2011). The search for signs of past life on Mars is a key NASA priority (National Research Council, 2011; Changela et al., 2021), demonstrated in 2021 by the arrival of the *Perseverance* rover on the Red Planet (Mangold et al., 2021). As of the time of this writing, neither extant life nor definitive signs of past life on Mars have been found; however, the habitability of Mars has been assessed to great detail (e.g., Cockell et al., 2012). For example, it has been shown that early

Mars had persistent liquid surface water, biogenic elements, and environments conducive to life (e.g., Grotzinger et al., 2015). While recent landing sites for habitability studies have focused on sedimentary environments (Kereszturi et al., 2016; Vago et al., 2018), relict hydrothermal settings may provide a better setting to investigate the astrobiological potential of early Mars (e.g., Michalski et al., 2018).

During the early period of Mars' history, volcanic/magmatic processes were widespread and liquid water was present in surface and near surface environments. The surface heat flux on early Mars was roughly an order of magnitude higher than at present (Hauck Ii and Phillips, 2002), and enormous amounts of crust were emplaced via volcanic and magmatic processes until ~3 billion years ago (e.g., Phillips et al., 2001; Craddock and Greeley, 2009; Carr and Head, 2010). Moreover, widespread liquid water was present at or near the surface during this time period (e.g., Hynek and Phillips, 2003; Fairén et al., 2003). Mars had an active, globally integrated, hydrologic cycle from ~3.8 to 3.6 Ga, based on the valley networks, which were incised at this time (Fassett and Head, 2008a; Hoke and Hynek, 2009; Hynek et al., 2010). Hundreds of paleolake basins have also been identified (e.g., Fassett and Head, 2008b; Goudge et al., 2016) and a number of these host fan delta deposits (e.g., Di Achille and Hynek, 2010; Wilson et al., 2021). After this time, significant water reserves remained in Mars' crust, as evidenced by the enormous outflow channels, which are thought to have been caused by confined aquifers bursting onto the surface through a cryosphere (e.g., Rotto and Tanaka, 1995; Andrews-Hanna and Phillips, 2007).

Given the abundant crustal/surface waters and rampant volcanism and magmatism, it is thought that large-scale hydrothermal alteration was common on early Mars, leading to extensive deposits of acid-sulfate alteration minerals (Bibring et al., 2005; Gendrin et al., 2005; Solomon et al., 2005; Ehlmann et al., 2011; Hynek et al., 2013). While surface waters may have been limited in time, volcanic activity likely occurred for much longer. With the lack of plate tectonics on Mars, the preserved geological record suggests intermittent summit eruptions occurred on individual volcanoes spanning 4 billion years (Robbins et al., 2011). Surface volcanic activity may have continued to <50,000 years ago (Horvath et al., 2021), and recent results from the *InSight* mission support a recently active volcano-tectonic system at Cerberus Fossae (Banerdt et al., 2020), which is believed to host an ice-saturated regolith (e.g., Moitra et al., 2021). Collectively, these observations suggest that subsurface hydrothermal activity may be ongoing within Mars' crust. In addition to volcanism, hydrothermal systems on Mars may also have been initiated from large impacts and could have provided a volumetrically large, long duration, cradle for the origin of life (Osinski et al., 2020). There are at least 78 large impact basins recorded to have formed prior to ~3.5 Ga (Robbins et al., 2013) with some likely hosting hydrothermal systems for up to 10 million years (Abramov and Kring, 2005).

Relict hydrothermal systems on Mars have been identified extensively on the surface *via* orbiters and landers obtaining mineralogy and geomorphology data. For example, the *Spirit* rover in Gusev crater found sulfate and silica accumulations suggesting acid-sulfate alteration occurred in fumarolic and/or hot spring environments next to Home Plate (Squyres et al., 2007; Squyres et al., 2008; Yen et al., 2008; Schmidt et al., 2009; Ruff et al., 2011). Hydrothermal processes have also been proposed for the *MER Opportunity* landing site (McCollom and Hynek, 2005) and at Gale crater, the home of the *Curiosity* rover (Yen et al., 2021). High temperature acid-sulfate alteration has also been hypothesized to have altered mineralogies present in Valles Marineris (Gendrin et al., 2005; Chojnacki and Hynek, 2008; Weitz et al., 2011; Thollot et al., 2012; Marcucci et al., 2013), the volcanic cone on the Nili Patera volcano (e.g., Skok et al., 2010), and numerous other volcanic edifices (Gulick, 1998; Tanaka et al., 1998; Dohm and Tanaka, 1999; Gulick, 2001; Hynek et al., 2010; El Maarry et al., 2012).

On Earth, hydrothermal environments often provide sources of heat, energy, and water for life (Walter and Des Marais, 1993; Schulze-Makuch et al., 2007; Hays et al., 2017). It is also hypothesized that the last universal common ancestor of life (LUCA) on Earth was likely a thermophile or hyperthermophile (Nisbet and Sleep, 2001; Giulio, 2003; Gaucher et al., 2008) potentially utilizing iron-sulfur redox chemistry in a hydrothermal setting (Martin and Russell, 2003; Wächtershäuser, 2006; Martin et al., 2008; Weiss et al., 2016). It is conceivable that life on Mars could have formed in a homologous manner in Martian hydrothermal environments and been sustained for billions of years through volcanism or impact-related hydrothermal activity. The condensation of volcanic vapors (fumaroles) and crustal hydrothermal circulation could have provided warm and moist habitats for life even while cold and dry conditions persisted globally. Understanding terrestrial life in environments analogous to Martian hydrothermal systems is crucial in order to characterize how life may have existed on Mars, which conditions extraterrestrial life could adapt to, and to better search for life on the Red Planet. Here, we characterize the taxonomic and functional diversity of microbial communities in the Poás Volcano in Costa Rica; arguably one of the most extreme Martian analog environments on Earth.

POÁS VOLCANO

The volcanic crater of Poás Volcano, Costa Rica (**Figure 1**) has been characterized as a Martian analog due to its mineralogical consistencies with relict Martian hydrothermal systems (Hynek et al., 2014; Black et al., 2015; Black et al., 2016; Rodríguez and van Bergen, 2017; Black and Hynek, 2018). The Poás Volcano is a basaltic andesite stratovolcano in the Central Cordillera of Costa Rica (Prosser and Carr, 1987). Poás has been active throughout the Holocene; phreatic to phreatomagmatic eruptions are common even in times of quiescence, such as between 1955 and 2017. These eruptions mostly consist of unpredictable steam-driven expulsions from the crater lake, Laguna Caliente (**Figure 1C**). A magmatic episode occurred from April to November 2017, and phreatomagmatic events resumed in 2019 (Salvage et al., 2018; Wang et al., 2020).

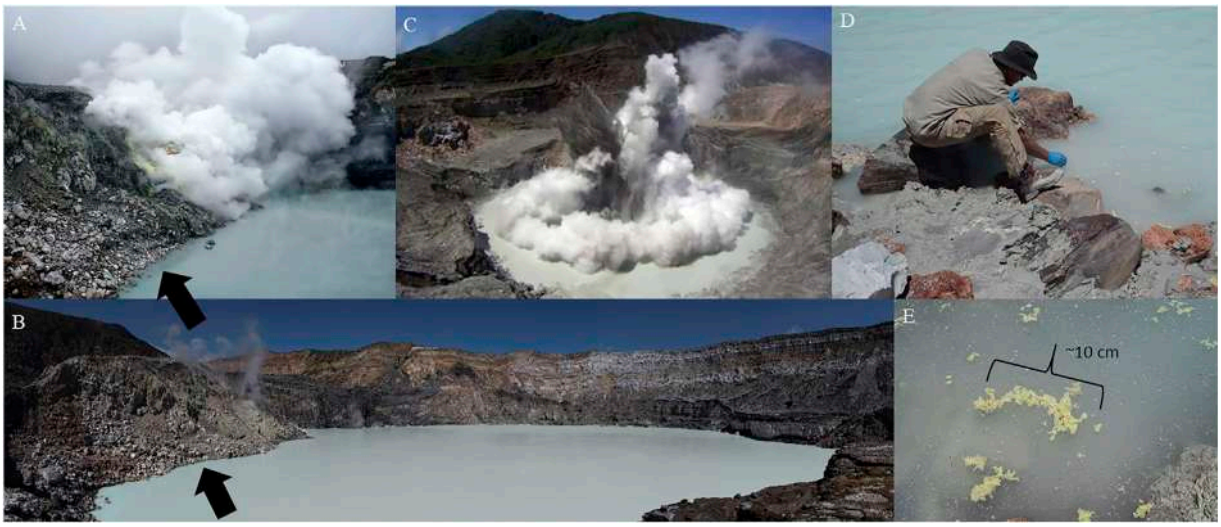

FIGURE 1 | (A) The active Poás Crater and Laguna Caliente during the November 20, 2013 field campaign, and **(B)** reduced activity during the March 23, 2017 field campaign. The arrows point to the same sampling site adjacent to fumarolic activity (10°11′48.09″N, 84°13′48.30″W). **(C)** A phreatic eruption in Poás Volcano, June 2014 (Courtesy of OVISCORI). **(D)** Sampling clumps of elemental sulfur floating on Laguna Caliente during the 2017 field campaign where fluids and lake bottom sediments were collected 2 m offshore. **(E)** A close-up of the sulfur clumps with dead insects.

Poás Volcano hosts Laguna Caliente, an ultra-acidic sulfurous crater lake that is primarily sourced through a subsurface groundwater system (Sanford et al., 1995). Acid-sulfate alteration of the parent rocks has led to an abundance of a variety of sulfates, Fe-oxides, and clays akin to those found on Mars in relict hydrothermal settings (Hynek et al., 2014; Black et al., 2015; Black et al., 2016; Rodríguez and van Bergen, 2017; Rodríguez and van Bergen, 2017; Black and Hynek, 2018). Poás is an extremely dynamic terrestrial environment with recorded temperatures ranging from near-ambient to boiling and pH values from −0.87 to 1.5; sometimes spanning these ranges over the course of days to weeks (Rowe et al., 1992b). Negative pH values are attributed to high normality (>1 M) of hydrogen ions in solution. Temperature and pH changes are reflective of an underlying magma body (<500 m depth to zero depth during eruptions) (Rymer and Brown, 1989; Rymer et al., 2000), fluctuating as a result of rising magma dendrites and magmatic gases interacting with meteoric and lake water (Rymer et al.,2000). Volcanic gases (HCl and H_2S and SO_2, which hydrolyze to H_2SO_4) contribute to the extreme acidity of the lake. Times of lower pH are a result of increased contribution from HCl and SO_2 relative to H_2S (Rowe et al., 1992a). The lake has historically exhibited a wide range of chemistries as well as redox potential (**Supplementary Tables S1, S2** in the Supplemental Information), including a variety of S and Fe redox chemistry. The large range of sulfur oxidation states (from 0 with elemental sulfur to +6 with sulfate; sulfite and thiosulfate were also detected, Martínez-Cruz et al., 2019) in this lake comprises a complex sulfur cycle which could provide metabolic options for chemolithotrophic archaea and bacteria (Friedrich, 1997; Hynek et al., 2018).

PRIOR MICROBIAL STUDIES AND THE *ACIDIPHILIUM* GENUS

On November 20, 2013, Laguna Caliente was sampled in order to characterize its microbiology for the first time (**Figure 1A**). This study was described in Hynek et al. (2018), which reported a "veritable monoculture" of a bacterium in the *Acidiphilium* genus in the phylum Proteobacteria. Nearly 98% of amplicons from 16S rRNA sequencing fell within a single Operational Taxonomic Unit (OTU), whose taxonomy was most closely related to *Acidiphilium angustum* strain KLB (at least 97% similarity).

Members of the *Acidiphilium* genus have been shown to grow in temperatures ranging from ~17°C–45°C, and in a pH range of ~1.5–7.5 with optimal growth at pH ~3 (Hiraishi et al., 1998; Küsel et al., 1999; Schippers, 2007; Li et al., 2020)—conditions less extreme than that of Laguna Caliente. Members of this genus have also been identified in, and isolated from, acid mine drainages, hydrothermal environments, a coal mine drainage, and another Mars analog in Rio Tinto, Spain (Harrison, 1981; Wichlacz et al., 1986; Lane et al., 1992; Kishimoto et al., 1995; González-Toril et al., 2003; Amils et al., 2007; San Martin-Uriz et al., 2011).

All members of the *Acidiphilium* genus are aerobic acidophiles, and these members have exhibited a wide range of environmental adaptations (Hiraishi et al., 1998; Dopson and Johnson, 2012). For example, some members of the *Acidiphilium* genus have been identified to oxidize elemental sulfur for growth (Rohwerder et al., 2003; Rohwerder and Sand, 2003; Ghosh and Dam, 2009) with some utilizing the bacterial Sox (sulfur oxidation) metabolic pathway (Liu et al., 2016). Other members of this genus are able to reduce Fe(III) (Lane et al., 1992; Küsel et al., 1999), reduce Cu(II) in the presence of iron (Johnson et al., 2017), and reduce Cr(VI) (Cummings et al.,

2007). Genes conferring nickel and arsenic resistance have also been identified in *Acidiphilium* spp. isolated from Rio Tinto, Spain (Mirete et al., 2017). The ability of acidophiles, like *Acidiphilium* spp., to live and grow in low pH has been attributed to highly impermeable cell membranes, reversed membrane potential, a predominance of secondary transporters, and methods to alleviate lowered pH for protons that cross through the cytoplasm (Baker-Austin and Dopson, 2007). Overall, members of the *Acidiphilium* genus have included obligate heterotrophs, facultative chemolithotrophs, and autotrophs (Hiraishi et al., 1998; Dopson and Johnson, 2012).

Environmental systems with extremely low microbial biodiversity, as described in Hynek et al. (2018), are rare on Earth. For comparison, the Iron Mountain Mine in California hosts an acid mine drainage with pH as low as −3.6, and a diverse microbial community that includes Bacteria, Archaea, and Eukarya was identified in a sample of pH ~0.5 (Nordstrom and Alpers, 1999; Edwards et al., 2000). It seems possible that in Laguna Caliente the combination of an extremely low pH, fluctuating temperatures (38°C–90°C, Rowe et al., 1992b), volcanic dynamics, and a high concentration of dissolved ions and toxic metals has restricted life in a way that only highly specialized bacteria can survive in this environment (Hynek et al., 2018; Wang et al., 2020).

To make predictions about how the organisms identified by Hynek et al. (2018) are able to survive in this challenging environment, samples were collected again by our team on March 28, 2017 (**Figures 1B,D**). In addition to describing the community makeup for temporal comparison to Hynek et al. (2018), we wanted to look specifically at the metabolic pathways and adaptations that could allow organisms to survive in such harsh conditions. Hydrothermal systems have the potential to be sterilizing by increasing temperatures, lowering pH, or inserting toxic chemicals to the environment. On Mars, the surface environment can also be sterilizing from incoming surface radiation and low atmospheric pressure. Thus, groundwater systems connected to hydrothermal systems are likely safe havens for single-celled organisms during volcanism-induced sterilization events. Because of this, if microorganisms were to exist in Martian hydrothermal systems, they likely would have required biological mechanisms to survive. An ability to survive on the fringes, such as in connected groundwater systems, would increase the chances for microorganisms to survive for extended periods of time. As a Martian analog, the Poás Volcano serves as a proxy for studying the adaptations that may have allowed any organisms to survive in hydrothermal systems on Mars. To accomplish the goals of this study, samples from both field campaigns were further scrutinized with shotgun metagenomics.

COLLECTION METHODS

The first field campaign occurred November 20, 2013, as described in Hynek et al. (2018), and the second field campaign occurred March 28, 2017. For both field campaigns, Laguna Caliente exhibited convective activity as evidenced by roiling of the lake's surface and adjacent active fumaroles. Sampling both years occurred at the same locale (**Figures 1A,B**).

Sampling in 2013 is described in more detail in Hynek et al. (2018), but to summarize, fluids from Laguna Caliente were collected aseptically in duplicate in sterile 50 ml Falcon tubes (Corning Incorporated, Corning, New York, United States) 2 m offshore, with the use of a sterile aluminum pole. In the 2017 sampling expedition, lake bottom sediment samples entrenched with lake fluids were collected using the same methods. Floating sulfur clump samples, also taken in the 2017 sampling expedition, were collected by hand closer to shore (**Figures 1D,E**) aseptically in duplicate in sterile 50 ml Falcon tubes with lake fluids entrenched. All samples were immediately stored on water ice. Within hours the samples were frozen to −4°C and within days were transferred to a −80°C freezer for later DNA extraction.

Temperature and pH were read by field instruments as well as pH paper for fidelity. Lake fluids were collected in sterile Falcon tubes and then filtered through 0.2 µm Sterivex filters (Cole-Parmer, Vernon Hills, Illinois, United States) and stored in the dark until analysis by ICP-MS and ICP-OES at Activation Laboratories Ltd. (Actlabs, Ancaster, Ontario, Canada) for cations, anions, and a full elemental scan.

ENVIRONMENTAL RESULTS

Mineralogical and fluid chemistry samples of Laguna Caliente were taken in both 2013 and 2017 (**Supplementary Tables S1, S2** in the Supplemental Information). For the 2017 field campaign, the temperature was 10°C lower than in the 2013 sampling and the pH was measured at 1.45 (compared to 0.29 in 2013). Compared to March 2013, the fumarolic activity was much less and there was no indication of significant HCl or H_2S in the gases, only SO_2 (**Figure 1**). The higher pH in the 2017 sampling is likely due to two factors; 1) lower observed volcanic activity, and 2) sampling after significant rainfall in the prior weeks (unlike our 2013 campaign), which could have diluted the lake fluids. The lower lake acidity in 2017 coincided with decreased concentrations of sulfate and chlorine (and many other elements). Nevertheless, the environmental conditions from 2017 still remained extreme for most mesophilic organisms.

Supplementary Table S1 in the Supplemental Information reports concentrations of elements in Laguna Caliente that have potential to be utilized in microbial metabolism (S and Fe). Additionally, concentrations of potentially hazardous elements to microorganisms that are discussed in the metagenomic results (Ag, As, Co, Cd, Cr, Cu, Ni, and Zn) are also included in **Supplementary Table S2** in the Supplemental Information.

MICROBIOLOGY METHODS

DNA was extracted from the −80°C frozen samples using the MoBio PowerMax Soil Kit (Qiagen, Germantown, MD, United States) following manufacturer's instructions. Duplicate extractions were performed using material from each sample (lake fluid, lake bottom sediment, sulfur clumps). The DNA from

the replicate extractions from each sample was combined and concentrated with Amicon Ultra-4 spin filters (MilliporeSigma, Burlington, MA, United States) three times for each sample to increase DNA concentration enough for downstream analysis.

For sequence-based analyses of 16S rRNA genes of the 2013 Laguna Caliente sample, we use the approaches described by Carini et al. (2016). To summarize, the V4 region of the 16S rRNA gene was PCR-amplified with barcoded primers (515F, 5′-GTGCCAGCMGCCGCGGTAA-3′ and 806R, 5′-GGACTACVSGGGTATCTAAT-3′ (Caporaso et al., 2010). Products from duplicate PCR reactions for each sample, as well as "no template" and "DNA extraction" negative controls, were cleaned, normalized, and pooled with the SequalPrepTM Normalization Plates (Thermo Fisher Scientific, Carlsbad, CA, United States) in the Fierer Lab at the University of Colorado (CU) Boulder, and sequenced on an Illumina MiSeq platform (Illumina, San Diego, CA, United States) by using v2 500-cycle paired-end kits at the CU Boulder Biofrontiers Sequencing Center. These sequence reads can be found in the supplementary material in Hynek et al. (2018).

16S rRNA gene sequences were processed using the DADA2 pipeline (Callahan et al., 2017). Sequences were quality filtered and clustered into amplicon sequence variants (ASVs). Taxonomic information was assigned to ASVs using a naive Bayesian classifier method (Wang et al., 2007), which takes the set of ASVs generated and compares them to a training set of reference sequences from the 16S rRNA bacterial and archaeal SILVA database (Quast et al., 2013; Yilmaz et al., 2014). A minimum bootstrapping threshold required to return a taxonomic classification of 50% similarity was used for analysis. ASVs associated with chloroplast, mitochondria, and eukaryotes were removed prior to downstream analyses.

For the metagenomic "shotgun" sequencing, three samples in total were sequenced. The same sample from Laguna Caliente in 2013 that underwent 16S rRNA sequencing was sequenced as well as two additional samples from the 2017 field campaign: a sulfur clump floating on the lake and bottom sediment from the shore of the lake - both mixed with lake fluid. These three samples were prepared using the Nextera XT DNA Library Prep Kit (Illumina, San Diego, CA, United States) by the University of Colorado BioFrontiers Institute. Afterwards, the samples were sequenced using a NovaSEQ 6000 Sequencing System (Illumina, San Diego, CA, United States) with paired-end 150 cycle 2 × 150 bp format by the Genomics and Microarray Core at the University of Colorado Denver Cancer Center with an targeted insert size of 250 bp. The sequencing data generated from these samples can be accessed in the NCBI Sequence Read Database, project accession number PRJNA760478.

Samples had between 2.4×10^7 and 5.2×10^7 reads for a total of 1.1×10^8 reads total across the three samples. Removal of adapter sequences from raw sequence data was done with Cutadapt (Martin, 2011). Quality filtering and trimming was performed with Sickle v.1.33 (-q 20 -I 50) (Joshi and Fass, 2011). After this trimming and filtering a total of 7.3×10^6 reads, just 7% of the total raw reads recovered from sequencing, remained for use in downstream analysis (average of 2.4×10^6 reads per sample). The relative abundance and diversity of bacteria and archaea in the metagenomic samples were classified by identifying 16S rRNA gene reads from the metagenomic sequence data using Metaxa2 (Bengtsson-Palme et al., 2015).

Assembly-free analysis on the adapter trimmed and quality filtered data was performed with SqueezeMeta on Reads v0.1.0, Sept 2019 with the alternative analysis mode sqm_reads.pl script (Tamames and Puente-Sánchez, 2019). With these settings paired end reads were grouped for annotation. Similarity searches for eggnog predictions (Huerta-Cepas et al., 2015) and KEGG classifications (Kanehisa and Goto, 2000) were done using Diamond (Buchfink et al., 2015). Annotated reads were rarified to 8917733, the lowest number of reads across the three samples using the "Vegan" package in R. The rarified table was normalized using MUSiCC to obtain accurate and biologically meaningful measures of gene abundance based on universal single copy genes (Manor and Borenstein, 2015).

Contigs were also generated from the trimmed and filtered sequence data using MEGAHIT, a NGS *de novo* assembler (Li et al., 2015). To identify and categorize specific iron genes and iron gene operons in these contigs, we used FeGenie (Braun, 2003; Garber et al., 2020).

MICROBIAL DIVERSITY RESULTS (16S AND METAGENOMIC SEQUENCING)

As described above, 16S rRNA genes sequences were recovered from both 16S rRNA sequencing and by extracting the 16S rRNA gene reads from the metagenomic sequence data using Metaxa2. In contrast with Hynek et al. (2018) who used OTUs, sequences were grouped with 100% similarity as Amplicon Sequence Variants (ASV) to categorize the microbes in the sample [see Callahan et al. (2017) for more explanation of why we chose to use ASVs instead of OTUs].

Re-processing the data from Hynek et al. (2018) as ASVs, instead of OTUs, produced similar results. Instead of ~98% of OTUs being assigned to *Acidiphilium* angustum, ~92% of ASVs were assigned to the *Acidiphilum* spp. (**Figure 2**). This slight difference is expected, as the adoption of ASVs occurred to help preserve the presence of rare taxa in sequencing data that were often hidden by OTU clustering (Callahan et al., 2017). This data clearly shows that *Acidiphilium* spp. is the overwhelmingly dominant genus in this system in 2013, supporting what was described by Hynek et al. (2018).

The taxonomic data recovered from the shotgun metagenomics shows an even wider spread of microbial diversity. The data from the 2013 Laguna Caliente fluid sample shows that ~64% of reads converge on *Acidiphilium* spp. ~3% of this sequence was assigned to *Asaia* spp., which is another acidophile that was first identified in a fluid of pH 3.5 (Moore et al., 2002). The 2017 sulfur clump data shows only ~32% of reads assigned to *Acidiphilium* spp. and the 2017 lake bottom sediment data shows that only ~2% of identified 16S sequences assigned to *Acidiphilium* spp. (**Figure 2**).

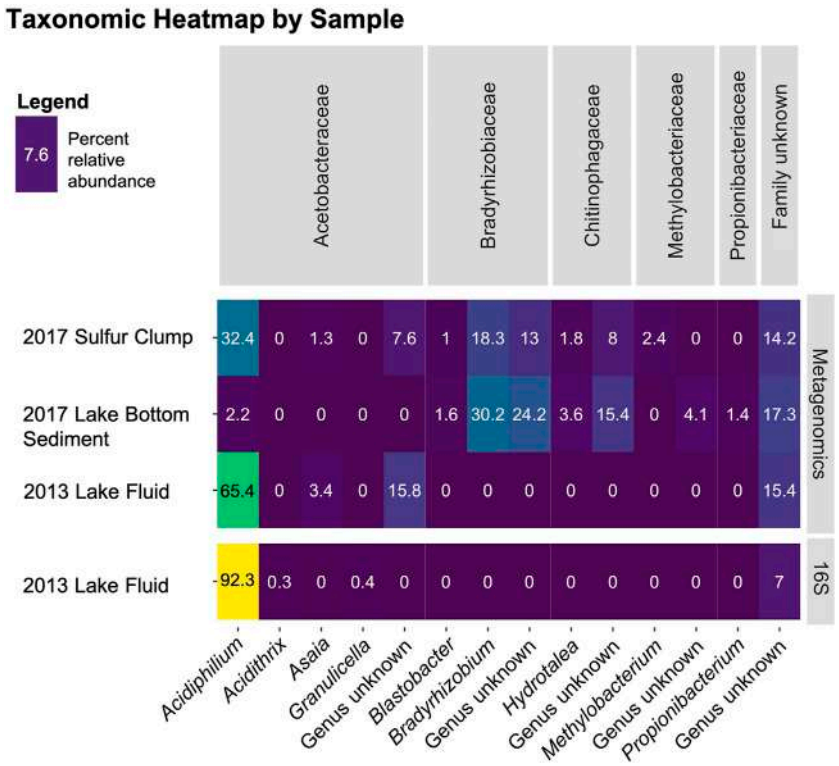

FIGURE 2 | Microbial communities of Laguna Caliente. The relative abundance of microbial communities in each of the four samples displayed were determined either by 16S rRNA marker gene sequencing or were recovered from metagenomic "shotgun" sequencing by Metaxa2 as indicated in the right panel. Identified bacterial families are shown across the top of the heatmap while genera are displayed across the bottom.

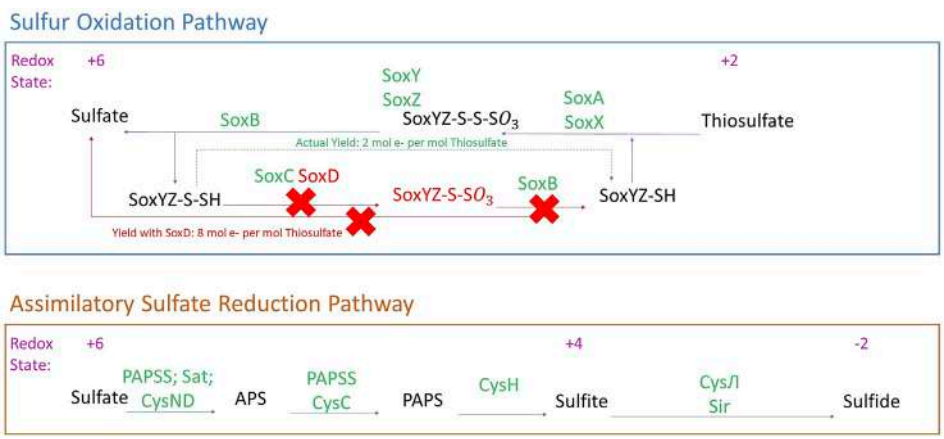

FIGURE 3 | Sulfur metabolism in Laguna Caliente metagenomic samples. Genes identified in the metagenomes are presented with green text. Genes and products not identified in the metagenomes are presented with red text. (Modified from Kanehisa and Goto, 2000).

METAGENOMIC RESULTS

As Laguna Caliente is an environment with high concentrations of sulfur in a variety of oxidation states, we investigated what sulfur metabolisms were present in the metagenome. Additionally, alternative types of metabolisms were investigated including complex carbon metabolisms, photosynthesis, and iron and arsenic oxidation. Many environmental adaptation genes were also investigated, such as heat shock operons, proton exporters, and heavy metal detoxifiers

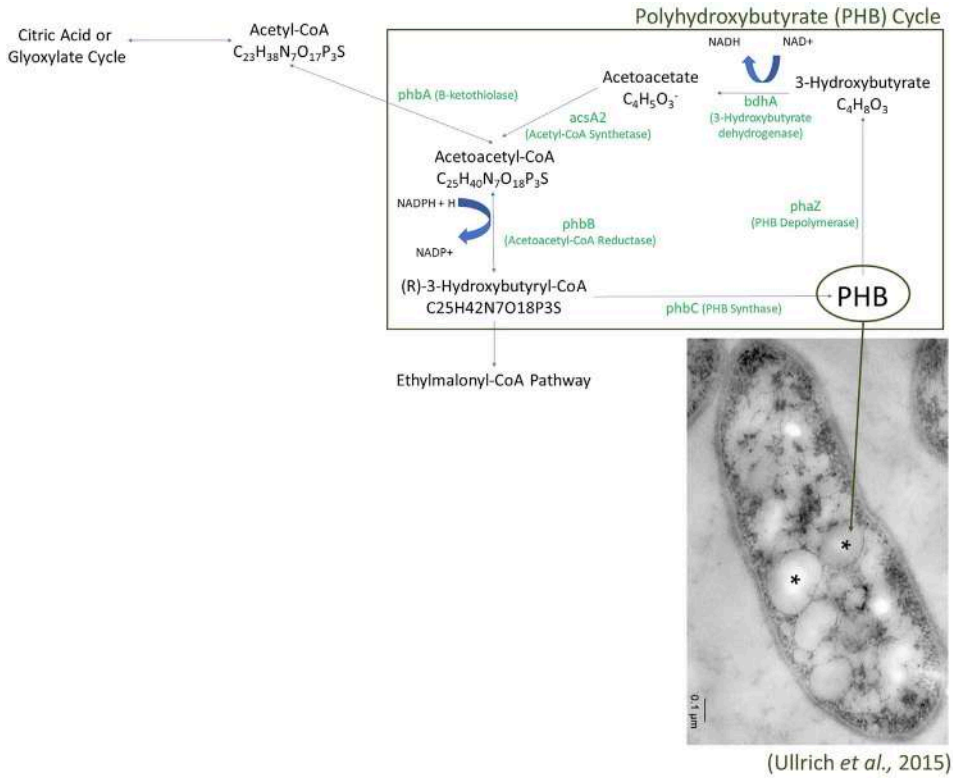

FIGURE 4 | The Polyhydroxybutyrate (PHB) Cycle as found in the Laguna Caliente metagenomic samples. Enzymes identified in the metagenomes are presented with green text.

that are commonly found in other organisms of the genus *Acidiphilium* (**Supplementary Table S3** in the Supplemental Information). Reads associated with these pathways were found in all three samples, unless noted otherwise. We acknowledge that while the metagenomics analyses used here can identify the presence/absence of genes and thus provide insights into potential functions, we cannot say whether or not these genes are active without metatranscriptomics.

Sulfur Metabolism

The metagenomic sequencing identified a wide range of sulfur metabolism genes in our samples (**Figure 3**). These genes indicate the ability to reduce inorganic sulfur from sulfate to sulfide (+6 to −2) using assimilatory sulfate reduction. Assimilatory sulfate reduction is a pathway that allows cells to further incorporate sulfide into carbon skeletons of amino acids to form cysteine or homocysteine (Brunold, 1993).

The metagenomes also host a nearly complete Sox system including *soxA, soxB, soxC, soxX, soxY*, and *soxZ*. However, we did not find *soxD* in the assembly-free analysis, and we did not search for it in the assembled data since that was used solely for the FeGenie analysis. With *soxD* absent, the heterotetrameric SoxCD complex would not be formed and sulfur-dependent cytochrome c reduction cannot be accomplished. Nevertheless, oxidation from thiosulfate to sulfate might still be accomplished; the SoxCD heterotetramer may be bypassed to allow for sulfur oxidation. In a full *soxXYZABCD* system, the yield is 8 mol electrons produced per mol of thiosulfate; however, with the SoxCD heterotetramer absent, the yield is reduced to 2 mol of electrons per mol of thiosulfate (Friedrich et al., 2001).

Simple and Complex Sugar Metabolism

The annotated reads also contained various pathways central to carbon metabolism in microorganisms. Genes related to the metabolism of simple sugars are present; gene regions related to glycolysis, gluconeogenesis, lactate fermentation, the pentose phosphate pathway, the citric acid cycle, and oxidative phosphorylation were all identified. Additionally, genes whose presence may indicate the utilization of more complex sugar molecules were also identified, including those assigned to the glyoxylate cycle, the ethylmalonyl-CoA pathway, the polyhydroxybutyrate cycle (**Figure 4**), the serine glyoxylate pathway, the methylglyoxal pathway, and the Entner-Doudoroff pathway (Yamauchi and Yamada, 1981; Ackermann et al., 1995; Okubo et al., 2010; Schneider et al., 2012). Identified genes and their abundance in the Laguna Caliente samples of the Entner-Doudoroff, methylglyoxal, and serine-glyoxylate pathways are reported in **Supplementary Table S4** in the Supplemental Information. Note that only the 2017 sulfur clump sample included genes for methylglyoxal synthase, which would allow for the full methylglyoxal pathway.

It has been suggested that the glyoxylate cycle and the ethylmalonyl-CoA pathway are anabolic pathways (Schneider et al., 2012; Chew et al., 2019), and the polyhydroxybutyrate cycle results in the creation of microbial plastic granules utilized in times of energy and carbon limitations (Ackermann et al., 1995). Peña-Ocaña et al. (2022) report metabolic maps and networks constructed from genes identified in mesophilic and hyperthermophilic samples from the El Chichón volcano crater lake that include some of the genes identified in the Laguna Caliente metagenomic samples, such as the Entner-Doudoroff pathway and sulfur oxidation.

Carbon Fixation/Photosynthesis

In addition to sugar metabolism genes, genes commonly utilized in photosynthesis were identified, including genes related to the Calvin Cycle and photorespiration. These included RuBisCO, phosphoribulokinase, fructose-1,6-bisphosphatase, photosystems I and II, light-harvesting complex I and II, cytochrome b_6f, and photosynthetic reaction center L and M subunits. Note that only the 2013 metagenome contained sequences encoding for photosystems I and II, light-harvesting complex I and II, and cytochrome b_6f.

Acid and Heat Response

While the trademark for acid-resistance in bacteria is an impermeable cell membrane characterized by a complex lipid bilayer (Baker-Austin and Dopson, 2007), metagenomic analysis can identify the presence of genes that encode for proton export that might confer acid resistance. All samples contained the full genetic pathways to encode for *nuo*, *cyo*, and F_1F_e-ATPase that when up-regulated confer acid resistance by proton efflux (Krulwich et al., 2011).

Genes related to the decarboxylase/antiporter-dependent acid-resistance systems (*AR2* and *AR3*) were identified. These genes include glutamate decarboxylase isozymes (*GadA* and *GadB*), arginine decarboxylase (*AdiA*), and cognate antiporters (*GadC* for glutamate and *AdiC* for arginine). Briefly, this system promotes intracellular conversion of glutamate to GABA and arginine to agmatine for efflux out of the cell. This system expels 1 mol of H+ per mol of glutamate or arginine promoting pH homeostasis and acid resistance (Foster, 2004).

The metagenome also contained many genes that confer heat resistance, including genes that are typically found in the heat-shock operons *hrcA-grpE-dnaJ, groES-groEL*, and *dnaK-sHSP*. The upregulation of these operons is known to confer heat resistance in thermophiles such as *Thermotoga maritima* (Wang et al., 2015). Additionally, increased dnaK mRNA and DnaK protein have been correlated in cells experiencing acid shock as well as in acid 'adapted' cells (Jayaraman et al., 1997).

Heavy Metals and Toxicity

Laguna Caliente hosts a high concentration of iron ions (276–631 ppm, **Supplementary Table S1** in the Supplemental Information). The metagenome contained numerous genes involving the transport and metabolism of iron. Iron uptake was found in the 2013 fluid and 2017 lake bottom sediment samples, marked by the presence of genes found in the *fbpABC* operon. Genes conferring the ability to reduce Fe(III) were not identified in the metagenome; however, the *Cyc2* gene was present in the 2013 fluid sample and the 2017 lake bottom sediment sample, which is a gene utilized in iron oxidation (Castelle et al., 2008). Specifically, the metagenome contained the gene sequence for cluster 2 of *Cyc2* that was found in an isolate of the acidophilic iron-oxidizing bacterium, *Acidithiobacillus ferrooxidans*. This cytochrome c is characterized by a relatively large redox potential (560 mV at pH 4.8) during the oxidation of Fe(II) to Fe(III) (Castelle et al., 2008).

Genes that code for the *Ton* system (*TonB-ExbB-ExbD*) protein complex were also present in all the samples. *TonB* can transport siderophores, hemes, and iron from transferrin/lactoferrin. It is understood to transport iron complexes the majority of the time; however, it is also known to uptake vitamin B_{12}, nickel chelates, and carbohydrates (Noinaj et al., 2010; Garber et al., 2020).

Chromate is a strong oxidant and a potential mutagen to cells (Cummings et al., 2007). Genes encoding for NAD(P)H-dependent chromate reductase were found in the metagenome. NAD(P)H-dependent chromate reductase reduces Cr(VI) to Cr(III) thereby conferring resistance to chromate.

Arsenic, which is very toxic to cells, was also found in high concentrations in Laguna Caliente (**Supplementary Table S2** in the Supplemental Information). Arsenic resistance is likely conferred by multiple arsenic resistance genes that were found in the metagenomes (**Supplementary Table S3** in the Supplemental Information). As(V) and As(III) enter cells utilizing the Pst/Pit and GlpF transporters, respectively (Kalia and Joshi, 2009); genes encoding for both transporters are found in the metagenomes. Once in the cell, arsenic can be detoxified and transported through multiple mechanisms. The *ars* operon, *arsRDABC*, reduces As(V) into As(III) (via ArsC) and exports As(III) out of the cell (*via* ArsAB) (Kalia and Joshi, 2009). The metagenome contained *arsA, arsB, arsC, and arsR*; while *arsD* was missing in the samples; *arsD* is often absent in bacteria. *arsD* encodes a negative regulatory protein and *arsR* encodes an arsenite inducible repressor (Kalia and Joshi, 2009). Genes encoding for the arsenic methyltransferase (ArsM) protein are also present in the metagenome; ArsM detoxifies As(III) by converting As(III) to trimethylarsine, which is then exported out of the cell *via* passive diffusion (Bentley and Chasteen, 2002; Kalia and Joshi, 2009). The samples also contained genes encoding for arsenite oxidase (Aox) protein. Aox allows cells to oxidize extracellular As(III) to As(V), thereby gaining energy from this process (Kalia and Joshi, 2009).

The metagenomes also contained genes that encode the *cusCBA* operon (**Supplementary Table S3** in the Supplemental Information). The *cusCBA* operon allows for metal efflux of Cu(I) and Ag(I). Additionally, genes encoding the Cue system (CopA and CueO) were also present. The Cue system detoxifies intracellular Cu(I) by exporting it to the periplasm (*via* CopA) and oxidizing the periplasmic Cu(I) to Cu(II) (*via* CueO) (Gudipaty et al., 2012). Note that genes conferring copper reduction were not found.

Genes encoding for the *cusCBA* operon were identified twice in the metagenome using the KEGG classification. The second identification of *cus* operon genes contains sequences that are homologous with two other metal efflux systems, Cnr and Czc. The KEGG classification system does not differentiate between these three systems using this sequence; i.e., they all have the same sequence ID's for each component (Cnr/Czc/Cus: C-K15725, A-K15726, B-K15727). While the data just presented on the genes encoding the *cusCBA* operon are likely to be unique to *cus*, the additional set of sequences may represent the *cnr* operon, the *czc* operon, the *cus* operon again, or up to all three operons. *cnrCBA* is the structural locus of the *cnr* operon, and the *cnrCBA* encodes an efflux pump that exports Co(II) and Ni(II) (Tibazarwa et al., 2000). The *czcCBA* operon encodes another homologous efflux pump protein complex that has the ability to export Co(II), Zn(II), and Cd(II) (Rensing et al., 1997). Ubiquitous in all microorganisms, multidrug efflux pumps may also export heavy metals in addition to other substrates (Blanco et al., 2016).

DISCUSSION

Both the metagenomic and 16S rRNA gene sequencing efforts show that the 2013 Laguna Caliente fluid sample contains >90% *Acidiphilium* (**Figure 2**). The 2017 samples, on the other hand, contain a larger diversity of bacteria including *Acidiphilium* spp. and *Asaia* spp., known acidophiles (**Figure 2**). However, members of the Bradyrhizobiaceae, Chitinophagaceae, and Methylobacteriaceae families were also represented. Some of these could be laboratory contaminants, but all are commonly found in soils and none of which are acidophiles (Kämpfer et al., 2011; Kovaleva et al., 2014; Cao et al., 2017; Ormeño-Orrillo and Martínez-Romero, 2019), so it is unlikely that they inhabited the harsh conditions of Laguna Caliente. More likely, since the 2017 campaign occurred after rainfall, these soil biome microbes were probably washed into the lake from the surrounding vegetated crater walls. It is also possible that a higher pH allowed for more biodiversity. However, considering the samples from 2017 contained more than just lake fluids (i.e., sulfur clumps, that also hosted dead insects (**Figure 1E**), or lake bottom sediment) and that the additional bacteria discovered are commonly found in soils, it is likely that these additional bacteria were sourced from the surrounding soils in the Poás Volcano crater. This is corroborated by the result that the 2017 lake bottom sediment sample had the lowest percentage of *Acidiphilium* spp. and the highest percentage of these soil taxa. Moving forward, samples from the lake fluid should be scrutinized more, and field campaigns should prioritize collection of samples farther away from the lake shore.

The samples all contained surprisingly high potential functional diversity for remarkably low biodiversity, especially for the 2013 Laguna Caliente fluid sample which was largely dominated by the genus *Acidiphilium*. Many of the genes related to carbon cycling pathways we identified utilize glyoxylate and the breaking down of it into malate to produce energy. It is more profound that there are many ways for this system of bacteria to create energy including sulfur oxidation, iron oxidation, arsenic oxidation, utilization of simple sugars, utilization of complex sugars, and carbon fixation. The finding of genes consistent with polyhydroxybutyrate (PHB) granule formation and utilization suggests that microorganisms in these communities may be creating energy reserves to use in times of energy limitations (Ackermann et al., 1995). For example, PHB granules have been found in *Acidiphilium* spp. JA12-A1 (Ullrich et al., 2015).

The chief question resulting from these findings is "why would a microbial community need so many ways to produce energy when there is an essentially unlimited source of energy (sulfur, in many oxidation states) present?" While sulfur oxidation through the Sox system yields less energy in the absence of *soxD* gene, there still remains an effectively unlimited supply of sulfur in various redox states present in Laguna Caliente to make up for the absence of *soxD* gene. We provide three potential explanations to this question.

Our first hypothesis is that since Laguna Caliente is limiting in organic and inorganic carbon (Barry, 2019); bacteria living in the lake would have to utilize carbon fixation, carbon storage (PHB granules), and carbon anabolism (glyoxylate cycle, ethylmalonyl-CoA pathway) to make up for this lack of organics.

Our second hypothesis for why we have identified genes related to so many metabolic pathways in the samples is that the bacteria would need a sufficiently high yield of ATP to survive in Laguna Caliente. We have identified various adaptations this sample may utilize to deal with the harsh conditions of the lake. Of these, the ATP-dependent molecular chaperone proteins utilize ATP directly to ensure proper protein folding in times of elevated heat, and in some cases, acidity (Jayaraman et al., 1997). Transport proteins also utilize a high amount of ATP for active transport; of the efflux pumps described in this paper, the multidrug efflux pump, F_1F_e-ATPase, *CopA*, *arsAB*, and the *Ton* system all use ATP to transport substrates across the cell membrane (Kalia and Joshi, 2009; Noinaj et al., 2010; Krulwich et al., 2011; Gudipaty et al., 2012; Blanco et al., 2016). Other environmental adaptation genes, such as those in the *cusCBA*, *cnrCBA*, *czcCBA* operons rely on secondary active transport, utilizing concentration gradients facilitated by ATP (Rensing et al., 1997; Tibazarwa et al., 2000; Long et al., 2012). The upregulation of glycolysis is also noted to occur in thermophiles to provide immediate energy to cope with heat stress (Wang et al., 2015).

Note that many of the genes and adaptations we discuss are also very common in microorganisms found in less extreme environments (e.g., the *Ton* system, the heat-shock operons, the multidrug efflux pumps, and acid-resistance genes). The confirmation of the ability for our bacteria to actually use these systems in times of environmental stress would have to be measured in the laboratory using other methods like transcriptomics. It has proven difficult to replicate the extreme conditions of Laguna Caliente *in vitro*, and to date, bacterial culturing and isolation experiments have been unsuccessful. While the metagenomic data does not prove that our samples utilize these systems and adaptations to survive, we show the *capabilities* of these bacteria. And while the presence of these genes in the metagenome do not prove these bacteria use these

genes to survive, it is highly likely that they would use the pathways available to them to survive in Laguna Caliente; an environment that is severely extreme and hostile to life. Thus, it is conceivable that an exceptionally high yield of ATP would be needed for the upkeep of various mechanisms to ensure survival in Laguna Caliente.

Our third hypothesis for the presence of numerous metabolic pathways in our sample is the most eccentric. We start with asking the question, "what if the presence of multiple metabolic pathways is the defining feature that allows this community to survive in a volcanically active environment?" Recall that the Poás Volcano exhibited occasional-to-frequent phreatic-to-phreatomagmatic eruptions in recent years (**Figure 1C**). These eruptions have the ability to make Laguna Caliente extremely hot, decrease the pH exponentially, and influx large amounts of environmental toxins. While life has proven persistent in a host of hostile conditions, it is probable that these eruptions could make Laguna Caliente too hostile for even these resolute microorganisms.

It is conceivable that bacteria in Laguna Caliente could be transported away from the lake and into the surrounding soils *via* water level fluctuations, groundwater diffusion, or phreatic eruptions. So, prior to a phreatic eruption there would exist microbes both in Laguna Caliente and in the surrounding soils and connected groundwater system. Then later, a dramatic eruption could sterilize life in Laguna Caliente potentially draining the lake, which is what occurred in April 2017. Nevertheless, bacteria in the surrounding soils would be able to survive farther away from the eruption using complex carbon metabolism such as multiple carbon anabolism pathways, photosynthesis, and PHB granules formed in times of higher energy availability. The combination of these complex carbon metabolisms, in addition to simple carbon pathways and sulfur, iron, and arsenic oxidation would allow microbes to survive in ever-changing conditions and environments in the Poás Volcano crater. Then, when milder conditions return in Laguna Caliente and the lake reforms and expands, certain bacteria would be returned to their native environment: either washed in from the surrounding surface or *via* a connected groundwater system associated with the lake. This could help explain the presence of so many energy metabolism pathways in a sample of such low biodiversity. This could also help explain the relative persistence of the identified microbes, particularly *Acidiphilium* spp., which is known to be able to tolerate a wide variety of challenging conditions (Hiraishi et al., 1998; Dopson and Johnson 2012; Ullrich et al., 2015), between the November 2013 and March 2017 field campaigns.

In April 2017 after the second sampling, Poás Volcano entered an eruptive phase for over 2 years. Laguna Caliente was drained during explosive eruptions that added tephra and lavas to the crater floor, effectively sterilizing it. In October 2019, surface volcanic activity waned enough for the crater lake to reform and we were able to sample it in November 2019. While the results of that expedition are ongoing, future expeditions to the Poás Volcano will continue to characterize both fluid samples of Laguna Caliente and surrounding soil samples to further scrutinize this theory of microbial persistence through volcanic eruptions.

IMPLICATIONS FOR MARS

All landed missions to Mars that have focused on water, habitability, and astrobiology this millennium have had landing sites in sedimentary environments. While the conditions on Mars were more habitable early in its history, with an active water cycle for up to millions of years (e.g., Hoke et al., 2011), it is likely that surface waters did not persist for much longer. The Gale crater lake might have lasted 10,000 years (Grotzinger et al., 2015). Formation timescales of deltas on Mars suggest 1,000s of years (Hoke et al., 2014). Hoke and Hynek (2009) argued that there was a ~200-million-year time period when fluvial valleys formed, albeit intermittently. Others argue that all the geomorphic fluviolacustrine features on Mars could have been formed from the melting of ice during punctuated events (e.g., Fastook and Head, 2015; Palumbo et al., 2018). To us, the geologically short duration of surface waters (e.g., Kereszturi, 2012) combined with harsh surface conditions (e.g., radiation, aridity, low temperature) imply a low probability for the origin and sustainment of life on Mars in sedimentary environments. Conversely, protracted groundwater and hydrothermal systems within the crust (e.g., Solomon et al., 2005; Ehlmann et al., 2011), and at individual volcanic centers active for most of Mars' history (Robbins et al., 2011) provide a much higher probability for Martian life. Additionally, even if life existed in the brief episodes of surface waters, it is likely that when Mars dried up, life would have condensed onto smaller habitable niches such as acid-sulfate hydrothermal systems, which were likely in existence for billions of years.

Hydrothermal environments are suitable habitats as they provide all the ingredients for life (Walter and Des Marais, 1993; Schulze-Makuch et al., 2007; Hays et al., 2017), and they were likely one of the most stable habitats on Mars due to persistent volcanism and continuous groundwater (Hynek et al., 2013), as well as within long-lived impact-generated hydrothermal systems (e.g., Abramov and Kring, 2005; Osinski et al., 2020). Relict Martian hydrothermal systems were likely as dynamic and at times as hostile to life as Laguna Caliente is at present. Hence, this environment might be key to understanding if and how life on the Red Planet existed.

While hydrothermal environments could provide warm and moist locales for life to thrive, a drastic environmental change, such as an influx of high temperature- or high acidity fluids, has the potential to sterilize any residential microorganisms. Outside of these habitable niches, the Martian surface can also be sterilizing with incoming surface radiation and hostile atmospheric conditions such as cold temperatures, low humidity, and low pressure. In the event of microbe-killing events in Martian hydrothermal environments, the most clement environment for refuge would be connected groundwater systems. So, in order to maximize survival in Martian hydrothermal environments, microbes would need to

be able to live in a variety of conditions such as hot, hydrothermal environments and connected groundwater systems. Thus, microbes on Mars would likely have to have had multiple adaptations to survive over millions or billions of years among hydrothermal features.

Our study is of considerable astrobiological interest because per our microbial community dominated by *Acidiphilium* spp., there appears to be various metabolic pathways and numerous adaptations that may possibly allow the community to survive in the ever-changing conditions and on the fringes of Laguna Caliente. The ability for *Acidiphilium* spp., in particular, to survive in a diverse set of extreme environments has been attributed to an abundant repertoire of genes acquired through horizontal gene transfer (HGT) (Li et al., 2020).

Like the microbial community in Laguna Caliente, any life in Martian hydrothermal environments would likely have developed considerable flexibility and tolerances to live in dynamic and extreme conditions. While our study suggests this bacterial community consists of highly evolved organisms suited for survival in the Poás Volcano, its rather low biodiversity suggests they live more independently compared to most described natural ecosystems. This makes it a rather simplistic system for maintaining survival in a hydrothermal environment. On the extreme end of this situation, single-species ecosystems are rare in nature, as very seldom can a singular species survive without symbiotic interactions with neighboring microbes (Chivian et al., 2008).

If life originated in the Noachian epoch (>3.7 bya) when Mars exhibited more widespread habitable conditions, we hypothesize that HGT events in the beginnings of Martian life, as was proposed to occur on Earth in the time of LUCA (e.g., Fournier et al., 2015), would benefit the development of functional diversity necessary to survive in extreme environments. Then in later times when global conditions became more hostile to life (aridification and acidification), microorganisms that live in communities with high functional diversity and low alpha diversity, like our microbial community dominated by *Acidiphilium* spp., would have the best chance of surviving in acid-sulfate hydrothermal systems. Thus, an independent single-celled organism (e.g., Chivian et al., 2008; Hynek et al., 2018) or a low biodiversity microbial community (described herein) that can survive in both Martian hydrothermal environments and in connected groundwater systems in times of volcanic dynamics may functionally resemble early Martian life.

One limitation of our study is that our microbial community likely utilizes aerobic metabolisms, and oxygen is scarce in the Martian atmosphere (Trainer et al., 2019), thereby making aerobic metabolism difficult. Nevertheless, aerobic methanotrophic metabolism has been proposed to be functional in the low temperatures, pressures, and oxygen concentrations present on Mars (Seto et al., 2019). Additionally, it has been suggested that sufficient oxygen for aerobic metabolisms would be present in briny near surface waters (Stamenković et al., 2018), such as hydrothermal systems. Although driven by abiotic processes, it has also been proposed that Mars underwent a large oxygenation event in the Late Noachian (Liu et al., 2021), which could have shaped metabolisms of future life. Oxygen may also be outgassed in hydrothermal environments or exist as free oxygen in fluids. Even if aerobic metabolisms could not be supported on Mars, it is probable that Martian microbes could develop analogous anaerobic metabolisms and environmental adaptations akin to our model community allowing for survival in extreme conditions and fringe environments. On Earth, obligate and facultative anaerobic acidophilic/acidotolerant thermophiles were cultivated from terrestrial hot springs and deep-sea hydrothermal vent chimneys, although their metabolic strategies were undetermined (Prokofeva et al., 2005).

While the low biodiversity and low biomass of our isolates from Laguna Caliente may suggest life on Mars is a difficult proposition, we argue that these findings show extreme perseverance of life in hostile and dynamic Mars-like conditions. Microorganisms on Earth have evolved to survive and thrive in a great host of conditions. If life on Mars began in a similar manner as life on Earth, it is conceivable that microorganisms on Mars could have evolved in an analogous manner to extremophiles on Earth, developing some of the adaptations found in this study.

CONCLUSION

Hydrothermal systems were likely the longest-lived habitable environment through Mars' history. This environment does not come without its challenges for life, which include potential sterilization events as a result of volcanic activity. The key solution for this challenge would be a self-sufficient microorganism or low biodiversity ecosystem that contains numerous adaptations and metabolisms capable of withstanding minor environmental changes and capable of surviving in connected groundwater systems during more extreme environmental fluctuations. This study addresses the challenges for life in Martian hydrothermal systems, using an analog system from Costa Rica, to show that life can in fact adapt to such environmental extremes. In the Poás Volcano, a microbial community largely dominated by *Acidiphilium* spp. appears to be a suitable model community that can even withstand phreatic eruptions. Our study shows that life contains the genetic potential and functional flexibility to survive in such extreme environments. Appropriately, we propose that acid-sulfate hydrothermal systems be prioritized in the search for life on Mars.

DATA AVAILABILITY STATEMENT

The datasets presented in this study can be found in online repositories. The names of the repository/repositories and accession number(s) can be found in the article/**Supplementary Material**.

ETHICS STATEMENT

Written informed consent was obtained from BH for the publication of any potentially identifiable images or data included in this article.

AUTHOR CONTRIBUTIONS

BH is the academic advisor of JW and ND, and he conceived this project. BH performed field sampling with GA. JW performed extractions of the samples. ND performed post-sequence processing of all the samples and submitted it to the NCBI Sequence Read Database. JW investigated the genes of interest from the sequence reads and wrote the first draft of the manuscript. ND, BH, and JW refined sections of the manuscript from the original draft. All authors contributed to manuscript revision, read, and approved the submitted version.

FUNDING

The Leadership Education for Advancement and Promotion (LEAP) program at the University of Colorado Boulder and NASA's Early Career Fellowship #NNX12AF20G helped fund this research.

ACKNOWLEDGMENTS

The authors would like to thank the Leadership Education for Advancement and Promotion (LEAP) program at the University of Colorado Boulder and NASA's Early Career Fellowship #NNX12AF20G for financial support. We sincerely appreciate the in-country support of Alvarado Induni Guillermo, Instituto Costarricense de Electricidad (ICE), and Observatorio Vulcanológico y Sismológico de Costa Rica (OVISCORI). We also are indebted to Alexis Templeton and Noah Fierer for use of their laboratory facilities to complete this work.

SUPPLEMENTARY MATERIAL

The Supplementary Material for this article can be found online at: https://www.frontiersin.org/articles/10.3389/fspas.2022.817900/full#supplementary-material

REFERENCES

Abramov, O., and Kring, D. A. (2005). Impact-induced Hydrothermal Activity on Early Mars. *J. Geophys. Res.* 110 (E12). doi:10.1029/2005JE002453

Ackermann, J.-u., Müller, S., Lösche, A., Bley, T., and Babel, w. (1995). Methylobacterium Rhodesianum Cells Tend to Double the DNA Content under Growth Limitations and Accumulate PHB. *J. Biotechnol.* 39 (1), 9–20. doi:10.1016/0168-1656(94)00138-3

Amils, R., González-Toril, E., Fernández-Remolar, D., Gómez, F., Aguilera, Á., and Rodríguez, N. (2007). Extreme Environments as Mars Terrestrial Analogs: The Rio Tinto Case. *Planet. Space Sci.* 55(3), 370–381. doi:10.1016/j.pss.2006.02.006

Andrews-Hanna, J. C., and Phillips, R. J. (2007). Hydrological Modeling of Outflow Channels and Chaos Regions on Mars. Journal of Geophysical Research. *Planets* 112 (E8). doi:10.1029/2006JE002881

Baker-Austin, C., and Dopson, M. (2007). Life in Acid: pH Homeostasis in Acidophiles. *Trends Microbiol.* 15 (4), 165–171. doi:10.1016/j.tim.2007.02.005

Banerdt, W. B., Smrekar, S. E., Banfield, D., Giardini, D., Golombek, M., Johnson, C. L., et al. (2020). Initial Results from the InSight mission on Mars. *Nat. Geosci.* 13 (3), 183–189. doi:10.1038/s41561-020-0544-y

Barry, P. (2019). Carbon and noble Gas Data from Costa Rica Seeps, Version 1.0. *Interdiscip. Earth Data Alliance (Ieda)*. Accessed 2020-10-18. doi:10.1594/IEDA/111271

Bengtsson-Palme, J., Hartmann, M., Eriksson, K. M., Pal, C., Thorell, K., Larsson, D. G. J., et al. (2015). metaxa2: Improved Identification and Taxonomic Classification of Small and Large Subunit rRNA in Metagenomic Data. *Mol. Ecol. Resour.* 15 (6), 1403–1414. doi:10.1111/1755-0998.12399

Bentley, R., and Chasteen, T. G. (2002). Microbial Methylation of Metalloids: Arsenic, Antimony, and Bismuth. Microbiology and Molecular Biology Reviews. *MMBR* 66 (2), 250–271. doi:10.1128/MMBR.66.2.250-271.2002

Bibring, J. P., Langevin, Y., Gendrin, A., Gondet, B., Poulet, F., Berthé, M., et al. (2005). Mars Surface Diversity as Revealed by the OMEGA/Mars Express Observations. *Science* 307 (5715), 1576. doi:10.1126/science.1108806

Black, S. R., and Hynek, B. M. (2018). Characterization of Terrestrial Hydrothermal Alteration Products with Mars Analog Instrumentation: Implications for Current and Future Rover Investigations. *Icarus* 307, 235–259. doi:10.1016/j.icarus.2017.10.032

Black, S. R., Hynek, B. M., and Alvarado, G. E. (2015). "Spectral Identification of Acid Sulfate Alteration Products in Costa Rica Volcanoes: Implications for Early Mars [abstract 2260]," in 46th Lunar and Planetary Science Conference, Houston (Lunar and Planetary Institute). LPI Contribution No. 1832.

Black, S. R., Hynek, B. M., Hoover, R., Beckerman, L. G., and Alvarado, G. E. (2016). "Characterization of Hydrothermal Alteration in Costa Rica: Mineralogy, Methodology, and Implications for Mars [abstract 2546]," in 47th Lunar and Planetary Science Conference, Houston (Lunar and Planetary Institute). LPI Contribution No. 1903.

Blanco, P., Hernando-Amado, S., Reales-Calderon, J. A., Corona, F., Lira, F., Alcalde-Rico, M., et al. (2016). Bacterial Multidrug Efflux Pumps: Much More Than Antibiotic Resistance Determinants. *Microorganisms* 4 (1). doi:10.3390/microorganisms4010014

Braun, V. (2003). Iron Uptake by *Escherichia coli*. *Front. Bioscience-Landmark* 8 (6), 1409–1421. doi:10.2741/1232

Brunold, C. (1993). "Regulatory Interactions between Sulfate and Nitrate Assimilation," in *Sulfur Nutrition and Assimilation in Higher PlantsRegulatory Agricultural and Environmental Aspects*. Editors L. J. de Kok, I. Stulen, H. Rennenberg, C. Brunold, Rauser, et al. (The Hague: SPB Academic Publishing), 61–76.

Buchfink, B., Xie, C., and Huson, D. H. (2015). Fast and Sensitive Protein Alignment Using DIAMOND. *Nat. Methods* 12 (1), 59–60. doi:10.1038/nmeth.3176

Callahan, B. J., McMurdie, P. J., and Holmes, S. P. (2017). Exact Sequence Variants Should Replace Operational Taxonomic Units in Marker-Gene Data Analysis. *ISME J.* 11 (12), 2639–2643. doi:10.1038/ismej.2017.119

Cao, M., Huang, J., Li, J., Qiao, Z., and Wang, G. (2017). Edaphobaculum Flavum Gen. nov., Sp. nov., a Member of Family Chitinophagaceae, Isolated from Grassland Soil. *Int. J. Syst. Evol. Microbiol.* 67 (11), 4475–4481. doi:10.1099/ijsem.0.002316

Caporaso, J. G., Kuczynski, J., Stombaugh, J., Bittinger, K., Bushman, F. D., Costello, E. K., et al. (2010). QIIME Allows Analysis of High-Throughput Community Sequencing Data. *Nat. Methods* 7 (5), 335–336. doi:10.1038/nmeth.f.303

Carini, P., Marsden, P. J., Leff, J. W., Morgan, E. E., Strickland, M. S., and Fierer, N. (2016). Relic DNA Is Abundant in Soil and Obscures Estimates of Soil

Microbial Diversity. *Nat. Microbiol.* 2 (3), 16242. doi:10.1038/nmicrobiol.2016.242

Carr, M. H., and Head, J. W. (2010). Geologic History of Mars. *Earth Planet. Sci. Lett.* 294 (3), 185–203. doi:10.1016/j.epsl.2009.06.042

Castelle, C., Guiral, M., Malarte, G., Ledgham, F., Leroy, G., Brugna, M., et al. (2008). A New Iron-oxidizing/O2-Reducing Supercomplex Spanning Both Inner and Outer Membranes, Isolated from the Extreme Acidophile Acidithiobacillus Ferrooxidans. *J. Biol. Chem.* 283 (38), 25803–25811. doi:10.1074/jbc.M802496200

Changela, H. G., Chatzitheodoridis, E., Antunes, A., Beaty, D., Bouw, K., Bridges, J. C., et al. (2021). Mars: New Insights and Unresolved Questions. *Int. J. Astrobiology* 20 (6), 394–426. doi:10.1017/S1473550421000276

Chew, S. Y., Chee, W. J. Y., and Than, L. T. L. (2019). The Glyoxylate Cycle and Alternative Carbon Metabolism as Metabolic Adaptation Strategies of Candida Glabrata: Perspectives from Candida Albicans and *Saccharomyces cerevisiae*. *J. Biomed. Sci.* 26 (1), 52. doi:10.1186/s12929-019-0546-5

Chivian, D., Brodie, E. L., Alm, E. J., Culley, D. E., Dehal, P. S., DeSantis, T. Z., et al. (2008). Environmental Genomics Reveals a Single-Species Ecosystem Deep within Earth. *Science* 322 (5899), 275. doi:10.1126/science.1155495

Chojnacki, M., and Hynek, B. M. (2008). Geological Context of Water-Altered Minerals in Valles Marineris, Mars. Journal of Geophysical Research. *Planets* 113 (E12). doi:10.1029/2007JE003070

Cockell, C. S., Balme, M., Bridges, J. C., Davila, A., and Schwenzer, S. P. (2012). Uninhabited Habitats on Mars. *Icarus* 217 (1), 184–193. doi:10.1016/j.icarus.2011.10.025

Craddock, R. A., and Greeley, R. (2009). Minimum Estimates of the Amount and Timing of Gases Released into the Martian Atmosphere from Volcanic Eruptions. *Icarus* 204 (2), 512–526. doi:10.1016/j.icarus.2009.07.026

Cummings, D. E., Fendorf, S., Singh, N., Sani, R. K., Peyton, B. M., and Magnuson, T. S. (2007). Reduction of Cr(VI) under Acidic Conditions by the Facultative Fe(III)-Reducing Bacterium Acidiphilium Cryptum. *Environ. Sci. Tech.* 41 (1), 146–152. doi:10.1021/es061333k

Davila, A. F. (2021). Life on Mars: Independent Genesis or Common Ancestor. *Astrobiology* 21 (7), 802–812. doi:10.1089/ast.2020.2397

Di Achille, G., and Hynek, B. M. (2010). Ancient Ocean on Mars Supported by Global Distribution of Deltas and Valleys. *Nat. Geosci.* 3 (7), 459–463. doi:10.1038/ngeo891

Dohm, J. M., and Tanaka, K. L. (1999). Geology of the Thaumasia Region, Mars: Plateau Development, valley Origins, and Magmatic Evolution. *Planet. Space Sci.* 47 (3), 411–431. doi:10.1016/S0032-0633(98)00141-X

Domagal-Goldman, S. D., Wright, K. E., Domagal-Goldman, S. D., Wright, K. E., Adamala, K., Arina de la Rubia, L., et al. (2016). The Astrobiology Primer v2.0. *Astrobiology* 16 (8), 561–653. doi:10.1089/ast.2015.1460

Dopson, M., and Johnson, D. B. (2012). Biodiversity, Metabolism and Applications of Acidophilic Sulfur-Metabolizing Microorganisms. *Environ. Microbiol.* 14 (10), 2620–2631. doi:10.1111/j.1462-2920.2012.02749.x

Edwards, K. J., Bond, P. L., Druschel, G. K., McGuire, M. M., Hamers, R. J., and Banfield, J. F. (2000). Geochemical and Biological Aspects of Sulfide mineral Dissolution: Lessons from Iron Mountain, California. *Chem. Geology.* 169 (3), 383–397. doi:10.1016/S0009-2541(00)00216-3

Ehlmann, B. L., Mustard, J. F., Clark, R. N., Swayze, G. A., and Murchie, S. L. (2011). Evidence for Low-Grade Metamorphism, Hydrothermal Alteration, and Diagenesis on Mars from Phyllosilicate Mineral Assemblages. *Clays and Clay Minerals* 59 (4), 359–377. doi:10.1346/CCMN.2011.0590402

Ehrenfreund, P., Röling, W. F. M., Thiel, C. S., Quinn, R., Sephton, M. A., Stoker, C., et al. (2011). Astrobiology and Habitability Studies in Preparation for Future Mars Missions: Trends from Investigating Minerals, Organics and Biota. *Int. J. Astrobiology* 10 (3), 239–253. doi:10.1017/S1473550411000140

El Maarry, M. R., Dohm, J. M., Marzo, G. A., Fergason, R., Goetz, W., Heggy, E., et al. (2012). Searching for Evidence of Hydrothermal Activity at Apollinaris Mons, Mars. *Icarus* 217 (1), 297–314. doi:10.1016/j.icarus.2011.10.022

Fairén, A. G., Dohm, J. M., Baker, V. R., de Pablo, M. A., Ruiz, J., Ferris, J. C., et al. (2003). Episodic Flood Inundations of the Northern plains of Mars. *Icarus* 165 (1), 53–67. doi:10.1016/S0019-1035(03)00144-1

Fassett, C. I., and Head, J. W. (2008a). The Timing of Martian valley Network Activity: Constraints from Buffered Crater Counting. *Icarus* 195 (1), 61–89. doi:10.1016/j.icarus.2007.12.009

Fassett, C. I., and Head, J. W. (2008b). Valley Network-Fed, Open-basin Lakes on Mars: Distribution and Implications for Noachian Surface and Subsurface Hydrology. *Icarus* 198 (1), 37–56. doi:10.1016/j.icarus.2008.06.016

Fastook, J. L., and Head, J. W. (2015). Glaciation in the Late Noachian Icy Highlands: Ice Accumulation, Distribution, Flow Rates, Basal Melting, and Top-Down Melting Rates and Patterns. *Sci. Planet. Space Sci.* 106, 82–98. doi:10.1016/j.pss.2014.11.028

Foster, J. W. (2004). *Escherichia coli* Acid Resistance: Tales of an Amateur Acidophile. *Nat. Rev. Microbiol.* 2 (11), 898–907. doi:10.1038/nrmicro1021

Fournier, G. P., Andam, C. P., and Gogarten, J. P. (2015). Ancient Horizontal Gene Transfer and the Last Common Ancestors. *BMC Evol. Biol.* 15, 70. doi:10.1186/s12862-015-0350-0

Friedrich, C. G. (1997). "Physiology and Genetics of Sulfur-Oxidizing Bacteria," in *Advances in Microbial Physiology*. Editor R. K. Poole (Academic Press), 235–289. doi:10.1016/s0065-2911(08)60018-1

Friedrich, C. G., Rother, D., Bardischewsky, F., Quentmeier, A., and Fischer, J. (2001). Oxidation of Reduced Inorganic Sulfur Compounds by Bacteria: Emergence of a Common Mechanism. *Appl. Environ. Microbiol.* 67 (7), 2873. doi:10.1128/AEM.67.7.2873-2882.2001

Garber, A. I., Nealson, K. H., Okamoto, A., McAllister, S. M., Chan, C. S., Barco, R. A., et al. (2020). FeGenie: A Comprehensive Tool for the Identification of Iron Genes and Iron Gene Neighborhoods in Genome and Metagenome Assemblies. *Front. Microbiol.* 11 (37). doi:10.3389/fmicb.2020.00037

Gaucher, E. A., Govindarajan, S., and Ganesh, O. K. (2008). Palaeotemperature Trend for Precambrian Life Inferred from Resurrected Proteins. *Nature* 451 (7179), 704–707. doi:10.1038/nature06510

Gendrin, A., Mangold, N., Bibring, J. P., Langevin, Y., Gondet, B., Poulet, F., et al. (2005). Sulfates in Martian Layered Terrains: The OMEGA/Mars Express View. *Science* 307 (5715), 1587. doi:10.1126/science.1109087

Ghosh, W., and Dam, B. (2009). Biochemistry and Molecular Biology of Lithotrophic Sulfur Oxidation by Taxonomically and Ecologically Diverse Bacteria and Archaea. *FEMS Microbiol. Rev.* 33 (6), 999–1043. doi:10.1111/j.1574-6976.2009.00187.x

Giulio, M. D. (2003). The Universal Ancestor Was a Thermophile or a Hyperthermophile: Tests and Further Evidence. *J. Theor. Biol.* 221 (3), 425–436. doi:10.1006/jtbi.2003.3197

González-Toril, E., Llobet-Brossa, E., Casamayor, E. O., Amann, R., and Amils, R. (2003). Microbial Ecology of an Extreme Acidic Environment, the Tinto River. *Appl. Environ. Microbiol.* 69 (8), 4853. doi:10.1128/AEM.69.8.4853-4865.2003

Goudge, T. A., Fassett, C. I., Head, J. W., Mustard, J. F., and Aureli, K. L. (2016). Insights into Surface Runoff on Early Mars from Paleolake basin Morphology and Stratigraphy. *Geology* 44 (6), 419–422. doi:10.1130/G37734.1

Grotzinger, J. P., Gupta, S., Malin, M. C., Rubin, D. M., Schieber, J., Siebach, K., et al. (2015). Deposition, Exhumation, and Paleoclimate of an Ancient lake deposit, Gale Crater. *Mars. Sci.* 350 (6257), aac7575. doi:10.1126/science.aac7575

Gudipaty, S. A., Larsen, A. S., Rensing, C., and McEvoy, M. M. (2012). Regulation of Cu(I)/Ag(I) Efflux Genes in *Escherichia coli* by the Sensor Kinase CusS. *FEMS Microbiol. Lett.* 330 (1), 30–37. doi:10.1111/j.1574-6968.2012.02529.x

Gulick, V. C. (1998). Magmatic Intrusions and a Hydrothermal Origin for Fluvial Valleys on Mars. *J. Geophys. Res. Planets* 103 (E8), 19365–19387. doi:10.1029/98JE01321

Gulick, V. C. (2001). Origin of the valley Networks on Mars: a Hydrological Perspective. *Geomorphology* 37 (3), 241–268. doi:10.1016/S0169-555X(00)00086-6

Harrison, A. P. (1981). Acidiphilium Cryptum Gen. nov., Sp. nov., Heterotrophic Bacterium from Acidic Mineral Environments. *Int. J. Syst. Evol. Microbiol.* 31 (3), 327–332. doi:10.1099/00207713-31-3-327

Hauck Ii, S. A., and Phillips, R. J. (2002). Thermal and Crustal Evolution of Mars. *J. Geophys. Res. Planets* 107 (E7), 6–1–6-19. doi:10.1029/2001JE001801

Hays, L. E., Graham, H. V., Des Marais, D. J., Hausrath, E. M., Horgan, B., McCollom, T. M., et al. (2017). Biosignature Preservation and Detection in Mars Analog Environments. *Astrobiology* 17 (4), 363–400. doi:10.1089/ast.2016.1627

Hiraishi, A., Nagashima, K. V. P., Matsuura, K., Shimada, K., Takaichi, S., Wakao, N., et al. (1998). Phylogeny and Photosynthetic Features of Thiobacillus Acidophilus and Related Acidophilic Bacteria: its Transfer to the Genus

Acidiphilium as Acidiphilium Acidophilum Comb. Nov. *Int. J. Syst. Evol. Microbiol.* 48 (4), 1389–1398. doi:10.1099/00207713-48-4-1389

Hoke, M. R. T., and Hynek, B. M. (2009). Roaming Zones of Precipitation on Ancient Mars as Recorded in valley Networks. Journal of Geophysical Research. *Planets* 114 (E8). doi:10.1029/2008JE003247

Hoke, M. R. T., Hynek, B. M., Di Achille, G., and Hutton, E. W. H. (2014). The Effects of Sediment Supply and Concentrations on the Formation Timescale of Martian Deltas. *Icarus* 228, 1–12. doi:10.1016/j.icarus.2013.09.017

Hoke, M. R. T., Hynek, B. M., and Tucker, G. E. (2011). Formation Timescales of Large Martian valley Networks. *Earth Planet. Sci. Lett.* 312 (1), 1–12. doi:10.1016/j.epsl.2011.09.053

Horvath, D. G., Moitra, P., Hamilton, C. W., Craddock, R. A., and Andrews-Hanna, J. C. (2021). Evidence for Geologically Recent Explosive Volcanism in Elysium Planitia, Mars. *Icarus* 365, 114499. doi:10.1016/j.icarus.2021.114499

Huerta-Cepas, J., Szklarczyk, D., Forslund, K., Cook, H., Heller, D., Walter, M. C., et al. (2015). eggNOG 4.5: a Hierarchical Orthology Framework with Improved Functional Annotations for Eukaryotic, Prokaryotic and Viral Sequences. *Nucleic Acids Res.* 44 (D1), D286–D293. doi:10.1093/nar/gkv1248

Hynek, B. M., Beach, M., and Hoke, M. R. T. (2010). Updated Global Map of Martian valley Networks and Implications for Climate and Hydrologic Processes. Journal of Geophysical Research. *Planets* 115 (E9). doi:10.1029/2009JE003548

Hynek, B. M., McCollom, T. M., Marcucci, E. C., Brugman, K., and Rogers, K. L. (2013). Assessment of Environmental Controls on Acid-Sulfate Alteration at Active Volcanoes in Nicaragua: Applications to Relic Hydrothermal Systems on Mars. *J. Geophys. Res. Planets* 118 (10), 2083–2104. doi:10.1002/jgre.20140

Hynek, B. M., McCollom, T. M., McHenry, L. J., and Alvarado, G. E. (2014). "Assessing Hydrothermal Alteration on Early Mars through Analog Environments in Nicaragua, Costa Rica, Ice-Land, and Hawaii [abstract 2172]," in 45thLunar and Planetary Science Conference, Houston (Lunar and Planetary Institute). LPI Contribution No. 1777.

Hynek, B. M., and Phillips, R. J. (2003). New Data Reveal Mature, Integrated Drainage Systems on Mars Indicative of Past Precipitation. *Geology* 31 (9), 757–760. doi:10.1130/G19607.1

Hynek, B. M., Rogers, K. L., Antunovich, M., Avard, G., and Alvarado, G. E. (2018). Lack of Microbial Diversity in an Extreme Mars Analog Setting. *Astrobiology* 18 (7), 923–933. Poás Volcano, Costa Rica. doi:10.1089/ast.2017.1719

Jayaraman, G. C., Penders, J. E., and Burne, R. A. (1997). Transcriptional Analysis of the Streptococcus Mutans hrcA, grpE and dnaK Genes and Regulation of Expression in Response to Heat Shock and Environmental Acidification. *Mol. Microbiol.* 25 (2), 329–341. doi:10.1046/j.1365-2958.1997.4671835.x

Johnson, D. B., Hedrich, S., and Pakostova, E. (2017). Indirect Redox Transformations of Iron, Copper, and Chromium Catalyzed by Extremely Acidophilic Bacteria. *Front. Microbiol.* 8, 211. doi:10.3389/fmicb.2017.00211

Kalia, K., and Joshi, D. N. (2009). "CHAPTER 72-Detoxification of Arsenic," in *Handbook of Toxicology of Chemical Warfare Agents*. Editor R. C. Gupta. (San Diego: Academic Press), 1083–1100. doi:10.1016/b978-012374484-5.00072-9*:*

Kämpfer, P., Lodders, N., and Falsen, E. (2011). Hydrotalea Flava Gen. nov., Sp. nov., a New Member of the Phylum Bacteroidetes and Allocation of the Genera Chitinophaga, Sediminibacterium, Lacibacter, Flavihumibacter, Flavisolibacter, Niabella, Niastella, Segetibacter, Parasegetibacter, Terrimonas, Ferruginibacter, Filimonas and Hydrotalea to the Family Chitinophagaceae Fam. Nov. *Int. J. Syst. Evol. Microbiol.* 61 (3), 518–523. doi:10.1099/ijs.0.023002-0

Kanehisa, M., and Goto, S. (2000). KEGG: Kyoto Encyclopedia of Genes and Genomes. *Nucleic Acids Res.* 28 (1), 27–30. doi:10.1093/nar/28.1.27

Kereszturi, A. (2012). Review of Wet Environment Types on Mars with Focus on Duration and Volumetric Issues. *Astrobiology* 12 (6), 586–600. doi:10.1089/ast.2011.0686

Kereszturi, A., Bradak, B., Chatzitheodoridis, E., and Ujvari, G. (2016). Indicators and Methods to Understand Past Environments from ExoMars Rover Drills. *Origins Life Evol. Biospheres* 46 (4), 435–454. doi:10.1007/s11084-016-9492-3

Kishimoto, N., Fukaya, F., Inagaki, K., Sugio, T., Tanaka, H., and Tano, T. (1995). Distribution of Bacteriochlorophyll a Among Aerobic and Acidophilic Bacteria and Light-Enhanced CO2-incorporation in Acidiphilium Rubrum. *FEMS Microbiol. Ecol.* 16 (4), 291–296. doi:10.1111/j.1574-6941.1995.tb00293.x

Kovaleva, J., Degener, J. E., and van der Mei, H. C. (2014). Methylobacterium and its Role in Health Care-Associated Infection. *J. Clin. Microbiol.* 52 (5), 1317. doi:10.1128/JCM.03561-13

Krulwich, T. A., Sachs, G., and Padan, E. (2011). Molecular Aspects of Bacterial pH Sensing and Homeostasis. *Nat. Rev. Microbiol.* 9 (5), 330–343. doi:10.1038/nrmicro2549

Küsel, K., Dorsch, T., Acker, G., and Stackebrandt, E. (1999). Microbial Reduction of Fe(III) in Acidic Sediments: Isolation of Acidiphilium Cryptum JF-5 Capable of Coupling the Reduction of Fe(III) to the Oxidation of Glucose. *Appl. Environ. Microbiol.* 65 (8), 3633. doi:10.1128/AEM.65.8.3633-3640.1999

Lane, D. J., Harrison, A. P., Jr., Stahl, D., Pace, B., Giovannoni, S. J., Olsen, G. J., et al. (1992). Evolutionary Relationships Among Sulfur- and Iron-Oxidizing Eubacteria. *J. Bacteriol.* 174 (1), 269–278. doi:10.1128/jb.174.1.269-278.1992

Li, D., Liu, C.-M., Luo, R., Sadakane, K., and Lam, T.-W. (2015). MEGAHIT: an ultra-fast single-node solution for large and complex metagenomics assembly via succinct de Bruijn graph. *Bioinformatics* 31 (10), 1674–1676. doi:10.1093/bioinformatics/btv033

Li, L., Liu, Z., Zhang, M., Meng, D., Liu, X., Wang, P., et al. (2020). Insights into the Metabolism and Evolution of the Genus Acidiphilium, a Typical Acidophile in Acid Mine Drainage. *mSystems* 5 (6), e00867–00820. doi:10.1128/mSystems.00867-20

Liu, J., Michalski, J. R., Tan, W., He, H., Ye, B., and Xiao, L. (2021). Anoxic Chemical Weathering under a Reducing Greenhouse on Early Mars. *Nat. Astron.* 5 (5), 503–509. doi:10.1038/s41550-021-01303-5

Liu, Y., Yang, H., Zhang, X., Xiao, Y., Guo, X., and Liu, X. (2016). Genomic Analysis Unravels Reduced Inorganic Sulfur Compound Oxidation of Heterotrophic *Acidophilic Acidicaldus* Sp. Strain DX-1. *Biomed. Res. Int.* 2016, 8137012. doi:10.1155/2016/8137012

Long, F., Su, C.-C., Lei, H.-T., Bolla, J. R., Do, S. V., and Yu, E. W. (2012). Structure and Mechanism of the Tripartite CusCBA Heavy-Metal Efflux Complex. Philosophical Transactions of the Royal Society of London. Series B. *Biol. Sci.* 367 (1592), 1047–1058. doi:10.1098/rstb.2011.0203

Mangold, N., Gupta, S., Gasnault, O., Dromart, G., Tarnas, J. D., Sholes, S. F., et al. (2021). Perseverance Rover Reveals an Ancient delta-lake System and Flood Deposits at Jezero Crater. *Mars. Sci.* 374 (6568), 711–717. doi:10.1126/science.abl4051

Manor, O., and Borenstein, E. (2015). MUSiCC: a Marker Genes Based Framework for Metagenomic Normalization and Accurate Profiling of Gene Abundances in the Microbiome. *Genome Biol.* 16 (1), 53. doi:10.1186/s13059-015-0610-8

Marcucci, E. C., Hynek, B. M., Kierein-Young, K. S., and Rogers, K. L. (2013). Visible-near-infrared Reflectance Spectroscopy of Volcanic Acid-Sulfate Alteration in Nicaragua: Analogs for Early Mars. *J. Geophys. Res. Planets* 118 (10), 2213–2233. doi:10.1002/jgre.20159

Martin, M. (2011). Cutadapt Removes Adapter Sequences from High-Throughput Sequencing readsNext Generation Sequencing Data AnalysisDO - 10.14806/ej.17.1.200. *EMBnet.journal* Vol. 17 (No 1). doi:10.14806/ej.17.1.200

Martin, W., Baross, J., Kelley, D., and Russell, M. J. (2008). Hydrothermal Vents and the Origin of Life. *Nat. Rev. Microbiol.* 6 (11), 805–814. doi:10.1038/nrmicro1991

Martin, W., and Russell, M. J. (2003). On the Origins of Cells: a Hypothesis for the Evolutionary Transitions from Abiotic Geochemistry to Chemoautotrophic Prokaryotes, and from Prokaryotes to Nucleated Cells. Philosophical Transactions of the Royal Society of London. Series B. *Biol. Sci.* 358 (1429), 59–85. doi:10.1098/rstb.2002.1183

Martínez-Cruz, M., van Bergen, M. J., Takano, B., Fernández-Soto, E., and Barquero-Hernández, J. (2019). "Behaviour of Polythionates in the Acid Lake of Poás Volcano: Insights into Changes in the Magmatic-Hydrothermal Regime and Subaqueous Input of Volatiles," in *Poás Volcano: The Pulsing Heart of Central America Volcanic Zone*. Editors F. Tassi, O. Vaselli, and R. A. Mora Amador (Cham: Springer International Publishing), 155–202. doi:10.1007/978-3-319-02156-0_7

McCollom, T. M., and Hynek, B. M. (2005). A Volcanic Environment for Bedrock Diagenesis at Meridiani Planum on Mars. *Nature* 438 (7071), 1129–1131. doi:10.1038/nature04390

Michalski, J. R., Onstott, T. C., Mojzsis, S. J., Mustard, J., Chan, Q. H. S., Niles, P. B., et al. (2018). The Martian Subsurface as a Potential Window into the Origin of Life. *Nat. Geosci.* 11 (1), 21–26. doi:10.1038/s41561-017-0015-2

Mirete, S., Morgante, V., and González-Pastor, J. E. (2017). "Acidophiles: Diversity and Mechanisms of Adaptation to Acidic Environments," in *Adaption of*

Microbial Life to Environmental Extremes: Novel Research Results and Application. Editors H. Stan-Lotter and S. Fendrihan (Cham: Springer International Publishing), 227–251. doi:10.1007/978-3-319-48327-6_9

Moitra, P., Horvath, D. G., and Andrews-Hanna, J. C. (2021). Investigating the Roles of Magmatic Volatiles, Ground Ice and Impact-Triggering on a Very Recent and Highly Explosive Volcanic Eruption on Mars. *Earth Planet. Sci. Lett.* 567, 116986. doi:10.1016/j.epsl.2021.116986

Moore, J. E., McCalmont, M., Xu, J., Millar, B. C., and Heaney, N. (2002). Asaia sp., an Unusual Spoilage Organism of Fruit-Flavored Bottled Water. *Appl. Environ. Microbiol.* 68 (8), 4130–4131. doi:10.1128/AEM.68.8.4130-4131.2002

National Research Council (2011). *Vision and Voyages for Planetary Science in the Decade 2013-2022*. Washington, DC: The National Academies Press.

Nisbet, E. G., and Sleep, N. H. (2001). The Habitat and Nature of Early Life. *Nature* 409 (6823), 1083–1091. doi:10.1038/35059210

Noinaj, N., Guillier, M., Barnard, T. J., and Buchanan, S. K. (2010). TonB-Dependent Transporters: Regulation, Structure, and Function. *Annu. Rev. Microbiol.* 64 (1), 43–60. doi:10.1146/annurev.micro.112408.134247

Nordstrom, D. K., and Alpers, C. N. (1999). Negative pH, Efflorescent Mineralogy, and Consequences for Environmental Restoration at the Iron Mountain Superfund Site, California. *Proc. Natl. Acad. Sci.* 96 (7), 3455. doi:10.1073/pnas.96.7.3455

Okubo, Y., Yang, S., Chistoserdova, L., and Lidstrom, M. E. (2010). Alternative Route for Glyoxylate Consumption during Growth on Two-Carbon Compounds by Methylobacterium Extorquens AM1. *J. Bacteriol.* 192 (7), 1813. doi:10.1128/JB.01166-09

Ormeño-Orrillo, E., and Martínez-Romero, E. (2019). A Genomotaxonomy View of the Bradyrhizobium Genus. *Front. Microbiol.* 10 (1334). doi:10.3389/fmicb.2019.01334

Osinski, G. R., Cockell, C. S., Pontefract, A., and Sapers, H. M. (2020). The Role of Meteorite Impacts in the Origin of Life. *Astrobiology* 20 (9), 1121–1149. doi:10.1089/ast.2019.2203

Palumbo, A. M., Head, J. W., and Wordsworth, R. D. (2018). Late Noachian Icy Highlands Climate Model: Exploring the Possibility of Transient Melting and Fluvial/lacustrine Activity through Peak Annual and Seasonal Temperatures. *Icarus* 300, 261–286. doi:10.1016/j.icarus.2017.09.007

Peña-Ocaña, B. A., Ovando-Ovando, C. I., Puente-Sánchez, F., Tamames, J., Servín-Garcidueñas, L. E., González-Toril, E., et al. (2022). Metagenomic and Metabolic Analyses of Poly-Extreme Microbiome from an Active Crater Volcano lake. *Environ. Res.* 203, 111862. doi:10.1016/j.envres.2021.111862

Phillips, R. J., Zuber, M. T., Solomon, S. C., Golombek, M. P., Jakosky, B. M., Banerdt, W. B., et al. (2001). Ancient Geodynamics and Global-Scale Hydrology on Mars. *Science* 291 (5513), 2587. doi:10.1126/science.1058701

Prokofeva, M. I., Kublanov, I. V., Nercessian, O., Tourova, T. P., Kolganova, T. V., Lebedinsky, A. V., et al. (2005). Cultivated Anaerobic Acidophilic/acidotolerant Thermophiles from Terrestrial and Deep-Sea Hydrothermal Habitats. *Extremophiles* 9 (6), 437–448. doi:10.1007/s00792-005-0461-4

Prosser, J. T., and Carr, M. J. (1987). Poás Volcano, Costa Rica: Geology of the summit Region and Spatial and Temporal Variations Among the Most Recent Lavas. *J. Volcanology Geothermal Res.* 33 (1), 131–146. doi:10.1016/0377-0273(87)90057-6

Quast, C., Pruesse, E., Yilmaz, P., Gerken, J., Schweer, T., Yarza, P., et al. (2013). The SILVA Ribosomal RNA Gene Database Project: Improved Data Processing and Web-Based Tools. *Nucleic Acids Res.* 41 (D1), D590–D596. doi:10.1093/nar/gks1219

Rensing, C., Pribyl, T., and Nies, D. H. (1997). New Functions for the Three Subunits of the CzcCBA Cation-Proton Antiporter. *J. Bacteriol.* 179 (22), 6871. doi:10.1128/jb.179.22.6871-6879.1997

Robbins, S. J., Achille, G. D., and Hynek, B. M. (2011). The Volcanic History of Mars: High-Resolution Crater-Based Studies of the Calderas of 20 Volcanoes. *Icarus* 211 (2), 1179–1203. doi:10.1016/j.icarus.2010.11.012

Robbins, S. J., Hynek, B. M., Lillis, R. J., and Bottke, W. F. (2013). Large Impact Crater Histories of Mars: The Effect of Different Model Crater Age Techniques. *Icarus* 225 (1), 173–184. doi:10.1016/j.icarus.2013.03.019

Rodríguez, A., and van Bergen, M. J. (2017). Superficial Alteration Mineralogy in Active Volcanic Systems: An Example of Poás Volcano, Costa Rica. *J. Volcanology Geothermal Res.* 346, 54–80. doi:10.1016/j.jvolgeores.2017.04.006

Rohwerder, T., Gehrke, T., Kinzler, K., and Sand, W. (2003). Bioleaching Review Part A. *Appl. Microbiol. Biotechnol.* 63 (3), 239–248. doi:10.1007/s00253-003-1448-7

Rohwerder, T., and Sand, W. (2003). The Sulfane Sulfur of Persulfides Is the Actual Substrate of the Sulfur-Oxidizing Enzymes from Acidithiobacillus and Acidiphilium Spp. *Microbiology* 149 (7), 1699–1710. doi:10.1099/mic.0.26212-0

Rotto, S., and Tanaka, K. L. (1995). *Geologic/geomorphologic Map of the Chryse Planitia Region of Mars*. IMAP.

Rowe, G. L., Brantley, S. L., Fernandez, M., Fernandez, J. F., Borgia, A., and Barquero, J. (1992a). Fluid-volcano Interaction in an Active Stratovolcano: the Crater lake System of Poás Volcano, Costa Rica. *J. Volcanology Geothermal Res.* 49 (1), 23–51. doi:10.1016/0377-0273(92)90003-V

Rowe, G. L., Ohsawa, S., Takano, B., Brantley, S. L., Fernandez, J. F., and Barquero, J. (1992b). Using Crater Lake Chemistry to Predict Volcanic Activity at Poás Volcano, Costa Rica. *Bull. Volcanology* 54 (6), 494–503. doi:10.1007/BF00301395

Ruff, S. W., Farmer, J. D., Calvin, W. M., Herkenhoff, K. E., Johnson, J. R., Morris, R. V., et al. (2011). Characteristics, Distribution, Origin, and Significance of Opaline Silica Observed by the Spirit Rover in Gusev Crater, Mars. Journal of Geophysical Research: Planets 116(E7). doi:10.1029/2010JE003767

Rymer, H., and Brown, G. (1989). Gravity Changes as a Precursor to Volcanic Eruption at Poás Volcano, Costa Rica. *Nature* 342 (6252), 902–905. doi:10.1038/342902a0

Rymer, H., Cassidy, J., Locke, C. A., Barboza, M. V., Barquero, J., Brenes, J., et al. (2000). Geophysical Studies of the Recent 15-year Eruptive Cycle at Poás Volcano, Costa Rica. *J. Volcanology Geothermal Res.* 97 (1), 425–442. doi:10.1016/S0377-0273(99)00166-3

Salvage, R. O., Avard, G., de Moor, J. M., Pacheco, J. F., Brenes Marin, J., Cascante, M., et al. (2018). Renewed Explosive Phreatomagmatic Activity at Poás Volcano, Costa Rica in April 2017. *Front. Earth Sci.* 6, 160. doi:10.3389/feart.2018.00160

San Martin-Uriz, P., Gomez Manuel, J., Arcas, A., Bargiela, R., and Amils, R. (2011). Draft Genome Sequence of the Electricigen Acidiphilium Sp. Strain PM (DSM 24941). *J. Bacteriol.* 193 (19), 5585–5586. doi:10.1128/JB.05386-11

Sanford, W. E., Konikow, L. F., Rowe, G. L., and Brantley, S. L. (1995). Groundwater Transport of Crater-lake Brine at Poa´s Volcano, Costa Rica. *J. Volcanology Geothermal Res.* 64 (3), 269–293. doi:10.1016/0377-0273(94)00080-Z

Schippers, A. (2007). "Microorganisms Involved in Bioleaching and Nucleic Acid-Based Molecular Methods for Their Identification and Quantification," in *Microbial Processing of Metal Sulfides*. Editors E. R. Donati and W. Sand. (DordrechtNetherlands: Springer), 3–33.:

Schmidt, M. E., Farrand, W. H., Johnson, J. R., Schröder, C., Hurowitz, J. A., McCoy, T. J., et al. (2009). Spectral, Mineralogical, and Geochemical Variations across Home Plate, Gusev Crater, Mars Indicate High and Low Temperature Alteration. *Earth Planet. Sci. Lett.* 281 (3), 258–266. doi:10.1016/j.epsl.2009.02.030

Schneider, K., Peyraud, R., Kiefer, P., Christen, P., Delmotte, N., Massou, S., et al. (2012). The Ethylmalonyl-CoA Pathway Is Used in Place of the Glyoxylate Cycle by Methylobacterium Extorquens AM1 during Growth on Acetate. *J. Biol. Chem.* 287 (1), 757–766. doi:10.1074/jbc.M111.305219

Schulze-Makuch, D., Dohm, J. M., Fan, C., Fairén, A. G., Rodriguez, J. A. P., Baker, V. R., et al. (2007). Exploration of Hydrothermal Targets on Mars. *Icarus* 189 (2), 308–324. doi:10.1016/j.icarus.2007.02.007

Seto, M., Noguchi, K., and Cappellen, P. V. (2019). Potential for Aerobic Methanotrophic Metabolism on Mars. *Astrobiology* 19 (10), 1187–1195. doi:10.1089/ast.2018.1943

Skok, J. R., Mustard, J. F., Ehlmann, B. L., Milliken, R. E., and Murchie, S. L. (2010). Silica Deposits in the Nili Patera Caldera on the Syrtis Major Volcanic Complex on Mars. *Nat. Geosci.* 3 (12), 838–841. doi:10.1038/ngeo990

Solomon, S. C., Aharonson, O., Aurnou, J. M., Banerdt, W. B., Carr, M. H., Dombard, A. J., et al. (2005). New Perspectives on Ancient Mars. *Science* 307 (5713), 1214. doi:10.1126/science.1101812

Squyres, S. W., Aharonson, O., Clark, B. C., Cohen, B. A., Crumpler, L., de Souza, P. A., et al. (2007). Pyroclastic Activity at Home Plate in Gusev Crater, Mars. *Science* 316 (5825), 738. doi:10.1126/science.1139045

Squyres, S. W., Arvidson, R. E., Ruff, S., Gellert, R., Morris, R. V., Ming, D. W., et al. (2008). Detection of Silica-Rich Deposits on Mars. *Science* 320 (5879), 1063. doi:10.1126/science.1155429

Stamenković, V., Ward, L. M., Mischna, M., and Fischer, W. W. (2018). O2 Solubility in Martian Near-Surface Environments and Implications for Aerobic Life. *Nat. Geosci.* 11 (12), 905–909. doi:10.1038/s41561-018-0243-0

Tamames, J., and Puente-Sánchez, F. (2019). SqueezeMeta, A Highly Portable, Fully Automatic Metagenomic Analysis Pipeline. *Front. Microbiol.* 9 (3349). doi:10.3389/fmicb.2018.03349

Tanaka, K. L., Dohm, J. M., Lias, J. H., and Hare, T. M. (1998). Erosional Valleys in the Thaumasia Region of Mars: Hydrothermal and Seismic Origins. *J. Geophys. Res. E: Planets* 103 (E13), 31407–31419. doi:10.1029/98je01599

Thollot, P., Mangold, N., Ansan, V., Le Mouélic, S., Milliken, R. E., Bishop, J. L., et al. (2012). Most Mars Minerals in a Nutshell: Various Alteration Phases Formed in a Single Environment in Noctis Labyrinthus. Journal of Geophysical Research. *Planets* 117 (E11). doi:10.1029/2011JE004028

Tibazarwa, C., Wuertz, S., Mergeay, M., Wyns, L., and van der Lelie, D. (2000). Regulation of the Cnr Cobalt and Nickel Resistance Determinant of Ralstonia Eutropha (Alcaligenes Eutrophus) CH34. *J. Bacteriol.* 182 (5), 1399. doi:10.1128/JB.182.5.1399-1409.2000

Trainer, M. G., Wong, M. H., McConnochie, T. H., Franz, H. B., Atreya, S. K., Conrad, P. G., et al. (2019). Seasonal Variations in Atmospheric Composition as Measured in Gale Crater, Mars. *J. Geophys. Res. Planets* 124 (11), 3000–3024. doi:10.1029/2019JE006175

Ullrich, S. R., Poehlein, A., Voget, S., Hoppert, M., Daniel, R., Leimbach, A., et al. (2015). Permanent Draft Genome Sequence of Acidiphilium Sp. JA12-A1. *Stand. Genomic Sci.* 10 (1), 56. doi:10.1186/s40793-015-0040-y

Vago, J. L., Coates, A. J., Jaumann, R., Korablev, O., Ciarletti, V., Mitrofanov, I., et al. (2018). "Chapter 12-Searching for Traces of Life with the ExoMars Rover," in *From Habitability to Life on Mars*. Editors N. A. Cabrol and E. A. Grin (Elsevier), 309–347. doi:10.1016/b978-0-12-809935-3.00011-6

Wächtershäuser, G. (2006). From Volcanic Origins of Chemoautotrophic Life to Bacteria, Archaea and Eukarya. Philosophical Transactions of the Royal Society of London. Series B. *Biol. Sci.* 361 (1474), 1787–1808. doi:10.1098/rstb.2006.1904

Walter, M. R., and Des Marais, D. J. (1993). Preservation of Biological Information in Thermal Spring Deposits: Developing a Strategy for the Search for Fossil Life on Mars. *Icarus* 101 (1), 129–143. doi:10.1006/icar.1993.1011

Wang, J., Hynek, B. M., et al. (2020). "Temporal and Metagenomic Studies of an Extreme Martian Analog Ecosystem: Poás Volcano, Costa Rica," in 51st Lunar and Planetary Science Conference, Houston, LPI (Lunar and Planetary Institute) Abstract 1774.

Wang, Q., Cen, Z., and Zhao, J. (2015). The Survival Mechanisms of Thermophiles at High Temperatures: An Angle of Omics. *Physiology* 30 (2), 97–106. doi:10.1152/physiol.00066.2013

Wang, Q., Garrity, G. M., Tiedje, J. M., and Cole, J. R. (2007). Naïve Bayesian Classifier for Rapid Assignment of rRNA Sequences into the New Bacterial Taxonomy. *Appl. Environ. Microbiol.* 73 (16), 5261. doi:10.1128/AEM.00062-07

Weiss, M. C., Sousa, F. L., Mrnjavac, N., Neukirchen, S., Roettger, M., Nelson-Sathi, S., et al. (2016). The Physiology and Habitat of the Last Universal Common Ancestor. *Nat. Microbiol.* 1 (9), 16116. doi:10.1038/nmicrobiol.2016.116

Weitz, C. M., Bishop, J. L., Thollot, P., Mangold, N., and Roach, L. H. (2011). Diverse Mineralogies in Two Troughs of Noctis Labyrinthus, Mars. *Geology* 39 (10), 899–902. doi:10.1130/G32045.1

Wichlacz, P. L., Unz, R. F., and Langworthy, T. A. (1986). Acidiphilium Angustum Sp. nov., Acidiphilium Facilis Sp. nov., and Acidiphilium Rubrum Sp. nov.: Acidophilic Heterotrophic Bacteria Isolated from Acidic Coal Mine Drainage. *Int. J. Syst. Evol. Microbiol.* 36 (2), 197–201. doi:10.1099/00207713-36-2-197

Wilson, S. A., Morgan, A. M., Howard, A. D., and Grant, J. A. (2021). The Global Distribution of Craters with Alluvial Fans and Deltas on Mars. *Geophys. Res. Lett.* 48 (4), e2020GL091653. doi:10.1029/2020GL091653

Yamauchi, M., and Yamada, Y. (1981). Glycolate Pathway and Serine Synthesis in Relation to CO2 Concentration in Tomato Leaves. *Plant Cel Physiol.* 22 (8), 1489–1498. doi:10.1093/oxfordjournals.pcp.a076302

Yen, A. S., Morris, R. V., Clark, B. C., Gellert, R., Knudson, A. T., Squyres, S., et al. (2008). Hydrothermal Processes at Gusev Crater: An Evaluation of Paso Robles Class Soils. Journal of Geophysical Research. *Planets* 113 (E6). doi:10.1029/2007JE002978

Yen, A. S., Morris, R. V., Ming, D. W., Schwenzer, S. P., Sutter, B., Vaniman, D. T., et al. (2021). Formation of Tridymite and Evidence for a Hydrothermal History at Gale Crater, Mars. *J. Geophys. Res. Planets* 126 (3), e2020JE006569. doi:10.1029/2020JE006569

Yilmaz, P., Parfrey, L. W., Yarza, P., Gerken, J., Pruesse, E., Quast, C., et al. (2014). The SILVA and "All-Species Living Tree Project (LTP)" Taxonomic Frameworks. *Nucleic Acids Res.* 42 (D1), D643–D648. doi:10.1093/nar/gkt1209

Conflict of Interest: The authors declare that the research was conducted in the absence of any commercial or financial relationships that could be construed as a potential conflict of interest.

Publisher's Note: All claims expressed in this article are solely those of the authors and do not necessarily represent those of their affiliated organizations, or those of the publisher, the editors and the reviewers. Any product that may be evaluated in this article, or claim that may be made by its manufacturer, is not guaranteed or endorsed by the publisher.

frontiers in Astronomy and Space Sciences

ORIGINAL RESEARCH
published: 07 February 2022
doi: 10.3389/fspas.2021.797591

Surface Morphologies in a Mars-Analog Ca-Sulfate Salar, High Andes, Northern Chile

Nancy W. Hinman[1], Michael H. Hofmann[1], Kimberly Warren-Rhodes[2], Michael S. Phillips[3], Nora Noffke[4], Nathalie A. Cabrol[5], Guillermo Chong Diaz[6], Cecilia Demergasso[7], Cinthya Tebes-Cayo[7], Oscar Cabestrero[6], Janice L. Bishop[2], Virginia C. Gulick[2,8], David Summers[2], Pablo Sobron[2], Michael McInenly[1], Jeffrey Moersch[3], Constanza Rodriguez[6], Philippe Sarazzin[2], Kevin L. Rhodes[9], Camila Javiera Riffo Contreras[6], David Wettergreen[10] and Victor Parro[11] on behalf of the SETI NAI team*

[1]Department of Geosciences, University of Montana, Missoula, MT, United States, [2]SETI Institute, Mountain View, CA, United States, [3]Department of Earth and Planetary Science, The University of Tennessee, Knoxville, TN, United States, [4]Ocean, Earth, and Atmospheric Sciences, Old Dominion University, Norfolk, VA, United States, [5]Carl Sagan Center, SETI Institute, Mountainview, CA, United States, [6]Departmento de Ciencias Geológicas, Catholic University of the North, Antofagasta, Chile, [7]Center for Biotechnology, Catholic University of the North, Antofagasta, Chile, [8]Ames Research Center, National Aeronautics and Space Administration (NASA), Moffet Field, CA, United States, [9]MAR Alliance, San Francisco, CA, United States, [10]Robotics Institute, Carnegie Mellon University, Pittsburgh, PA, United States, [11]Center for Astrobiology, Spanish National Research Council (CSIC), Madrid, Spain

OPEN ACCESS

Edited by:
David Flannery, Queensland University of Technology, Brisbane, Australia

Reviewed by:
Akos Kereszturi, Hungarian Academy of Sciences (MTA), Hungary
Monica Pondrelli, Università d'Annunzio, Pescara, Italy

***Correspondence:**
Nancy W. Hinman
nancy.hinman@umontana.edu

Specialty section:
This article was submitted to Astrobiology, a section of the journal Frontiers in Astronomy and Space Sciences

Received: *18 October 2021*
Accepted: *01 December 2021*
Published: *07 February 2022*

Citation:
Hinman NW, Hofmann MH, Warren-Rhodes K, Phillips MS, Noffke N, Cabrol NA, Chong Diaz G, Demergasso C, Tebes-Cayo C, Cabestrero O, Bishop JL, Gulick VC, Summers D, Sobron P, McInenly M, Moersch J, Rodriguez C, Sarazzin P, Rhodes KL, Riffo Contreras CJ, Wettergreen D and Parro V (2022) Surface Morphologies in a Mars-Analog Ca-Sulfate Salar, High Andes, Northern Chile. Front. Astron. Space Sci. 8:797591. doi: 10.3389/fspas.2021.797591

Salar de Pajonales, a Ca-sulfate salt flat in the Chilean High Andes, showcases the type of polyextreme environment recognized as one of the best terrestrial analogs for early Mars because of its aridity, high solar irradiance, salinity, and oxidation. The surface of the salar represents a natural climate-transition experiment where contemporary lagoons transition into infrequently inundated areas, salt crusts, and lastly dry exposed paleoterraces. These surface features represent different evolutionary stages in the transition from previously wetter climatic conditions to much drier conditions today. These same stages closely mirror the climate transition on Mars from a wetter early Noachian to the Noachian/Hesperian. Salar de Pajonales thus provides a unique window into what the last near-surface oases for microbial life on Mars could have been like in hypersaline environments as the climate changed and water disappeared from the surface. Here we open that climatological window by evaluating the narrative recorded in the salar surface morphology and microenvironments and extrapolating to similar paleosettings on Mars. Our observations suggest a strong inter-dependence between small and large scale features that we interpret to be controlled by extrabasinal changes in environmental conditions, such as precipitation-evaporation-balance changes and thermal cycles, and most importantly, by internal processes, such as hydration/dehydration, efflorescence/deliquescence, and recrystallization brought about by physical and chemical processes related to changes in groundwater recharge and volcanic processes. Surface structures and textures record a history of hydrological changes that impact the mineralogy and volume of Ca-sulfate layers comprising most of the salar surface. Similar surface features on Mars, interpreted as products of freeze-thaw cycles, could, instead, be products of water-driven, volume changes in salt deposits. On Mars, surface manifestations of such salt-related processes would point to potential water sources. Because hygroscopic salts have been invoked as sources of localized, transient water sufficient to support terrestrial life, such structures might be good targets for biosignature exploration on Mars.

Keywords: mars, evaporite, salt pan, gypsum (CaSO 2H O) 4 2, Chile, Andes, Salar

1 INTRODUCTION

The Andean Salar de Pajonales (3,537 m asl, 25°08′40″ S, 68°49′12″ W; **Figure 1**) is an evaporitic basin located on the western margin of the High Andes in the Altiplano[1]. At present, it is in the desiccation period of wetting and drying cycles, comprising lagoons/salt ponds, salt crusts, infrequently inundated areas, and dry exposed paleoterraces (Chong Diaz et al., 2020).

The hydrological progression from active lagoons to exposed salt paleoterraces forms a natural climate-transition experiment, where each salar surface represents a different stage of evolution in the wet-to-dry transitions during (micro-)cycles of climate change over geological time scales. The climate transition exemplified at Salar de Pajonales partly mirrors that postulated for early Mars (Kite, 2019; Wordsworth et al., 2021), thus making it a unique terrestrial analog for early climate change on that planet (Cabrol et al., 2009; Cabrol et al., 2010; Cabrol, 2018; Farías and Acuña, 2020; Pueyo et al., 2021).

At present, the High Andes are characterized by daily occurrences of dust devils and enhanced evaporation (-1,500 mm/yr) (Cabrol and Grin, 2010; Benison, 2017). Indeed, surface measurements in the High Andes recorded the highest solar radiation levels on Earth, including UVB (Cabrol et al., 2014; Albarracin et al., 2015; Häder and Cabrol, 2018; Häder and Cabrol, 2020). The thin atmosphere produces sudden and sharp daily temperature (T) and relative humidity (Warren-Rhodes et al., in review; Kereszturi et al., 2020) fluctuations that generate high UV/T ratios further extending the Salar de Pajonales region's environmental analogies to Martian conditions.

Salar de Pajonales furnishes a window into the possible last microbial refugia on Mars as the climate shifted and water disappeared from the surface (Davila and Schulze-Makuch, 2016) Here we open that climatological window by evaluating the morphological and mineralogical properties of the salar and its implications for evaporitic basins on Mars during the Noachian through early Hesperian (Cabrol et al., 2018; Kite, 2019; Wordsworth et al., 2021). We test the hypothesis that hydrological processes on a time scale relevant to recent climate changes, coupled with volcanic processes, are the major control on surface morphology in this Martian analog. If true, then these morphologies could reflect similar hydrological conditions during the wetter climate of early Mars and could guide site and sample selection—going beyond the "follow the water" model for on-going and upcoming Mars missions.

1.1 Site Overview

Salar de Pajonales (**Figure 1**) is a large (104 km^2) salt flat that lies in a high elevation basin on the western margin of the High Andes in northern Chile to the east of the Atacama Desert—a well-described Martian analog (Cabrol et al., 2001; Cabrol et al., 2007; Gómez-Silva et al., 2008; Gómez-Silva, 2010; Artieda et al., 2015; Wilhelm et al., 2018; Kereszturi et al., 2020).

The Andes Mountain arise from the subduction of the Nazca plate beneath the South American Plate since the Upper Triassic—Early Jurassic (Haschke et al., 2002; Haschke et al., 2006). The subduction activity created the Andean arc magmatism, which has been practically continuous to the present (Charrier et al., 2007). Along this geological time span different paleogeographic changes took place. The physiographic provinces change with latitude but follow a general discontinuous pattern of N-S trending orogens separated by intermontane valleys. In Northern Chile (~18° S to 27° S), the order from west-to-east is the Coastal Cordillera, the Central Depression (Longitudinal Valley), the PreCordillera, and the Preandean Depression (Salar de Atacama/Salar de Punta Negra Depression), the Western or Volcanic Cordillera, which overlies the Altiplano-Puno of Northern Chile and, in Argentina, the Eastern Cordillera or Cordillera Oriental (Eocene to Pliocene), and the Subandean

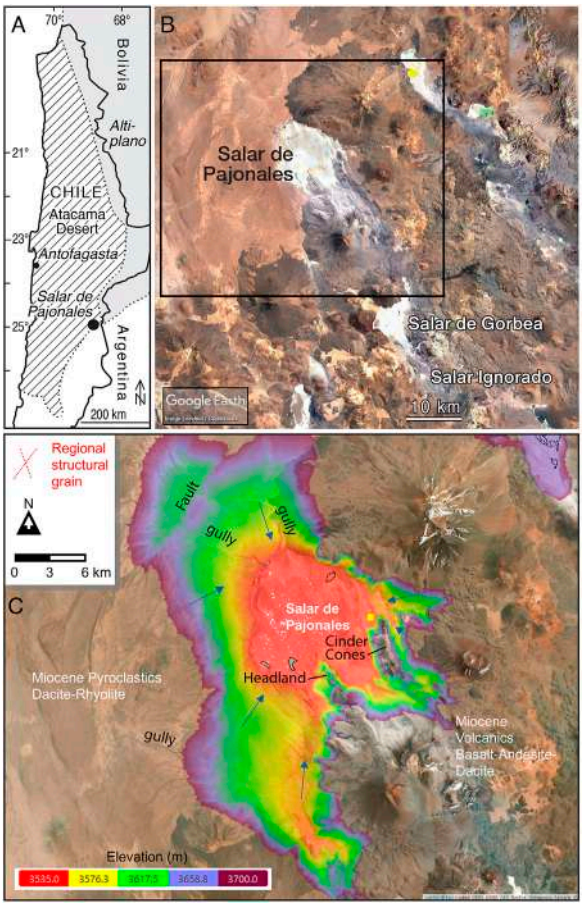

FIGURE 1 | Location of study area. **(A)** Map of Chile. **(B)** Overview of Salar de Pajonales. **(C)** Truncated digital elevation model (DEM) of the study site composed in the Cartalytics (www.cltix.com) spatial data software; aerial imagery is downloaded from the Leaflet open-source library (https://leafletjs.com/).

[1]It should be noted that this high elevation desert is known as the Puna in Argentina and the (Chilean) Altiplano in Chile and Bolivia, and is sometimes referred to as the Atacama Altiplano or as an extension of the Atacama Desert in Chile (e.g., Farias and Acuña, 2020; Wierzchos et al., 2020). This observation is provided to clarify the physiographic location of Salar de Pajonales relative to other high-elevation study sites.

and Santa Bárbara Ranges (Jordan et al., 1983; Rehak et al., 2010; DeCelles et al., 2015; Quade et al., 2015; Reiners et al., 2015; Chong Diaz et al., 2020; Wierzchos et al., 2020).

The physiographic regions of Northern Chile (18°–27°S) are characterized by a temporal and compositional progression of Cenozoic salt deposits at the surface most often expressed as salt flats (e.g., Artieda et al., 2015; Finstad et al., 2016; Alonso and Rojas, 2020; Chong Diaz et al., 2020). In west-to-east order, the Coastal Range hosts the oldest salt flats; these are inactive and fossilized. Inland to the east are the salt flats of the Central Depression and the Preandean salt flats located at the western border of the Precordillera (i.e., Salar de Atacama). The youngest are the Andean salt flats and saline lakes emplaced in basins of the Altiplano.

Salar de Pajonales is located in the Altiplano at the foothills of the Sierra de Varas, which form the western side of the endorheic depression (Riquelme et al., 2007; Pfeiffer et al., 2018). Miocene to Recent volcanoes of the Western Cordillera form the salar's eastern border (**Figure 1**).

Oligocene to Holocene volcanic rocks of the Altiplano comprise basaltic to dacitic and rhyolitic extrusives that erupted from 10–11 Ma to <1 Ma (DeCelles et al., 2015), and volcanic activity continues today (Quade et al., 2015). The main eruptive centers near the salar are Lastarria to the east and Llullaillaco to the north in the Western Cordillera (Risacher and Alonso, 2001; Robidoux et al., 2020) (**Supplementary Figure S1**). Lastarria has not erupted in recorded history but continues intense fumarolic activity (Global Volcanism Program, 2013). Llullaillaco erupted most recently in the 19th Century (Casertano, 1963). This volcanic activity influences the chemistry of the adjacent salars (Risacher et al., 2003; Chong Diaz et al., 2020). Salar de Pajonales is thus set within the wider Andean landscape (Artieda et al., 2015) of sulfur-rich volcanic, hydrothermal, lacustrine, and aeolian deposits (Chong Diaz et al., 2020).

Salar de Pajonales is a hydrologically active evaporitic system. Brines that fill the remaining active lagoons in the lower elevation portions of Salar de Pajonales are formed by a combination of atmospheric aerosol input, volcanic emissions, chemical weathering of country rock, and high rates of evaporation relative to precipitation (Risacher et al., 2003; Chong Diaz et al., 2020; Otalora et al., 2020; Pueyo et al., 2021). During the transition to the more arid climate of today, episodic evaporation of the brines and inundation of the basin left an evaporite package several meters thick (**Figure 2**; see below). At present, the basin receives recharge from both surface water (Risacher et al., 2003) and, by inference from other endorheic basins, groundwater, which originates from the volcanic arc of the Andes to the east (Urrutia et al., 2018; Chong Diaz et al., 2020; Pueyo et al., 2021).

1.2 Climate

Climate records, extensively reviewed by Pfeiffer et al. (2018) from the Atacama Desert, Altiplano, and Puna indicate wet periods since the Pleistocene, most notably during the Minchin phase (35–23 ka), the MIS 2 (~26.5–22 ka), the Tauca highstand (~17.5–15 ka), and in late glacial times (i.e., Younger Dryas, 13–10 ka; Coipasa, ~13–11 ka) (e.g., for Chile: Geyh et al., 1999; Ward et al., 2015; Ward et al., 2017; Pfeiffer et al., 2018; Palacios et al., 2020)[2]. At present, there are no confirmed glacial

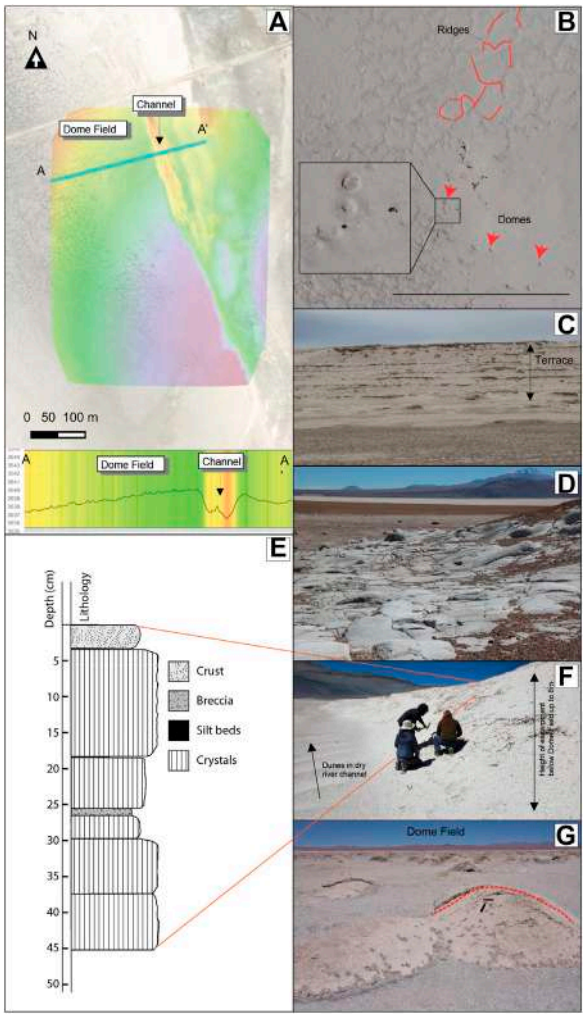

FIGURE 2 | (A) Shaded DEM of study area with A-A′ elevation transect. Maps and cross section were created in Cartalytics (www.cltix.com); aerial imagery is downloaded from the Leaflet open-source library (https://leafletjs.com/). **(B)** Air photo of study site with Domes (red arrows) and randomly oriented ridge segments that connect to form irregular Megapolygons (outlined in dashed red lines). **(C)** Paleoterraces of exposed gypsum beds. **(D)** Rhyolite surface eroded by abrasive flooding. Field of vew ca 25 m. **(E)** Drainage cut through gypsum bed looking south. The Dome Field is to the right on the top of the gypsum terrace. **(F)** Stratigraphy column illustrating cyclic deposition in the upper 0.5 m of salar surface at the Dome Field. The surface layer is a coherent but breakable crust of cemented grains extending downward between crystals from the underlying layer. Crystal beds are vertically oriented selenite. Silt beds are thin, recessive laminar beds comprising detrital crystals and grains. Breccia layers comprise flat lying selenite that is very friable. **(G)** Dome field looking west. A dashed red line highlights the dome in the center right.

[2]The dates are somewhat different to the east in the Bolivian Altiplano, but the sequence remains the same (Chepstow-Lusty et al., 2005).

landforms recorded in the Salar de Pajonales area (Palacios et al., 2020), suggesting that glacial processes did not directly influence the basin during the last glacial period. Gypsum beds exposed in paleoterraces testify to higher lake stands and thicker lake fill, much of which has been removed by surface runoff (**Figures 2C,E**).

During the late glacial wet periods, precipitation is inferred to have been 2–5 times higher than present day (~200 mm/yr; (Grosjean et al., 2001; Latorre et al., 2006; Ward et al., 2015). Lake levels in the Altiplano reached their maximum between 10.8 and 9.2 ka and disappeared sometime between 8.4 and 8.0 ka (Geyh et al., 1999). Since then, the climate has been extremely arid except for brief wetter periods, the most recent being probably from the same time (1.39+/− 0.10 ka) as that of the Gorbea and Ignorado salt flats located ~40 km south of Salar de Pajonales and at higher elevation (**Figure 1**; ~4000 m asl (Pueyo et al., 2021). Other climate records, found in fossilized rodent middens, wetland deposits, and archeological sites also reflect wetter time periods within the last 90 ka (Chepstow-Lusty et al., 2005; Maldonado et al., 2005; Díaz et al., 2012; Pfeiffer et al., 2021).

Historic, significant rainfall events, which occur episodically, flood salar surfaces and lead to increased biodiversity (Schulze-Makuch et al., 2018; Ortega et al., 2019; Pfeiffer et al., 2021). The frequency and intensity of these freshening events have changed over the last 106 ka based on a 100 m core from Salar de Atacama (Bobst et al., 2001). Such events are controlled by the complex hydrometeorological patterns of the southern Pacific Ocean. The more usual configuration of SE Trade Winds bringing moisture-depleted air over the Andes is disrupted episodically (Garreaud et al., 2009; Diederich et al., 2020). These interruptions are known as El Niño events, which are linked to high sea-surface temperatures in the eastern Pacific Ocean (Garreaud et al., 2009; Bozkurt et al., 2016; Urrutia et al., 2019). This relatively common weather pattern, which is part of the El Niño Southern Oscillation (ENSO), disrupts the southeasterly trade winds and allows moist air to flow inland from the warm Pacific Ocean leading to austral winter precipitation events in parts of the Atacama desert (Houston and Hartley, 2003; Houston, 2006; Diederich et al., 2020; Meseguer-Ruiz et al., 2020). However, El Niño events have a different effect on the Altiplano. There they lead to negative precipitation while La Niña years yield wetter seasons (Garreaud et al., 2003; Urrutia et al., 2019). These extreme events are associated with the Madden-Julian Oscillation during which sea surface temperatures increase in the southeastern Pacific Ocean, effectively blocking the normal westerly Ferrell-cell flow and diverting moisture toward north-central Chile (Ortega et al., 2019). Monsoonal summer rain events are tied to normal northeasterly airflow from the Atlantic Ocean, over the Amazon basin, and to the Andean mountain range (Garreaud, 2000; Garreaud et al., 2003; Diederich et al., 2020).

Salar de Pajonales lies in the Arid Diagonal on the divide between regions of dominantly winter rain (generally to the west and south) and dominantly summer (monsoonal) rain (generally to the east and north) (Betancourt et al., 2000; Diederich et al., 2020; Hooper et al., 2020; Palacios et al., 2020, see their **Figure 1**) and is subject to infrequent freshening events (Bozkurt et al., 2016). Recent rainfall events caused significant flooding and destruction along rivers in the southern reaches of the Atacama Desert (Barrett et al., 2016; Bozkurt et al., 2016; Wilcox et al., 2016; Valdés-Pineda et al., 2017; Cabre et al., 2020) but were insufficient, in large part, to mobilize hillslopes. Most fluvial features suggest that much larger rain events occurred in the Pleistocene (Pfeiffer et al., 2021). At that time, large river systems drained westward into the Central Depression (Garcia et al., 2011). Unlike the Calama Basin where the Rio Loa cuts through the Domeyko Cordillera (De Wet et al., 2020), there is no geomorphic evidence of large rivers that drained to the Pacific Ocean from the Salar de Pajonales area. However, post-glacial flooding events are inferred along the eastern and much of the southern margin of the salar where large portions of volcanic rhyolitic basement are eroded flat by abrasive flooding (**Figure 2D**, Chong Diaz, unpubl.).

2 METHODS

Here, we used field observations to spatially resolve surface features that can be explored for different textural surfaces as defined by distinct physical, chemical, and hydrological conditions. Detailed descriptions are provided in the figure caption illustrating each characteristic (see below). Additional laboratory analyses confirmed and augmented field observations. This paper relates and refers to two other works that present results about the surface features, the threshold for detection from drone and satellite imagery, and on the distribution of microbial colonies within habitats (Phillips et al., 2021 in prep.; Warren-Rhodes et al., in review).

2.1 Site Selection

The Dome Field study site is in the eastern area of Salar de Pajonales. It stands about 8 m above a dry river channel that bounds the study area on the eastern and southern sides (**Figure 2**). From the study site, the salar surface slopes irregularly toward the west eventually giving way to water-saturated salt flats and ponds. Within the larger Martian analog site, this Dome Field was selected because of the presence of endolithic photosynthetic microbial communities (Warren-Rhodes et al., in review). The features described herein provided visual access to the subsurface allowing us to probe the processes leading to the development of the surface morphology.

2.2 Field observations

Visual observations of the shape, size, and distribution of surface features were made during three field campaigns (Oct. 2016–Oct. 2019).

2.3 Aerial imagery

Aerial images were collected with a Phantom 4 Professional drone at an elevation of 120 m above the salar surface, which corresponds to a ground sampling distance of ~2.5–3.0 cm. An orthophotomosaic (OPM) and digital elevation model (DEM)

were generated from the images using Pix4D, a structure from motion software package, to enable measurements and analyses of landforms and textures. See Phillips et al. (2021) (in prep.) for additional information.

2.4 Sample Collection

Fist-sized samples were collected from the surface down to a maximum depth of 12 cm with a rock hammer and placed in plastic bags. The samples were selected to represent the range of surface types and textures.

2.5 Photomosaic

Samples were photographed with a hand-held camera (Sony alpha 6,000) and/or a Insight Spot 4 camera (Diagnostic Instruments, Sterling Heights, MI) mounted on a Leica MZ95 stereoscope (Wetzlar, Germany). Photomosaics were prepared using the Adobe Photoshop automated merge function.

2.6 X-ray diffractometry

Field samples were analyzed at two laboratories and the results were compared. One set was powdered (<63 μm) and analyzed from 2 to 70°2Θ at a step size of 0.017°2Θ with a PANalytical X-Pert Pro MPD X-ray diffractometer with a Cu X-ray tube (Kα1 1.54060Å, 45 mA, 40 kV). The data were pattern-matched and Reitveld-refined with High Score Plus (Malvern PANalytical, Inc., Netherlands) using the ICDD PDF-4 Minerals database (ICDD, Newtown Square, PA). The other set was powdered (<20 μm) and analyzed from 2 to 65°2Θ at a step size of 0.02°2Θ on a Bruker D8 Advance diffractometer with Cu X-ray tube (Kα1 1.54051Å, 30 mA, 40 kV). The data were pattern-matched with Sieve (ICDD, Newtown Square, PA, United States) and quantified with the software, DIFFRAC. EVA (Bruker, Billerica, MA, United States) using the ICDD PDF-2 and PDF-4/Minerals database. Major minerals were detected (signal/noise 3) by both systems.

2.7 Optical microscopy

Twenty three field samples were selected for thin section preparation to represent different textures and provide spatial distribution. Samples were stabilized with blue-dyed resin and vertically oriented prior to cutting. Single-side polished, 30 μm, thin sections were prepared by Spectrum Petrographics, Inc. (Vancouver, WA, United States). Samples were imaged in transmitted and reflected light modes with a Leica DMLP petrographic microscope equipped with a Leica MC170HD camera.

2.8 Spectroscopy

Raman spectroscopy measurements were performed on a custom Raman spectrometer with a Raman probe (Impossible Sensing, St. Louis, MO, United States). We performed our Raman analyses in the field using optical fibers housed in a single cable to transmit the laser (532 nm) to the sample and to transfer the Raman signal from the sample to a TE-cooled CCD spectrometer and detection system. The recorded spectra were compared to existing spectral databases of minerals (Lafuente et al., 2015). Infrared (IR) spectra were taken with using Thermo Scientific Nicolet iN10 MX FTIR Microscope. Spectra were taken in "reflectance mode." In that mode, the beam passes through the sample, is reflected off the gold surface, and passes through the sample again. The spectrum are absorption spectra, not reflectance spectra, the light passes through the sample. The spectra were taken at 4 cm^{-1} resolution with liquid nitrogen cooling of the detector. Spectra were taken from 7,000 cm^{-1} to 700 cm^{-1}. We used a square IR beam with a width of 75 μm. Powder samples were placed on top of a gold-coated glass slide. The particles were smaller than the beam, so aggregates of particles were observed to maximize signal.

3 RESULTS

Diffraction data from powdered samples showed that the study site comprised almost entirely gypsum (**Supplementary Figure S2**). XRD or Raman and VNIR spectra show additional Ca-sulfate phases, along with small quantities of calcite, halite, magnetite, and plagioclase (**Table 1**, **Supplementary Figure S2**).

These gypsum deposits are bedded on a decimeter scale, and a cyclic deposition can be inferred from the stacking of thin beds comprising well-developed gypsum crystals inter-layered with thinner beds of gypsum breccia (**Figure 2**). The lateral continuity of individual gypsum layers is unknown, but a largely layer-cake stratigraphy within the study area can be inferred.

In this gypsum-dominated environment, surface structures can be distinguished into two groups based on spatial scale (**Table 2**). Macroscale structures have dimensions centered on the meter scale and above. They affect multiple gypsum layers, however, the maximum depth to which these feature extend into the subsurface cannot be determined by our available dataset. These macroscale structures are distinct from centimeter to millimeter scale structures, herein called microscale structures. The latter only affect the surfaces of individual, thin beds. Further, the microscale structures are often superimposed on the macroscale structures. Surfaces of microscale structures have one or more textures at the centimeter to millimeter scale.

All of our interpretations on these geomorphic structures, independent of scale, are based on observations of the surface layer; our data do not allow interpretation of facies stacking and associated morphologic structures with depth.

3.1 Macroscale Structures

Macroscale structures are summarized in **Table 2** and include PolygonRidges, Megapolygons, Domes, and Quasi-Flat areas. We describe these endmembers below but recognize that there is overlap among the structures. For example, PolygonRidges may incorporate Domes as part of their structure.

3.1.1 PolygonRidges

As termed by Phillips et al. (2021), PolygonRidges are the most recognizable structures in the study area (**Table 2**; **Figure 3**). They are elongate topographic features with variable surface texture and generally a maximum of a few tens of meters long (**Table 2**; **Figures 3A,B**). From above, the ridges form a honeycomb pattern (**Figure 2B**). They were defined as

TABLE 1 | Mineralogical detections by different methods.

	XRD	Raman	IR	Petrography
Gypsum	x	x	x	x
Anhydrite	—	x	x	x
Bassanite	—	—	x	—
Halite	x	—	—	—
Calcite	x	—	—	x
Magnetite	x	—	—	—
Plagioclase	—	—	—	x
Chromate	—	x	—	—

structures with a length to width ratio (L:W) value of >2:1 and are said to be continuous when the distance between ridge segments was less than the width of the ridge, i.e., the separation was less than ~ 2 m. PolygonRidge crests fall into two types: intact and eroded (**Figure 4**). In addition to the two crest types, ridges may have rough or spiny (i.e., having extruded crystals) macroscale surface textures, or both (**Figure 3C**); few smooth ridges were observed. These PolygonRidges show no preferred orientation relative to the tectonic stress field as determined qualitatively from aerial photographs and digital elevation models (**Figure 2**).

3.1.2 Megapolygons

Easily seen in drone images, Megapolygons were irregularly shaped and discontinuously bounded by PolygonRidges (**Table 2**; **Figure 2B**). Their interiors were overall relatively flat but might encompass low ridges or small domes with relief of less than 1 m.

3.1.3 Domes

Domes are the most characteristic features in our study area (**Table 2**; **Figures 3A,C**) They are convex-upward, quasi-circular, topographic highs and are defined as structures with 1: 1 < L:W < 2:1 and heights that varied continuously between circa 0.1 and 2.0 m. All domes that breached during sampling had lined convex-upward cavities below the surface gypsum layer. Most Domes had surface cracks, some of which widened into circular holes that connected the cavity to the surface (**Figure 4D**). The ceilings of cavities and edges of the holes were lined with an undulating layer of hard, white gypsum often with fractures and sometimes damp (i.e., moisture was present; **Figure 5D**). The Domes, some of which are partially collapsed, had surface textures that are either uniform or had gradual or abrupt transitions between textures (**Figure 3C**). Some surfaces had micropolygons, which are tiles in which the micropolygon interiors (MP Interiors) are flat and micropolygon rims (MP Rims) demarcate the margins (**Table 2**). These surfaces had combinations of smooth, rough, or spiny textures, which allowed further separation of Domes into sub-types (**Figure 3C**, **Figures 5A–C**).

3.1.4 Quasi-Flat Areas

Quasi-Flat areas have minimal positive relief and constitute the space between Domes and PolygonRidges (**Figure 3A**). Some surfaces comprise rimmed, irregular micropolygons lacking surface texture (smooth) or they are covered with duricrust,

TABLE 2 | Macroscale and microscale structures and textures observed in the field at Salar de Pajonales.

Megascale structures and combinations					
Name	**Dimensions (m)**	**Relief (cm)**	**Length to width**	**Continuity[a]**	**Figure**
Domes	<7.5 diameter	10–200	1:1 < L:W < 2:1	na	3a - ground view
PolygonRidge	<2.5 wide	10–200	>2:1	0–2	3b - ground view
Quasi-Flat areas	10s across	<5	~1:1	0–2	3c - ground view
Megapolygon	10s across	<200	na	0–2	2 aerial view
Macroscale Surface Textures					
	Surface Relief (cm)	**Maximum visible crystal size (cm)**		**Duricrust[b]**	
Smooth	<7	na		1–2	4a
Rough	<10	na		2	4b
Spiny	<20	15–18		0–1	4c
Ridge Types					
Intact	<200	na			4d
Eroded	<100	15–18			4f
Centimeter to Millimeter Scale Structures and Combinations					
Micropolygon (MP)	<2	na		na	5a
MP rims	<2 cm	not exposed	white, brown	0–2	5a
MP interior	<0.5 cm	not exposed	white, tan	0	5a
Microscale Surface Features					
Fractures or cracks	<20 cm	not fully exposed	white, gray, brown	na	5c
Centimeter to Millimeter Scale Surface Cover					
Duricrust, Gypcrete	<2 mm	na	brown, tan	na	6a
Bulbous, Rugosic Texture	<2 cm	na	white, tan	1–2	6b
Spines	up to 15	up to 18 cm	white, tan	0–1	6c
Regolith	<1 cm	up to 18 cm	white to brown to black	0–1	6d

[a]*0 = discontinuous, 1 = continuous with gaps, 2 = continuous.*

[b]*0 = no duricrust, 1 = partial duricrust, 2 = completely covered with duricrust.*

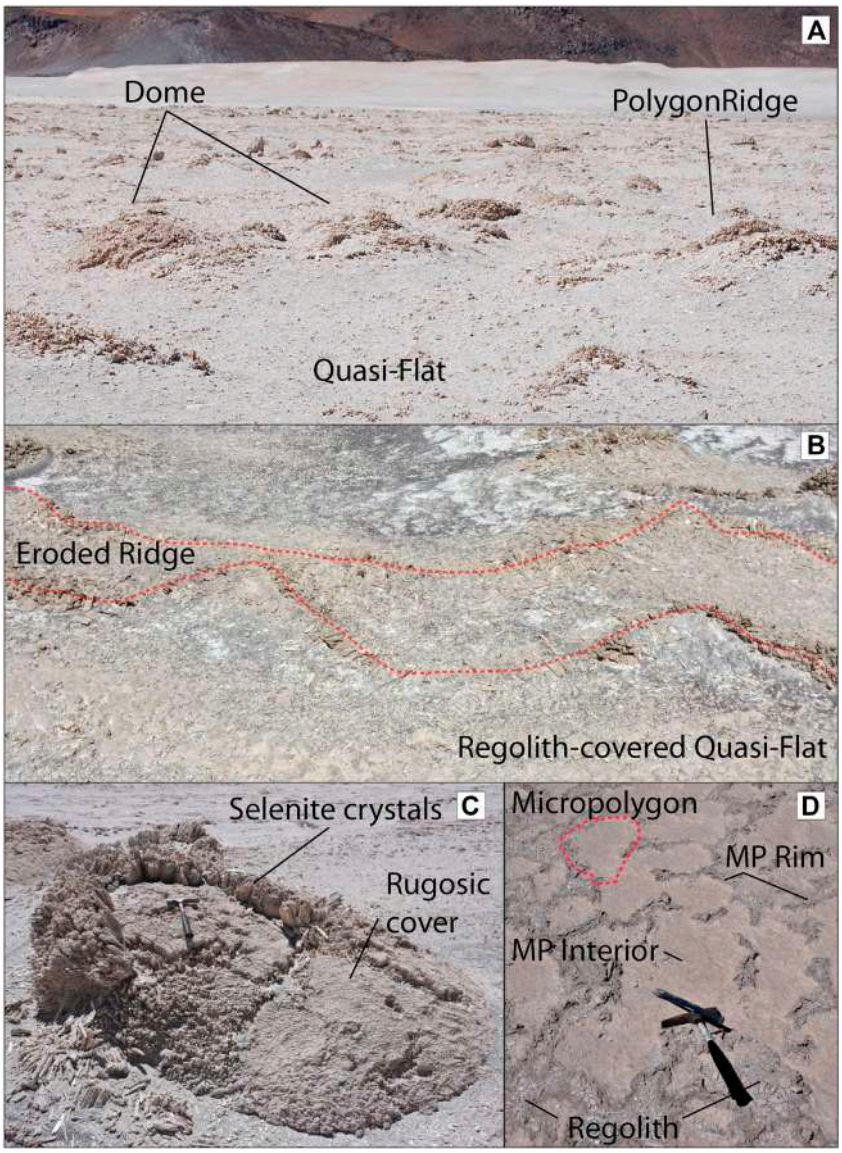

FIGURE 3 | Morphologies of PolygonRidges, Domes, and Quasi-Flats. **(A)** Landscape view identifying PolygonRidges, Domes, and Quasi-Flats. Field of view is ca. 12 m at the bottom edge. **(B)** Ground view of eroded PolygonRidge and regolith-covered Quasi-Flat. Dashed red line delineates eroded ridge margins. On ridge margins, selenite crystals are randomly oriented. Regolith occupies the space between the selenite crystals. Field of view is ca. 8 m. **(C)** Dome with rough surface and fractures. Rough surfaces had combinations of irregular micropolygons comprising MP Interiors, which are irregular tiles with diameters of 10–30 cm that are separated from each other by cracks or rims. MP Rims are narrow (3–5 cm) sinuous topographic highs (<ca. 2 cm). Rough surfaces had a layer of duricrust and/or bulbous (i.e., platey, rugosic, or knobby) cover. Both rough and smooth surfaces (see 3D) had fractures, which were sinuous, semi-continuous cracks that were vertically displaced up to ca. 20 cm. Intact, growth-aligned crystals were visible on the upward-thrust side of the fractures. **(D)** Quasi-Flats with regolith, micropolygons, MP interiors, and MP Rims. MP interiors could be bare, hard, smooth surfaces with selenite crystals truncated across the growth plane or could be covered with regolith. MP Rims were gray/brown, cemented, sand-sized or finer material present as elongate, positive topographic features. The profile of MP Rims comprised a central, grain-filled, cm-scale-deep furrow and two parallel edges that thinned towards and blended into the MP Interiors.

bulbous material, gypcrete (strongly indurated rock comprising gypsum), and regolith (**Table 2**; **Figure 5**). Other Quasi-Flat areas lack micropolygons. These surfaces are covered with duricrust, bulbous material, gypcrete, and regolith, whereas smooth surfaces do not occur. Micropolygons had similar shapes to those present on Domes except that the MP Interiors may be smooth, and the MP Rims appear partly eroded.

3.2 Centimeter to Millimeter Scale Features

Upon closer examination, some macroscale features (i.e., Domes, PolygonRidges, and Quasi-Flats; **Figure 3** and **Table 2**) were not just distinguishable by their large-scale morphology but also by a variety of gypsum types (**Figure 6**).

The most common crystal habit for gypsum is fishtail twinned selenite. Twins are bottom-nucleated and originated from a

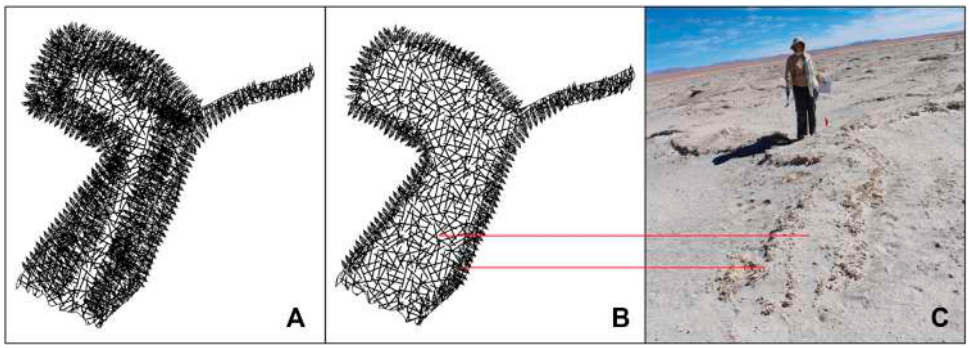

FIGURE 4 | Sketch of intact ridge **(A)** and eroded ridge **(B)**. Intact ridges are short segments of upwardly convex linear structure with rough surfaces as defined for domes and with an intact surface bed (roof), and ii) eroded ridges are defined by two quasi-parallel, sinuous lines of randomly oriented spines of similar length (<18 cm) between which are areas of mixed regolith. **(C)** Image of eroded ridge showing branching form. Person for scale.

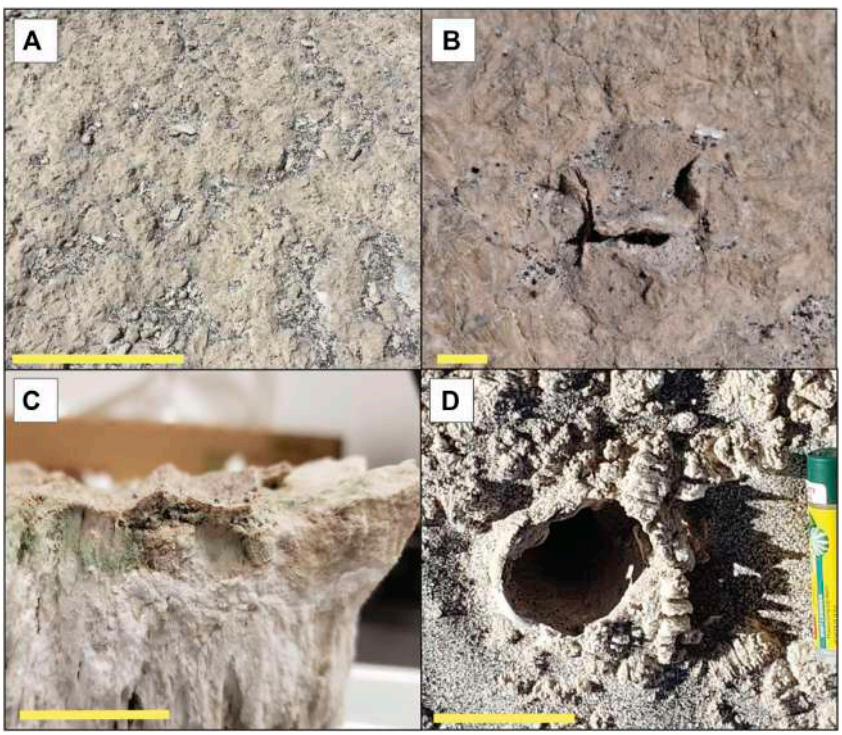

FIGURE 5 | Surface textures and holes. **(A)** View of rugosic texture and regolith from above. Scale bar is ca. 50 cm. **(B)** Partially detached duricrust on smooth surface. Scale bar is 1 cm. **(C)** Partially detached duricrust. Note pigments below duricrust. Scale bar is 1 cm. **(D)** Lined hole in bulbous texture with regolith. Scale bar is 5 cm.

horizontal, likely erosional, surface. They terminate perpendicular to the growth direction at another likely erosional surface (**Figure 6A**). Petrographic analysis reveals growth fronts visible in hand specimens and in thin sections of the crystals (**Figure 6** and **Figure 7**). On spiny dome surfaces, some twinned crystals increase, while others decrease in size resulting in more crystal-nucleation sites at the base of the gypsum layer than extend through the height of the crystal layer. Selenite domains are rigid and coherent.

Alabaster is a less common habit, most often occurring at the bottom of PolygonRidges and Domes at the juncture of these structures and the salar surface but also inter-grown with selenite and filling vertical slot pores (**Figures 6**, **7**). Alabaster was not observed in spines but could be observed associated with un-erupted crystals. When intermingled, alabaster and selenite domains were sometimes difficult to visually distinguish in the field, but the presence of alabaster could usually be determined by its physical properties. Domains

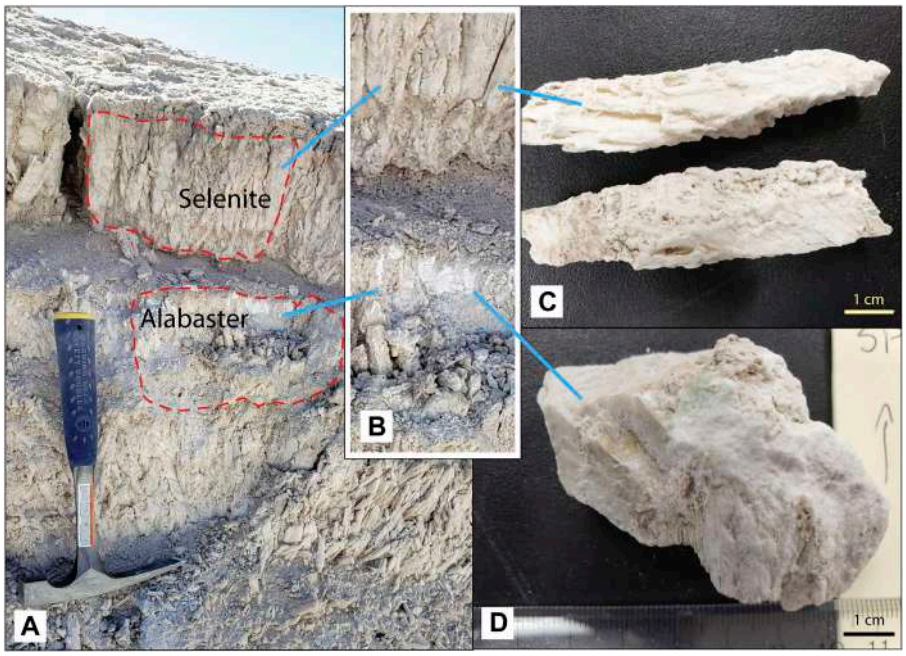

FIGURE 6 | Crystal and alabaster textures. **(A)** Surface bed of in-place crystals caps sediment package with alabaster domains. **(B)** Close up of selenite and alabaster in **(A)**. **(C)** Selenite crystal. Scale bar is 1 cm. **(D)** Alabaster. Arrow indicates up direction. Scale bar is 1 cm.

dominated by alabaster were powdery and easily crumbled between fingers and yet were difficult to break with a rock hammer; the alabaster became somewhat thixotropic under hammer pressure.

Surface cover is present over both habits; duricrust, bulbous texture, rugosic (wrinkly) texture, gypcrete, or regolith is present and could form from a combination of physical (changes in temperature or hydration) and mineralogical (phase changes) as invoked here for larger structures and biological processes (Warren-Rhodes et al., in review). It likely stabilizes the alabaster surface and prevents mechanical erosion. Selenite sometimes has a surface cover (**Figure 5**, **Figure 8**). Duricrust and bulbous texture are diagnostic for the presence of alabaster (Warren-Rhodes et al., in review). Among selenite crystals, those occurring in MP Interiors or on surfaces of smooth and rough domes have duricrust, bulbous texture, rugosic texture, or gypcrete surfaces and are often denser at the surface than at depth, while erupted selenite has surface cover less frequently. Loose material, i.e., regolith, covered some of the surfaces.

Taken together, the observations across spatial scales record a history of conditions/mechanisms causing morphologies at the macroscale (Domes, PolygonRidges, Megapolygons, and Quasi-Flats) and microscale (surface-cover type and selenite or alabaster crystal domains).

4 DISCUSSION

Our observations suggest a strong inter-dependency between small and large spatial scale features that we interpret to be controlled by extrabasinal changes in environmental conditions (e.g., relative humidity, precipitation, and temperature as controlled by climate). The environmental parameters may include precipitation-evaporation balance changes and thermal cycles and most importantly, internal processes of hydration/dehydration, efflorescence/deliquescence, and recrystallization typical for chemical sedimentary systems.

This section first discusses the macroscale features, followed by the microscale features, the origin and timing of their formation, and lastly the implications for Mars exploration.

4.1 Processes Controlling the Formation of Macroscale Features

4.1.1 PolygonRidges and Megapolygons in Salars

PolygonRidges as geomorphic features can form through a wide variety of geologic processes, including warping due to pressure or shrinkage caused by tectonic or other processes, during deposition, and as remnants of erosion. The gypsum ridges in the salar are part of a polygonal network that enclosed Megapolygons without any aligned distribution (**Figure 2B**). All PolygonRidges were about the same height. We attribute this to ongoing constructional processes in the salar that exceed erosion rates.

Tectonic and volcanic processes in the actively uplifting Cordillera are constantly at play. However, the dominant regional structures related to the ongoing tectonic shortening and uplift are oriented in a NE-SW and NW-SE direction (**Figures 1B,C**), whereas the polygonal patterns are not aligned. The Dome Field itself is aligned with a series of

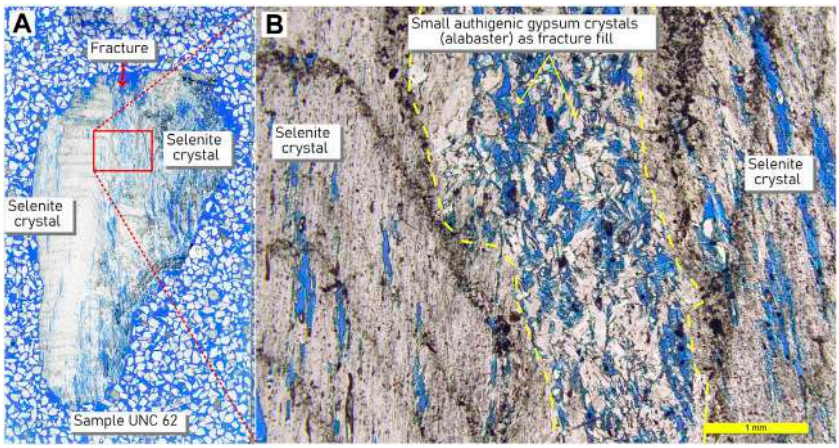

FIGURE 7 | Petrographic thin section showing growth fronts in selenite crystal habit. **(A)** Scan of petrographic thin section. **(B)** Close-up of area within red box in A. Selenite crystal with growth fronts and small patches of alabaster with slot pores. Such growth fronts were ≤2 mm thick and comprised an opaque black layer separating layers of selenite gypsum. Pores can be filled with intraclastic gypsum grains, secondary gypsum crystals, and/or volcanic detritus and may be adjacent to alabaster domains. Slide background is a mixture of mineral grains to show slide thickness during preparation.

cinder cones that are strung along the direction of one of the main regional structural grains (**Figure 1**). However, tectonic forces act on long timescales, and a degradation of ridge axes would be expected to reflect their erosion between tectonic events, contrary to the observed roughness on the ridges and overall high topographic relief. Although some PolygonRidges were over 100 m long, most measured tens of meters in length but maintained an overall consistent height. Tectonic ridges that comprise fault scarps related to regional forces would be expected to have lateral continuity of hundreds of meters and kilometers with heights that scale to the length and taper towards the tip of the faults. No such continuity is observed on the relatively local scale of the ridges in the Dome Field, and we do not attribute the PolygonRidges to tectonic forces.

Instead, we propose the PolygonRidges in the Dome Field reflect intrabasinal volume changes associated with wetting and drying cycles, i.e., hydration-dehydration or recrystallization cycles, along with increases in salt volume during transport and evaporation of saturated brines. **Figure 9** illustrates gypsum-specific processes based on Warren's (2016) model for ridge formation in evaporites; a model we propose is largely apropos to ridge formation in the salar. The original salar surface formed during a time of inundation, has become exposed, and has since been flattened by mechanical and chemical weathering (**Figure 9A**). Chemical weathering occurs in subsequent rain events during which selenite crystals dissolve and recrystallize into a dense gypsum surface layer (**Figure 6A**). Such horizons in the subsurface can undergo extensive dissolution and reprecipitation, as water chemistry changes, with associated volume changes over time (**Figure 9B**). These horizons can promote lateral water flow and additional salt dissolution to destabilize the salar surface, which leads to the PolygonRidges. The spacing of the ridges would depend on the amount of water flow, and therefore destabilization, in the subsurface; more water flow in the subsurface (volume or frequency) would lead to more closely spaced ridges, i.e., smaller Megapolygons.

4.1.2 Domes in Salars

Domical structures within an evaporite basin can form by several processes that largely hinge on volume changes associated with wetting and drying cycles, with an associated change in salt volume during dilution and evaporation of saturated brines.

Domes are common features in gypsum evaporites (Warren, 2016). Their origin is most often attributed to volume changes associated with recrystallization brought on by cycles of hydration-dehydration reactions. The details of this process vary. Artieda (2013) suggests that after *in situ* dissolution and precipitation events, secondary gypsum fills pores, increasing volume and pressure, leading to lateral gypsum expansion to form domes, called "tumuli." Calaforra and Pulidobosch (1997) offer the alternative that the volume increase is caused by recrystallization from anhydrite to gypsum. They agree with Artieda (2013) that infilling the gypsum matrix within macro-crystalline gypsum could also cause the volume to increase. Gutiérrez (2005) suggests that tumuli may form from changes in volume due to wetting and drying of a thin layer below the surface gypsum bed, which Warren (2016) attributes to efflorescence within the surface bed. We propose a very similar genesis—i.e., the result of volume changes in the evaporites during multiple hydration cycles—for the formation of the domes in the salar. This leads to warping of the salar surface.

Warping only affects the uppermost gypsum bed giving clear evidence for a control associated with surface processes, rather than deep-rooted tectonic forces. Textural transitions also occur on the sub-centimeter scale. As a result, we agree with Warren (2016) and attribute the presence of alabaster in the proximity of or filling small cracks in the deformed selenite crust to efflorescence (**Figure 7B**). Efflorescence involves the precipitation of salt from brine. The brine is transported as

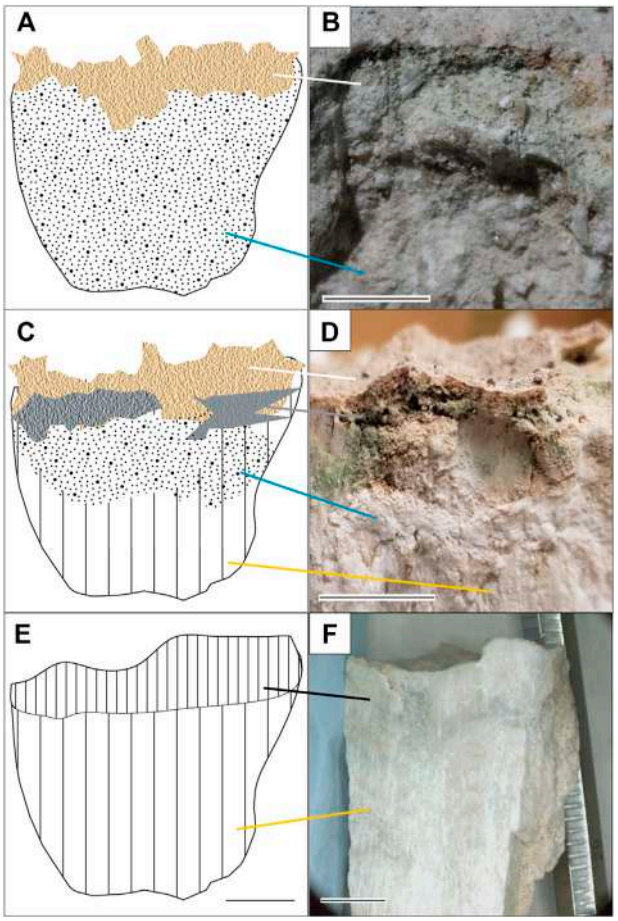

FIGURE 8 | Surface textures on gypsum. **(A)** Duricrust comprises a tan crust (white line) that overlies and is fully attached to the alabaster gypsum surface (blue line). Gypsum may have either selenite or alabaster habit, but alabaster is used here to match the image. Scale bar for **(A,C,E)** is ca. 1 cm. **(B)** Image of duricrust. Scale bar is 1 cm. **(C)** Bulbous texture comprises detached duricrust (white line) over the gypsum surface, which is drawn here as alabaster (blue line) above selenite (yellow lone) to match the example. Gray line connects void space beneath the detached crust. Duricrust and bulbous texture are diagnostic for the presence of alabaster (Warren-Rhodes et al., in review). **(D)** Image of duricrust and bulbous texture. Scale bar is 1 cm. **(E)** Gypcrete comprises a denser selenite texture (black line) where pore space has been filled with secondary gypsum. Gypcrete overlies selenite (yellow line). **(F)** Image of gypcrete. Scale bar is 1 cm.

salt-saturated vapor until it condenses in pores. When conditions become warmer or dryer, the water evaporates again, leaving the salt behind to increase the mineral volume. The presence of anhydrite remnants in some of our samples suggests episodic complete dehydration of the Ca-sulfate phase. The decrease in volume associated with the dehydration (recrystallization to anhydrite) and increase in volume with subsequent hydration (recrystallization to gypsum) is another process we consider as a mechanism for dome formation. These processes could be aided by accompanying changes in brine chemistry brought about by changes in volcanic activity and groundwater recharge. Consequently, a water-related process, one with multiple episodes of wetting and drying, is the most reasonable explanation for the formation of tumuli in the salar, an explanation in line with the formation processes proposed for similarly sized tumuli elsewhere (Gutiérrez and Cooper, 2013). Holes, interpreted to be gas vents lie within two larger gas domes and provide individual sites for water vapor and gas exchange leading to focused warping to form Domes (Hofmann et al., in review).

4.1.3 Quasi-Flat Areas in Salars

Quasi-Flat areas had surface characteristics different from Domes and PolygonRidges except for the presence of polygonal features, which could be found on Domes. Rims separate MP Interiors on the solid, quasi-flat salar surface. The arrangement of the MP Interiors and rims forms the "patterned ground" referenced in Phillips et al. (2021) and Warren-Rhodes et al. (in review).

The MP Interiors and MP Rims (**Table 2**) may have formed during wetter times if thin microbial mats had covered the surface of the shallow salar. Wetting and drying cycles may contribute to both abiotic and biological processes during which a thin surface layer experiences cycles of hydration and

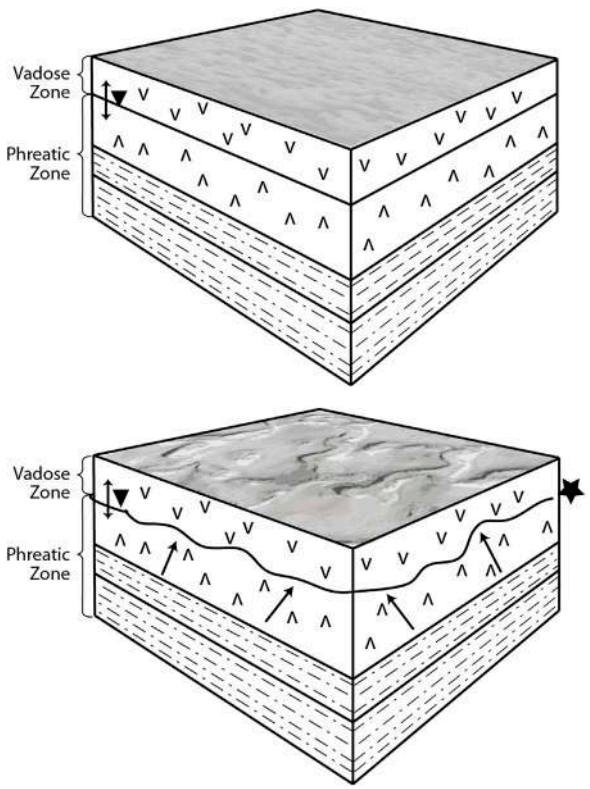

FIGURE 9 | Drawing of proposed sequence of ridge formation. The upper sketch is the starting point for the evaporitic-sediment package. The inferred basal lakebeds become more salt-rich (calcite, gypsum and halite (^s) with increasing evaporation. The gypsum surface beds (^s) form during freshening events. The lower sketch shows a somewhat wetter time when the Ca-Na-Cl-SO_4 mixture (highlighted by ★) precipitates minerals that force the surface upward (arrows) forming expansion ridges in pseudo polygonal patterns. Modified from Warren (2016).

dehydration, leading to development of rims around polygonal tiles, called tepees (mainly abiotic origin) or petees (mainly biotic origin) (Noffke, 2010; Warren, 2016). In the Dome Field, elevated micropolygon margins and shrinkage cracks are both present, forming irregular rims of sand-sized and finer particles bound together by tan to gray gypsum cement. The sometimes smooth, interior flat surfaces may crack secondarily into shrinkage structures, exposing the barren deposits beneath. Both the surfaces of the micropolygons and MP Rims have been abraded by wind and degraded by episodic rain events during which water pools in MP Interiors and infiltrates preferentially into rims (Warren-Rhodes et al., in review). Although our data do not yet allow us to determine the biogenic or abiotic origin of these flats and micropolygons, the laminae size, occurrence of microbial layers, and the substrate composition (gypsum) suggest that physical processes might play the primary role while biologic processes might be secondary and may serve to exaggerate the physically induced micro-morphology.

There are alternative explanations for the formation of micropolygons. Artieda et al. (2015) report different types of halite polygonal structures in Salar Grande and Yungay basins and attribute the differences to an evolutionary process whereby regular, flat polygons transform first into well-developed tepees with open, axial troughs and then into nodular, heavily uplifted, highly deformed, fin-like near vertical structures with distinct internal zonation. Deliquescence serves to enrich the salt content along the margins of the polygons and increasing the height of the rims (Artieda et al., 2015). These structures appear to require deliquescent salts and limited precipitation and would be incompatible with the much less soluble Ca-sulfate matrix, although we cannot rule out that other salts played some role. Nevertheless, the structures observed at the Dome Field do not require such processes.

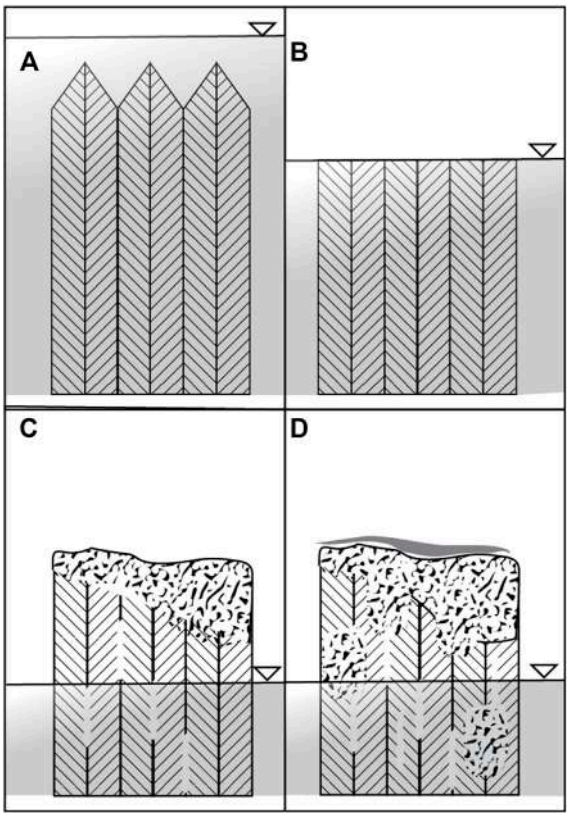

FIGURE 10 | Scenario for textural changes in gypsum at the salar surface caused by climate change, which is depicted as a change in water table elevation and the thickness of the saturated zone (shaded area). **(A)** Bottom-nucleated selenite forms on the bed of a shallow saline lake. **(B)** The surface is eroded during arid times. Changes in the water table lead to variable saturation and salt transport in vadose zone. **(C)** Surface crust and slot pores develop. **(D)** Additional alabaster zones develop further enhancing water availability.

4.2 Centimeter and Millimeter Scale Features

Mineralogical transformations between gypsum, the dominant mineral, and its dehydrated form, anhydrite involve a 39% change in volume (Jowett et al., 1993); gypsum dehydrates to the denser anhydrite leading to slot pore formation on a millimeter scale and surface-crack formation and structural collapse on a centimeter to meter scale. Cracks then enable water transport leading to rehydration of anhydrite to gypsum. These dehydration-rehydration cycles lead to expansion and contraction of the salar surface (Charola et al., 2007). In addition, salts accumulate at the surface by efflorescence, increasing the volume of solids at the surface. Associated deliquescence results in a decrease in volume of solids at the salar surface. All three processes—recrystallization, dehydration-hydration, and efflorescence - are probably at work, and all three point to the role of water, and therefore climate, on the surface morphology.

Changes in mineral habit affect porosity (Yilmaz and Karacan, 2005) and thus the ability of the gypsum materials to transport water (Koponen et al., 1997). Thus, the more porous alabaster has greater permeability than does less porous selenite. The sequence of wetting and drying cycles leads to the current distribution of selenite and alabaster habits (**Figure 10**). In the initial stages, bottom-nucleated selenite formed on the bed of a shallow saline lake during freshening events. During more arid times, the surface would be eroded. Climate could drive changes in the water table, which, along with surface precipitation, could cause variations in the depth and saturation of the vadose zone. Temperature could also play a role. Meteoric water could infiltrate and freeze in the surface layer as temperature decreases (Warren-Rhodes et al., in review). The associated volume changes could lead to formation of slot pores further enhancing water transport and retention.

Quasi-Flat areas and Domes have either smooth surfaces or low relief covers of duricrust, bulbous cover, or gypcrete. Duricrust forms during lithification of biological soil crust, by physical deposition processes (Davis et al., 2010) or by capillary migration and evaporation of soil water (Wierzchos et al., 2011). At the Dome Field, there is ample evidence microbial communities populate the shallow subsurface even under

today's hyperarid conditions (Warren-Rhodes et al., in review). We can infer that, during wetter times, microbial mats may have covered the salar surface as they do in other saline environments (Des Marais, 2010; Noffke, 2010). The EPS from the mat would have bound detrital grains from volcanic and local sources (Noffke, 2010) and been in contact with salt-saturated solutions, either halite or gypsum, depending on the degree of concentration. Gypsum-saturated solutions would infuse the microbial mat and serve to lithify the EPS prior to saturation with respect to halite. The detritus-bearing surface layer points toward the relevance of EPS mineralization as a process for forming duricrust at the Dome Field. However Wierzchos et al.'s (2011), model describes duricrust formation in systems saturated with respect to halite, which is much more soluble than gypsum. Warren-Rhodes et al.'s (in review) model promotes capillary migration as a cause for the formation of a denser gypsum surface layer, i.e., gypcrete, but does not mention formation of duricrust. Efflorescence also has a role in shaping the salar surface. As a potential cause for dome formation (Warren, 2016), efflorescence may contribute to the formation of gypcrete and bulbous cover by transporting salt-saturated solutions to the surface where they deposit Ca-sulfate minerals and change the texture and rigidity of the surface horizon. Bulbous cover likely evolves over time as fresh water from precipitation events seeps into slot pores leading to recrystallization from selenite to alabaster. Over time, the surface becomes knobby, and such knobs would indicate where alabaster would be found (Warren-Rhodes et al., in review).

4.3 Origin and Evolution of Surface Forms—The Role of Water

The surface structures and textures at the Dome Field record a history of hydrological changes that affect the mineralogy and volume of Ca-sulfate in beds that comprise the salar surface and are visible as paleoterraces (**Figures 2C,E**). Several mechanisms for surface structure formation are presented in **Table 3**. The most likely scenarios involve water-related processes.

Changes in groundwater lead to Megapolygon-defining surface ridges due to expansion and contraction in response to mineral precipitation. Cycles of wetting and drying accompanied by vapor exchange in vents or salt cones lead to focused warping of the surface Ca-sulfate bed to form Domes, i.e., tumuli. Water ponds in Quasi-Flat areas lead to smaller polygonal patterns of tepees, petees, and shrinkage cracks. In the course of their formation, mineralogical transformation and recrystallization affect the texture and porosity of the surface material. The transition from primary selenite crystals to secondary alabaster is accompanied by a change in porosity that would enable water transport. Indeed, water is the driving factor in the distribution of photosynthetic life among all macro- and micro-scale structures at Pajonales (Warren-Rhodes et al., in review). Evidence of this selenite-to-alabaster transition takes the form of surface textures: duricrust, bulbous cover, and gypcrete are indicators of selenite-alabaster transitions. These climate-related changes in hydrological conditions are evident at the macro to microscale at the Dome Field.

The timing of formation remains uncertain. It is not entirely clear whether PolygonRidges and Domes are contemporaneous. One observation would suggest that the PolygonRidges predate the Domes: intact ridges are rare and most are eroded, unlike domes for which a substantial number are intact. Most of the ridges have collapsed, which suggests loss of structural integrity and eroded to axial deposits of intraclastic selenite detritus and regolith (**Figure 4**). It is possible that this collapse is linked to climate-related, water-table-elevation cycles, which caused dissolution of salt or hydration and dehydration of mixed chloride-sulfate salts in the subsurface (Bishop et al., 2021) that led to volume changes and destabilization of the surface (**Figure 9**). This would lead to linear features creating quasi-tiles, such as, PolygonRidges and Megapolygons. In contrast, more local focii would lead to circular features, like Domes, which would accommodate the volume changes from a central point rather than from a landscape-scale pressure field. This would suggest that the PolygonRidges represent longer-term processes, which would explain their degraded condition. An alternative observation is that Domes have a shape with more structural integrity than do PolygonRidges and therefore, would not rule out contemporaneous formation and must be considered, along with genetic mechanisms.

4.4 Implications for Mars Exploration

Salar de Pajonales is an excellent analog for evaporitic basins on Mars because of its high UV radiation, relatively thin atmosphere, broad diurnal and annual temperature variations, volcanic and hydrothermal activity, mineralogy, morphology, geomorphology, salt abundance, and aridity (Cabrol et al., 2001; Bada et al., 2003; McKay et al., 2003; Wettergreen et al., 2005; Grunthaner et al., 2006; Warren-Rhodes et al., 2007a; Warren-Rhodes et al., 2007b; Cabrol et al., 2007; Piatek et al., 2007; Gómez-Silva et al., 2008; Cabrol et al., 2010; Cabrol and Grin, 2010; Fairen et al., 2010; Fiahaut et al., 2017; Cabrol et al., 2018; Wilhelm et al., 2018). Our evidence suggests that repeated wetting and drying cycles are responsible for the geomorphic and petrographic characteristics of surface structures at the Dome Field.

PolygonRidges and Domes are topographic modifications caused by wetting and drying of Ca-sulfate salts on the existing salar surface and in the subsurface. The effects of water on the volume changes in Ca-sulfate minerals, coupled with the ability of gypsum to form indurated beds, may be key to the formation of these macroscale surface structures (Domes, in particular); we are not aware of any occurrences of Domes in exposed evaporite beds dominated by minerals other than gypsum. Changes on the microscale are equally important. Specifically, the changes in porosity and pore structure signal the effects of water on the habit, texture, and mineralogy of the gypsum beds. Pores isolated by reprecipitation, efflorescence, or mechanical closure might serve as micro-reservoirs. Consequently, it may be possible that gypsum evaporite beds and structures could retain water in pore spaces or along crystal surfaces despite overall salar desiccation. Thus Ca-sulfate surface structures could pinpoint evidence of water-related processes and mimic surface patterns—"patterned ground" or "polygonal

TABLE 3 | Possible mechanisms for formation of the macroscale features.

Structure	Process				
	Tectonic processes	Hydration-dehydration	Salt-mineral recrystallization	Efflorescence-deliquescence	Artesian springs
PolygonRidge	Ridges are not aligned with regional structural grain and are localized	Can result in volume change over a broad area in the subsurface	Can result in volume change over a broad area in the subsurface	NA	NA
Domes	NA	Can provide volume change but needs an alternative mechanism to focus process	Can provide volume change but needs an alternative mechanism to focus process	Can provide volume change but needs an alternative mechanism to focus process	Springs do not produce subsurface hollows and surface warping
Quasi-Flats	NA	Can produce the micropolygons and rims	Can produce the micropolygons and rims	Can produce the cover textures (duricrust, gypcrete, rugosic, and bulbous) micropolygons and rims	NA
	unlikely	NA—not applicable			
	possible				
	likely				

networks"—at mid-to higher latitudes on the Martian surface (Malin and Edgett, 2000; Mangold et al., 2004; Langsdorf and Britt, 2005; Mangold, 2005; Levy et al., 2009). Such polygonal patterned ground manifests itself at two scales at Salar de Pajonales—Megapolygons (tens of meters) and micropolygons (tens of centimeters), which represent the combined effects of polyextreme conditions on salar materials at different spatial and temporal scales.

Terrestrial polygons formed by desiccation processes in playa environments can range from diameters of centimeters (micropolygons) to up to 300 m (megapolygons) (Neal et al., 1968; Brooker et al., 2018). The larger polygons are thought to form by periods of intense evaporation due to increased aridity, combined with lowering of the ground-water table (Neal et al., 1968; El-Maarry et al., 2014; Brooker et al., 2018). Polygonal surface patterns (patterned ground) on Mars range in diameter from meters to tens of kilometers and, like terrestrial polygons, can form by several different processes and reflect a variety of past climatic conditions (Pechmann, 1980; Seibert and Kargel, 2001; Mangold, 2005; Soare et al., 2005; Morgenstern et al., 2007; Soare et al., 2008; Lefort et al., 2009; Levy et al., 2009).

The polygonal surface patterns documented to date on Mars are fairly young (~0.1–1 Ma) and, at low latitudes, have been attributed to thermal cracking (Levy et al., 2009) or, at high latitudes, to freeze-thaw cycles (Malin and Edgett, 2000; Mangold et al., 2004; Langsdorf and Britt, 2005; Mangold, 2005). In their model for low-latitude patterned ground, Levy et al. (2009) propose that cracks form through thermal expansion and contraction of subsurface ice. Ridges form along margins of the cracks leading to the observed polygonal patterns. But such ridges could form by hydrochemical processes as well. An alternative explanation for ridges on Mars may be destabilization of hydrated salts in the subsurface. Bishop et al. (2021) proposed such a model for recurring slope lineae (RSL). In their model, RSL occur as a consequence of seasonal hydration and dehydration of subsurface chloride-sulfate salts leading to slope failure. Ridge formation by a similar process, but over a longer time scale, may be occurring at Salar de Pajonales and would reflect changes in groundwater level (i.e., water table). Elevation changes in the water table could be attributed to changes in groundwater recharge and therefore to climate. Thus, it's possible the megapolygon-scale patterned ground illustrates salt-related expansion and contraction in the subsurface as a function of changes in the elevation of the water table. Similar changes in groundwater may have been common during the Noachian/Hesperian transition on Mars and contributed to the formation of patterned ground.

While PolygonRidge formation reflects changes in the subsurface (tens to hundreds of meters), Dome formation points to wetting and drying cycles at shallower depths (meters to tens of meters). On Mars, volume changes associated with recrystallization, hydration and dehydration, and efflorescence–deliquescence processes could create or modify porosity pathways for water-exchange in the shallow subsurface. Evidence for efflorescence-deliquescence transitions for chlorate salts (Fernanders et al., 2022) supports proposed occurrence of deliquescence on Mars (e.g., Pál and Kereszturi, 2020; Nazari-Sharabian et al., 2020 and references therein). Water exchanged in this manner may point towards oases for life during the last stages of dehydration (Davila and Schulze-Makuch, 2016). Dundas and Mcewen (2010) interpreted mounds observed in Mars Reconnaissance Orbiter (MRO) High Resolution Imaging Science Experiment (HiRISE) camera images as pingos, which are mounds created by over-pressured groundwater that freezes beneath an impermeable layer, usually frozen ground (Angel de Pablo and Komatsu, 2009; Burr et al., 2009). Angel de Pablo and Komatsu (2009) attribute similar structures in the Utopia basin on Mars to pingos as well. On Earth, pingo ponds are often associated with depressions formed after the ice core melts, but pingos in their initial phase are mounds that formed during pressurization of groundwater in the subsurface (Burr et al., 2009). Volume changes in sulfate salts could occur not as a consequence of freezing but rather of changes in water content in Ca-sulfate systems (Warren, 2016). The resulting tumuli occur as tumuli fields, of which the Dome Field is an example. This provides an alternative explanation for the formation of mounds on Mars; one in which an impermeable surface layer is pushed upwards by the force of

mineral transformation, rather than freeze-thaw, processes over time.

Desiccation polygons have been identified at the centimeter scale on the floor of Gale Crater using data from the Mars Science Laboratory (MSL) Curiosity rover (Stein et al., 2018) as well as by both MER Spirit and Opportunity rovers. In Gale Crater, ChemCam Laser Induced Breakdown Spectrometer (LIBS) and Alpha-Particle X-Ray Spectrometer (APXS), identified parallel bedding seams of Ca-sulfate ($CaSO_4$) running through a gray sandstone unit which is overlain by a ~1 cm thick red mudstone unit (Stein et al., 2018). $CaSO_4$ veins run through most of the polygonal ridges and sometimes cut across them. In addition, sulfate-mineralized fractures are present throughout the region and are attributed to hydraulic fracturing (Grotzinger et al., 2014; Caswell and Milliken, 2017; Young and Chan, 2017). The eventual transformation of desiccation cracks into ridges likely formed by persistent flows of sulfate-rich waters through the cracks and eventually formed the ridges. The discovery of these desiccation polygons in Gale Crater suggests a history of oscillating lake levels, which confirms the existence of a paleolake that rose and fell dramatically over time (Stein et al., 2018).

Gulick et al. (2019) studied the gullies and landforms surrounding the central peak of Lyot Crater (~220 km in diameter), which is located on the edge of the Northern Lowlands of Mars (50.4°N and 29.3°E). The crater floor located just to the west of the central peak region marks the lowest elevation (-7,034 m) in the northern hemisphere (50.6030°N, 29.16503°E) (Gulick et al., 2019). It is also the youngest major impact basin on Mars (Amazonian age, <3 Ga; Greeley and Guest, 1987; Tanaka et al., 2014). In their study, Gulick et al. (2019) mapped the gullies and landforms in this region. They identified two scales of polygonal landforms, numerous depressions connected by a system of channel forms that trended downslope, a pristine-appearing 200-m diameter impact crater with lobate ejecta, gullies on the western slope of the central peak, and evidence for a paleolake just west of the central peak region. Because the central peak region would reflect the last vestiges of hydrothermal activity of this large impact crater, the adjacent paleolake likely experienced evaporation similar to Salar de Pajonales. Because current temperatures and pressures are consistent with a climate where liquid water could flow seasonally if present, Gulick et al. (2019) concluded that Lyot's central peak and paleolake region likely provided a unique microclimate where westerly winds blowing across the paleolake deposited water vapor to the central peak's western slopes. Seasonal and hydrothermally induced snowmelt on the slopes could eventually have formed the gullies. As this local hydrological cycle ebbed due to decreasing hydrothermal activity, this region would have formed an evaporative basin similar to that of Salar de Pajonales.

A follow up study by Glines and Gulick (in review) included a more detailed mapping study of the features and landforms in this region of Lyot Crater floor. In additional to several other features, they characterized the two types of polygons. The first being the low-centered dark-toned polygons with prominent raised ridges, which are up to ~10 m in diameter and are located downslope of the system of depressions and channels. The second type are fractures outlining extensive high-centered polygons ~500–1,000 m in diameter located in light-toned regions. These are located southeast of the central peak region and were mapped in the original Gulick et al. (2019) study. Although, HiRISE would not have resolved the cm-scale polygons identified in Salar de Pajonales, polygons were identified down to the HiRISE meter-scale spatial resolution. Surface exploration of this young, low elevation region might reveal additional smaller scale features similar to those identified in Salar de Pajonales.

El-Maarry et al. (2014) completed a systematic study of potential desiccation polygons (PDPs) from orbit using images from the HiRISE camera. They found that PDPs tend to be located in regional depressions such as impact craters or flat plains and are associated with light-toned phyllosilicate-rich terrains. PDPs observed from orbit range from 1- to 30-m wide, although those observed at the surface by all three rovers are centimeter scale. El-Maarry et al. (2014) pointed out that the size range may reflect variable hydrological conditions where the smaller polygons observed at the rover scale may have formed through surface evaporation while the larger PDPs may suggest fluctuating water tables like what is proposed in this paper for Salar de Pajonales.

Based on our results, surface manifestations, such as domes and polygons, of salt-related processes on Mars could point to potential water sources. Because hygroscopic salts have been invoked as sources of localized, transient water sufficient to support terrestrial life (Davila et al., 2010; Hallsworth, 2020), areas displaying such structures would be good targets for biosignature exploration on Mars.

4.5 Summary and Future Directions

The Salar de Pajonales is currently in a desiccation period of a series of wetting and drying cycles. The salar surface types—lagoons, salt crusts, infrequently inundated areas, and dry exposed paleoterraces (Chong Diaz et al., 2020)– spatially reflect climate changes that partly mirror similar climate transitions postulated for early Mars. These intermittently moist areas offer a glimpse into the possible last microbial refugia on Mars as the climate changed and water vanished from the surface (Davila and Schulze-Makuch et al., 2016).

Different salar surface types offer opportunities to follow morphological transformations that create distinct environmental conditions for life. These morphologies could reflect similar hydrological conditions during the wetter climate of early Mars. Focusing on the Dome Field, an exposed paleoterrace, we identified surface structures that can be identified by drone imagery (Phillips et al., 2021) and explored for different textural surfaces as defined by distinct physical, chemical, and hydrological conditions.

The Dome Field comprises gypsum deposits that infer a cyclic deposition of thin beds comprising well-developed gypsum crystals inter-layered with thinner beds of gypsum breccia and laminar sediments (**Figure 2**). Surface characteristics fall into two distinct groups based on spatial scale. Macroscale structures (meter-scale; PolygonRidges, which encircle Megapolygons; Domes; and Quasi-Flats) formed by volume changes associated with water-related processes, and microscale

structures, which are attributed to water-brine-related processes active within the upper gypsum bed. Our observations suggest a strong inter-dependency between these structures across scales that we interpret to represent changes in environmental parameters related to changing climate.

Polygonal surface patterns on Mars have a bimodal size range similar to what we observe at Salar de Pajonales. At Salar de Pajonales, we attribute these changes to hydrological conditions where smaller scale polygons observed at the rover scale may have formed through surface evaporation, and larger potential desiccation polygons may suggest groundwater fluctuations. Thus domes and polygons on Mars could represent potential water sources and, hence, brine transport, creating excellent targets for biosignature exploration on Mars.

This research is part of a larger effort to determine remote-sensing thresholds of detection for the surface structures described here (Phillips et al., 2021 in prep), to establish the distribution and predictability of biosignatures within the salar (Warren-Rhodes et al., in review), and to test the hypothesis of underlying unique geologic conditions in the Dome Field (Hofmann et al., in review). Consequently, we focused on the Dome Field where both the structures and the biosignatures are present. However, a complete study of the facies distribution in the Dome Field and across the larger Salar de Pajonales evaporitic basin could provide further context for the geologic and climatic controls on the observed structures and would further help to strengthen the site as a Martian analog. In this study and the accompanying papers mentioned above, our focus is on a smaller area to provide a more detailed picture of the interrelationships of structure, life, and water and our ability to detect relevant targets.

DATA AVAILABILITY STATEMENT

The original contributions presented in the study are included in the article/**Supplementary Material**, further inquiries can be directed to the corresponding author.

AUTHOR CONTRIBUTIONS

NWH, KWR, MP, and NAC conceived and designed the study. NWH, MHH, KWR, MP, NAC, CT-C, OC, GCD, CD, JLB, VCG, DS, PS, MM, JM, NN, CR, PS, KLR, CJR, and DW analyzed and interpreted the data. NWH, MHH, KWR, MP, NN, NAC, CT-C, OC, CR, KLR, CJR, DW, and VP conducted the investigation. NAC acquired the funding. NWH, MHH, KWR, MP, NAC, GCD, JM, NN, KLR wrote the manuscript.

FUNDING STATEMENT

This study was supported by the NASA Astrobiology Institute (NAI) *via* Grant No. NNA15BB01A (N. A. Cabrol, PI).

ACKNOWLEDGMENTS

NWH acknowledges Nancy E. Hulbirt, Suntikoon Supanut, and Brianna McKay for assistance with figures and data entry. Campoalto provided logistical support in Chile. MHH acknowledges Cartalytics for the free use of their software.

SUPPLEMENTARY MATERIAL

The Supplementary Material for this article can be found online at: https://www.frontiersin.org/articles/10.3389/fspas.2021.797591/full#supplementary-material

Supplementary Figure S1 | Profile across the western Andean front. **(A)** Shaded DEM. **(B)** Map. **(C)** Satellite image. **(D)** Profile along green line in **(A,B,C)** from west to east. Maps and cross section were created in Cartalytics (www.cltix.com); aerial imagery and topo map are downloaded from the Leaflet open-source library (www.cltix.com).

Supplementary Figure S2 | Spectra of gypsum samples from Salar de Pajonales. **(A)** X-ray diffractogram showing gypsum and calcite peaks. **(B)** Raman spectra with gypsum and anhydrite bands labeled. **(C)** IR spectra with gypsum and anhydrite bands labeled.

REFERENCES

Albarracín, V. H., Kurth, D., Ordoñez, O. F., Belfiore, C., Luccini, E., Salum, G. M., et al. (2015). High-up: A Remote Reservoir of Microbial Extremophiles in Central Andean Wetlands. *Front. Microbiol.* 6, 1404. doi:10.3389/fmicb.2015.01404

Alonso, R. N., and Rojas, W. (2020). "Origin and Evolution of the Central Andes: Deserts, Salars, Lakes, and Volcanoes," in *Microbial Ecosystems in Central Andes Extreme Environments* (Cham: Springer), 3–19. doi:10.1007/978-3-030-36192-1_1

Angel de Pablo, M., and Komatsu, G. (2009). Possible Pingo fields in the Utopia basin, Mars: Geological and Climatical Implications. *Icarus* 199, 49–74. doi:10.1016/j.icarus.2008.09.007

Artieda, O., Davila, A., Wierzchos, J., Buhler, P., Rodríguez-Ochoa, R., Pueyo, J., et al. (2015). Surface Evolution of Salt-Encrusted Playas under Extreme and Continued Dryness. *Earth Surf. Process. Landforms* 40, 1939–1950. doi:10.1002/esp.3771

Artieda, O. (2013). Morphology and Micro-fabrics of Weathering Features on Gyprock Exposures in a Semiarid Environment (Ebro Tertiary Basin, NE Spain). *Geomorphology* 196, 198–210. doi:10.1016/j.geomorph.2012.03.020

Bada, J., Zent, A., Grunthaner, F., Quinn, R., Navarro-Gonzalez, R., Gomez-Silva, B., et al. (2003). "ASTROBIOLAB: A mobile Biotic and Soil Analysis Laboratory," in Sixth International Conference on Mars, Pasadena, Calif: Citeseer, Germany, 10 May 1842 (Springer).

Barrett, B. S., Campos, D. A., Veloso, J. V., and Rondanelli, R. (2016). Extreme Temperature and Precipitation Events in March 2015 in central and Northern Chile. *J. Geophys. Res. Atmos.* 121, 4563–4580. doi:10.1002/2016jd024835

Benison, K. C. (2017). Gypsum Gravel Devils in Chile: Movement of Largest Natural Grains by Wind? *Geology* 45, 423–426. doi:10.1130/g38901.1

Betancourt, J. L., Latorre, C., Rech, J. A., Quade, J., and Rylander, K. A. (2000). A 22,000-year Record of Monsoonal Precipitation from Northern Chile's Atacama Desert. *Science* 289, 1542–1546. doi:10.1126/science.289.5484.1542

Bishop, J. L., Yeşilbaş, M., Hinman, N. W., Burton, Z. F. M., Englert, P. A. J., Toner, J. D., et al. (2021). Martian Subsurface Cryosalt Expansion and Collapse as Trigger for Landslides. *Sci. Adv.* 7, eabe4459. doi:10.1126/sciadv.abe4459

Bobst, A. L., Lowenstein, T. K., Jordan, T. E., Godfrey, L. V., Ku, T.-L., and Luo, S. (2001). A 106ka paleoclimate record from drill core of the Salar de Atacama, northern Chile. *Palaeogeogr. Palaeoclimatol. Palaeoecol.* 173, 21–42. doi:10.1016/s0031-0182(01)00308-x

Bozkurt, D., Rondanelli, R., Garreaud, R., and Arriagada, A. (2016). Impact of Warmer Eastern Tropical Pacific SST on the March 2015 Atacama Floods. *Monthly Weather Rev.* 144, 4441–4460. doi:10.1175/mwr-d-16-0041.1

Brooker, L. M., Balme, M. R., Conway, S. J., Hagermann, A., Barrett, A. M., Collins, G. S., et al. (2018). Clastic Polygonal Networks Around Lyot Crater, Mars: Possible Formation Mechanisms from Morphometric Analysis. *Icarus* 302, 386–406. doi:10.1016/j.icarus.2017.11.022

Burr, D. M., Tanaka, K. L., and Yoshikawa, K. (2009). Pingos on Earth and Mars. *Planet. Space Sci.* 57, 541–555. doi:10.1016/j.pss.2008.11.003

Cabré, A., Remy, D., Aguilar, G., Carretier, S., and Riquelme, R. (2020). Mapping Rainstorm Erosion Associated with an Individual Storm from InSAR Coherence Loss Validated by Field Evidence for the Atacama Desert. *Earth Surf. Process. Landforms* 45, 2091–2106. doi:10.1002/esp.4868

Cabrol, N. A., Chong-Diaz, G., Stoker, C. R., Gulick, V. C., Landheim, R., Lee, P., et al. (2001). Nomad Rover Field Experiment, Atacama Desert, Chile: 1. Science Results Overview. *J. Geophys. Res.* 106, 7785–7806. doi:10.1029/1999je001166

Cabrol, N. A., Feister, U., Hã¤der, D.-P., Piazena, H., Grin, E. A., and Klein, A. (2014). Record Solar UV Irradiance in the Tropical Andes. *Front. Environ. Sci.* 2, 19, 2014 . Article No.: 19. doi:10.3389/fenvs.2014.00019

Cabrol, N. A., Grin, E. A., Chong, G., Häder, D. P., Minkley, E., Yu, Y., et al. (2010). "Dynamics of Declining lake Habitat in Changing Climate," in *Lakes on Mars* (Elsevier), 347–369. doi:10.1016/b978-0-444-52854-4.00013-1

Cabrol, N. A., and Grin, E. A. (2010). *Lakes on Mars*. Elsevier.

Cabrol, N. A., Grin, E. A., Zippi, P., Noffke, N., and Winter, D. (2018). "Evolution of Altiplanic Lakes at the Pleistocene/holocene Transition: a Window into Early mars Declining Habitability, Changing Habitats, and Biosignatures," in *From Habitability to Life on Mars* (Elsevier), 153–177. doi:10.1016/b978-0-12-809935-3.00006-2

Cabrol, N. A., McKay, C. P., Grin, E. A., Kiss, K. T., Ács, É., Tóth, B., et al. (2009). *Signatures of Habitats and Life in Earth's High-Altitude Lakes: Clues to Noachian Aqueous Environments on Mars*.

Cabrol, N. A. (2018). The Coevolution of Life and Environment on Mars: An Ecosystem Perspective on the Robotic Exploration of Biosignatures. *Astrobiology* 18, 1–27. doi:10.1089/ast.2017.1756

Cabrol, N. A., Wettergreen, D., Warren-Rhodes, K., Grin, E. A., Moersch, J., Diaz, G. C., et al. (2007). Life in the Atacama: Searching for Life with Rovers (Science Overview). *J. Geophys. Res. Biogeosciences* 112, 1. doi:10.1029/2006jg000298

Calaforra, J. M., and Pulido-Bosch, A. (1997). Peculiar Landforms in the gypsum Karst of Sorbas (southeastern Spain). *Carbonates Evaporites* 12, 110–116. doi:10.1007/bf03175809

Casertano, L. (1963). General Characteristics of Active Andean Volcanoes and a Summary of Their Activities during Recent Centuries. *Bull. Seismological Soc. America* 53, 1415–1433. doi:10.1785/bssa0530061415

Caswell, T. E., and Milliken, R. E. (2017). Evidence for Hydraulic Fracturing at Gale Crater, Mars: Implications for Burial Depth of the Yellowknife Bay Formation. *Earth Planet. Sci. Lett.* 468, 72–84. doi:10.1016/j.epsl.2017.03.033

Charola, A. E., Puhringer, J., and Steiger, M. (2007). Gypsum: a Review of its Role in the Deterioration of Building Materials. *Environ. Geology* 52, 207–220. doi:10.1007/s00254-006-0566-9

Charrier, R., Pinto, L., and Rodríguez, M. P. (2007). "Tectonostratigraphic Evolution of the Andean Orogen in Chile," in *The Geology of Chile*, 21–114.

Chepstow-Lusty, A., Bush, M. B., Frogley, M. R., Baker, P. A., Fritz, S. C., and Aronson, J. (2005). Vegetation and Climate Change on the Bolivian Altiplano between 108,000 and 18,000 Yr Ago. *Quat. Res.* 63, 90–98. doi:10.1016/j.yqres.2004.09.008

Chong Diaz, G., Demergasso, C., Urrutia Meza, J., and Vargas a, M. (2020). The Saline Domain of Northern Chile and its Industrial mineral Deposits. *Boletin De La Sociedad Geologica Mexicana* 72, 1. doi:10.18268/bsgm2020v72n3a020720

Davila, A. F., Duport, L. G., Melchiorri, R., Jänchen, J., Valea, S., De Los Rios, A., et al. (2010). Hygroscopic Salts and the Potential for Life on Mars. *Astrobiology* 10, 617–628. doi:10.1089/ast.2009.0421

Davila, A. F., and Schulze-Makuch, D. (2016). The Last Possible Outposts for Life on Mars. *Astrobiology* 16, 159–168. doi:10.1089/ast.2015.1380

Davis, W. L., De Pater, I., and McKay, C. P. (2010). Rain Infiltration and Crust Formation in the Extreme Arid Zone of the Atacama Desert, Chile. *Planet. Space Sci.* 58, 616–622. doi:10.1016/j.pss.2009.08.011

De Wet, C. B., De Wet, A. P., Godfrey, L., Driscoll, E., Patzkowsky, S., Xu, C., et al. (2020). Pliocene Short-Term Climate Changes Preserved in continental Shallow Lacustrine-Palustrine Carbonates: Western Opache Formation, Atacama Desert, Chile. *Geol. Soc. America Bull.* 132, 1795–1816. doi:10.1130/b35227.1

DeCelles, P. G., Zandt, G., Beck, S. L., Currie, C. A., Ducea, M. N., Kapp, P., et al. (2015). Cyclical Orogenic Processes in the Cenozoic central Andes. *Memoir Geol. Soc. America* 212, 459–490. Geodynamics of a Cordilleran Orogenic System: the Central Andes of Argentina and Northern Chile. doi:10.1130/2015.1212(22)

Díaz, F. P., Latorre, C., Maldonado, A., Quade, J., and Betancourt, J. L. (2012). Rodent Middens Reveal Episodic, Long-distance Plant Colonizations across the Hyperarid Atacama Desert over the Last 34,000 Years. *J. Biogeogr.* 39, 510–525.

Diederich, J. L., Wennrich, V., Bao, R., Buettner, C., Bolten, A., Brill, D., et al. (2020). A 68 Ka Precipitation Record from the Hyperarid Core of the Atacama Desert in Northern Chile. *Glob. Planet. Change* 184. doi:10.1016/j.gloplacha.2019.103054

Dundas, C. M., and Mcewen, A. S. (2010). An Assessment of Evidence for Pingos on Mars Using HiRISE. *Icarus* 205, 244–258. doi:10.1016/j.icarus.2009.02.020

El-Maarry, M. R., Watters, W., Mckeown, N. K., Carter, J., Noe Dobrea, E., Bishop, J. L., et al. (2014). Potential Desiccation Cracks on Mars: A Synthesis from Modeling, Analogue-Field Studies, and Global Observations. *Icarus* 241, 248–268. doi:10.1016/j.icarus.2014.06.033

Fairén, A. G., Davila, A. F., Lim, D., Bramall, N., Bonaccorsi, R., Zavaleta, J., et al. (2010). Astrobiology through the Ages of Mars: The Study of Terrestrial Analogues to Understand the Habitability of Mars. *Astrobiology* 10, 821–843. doi:10.1089/ast.2009.0440

Farías, M. E., and Acuña, L. A. S. (2020). "Modern Microbial Mats and Endoevaporite Systems in Andean Lakes: A General Approach," in *Microbial Ecosystems in Central Andes Extreme Environments* (Springer), 21–33.

Fernanders, M. S., Gough, R. V., Chevrier, V. F., Schiffman, Z. R., Ushijima, S. B., Martinez, G. M., et al. (2022). Water Uptake by Chlorate Salts under Mars-relevant Conditions. *Icarus* 371, 114715. doi:10.1016/j.icarus.2021.114715

Fiahaut, J., Martinot, M., Bishop, J. L., Davies, G. R., and Potts, N. J. (2017). Remote Sensing and *In Situ* Mineralogic Survey of the Chilean Salars: An Analog to Mars Evaporate Deposits? *Icarus* 282, 152–173.

Finstad, K., Pfeiffer, M., McNicol, G., Barnes, J., Demergasso, C., Chong, G., et al. (2016). Rates and Geochemical Processes of Soil and Salt Crust Formation in Salars of the Atacama Desert, Chile. *Geoderma* 284, 57–72. doi:10.1016/j.geoderma.2016.08.020

García, M., Riquelme, R., Farías, M., Hérail, G., and Charrier, R. (2011). Late Miocene-Holocene canyon Incision in the Western Altiplano, Northern Chile: Tectonic or Climatic Forcing? *J. Geol. Soc.* 168, 1047–1060. doi:10.1144/0016-76492010-134

Garreaud, R. D., Vuille, M., Compagnucci, R., and Marengo, J. (2009). Present-day South American Climate. *Palaeogeogr. Palaeoclimatol. Palaeoecol.* 281, 180–195. doi:10.1016/j.palaeo.2007.10.032

Garreaud, R. (2000). Intraseasonal Variability of Moisture and Rainfall over the South American Altiplano. *Mon. Wea. Rev.* 128, 3337–3346. doi:10.1175/1520-0493(2000)128<3337:ivomar>2.0.co;2

Garreaud, R., Vuille, M., and Clement, A. C. (2003). The Climate of the Altiplano: Observed Current Conditions and Mechanisms of Past Changes. *Palaeogeogr. Palaeoclimatol. Palaeoecol.* 194, 5–22. doi:10.1016/s0031-0182(03)00269-4

Geyh, M. A., Grosjean, M., Núñez, L., and Schotterer, U. (1999). Radiocarbon Reservoir Effect and the Timing of the Late-Glacial/early Holocene Humid Phase in the Atacama Desert (Northern Chile). *Quat. Res.* 52, 143–153. doi:10.1006/qres.1999.2060

Glines, N. H., and Gulick, V. C. (in review). *Paleolakes and Channels on the Floor of Lyot Crater*. Mars: Icarus.

Global Volcanism Program (2013). *Lastarria (355120) Volcanoes of the World*. Washington, D.C.: Smithsonian Institute. v.4.10.2 (24 Aug 2021) [Online] (Accessed Aug 25, 2021).

Gómez-Silva, B. (2010). "On the Limits Imposed to Life by the Hyperarid Atacama Desert in Northern Chile," in *Astrobiology: Emergence, Search and Detection of Life* (United States: American Scientific Publishers), 199–213.

Gómez-Silva, B., Rainey, F. A., Warren-Rhodes, K. A., McKay, C. P., and Navarro-González, R. (2008). "Atacama Desert Soil Microbiology," in *Microbiology of Extreme Soils* (Springer), 117–132.

Greeley, R., and Guest, J. (1987). *Geologic Map of the Eastern Equatorial Region of Mars*. USGS Miscellaneous Investigations Series Map I–1802–B, as part of the Atlas of Mars, 1:15,000,000 Geologic Series. Reston, VA: US Geological Survey.

Grosjean, M., Van Leeuwen, J. F. N., Van Der Knaap, W. O., Geyh, M. A., Ammann, B., Tanner, W., et al. (2001). A 22,000 14C Year BP Sediment and Pollen Record of Climate Change from Laguna Miscanti (23°S), Northern Chile. *Glob. Planet. Change* 28, 35–51. doi:10.1016/s0921-8181(00)00063-1

Grotzinger, J. P., Sumner, D. Y., Kah, L. C., Stack, K., Gupta, S., Edgar, L., et al.Team, M.S.L.S. (2014). A Habitable Fluvio-Lacustrine Environment at Yellowknife Bay, Gale Crater, Mars. *Science* 343, 1242777. doi:10.1126/science.1242777

Grunthaner, F. J., Willis, P., Amashukeli, X., Bada, J. L., Aubrey, A., Mathies, R. A., et al. (2006). The Urey Instrument: Ultra-sensitive Chiral Biomarker Detection with Correlated Soil Oxidant Profiling. *Astrobiology* 6, 242–243.

Gulick, V. C., Glines, N., Hart, S., and Freeman, P. (2019). Geomorphological Analysis of Gullies on the central Peak of Lyot Crater, Mars. *Geol. Soc. Lond. Spec. Publications* 467, 233–265. doi:10.1144/sp467.17

Gutiérrez, F., and Cooper, A. (2013). *6.33 Surface Morphology of Gypsum Karst*.

Gutiérrez, M. (2005). "Desert Lakes: Playa Lakes and Sebkhas," in *Developments in Earth Surface Processes*. Editor M. Gutiérrez (Amsterdam, Netherlands: Elsevier), 383–405.

Häder, D.-P., and Cabrol, N. A. (2018). "UV and Life Adaptation Potential on Early Mars: Lessons from Extreme Terrestrial Analogs," in *From Habitability to Life on Mars* (Elsevier), 233–248.

Häder, D. P., and Cabrol, N. A. (2020). Monitoring of Solar Irradiance in the High Andes. *Photochem. Photobiol.* 96, 1133–1139. doi:10.1111/php.13276

Hallsworth, J. E. (2020). Salt Deliquescence Can Support Extraterrestrial Life. *Nat. Astron.* 4, 739–740. doi:10.1038/s41550-020-1081-8

Haschke, M., Gunther, A., Melnick, D., Echtler, H., Reutter, K. J., Scheuber, E., et al. (2006). Central and Southern Andean Tectonic Evolution Inferred from Arc Magmatism. *Andes: Active Subduction Orogeny* 1, 337–353. doi:10.1007/978-3-540-48684-8_16

Haschke, M. R., Scheuber, E., Gunther, A., and Reutter, K.-J. (2002). Evolutionary Cycles during the Andean Orogeny: Repeated Slab Breakoff and Flat Subduction? *Terra Nova* 14, 49–55. doi:10.1046/j.1365-3121.2002.00387.x

Hofmann, M. H., Hinman, N. W., Phillips, M. P., McInenly, M., Chong Diaz, G., Noffke, N., et al. (in review). An Integrated Process Model of gypsum Dome Morphology Formation and its Relevance in the Search for Life on Mars. *Scientific Rep.* 1, 1.

Hooper, J., Marx, S. K., May, J.-H., Lupo, L. C., Kulemeyer, J. J., Pereira, E. d. l. Á., et al. (2020). Dust Deposition Tracks Late-Holocene Shifts in Monsoon Activity and the Increasing Role of Human Disturbance in the Puna-Altiplano, Northwest Argentina. *The Holocene* 30, 519–536. doi:10.1177/0959683619895814

Houston, J., and Hartley, A. J. (2003). The central Andean West-Slope Rainshadow and its Potential Contribution to the Origin of HYPER-ARIDITY in the Atacama Desert. *Int. J. Climatol.* 23, 1453–1464. doi:10.1002/joc.938

Houston, J. (2006). Variability of Precipitation in the Atacama Desert: Its Causes and Hydrological Impact. *Int. J. Climatol.* 26, 2181–2198. doi:10.1002/joc.1359

Jordan, T. E., Isacks, B. L., Ramos, V. A., and Allmendinger, R. W. (1983). Mountain Building in the central Andes. *Episodes* 3, 20–26.

Jowett, E. C., Cathles, L. M., and Davis, B. W. (1993). Predicting Depths of gypsum Dehydration in Evaporitic Sedimentary Basins. *AAPG Bulletin-American Assoc. Pet. Geologists* 77, 402–413. doi:10.1306/bdff8c22-1718-11d7-8645000102c1865d

Kereszturi, A., Aszalós, J. M., Heiling, Z., Ignéczi, Á., Kapui, Z., Király, C., et al. (2020). Cold, dry, windy, and UV irradiated: Surveying Mars-relevant conditions in Ojos del Salado Volcano (Andes Mountains, Chile). *Astrobiology* 20, 677–683. doi:10.1089/ast.2019.2165

Kite, E. S. (2019). Geologic Constraints on Early Mars Climate. *Space Sci. Rev.* 215, 2019. doi:10.1007/s11214-018-0575-5

Koponen, A., Kataja, M., and Timonen, J. (1997). Permeability and Effective Porosity of Porous media. *Phys. Rev. E.* 56, 3319–3325. doi:10.1103/physreve.56.3319

Lafuente, B., Downs, R. T., Yang, H., and Stone, N. (2015). "The Power of Databases: The RRUFF Project," in *Highlights in Mineralogical Crystallography*. Editors T. Armbruster and R. M. Danisi (Berlin, Germany: W. De Gruyter), 1–30.

Langsdorf, E., and Britt, D. (2005). "Classification and Distribution of Patterned Ground in the Southern Hemisphere of Mars," in 36th Annual Lunar and Planetary Science Conference.

Latorre, C., Betancourt, J. L., and Arroyo, M. T. K. (2006). Late Quaternary Vegetation and Climate History of a Perennial River canyon in the Río Salado basin (22°S) of Northern Chile. *Quat. Res.* 65, 450–466. doi:10.1016/j.yqres.2006.02.002

Lefort, A., Russell, P. S., Thomas, N., Mcewen, A. S., Dundas, C. M., and Kirk, R. L. (2009). Observations of Periglacial Landforms in Utopia Planitia with the High Resolution Imaging Science Experiment (HiRISE). *J. Geophys. Research-Planets* 114, e4. doi:10.1029/2008je003264

Levy, J., Head, J., and Marchant, D. (2009). Thermal Contraction Crack Polygons on Mars: Classification, Distribution, and Climate Implications from HiRISE Observations. *J. Geophys. Research-Planets* 114, e1. doi:10.1029/2008je003273

Maldonado, A., Betancourt, J. L., Latorre, C., and Villagran, C. (2005). Pollen Analyses from a 50 000-yr Rodent Midden Series in the Southern Atacama Desert (25° 30′ S). *J. Quat. Sci.* 20, 493–507. doi:10.1002/jqs.936

Malin, M. C., and Edgett, K. S. (2000). Evidence for Recent Groundwater Seepage and Surface Runoff on Mars. *Science* 288, 2330–2335. doi:10.1126/science.288.5475.2330

Mangold, N. (2005). High Latitude Patterned Grounds on Mars: Classification, Distribution and Climatic Control. *Icarus* 174, 336–359. doi:10.1016/j.icarus.2004.07.030

Mangold, N., Maurice, S., Feldman, W. C., Costard, F., and Forget, F. (2004). Spatial Relationships between Patterned Ground and Ground Ice Detected by the Neutron Spectrometer on Mars. *J. Geophys. Research-Planets* 109, 1. doi:10.1029/2004je002235

Marais, D. J. D. (2010). "Marine Hypersaline Microcoleus-Dominated Cyanobacterial Mats in the Saltern at Guerrero Negro, Baja California Sur, Mexico: A System-Level Perspective," in *Microbial Mats* (Springer), 401–420. doi:10.1007/978-90-481-3799-2_21

McKay, C. P., Friedmann, E. I., Gómez-Silva, B., Cáceres-Villanueva, L., Andersen, D. T., and Landheim, R. (2003). Temperature and Moisture Conditions for Life in the Extreme Arid Region of the Atacama Desert: Four Years of Observations Including the El Niño of 1997-1998. *Astrobiology* 3, 393–406. doi:10.1089/153110703769016460

Meseguer-Ruiz, O., Ponce-Philimon, P. I., Baltazar, A., Guijarro, J. A., Serrano-Notivoli, R., Olcina Cantos, J., et al. (2020). Synoptic Attributions of Extreme Precipitation in the Atacama Desert (Chile). *Clim. Dyn.* 55, 3431–3444. doi:10.1007/s00382-020-05455-4

Morgenstern, A., Hauber, E., Reiss, D., Van Gasselt, S., Grosse, G., and Schirrmeister, L. (2007). Deposition and Degradation of a Volatile-Rich Layer in Utopia Planitia and Implications for Climate History on Mars. *J. Geophys. Research-Planets* 112, E06010. doi:10.1029/2006je002869

Nazari-Sharabian, M., Aghababaei, M., Karakouzian, M., and Karami, M. (2020). Water on Mars-A Literature Review. *Galaxies* 8, 40. doi:10.3390/galaxies8020040

Neal, J. T., Langer, A. M., and Kerr, P. F. (1968). Giant Desiccation Polygons of Great Basin Playas. *Geol. Soc. America Bull.* 79, 69. doi:10.1130/0016-7606(1968)79[69:gdpogb]2.0.co;2

Noffke, N. (2010). *Geobiology: Microbial Mats in sandy Deposits from the Archean Era to Today*. Springer Science & Business Media.

Ortega, C., Vargas, G., Rojas, M., Rutllant, J. A., Muñoz, P., Lange, C. B., et al. (2019). Extreme ENSO-Driven Torrential Rainfalls at the Southern Edge of the Atacama Desert during the Late Holocene and Their Projection into the 21th century. *Glob. Planet. Change* 175, 226–237. doi:10.1016/j.gloplacha.2019.02.011

Otálora, F., Criado-Reyes, J., Baselga, M., Canals, A., Verdugo-Escamilla, C., and García Ruiz, J. M. (2020). Hydrochemical and mineralogical evolution through evaporitic processes in Salar de Llamara brines (Atacama, Chile). *ACS Earth Space Chem.* 4, 882–896. doi:10.1021/acsearthspacechem.0c00085

Pál, B., and Kereszturi, Á. (2020). Annual and Daily Ideal Periods for Deliquescence at the landing Site of InSight Based on GCM Model Calculations. *Icarus* 340, 113639. doi:10.1016/j.icarus.2020.113639

Palacios, D., Stokes, C. R., Phillips, F. M., Clague, J. J., Alcala-Reygosa, J., Andres, N., et al. (2020). The Deglaciation of the Americas during the Last Glacial Termination. *Earth-Science Rev.* 203. doi:10.1016/j.earscirev.2020.103113

Pechmann, J. C. (1980). The Origin of Polygonal Troughs on the Northern plains of Mars. *Icarus* 42, 185–210. doi:10.1016/0019-1035(80)90071-8

Pfeiffer, M., Latorre, C., Santoro, C. M., Gayo, E. M., Rojas, R., Carrevedo, M. L., et al. (2018). Chronology, Stratigraphy and Hydrological Modelling of Extensive Wetlands and Paleolakes in the Hyperarid Core of the Atacama Desert during the Late Quaternary. *Quat. Sci. Rev.* 197, 224–245. doi:10.1016/j.quascirev.2018.08.001

Pfeiffer, M., Morgan, A., Heimsath, A., Jordan, T., Howard, A., and Amundson, R. (2021). Century Scale Rainfall in the Absolute Atacama Desert: Landscape Response and Implications for Past and Future Rainfall. *Quat. Sci. Rev.* 254, 106797. doi:10.1016/j.quascirev.2021.106797

Phillips, M. S., Moersch, J. E., Cabrol, N. A., Candela, A., Wettergreen, D., Warren-Rhodes, K., et al.Team, T.S.I.N. (2021). *Establishing Thresholds of Identification*

for Planetary Features Using Deep Learning: Application to Habitats in a Mars-analog Landscape.

Piatek, J. L., Hardgrove, C., Moersch, J. E., Drake, D. M., Wyatt, M. B., Rampey, M., et al. (2007). Surface and Subsurface Composition of the Life in the Atacama Field Sites from Rover Data and Orbital Image Analysis. *J. Geophys. Research-Biogeosciences* 112, 1. doi:10.1029/2006jg000317

Pueyo, J., Demergasso, C., Escudero, L., Chong, G., Cortéz-Rivera, P., Sanjurjo-Sánchez, J., et al. (2021). On the Origin of saline Compounds in Acidic Salt Flats (Central Andean Altiplano). *Chem. Geology* 1, 120155. doi:10.1016/j.chemgeo.2021.120155

Quade, J., Dettinger, M., Carrapa, B., Decelles, P., Murray, K., Huntington, K., et al. (2015). The Growth of the central Andes, 22 S–26 S. *Geol. Soc. Am. Mem.* 12, 277–308. doi:10.1130/2015.1212(15)

Rehak, K., Bookhagen, B., Strecker, M. R., and Echtler, H. P. (2010). The Topographic Imprint of a Transient Climate Episode: the Western Andean Flank between 15·5° and 41·5°S. *Earth Surf. Process. Landforms* 35, 1516–1534. doi:10.1002/esp.1992

Reiners, P. W., Thomson, S. N., Vernon, A., Willett, S. D., Zattin, M., Einhorn, J., et al. (2015). Geodynamics of a Cordilleran Orogenic System: the Central Andes of Argentina and Northern Chile. *Geol. Soc. America* 212, 215–249. doi:10.1130/MEM212

Riquelme, R., Hérail, G., Martinod, J., Charrier, R., and Darrozes, J. (2007). Late Cenozoic Geomorphologic Signal of Andean Forearc Deformation and Tilting Associated with the Uplift and Climate Changes of the Southern Atacama Desert (26°S-28°S). *Geomorphology* 86, 283–306. doi:10.1016/j.geomorph.2006.09.004

Risacher, F., and Alonso, H. (2001). Geochemistry of Ash Leachates from the 1993 Lascar Eruption, Northern Chile. Implication for Recycling of Ancient Evaporites. *J. Volcanology Geothermal Res.* 109, 319–337. doi:10.1016/s0377-0273(01)00198-6

Risacher, F., Alonso, H., and Salazar, C. (2003). The Origin of Brines and Salts in Chilean Salars: a Hydrochemical Review. *Earth-Science Rev.* 63, 249–293. doi:10.1016/s0012-8252(03)00037-0

Robidoux, P., Rizzo, A. L., Aguilera, F., Aiuppa, A., Artale, M., Liuzzo, M., et al. (2020). Petrological and noble Gas Features of Lascar and Lastarria Volcanoes (Chile): Inferences on Plumbing Systems and Mantle Characteristics. *Lithos* 370, 105615. doi:10.1016/j.lithos.2020.105615

Schulze-Makuch, D., Wagner, D., Kounaves, S. P., Mangelsdorf, K., Devine, K. G., De Vera, J.-P., et al. (2018). Transitory Microbial Habitat in the Hyperarid Atacama Desert. *Proc. Natl. Acad. Sci. USA* 115, 2670–2675. doi:10.1073/pnas.1714341115

Seibert, N. M., and Kargel, J. S. (2001). Small-scale Martian Polygonal Terrain: Implications for Liquid Surface Water. *Geophys. Res. Lett.* 28, 899–902. doi:10.1029/2000gl012093

Soare, R. J., Burr, D. M., and Wan Bun Tseung, J. M. (2005). Possible Pingos and a Periglacial Landscape in Northwest Utopia Planitia. *Icarus* 174, 373–382. doi:10.1016/j.icarus.2004.11.013

Soare, R. J., Osinski, G. R., and Roehm, C. L. (2008). Thermokarst Lakes and Ponds on Mars in the Very Recent (Late Amazonian) Past. *Earth Planet. Sci. Lett.* 272, 382–393. doi:10.1016/j.epsl.2008.05.010

Stein, N., Grotzinger, J. P., Schieber, J., Mangold, N., Hallet, B., Sumner, D. Y., et al. (2018). Desiccation Cracks Provide Evidence of lake Drying on Mars, Sutton Island Member, Murray Formation, Gale Crater. *Geology* 46, E450. doi:10.1130/g45237y.1

Tanaka, K. L., Skinner, J. A., Jr, Dohm, J. M., Irwin, R. P., III, Kolb, E. J., Fortezzo, C. M., et al. (2014). *Geologic Map of Mars*.

Urrutia, J., Herrera, C., Custodio, E., Jódar, J., and Medina, A. (2019). Groundwater Recharge and Hydrodynamics of Complex Volcanic Aquifers with a Shallow saline lake: Laguna Tuyajto, Andean Cordillera of Northern Chile. *Sci. Total Environ.* 697, 134116. doi:10.1016/j.scitotenv.2019.134116

Urrutia, J., Jódar, J., Medina, A., Herrera, C., Chong, G., Urqueta, H., et al. (2018). Hydrogeology and Sustainable Future Groundwater Abstraction from the Agua Verde Aquifer in the Atacama Desert, Northern Chile. *Hydrogeol. J.* 26, 1989–2007. doi:10.1007/s10040-018-1740-3

Valdés-Pineda, R., V Aldés, J. B., and Garcia-Chevesich, P. (2017). Modelación de crecidas aluvionales en la Cuenca del Río Copiapó, Chile. *Ingeniería Del. Agua* 21, 135–152. [S.l.]. doi:10.4995/ia.2017.7366

Ward, D. J., Cesta, J. M., Galewsky, J., and Sagredo, E. (2015). Late Pleistocene Glaciations of the Arid Subtropical Andes and New Results from the Chajnantor Plateau, Northern Chile. *Quat. Sci. Rev.* 128, 98–116. doi:10.1016/j.quascirev.2015.09.022

Ward, D., Thornton, R., and Cesta, J. (2017). Across the Arid diagonal: Deglaciation of the Western Andean Cordillera in Southwest Bolivia and Northern Chile. *Cig.* 43, 667–696. doi:10.18172/cig.3209

Warren, J. K. (2016). *Evaporites: A Geological Compendium*. Springer.

Warren-Rhodes, K., Cabrol, N. A., Phillips, M., Tebes Cayo, C., Hinman, N. W., Rhodes, K. L., et al. (in review). Decoding Microbial Spatial Patterns as a Blueprint for Biosignature Detection on Mars and Beyond. *Astrobiology* 15, 998. doi:10.1089/ast.2015.1374

Warren-Rhodes, K., Weinstein, S., Dohm, J., Piatek, J., Minkley, E., Hock, A., et al. (2007a). Searching for Microbial Life Remotely: Satellite-To-Rover Habitat Mapping in the Atacama Desert, Chile. *J. Geophys. Research-Biogeosciences* 112, 1. doi:10.1029/2006jg000283

Warren-Rhodes, K., Weinstein, S., Piatek, J. L., Dohm, J., Hock, A., Minkley, E., et al. (2007b). Robotic Ecological Mapping: Habitats and the Search for Life in the Atacama Desert. *J. Geophys. Research-Biogeosciences* 112, 1. doi:10.1029/2006jg000301

Wettergreen, D., Cabrol, N., Baskaran, V., Calderón, F., Heys, S., Jonak, D., et al. (2005). "Second Experiments in the Robotic Investigation of Life in the Atacama Desert of Chile," in Proc. 8th International Symposium on Artificial Intelligence, Robotics and Automation in Space: Citeseer).

Wierzchos, J., Ascaso, C., Artieda, O., and Casero, M. C. (2020). "The Desert Polyextreme Environment and Endolithic Habitats," in *Microbial Ecosystems in Central Andes Extreme Environments: Biofilms, Microbial Mats, Microbialites and Endoevaporites*. Editor M. E. Farías (Switzerland: Springer), 37–49. doi:10.1007/978-3-030-36192-1_3

Wierzchos, J., Cámara, B., De Los Ríos, A., Davila, A. F., Sánchez Almazo, I. M., Artieda, O., et al. (2011). Microbial Colonization of Ca-Sulfate Crusts in the Hyperarid Core of the Atacama Desert: Implications for the Search for Life on Mars. *Geobiology* 9, 44–60. doi:10.1111/j.1472-4669.2010.00254.x

Wilcox, A. C., Escauriaza, C., Agredano, R., Mignot, E., Zuazo, V., Otárola, S., et al. (2016). An Integrated Analysis of the March 2015 Atacama Floods. *Geophys. Res. Lett.* 43, 8035–8043. doi:10.1002/2016gl069751

Wilhelm, M. B., Davila, A. F., Parenteau, M. N., Jahnke, L. L., Abate, M., Cooper, G., et al. (2018). Constraints on the Metabolic Activity of Microorganisms in Atacama Surface Soils Inferred from Refractory Biomarkers: Implications for Martian Habitability and Biomarker Detection. *Astrobiology* 18, 955–966. doi:10.1089/ast.2017.1705

Wordsworth, R., Knoll, A. H., Hurowitz, J., Baum, M., Ehlmann, B. L., Head, J. W., et al. (2021). A Coupled Model of Episodic Warming, Oxidation and Geochemical Transitions on Early Mars. *Nat. Geosci.* 14, 127–132. doi:10.1038/s41561-021-00701-8

Yilmaz, I., and Karacan, E. (2005). Slaking Durability and its Effect on the Doline Formation in the gypsum. *Environ. Geol.* 47, 1010–1016. doi:10.1007/s00254-005-1234-1

Young, B. W., and Chan, M. A. (2017). Gypsum Veins in Triassic Moenkopi Mudrocks of Southern Utah: Analogs to Calcium Sulfate Veins on Mars. *J. Geophys. Res. Planets* 122, 150–171. doi:10.1002/2016je005118

Conflict of Interest: The authors declare that the research was conducted in the absence of any commercial or financial relationships that could be construed as a potential conflict of interest.

Publisher's Note: All claims expressed in this article are solely those of the authors and do not necessarily represent those of their affiliated organizations, or those of the publisher, the editors and the reviewers. Any product that may be evaluated in this article, or claim that may be made by its manufacturer, is not guaranteed or endorsed by the publisher.

frontiers in Astronomy and Space Sciences

ORIGINAL RESEARCH
published: 09 February 2022
doi: 10.3389/fspas.2022.794932

Selection of Amino Acid Chirality Induced by Cyclic Dipeptide Synthesis in Plausible Prebiotic Conditions

Yeting Guo[1], Yumeng Zhang[2], Jianxi Ying[1], Yan Liu[2], Gaiyun Zhang[3]* and Yufen Zhao[1,2,4]**

[1]Institute of Drug Discovery Technology, Ningbo University, Ningbo, China, [2]College of Chemistry and Chemical Engineering, Xiamen University, Xiamen, China, [3]Key Laboratory of Marine Biogenetic Resources, Third Institute of Oceanography, Ministry of Natural Resources, Xiamen, China, [4]Key Laboratory of Bioorganic Phosphorus Chemistry and Chemical Biology (Ministry of Education), Department of Chemistry, Tsinghua University, Beijing, China

The biological system uses L-amino acids (L-AAs) to construct peptides. The selection of AA chirality in the prebiotic Earth still remains a mystery. Here we report the intrinsic mechanism of AA chiral selection in the formation of prebiotic proline-containing cyclic dipeptide (DKPs). The DKPs were synthesized by equal amounts of L-AA and D-AA with L-Pro that exhibited a clear preference for D-AA as opposed to L-AA. And surprisingly, the L-AA was preferred over D-AA in the mirror-image system with D-Pro. These results indicate that prebiotic DKPs synthesis has a certain selectivity for AA chirality preceded the biological enzymatic catalysis.

Keywords: chiral selection, amino acid, cyclic dipeptide, prebiotic chemistry, origin of life

OPEN ACCESS

Edited by:
Yiliang Li,
The University of Hong Kong, Hong Kong SAR, China

Reviewed by:
Albert Rimola,
Universitat Autònoma de Barcelona, Spain
Terence Phillip Kee,
University of Leeds, United Kingdom

****Correspondence:***
Jianxi Ying
yingjianxi@nbu.edu.cn
Gaiyun Zhang
zhgyun@tio.org.cn
Yufen Zhao
zhaoyufen@nbu.edu.cn

Specialty section:
This article was submitted to Astrobiology, a section of the journal Frontiers in Astronomy and Space Sciences

Received: *14 October 2021*
Accepted: *21 January 2022*
Published: *09 February 2022*

Citation:
Guo Y, Zhang Y, Ying J, Liu Y, Zhang G and Zhao Y (2022) Selection of Amino Acid Chirality Induced by Cyclic Dipeptide Synthesis in Plausible Prebiotic Conditions. Front. Astron. Space Sci. 9:794932. doi: 10.3389/fspas.2022.794932

1 INTRODUCTION

Life on Earth has a unique characteristic of chiral selection, e.g., L-amino acids (L-AAs) in proteins and D-nucleosides in nucleic acids (Bondy and Harrington, 1979; Bonner, 2000; Tamura, 2008). It is widely known that the chirality of biomolecules is catalyzed by bio-enzymes. The process of enzymatic catalyzed chirality is extremely precise and complex and cannot be realized at the beginning of life. However, the question of prebiotic chiral selection in biomolecule remains an abstruse problem. For the chemical origin of life, the simpler forms must have driven the prebiotic chiral selection process. Something as simple as intrinsic reactivity may have driven the prebiotic evolution process (Joshi et al., 2000; Rikken and Raupach, 2000; Hazen and Sholl, 2003; Ying et al., 2018a; Guasti, 2019; Yachmenev et al., 2019; Ye et al., 2019).

Cyclic dipeptides (DKPs), as one kind of the simplest peptide derivatives, have been found to have chiral catalysis properties (Prasad, 1995; Poullennec et al., 2002; Borthwick, 2012; Manchineella et al., 2013). DKPs might have chiral catalytic characteristics previous to the appearance of the bio-enzymes within the prebiotic chemical evolution. Consequently, it is reasonable to consider that DKPs ought to have played a crucial function in this process (Huber et al., 2003; Ying et al., 2018b). The synthesis of DKPs has been implemented under different conditions (Botti et al., 1996; Trauger et al., 2000; Lambert et al., 2001; Jainta et al., 2008; Nonappa et al., 2011; Borthwick, 2012), but there are limited reports involving plausible prebiotic chemical inventory, i.e., aqueous environment (Parker et al., 2014; Ying et al., 2018b; Guo et al., 2021). P_3m may have existed in the prebiotic environment. Yamagata found volcanic production of polyphosphates including P_3m (Yamagata et al., 1991). Rabinowitz demonstrated that some amino acids, such as Gly and Ala, could be condensed to dipeptides in aqueous solutions with maximum yield by treatment of P_3m which may play an important role in the prebiotic synthesis of peptides (Rabinowitz et al., 1969).

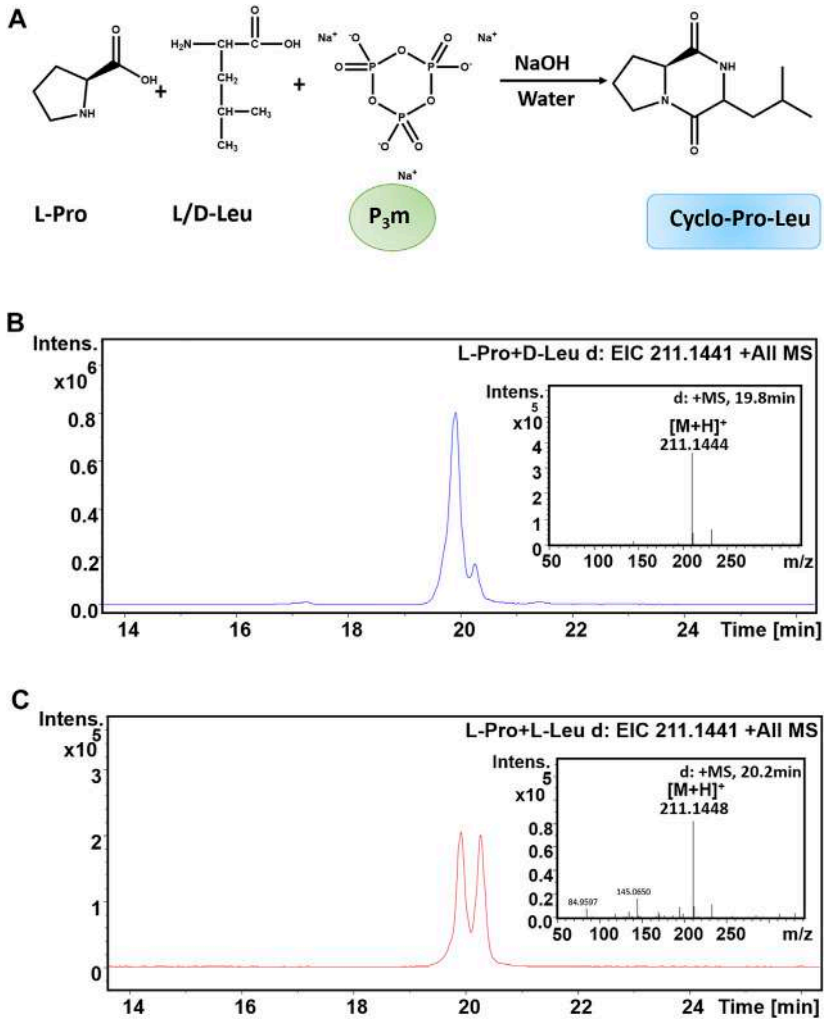

FIGURE 1 | Formation of cyclo-L-Pro-Leu from a reaction mixture of L-Pro, L/D-Leu and P_3m in an alkaline aqueous solution (pH = 11.7). The calculated value of cyclo-Pro-Leu $[M + H]^+$ is 211.1441. **(A)** Reaction scheme. **(B)** EIC-MS spectrum of the cyclo-L-Pro-L-Leu from the L-Pro reaction with L-Leu. **(C)** EIC-MS profile of the cyclo-L-Pro-D-Leu from the L-Pro reaction with D-Leu.

We recently reported the formation of DKPs from free AAs with the presence of trimetaphosphate (P_3m) in aqueous solution (Ying et al., 2018b). Meanwhile, we found proline-containing DKPs (cyclo-Pro-AAs) can spontaneously be acquired from linear dipeptides under aqueous environment. Notably, the yields of DKPs had been suffering from the sequence of linear dipeptides and whether the reaction contains P_3m (Guo et al., 2021). These findings are very useful to understand the formation of DKPs and provide some guidelines for properly know-how the function of DKPs in the process of prebiotic chemistry.

In our assay, cyclo-Pro-AAs were detected in L-Pro reaction with L-AAs (Ying et al., 2018b). How the effect of Pro and AAs chirality on the formation of cyclo-Pro-AAs in plausible prebiotic situations has not been mentioned. In other words, it was unclear whether the chirality of Pro and another AA (components of cyclo-Pro-AA) have effect on the corresponding DKPs synthesis. In this paper, we experimentally explored the amino acid chiral selection in the process of prebiotic DKPs synthesis.

2 MATERIALS AND METHODS

A sealed tube was charged with L-Pro or D-Pro (.05 mmol, .5 equiv.), L-AA or D-AA (.1 mmol, 1 equiv.) and P_3m (.1 mmol, 1 equiv.) in water (1 ml) under regular air compositions. The pH of reaction mixtures were adjusted to 11.7 with 10 M NaOH. Then, the samples were carried out in an incubator at 35°C for 6 days. After cooling at room temperature, the mixture were filtered with the .22 μm filter for HPLC-MS analysis.

2.1 Materials

L-proline (L-Pro), L-alanine (L-Ala), L- arginine (L-Arg), L-leucine (L-Leu), L- Methionine (L-Met), D-proline (D-Pro),

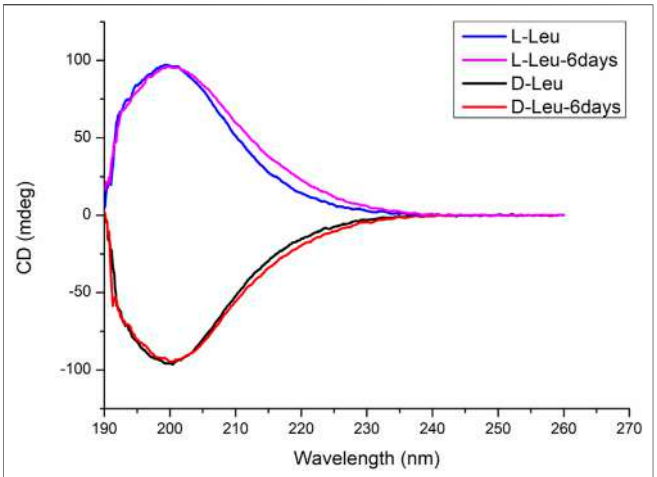

FIGURE 2 | CD spectra of four chiral Leu. Blue line: the CD spectrum is derived from freshly prepared L-Leu aqueous solutions. Purple line: the CD spectrum of L-Leu in an initial pH 11.7 at 35°C for 6 days Black line: the CD spectrum is derived from freshly prepared D-Leu aqueous solutions. Red line: the CD spectrum of D-Leu in an initial pH 11.7 at 35°C for 6 d. The results showed that L-Leu or D-Leu did not undergo chiral racemization in the experiment reaction conditions.

D-alanine (D-Ala), D- arginine (D-Arg), D-leucine (D-Leu) and D- methionine (D-Met) were purchased from MACKLIN (China). Trimetaphosphate (P_3m) was purchased from Sigma Aldrich (United States). NaOH was obtained from Energy Chemical (China). Analytical reagents methanol (High Performance Liquid Chromatography (HPLC) grade) was purchased from SpectrumChemical. HPLC grade formic acid was purchased from Sigma Aldrich (United States). Ultrapure water (Millipore, 18.2 MΩ) was used to prepare the aqueous solutions and the mobile phase.

2.2 General Procedure for Trapping the Proline-Containing DKPs (Cyclo-Pro-AAs)

For Cyclo-L-Pro-AAs, .1 mmol L-/D-AA was mixed with .05 mmol L-Pro in 1 ml trimetaphosphate (P_3m, .1 mmol) aqueous solutions, respectively. The pH of the mixtures was adjusted to 11.7 with 10 M NaOH. Then, the samples were carried out at 35°C for 6 days.

For Cyclo-D-Pro-AAs, .1 mmol L-/D-AA was mixed with .05 mmol D-Pro in 1 ml P_3m aqueous solutions, respectively. The pH of mixtures was adjusted to 11.7 with 10 M NaOH. Then, the samples were carried out at 35°C for 6 days.

2.3 Analytical Methods of HPLC- Mass Spectrometry

MS was performed using Bruker micrOTOF-Q Ⅱmass spectrometer in positive-ion mode. The MS main spectrometer parameters were as follows: capillary voltage: 4,500 V; nebulizer pressure: 2 bar; dry gas: 8 L min^{-1}; dry temperature: 200°C. Mass spectra were recorded in the mass range from m/z 50 to m/z 1,000. The 1/10 eluate sample was introduced into electrospray ionization-MS (ESI-MS) through a splitting three-way pipe. In order to detect the reaction product online, we set up the divert valve of the MS spectrometer parameters as follows: 1) when the divert valve was set to waste position in the first 3 min, so that the HPLC flows directly to waste tank; 2) and then, when the divert valve was switched to source position, the valve can be used for HPLC flows immediately to MS ion source.

The HPLC was performed on Agilent HPLC systems series 1,260 Infinity. The mobile phase A was .1% formic acid and mobile phase B was methanol. The gradient elution program was used: 5%–30% B: 0–15 min; 30%–70% B: 15–20 min; 70% B: 20–22 min; 70%–5% B: 22–24 min; 5% B: 24–29 min. The column was kept at ambient temperature. The HPLC flow rate was .8 ml min^{-1} with TC- C18 column (4.6 mm × 150 mm, 5 μm, Agilent).

2.4 Analytical Methods of Circular Dichroism

CD were performed on a 1700 JASCO circular dichroism spectrometer. The samples for the CD measurements were prepared in 1 mm cuvette. The CD instrument parameters were as follows: scanning speed: 50 nm min^{-1}; bandwidth: 1 nm; sheath gas flow rate: 3 L min^{-1}; data pitch: .1 nm. CD were registered in the scan range from 190 to 260 nm.

3 RESULTS AND DISCUSSION

Initially, we investigated whether the chirality of amino acid (AA, one of components of cyclo-Pro-AA) would affect the formation of cyclo-Pro-AAs. The synthesis of chiral cyclo-Pro-Leu using equal amounts of D-Leu and L-Leu with L-Pro and trimetaphosphate (P_3m) was carried out at an initial pH 11.7 at 35°C for 6 days, respectively. The pH was not adjusted during the whole process. The reaction was quenched with 4 M HCl solution. All the experimental data reported here were obtained after repeating the experiments three times. The resulting reactions were monitored by HPLC-high resolution mass spectrometry (HPLC-HRMS).

The reaction of D-Leu with L-Pro showed an extracted ion chromatogram (EIC) of m/z 211.1441 with retention times, respectively, of 19.8 and 20.2 min, which correspond to cyclo-Pro-Leu molecular ions $[M + H]^+$ (**Figures 1A,B**). This result indicated that the cyclo-Pro-Leu has two isomers. There are two reasons for this phenomenon. One is the racemization of D-Leu or L-Pro during the reaction. Another possibility is that enantioselection occurred during the cyclo-L-Pro-D-Leu formation. To explain this confusion, we then investigated whether the chiral amino acids used in the experiment were racemized under the above reaction conditions (that is an initial pH 11.7 at 35°C for 6 days). The results showed that these chiral amino acids did not undergo chiral racemization (**Figure 2**). So, the two isomers may be the result of the condensations reaction itself, in which two different stereoisomer products were formed from the reaction of L-Pro and D-Leu. Therefore, the yield of cyclo-L-Pro-D-Leu is the sum of these two peaks of 19.8 min and 20.2 min (**Figures 1A,B**). Similarly, in **Figure 1C**, the yield of cyclo-L-Pro-L-Leu is the sum of peak 19.8 min and peak 20.2 min (**Figures 1A,C**).

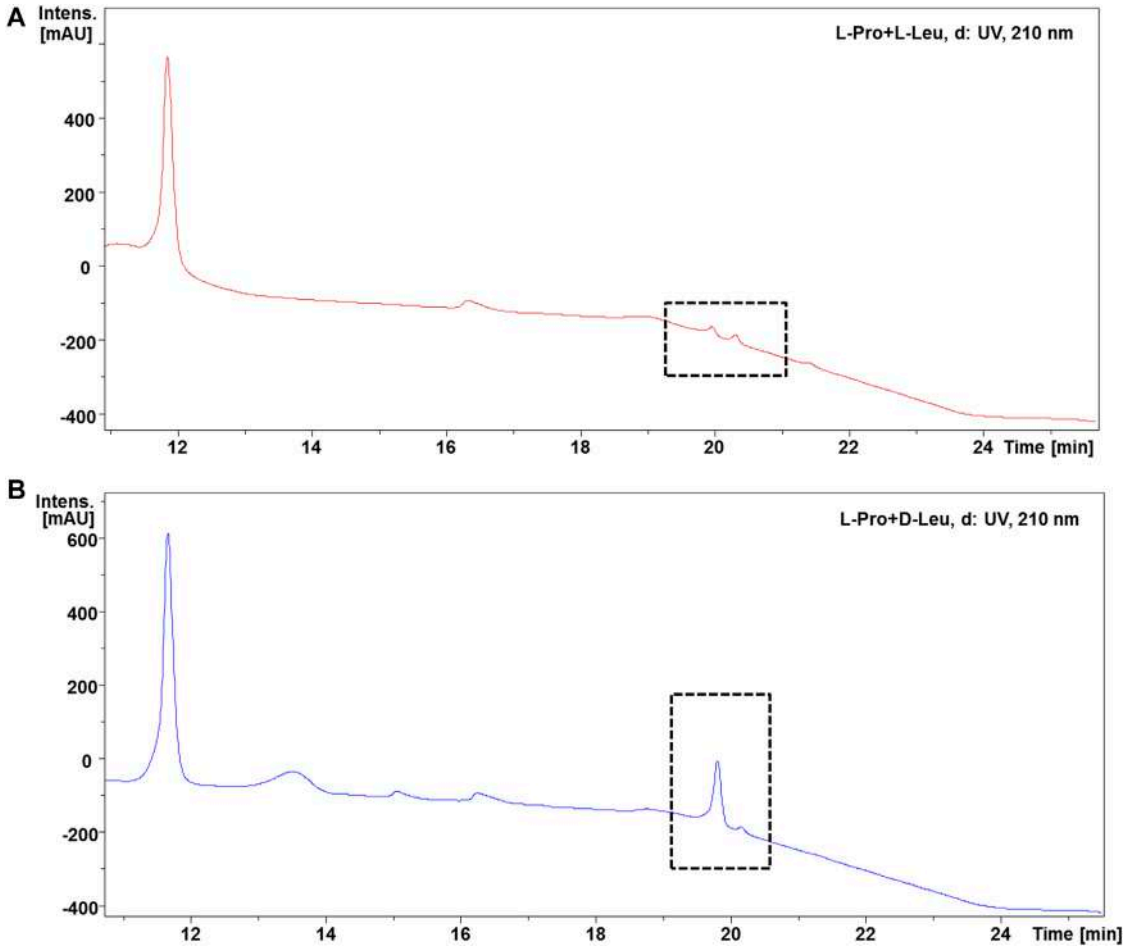

FIGURE 3 | HPLC spectra analysis of cyclo-Pro-Leu products. **(A)**: HPLC profile for the reaction products cyclo-L-Pro-L-Leu of L-Leu with L-Pro and P_3m in aqueous solution. **(B)**: HPLC spectrum of products cyclo-L-Pro-D-Leu from the reaction system with D-Leu, L-Pro and P_3m. The peaks in the gridlines represent corresponding products cyclo-Pro-Leu. The peak with retention time of 11.9 min was cyclo-Pro-Pro.

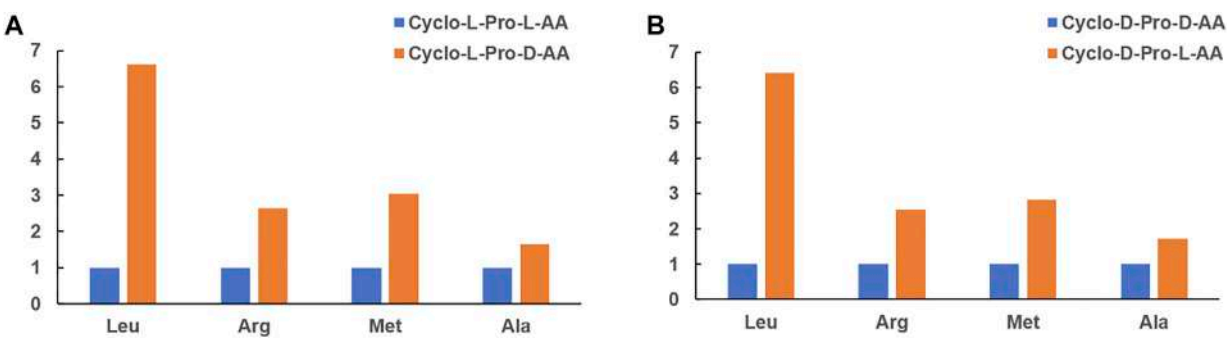

FIGURE 4 | The relative intensity of UV- absorption of the cyclo-Pro-AAs at 210 nm in these reactions. **(A)** Bar graph representation of the reaction L-Pro with four L-/D-AAs, respectively. **(B)** Bar graph representation of the reaction D-Pro with four L-/D-AAs, respectively.

These results indicated that both L-Leu and D-Leu with L-Pro can form corresponding chiral cyclo-Pro-Leu under alkaline aqueous solution, respectively. And remarkably, it showed that the formation of cyclo-L-Pro-D-Leu was preferred over that of cyclo-L-Pro-L-Leu by a ratio of about 6.61: 1, i.e., D-Leu was preferred over L-Leu in the presence of L-Pro (**Figures 3**, **4**). Moreover, when the

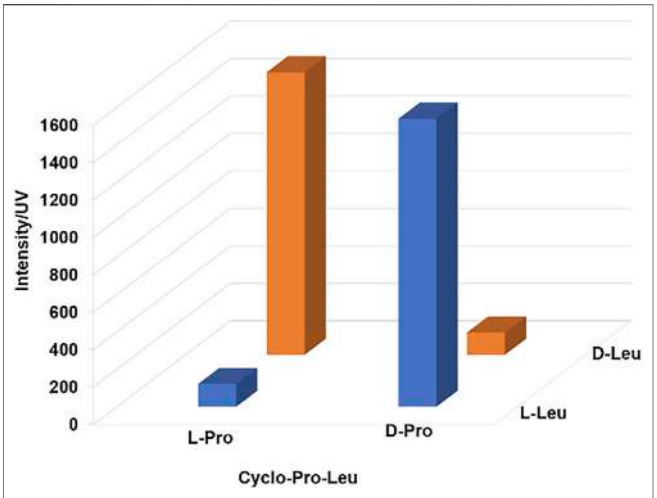

FIGURE 5 | Effect of chirality of Pro and Leu on the cyclo-Pro-Leu formation. These reactions were carried out under standard conditions.

chirality of Pro was changed into the D-configuration, the results showed that the yield of cyclo-D-Pro-L-Leu from L-Leu was higher than that cyclo-D-Pro-D-Leu from D-Leu, which was improved to 6.42-fold (**Figure 4**; **Supplementary Figures S2–S3**). As in our previous study, cyclo-Pro-Pro was the primary product of Pro reaction with other amino acids in the P_3m alkaline solution, while cyclo-Pro-Leu (heterocyclic dipeptides) were relatively rare (Ying et al., 2018b). The formation of cyclo-Pro-Pro did not involve chiral selection, so the cyclo-Pro-Pro was not considered in this study.

Moreover, analogous experiments were also performed with the other three L-/D-AAs (Arg, Met and Ala) revealing similar selectivity for the cyclo-L-Pro-AAs and cyclo-D-Pro-AAs species. That was L-Pro preferentially reacted with the D-AA to form cyclo-L-Pro-AA while D-Pro chose L-AA more than D-AA to form cyclo-D-Pro-AA (**Figure 4**; **Supplementary Figures S1, S4–S15**). It was further shown that the yield of heterochiral cyclo-Pro-AA was higher than that of homochiral cyclo-Pro-AA (**Figure 5**; **Supplementary Figure S16**).

In the case of Ala, the reaction with L-/D-Pro showed EIC (m/z 169.0972) of cyclo-Pro-Ala yielding one peak with the retention time of 8.6 min (**Supplementary Figures S12–S15**). The unusual behavior of Ala was attributed to the small polarity difference between two stereoisomers of cyclo-Pro-Ala, which results in their retention times being almost identical in the HPLC-MS.

Taken together, our data showed that chiral selection of amino acids can occur during the process of AAs reaction with Pro generating cyclo-Pro-AAs. These results revealed that the formation of cyclo-Pro-AAs for the reaction of L-/D-AA and Pro exhibit an intrinsic chiral selection at the molecular level. **Figure 4** shows that the chiral selectively was about 1.65–6.61 fold for each case, respectively. Alata argues that cyclic dipeptide was a planar structure when it was formed by amino acids with small side chains (e.g., glycine). When the side chain groups of amino acids are larger, a planar structure is produced only when the amino acids have opposite chirality which had smaller formation energy (Alata et al., 2017). It is coincided with our results. In other words, heterochiral cyclic dipeptides are formed more than homochiral cyclic dipeptides. Pro is thought to have existed in the prebiotic environment and was one of the first amino acids to be biologically encoded (Zaia et al., 2008). Cis-trans isomerization reactions usually limit the rate of peptide and protein folding (Wedemeyer et al., 2002). Pro can kink the helix, terminate the helix, and form amide hydrogen without the helix (Counterman and Clemmer, 2004). We speculate that Pro may have provided a special contribution to the evolution of peptides due to its aforementioned properties. Studying the formation and structure of Pro-containing DKP may be a key step in prebiotic peptides. According to previous studies, some characteristic environmental factors could achieve chiral enrichment of amino acids from the initial racemic mixing in the early Earth (Bondy and Harrington, 1979; Hazen et al., 2001; Wedyan and Preston, 2005; Breslow and Cheng, 2009; Fraser et al., 2011a; Fraser et al., 2011b). During the long-term evolution of the Earth, some environmental conditions led to selective enrichment of L-AA under a prebiotic environment (Bondy and Harrington, 1979; Breslow and Cheng, 2009). In the above mentioned case, D-AAs are more likely to participate in the formation of cyclic dipeptides in the presence of L-Pro of enantio-enrichment, resulting in more L-AAs to take part in other reactions (e.g., linear dipeptides synthesis). Although this chiral selection is under weak pressure, it could lead to an overpowering preference to use L-amino acids in the biological system over the long period of the prebiotic evolution process.

4 CONCLUSION

In conclusion, reactions of L-/D-amino acids (AAs) with Pro can shape the corresponding chiral cyclo-Pro-AAs in the alkaline aqueous solution. Furthermore, the chiral selectivity of AAs, during the cyclo-Pro-AAs formation, has been found at the molecular level. In other words, cyclo-Pro-AAs can be synthesized by L-Pro with a clear preference for D-AA over L-AA. Vice-versa, L-AA was preferred over D-AA in the presence of D-Pro. These findings are very helpful to understand the chiral selection of AA in the prebiotic chemical evolution. Therefore, we believe that the fixed chirality of AA in biosystem peptides is not necessarily determined in a certain process, but may be caused by the confluence of multiple processes.

DATA AVAILABILITY STATEMENT

The original contributions presented in the study are included in the article/**Supplementary Material**, further inquiries can be directed to the corresponding authors.

AUTHOR CONTRIBUTIONS

YZ conceived the research. JY designed the experiments. YG jointly performed key research and experiments. YZ and YL performed HPLC-MS. YZ, JY, and GZ wrote the paper.

FUNDING

This work was supported by the National Natural Science Foundation of China (Nos. 42003062, 91856126 and 21778042), Scientific Research Grant of Ningbo University (No. 215-432000282), Ningbo Top Talent Project (No. 215-432094250) and Scientific Research Foundation of Key Laboratory of Marine Biogenetic Resources, Third Institute of Oceanography, Ministry of Natural Resources (No. HY202104).

ACKNOWLEDGMENTS

We thank Songsen Fu (Ningbo University) and Yile Wu (Ningbo University) for many constructive comments on this manuscript.

SUPPLEMENTARY MATERIAL

The Supplementary Material for this article can be found online at: https://www.frontiersin.org/articles/10.3389/fspas.2022.794932/full#supplementary-material

REFERENCES

Alata, I., Pérez-Mellor, A., Ben Nasr, F., Scuderi, D., Steinmetz, V., Gobert, F., et al. (2017). Does the Residues Chirality Modify the Conformation of a Cyclo-Dipeptide? Vibrational Spectroscopy of Protonated Cyclo-Diphenylalanine in the Gas Phase. *J. Phys. Chem. A.* 121, 7130–7138. doi:10.1021/acs.jpca.7b06159

Bondy, S. C., and Harrington, M. E. (1979). L Amino Acids and D-Glucose Bind Stereospecifically to a Colloidal clay. *Science* 203, 1243–1244. doi:10.1126/science.424749

Bonner, W. A. (2000). Parity Violation and the Evolution of Biomolecular Homochirality. *Chirality* 12, 114–126. doi:10.1002/(sici)1520-636x(2000)12:3<114:aid-chir3>3.0.co;2-n

Borthwick, A. D. (2012). 2,5-Diketopiperazines: Synthesis, Reactions, Medicinal Chemistry, and Bioactive Natural Products. *Chem. Rev.* 112, 3641–3716. doi:10.1021/cr200398y

Botti, P., Pallin, T. D., and Tam, J. P. (1996). Cyclic Peptides from Linear Unprotected Peptide Precursors through Thiazolidine Formation. *J. Am. Chem. Soc.* 118, 10018–10024. doi:10.1021/ja954278g

Breslow, R., and Cheng, Z.-L. (2009). On the Origin of Terrestrial Homochirality for Nucleosides and Amino Acids. *Proc. Natl. Acad. Sci.* 106, 9144–9146. doi:10.1073/pnas.0904350106

Counterman, A. E., and Clemmer, D. E. (2004). Anhydrous Polyproline Helices and Globules. *J. Phys. Chem. B* 108, 4885–4898. doi:10.1021/jp036454a

Fernández Guasti, M. (2019). Chirality, Helicity and the Rotational Content of Electromagnetic fields. *Phys. Lett. A* 383, 3180–3186. doi:10.1016/j.physleta.2019.06.002

Fraser, D. G., Fitz, D., Jakschitz, T., and Rode, B. M. (2011a). Selective Adsorption and Chiral Amplification of Amino Acids in Vermiculite clay-implications for the Origin of Biochirality. *Phys. Chem. Chem. Phys.* 13, 831–838. doi:10.1039/c0cp01388a

Fraser, D. G., Greenwell, H. C., Skipper, N. T., Smalley, M. V., Wilkinson, M. A., Demé, B., et al. (2011b). Chiral Interactions of Histidine in a Hydrated Vermiculite clay. *Phys. Chem. Chem. Phys.* 13, 825–830. doi:10.1039/c0cp01387k

Guo, Y., Ying, J., Sun, D., Zhang, Y., Zheng, M., Ding, R., et al. (2021). Cyclic Dipeptides Formation from Linear Dipeptides under Potentially Prebiotic Earth Conditions. *Front. Chem.* 9, 398. doi:10.3389/fchem.2021.675821

Hazen, R. M., Filley, T. R., and Goodfriend, G. A. (2001). Selective Adsorption of L- and D-Amino Acids on Calcite: Implications for Biochemical Homochirality. *Pnas* 98, 5487–5490. doi:10.1073/pnas.101085998

Hazen, R. M., and Sholl, D. S. (2003). Chiral Selection on Inorganic Crystalline Surfaces. *Nat. Mater* 2, 367–374. doi:10.1038/nmat879

Huber, C., Eisenreich, W., Hecht, S., and Wächtershäuser, G. (2003). A Possible Primordial Peptide Cycle. *Science* 301, 938–940. doi:10.1126/science.1086501

Jainta, M., Nieger, M., and Bräse, S. (2008). Microwave-Assisted Stereoselective One-Pot Synthesis of Symmetrical and Unsymmetrical 2,5-Diketopiperazines from Unprotected Amino Acids. *Eur. J. Org. Chem.* 2008, 5418–5424. doi:10.1002/ejoc.200800605

Joshi, P. C., Ferris, J. P., and Pitsch, S. (2000). Homochiral Selection in the Montmorillonite-Catalyzed and Uncatalyzed Prebiotic Synthesis of RNA. *Chem. Commun.*, 2497–2498. doi:10.1039/b007444f

Lambert, J. N., Mitchell, J. P., and Roberts, K. D. (2001). The Synthesis of Cyclic Peptides. *J. Chem. Soc. Perkin Trans.* 1, 471–484. doi:10.1039/b001942i

Manchineella, S., Prathyusha, V., Priyakumar, U. D., and Govindaraju, T. (2013). Solvent-Induced Helical Assembly and Reversible Chiroptical Switching of Chiral Cyclic-Dipeptide-Functionalized Naphthalenediimides. *Chem. Eur. J.* 19, 16615–16624. doi:10.1002/chem.201303123

Nonappa, N., Ahonen, K., Lahtinen, M., and Kolehmainen, E. (2011). Cyclic Dipeptides: Catalyst/promoter-free, Rapid and Environmentally Benign Cyclization of Free Amino Acids. *Green. Chem.* 13, 1203–1209. doi:10.1039/c1gc15043j

Parker, E. T., Zhou, M., Burton, A. S., Glavin, D. P., Dworkin, J. P., Krishnamurthy, R., et al. (2014). A Plausible Simultaneous Synthesis of Amino Acids and Simple Peptides on the Primordial Earth. *Angew. Chem. Int. Ed.* 53, 8132–8136. doi:10.1002/anie.201403683

Poullennec, K. G., Kelly, A. T., and Romo, D. (2002). Highly Diastereoselective Desymmetrizations of Cyclo(Pro,Pro): An Enantioselective Strategy toward Phakellstatin and Phakellin. *Org. Lett.* 4, 2645–2648. doi:10.1021/ol026140q

Prasad, C. (1995). Bioactive Cyclic Dipeptides. *Peptides* 16, 151–164. doi:10.1016/0196-9781(94)00017-z

Rabinowitz, J., Flores, J., Krebsbach, R., and Rogers, G. (1969). Peptide Formation in the Presence of Linear or Cyclic Polyphosphates. *Nature* 224, 795–796. doi:10.1038/224795a0

Rikken, G. L. J. A., and Raupach, E. (2000). Enantioselective Magnetochiral Photochemistry. *Nature* 405, 932–935. doi:10.1038/35016043

Tamura, K. (2008). Origin of Amino Acid Homochirality: Relationship with the RNA World and Origin of tRNA Aminoacylation. *Biosystems* 92, 91–98. doi:10.1016/j.biosystems.2007.12.005

Trauger, J. W., Kohli, R. M., Mootz, H. D., Marahiel, M. A., and Walsh, C. T. (2000). Peptide Cyclization Catalysed by the Thioesterase Domain of Tyrocidine Synthetase. *Nature* 407, 215–218. doi:10.1038/35025116

Wedemeyer, W. J., Welker, E., and Scheraga, H. A. (2002). Proline Cis–Trans Isomerization and Protein Folding. *Biochemistry* 41, 14637–14644. doi:10.1021/bi020574b

Wedyan, M., and Preston, M. R. (2005). Isomer-selective Adsorption of Amino Acids by Components of Natural Sediments. *Environ. Sci. Technol.* 39, 2115–2119. doi:10.1021/es040474o

Yachmenev, A., Onvlee, J., Zak, E., Owens, A., and Küpper, J. (2019). Field-Induced Diastereomers for Chiral Separation. *Phys. Rev. Lett.* 123, 243202. doi:10.1103/PhysRevLett.123.243202

Yamagata, Y., Watanabe, H., Saitoh, M., and Namba, T. (1991). Volcanic Production of Polyphosphates and its Relevance to Prebiotic Evolution. *Nature* 352, 516–519. doi:10.1038/352516a0

Ye, X., Cui, J., Li, B., Li, N., Wang, R., Yan, Z., et al. (2019). Enantiomer-selective Magnetization of Conglomerates for Quantitative Chiral Separation. *Nat. Commun.* 10, 1964. doi:10.1038/s41467-019-09997-y

Ying, J., Fu, S., Li, X., Feng, L., Xu, P., Liu, Y., et al. (2018a). A Plausible Model Correlates Prebiotic Peptide Synthesis with the Primordial Genetic Code. *Chem. Commun.* 54, 8598–8601. doi:10.1039/c8cc04767g

Ying, J., Lin, R., Xu, P., Wu, Y., Liu, Y., and Zhao, Y. (2018b). Prebiotic Formation of Cyclic Dipeptides under Potentially Early Earth Conditions. *Sci. Rep.* 8, 936. doi:10.1038/s41598-018-19335-9

Zaia, D. A. M., Zaia, C. T. B. V., and De Santana, H. (2008). Which Amino Acids Should Be Used in Prebiotic Chemistry Studies? *Orig Life Evol. Biosphbiospheres* 38, 469–488. doi:10.1007/s11084-008-9150-5

Conflict of Interest: The authors declare that the research was conducted in the absence of any commercial or financial relationships that could be construed as a potential conflict of interest.

frontiers in Astronomy and Space Sciences

ORIGINAL RESEARCH
published: 22 February 2022
doi: 10.3389/fspas.2022.794067

Nebula-Relay Hypothesis: The Chirality of Biological Molecules in Molecular Clouds

Lei Feng[1,2,3]*

[1]Key Laboratory of Dark Matter and Space Astronomy, Purple Mountain Observatory, Chinese Academy of Sciences, Nanjing, China, [2]School of Astronomy and Space Science, University of Science and Technology of China, Hefei, China, [3]Joint Center for Particle, Nuclear Physics and Cosmology, Nanjing University - Purple Mountain Observatory, Nanjing, China

The chiral puzzle of biological molecules is thought to be closely related to the origin of life and is still a mystery so far. Previously, we proposed a new model on the origin of life, Nebula-Relay hypothesis, which assumed that the life on Earth originated at the planetary system of the Sun's predecessor star and then filled in the pre-solar nebula after its death. As primitive lives existed in the pre-solar nebula for a long time, did the chiral biomolecules form during this period? We explore such a possibility in this work and find that the ultra-low temperature environment of molecular clouds is beneficial to generating the chiral polymer chain of biological molecules.

Keywords: chirality, Nebula-Relay hypothesis, molecular cloud, biological molecules, peptide chain

OPEN ACCESS

Edited by:
Yiliang Li,
The University of Hong Kong, Hong Kong SAR, China

Reviewed by:
Jan Hendrik Bredehöft,
University of Bremen, Germany
Josep M. Trigo-Rodríguez,
Institute of Space Sciences (CSIC), Spain

***Correspondence:**
Lei Feng
fenglei@pmo.ac.cn

Specialty section:
This article was submitted to Astrobiology, a section of the journal Frontiers in Astronomy and Space Sciences

Received: *13 October 2021*
Accepted: *25 January 2022*
Published: *22 February 2022*

Citation:
Feng L (2022) Nebula-Relay Hypothesis: The Chirality of Biological Molecules in Molecular Clouds. Front. Astron. Space Sci. 9:794067. doi: 10.3389/fspas.2022.794067

1 INTRODUCTION

Symmetry usually refers to the invariance of an object under some transformations, such as translation, reflection, and rotation. It is also a fundamental aspect of biological molecules. In chemistry, if a molecule or ion cannot be superposed on its mirror image by any transform, we call them enantiomers. These two enantiomers are usually labeled as "right(left)-handed" or D(L) forms. It is the nature of chirality and an intrinsic property of natural chemical molecules. Unlike typical chemical synthesis, chirality is broken in the biochemical processes of living systems. For example, there are only L-amino acids in proteins and D-ribose in ribonucleic acids for almost all creatures on Earth. The origin of biological chiral is an intractable mystery that has plagued us for a long time and is thought to be related to the origination of life.

Generally speaking, there are two most persuasive and popular models, i.e., abiogenesis (Alexander Oparin, 2021; Haldane, 2021) and panspermia theory (Davies, 1988). The famous Miller–Urey experiment (Miller, 1953) proved that amino acids (constituents of the proteins) could be synthesized in the reaction chamber, which simulates the environment of the early earth. However, equivalent left- and right-handed amino acids are produced in this experiment. Some new experiments demonstrated the catalytic action of chondritic meteorite minerals in mild aqueous environments (Rotelli et al., 2016; Cabedo et al., 2021), which is very instructive for this field. Alexander et al. (2017) and Alexander et al. (2018) pointed out that the insoluble organic materials in comets are potential sources of volatiles for the terrestrial planets in the solar system. Anyway, the origin of life is much more complicated than we thought, and new mechanisms need to be introduced into the origination model of life.

There are many discussions about chiral puzzle already. One possible explanation is proposed by Vester–Ulbricht, who assume that left-handed electrons, produced by parity-violating beta decays, interact with biological precursor molecules and destroy one type of enantiomer more significantly

(Vester et al., 1959; Ulbricht and Vester, 1962) than another. The circularly polarized bremsstrahlung produced by the longitudinally spin-polarized beta electrons, they guess, is the reason which preferentially photolyzes certain chiral molecules (Ulbricht and Vester, 1962).

Some studies pointed out that the interaction between beta electrons and chiral molecules can induce a left–right asymmetry of order $\sim 10^{-6}$ (Zeldovithe and Sakyan, 1980; Wang and Luo, 1985). Several experiments were designed to search evidence of the above scenario, but no one achieved positive and repeatable results (Bonner et al., 1979; Hodge et al., 1979; Bonner, 1991; Bonner, 2000; Fitz et al., 2007). Circularly polarized light has been detected in molecular clouds. For example, the authors reported a high degree of circular polarization of as much as 22% in NGC 6334 in Kwon et al. (2013). According to the Vester–Ulbricht hypothesis, chiral amino acids can be synthesized under such an environment.

Carbonaceous chondrites are the only rocks that can provide original records of pre-solar nebula processes. The famous Murchison meteorite is one kind of carbonaceous chondrite which is rich in organic compounds and contends more than fifteen types of amino acids (Wolman et al., 1972). Some types of amino acids were found to have an excess of the L-configuration (Engel and Nagy, 1982; Cronin and Pizzarello, 1997; Engel and Macko, 1997), but there are also many objections (Bada et al., 1983; Pizzarello and Cronin, 1998). Schmitt-Kopplin and his collaborators had identified 70 amino acids in Murchison meteorite (Schmitt-Kopplin et al., 2010). Several amino acids are also distinguished from a carbonaceous chondrite at Mukundpura, India (Rudraswami et al., 2019). There are ninety two types of amino acids identified in meteorites according to current research studies (Cronin et al., 1995; Martins et al., 2009; Glavin et al., 2010; Elsila et al., 2016; Burton and Berger, 2018). These facts may hint that there are amino acids in molecular clouds.

This paper is organized as follows: In **Section 2**, we briefly introduce the Nebula-Relay hypothesis. Then, we present the calculation method we used in this manuscript in **Section 3**. The main results are presented in **Section 4**, and the conclusions are summarized in **Section 5**.

2 NEBULA-RELAY HYPOTHESIS

In panspermia theory, it is presumed that primitive lives spread to Earth from other planets in the solar system or other planetary systems in the Milky Way. However, it does not solve the problem of how and where life originated, let alone the chiral puzzle of biological molecules.

Feng (2021) proposed a new hypothesis on the origin of Earth's life, named "Nebula-Relay hypothesis" or "local panspermia." The original intention of our hypothesis is that life on Earth may appear too early (Dodd et al., 2017). We assume that the chemical origin theory is correct but takes billions of years. Then, we believe that primitive life formed on the planet system of the sun's predecessor star and filled in the produced pre-solar nebula after the death of the predecessor star. So, the history of Earth's life can be divided into three epochs: the origin of life on the planetary system of the Sun's predecessor star, primitive life epoch in the pre-solar nebula, and Earth life epoch.

In epoch I, primitive creatures were formed on the planet of the pre-solar star through complex physicochemical interactions. The environment of the pre-solar planet may be similar to that of the early Earth, and then explorations on the origin of Earth's life are inspiring and informative. Rotelli et al. (2016) pointed out that most of the complex organic compounds were produced by the catalytic action of minerals under the presence of heat and water. Complex organics in meteorites can also be generated in their parent asteroids through Fischer–Tropsch catalytic reactions (Cabedo et al., 2021). Nuth et al. (2020) studied the complex carbon cycle on the evolving asteroid through thermal or hydrous metamorphic processes.

Cosmic ray (CR, also including the contribution of nearby bright stars) particles collide with the gas in nebula and produce low-energy secondary particles. It reduces high-energy CR particles and protects primitive life from lethal radiation. So, we propose that low-energy secondary electrons and (or) photons of CR are the energy source of living creatures in molecular clouds (Feng, 2021).

There are differences between this model and ordinary panspermia theory. Different from the shuttle of seeds in panspermia, primitive life in this model occurred on the local place at the pre-solar epoch and scattered in the pre-solar nebula. Homologous lives are almost everywhere in the solar system, and we can search for the traces of these homologous creatures to test this model. As the energy comes from the cosmic ray and the encapsulation of the meteorite prevents this process, there are no living forms in meteorite materials. Although challenging, their fossils might be found in meteorites.

Can the chiral puzzle be satisfactorily explained in the Nebula-Relay hypothesis? We explore this problem in this article and try to prove that the low-temperature environment is conducive to the production of biological chirality.

3 SOME PHYSICAL BACKGROUNDS

The previous section shows that the chiral biomolecules could be achieved through their interaction with longitudinally spin-polarized beta electrons or circularly polarized light. However, no significant chiral differences were found in the amino acids of meteorites. In other words, the difference between enantiomers is tiny.

This work aims to achieve the chirality of biomolecules with such a slight left–right deviation. Following the calculation method in Luo (1994), we try to explore the amplification of left–right asymmetry through the polymerization process in the low-temperature environment of molecular cloud, i.e., the production of homochiral polymers.

Firstly, we suppose that the distribution of chiral monomers satisfies the Boltzmann distribution, i.e., $n_{L,D} \sim \exp(-E_{L,D}/K_B T)$, where $E_{L,D}$ is the energy of L(D)-form chiral monomer, respectively, and K_B is the Boltzmann constant. The following formula can describe the polarization of chiral monomers:

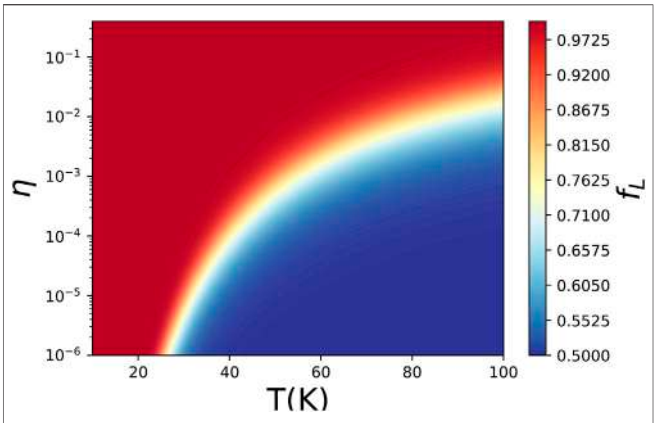

FIGURE 1 | Probability of L-type monomer in the polymer chain.

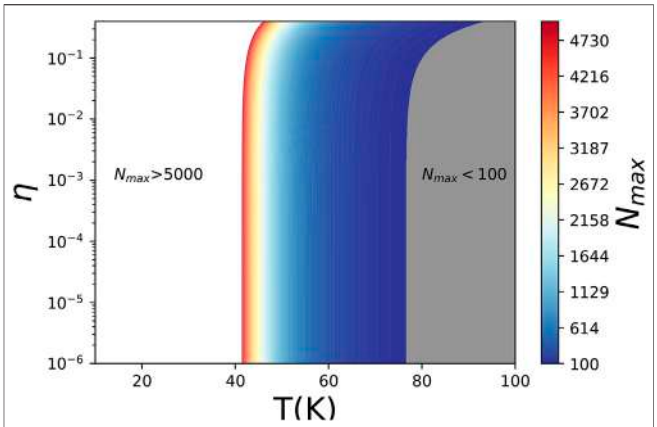

FIGURE 2 | Dependence of the maximum pure L-type chain length N on η and temperature.

$$\eta = (n_L - n_D)/(n_L + n_D) = \tanh J, \tag{1}$$

where

$$J = (E_D - E_L)/2K_BT. \tag{2}$$

Then, we focus on the recombined energy of neighboring monomers $E_{LL,DD,LD,DL}$ and set $E_{LL} = E_{DD}$, $E_{LD} = E_{DL}$ for symmetry consideration. The chiral interaction energy is defined as follows:

$$U = (E_{LD} - E_{LL})/2K_BT. \tag{3}$$

If $U > 0$, the system tends to state the identical chiral monomers stick together. We then define stereoselectivity γ to describe the difference of probabilities of adding distinct chiral monomers as in Luo (1994), which is

$$\gamma = \tanh U = \frac{\exp(-E_{LL}/K_BT) - \exp(-E_{LD}/K_BT)}{\exp(-E_{LL}/K_BT) + \exp(-E_{LD}/K_BT)}. \tag{4}$$

To form a pure L-form polymer chain with length N_c and relatively high probability, there must be (Avetisov et al., 1991)

$$\frac{(1-\eta)(1-\gamma)}{2(1+\eta\gamma)} < N_c^{-1}. \tag{5}$$

The Hamiltonian of the system is described by

$$H = -K_BT\left(J\sum_i \sigma_i + U\sum_i \sigma_i\sigma_{i+1}\right), \tag{6}$$

where the chirality of each monomer is described by the spin σ_i ($\sigma_i = \pm 1$ denotes L- and D-form chiral molecular). As in Luo (1994), a statistical ensemble with the above Hamiltonian can be used to calculate the equilibrium distribution of chiral monomers through the Ising model (Huang, 1963). The chiral polarization of polymer f_L can be calculated through the following formula:

$$f_L = \frac{1}{2}\left\{1 + \sinh J \Big/ \left[\sinh^2 J + e^{-4U}\right]^{1/2}\right\}, \tag{7}$$

where $f_{L(D)}$ denotes the probability of L(D)-form monomer in the chain and $f_L + f_D = 1$. $f_L = 1$ denotes the pure L-form monomer and vice versa. It is obvious that if $\exp^{-4U} \ll \sinh J$, $f_L \sim 1$.

Combining amino acids into peptide chains is an exothermic reaction in nature, and reactions between homochiral molecules release more heat. Therefore, more energy is required to decompose the bonds of homochiral molecules during the photolysis/radiolysis process, but L-D chemical bond is much easier to break down. This effect would further amplify pure L-form polymer chains, although we do not consider this effect here.

4 CHIRAL OF BIOMOLECULES IN A LOW-TEMPERATURE ENVIRONMENT

The typical temperature of molecular cloud is about 10 ~ 50 K but has significant differences in different regions. Wilson et al. (1997) pointed out that molecular clouds with H II regions have temperatures of 15–100 K, and even larger in the giant H II region. Therefore, we set 10 K < T < 100 K and $E_{LD} - E_{LL}$ = 700 Cal/mol (1% of C-N bound energy) in following calculations.

The probability of L-form monomer in the polymer chain is shown in **Figure 1**. It is easy to see that low temperature and large polarization of chiral monomers could enlarge the probability of an L-form monomer. At low temperature (T < 25 K), a tiny deviation between L and D types of monomers could induce a left-handed chain, which is consistent with the critical temperature in Luo (1994) with polarization 10^{-6}. For $\eta \sim 10^{-2}$, temperatures below 100 K are all suitable.

According to **Eq. 5**, we define the maximum permissible length of pure L-type polymer chain N_{max} as follows:

$$N_{max} = \left[\frac{2(1+\eta\gamma)}{(1-\eta)(1-\gamma)}\right]. \tag{8}$$

The relation between N_{max} and (η, γ) is shown in **Figure 2**. From the figure, we can see that the maximum length of pure

L-type chain is less than 100 as $T > 80$ K because η and γ decrease sharply with increasing temperature.

During the formation of the solar system, the temperature increased in high-density areas. But the temperature in the other regions is still relatively low. Moreover, the left-handed biological system has already formed, and temperature changes no longer affect the chirality of biomolecules.

5 SUMMARY AND DISCUSSIONS

In this article, we calculate the probability of generating homochiral polymers in the nebula environment with a slight deviation in the density of the left- and right-handed monomers. We intend to explain the chiral puzzle of biomolecules. Our calculations show that chiral polymers can be naturally induced in an ultra-low temperature molecular cloud environment because the polarization and stereoselectivity of chiral biomolecules are much smaller than the homeothermy one. Moreover, a pure left-handed polymer chain can be much longer in a low-temperature environment. Furthermore, this model might be tested through low-temperature experiments.

DATA AVAILABILITY STATEMENT

The original contributions presented in the study are included in the article/Supplementary Materials, further inquiries can be directed to the corresponding author.

AUTHOR CONTRIBUTIONS

The author confirms being the sole contributor of this work and has approved it for publication.

FUNDING

This work was supported by the National Natural Science Foundation of China (Grant No. 11 773 075) and the Youth Innovation Promotion Association of Chinese Academy of Sciences (Grant No. 2016 288).

ACKNOWLEDGMENTS

The author thanks Dr. Lei Zu and Zi-Qing Xia for their generous help in perfecting this article.

REFERENCES

Alexander, C. M. O. D., Cody, G. D., De Gregorio, B. T., Nittler, L. R., and Stroud, R. M. (2017). The Nature, Origin and Modification of Insoluble Organic Matter in Chondrites, the Major Source of Earth's C and N. *Geochemistry* 77, 227–256. doi:10.1016/j.chemer.2017.01.007

Alexander, C. M. O'D., McKeegan, K. D., and Altwegg, K. (2018). Water Reservoirs in Small Planetary Bodies: Meteorites, Asteroids and Comets. *Space Sci. Rev.* 214 (36), 47. doi:10.1007/s11214-018-0474-9

Alexander Oparin (2021). *The Origin of Life*. 9780486495224.

Avetisov, V. A., Kuz'min, V. V., and Goldanskii, V. I. (1991). Handedness, Origin of Life and Evolution. *Phys. Today* 44, 33–41. doi:10.1063/1.881264

Bada, J. L., Cronin, J. R., Ho, M.-S., Kvenvolden, K. A., Lawless, J. G., Miller, S. L., et al. (1983). On the Reported Optical Activity of Amino Acids in the Murchison Meteorite. *Nature* 301 (5900), 494–496. doi:10.1038/301494a0

Bonner, W. A., Blair, N. E., and Flores, J. J. (1979). Attempted Asymmetric Radiolysis of D,L-tryptophan with 32P β Radiation. *Nature* 281, 150–151. doi:10.1038/281150a0

Bonner, W. A. (2000). Parity Violation and the Evolution of Biomolecular Homochirality. *Chirality* 12, 114–126. doi:10.1002/(sici)1520-636x(2000)12:3<114::aid-chir3>3.0.co;2-n

Bonner, W. A. (1991). The Origin and Amplification of Biomolecular Chirality. *Origins Life Evol. Biosph.* 21, 59–111. doi:10.1007/bf01809580

Burton, A., and Berger, E. (2018). Insights into Abiotically-Generated Amino Acid Enantiomeric Excesses Found in Meteorites. *Life* 8, 14. doi:10.3390/life8020014

Cabedo, V., Llorca, J., Trigo-Rodriguez, J. M., and Rimola, A. (2021). Study of Fischer-tropsch-type Reactions on Chondritic Meteorites. *A&A* 650, A16023. doi:10.1051/0004-6361/202039991

Cronin, J. R., Cooper, G. W., and Pizzarello, S. (1995). Characteristics and Formation of Amino Acids and Hydroxy Acids of the Murchison Meteorite. *Adv. Space Res.* 15, 91–97. doi:10.1016/s0273-1177(99)80068-4

Cronin, J. R., and Pizzarello, S. (1997). Enantiomeric Excesses in Meteoritic Amino Acids. *Science* 275 (5302), 951–955. doi:10.1126/science.275.5302.951

Davies, R. E. (1988). Panspermia: Unlikely, Unsupported, but Just Possible. *Acta Astronautica* 17, 129–135. doi:10.1016/0094-5765(88)90136-1

Dodd, M. S., Papineau, D., Grenne, T., Slack, J. F., Rittner, M., Pirajno, F., et al. (2017). Evidence for Early Life in Earth's Oldest Hydrothermal Vent Precipitates. *Nature* 543, 764360–764364. doi:10.1038/nature21377

Elsila, J. E., Aponte, J. C., Blackmond, D. G., Burton, A. S., Dworkin, J. P., and Glavin, D. P. (2016). Meteoritic Amino Acids: Diversity in Compositions Reflects Parent Body Histories. *ACS Cent. Sci.* 2, 370–379. doi:10.1021/acscentsci.6b00074

Engel, M. H., and Macko, S. A. (1997). Isotopic Evidence for Extraterrestrial Non-Racemic Amino Acids in the Murchison Meteorite. *Nature* 389 (6648), 265–268. doi:10.1038/38460

Engel, M. H., and Nagy, B. (1982). Distribution and Enantiomeric Composition of Amino Acids in the Murchison Meteorite. *Nature* 296 (5860), 837–840. doi:10.1038/296837a0

Feng, L. (2021). Nebula-Relay Hypothesis: Primitive Life in Nebula and Origin of Life on Earth[J]. *Acta Astronomica Sinica* 62 (3), 28. [arXiv: 1910.06396].

Fitz, D., Reiner, H., Plankensteiner, K., and Michael Rode, B. (2007). Possible Origins of Biohomochirality. *Ccb* 1, 41–52. doi:10.2174/2212796810701010041

Glavin, D. P., Callahan, M. P., Dworkin, J. P., and Elsila, J. E. (2010). The Effects of Parent Body Processes on Amino Acids in Carbonaceous Chondrites. *Meteorit. Planet. Sci.* 45, 1948–1972. doi:10.1111/j.1945-5100.2010.01132.x

Haldane, J. B. S. (2021). The Origin of Life. *Rationalist Annu.* 148, 3–10.

Hodge, L. A., Dunning, F. B., Walters, G. K., White, R. H., and Schroepfer, G. J. (1979). Degradation of DL-Leucine with Longitudinally Polarised Electrons. *Nature* 280, 250–252. doi:10.1038/280250a0

Huang, K. S. (1963). *Statistical Mechanics*. New York: Wiley, 346.

Kwon, J., Tamura, M., Lucas, P. W., Hashimoto, J., Kusakabe, N., Kandori, R., et al. (2013). Near-infrared Circular Polarization Images of Ngc 6334-v. *ApJ* 765, L6. doi:10.1088/2041-8205/765/1/l6

Luo, L. F. (1994). *Acta Scientiarum Naturalium Universitatis Intramongolicae (Neimenggu)* 25, 282. [C2 of this collected works].

Martins, Z., Sephton, M., and Hughes, A. (2009). "Amino Acids," in *Peptides and Proteins in Organic Chemistry: Origins and Synthesis of Amino Acids* (Weinheim, Germany: Wiley VCH), Vol. 1.

Miller, S. L. (1953). Production of Amino Acids under Possible Primitive Earth Conditions. *Science* 117, 3046. doi:10.1126/science.117.3046.528

Nuth, J. A., Ferguson, F. T., Hill, H. G. M., and Johnson, N. M. (2020). Did a Complex Carbon Cycle Operate in the Inner Solar System? *Life* 10 (9), 206. doi:10.3390/life10090206

Pizzarello, S., and Cronin, J. R. (1998). Alanine Enantiomers in the Murchison Meteorite. *Nature* 394 (6690), 236. doi:10.1038/28306

Rotelli, L., Trigo-Rodríguez, J. M., Moyano-Cambero, C. E., Carota, E., Botta, L., Di Mauro, E., et al. (2016). The Key Role of Meteorites in the Formation of Relevant Prebiotic Molecules in a Formamide/water Environment. *Sci. Rep.* 6, 38888. doi:10.1038/srep38888

Rudraswami, N. G., Naik, A. K., Tripathi, R. P., Bhandari, N., Karapurkar, S. G., Prasad, M. S., et al. (2019). Chemical, Isotopic and Amino Acid Composition of Mukundpura CM2.0 (CM1) Chondrite: Evidence of Parent Body Aqueous Alteration. *Geosci. Front.* 10 (2), 495–504. doi:10.1016/j.gsf.2018.02.001

Schmitt-Kopplin, P., Gabelica, Z., Gougeon, R. D., Fekete, A., Kanawati, B., Harir, M., et al. (2010). High Molecular Diversity of Extraterrestrial Organic Matter in Murchison Meteorite Revealed 40 Years after its Fall. *Proc. Natl. Acad. Sci. U S A.* 107 (7), 2763–2768. doi:10.1073/pnas.0912157107

Ulbricht, T. L. V., and Vester, F. (1962). Attempts to Induce Optical Activity with Polarized β-radiation. *Tetrahedron* 18, 629–637. doi:10.1016/s0040-4020(01)92714-0

Vester, F., Ulbricht, T. L. V., and Krauch, H. (1959). Optische Aktivität und die Paritätsverletzung im β-Zerfall. *Naturwissenschaften* 46, 68. doi:10.1007/bf00599091

Wang, J., and Luo, L. F. (1985). *Scientia Sinica B* 28, 1265.

Wilson, C. D., Walker, C. E., and Thornley, M. D. (1997). The Density and Temperature of Molecular Clouds in M33. *ApJ* 483, 210–219. doi:10.1086/304216

Wolman, Y., Haverland, W. J., and Miller, S. L. (1972). Nonprotein Amino Acids from Spark Discharges and Their Comparison with the Murchison Meteorite Amino Acids. *Proc. Natl. Acad. Sci.* 69 (4), 809–811. doi:10.1073/pnas.69.4.809

Zeldovithe, Y. B., and Sakyan, D. B. (1980). *J.Exp.Theor.Phys* 78, 233.

Conflict of Interest: The author declares that the research was conducted in the absence of any commercial or financial relationships that could be construed as a potential conflict of interest.

Publisher's Note: All claims expressed in this article are solely those of the authors and do not necessarily represent those of their affiliated organizations, or those of the publisher, the editors, and the reviewers. Any product that may be evaluated in this article, or claim that may be made by its manufacturer, is not guaranteed or endorsed by the publisher.

frontiers in Microbiology

ORIGINAL RESEARCH
published: 28 March 2022
doi: 10.3389/fmicb.2022.800219

Oligotrophic Growth of Nitrate-Dependent Fe^{2+}-Oxidising Microorganisms Under Simulated Early Martian Conditions

Alex Price[1], Michael C. Macey[1], Victoria K. Pearson[2], Susanne P. Schwenzer[1], Nisha K. Ramkissoon[1] and Karen Olsson-Francis[1]*

[1]School of Environment, Earth and Ecosystem Sciences, Faculty of Science, Technology, Engineering, and Mathematics, The Open University, Milton Keynes, United Kingdom, [2]School of Physical Sciences, Faculty of Science, Technology, Engineering, and Mathematics, The Open University, Milton Keynes, United Kingdom

Nitrate-dependent Fe^{2+} oxidation (NDFO) is a microbially mediated process observed in many anaerobic, low-nutrient (oligotrophic) neutral–alkaline environments on Earth, which describes oxidation of Fe^{2+} to Fe^{3+} in tandem with microbial nitrate reduction. Evidence suggests that similar environments existed on Mars during the Noachian epoch (4.1–3.7 Ga) and in periodic, localised environments more recently, indicating that NDFO metabolism could have played a role in a potential early martian biosphere. In this paper, three NDFO microorganisms, *Acidovorax* sp. strain BoFeN1, *Pseudogulbenkiania* sp. strain 2002 and *Paracoccus* sp. strain KS1, were assessed for their ability to grow oligotrophically in simulated martian brines and in a minimal medium with olivine as a solid Fe^{2+} source. These simulant-derived media were developed from modelled fluids based on the geochemistry of Mars sample locations at Rocknest (contemporary Mars soil), Paso Robles (sulphur-rich soil), Haematite Slope (haematite-rich soil) and a Shergottite meteorite (common basalt). The Shergottite medium was able to support growth of all three organisms, while the contemporary Mars medium supported growth of *Acidovorax* sp. strain BoFeN1 and *Pseudogulbenkiania* sp. strain 2002; however, growth was not accompanied by significant Fe^{2+} oxidation. Each of the strains was also able to grow in oligotrophic minimal media with olivine as the sole Fe^{2+} source. Biomineralised cells of *Pseudogulbenkiania* sp. strain 2002 were identified on the surface of the olivine, representing a potential biosignature for NDFO microorganisms in martian samples. The results suggest that NDFO microorganisms could have thrived in early martian groundwaters under oligotrophic conditions, depending on the local lithology. This can guide missions in identifying palaeoenvironments of interest for biosignature detection. Indeed, biomineralised cells identified on the olivine surface provide a previously unexplored mechanism for the preservation of morphological biosignatures in the martian geological record.

Keywords: oligotrophy, iron, nitrate, Mars, NDFO, NRFeOx, simulant

OPEN ACCESS

Edited by:
Maggie CY Lau Vetter, Institute of Deep-Sea Science and Engineering (CAS), China

Reviewed by:
Donald Pan, Shanghai Jiao Tong University, China
Binlong Ye, The University of Hong Kong, Hong Kong SAR, China

****Correspondence:***
Alex Price
alex.price@open.ac.uk

Specialty section:
This article was submitted to Extreme Microbiology, a section of the journal Frontiers in Microbiology

Received: *22 October 2021*
Accepted: *24 February 2022*
Published: *28 March 2022*

Citation:
Price A, Macey MC, Pearson VK, Schwenzer SP, Ramkissoon NK and Olsson-Francis K (2022) Oligotrophic Growth of Nitrate-Dependent Fe^{2+}-Oxidising Microorganisms Under Simulated Early Martian Conditions. Front. Microbiol. 13:800219. doi: 10.3389/fmicb.2022.800219

INTRODUCTION

Oligotrophic environments comprise much of the microbial biosphere on Earth and include many locations where certain conditions can be considered analogous to extraterrestrial locations, such as Mars (Bonilla-Rosso et al., 2012; Schmidt et al., 2018; Parro et al., 2019). A wide variety of biogeochemical cycles operate in these oligotrophic ecosystems, meaning that investigation of the myriad microbial processes hosted here can yield insights into both the terrestrial biosphere and potential extinct or extant biospheres on Mars.

Owing to the Fe-rich composition of the martian surface (Bertka and Fei, 1998; Halliday et al., 2001; Papike, 2018) the feasibility of Fe biogeochemical cycling has been discussed previously (Nixon et al., 2012). Studies have predominantly focused on aerobic Fe oxidation and organotrophic Fe reduction as plausible metabolisms on Mars (Amils et al., 2011; Popa et al., 2012; Bauermeister et al., 2014; Nixon, 2014). However, the detection of nitrates (70–1,100 ppm) in mudstone deposits at Gale crater (a circumneutral palaeolake environment; Stern et al., 2015) and from the meteorite EETA79001 (Kounaves et al., 2014), together with the confirmation of complex organics (Eigenbrode et al., 2018), have expanded the list of plausible electron donors and acceptors on Mars to include reduced organic compounds and oxidised nitrogen species.

Nitrate-dependent Fe^{2+} oxidation (NDFO) metabolism—also known as nitrate-reducing Fe oxidation (NRFeOx)—was recognised as a geobiological process over two decades ago in anoxic soils, waters and sediments (Hafenbradl et al., 1996; Straub et al., 1996; Benz et al., 1998). Although the biochemical mechanisms are yet to be fully resolved, isolates and enrichment cultures have been identified that couple Fe^{2+} oxidation with nitrate reduction during apparent autotrophic and mixotrophic growth, as well as Fe^{2+} oxidation caused by organotrophic denitrification (Straub et al., 1996; Weber et al., 2006b; Muehe et al., 2009; Carlson et al., 2013). Some claims of autotrophic growth by NDFO organisms are controversial [see discussion in Bryce et al., 2018]. One reason is that results could be obfuscated by the potential for both the carry-over of internal carbon sources within washed cells or by low-level residual organic carbon within batch culture apparatus and media components.

Circumneutral–alkaline conditions, such as those described for lacustrine environments on early Mars (Grotzinger et al., 2014), are required for NDFO to be an energy-yielding process (Weber et al., 2006a). NDFO provides less energy ($-481.15\,kJ\,mol^{-1}\ NO^{3-}$) than both organotrophic denitrification ($-556\,kJ\,mol^{-1}\ NO^{3-}$) and organotrophic nitrate ammonification ($-623\,kJ\,mol^{-1}\ NO^{3-}$; Strohm et al., 2007). However, the process is exergonic at circumneutral pH ($\Delta G^{o\prime} = -481.15\,kJ\,mol^{-1}\ NO^{3-}$, $-96.23\,kJ\,mol^{-1}$ Fe) and, theoretically, provides enough energy to sustain growth under mixotrophic (Muehe et al., 2009; Weber et al., 2009) or autotrophic conditions, although this would require 26 moles Fe^{2+} to fix 1 mole C (Laufer et al., 2016; Bryce et al., 2018). NDFO could, therefore, have represented an important microbial process under circumneutral, near-surface conditions on early Mars (Price et al., 2018). However, most experiments using these organisms have used high Fe^{2+} (10 mM) that are not representative of typical oligotrophic aqueous environments on early Mars (Weber et al., 2006b; Miot et al., 2009a).

To address the plausibility of NDFO as a potential metabolism under oligotrophic early martian conditions, simulation experiments are required. Prior laboratory-based work has assessed the habitability of Mars across a range of chemical, pH, redox and physical conditions (Allen et al., 1997; Peters et al., 2008; Böttger et al., 2012; Stevens et al., 2018). Various brine-derived media have been developed to recreate aqueous environments representative of different martian locations and historical periods. For example, Fox-Powell et al. (2016) utilised the thermodynamically modelled brines (derived from weathering of a generalised synthetic martian basalt) of Tosca et al. (2011) to develop growth media, which could be used to study the impact of ionic strength on habitability. Despite the contribution made to our understanding of martian fluid chemistry and habitability, these brines were not suitable for this investigation for two reasons. Firstly, the ionic concentrations of these highly saline brines are intended to represent the evaporative conditions of the Hesperian era, rather than the hydrologically active Noachian period that carries the most interest in terms of NDFO and Fe^{2+} oxidising metabolisms more generally on Mars. Secondly, the modelled brines assumed that all Fe is present entirely in the ferrous form (Fe^{2+}), which could be unrealistic when considering the variability in Fe oxidation state across martian environments and have a bearing on the viability of an Fe^{2+}-oxidising metabolism.

To address these issues and create a link to *in situ* data, we have developed martian brines based on a suite of simulants (Ramkissoon et al., 2019). These simulants themselves are based on the geochemical composition of four different martian lithologies: (1) the sulphur-rich (SR) Paso Robles regolith found at Columbia Hills, Gusev crater; (2) a haematite-rich (HR) deposit discovered at Meridiani Planum (Rieder et al., 2004; Lane et al., 2008); (3) the Rocknest regolith at Gale crater (Blake et al., 2013) as a contemporary Mars (CM) simulant due to similarity to the global Mars mean regolith composition (Ramkissoon et al., 2019); and (4) a Shergottite (SG) meteorite (Bridges and Warren, 2006), representative of the Fe-rich basaltic material that dominates the martian surface (Bish et al., 2013; Ehlmann and Edwards, 2014). These four environments represent some of the diverse lithologies present on Mars, allowing for a nuanced assessment of habitability for NDFO microorganisms. These four source lithologies are not all Noachian, but the dilution used to create the media is relevant to this time period. In this study, we use these four brines to represent near-surface aqueous environments, thought to have been widespread on Noachian Mars and which may retain traces of life (Ehlmann et al., 2011).

Biosignature preservation in the martian near-surface geological record is a key issue concerning the detection of any hypothetical early martian biosphere. Microbial Fe^{2+} oxidation is responsible for numerous instances of mineralised microfossils in the terrestrial geological record (Chan et al., 2011; Chi Fru et al., 2013; Crosby et al., 2014), and NDFO specifically has

been shown to promote biomineralisation of cells (Kappler et al., 2005; Miot et al., 2009a; Klueglein et al., 2014), which we have previously proposed as a potential mechanism for morphological biosignature generation on Mars (Price et al., 2018).

Potential targets for the investigation of such biosignatures on Mars could be palaeoenvironments where aqueous fluids have interacted with olivine. Olivine has been demonstrated to act as a solid Fe^{2+} source for microaerophilic Fe oxidation, enhanced by microbial weathering and dissolution of the mineral surface (Popa et al., 2012). This mineral is also a major constituent of many martian meteorites [including the Chassignites and some Shergottites (Floran et al., 1978; Nyquist et al., 2001; Goodrich, 2002; Beck et al., 2006)]. Olivine has been detected from martian orbit in close association to hydrous minerals (Ehlmann et al., 2008) and is a constituent of rocks found on the martian surface (McSween et al., 2006; McSween, 2015; Filiberto, 2017). As such, olivine is assessed here as a substrate for NDFO growth and subsequently examined for cellular structures indicating biomineralisation.

This paper is the first to explore the proposition that oligotrophic NDFO could have contributed to chemotrophic growth in near-surface fluids on early Mars, using nitrates and Fe^{2+}-rich lithology as sources of electron acceptors and donors. We test the specific suitability of multiple putative early martian environments for NDFO, using a suite of media of varying compositions and an olivine bedrock analogue. In calculating the ionic compositions of these brines to match those expected for subsurface groundwaters we can apply the results of this research to habitability of both the early martian crust and potential extant subsurface reservoirs. The olivine surfaces will be inspected for signs of NDFO-driven biomineralisation behaviours that may enhance morphological biosignature preservation. In assessing the viability of NDFO in ancient martian environments and cell structure preservation on mineral surfaces, the results of this study can inform target selection for *in situ* life detection efforts, such as the Mars 2020 Perseverance rover and ExoMars Rosalind Franklin rover, and sample collection for future return. Finally, we quantify the carry-over effect in our study, examining organic carbon across blanks and media inoculated with washed and starved cells.

MATERIALS AND METHODS

Microorganisms

Three bacterial strains, *Pseudogulbenkiania* sp. strain 2002 (DSM-18807), *Paracoccus* sp. strain KS1 (DSM-11072) and *Acidovorax* sp. strain BoFeN1 were used in this study to investigate oligotrophic growth in simulated martian fluids and separately on a Mars-relevant mineral substrate (**Supplementary Figure S1**). The selected strain represents three proposed categories of NDFO. *Pseudogulbenkiania* sp. strain 2002 has been reported as performing autotrophic NDFO (Weber et al., 2006b), *Acidovorax* sp. strain BoFeN1 is thought to grow mixotrophically by NDFO (Muehe et al., 2009), and *Paracoccus* sp. strain KS1 is an organotrophic denitrifier (Iordan et al., 1995). All strains were acquired from DSMZ (German Collection of Microorganisms and Cell Cultures in Leibniz, Germany) except *Acidovorax* sp. strain BoFeN1, which was obtained from the IMPMC (Institut de Minéralogie, de Physique des Matériaux et de Cosmochimie in Paris, France).

The headspace used in these experiments (90% N_2, 10% CO_2, 1 bar) is not intended as a facsimile of the martian atmosphere, which is now dominated by (95.9%) CO_2 and thought to have been so in early martian history (Ramirez et al., 2014; Jakosky et al., 2017; Kurokawa et al., 2018). However, given the estimates of >0.5 bar atmospheric pressure on Noachian Mars (Kurokawa et al., 2018), the $ppCO_2$ is a reasonable approximation for the scope of the experiments.

Anaerobic nutrient medium (L^{-1}: 5.0 g of peptone, 3.0 g of meat extract, 5.0 g of $Na_2S_2O_3.5H_2O$) was used for routine growth of *Pseudogulbenkiania sp*. strain 2002, *Paracoccus sp*. strain KS1 and *Acidovorax sp*. strain BoFeN1. All cultures were incubated statically at 30°C for 48 h prior to inoculation.

Mars Simulant-Derived Media

To investigate microbial growth in simulated martian aqueous conditions, the selected strains were grown in four Mars simulant-derived media, which were based on the geochemical composition of the following lithologies: contemporary Mars (CM), sulphur-rich (SR), haematite-rich (HR) and Shergottite (SG). The fluid ion chemistries (**Supplementary Table S1**) were calculated assuming complete mineral dissolution—without secondary mineral precipitation—of 1 g simulant in 1 l water, giving a water/rock ratio (W/R) of 1,000 (Ramkissoon et al., 2019). This value was chosen to represent the W/R of fluids within bedrock fractures, in a near-surface martian environment. Given the uncertainty over the longevity of open water bodies on Mars, subsurface aqueous environments were chosen as representative of a more stable martian aqueous environment.

The composition of the media (**Table 1**) was calculated based on the predicted ion concentrations listed in the **Supplementary Data**. The insoluble components listed in **Table 1** (FeO, Fe_2O_3, $3Al_2O_3{\cdot}2SiO_2$, $3MgO{\cdot}4SiO_2{\cdot}H_2O$, SiO_2, TiOH, $Ca(OH)_2$) were suspended in anoxic milli-Q water (1 mg L^{-1} resazurin) under N_2 flushing, sealed and autoclaved at 121°C for 15 min. The soluble components were prepared as stock solutions in anoxic milli-Q water and filter-sterilised with a 0.2 µm filter and added to achieve the final concentrations shown in **Table 1**.

Under anoxic conditions in a COY anaerobic chamber, 30 ml of media was dispensed into 50 ml Wheaton bottles and sealed with blue butyl stoppers. The headspaces were flushed with a 90% N_2/10% CO_2 headspace to remove the 5% H_2 component of the COY anoxic atmosphere. Initial pH for these media is given in **Supplementary Table S2**.

Prior to inoculation, the cells were washed to remove any excess growth medium. For this, 1 ml of exponentially grown cells were harvested by centrifugation at 3000 × *g*, for 10 min. All manipulations were conducted anaerobically in the COY chamber, with sealed microcentrifuge tubes removed for the centrifugation steps. The cell pellet was washed twice with

TABLE 1 | Chemical composition of the contemporary Mars (CM), sulphur-rich (SR), haematite-rich (HR) and Shergottite (SG) media.

	Simulant			
	CM	**SR**	**HR**	**SG**
Component	Concentration (μM)			
$NaNO_3$	1,000	618.28	746.05	–
$Mg(NO_3)_2$	–	190.86	126.98	500
Na_2S	–	–	11.56	31.59
$MnCl_2$	14.71	10.42	11.56	9.87
K_2HPO_4	19.83	–	72.04	78.70
NaOH	42.45	–	–	461.10
KOH	233.55	–	98.95	–
$Ca(OH)_2$	1381.81	1510.99	1020.33	1692.42
$FeSO_4$	226.29	2300.89	533.84	–
FeO	2392.10	578.66	1429.27	2253.63
Fe_2O_3	–	–	961.19	75.66
$3AL_2O_3.2SiO_2$	329.69	164.92	233.26	211.81
$3MgO.4SiO_2.H_2O$	506.55	–	1597.01	685.33
SiO_2	4665.92	3271.76	–	5420.55
TiOH	92.27	58.41	61.95	31.64
$MnSO_4$	19.04	5.65	746.05	18.59
Na_2HPO_4	–	–	126.98	1.63
$Fe_2(SO_4)_3$	220.41	210.15	11.564	–
KH_2PO_4	–	420.45	11.56	–
$MgSO_4$	–	1131.97	72.04	–

sterile simulant-derived media and resuspended to a final cell density of 10^9 cells ml^{-1} based on cell counts at 100 × magnification. A 1% inoculum was used to inoculate the bottles, which gave an initial concentration of 10^7 cells ml^{-1}. The bottles were incubated at 25°C, without shaking, for 10 days. Each experiment was carried out in triplicate with abiotic controls prepared in parallel.

Olivine Media Growth Cultures

To investigate growth on the surface of olivine. and potential associated biosignature formation, the strains were grown in a minimal medium using olivine as the sole source of Fe^{2+}. The olivine was sourced from the Upper Loire region of France and purchased from Richard Tayler Minerals. The elemental composition and forsterite value (Fo_{84}; $Mg_{1.68}Fe_{0.32}SiO_4$) of the olivine was determined by Electron Probe Micro-Analysis (EPMA; Cameca SX 100 microprobe). Standard silicate analysis conditions were used (column conditions: 20 keV, 20 nA; beam size: 10 μm). Each culture and control contained 5 g of olivine (0.5–1 mm grain size), which had been sonicated in acetone and washed with milli-Q water to remove organics. Additionally, 1 cm^3 polished olivine cubes, which had been acetone-washed, were added.

The olivine was added as the sole electron donor to the anoxic minimal medium (L^{-1}: 0.3 g of NH_4Cl, 0.4 g of $MgCl_2.6H_2O$, 0.1 g of $CaCl_2.2H_2O$, 0.6 g of K_2HPO_4, 50 mg of $MgSO_4$, 30 mM $NaHCO_3$, 4 mM $NaNO_3$, 1 mg resazurin) after N_2 sparging for 15 min. The $NaHCO_3$ and $NaNO_3$ (0.2 μm-filtered sterilised) were added after autoclaving from 1 M stock solutions. The pH was altered to 7 using 0.1 M HCL or 0.1 M NaOH and 50 ml aliquots was dispensed into 125 ml Wheaton bottles, which were sealed with blue butyl stoppers and flushed with a 90% N_2/10% CO_2 headspace.

The inoculum was washed and resuspended to a concentration of 10^7 cells ml^{-1} cells, as described in the section above. A 1% inoculum was used to inoculate the medium (initial concentration of 10^5 cells ml^{-1}), and the bottles were incubated at 25°C, without shaking, for 146 days. Each experiment was carried out in triplicate with abiotic controls prepared identically in parallel.

Organic Carry-Over

Non-purgeable organic carbon (NPOC) analysis was employed to compare washed cells with washed *and* nutrient-starved cells in order to quantify intracellular organic carbon carried into the experiment within inoculated cells.

Each strain was grown in anaerobic nutrient media for 48 h at 30°C, before twice washing, as described above, and resuspending in the test media (CM, SR, HR, SG and olivine minimal medium). The suspensions were used to inoculate anaerobic 30 ml cultures (100% N_2 headspace) of the corresponding media, to give initial concentrations of 10^7 cells ml^{-1}, and incubated at 25°C for 48 h.

Two sets of 10 ml samples were collected, at 0 and 48 h. The samples were frozen at −20°C, heated to 90°C, and sonicated for 10 min to lyse cells. Cell debris was then removed using 0.2 μm filters. NPOC was quantified in lysed samples using a Shimadzu TOC-L CPH analyser with associated ASI-V auto-sampler (detection limit = 1 mg L^{-1}) by the British Geological Survey (Keyworth, UK; Marriott et al., 2020). The analysis used a Peak Scientific 42-1,040 TOC gas generator for carrier gas of high purity air, with TOC Control V Software (version 1.09) package was used to control the analyser and acquire data. Extracted fluid (<6 ml) was pipetted into glass tubes, capped by aluminium foil and placed into the sample carousel for analysis. A Certified Reference Material (CRM 100 mg L^{-1} Carbon from National Institute of Standards and Technology—ERA®) was used (10 mg L^{-1}) of C during each analytical run to test performance. Sample and calibration standards were run together, and the results accepted with a coefficient of variation (CV) <5% at concentrations greater than three times the quantification limit, or <20% at concentrations less than three times the quantification limit. The analytical error was estimated at 8%.

Monitoring Microbial Growth

To monitor microbial growth in the four Mars simulant-derived media, protein biomass was measured using a modified Bradford assay (Miot et al., 2009a). Tamm reagent was used to dissolve the Fe^{3+} oxides in the media to overcome suspected interference of metal oxides with the action of the Bradford reagent and cell stains. A secondary function of Tamm reagent is cell lysis (Vodyanitskii, 2001), meaning protein quantification was preferred to cell counts in the simulant-derived media cultures. Cell counts were taken from 100 μl samples in the olivine cultures using a Baclight cell viability kit (Invitrogen) and analysed using a Leica DMRB microscope equipped with

epifluorescence (Leica Microsystem, Bensheim, Germany). The growth rate constant (k) for the log phase of growth was determined by plotting the natural log of the protein concentration and cell counts over time (Pirt, 1975).

Chemical Analysis

To monitor the concentration of Fe^{2+} and total Fe throughout the Mars simulant-derived media experiments, the Ferrozine method was used. At each time point, two 20 µl samples from each culture and control were collected anaerobically and diluted *via* a 0.2 µm filter into 980 µl of a 0.5 M HCl solution and 980 µl of a reducing solution (0.5 M HCl, 0.3 M Hydroxylamine hydrochloride), respectively, and incubated at 4°C for 1 h. The HCl solution prevents abiotic oxidation of Fe^{2+} in the sample, allowing determination of Fe^{2+} concentration. The reducing solution converts all Fe^{3+} in the sample to Fe^{2+}, which can then be measured to give a total Fe (Fe_{total}) concentration from which Fe^{2+}/Fe^{3+} can be deduced. A 20 µl aliquot of each digested sample was mixed with 980 µl of Ferrozine solution in a cuvette and absorbance measured at 562 nm on a spectrophotometer. Sample concentrations were calculated from a standard curve at 10 mM, 5 mM, 1 mM and 500 µM $FeSO_4$.

Inductively coupled plasma mass spectrometry (ICP-MS) was used to measure the initial and final Fe concentrations during the olivine experiment. Ferrozine could not be used because of the low concentrations of dissolved Fe in solution. An aliquot (9 ml) was extracted under anaerobic conditions using a N2-flushed sterile syringe at day 146. The sample was filtered through a 0.2 µm sterile filter into 1 ml aliquots of 20% HNO_3 solution, resulting in 2% final HNO3 concentration. ICP-MS was conducted using an Agilent 7,500 s with New Wave 213 laser system at The Open University, United Kingdom. Detection limits of the instrument are listed in **Supplementary Table S3**.

The nitrite concentration was measured using the Griess reagent assay, in which sulfanilic acid reacts with 1-naphthylamine to produce red-pink azo compounds in the presence of nitrite ions (Griess, 1879). For monitoring nitrite concentrations, a 100 µl aliquot of culture was transferred into sterile 1.5 ml microcentrifuge tubes and centrifuged at 15,500 × g for 10 min. In parallel, nitrite standards were prepared by diluting 100 mM $NaNO_2$ with 0.1 M NaOH solution, to give 100 µM, 50 µM, 25 µM, 10 µM, 5 µM, 2.5 µM and 1 µM $NaNO_2$ concentrations. The standards (in triplicate) and the culture supernatants (50 µl) were transferred to a 96-well flat-bottomed, optically clear ELISA microplate. 100 µl of 1 × Griess reagent solution (Sigma-Aldrich) was added to each well. After 15 min, the absorbance was read using a Bio-tek ELx808 microplate reader with a 540 nm filter, using KC4 software for the data output.

The nitrate concentration was measured using an ELIT 0821 ion selective NO_3^- electrode with ELIT 003 lithium acetate reference electrode (Nico2000) connected to a conductivity meter (HANNA instruments), as per the manufacturer's instructions. The electrode was calibrated by placing the electrode in 5 ml of electrode buffer solution and waiting for equilibrium to be reached.

pH was measured using a Thermo Scientific Orion Three Star pH meter with a two-point calibration using Omega Buffer solutions at pH 4 and 7 at the start and end points of the experiment.

Morphological Analyses

To investigate morphological biosignatures, the olivine cubes were removed from the culture after 146 days. After drying in covered, sterile glass vials under a 85% N_2/10% CO_2/5% H_2 atmosphere for 2 days, the rocks were gold-coated under vacuum. Analysis was carried out under vacuum with a Zeiss Supra 55 VP Field Emission Gun Scanning Electron Microscope (FEG-SEM), using SE2 and Cent detectors at ´100 to ´50,000 magnifications. For imaging, working distances of 4.1–10.1 mm and accelerating voltages of 3–20 kV were used. Energy-dispersive X-ray spectroscopic (EDS) analysis was performed using the integrated Aztec Energy v3.3 system (Oxford Instruments).

Statistics

Significant differences between the cultures and controls were tested using a 2-tailed paired Student's t-test. Pooled biotic samples were tested for significance against controls using a 2-tailed 2-sample t-test assuming equal variance. Correlations were calculated using Pearson's coefficient of linear correlation.

RESULTS

Mars Simulant-Derived Media Experiment

Initial Conditions

The initial pH of the four simulant-derived media was similar (6.69–7.00), with sulphur-rich (SR) the most acidic and Shergottite (SG) the most alkaline, as shown in **Supplementary Table S2**. Initial nitrate ion concentration was equalised across the four media at 1 mM, whereas dissolved Fe^{2+} ranged from ~2.3 mM in SR to below detection limits in SG (where Fe was present as insoluble FeO; **Table 1**).

Growth In Martian Simulant-Derived Media

The Shergottite (SG) and contemporary Mars (CM) media were able to support growth (**Figure 1A**), whereas no significant growth was observed for any organism in the haematite-rich (HR) or sulphur-rich (SR) media (**Supplementary Figure S2**).

For the SG medium, the mean specific growth rates (k) for the triplicates were 0.25, 0.15, and 0.10 day^{-1} for *Pseudogulbenkiania* sp. strain 2002, *Paracoccus* sp. strain KS1 and *Acidovorax* sp. strain BoFeN1, respectively. In the CM medium, k was similar for *Pseudogulbenkiania* sp. strain 2002 (0.14 day^{-1}) and *Acidovorax* sp. strain BoFeN1 (0.13 day^{-1}). No significant protein concentrations were detected over 10 days in normalised data for *Paracoccus* sp. strain KS1 in CM, thus growth of *Paracoccus sp*. Strain KS1 cannot be confirmed. Significant differences between growth in SG and CM media were not established for any strain.

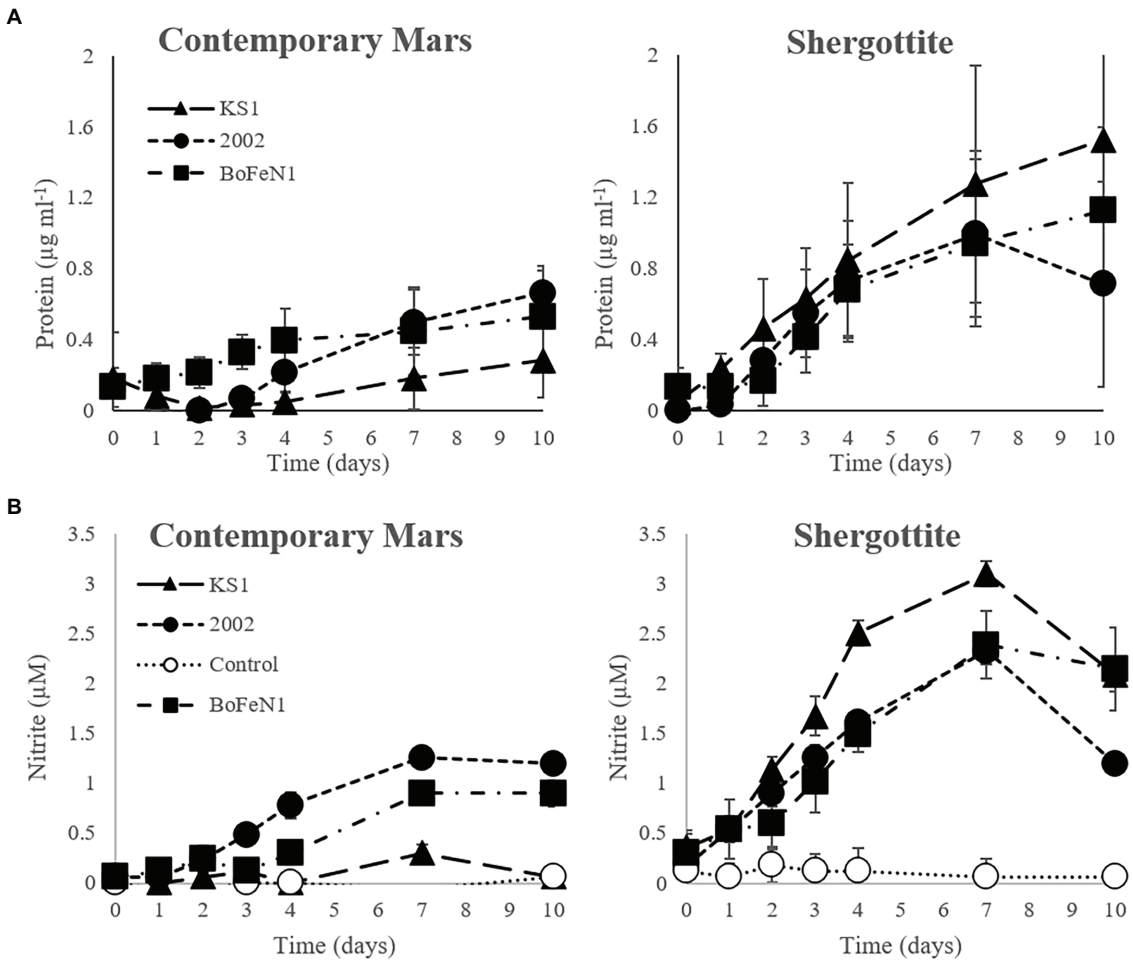

FIGURE 1 | (A) Protein and **(B)** nitrite concentration over time in the contemporary Mars (CM) and Shergottite (SG) simulant media for *Paracoccus* sp. strain KS1, *Pseudogulbenkiania* sp. strain 2002, *Acidovorax* sp. strain BoFeN1 (± standard error of triplicates). Protein values are normalised against the abiotic control.

Nitrite Production and Nitrate Reduction

There was an overall positive correlation between nitrite and protein concentrations in both the CM and SG media (**Supplementary Figure S3**). Furthermore, strains that produced a significant increase in protein concentration in the CM (*Pseudogulbenkiania* sp. strain 2002 and *Acidovorax* sp. strain BoFeN1) and SG (all strains) media, demonstrated positive correlations between nitrite concentration (**Figure 1B**) and protein, detailed in **Supplementary Table S4**. Negative correlations were observed both between the nitrate and nitrite concentrations ($\rho = -0.87$ at day 10) and between nitrate and protein ($\rho = -0.89$ at day 10) across the same strains in CM and SG media (**Supplementary Figure S4**), indicating more extensive consumption of nitrate in growing cultures. The maximum protein and nitrite concentrations were observed in the *Paracoccus* sp. strain KS1 SG cultures. The maximum nitrite concentrations (at day 7) were significantly greater ($p < 0.05$) for each strain in the SG medium compared to the values in the corresponding CM medium. There was no significant production of nitrite or nitrate consumption in the abiotic controls for the simulant-derived media ($p < 0.05$).

Fe Oxidation State

Over the duration of the experiment, the Fe in the CM media became reduced in both the biotic and abiotic controls (**Supplementary Figure S5**). The mean Fe^{2+}/Fe_{total} ratios (shown in **Table 2**) were lower in the three CM biotic culture sets than in the control and there were inverse correlations between Fe^{2+}/Fe_{total} relative to the control and microbial growth in the CM media for *Paracoccus* sp. strain KS1 ($\rho = -0.43$), *Pseudogulbenkiania* sp. strain 2002 ($\rho = -0.45$) and *Acidovorax* sp. strain BoFeN1 ($\rho = -0.92$; **Supplementary Data**). However, these trends did not result in significant differences in Fe^{2+}/Fe_{total} ratios between the CM cultures and controls within the timeframe of the experiment, either when cultures were considered in organism-specific groups (*Acidovorax* sp. strain BoFeN1 $p = 0.22$, *Pseudogulbenkiania* sp. strain 2002 $p = 0.36$, *Paracoccus* sp. strain KS1 $p = 0.06$) or a pooled biotic sample set ($p = 0.09$). Macroscopic Fe oxide precipitates were not observed in any

TABLE 2 | Change in dissolved Fe, nitrate, Fe^{2+}/Fe_{total} ratios and pH for Mars simulant-derived media cultures and abiotic controls over 10 days (± standard error of triplicates), growth rate (*k*) and doubling time of growing cultures.

Media	Inoculum	ΔNO_3^-	$\Delta Fe^{2+}/Fe_{total}$	End point pH	ΔpH	*k* (day^{-1})	Doubling time (days)
Contemporary Mars	*Paracoccus* sp. strain KS1	−2.32% (±4.49)	+0.163 (±0.056)	6.28 (±0.06)	−0.47 (±0.06)	0.06	5.10
	Pseudogulbenkiania sp. strain 2002	−14.17% (±2.93)	+0.171 (±0.026)	6.39 (±0.07)	−0.36 (±0.07)	0.14	2.11
	Acidovorax sp. strain BoFeN1	−9.95% (±3.07)	+0.178 (±0.048)	6.21 (±0.03)	−0.54 (±0.03)	0.13	2.26
	Control	−2.61% (±1.28)	+0.266 (±0.061)	6.28 (±0.07)	−0.47 (±0.07)	–	–
Sulphur-rich	*Paracoccus* sp. strain KS1	−2.46% (±3.40)	−0.090 (±0.154)	5.85 (±0.02)	−0.84 (±0.02)	–	–
	Pseudogulbenkiania sp. strain 2002	−3.96% (±3.67)	−0.130 (±0.093)	5.86 (±0.02)	−0.83 (±0.02)	–	–
	Acidovorax sp. strain BoFeN1	−3.96% (±3.67)	−0.140 (±0.150)	5.76 (±0.05)	−0.93 (±0.05)	–	–
	Control	−2.61% (±1.28)	−0.062 (±0.161)	5.79 (±0.01)	−0.90 (±0.01)	–	–
Haematite-rich	*Paracoccus* sp. strain KS1	−5.67% (±1.22)	+0.051 (±0.055)	6.36 (±0.03)	−0.36 (±0.03)	–	–
	Pseudogulbenkiania sp. strain 2002	−2.54% (±2.50)	−0.122 (±0.056)	6.34 (±0.02)	−0.38 (±0.02)	–	–
	Acidovorax sp. strain BoFeN1	−2.61% (±1.28)	−0.027 (±0.113)	6.30 (±0.04)	−0.42 (±0.04)	–	–
	Control	−0.96% (±2.63)	−0.066 (±0.072)	6.31 (±0.02)	−0.41 (±0.02)	–	–
Shergottite	*Paracoccus* sp. strain KS1	−20.85% (±1.79)	–	6.70 (±0.01)	−0.30 (±0.01)	0.15	2.02
	Pseudogulbenkiania sp. strain 2002	−11.45% (±2.27)	–	6.74 (±0.06)	−0.26 (±0.06)	0.25	1.22
	Acidovorax sp. strain BoFeN1	−9.75% (±4.55)	–	6.63 (±0.03)	−0.37 (±0.03)	0.10	2.91
	Control	−1.04% (±1.28)	–	6.67 (±0.07)	−0.33 (±0.07)	–	–

of the cultures. Dissolved Fe was not detected in SG media by the Ferrozine assay, as the Fe sources used were insoluble.

pH

Overall, the pH decreased and there were no significant differences between the biotic and abiotic experiments after 10 days ($p > 0.05$), except for *Pseudogulbenkiania* sp. strain 2002 grown in the SG medium where pH decreased less than in the abiotic control ($p = 0.02$). Values are shown in **Table 2**.

Olivine Culture Experiment

Microbial Growth With Olivine as a Sole Source of Fe

Each of the strains was able to grow in the minimal medium using olivine as a sole source of Fe^{2+} (**Figure 2**). The specific growth rates varied between 0.07 and 0.37, as shown in **Table 3**. There was a negative correlation ($\rho = -0.67$) between maximum cell numbers and nitrate concentration at the end of the experiment (**Supplementary Figure S6**), meaning growth is positively correlated to nitrate consumption.

ICP-MS analysis after 146 days (**Table 3**) demonstrated that the concentration of Fe was significantly lower in the aqueous media of the biotic experiments compared to that of the abiotic control ($p < 0.05$), indicating that Fe is being removed from solution. However, no macroscopic Fe oxide precipitates were observed.

The pH of the cultures and abiotic controls increased significantly over the course of the experiment ($p < 0.05$), as shown in **Table 3**. However, there were no significant differences in the end point pH between any of the cultures and the abiotic control ($p > 0.05$).

Morphological Biosignatures

FEG-SEM analysis was performed on olivine cubes after 146 days of incubation. Cell-like features were observed on the mineral surface in *Pseudogulbenkiania* sp. strain 2002 and *Paracoccus* sp. strain KS1 cultures. For *Pseudogulbenkiania* sp. strain 2002, the individual features measured approximately 1.5–2 μm in diameter. The clusters typically composed of between 50 and 100 coccoid units, which were covered by a layer of nanometre-scale dendritic features (**Figure 3**). EDS analysis demonstrated a co-location between the coccoid features and regions with elevated C (11.7 ± 0.4 wt%) when compared with the underlying substrate (4.0 ± 0.3 wt%; **Figure 3B**).

Individual coccobacillal (ovoid) structures, flatter than those observed in the *Pseudogulbenkiania* sp. strain 2002 cultures and ~ 1 μm in diameter, were also observed attached to the mineral surface of the *Paracoccus* sp. strain KS1 olivine cube. The thickest of these features were also co-located with areas of elevated carbon (6.0 ± 0.4 wt%) relative to the substrate (1.8 ± 0.3 wt%; **Figure 3C**). No features suggestive of biological processes were observed on the olivine mineral surfaces in the abiotic control.

Residual and Carried Over Organic Carbon

No significant differences ($p = <0.05$ in all cases) in NPOC were found between starved and non-starved inocula. This was true across the five media used and for each of the organisms, as well as in abiotic controls. The mean normalised NPOC concentrations are given in **Supplementary Table S5**, with significance values. There was a detectable baseline of residual organic carbon in the five blank media ranging from 2.23 $mg\,L^{-1}$ in CM to 4.51 $mg\,L^{-1}$ in SG.

DISCUSSION

Nitrate Reduction Drives Growth in Simulated Martian Environments

The presence of nitrates in modern and ancient martian surface samples (Stern et al., 2015) greatly diversified the range of metabolisms hypothetically possible, bringing autotrophic and

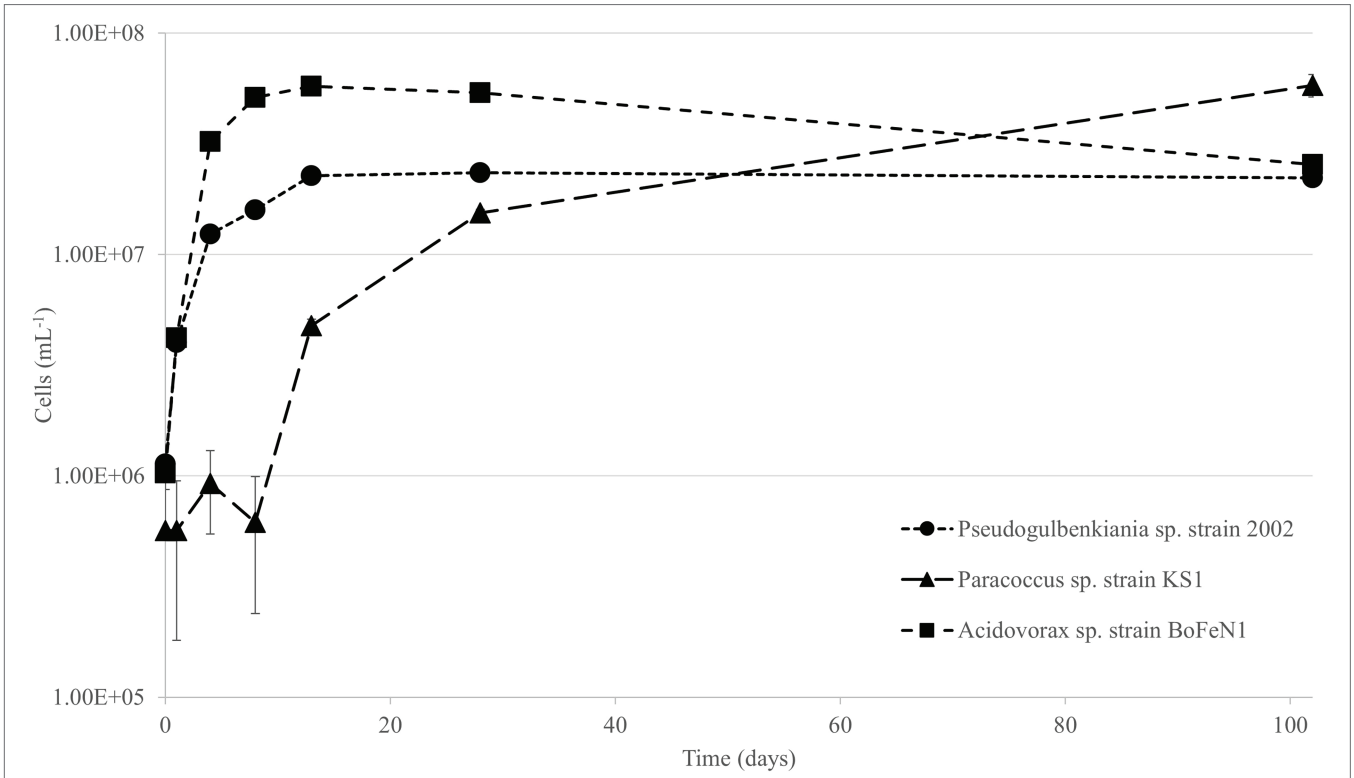

FIGURE 2 | Viable cell counts over time for *Pseudogulbenkiania* sp. strain 2002, *Paracoccus* sp. strain KS1 and *Acidovorax* sp. strain BoFeN1. Error bars represent ± standard error.

TABLE 3 | Final Fe concentrations, changes in nitrate and pH for inoculated olivine culture series and abiotic controls (± standard error of triplicates), growth rate (*k*) and doubling time for growing cultures.

Series	ΔFe_{total} (μM)	ΔNO_3^-	ΔpH	*k* (day^{-1})	Doubling time (days)
Paracoccus sp. strain KS1	+0.182 (±0.029)	−40.28% (±3.79)	+0.12 (±0.00)	0.07	4.31
Pseudogulbenkiania sp. strain 2002	+0.154 (±0.025)	−34.80% (±3.07)	+0.15 (±0.04)	0.26	1.16
Acidovorax sp. strain BoFeN1	+0.140 (±0.027)	−27.93% (±0.76)	+0.14 (±0.02)	0.37	0.80
Control	+1.000 (±0.017)	−10.20% (±0.95)	+0.13 (±0.01)	–	–

heterotrophic forms of nitrate reduction and denitrification to the fore.

The abundances of nitrate on Mars in scooped dust and drilled sediment are in the range of 70–1,100 ppm (Stern et al., 2015), equivalent to ~1–16 mM and sufficient to drive nitrogen-based metabolisms in the presence of potential active nitrate formation mechanisms, such as volcanic lightning, impact-generated and radiation-catalysed nitrogen fixation reactions (Mahaffy et al., 2013; Smith et al., 2014; Stern et al., 2015). Denitrifying microbes are typically active in environments with lower nitrate concentrations (<1 ppm), but occur across a wide range of concentrations and have been described performing denitrification at up to 36,000 ppm (0.58 M) on Earth, albeit at an impaired rate (Glass and Silverstein, 1999; Tomasek et al., 2017).

The growth of *Acidovorax* sp. strain BoFeN1, *Pseudogulbenkiania* sp. strain 2002 and *Paracoccus* sp. strain KS1 with olivine and in the SG simulant media, and the two former strains in the CM simulant media, suggests that growth by nitrate reduction is possible on both martian mineral substrates and in simulated martian fluid chemistries. This is relevant for early biospheres on Mars, given the availability of nitrate as an electron acceptor within the context of the early surface environment (Stern et al., 2015), and the near absence of molecular oxygen.

Oligotrophic Mixotrophy Over Autotrophy

Of the microorganisms investigated here, autotrophic growth by NDFO has only been reported in *Pseudogulbenkiania* sp. strain 2002, which was claimed to have grown consistently across repeated transfers (Weber et al., 2006b). In comparison with the olivine cultures in this study, the autotrophic growth observed by Weber et al. (2006b) occurred with a higher growth rate. However, there was no limitation of Fe^{2+} in that previous

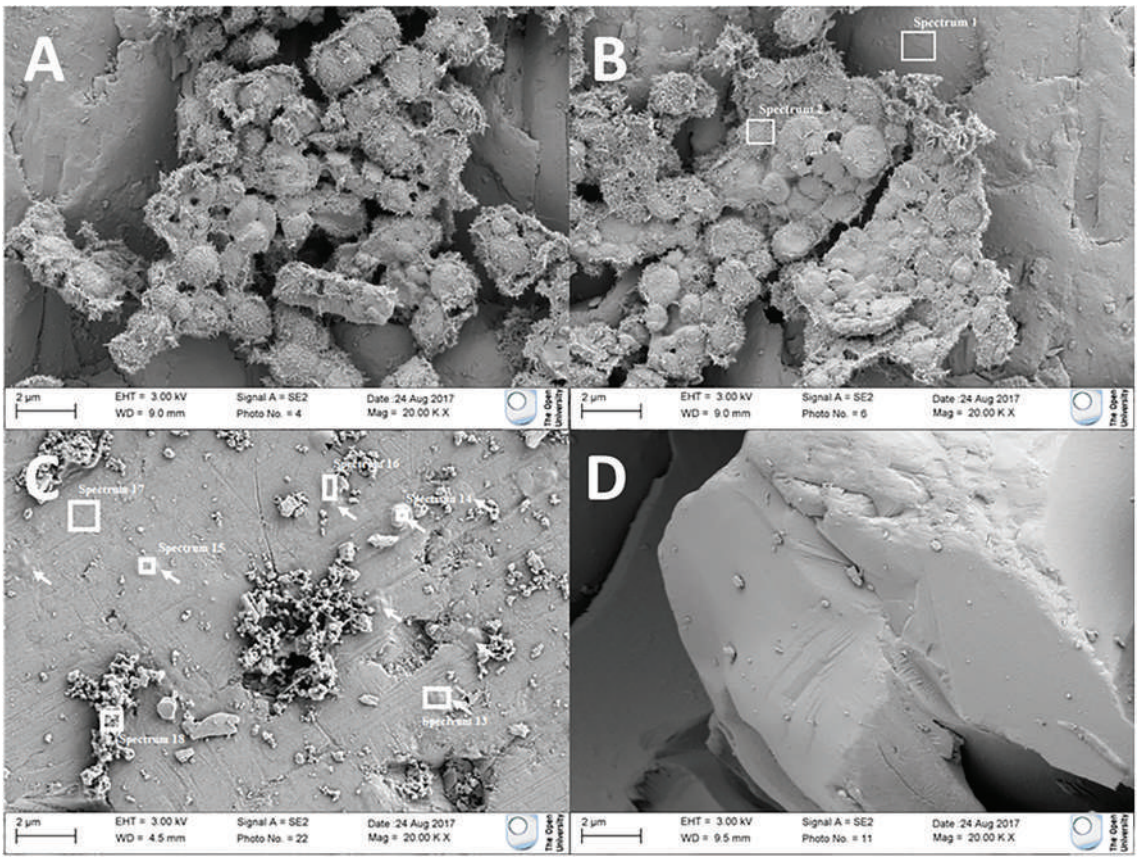

FIGURE 3 | Electron micrographs of **(A,B)** coccoid features adhered to olivine after culture with Pseudogulbenkiania sp. strain 2002. **(C)** Flattened, rounded features (indicated by arrows) adhered to the olivine surface after culture with *Paracoccus* sp. strain KS1. Target areas for electron dispersive X-ray spectroscopic (EDS) analysis are shown with white boxes. No such features were observed in **(D)** the abiotic control.

study, which invoked an initial concentration of 10 mM. Under the Fe^{2+}-limited conditions of this experiment (only solid-state Fe and <1 µM Fe in solution), it is unsurprising that we observed a lower growth rate here.

Although *Acidovorax* sp. strain BoFeN1 and *Paracoccus* sp. strain KS1 had previously been thought to require an organic co-substrates for NDFO-associated growth (Iordan et al., 1995; Kappler et al., 2005), both strains grew on olivine and in SG cultures with no organic media component. The reason for this is likely the low-but-detectable baseline concentration of organic carbon which was detected in all of the blank media, identified in this case as originating from the media components. The NPOC concentrations detected (~2.2–4.5 mg L^{-1}) were equivalent to the presence of ~12–25 µM glucose, meaning these compounds could be serving as a co-electron donor for growth by mixotrophic NDFO in otherwise autotrophic cultures. This conclusion supports the assertion by Bryce et al. (2018) that true autotrophic growth by NDFO has only been conclusively demonstrated in one instance—the so-called 'KS' co-culture (Straub et al., 1996; Blöthe and Roden, 2009) – and that most reported NDFO strains are in fact mixotrophic or organotrophic denitrifiers. Even so, the growth of strains as metabolically and phylogenetically diverse as *Acidovorax* sp. strain BoFeN1, *Pseudogulbenkiania* sp. strain 2002 and *Paracoccus* sp. strain KS1 under low Fe^{2+} availability and oligotrophic, anoxic conditions supports the suitability of NDFO organisms to circumneutral early martian environments, which are now thought to have been replete with organic carbon compounds (Eigenbrode et al., 2018).

Diverse Martian Chemistries Affect NDFO Habitability

The Shergottite meteorites, upon which the SG medium is based (Ramkissoon et al., 2019), are proposed to be representative of martian basaltic terrains (Treiman, 2003). With that in mind, the growth of all three strains in the SG medium indicates that the geochemical composition of basaltic environments could support the proliferation of NDFO microbes if sufficient nitrate was present as a result of various formation mechanisms (Stern et al., 2015, 2017; **Figure 4**). This finding has implications for life at both the early surface of Mars, and in the subsurface, where basalts of this type have been abundant throughout the planet's history (Bertka and Fei, 1998; Bridges and Warren, 2006; Steele et al., 2012). Compared to the other simulant-derived media, the SG medium is particularly characterised

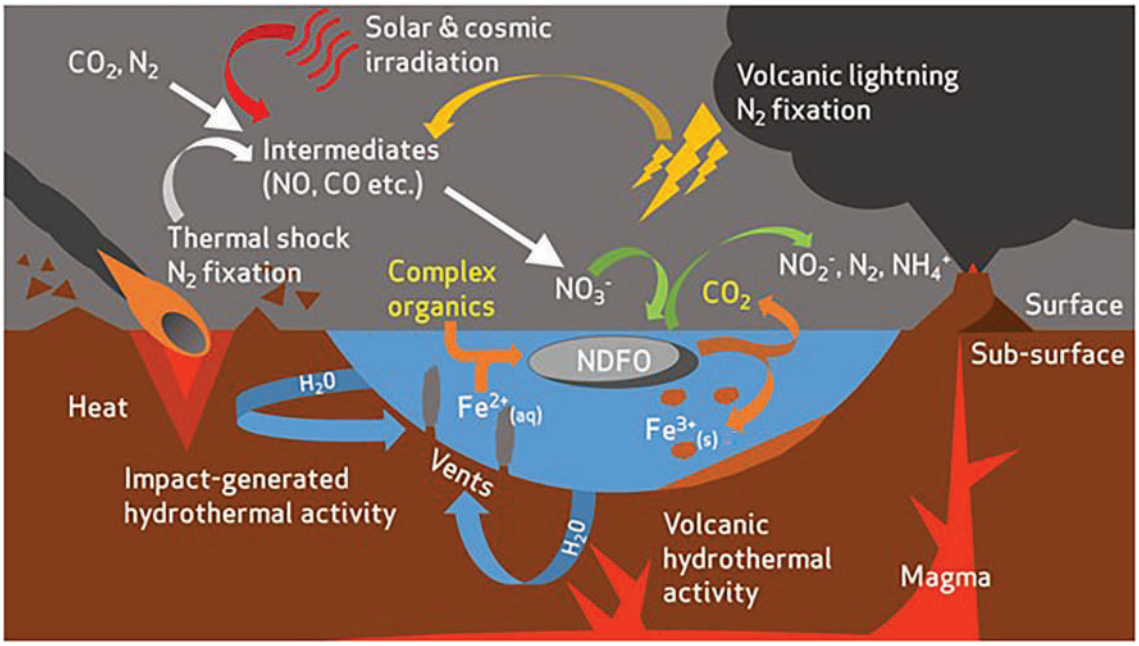

FIGURE 4 | Overview of potential redox substrate sources for nitrate-dependent Fe^{2+}-oxidising microorganisms in the early Mars environment [modified from Price et al., 2018]. Complex organics are present as an additional electron donor and carbon source for microbial life. Organics act as a co-substrate with Fe^{2+} to drive respiratory nitrate reduction and ATP production in NDFO-performing microorganisms. CO_2 is produced as a metabolite from oxidation of organics.

by the presence of insoluble Fe components. Paired with the growth of all three strains on an olivine substrate, this finding suggests that oligotrophic NDFO may perform optimally under Fe^{2+} limitation, possibly due to additional ATP consumption for metal efflux under high Fe^{2+} conditions.

The CM medium contains greater concentrations of dissolved Fe^{2+}, Fe^{3+} and sulphate in comparison to SG medium. It is derived from a simulant of aeolian dust at Gale crater and better represents the modern global composition of the weathered martian surface (Ramkissoon et al., 2019), so, the confirmed growth of *Pseudogulbenkiania* sp. strain 2002 and *Acidovorax sp*. strain BoFeN1 (evidence for growth of *Paracoccus* sp. strain KS1 was inconclusive) could mean that near-surface aqueous environments with regolith of a similar composition could support NDFO organisms. Habitation of hypothetical modern and ancient fluids by NDFO microbes is made more plausible by the evidence for Amazonian hydrological activity (Adeli et al., 2016; Butcher et al., 2017). Butcher et al. (2017) described eskers, subglacial landforms caused by basal melting and subsequent erosion, revealed by retreating glaciers in areas of elevated geothermal heat flux. The existence of these features indicates that Mars has hosted large-scale mixing of meltwater with modern surface geology, potentially providing environments similar to the CM media in this experiment. If a putative early biosphere existed and retreated to the deep subsurface, as others have suggested (Michalski et al., 2013), localised geothermal activity paired with glacial basal melting could have provided an opportunity to periodically replenish the near-surface environments with extant microbes and generate more recent biosignatures.

The HR and SR media, in which no strain grew, hold some key differences in initial chemistry and progression of physicochemical conditions throughout the experiment, which may help to explain the observed variation in habitability. The HR media contained a higher dissolved concentration of Fe^{2+} than either SG or CM. Counterintuitively, this may have had an inhibitory effect on the strains tested. Carlson et al. (2012) describe the toxic reactions of Fe^{2+} with oxidised nitrogen species, which may have inhibited growth if the cultures were not able to acclimatise following inoculation. Alternatively, the cells may have undergone rapid encrustation leading to loss of viability, as described previously for *Acidovorax* sp. strain BoFeN1 (Miot et al., 2009a).

The concentration of sulphates (>3.6 mM) in SR media greatly exceeded either CM (0.47 mM) or SG (0.05 mM) and caused acidification. For example, after 10 days the pH had dropped below the reported range (pH < 6) for NDFO metabolism. Acidification reduces the energetic favourability of the redox potential NDFO couple for sustaining microbial growth and carbon fixation (Weber et al., 2006a). The acidification could also be exacerbated by the reaction of the 10% CO_2 headspace component with water to form carbonic acid and the lack of buffer capacity in solution, as the other three simulant media also became acidified (albeit to a lesser extent than SR; **Supplementary Table S2**). The martian atmosphere is, and has been, primarily composed of CO_2 throughout history, so the acidifying effects of this on

long-lived hydrological systems in contact with the atmosphere are important to note when considering habitability for pH-dependent metabolisms, such as NDFO. Indeed, acidified oceans (pH < 6.2) have been proposed on early Mars as a consequence of a CO_2 (0.8–4 bar) atmosphere (Fairén et al., 2004). If true, these conditions would inhibit NDFO as a viable metabolism across surface-exposed water bodies of early Mars. However, basaltic rocks (relevant to the olivine and SG cultures) act as a buffer and systems are generally neutral to alkaline when not in direct contact with the atmosphere or any other source of acidification (Zolotov and Mironenko, 2007; McAdam et al., 2008). Direct geochemical analysis of rocks *in situ* at Gale crater (upon which CM is based) also show that circumneutral systems did persist on early Mars (Grotzinger et al., 2014), particularly in the subsurface, where they could even exist today (Michalski et al., 2013).

Fe Oxidation State

Despite evidence for both microbial growth and microbially mediated nitrate to nitrite reduction in the SG and CM simulant media, there was no significant oxidation of Fe^{2+}. This contrasts with expectations for active NDFO-based energy metabolisms in growing cultures (Miot et al., 2014a). For example, Weber et al. (2006b) observed that *Pseudogulbenkiania* sp. strain 2002 oxidised ~2 mM Fe^{2+} of a medium containing 10 mM Fe^{2+} over 7 days during autotrophic growth. *Acidovorax* sp. strain BoFeN1 oxidised ~2 mM of 4 mM total Fe^{2+} during autotrophic culture over 20 days (Kappler et al., 2005). These studies included higher concentrations of both Fe^{2+} and nitrate than any of the media tested here, which may account for some of the difference in the extent of Fe^{2+} oxidation when compared to the CM and SG martian simulant-derived media. It is also possible the growth observed here in CM (>1 μg ml^{-1} protein) may be insufficient to generate significant Fe oxidation relative to the control, given the sensitivity of the ferrozine assay. In comparison, Miot et al. (2009a) recorded ~65 μg ml^{-1} protein generated during mixotrophic oxidation of 5.4 mM Fe^{2+} by *Acidovorax* sp. strain BoFeN1.

There were no significant differences in Fe oxidation state between the inoculated cultures and controls for any of the simulant-derived media, which suggests that the reducing trend in the CM Fe^{2+}/Fe_{total} ratios over time were predominantly the result of an abiotic chemical factor. It is noteworthy that in all of the CM cultures which showed evidence of microbial growth, the mean Fe oxidation state was more oxidised (Fe^{2+}/Fe_{total} = 0.41–0.43) after 10 days than in the CM control (Fe^{2+}/Fe_{total} = 0.48). Furthermore, there was a negative correlation between microbial growth and the Fe^{2+}/Fe_{total} ratio—greater growth leads to greater Fe oxidation—relative to the control in CM media. That correlation suggests that growth had an oxidising effect on the media and sufficient microbial growth by nitrate reduction to nitrite in this media could produce significant patterns of Fe oxidation. However, observing this effect definitively may require a longer experiment duration, a more sensitive method for monitoring Fe oxidation state or a defined organic co-substrate to increase microbial activity.

Oligotrophic Growth on Olivine

All three strains were able to grow using olivine as a sole source of Fe^{2+}. The end point concentration of dissolved Fe was highest in the abiotic control, despite Fe being absent from the initial media composition. It can be assumed that this represents Fe (namely, Fe^{2+}) leached abiotically from the olivine substrate over the duration of the experiment, which is in line with olivine dissolution kinetics at circumneutral pH proposed by Wogelius and Walther (1991) and represents a rate-limiting factor for microbial Fe^{2+} oxidation. The Fe concentrations accumulated from olivine dissolution over the course of the experiment reached a maximum of ~1 μM. In comparison, the initial Fe^{2+} concentration was ~226 μM in the CM media, whereas dissolved Fe^{2+} was below the limit of detection in SG. A similar experiment demonstrated that neutrophilic growth by microaerophilic bacteria could occur under microoxic (1.6% O_2) conditions using olivine sand as a sole Fe source (although Fo_{91} compared with Fo_{84} in this study; Popa et al., 2012). That isolate, *Pseudomonas* sp. strain HerB, was able to grow with the same ratio of olivine mass to media volume and the same temperature and pH range as in the experiments described in this study. This adds credence to the conclusion that the rate of dissolution and concentration of Fe seen in the results presented here are indeed sufficient to help drive microbial growth. Furthermore, the anaerobic conditions and use of nitrate as an electron acceptor in the experiments detailed here may represent early martian environments more closely as they are now better understood.

Soluble Fe^{2+} concentrations were lower than the control in the actively growing cultures of *Acidovorax* sp. strain BoFeN1, *Pseudogulbenkiania* sp. strain 2002 and *Paracoccus* sp. strain KS1. Although formation of macroscopic Fe^{3+} precipitates was not observed, the most likely explanation in the context of this experiment is that micromolar Fe^{2+} is being scavenged and oxidised during NDFO, resulting in the precipitation of microscopic insoluble Fe^{3+} compounds, as has been described extensively in the literature (Schädler et al., 2009; Miot et al., 2009a, 2014a, 2015; Pantke et al., 2012). The consumption of Fe^{2+} and nitrate, together with evidence of growth from cell counts, suggests that microbial growth facilitated by NDFO has occurred. Growth of *Acidovorax* sp. strain BoFeN1 using Fe^{2+} from olivine (in which soluble Fe^{2+} was detectably consumed) was significantly greater than when grown in the SG and CM media (in which microbial Fe^{2+} consumption was not detectable). This disparity is likely to be due to the higher initial nitrate concentration in the olivine cultures (4 mM), compared to the simulant-derived media (1 mM).

Biogenicity and NDFO Detection on Mars

SEM analysis of the olivine mineral surfaces showed features with aspects suggesting biogenic origin, some of which were supported by results from EDS analyses. The clustered features observed with the *Pseudogulbenkiania* sp. strain 2002 (**Figure 3**)

were morphologically similar to that of *Pseudogulbenkiania* sp. strain 2002 cells, which have been visualised previously (Zhao et al., 2013). The largest clusters of mineralised cells (*Pseudogulbenkiania* sp. strain 2002; **Supplementary Figure S7**) retained detectable, elevated carbon signatures. These biomineralised microbial structures demonstrate a mechanism for morphological biosignature production from oligotrophic NDFO cultures. As in the *Pseudogulbenkiania* sp. strain 2002 culture, the carbon signature (**Supplementary Figure S8**) detected in the *Paracoccus* sp. strain KS1 culture (**Figure 3C**) provides supporting evidence for the biogenicity of these features. Furthermore, transmission electron microscopy has previously demonstrated the nucleation of ferric minerals in the periplasm of *Acidovorax* sp. strain BoFeN1 (Kappler et al., 2005; Schädler et al., 2009; Miot et al., 2009a, 2014a, 2015; Pantke et al., 2012; Zhou et al., 2016).

The difficulty in terms of *in situ* detection on Mars, however, is the scale of these structures (~1–200 μm). For reference, the spot sizes on the Raman Laser Spectrometer (Rosalind Franklin rover) and Scanning Habitable Environments With Raman & Luminescence for Organics & Chemicals (SHERLOC) instrument (Perseverance rover) are both 50 μm (Beegle et al., 2015; Rull et al., 2017). The consequence of this is that small biomineralised structures would be difficult to identify, even if located in the path of the beam. Even so, the features observed in this study suggest that olivine-rich rocks with historical exposure to circumneutral fluids are a logical starting point for these biosignature-oriented missions, which aim to investigate preserved Noachian sedimentary environments at Oxia Planum and Jezero crater (3.8–3.9 Ga), respectively (Goudge et al., 2018; Quantin-Nataf et al., 2019). A logical progression from the results of this paper would be to investigate NDFO encrustations using ground-based Raman instruments, in order to better interpret future rover data.

Our knowledge of the long-term effects of geological processing on NDFO-mediated cell encrustations is limited. However, Glasauer et al. (2013) combined laboratory encrustation experiments using a NDFO isolate with field observations to highlight the importance of the redox environment in fossilisation, finding that reductive dissolution could inhibit Fe biomineralisation; in testing the diagenetic maturation of organo-ferric structures from microaerobic Fe oxidisers, Picard et al. (2015) found that Fe^{3+} oxides could enhance structural and chemical preservation of biological material under high temperature and pressure and that spectroscopy could be used to identify these biosignatures in the rock record. Meanwhile, other Fe encrustations have been proposed as some of the earliest evidence for life on Earth (Li et al., 2013). Further artificial maturation experiments and identification of NDFO structures in terrestrial samples should be pursued to better understand how these biosignatures may present in target rocks on Mars.

The growth of strains in the basaltic SG medium supports this assessment, while growth in CM medium validates the hypothesis that circumneutral, sedimentary palaeoenvironments on Mars are ideal targets for NDFO biosignature detection. Likewise, the lack of microbial metabolism or growth among the tested strains in HR and SR media can be useful in guiding target selection. The acidifying, high-sulphate conditions in SR cultures are not conducive to circumneutral NDFO activity, meaning acidic sulphur-rich martian palaeoenvironments are poor candidates to host biomineralised NDFO cells. However, previous work has established the possibility of other metabolisms which may have been suited to such locations (Amils et al., 2014; Bauermeister et al., 2014). Similarly, the oxidised conditions of Fe^{3+}-rich HR media may be unsuitable for NDFO organisms and suggests haematite-dominated martian lithologies would not represent good targets for NDFO biosignature detection. However, as Fe^{2+} oxidisers, these microbes are capable of producing a broad range of Fe^{3+} oxides under reducing conditions (Kappler et al., 2005; Schädler et al., 2009; Miot et al., 2009b, 2014a,b; Pantke et al., 2012). Therefore, oxidised features in otherwise reduced habitable palaeoenvironments would represent logical targets for analysis and sample caching. For identification of structures on the scale of those observed in this study, Mars sample return is vital.

The evident difficulty in determining biogenicity from morphology, even in batch cultures where the original morphology of the cells is known, serves to highlight a necessity for multiple lines of evidence when investigating potential biosignatures on Earth and Mars. Indeed, some have suggested that many putative microfossils in the rock record on Earth may require reclassification (McMahon et al., 2021). The verification of biogenicity based on morphology has led to many contentious claims about evidence of life in both ancient terrestrial rocks and martian meteorites (McKay et al., 1996; Mojzsis et al., 1996). The results of this experiment suggest that pairing morphology and elemental observations with alternative methods of determining the past presence of biological Fe metabolism, such as isotope fractionation patterns (Anand et al., 2006), should be investigated.

CONCLUSION

This is the first study to experimentally investigate nitrate-dependent Fe^{2+} oxidation as a plausible metabolism for early Mars, monitoring microbial growth and NDFO under simulated martian chemical conditions and on Mars-relevant olivine mineral surfaces.

All three tested strains were confirmed to have grown in the SG media and at least two strains in the CM media, based on protein, nitrite and nitrate data, which suggests some aqueous environments on early Mars were potentially habitable for NDFO microorganisms. However, there was no significant Fe oxidation or removal of soluble Fe from solution to form Fe^{3+} oxide precipitates by cultures in any of the simulant-derived media relative to their abiotic controls, suggesting that NDFO by actively growing microbes under these conditions did not dominate the overall redox chemistry of the media.

All three strains were also able to grow under anoxic, oligotrophic conditions by respiring nitrate and utilising Fe^{2+}

released by dissolution from an olivine substrate. This capability holds implications for the habitability of early Mars, where comparable conditions are likely to have existed. Signs of biomineralisation were observed on some of the olivine surfaces, demonstrating that NDFO could be a mechanism for preservation of morphological biosignatures from the early martian environment for detection in the present day. However, the small size of biomineralised features complicates *in situ* detection and necessitates Mars sample return.

DATA AVAILABILITY STATEMENT

The raw data supporting the conclusions of this article will be made available by the authors, without undue reservation.

AUTHOR CONTRIBUTIONS

AP conducted all experimental work in this study, with exceptions noted in the acknowledgements. AP developed the concepts underpinning this work in discussion with KO-F, VP, and SS. NR and MM developed the simulants and methods to derive media composition, respectively. All authors contributed to development of the manuscript, which was primarily authored by AP.

FUNDING

This work was supported by studentship funding from the Science and Technology Facilities Council and The Open University, as well as an Expanding Excellence in England (E3) grant from Research England (grant no. 124.18).

ACKNOWLEDGMENTS

The majority of data contained in this paper derives from the PhD thesis of the first author (Price, 2020). Non-purgeable organic carbon analyses were conducted externally at the British Geological Survey, with the assistance of Andy Marriott and Andrea Mills and at the Open University by Tim Barton. The *Acidovorax* sp. strain BoFeN1 microorganism and some conceptual input for this study were contributed by Jennyfer Miot of Institut de Minéralogie, de Physique des Matériaux et de Cosmochimie (IMPMC), Sorbonne Université-CNRS-MNHN, Paris.

SUPPLEMENTARY MATERIAL

The Supplementary Material for this article can be found online at: https://www.frontiersin.org/articles/10.3389/fmicb.2022.800219/full#supplementary-material

REFERENCES

Adeli, S., Hauber, E., Kleinhans, M., Le Deit, L., Platz, T., Fawdon, P., et al. (2016). Amazonian-aged fluvial system and associated ice-related features in Terra Cimmeria, Mars. *Icarus* 277, 286–299. doi: 10.1016/j.icarus.2016.05.020

Allen, C.C., Morris, R.V., Lindstrom, D.J., Lindstrom, M., and Lockwood, J. (1997). "JSC Mars-1-Martian regolith simulant." in *Lunar and Planetary Science Conference 1997; March 17-21, 1997; Houston*.

Amils, R., Fernández-Remolar, D., and Team, T. I. (2014). Río tinto: a geochemical and mineralogical terrestrial analogue of Mars. *Life* 4, 511–534. doi: 10.3390/life4030511

Amils, R., González-Toril, E., Aguilera, A., Rodrıguez, N., Fernández-Remolar, D., Gómez, F., et al. (2011). From Rıo Tinto to Mars: the terrestrial and extraterrestrial ecology of acidophiles. *Adv. Appl. Microbiol.* 77, 41–70. doi: 10.1016/B978-0-12-387044-5.00002-9

Anand, M., Russell, S., Blackhurst, R., and Grady, M. (2006). Searching for signatures of life on Mars: an Fe-isotope perspective. *Philos. Trans. R. Soc. Lond., B, Biol. Sci.* 361, 1715–1720. doi: 10.1098/rstb.2006.1899

Bauermeister, A., Rettberg, P., and Flemming, H.-C. (2014). Growth of the acidophilic iron–sulfur bacterium *Acidithiobacillus ferrooxidans* under Mars-like geochemical conditions. *Planet. Space Sci.* 98, 205–215. doi: 10.1016/j.pss.2013.09.009

Beck, P., Barrat, J. A., Gillet, P., Wadhwa, M., Franchi, I. A., Greenwood, R. C., et al. (2006). Petrography and geochemistry of the chassignite Northwest Africa 2737 (NWA 2737). *Geochim. Cosmochim. Acta* 70, 2127–2139. doi: 10.1016/j.gca.2006.01.016

Beegle, L., Bhartia, R., White, M., DeFlores, L., Abbey, W., Yen-Hung, W., et al. (2015). "SHERLOC: Scanning habitable environments with Raman & luminescence for organics & chemicals." in *2015 IEEE Aerospace Conference, Big Sky*; March 7-14, 2015; 1–11.

Benz, M., Brune, A., and Schink, B. (1998). Anaerobic and aerobic oxidation of ferrous iron at neutral pH by chemoheterotrophic nitrate-reducing bacteria. *Arch. Microbiol.* 169, 159–165. doi: 10.1007/s002030050555

Bertka, C. M., and Fei, Y. (1998). Density profile of an SNC model Martian interior and the moment-of-inertia factor of Mars. *Earth Planet. Sci. Lett.* 157, 79–88. doi: 10.1016/S0012-821X(98)00030-2

Bish, D. L., Blake, D. F., Vaniman, D. T., Chipera, S. J., Morris, R. V., Ming, D. W., et al. (2013). X-ray diffraction Results from Mars science laboratory: mineralogy of Rocknest at gale crater. *Science* 341:1238932. doi: 10.1126/science.1238932

Blake, D. F., Morris, R. V., Kocurek, G., Morrison, S. M., Downs, R. T., Bish, D., et al. (2013). Curiosity at gale crater, Mars: characterization and analysis of the Rocknest sand shadow. *Science* 341:1239505. doi: 10.1126/science.1239505

Blöthe, M., and Roden, E. E. (2009). Composition and activity of an autotrophic Fe (II)-oxidizing, nitrate-reducing enrichment culture. *Appl. Environ. Microbiol.* 75, 6937–6940. doi: 10.1128/AEM.01742-09

Bonilla-Rosso, G., Peimbert, M., Alcaraz, L. D., Hernández, I., Eguiarte, L. E., Olmedo-Alvarez, G., et al. (2012). Comparative Metagenomics of two microbial Mats at Cuatro Ciénegas Basin II: community structure and composition in oligotrophic environments. *Astrobiology* 12, 659–673. doi: 10.1089/ast.2011.0724

Böttger, U., de Vera, J. P., Fritz, J., Weber, I., Hübers, H. W., and Schulze-Makuch, D. (2012). Optimizing the detection of carotene in cyanobacteria in a martian regolith analogue with a Raman spectrometer for the ExoMars mission. *Planet. Space Sci.* 60, 356–362. doi: 10.1016/j.pss.2011.10.017

Bridges, J. C., and Warren, P. H. (2006). The SNC meteorites: basaltic igneous processes on Mars. *J. Geol. Soc.* 163, 229–251. doi: 10.1144/0016-764904-501

Bryce, C., Blackwell, N., Schmidt, C., Otte, J., Huang, Y.-M., Kleindienst, S., et al. (2018). Microbial anaerobic Fe(II) oxidation – ecology, mechanisms and environmental implications. *Environ. Microbiol.* 20, 3462–3483. doi: 10.1111/1462-2920.14328

Butcher, F. E. G., Balme, M. R., Gallagher, C., Arnold, N. S., Conway, S. J., Hagermann, A., et al. (2017). Recent basal melting of a mid-latitude glacier on Mars. *J. Geophys. Res. Planets* 122, 2445–2468. doi: 10.1002/2017JE005434

Carlson, H. K., Clark, I. C., Blazewicz, S. J., Iavarone, A. T., and Coates, J. D. (2013). Fe (II) oxidation is an innate capability of nitrate-reducing bacteria that involves abiotic and biotic reactions. *J. Bacteriol.* 195, 3260–3268. doi: 10.1128/JB.00058-13

Carlson, H. K., Clark, I. C., Melnyk, R. A., and Coates, J. D. (2012). Toward a mechanistic understanding of anaerobic nitrate-dependent iron oxidation: balancing electron uptake and detoxification. *Front. Microbiol.* 3:57. doi: 10.3389/fmicb.2012.00057

Chan, C. S., Fakra, S. C., Emerson, D., Fleming, E. J., and Edwards, K. J. (2011). Lithotrophic iron-oxidizing bacteria produce organic stalks to control mineral growth: implications for biosignature formation. *ISME J.* 5, 717–727. doi: 10.1038/ismej.2010.173

Chi Fru, E., Ivarsson, M., Kilias, S. P., Bengtson, S., Belivanova, V., Marone, F., et al. (2013). Fossilized iron bacteria reveal a pathway to the biological origin of banded iron formation. *Nat. Commun.* 4:2050. doi: 10.1038/ncomms3050

Crosby, C. H., Bailey, J. V., and Sharma, M. (2014). Fossil evidence of iron-oxidizing chemolithotrophy linked to phosphogenesis in the wake of the great oxidation event. *Geology* 42, 1015–1018. doi: 10.1130/G35922.1

Ehlmann, B. L., and Edwards, C. S. (2014). Mineralogy of the Martian surface. *Annu. Rev. Earth Planet. Sci.* 42, 291–315. doi: 10.1146/annurev-earth-060313-055024

Ehlmann, B. L., Mustard, J. F., Fassett, C. I., Schon, S. C., Head, J. W. III, Des Marais, D. J., et al. (2008). Clay minerals in delta deposits and organic preservation potential on Mars. *Nat. Geosci.* 1, 355–358. doi: 10.1038/ngeo207

Ehlmann, B. L., Mustard, J. F., Murchie, S. L., Bibring, J.-P., Meunier, A., Fraeman, A. A., et al. (2011). Subsurface water and clay mineral formation during the early history of Mars. *Nature* 479, 53–60. doi: 10.1038/nature10582

Eigenbrode, J. L., Summons, R. E., Steele, A., Freissinet, C., Millan, M., Navarro-González, R., et al. (2018). Organic matter preserved in 3-billion-year-old mudstones at Gale crater, Mars. *Science* 360, 1096–1101. doi: 10.1126/science.aas9185

Fairén, A. G., Fernández-Remolar, D., Dohm, J. M., Baker, V. R., and Amils, R. (2004). Inhibition of carbonate synthesis in acidic oceans on early Mars. *Nature* 431, 423–426. doi: 10.1038/nature02911

Filiberto, J. (2017). Geochemistry of Martian basalts with constraints on magma genesis. *Chem. Geol.* 466, 1–14. doi: 10.1016/j.chemgeo.2017.06.009

Floran, R. J., Prinz, M., Hlava, P. F., Keil, K., Nehru, C. E., and Hinthorne, J. R. (1978). The Chassigny meteorite: a cumulate dunite with hydrous amphibole-bearing melt inclusions. *Geochim. Cosmochim. Acta* 42, 1213–1229. doi: 10.1016/0016-7037(78)90115-1

Fox-Powell, M. G., Hallsworth, J. E., Cousins, C. R., and Cockell, C. S. (2016). Ionic strength is a barrier to the habitability of Mars. *Astrobiology* 16, 427–442. doi: 10.1089/ast.2015.1432

Glasauer, S., Mattes, A., and Gehring, A. (2013). Constraints on the preservation of ferriferous microfossils. *Geomicrobiol J.* 30, 479–489. doi: 10.1080/01490451.2012.718408

Glass, C., and Silverstein, J. (1999). Denitrification of high-nitrate, high-salinity wastewater. *Water Res.* 33, 223–229. doi: 10.1016/S0043-1354(98)00177-8

Goodrich, C. A. (2002). Olivine-phyric martian basalts: a new type of shergottite. *Meteorit. Planet. Sci.* 37, 31.

Goudge, T. A., Mohrig, D., Cardenas, B. T., Hughes, C. M., and Fassett, C. I. (2018). Stratigraphy and paleohydrology of delta channel deposits, Jezero crater, Mars. *Icarus* 301, 58–75. doi: 10.1016/j.icarus.2017.09.034

Griess, P. (1879). Bemerkungen zu der Abhandlung der HH. Weselsky und Benedikt "Ueber einige Azoverbindungen". *Ber. Dtsch. Chem. Ges.* 12, 426–428. doi: 10.1002/cber.187901201117

Grotzinger, J. P., Sumner, D., Kah, L., Stack, K., Gupta, S., Edgar, L., et al. (2014). A habitable fluvio-lacustrine environment at Yellowknife Bay, gale crater, Mars. *Science* 343:1242777. doi: 10.1126/science.1249944

Hafenbradl, D., Keller, M., Dirmeier, R., Rachel, R., Roßnagel, P., Burggraf, S., et al. (1996). Ferroglobus placidus gen. Nov., sp. nov., a novel hyperthermophilic archaeum that oxidizes Fe^{2+} at neutral pH under anoxic conditions. *Arch. Microbiol.* 166, 308–314. doi: 10.1007/s002030050388

Halliday, A. N., Wänke, H., Birck, J. L., and Clayton, R. N. (2001). The accretion, composition and early differentiation of Mars. *Space Sci. Rev.* 96, 197–230. doi: 10.1023/A:1011997206080

Iordan, S. L., Kraczkiewicz-Dowjat, A. J., Kelly, D. P., and Wood, A. P. (1995). Novel eubacteria able to grow on carbon disulfide. *Arch. Microbiol.* 163, 131–137. doi: 10.1007/BF00381787

Jakosky, B., Slipski, M., Benna, M., Mahaffy, P., Elrod, M., Yelle, R., et al. (2017). Mars' atmospheric history derived from upper-atmosphere measurements of 38Ar/36Ar. *Science* 355, 1408–1410. doi: 10.1126/science.aai7721

Kappler, A., Schink, B., and Newman, D. K. (2005). Fe (III) mineral formation and cell encrustation by the nitrate-dependent Fe (II)-oxidizer strain BoFeN1. *Geobiology* 3, 235–245. doi: 10.1111/j.1472-4669.2006.00056.x

Klueglein, N., Zeitvogel, F., Stierhof, Y.-D., Floetenmeyer, M., Konhauser, K. O., Kappler, A., et al. (2014). Potential role of nitrite for abiotic Fe (II) oxidation and cell encrustation during nitrate reduction by denitrifying bacteria. *Appl. Environ. Microbiol.* 80, 1051–1061. doi: 10.1128/AEM.03277-13

Kounaves, S. P., Carrier, B. L., O'Neil, G. D., Stroble, S. T., and Claire, M. W. (2014). Evidence of martian perchlorate, chlorate, and nitrate in Mars meteorite EETA79001: implications for oxidants and organics. *Icarus* 229, 206–213. doi: 10.1016/j.icarus.2013.11.012

Kurokawa, H., Kurosawa, K., and Usui, T. (2018). A lower limit of atmospheric pressure on early Mars inferred from nitrogen and argon isotopic compositions. *Icarus* 299, 443–459. doi: 10.1016/j.icarus.2017.08.020

Lane, M. D., Bishop, J. L., Darby Dyar, M., Hyde, B. C., King, P. L., and Parente, M. (2008). Mineralogy of the Paso Robles soils on Mars. *Am. Mineral.* 93, 728–739. doi: 10.2138/am.2008.2757

Laufer, K., Røy, H., Jørgensen, B. B., and Kappler, A. (2016). Evidence for the existence of autotrophic nitrate-reducing Fe(II)-oxidizing bacteria in marine coastal sediment. *Appl. Environ. Microbiol.* 82, 6120–6131. doi: 10.1128/AEM.01570-16

Li, J., Benzerara, K., Bernard, S., and Beyssac, O. (2013). The link between biomineralization and fossilization of bacteria: insights from field and experimental studies. *Chem. Geol.* 359, 49–69. doi: 10.1016/j.chemgeo.2013.09.013

Mahaffy, P. R., Webster, C. R., Atreya, S. K., Franz, H., Wong, M., Conrad, P. G., et al. (2013). Abundance and isotopic composition of gases in the martian atmosphere from the curiosity rover. *Science* 341, 263–266. doi: 10.1126/science.1237966

Marriott, A. L., Kelly, T. J., Sarkar, S. K., Chenery, S. R. N., Rakshit, D., Bhattacharya, B. D., et al. (2020). Elemental composition of aquaculture fish from West Bengal, India: nutrition versus food safety. *Environ. Geochem. Health* 42, 1211–1228. doi: 10.1007/s10653-019-00401-8

McAdam, A. C., Zolotov, M. Y., Mironenko, M. V., and Sharp, T. G. (2008). Formation of silica by low-temperature acid alteration of Martian rocks: physical-chemical constraints. *J. Geophys. Res. Planets* 113. doi: 10.1029/2007JE003056

McKay, D. S., Gibson, E. K., Thomas-Keprta, K. L., Vali, H., Romanek, C. S., Clemett, S. J., et al. (1996). Search for past life on Mars: possible relic biogenic activity in Martian meteorite ALH84001. *Science* 273, 924–930. doi: 10.1126/science.273.5277.924

McMahon, S., Ivarsson, M., Wacey, D., Saunders, M., Belivanova, V., Muirhead, D., et al. (2021). Dubiofossils from a Mars-analogue subsurface palaeoenvironment: the limits of biogenicity criteria. *Geobiology* 19, 1–16. doi: 10.1111/gbi.12445

McSween, H. Y. Jr. (2015). Petrology on Mars†. *Am. Mineral.* 100, 2380–2395. doi: 10.2138/am-2015-5257

McSween, H. Y., Wyatt, M. B., Gellert, R., Bell, J. F. III, Morris, R. V., Herkenhoff, K. E., et al. (2006). Characterization and petrologic interpretation of olivine-rich basalts at Gusev crater, Mars. *J. Geophys. Res. Planets* 111. doi: 10.1029/2005JE002477

Michalski, J. R., Cuadros, J., Niles, P. B., Parnell, J., Rogers, A. D., and Wright, S. P. (2013). Groundwater activity on Mars and implications for a deep biosphere. *Nat. Geosci.* 6, 133–138. doi: 10.1038/ngeo1706

Miot, J., Benzerara, K., Morin, G., Kappler, A., Bernard, S., Obst, M., et al. (2009a). Iron biomineralization by anaerobic neutrophilic iron-oxidizing bacteria. *Geochim. Cosmochim. Acta* 73, 696–711. doi: 10.1016/j.gca.2008.10.033

Miot, J., Benzerara, K., Obst, M., Kappler, A., Hegler, F., Schädler, S., et al. (2009b). Extracellular iron biomineralization by photoautotrophic iron-oxidizing bacteria. *Appl. Environ. Microbiol.* 75, 5586–5591. doi: 10.1128/AEM.00490-09

Miot, J., Li, J., Benzerara, K., Sougrati, M. T., Ona-Nguema, G., Bernard, S., et al. (2014a). Formation of single domain magnetite by green rust oxidation promoted by microbial anaerobic nitrate-dependent iron oxidation. *Geochim. Cosmochim. Acta* 139, 327–343. doi: 10.1016/j.gca.2014.04.047

Miot, J., Recham, N., Larcher, D., Guyot, F., Brest, J., and Tarascon, J.-M. (2014b). Biomineralized α-Fe_2O_3: texture and electrochemical reaction with Li. *Energy Environ. Sci.* 7, 451–460. doi: 10.1039/c3ee41767k

Miot, J., Remusat, L., Duprat, E., Gonzalez, A., Pont, S., and Poinsot, M. (2015). Fe biomineralization mirrors individual metabolic activity in a nitrate-dependent Fe (II)-oxidizer. *Front. Microbiol.* 6:879. doi: 10.3389/fmicb.2015.00879

Mojzsis, S. J., Arrhenius, G., McKeegan, K. D., Harrison, T. M., Nutman, A. P., and Friend, C. R. L. (1996). Evidence for life on earth before 3,800 million years ago. *Nature* 384, 55–59. doi: 10.1038/384055a0

Muehe, E. M., Gerhardt, S., Schink, B., and Kappler, A. (2009). Ecophysiology and the energetic benefit of mixotrophic Fe (II) oxidation by various strains of nitrate-reducing bacteria. *FEMS Microbiol. Ecol.* 70, 335–343. doi: 10.1111/j.1574-6941.2009.00755.x

Nixon, S.L. (2014). Microbial iron reduction on Earth and Mars. PhD thesis, University of Edinburgh.

Nixon, S. L., Cockell, C. S., and Tranter, M. (2012). Limitations to a microbial iron cycle on Mars. *Planet. Space Sci.* 72, 116–128. doi: 10.1016/j.pss.2012.04.003

Nyquist, L.E., Bogard, D.D., Shih, C.-Y., Greshake, A., Stöffler, D., and Eugster, O. (2001). "*Ages and Geologic Histories of Martian Meteorites*," Springer Netherlands, 105–164.

Pantke, C., Obst, M., Benzerara, K., Morin, G., Ona-Nguema, G., Dippon, U., et al. (2012). Green rust formation during Fe (II) oxidation by the nitrate-reducing Acidovorax sp. strain BoFeN1. *Environ. Sci. Technol.* 46, 1439–1446. doi: 10.1021/es2016457

Papike, J. J. (2018). "Chapter 7. Comparative planetary mineralogy: chemistry of melt-deriyed pyroxene, feldspar, and olivine," in *Planetary Materials*. ed. J. J. Papike (Washington DC, USA: De Gruyter), 1007–1018.

Parro, V., Puente-Sánchez, F., Cabrol, N. A., Gallardo-Carreño, I., Moreno-Paz, M., Blanco, Y., et al. (2019). Microbiology and nitrogen cycle in the benthic sediments of a glacial oligotrophic deep Andean Lake as Analog of ancient Martian Lake-beds. *Front. Microbiol.* 10:929. doi: 10.3389/fmicb.2019.00929

Peters, G. H., Abbey, W., Bearman, G. H., Mungas, G. S., Smith, J. A., Anderson, R. C., et al. (2008). Mojave Mars simulant—characterization of a new geologic Mars analog. *Icarus* 197, 470–479. doi: 10.1016/j.icarus.2008.05.004

Picard, A., Kappler, A., Schmid, G., Quaroni, L., and Obst, M. (2015). Experimental diagenesis of organo-mineral structures formed by microaerophilic Fe(II)-oxidizing bacteria. *Nat. Commun.* 6:6277. doi: 10.1038/ncomms7277

Pirt, S.J. (1975). *Principles of Microbe and Cell Cultivation*. Oxford: Blackwell Scientific Publications.

Popa, R., Smith, A. R., Popa, R., Boone, J., and Fisk, M. (2012). Olivine-respiring bacteria isolated from the rock-ice interface in a lava-tube cave, a Mars analog environment. *Astrobiology* 12, 9–18. doi: 10.1089/ast.2011.0639

Price, A. (2020). Microbial Nitrate Dependent Fe^{2+} Oxidation: A Potential Early Mars Metabolism. PhD, The Open University.

Price, A., Pearson, V. K., Schwenzer, S. P., Miot, J., and Olsson-Francis, K. (2018). Nitrate-dependent iron oxidation: a potential Mars metabolism. *Front. Microbiol.* 9:513. doi: 10.3389/fmicb.2018.00513

Quantin-Nataf, C., Carter, J., Mandon, L., Balme, M., Fawdon, P., Davis, J., et al. (2019). "ExoMars at Oxia Planum, probing the aqueous-related Noachian environments." in *Ninth International Conference on Mars 2019*. July 22-26, 2019.

Ramirez, R. M., Kopparapu, R., Zugger, M. E., Robinson, T. D., Freedman, R., and Kasting, J. F. (2014). Warming early Mars with CO_2 and H_2. *Nat. Geosci.* 7, 59–63. doi: 10.1038/ngeo2000

Ramkissoon, N. K., Pearson, V. K., Schwenzer, S. P., Schröder, C., Kirnbauer, T., Wood, D., et al. (2019). New simulants for martian regolith: controlling iron variability. *Planet. Space Sci.* 179:104722. doi: 10.1016/j.pss.2019.104722

Rieder, R., Gellert, R., Anderson, R. C., Brückner, J., Clark, B. C., Dreibus, G., et al. (2004). Chemistry of rocks and soils at Meridiani Planum from the alpha particle X-ray spectrometer. *Science* 306, 1746–1749. doi: 10.1126/science.1104358

Rull, F., Maurice, S., Hutchinson, I., Moral, A., Perez, C., Diaz, C., et al. (2017). The Raman laser spectrometer for the ExoMars rover Mission to Mars. *Astrobiology* 17, 627–654. doi: 10.1089/ast.2016.1567

Schädler, S., Burkhardt, C., Hegler, F., Straub, K., Miot, J., Benzerara, K., et al. (2009). Formation of cell-iron-mineral aggregates by phototrophic and nitrate-reducing anaerobic Fe (II)-oxidizing bacteria. *Geomicrobiol J.* 26, 93–103. doi: 10.1080/01490450802660573

Schmidt, S. K., Gendron, E. M. S., Vincent, K., Solon, A. J., Sommers, P., Schubert, Z. R., et al. (2018). Life at extreme elevations on Atacama volcanoes: the closest thing to Mars on earth? *Antonie Van Leeuwenhoek* 111, 1389–1401. doi: 10.1007/s10482-018-1066-0

Smith, M. L., Claire, M. W., Catling, D. C., and Zahnle, K. J. (2014). The formation of sulfate, nitrate and perchlorate salts in the martian atmosphere. *Icarus* 231, 51–64. doi: 10.1016/j.icarus.2013.11.031

Steele, A., McCubbin, F., Fries, M., Kater, L., Boctor, N., Fogel, M., et al. (2012). A reduced organic carbon component in martian basalts. *Science* 337, 212–215. doi: 10.1126/science.1220715

Stern, J. C., Sutter, B., Freissinet, C., Navarro-González, R., McKay, C. P., Archer, P. D., et al. (2015). Evidence for indigenous nitrogen in sedimentary and aeolian deposits from the curiosity rover investigations at Gale crater, Mars. *Proc. Natl. Acad. Sci.* 112, 4245–4250. doi: 10.1073/pnas.1420932112

Stern, J. C., Sutter, B., Jackson, W. A., Navarro-González, R., McKay, C. P., Ming, D. W., et al. (2017). The nitrate/(per)chlorate relationship on Mars. *Geophys. Res. Lett.* 44, 2643–2651. doi: 10.1002/2016GL072199

Stevens, A. H., Steer, E., McDonald, A., Amador, E. S., and Cockell, C. S. (2018). Y-Mars: an Astrobiological analogue of Martian mudstone. *Earth Space Sci.* 5, 163–174. doi: 10.1002/2017EA000318

Straub, K. L., Benz, M., Schink, B., and Widdel, F. (1996). Anaerobic, nitrate-dependent microbial oxidation of ferrous iron. *Appl. Environ. Microbiol.* 62, 1458–1460. doi: 10.1128/aem.62.4.1458-1460.1996

Strohm, T. O., Griffin, B., Zumft, W. G., and Schink, B. (2007). Growth yields in bacterial denitrification and nitrate ammonification. *Appl. Environ. Microbiol.* 73, 1420–1424. doi: 10.1128/AEM.02508-06

Tomasek, A., Kozarek, J. L., Hondzo, M., Lurndahl, N., Sadowsky, M. J., Wang, P., et al. (2017). Environmental drivers of denitrification rates and denitrifying gene abundances in channels and riparian areas. *Water Resour. Res.* 53, 6523–6538. doi: 10.1002/2016WR019566

Tosca, N. J., McLennan, S. M., Lamb, M. P., and Grotzinger, J. P. (2011). Physicochemical properties of concentrated Martian surface waters. *J. Geophys. Res. Planets* 116:E05004. doi: 10.1029/2010JE003700

Treiman, A. H. (2003). Chemical compositions of martian basalts (shergottites): Some inferences on b; formation, mantle metasomatism, and differentiation in Mars. *Meteorit. Planet. Sci.* 38, 1849–1864. doi: 10.1111/j.1945-5100.2003.tb00019.x

Vodyanitskii, Y. N. (2001). On the dissolution of iron minerals in Tamm's reagent. *Eurasian Soil Sci.* 34, 1086–1096.

Weber, K. A., Achenbach, L. A., and Coates, J. D. (2006a). Microorganisms pumping iron: anaerobic microbial iron oxidation and reduction. *Nat. Rev. Microbiol.* 4, 752–764. doi: 10.1038/nrmicro1490

Weber, K. A., Hedrick, D. B., Peacock, A. D., Thrash, J. C., White, D. C., Achenbach, L. A., et al. (2009). Physiological and taxonomic description of the novel autotrophic, metal oxidizing bacterium, *Pseudogulbenkiania* sp. strain 2002. *Appl. Microbio. Biotechnol.* 83, 555–565. doi: 10.1007/s00253-009-1934-7

Weber, K. A., Pollock, J., Cole, K. A., O'Connor, S. M., Achenbach, L. A., and Coates, J. D. (2006b). Anaerobic nitrate-dependent iron (II) bio-oxidation by a novel lithoautotrophic betaproteobacterium, strain 2002. *Appl. Environ. Microbiol.* 72, 686–694. doi: 10.1128/AEM.72.1.686-694.2006

Wogelius, R. A., and Walther, J. V. (1991). Olivine dissolution at 25 C: effects of pH, CO_2, and organic acids. *Geochim. Cosmochim. Acta* 55, 943–954. doi: 10.1016/0016-7037(91)90153-V

Zhao, L., Dong, H., Kukkadapu, R., Agrawal, A., Liu, D., Zhang, J., et al. (2013). Biological oxidation of Fe(II) in reduced nontronite coupled with nitrate reduction by *Pseudogulbenkiania* sp. Strain 2002. *Geochimica et Cosmochimica Acta* 119, 231–247. doi: 10.1016/j.gca.2013.05.033

Zhou, J., Wang, H., Yang, K., Ji, B., Chen, D., Zhang, H., et al. (2016). Autotrophic denitrification by nitrate-dependent Fe(II) oxidation in a continuous up-flow biofilter. *Bioprocess Biosyst. Eng.* 39, 277–284. doi: 10.1007/s00449-015-1511-7

Zolotov, M. Y., and Mironenko, M. V. (2007). Timing of acid weathering on Mars: a kinetic-thermodynamic assessment. *J. Geophys. Res. Planets* 112:E07006. doi: 10.1029/2006JE002882

Conflict of Interest: The authors declare that the research was conducted in the absence of any commercial or financial relationships that could be construed as a potential conflict of interest.

Publisher's Note: All claims expressed in this article are solely those of the authors and do not necessarily represent those of their affiliated organizations, or those of the publisher, the editors and the reviewers. Any product that may be evaluated in this article, or claim that may be made by its manufacturer, is not guaranteed or endorsed by the publisher.

frontiers | Frontiers in Astronomy and Space Sciences

ORIGINAL RESEARCH
published: 23 May 2022
doi: 10.3389/fspas.2022.875547

Weathering of Chlorite Illite Deposits in the Hyperarid Qaidam Basin: Implications to Post-Depositional Alteration on Martian Clay Minerals

Yu Sun[1], Yiliang Li[2,3], Chaoqun Zhang[1], Xiaorong Qin[4,5], Jianxun Shen[1], Hongping He[4,5] and Yongxin Pan[1,5]*

[1]Key Laboratory of Earth and Planetary Physics, Institute of Geology and Geophysics, Chinese Academy of Sciences (CAS), Beijing, China, [2]Department of Earth Sciences, University of Hong Kong, Pokfulam, Hong Kong SAR, China, [3]CAS Center for Excellence in Comparative Planetology, Hefei, China, [4]CAS Key Laboratory of Mineralogy and Metallogeny/Guangdong Provincial Key Laboratory of Mineral Physics and Materials, Guangzhou Institute of Geochemistry, Chinese Academy of Sciences, Guangzhou, China, [5]University of Chinese Academy of Sciences, Beijing, China

Chlorite is the second-most common class of clay minerals on the Martian surface and has been found to coexist with illite in some regions. Although previous studies have paid much attention to the formation of this assemblage, the post-depositional evolution cannot be neglected because the aqueous activities may alter the mineral assemblage and distribution. Here, we report on the post-depositional weathering of lacustrine-fluvial deposits collected from yardangs and dune-covering lake beds in the western Qaidam Basin, one of the largest and highest terrestrial Mars analogs. Mineralogical analysis shows that Fe-clinochlore and illite are the main clay components deposited as detrital particles. Electron microscopic observations of small rusty concretions from yardang deposits revealed that iron was released from clinochlore and formed ferrihydrite in fractures. We suggest that the activities of ephemeral waters after the deposition provide the major source of water that influences the migration of Fe in a long-lasting hyperarid climate. A similar iron-releasing mechanism could have occurred in Nili Fossae on Mars because multiple aqueous activities have shaped the terrains where chlorite illite deposits were identified by orbital near-infrared reflectance spectroscopy. Thus, reconstruction of the aqueous history of ancient Mars from surface minerals requires consideration of post-depositional processes, since groundwater/meteoric water may continuously interact with clay mineral-bearing deposits on Mars after their formation.

Keywords: chlorite, illite, Qaidam Basin, Mars, weathering

OPEN ACCESS

Edited by:
Alberto Fairén, Center for Astrobiology (CSIC), Spain

Reviewed by:
Elizabeth Rampe, National Aeronautics and Space Administration (NASA), United States
Thomas Bristow, National Aeronautics and Space Administration (NASA), United States

****Correspondence:***
Yu Sun
sunyu@mail.iggcas.ac.cn

Specialty section:
This article was submitted to Astrobiology, a section of the journal Frontiers in Astronomy and Space Sciences

Received: *14 February 2022*
Accepted: *25 April 2022*
Published: *23 May 2022*

Citation:
Sun Y, Li Y, Zhang C, Qin X, Shen J, He H and Pan Y (2022) Weathering of Chlorite Illite Deposits in the Hyperarid Qaidam Basin: Implications to Post-Depositional Alteration on Martian Clay Minerals. Front. Astron. Space Sci. 9:875547. doi: 10.3389/fspas.2022.875547

INTRODUCTION

The global distribution of clay minerals on the Martian surface demonstrates the liquid water activity on ancient Mars (Poulet et al., 2005; Bibring et al., 2006; Bishop, 2018). Among clay members of the phyllosilicate group identified from the orbital datasets of Mars, the content of chlorite is higher than that of all the other members with the exception of smectite (Ehlmann et al., 2011a; Ehlmann et al., 2011b). Similar to smectite, Martian chlorite is also rich in Fe and Mg (Ehlmann et al., 2011a). Chlorite is a hydrous phyllosilicate-type mineral with an interlayer hydroxide octahedral sheet between two structural layered units, forming a special 2:1:1 layered structure (Kohut and Warren,

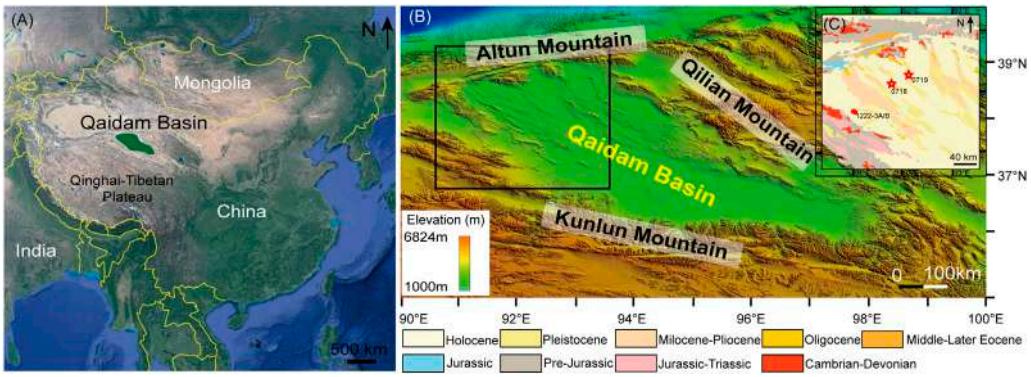

FIGURE 1 | The location of the Qaidam Basin and the geological map of the study area. **(A)** The location (green area) of the Qaidam Basin on the Tibetan Plateau. **(B)** Digital elevation model map of the Qaidam Basin, with the black open square marking our study area. **(C)** The geological map of the study area and the sampling sites (Cheng et al., 2019).

2002). According to different enriched metallic elements that occupy the octahedral sheet, chlorite can be divided into four subtypes—clinochlore (Mg^{2+}-rich), chamosite (Fe^{2+}-rich), nimite (Ni^{2+}-rich), and pennantite (Mn^{2+}-rich) (Kohut and Warren, 2002). However, due to element substitutions, clinochlore can also be rich in Fe^{2+} (Smyth et al., 1997), as Fe^{2+} and Mg^{2+} are the dominant divalent cations in the octahedral sheets (Aja et al., 2015). Chlorite can be formed through the diagenesis of smectite, hydrothermal alteration, and metamorphism, and it could be further weathered to vermiculite in warm and wet terrestrial surface conditions (Ehlmann et al., 2011a).

On Mars, chlorite has been identified mainly by visible/near-infrared (VNIR) spectra obtained by the Compact Reconnaissance Imaging Spectrometer for Mars (CRISM) onboard the Mars Reconnaissance Orbiter (MRO) and Observatoire pour la Minéralogie, l'Eau, les Glaces et l'Activité (OMEGA) onboard the Mars Express orbiter (Poulet et al., 2005; Ehlmann et al., 2011b). In some cases, chlorite coexists with prehnite near craters, indicating the presence of hydrothermal activity driven by impacts (Ehlmann et al., 2009; Ehlmann et al., 2011a). Alteration mineral assemblages are also discovered in central peaks of craters where chlorite is associated with Fe, Mg-smectite, analcime, and hydrated silica (Milliken et al., 2008; Ehlmann et al., 2009).

Another phyllosilicate, illite, is structurally a 2:1 type of phyllosilicate composed of two tetrahedral sheets sandwiched by one octahedral sheet (T-O-T) (Ehlmann et al., 2009). Although illite is indistinguishable from muscovite in CRISM and OMEGA data (Ehlmann et al., 2009), it may coexist with chlorite as the main weathering-derived clay member on Mars. In the region of Nili Fossae, both chlorite and illite are identified based on the CRISM data (Ehlmann et al., 2009). Considering the mineral composition and the aqueous history of this region, (Ehlmann et al., 2009), suggest that the fluvial activity and sapping channel formation could affect the distribution of these minerals. Therefore, the post-depositional effects caused by later water activity are significant for understanding the aqueous history and the mineral transformation during the long evolution of the Martian paleoclimate.

The Qaidam Basin, located on the northern edge of the Tibetan Plateau (**Figure 1A**), has formed a vast area of playas and eolian landscapes due to the blocking of moisture by surrounding mountain ranges of >5,000-m altitude (**Figure 1B**) and the resultant prolonged hyperarid climate (Han et al., 2014). After a similar climate transition from wet to dry, the surface landforms and changing surface environments of the Qaidam Basin are analogous to those proposed for ancient Mars (Kong et al., 2018). The basin has maintained high aridity, with a current evaporation rate of 2,590 mm/yr and a precipitation rate of <20 mm/yr (Kong et al., 2018). The average annual surface temperature of the western Qaidam basin is 3.5°C, with the maximum monthly average air temperature of 16°C in July and the minimum monthly average air temperature of −10.7°C in January (Kong et al., 2018). Thus, numerous previous studies exemplify Qaidam as one of the highest environmental Mars analogs (Xiao et al., 2016; Anglés and Li, 2017; Sun et al., 2019; Sun et al., 2021). Here, we report alteration of chlorite illite-bearing deposits in two areas: weathered yardang (basin center) and dune-covered (basin margin) deposits in the western Qaidam Basin. By evaluating the post-depositional effects on these deposits in a dry and cold Mars analogous environment, this study seeks to provide constraints on the evolution of widespread iron-bearing phyllosilicate on Mars.

SAMPLES AND METHODS

Four samples of this study were collected in lacustrine-fluvial deposits from western Qaidam Basin: the yardang samples (named 0718 and 0719) at N38°2′6.4″, E91°51′8.39″, and N38°12′40.716″, E92°4′15.276″, respectively; the dune-covered samples (named 1222-3A and 3B) at N37°50′58.6″, E91°4′6.5″ (**Figure 1C**). These samples were collected in the vast area of the Holocene playa (**Figure 1C**), representing the last massive liquid water event (Han et al., 2014) that has been shaping the depocenter of the western Qaidam Basin ever since. After the disappearance of the northwestern center of the mega-lake, the

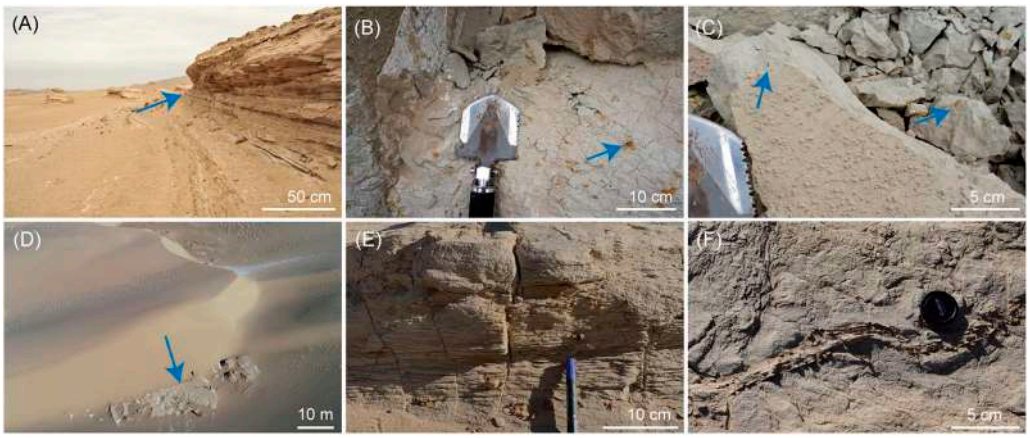

FIGURE 2 | Sampling sites and samples from the western Qaidam Basin. **(A)** Deposits are exposed on the side of a yardang (blue arrow). **(B,C)** Yardang samples (0718 and 0719) with rusty concretions (blue arrows). **(D)** Deposits (yellow arrow) are covered by sand dunes from the view of a drone. **(E,F)** Dune-covering samples (1222-3A and 3B).

surface is featured by strong wind-sculpted yardang fields (Xiao et al., 2016). Thin layers of carbonate ooids were found actively formed 38,000 years ago near the yardang sampling area (Sun et al., 2019), indicating that these deposits should be exposed later than this period. Otherwise, evaporites would have cemented the deposits. In the western Qaidam Basin, yardang fields display various morphologies and sizes due to winds with different strengths and directions. The yardang fields now cover an area of 3.88×10^4 km^2 in the Qaidam Basin (Xiao et al., 2016). The two yardang samples were collected on the lower side of the weathered yardangs (**Figures 1C**, **2A**). Samples displayed grey surfaces with rusty small concretions (**Figures 2B,C**). Sand dunes in the desert, however, have only developed in particular zones in the basin. The dune-covered samples were collected on a fluvial fan of Kunlun Mountain, which is partially covered by a series of barchan dunes (**Figures 1C**, **2D**). These deposits were layered and loose (**Figure 2E**). Iron-bearing veins exist in these deposits (**Figure 2F**). Two samples were collected with clean tools from the same site but in different layers and sealed with parafilm tapes to prevent exposure to air moisture during transport to the laboratory.

In addition to the four sediment samples, we collected two purified clay minerals (see **Supplementary Figure S1** for more component information), clinochlore (from Liaoning, China) and illite (from Zhejiang, China), as positive controls in spectral measurements.

The mineral compositions of these samples were determined using a Rigaku MiniFlex-400 X-ray diffractometer (XRD) at the Guangzhou Institute of Geochemistry, Chinese Academy of Sciences (CAS). The diffractometer is equipped with a Hybrid pixel array detector, a Cu source, and a Ni filter. Prior to bulk XRD measurements, samples were ground into fine powder (70 μm) using agate mortar. The samples were loaded into rectangular Al holders and tableted for measurements. Data were collected between 3° and 70° with a step size of 0.01 and a dwell time of 1°s in each step. To identify the composition of the rusty parts from these deposits, the rusty concretions were separated with clean tweezers based on different colors and ground for further XRD measurements.

Spectroscopic analysis was conducted on a Malvern Panalytical TerraSpec 4 Hi-Res spectrometer at the Institute of Geology and Geophysics (IGG), CAS. Before the spectroscopic analysis, samples were oven-dried at 80°C overnight and separated into bulk clay and rusty parts with tweezers, followed by mild grinding into fine powder. Microstructure and morphology of small particles were recorded using an FEI Apreo S scanning electron microscope (SEM) equipped with a Bruker XFlash 60 energy dispersive spectrometer (EDS) detector and a JEOL JEM-2100 transmission electron microscope (TEM) at IGGCAS. To obtain the natural morphology of the minerals, we use small tweezers to pick out the rusty parts and fix them on the conductive adhesive for direct SEM observation. The samples for TEM observation were ground with an agate mortar for 5 min, dispersed in alcohol, and dropped on the copper grid for analysis.

The rusty concretions were separated from the samples and were ground into fine powder for ^{57}Fe Mössbauer spectroscopy measurements at room temperature in the transmission mode operating in constant acceleration mode using a Silver Double Limited WSS-10 spectrometer. The Mössbauer source was a ^{57}Co in the Rh matrix. The velocity drive transducer was operated in a triangular waveform mode over energy ranges of ±15 mm/s. The spectroscopic center was calibrated using an α-Fe foil. The spectrum was analyzed with the Mosswinn 4.0 program. Subspectra attributed to different phases were determined based on their hyperfine parameters [i.e., isomer (IS), quadrupole splitting (QS), and linewidths].

RESULTS

As shown by the XRD patterns, the mineral components of these deposits were quartz ($d_{(101)}$ = 3.34 Å), albite ($d_{(002)}$ = 3.18 Å), minor carbonate ($d_{(104)}$ = 3.03 Å), and clay minerals identified as Fe-clinochlore and illite in accordance with their main d values

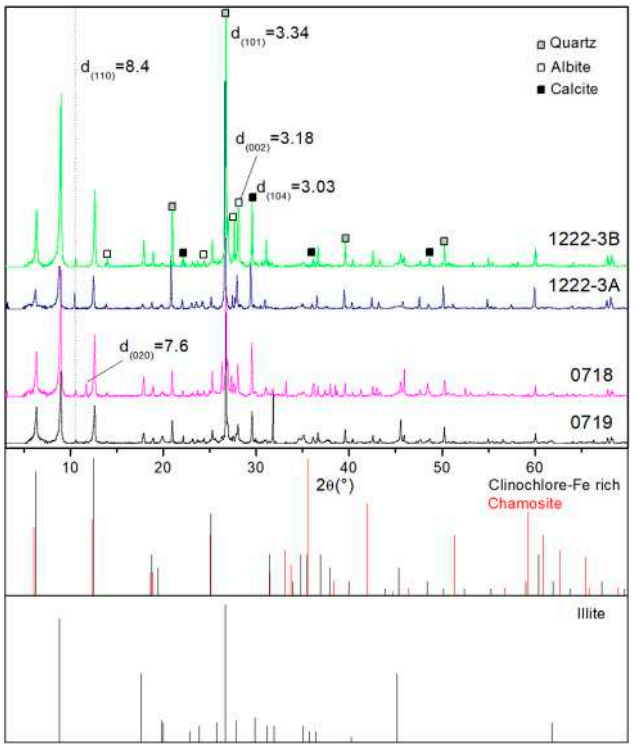

FIGURE 3 | X-ray diffractograms of the four sediment samples.

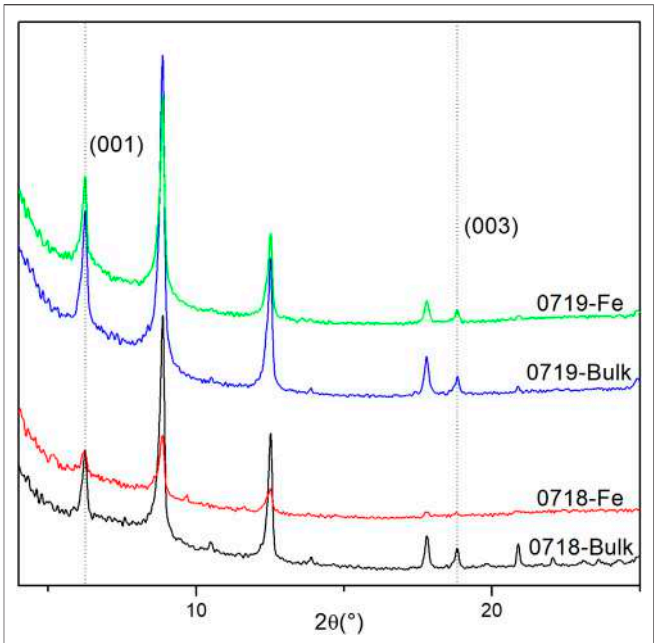

FIGURE 4 | X-ray diffraction patterns between 5° and 18° of the bulk deposits and rusty parts from samples 0718 and 0719. The $d_{(001)}$ values are the same as the bulk measurements.

($d_{(001)}$ = 13.90 Å and $d_{(002)}$ = 9.90 Å) and the overall pattern features (**Figure 3**). The yardang samples contained minor gypsum ($d_{(020)}$ = 7.6 Å), reflecting the evaporation of liquid water in the basin center. The dune-covered deposits displayed characteristic XRD peaks of amphibole ($d_{(110)}$ = 8.4 Å) (**Figure 3**), implying that the debris from nearby mountains was only partially weathered.

The XRD patterns of the rusty parts (named 0718-Fe and 0719-Fe) display the same features as the bulk samples (**Figure 4**), indicating no new well-crystallized phase was formed. The intensity ratio of $d_{(001)}/d_{(003)}$ in XRD patterns was used to determine the Fe content in clinochlore (Ryan and Reynolds, 1997). The ratios are 8.84, 4.6 for 0719-Bulk and 0719-Fe; 4.4, 4.2 for 0718-Bulk and 0718-Fe. The decrease of the $d_{(001)}/d_{(003)}$ ratio indicated that Fe migrated from clinochlore to the rusty parts.

SEM micrographs of the bulk samples showed poor morphology of these clay minerals with grain sizes <2 μm (**Figures 5A–C**), indicating a debris origin (Wilson, 1999). Halite was observed in the yardang-type samples (**Figure 5B**). In the rusty parts, nanoparticles are distributed on the surface of the clay grains (**Figure 5D**). Backscattered electron imaging associated with the elemental mapping of the same area illustrated that these materials were Fe-enriched (**Figures 5E,F**) but Mg, Al, Si-depleted compared to the surrounding clay grains (**Figures 5G–I**). EDS results confirmed that clinochlore in these samples was enriched with Fe, and the content of Fe in the clay mineral was decreased near the Fe enriched area (see **Supplementary Table S1**).

Under TEM (**Figure 6A**), nanoparticles were intimately mixed with clinochlore. The magnified image of these minerals again displayed nanophase aggregates with a diameter of <5 nm (**Figure 6B**). The high-resolution TEM image revealed that the d-spacing of the nanoparticle was 2.5 Å (**Figure 6B**), which corresponded to the 110 panels of ferrihydrite or nano-hematite (Jiang et al., 2018).

Mössbauer spectroscopy of the rusty parts provided further identification of the Fe-bearing materials. The spectrum was fitted with two subspectra (**Figure 7**). The doublet with IS, QS values of 1.12 mm/s, and 2.73 mm/s (green) corresponded to the Fe^{2+} in the octahedron of chlorite (Pollak and Stevens, 1986). Another doublet with IS, QS values of 0.37 mm/s, 0.61 mm/s (pink) indicated that the octahedral sites of Fe^{3+} were relatively disordered, which should be attributed to ferrihydrite as additionally supported by the TEM observations (Murad, 1996).

The NIR spectra of these Qaidam samples displayed combinative features of both clinochlore and illite (**Figure 8**). The -OH overtone at 1.414 μm was much weaker than the pure clinochlore and illite. The H-O-H combination band at 1.931 μm should be attributed to the coupling of the signals from both clinochlore and illite, which moved to a higher wavelength indicative of the increasing content of illite (**Figure 8**). The 2.211 μm absorption was due to the Al-OH in illite (Ehlmann et al., 2009), while the ~2.347 μm absorption was a combination of M-OH (M could be Fe, Mg, or the mix of these cations) in clinochlore and illite (Bishop et al., 2008). The CRISM data reported by (Ehlmann et al., 2009) demonstrated a similar NIR pattern with 1.4, 1.9, 2.2, and ~2.3 μm absorptions as compared to the Qaidam samples in this study, indicating the deposition of the chlorite illite assemblage in the Nili Fossae region on Mars.

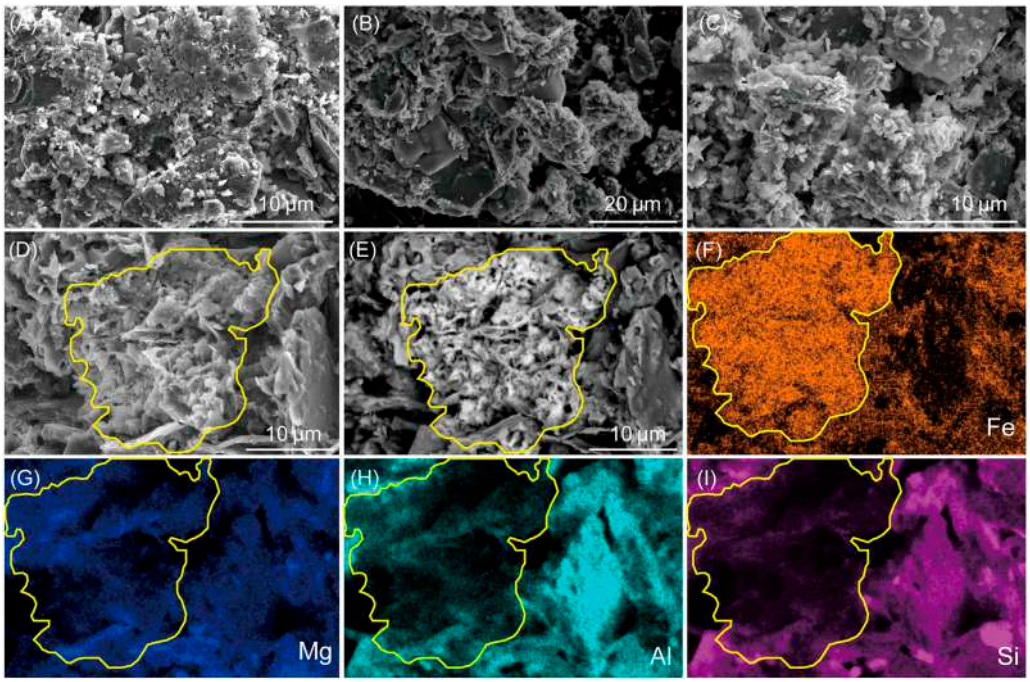

FIGURE 5 | SEM micrographs of the clay minerals. **(A)** Clay morphology from sample 0718. **(B)** Clay morphology from sample 0719. **(C)** Clay morphology from sample 1222-3A. **(D)** Amorphous materials on the surface of clay grains. **(E)** Backscattered electron image of the amorphous materials. **(F)** Distribution of Fe in the same area as **(E)**. **(G)** Distribution of Mg in the same area as **(E)**. **(H)** Distribution of Al in the same area as **(E)**. **(I)** Distribution of Si in the same area as **(E)**.

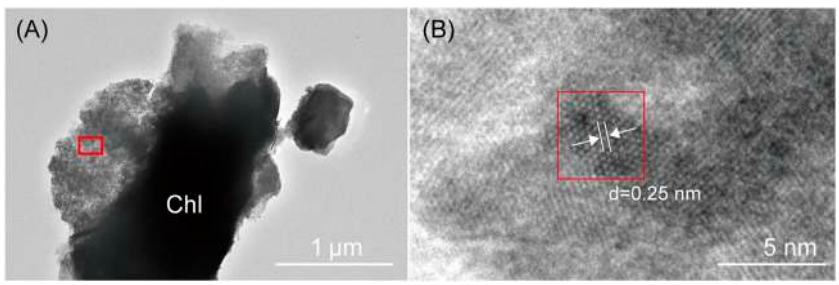

FIGURE 6 | TEM micrographs of the rusty parts from 0718. **(A)** Fe-bearing materials associated with chlorite. **(B)** High-resolution TEM image of the Fe-bearing materials and the Fourier transform of a single crystal framed in the red rectangle.

DISCUSSION

The Alteration of Clinochlore

As indicated by the XRD and EDS results, chlorite in the deposits was characterized as Fe-rich clinochlore because the chamosite has a different XRD pattern (Kohut and Warren, 2002). These minerals are detrital and sourced from the physical weathering of metamorphic and granitic parent rocks from the surrounding mountains (Miao et al., 2016). However, in the presence of post-depositional aqueous activity, the stability of clinochlore is affected. The deposits are loose and porous which provides intergranular space for the percolation of water. Previous experiments demonstrate that even in neutral to alkaline fluids, chlorite can be partially altered to release iron to the aqueous repository (Malmström et al., 1996).

Along with the release of iron, the crystallinity of clinochlore decreases. Afterward, iron precipitates near the spots of weathering where the liquid water availability declines. The decreased intensity in XRD patterns and the reduction of Fe content determined by EDS provide both the structural and compositional evidence to support the above-proposed scenarios. Combined with the amorphous crystallinity and the Mössbauer hyperfine parameters, the post-weathering iron-bearing mineral was determined to be ferrihydrite. The SEM observations furnish the transformation of clay minerals with extra constraints as the content of Mg, Al, and Si decreases during the formation of amorphous ferrihydrite.

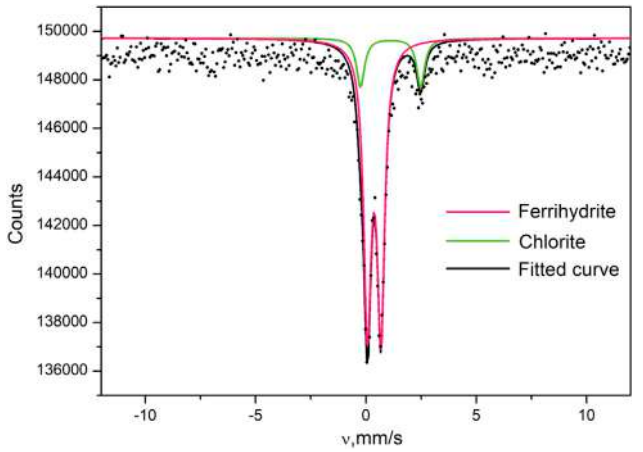

FIGURE 7 | ^{57}Fe Mössbauer spectrum of the rusty parts from 0719 recorded at room temperature.

The clinochlore upon further weathering would be transformed to vermiculite and kaolinite associated with the evolution of Fe minerals from goethite to hematite in warm and wet conditions (Aspandiar and Eggleton, 2002a, b). However, as shown in **Figure 9**, the weathering reaction in the western Qaidam Basin is at the early stage which is hindered by the lack of liquid water in the prolonged hyperarid climate (Han et al., 2014). Rainwater or snowmelt can intermittently occur but be rapidly evaporated soon after the commencement of the weathering process. The low water availability may also be the reason that the weathering can only form amorphous iron hydroxides in the western Qaidam Basin.

Comparatively, illite is more stable than chlorite when exposed to post-depositional environments (Wilson, 1999). Considering the hyperarid climate in western Qaidam Basin, the alternation of illite is even negligible. Therefore, chlorite rather than illite is notably affected by post-depositional aqueous activity in the Qaidam deposits.

Chlorite Illite Deposits on Mars

Martian chlorite illite deposits have previously been identified in Nili Fossae by NIR spectroscopy (**Figure 8**). In the region of Nili Fossae, alluvial activity shaped the stratigraphy of the area and left traces of large-scale flood events (Ehlmann et al., 2009; Mangold et al., 2007). The aqueous activity plays an important role in the mineralogy of these chlorite illite deposits because chlorite could be easily weathered to T-O-T clay minerals and iron hydroxide/oxides in the presence of liquid water (Aspandiar and Eggleton, 2002a, b). This process is essential to Martian deposits as liquid water might only be present occasionally for a long period through the geological time of Mars (Fairén, 2010; Bishop et al., 2018).

Cold and dry environments (e.g., permafrost areas, polar dry valleys, and the Qaidam Basin) where chlorite illite deposits distributed extensively are universally dominated by physical weathering (Bishop et al., 2008). Similar weathering processes

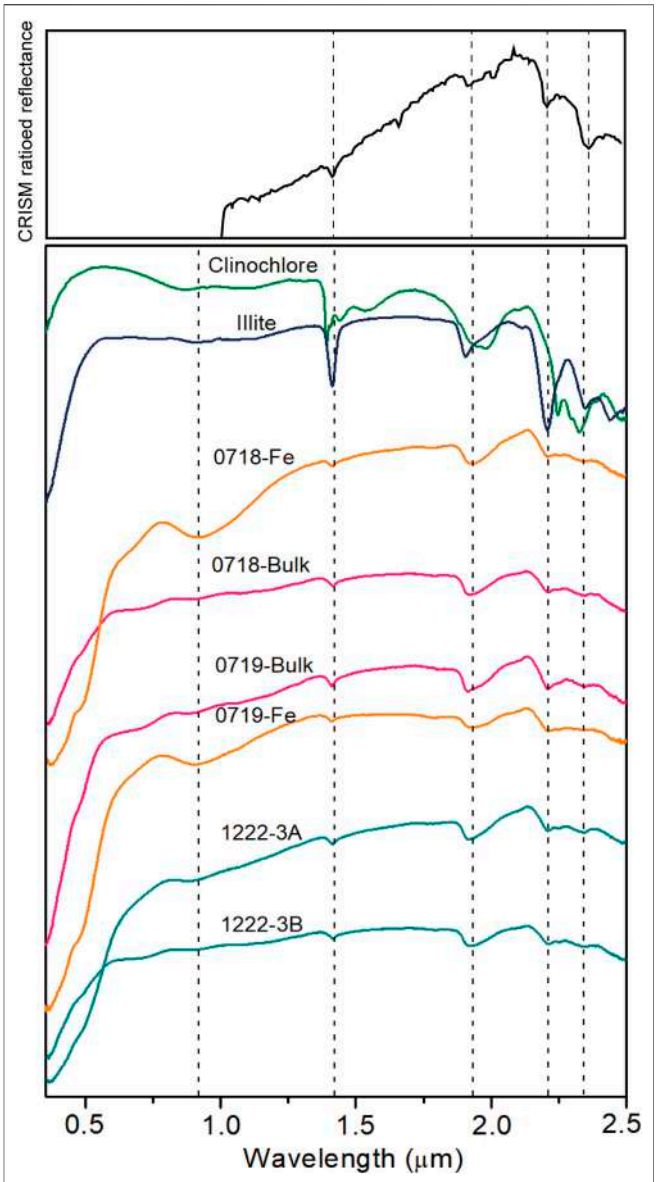

FIGURE 8 | NIR spectra of the Qaidam lacustrine-fluvial deposits and the CRISM spectrum (Ehlmann et al., 2009) from the Nili Fossae region (top).

have likely existed on early Mars. By analyzing the rates of clay formation (Bishop et al., 2018), suggested that clay minerals on Mars could have formed in a relatively short geological time (tens of thousands of years), which is consistent with a more durable dry and cold climate model of early Mars (Mangold, 2021; Wordsworth et al., 2021).

On the Martian surface, chlorite is more common than illite due to the lack of K^+ in most sedimentary remains (Ehlmann et al., 2009). (Ehlmann et al., 2011a) suggested that the Martian chlorite illite deposits were formed through diagenesis or subsurface low-grade metamorphism and were then transported by alluvial activities, which is comparable to the scenario in the western Qaidam Basin. Our results indicate

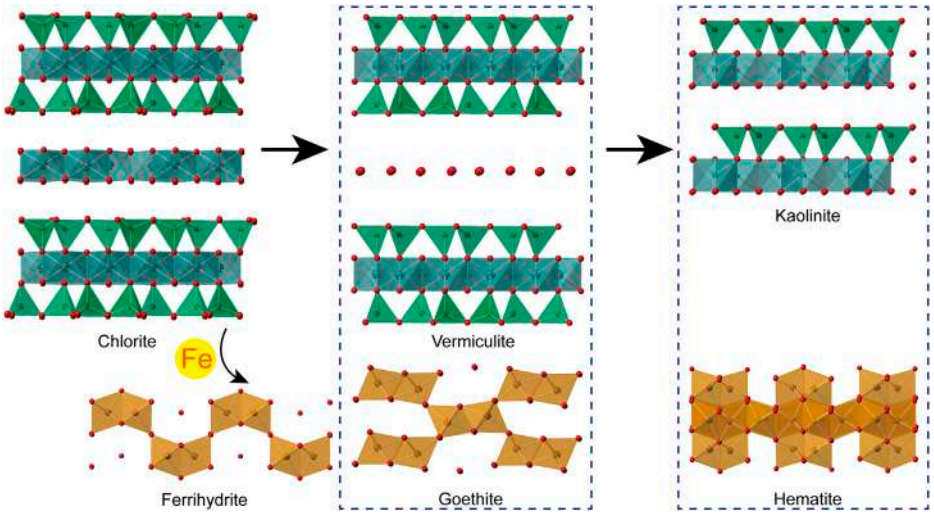

FIGURE 9 | The weathering process of chlorite (modified after Aspandiar and Eggleton, 2002a).

that subtle changes can still be happening with regional transient liquid activity. The most concentrated carbonate deposits on Mars are identified in the channel of Nili Fossae, which excludes the plausibility of extensive alteration from acidic fluids in this region (Ehlmann et al., 2009). Such situations and environments have dominated much of Martian history, which might leave possible aqueous information over minerals after the great change in global climate (McLennan et al., 2019).

The weathering process in Qaidam Basin is primarily driven by diagenesis, a process that might also play an important role in elemental migration on Mars. The abundance and mobility of Fe in the surface environment greatly affected the surface mineralogy of Mars (Tosca et al., 2008). The formation of widespread clay minerals is suggested to occur in the first billion years of Mars when the surface was aqueous and alkaline (Bibring et al., 2006; Ehlmann and Edwards, 2014). However, Fe can be released from clay materials easily to form nanophase hydroxides/oxides in the presence of limited liquid water. The post-depositional weathering process is likely still ongoing on the Martian surface, which could display a similar alteration tendency to the scenario in the Qaidam Basin. Although ferrihydrite is metastable in most terrestrial environments (Dehouck et al., 2017), evaluated the possibility of its presence on Mars by examining its transformation in varied conditions. The Mössbauer spectrographs acquired by the Spirit and Opportunity rovers and the XRD results from the CheMin onboard the Curiosity rover suggest the widespread occurrence of ferrihydrite (Rampe et al., 2016) or nanocrystalline hematite (Rampe et al., 2020) on Mars. Burial and heating of sediments would favor the transformation of these amorphous components into goethite and well-crystallized hematite; however, these scenarios might not occur after the weathering of Fe-clay minerals in Martian sediments. Despite the neutral to alkaline conditions in Nili Fossae, acidity has evolved in most regions on Mars since the beginning of Hesperian (Zolotov and Mironenko, 2007), which can enhance the Fe-clay weathering and provide more sources for the widespread iron-bearing materials on Mars.

CONCLUSION

Through the mineralogical study of chlorite illite deposits in the western Qaidam Basin, we observed the post-depositional effects on the change of chlorite composition and structure under hyperarid climatic conditions. Due to the ephemeral water activity, iron is released from Fe-clinochlore and forms amorphous ferric oxyhydroxides in the sediments. Similar NIR spectra are characterized in the Nili Fossae region on Mars, indicating the presence of chlorite illite deposits. Diagenesis in the Qaidam Basin and the resulting chemical weathering of chlorite may inform the evolution of chlorite and precipitation of secondary iron phases on the Martian surface.

DATA AVAILABILITY STATEMENT

The datasets [ANALYZED] for this study can be found in the [Mendeley] https://data.mendeley.com/datasets/xrrkt26zgt/1.

AUTHOR CONTRIBUTIONS

YS and YL planned this research. YS collected the samples and performed most experiments. CZ and XQ contributed to the analysis of XRD and NIR measurements. JS helped with the language. HH

and YP coordinated laboratory analyses and made constructive suggestions.

FUNDING

This research was supported by NSFC (41621004 to YP), the CAS Strategic Priority Research Program (XDA17010501 to LT), and the National Natural Science Foundation of China (41921003). YL is funded by grants from the Research Grants Council of Hong Kong (RIF Project No: R5043-19).

ACKNOWLEDGMENTS

We thank Dr. Xu Tang for his help with the TEM experiments.

SUPPLEMENTARY MATERIAL

The Supplementary Material for this article can be found online at: https://www.frontiersin.org/articles/10.3389/fspas.2022.875547/full#supplementary-material

REFERENCES

Aja, S., Omotoso, O., Bertoldi, C., Dachs, E., and Benisek, A. (2015). The Structure and Thermochemistry of Three Fe-Mg Chlorites. *Clays Clay Min.* 63 (5), 351–367. doi:10.1346/ccmn.2015.0630502

Anglés, A., and Li, Y. (2017). The Western Qaidam Basin as a Potential Martian Environmental Analogue: An Overview. *J. Geophys. Res. Planets* 122 (5), 856–888. doi:10.1002/2017je005293

Aspandiar, M. F., and Eggleton, R. A. (2002b). Weathering of Chlorite: II. Reactions and Products in Microsystems Controlled by Solution Avenues. *Clays Clay Min.* 50 (6), 699–709. doi:10.1346/000986002762090100

Aspandiar, M. F., and Eggleton, R. A. (2002a). Weathering of Chlorite: I. Reactions and Products in Microsystems Controlled by the Primary Mineral. *Clays Clay Min.* 50 (6), 685–698. doi:10.1346/000986002762090227

Bibring, J.-P., Langevin, Y., Mustard, J. F., Poulet, F., Arvidson, R., Gendrin, A., et al. (2006). Global Mineralogical and Aqueous Mars History Derived from OMEGA/Mars Express Data. *Science* 312, 5772400–5772404. doi:10.1126/science.1122659

Bishop, J. L., Dobrea, E. Z. N., McKeown, N. K., Parente, M., Ehlmann, B. L., Michalski, J. R., et al. (2008). Phyllosilicate Diversity and Past Aqueous Activity Revealed at Mawrth Vallis, Mars. *Science* 321 (5890), 830–833. doi:10.1126/science.1159699

Bishop, J. L., Fairén, A. G., Michalski, J. R., Gago-Duport, L., Baker, L. L., Velbel, M. A., et al. (2018). Surface Clay Formation during Short-Term Warmer and Wetter Conditions on a Largely Cold Ancient Mars. *Nat. Astron.* 2 (3), 206–213. doi:10.1038/s41550-017-0377-9

Bishop, J. L. (2018). "Remote Detection of Phyllosilicates on Mars and Implications for Climate and Habitability," in *From Habitability to Life on Mars* (Elsevier), 37–75. doi:10.1016/b978-0-12-809935-3.00003-7

Cheng, F., Garzione, C. N., Jolivet, M., Guo, Z., Zhang, D., Zhang, C., et al. (2019). Initial Deformation of the Northern Tibetan Plateau: Insights from Deposition of the Lulehe Formation in the Qaidam Basin. *Tectonics* 38 (2), 741–766. doi:10.1029/2018tc005214

Dehouck, E., McLennan, S. M., Sklute, E. C., and Dyar, M. D. (2017). Stability and Fate of Ferrihydrite during Episodes of Water/rock Interactions on Early Mars: An Experimental Approach. *J. Geophys. Res. Planets* 122 (2), 358–382. doi:10.1002/2016je005222

Ehlmann, B. L., and Edwards, C. S. (2014). Mineralogy of the Martian Surface. *Annu. Rev. Earth Planet. Sci.* 42, 291–315. doi:10.1146/annurev-earth-060313-055024

Ehlmann, B. L., Mustard, J. F., Clark, R. N., Swayze, G. A., and Murchie, S. L. (2011a). Evidence for Low-Grade Metamorphism, Hydrothermal Alteration, and Diagenesis on Mars from Phyllosilicate Mineral Assemblages. *Clays Clay Min.* 59 (4), 359–377. doi:10.1346/ccmn.2011.0590402

Ehlmann, B. L., Mustard, J. F., Murchie, S. L., Bibring, J.-P., Meunier, A., Fraeman, A. A., et al. (2011b). Subsurface Water and Clay Mineral Formation during the Early History of Mars. *Nature* 479, 737153–737160. doi:10.1038/nature10582

Ehlmann, B. L., Mustard, J. F., Swayze, G. A., Clark, R. N., Bishop, J. L., Poulet, F., et al. (2009). Identification of Hydrated Silicate Minerals on Mars Using MRO-CRISM: Geologic Context Near Nili Fossae and Implications for Aqueous Alteration. *J. Geophys. Res.* 114, E2. doi:10.1029/2009je003339

Fairén, A. G. (2010). A Cold and Wet Mars. *Icarus* 208 (1), 165–175. doi:10.1016/j.icarus.2010.01.006

Han, W., Fang, X., Ye, C., Teng, X., and Zhang, T. (2014). Tibet Forcing Quaternary Stepwise Enhancement of Westerly Jet and Central Asian Aridification: Carbonate Isotope Records from Deep Drilling in the Qaidam Salt Playa, NE Tibet. *Glob. Planet. Change* 116 (3), 68–75. doi:10.1016/j.gloplacha.2014.02.006

Jiang, Z., Liu, Q., Roberts, A. P., Barrón, V., Torrent, J., and Zhang, Q. (2018). A New Model for Transformation of Ferrihydrite to Hematite in Soils and Sediments. *Geology* 46 (11), 987–990. doi:10.1130/g45386.1

Kohut, C. K., and Warren, C. J. (2002). "Chlorites," in *Chlorites: Soil Mineralogy with Environmental Applications* (Madison, WI: Soil Science Society of America, Inc.), 7, 531–553. doi:10.2136/sssabookser7.c17

Kong, F., Zheng, M., Hu, B., Wang, A., Ma, N., and Sobron, P. (2018). Dalangtan Saline Playa in a Hyperarid Region on Tibet Plateau: I. Evolution and Environments. *Astrobiology* 18 (10), 1243–1253. doi:10.1089/ast.2018.1830

Malmström, M., Banwart, S., Lewenhagen, J., Duro, L., and Bruno, J. (1996). The Dissolution of Biotite and Chlorite at 25 °C in the Near-Neutral pH Region. *J. Contam. Hydrol.* 21 (1-4), 201–213. doi:10.1016/0169-7722(95)00047-X

Mangold, N. (2021). Intermittent Warmth on Young Mars. *Nat. Geosci.* 14 (3), 112–113. doi:10.1038/s41561-021-00700-9

Mangold, N., Poulet, F., Mustard, J. F., Bibring, J.-P., Gondet, B., Langevin, Y., et al. (2007). Mineralogy of the Nili Fossae Region with OMEGA/Mars Express Data: 2. Aqueous Alteration of the Crust. *J. Geophys. Res.* 112, E8. doi:10.1029/2006JE002835

McLennan, S. M., Grotzinger, J. P., Hurowitz, J. A., and Tosca, N. J. (2019). The Sedimentary Cycle on Early Mars. *Annu. Rev. Earth Planet. Sci.* 47, 91–118. doi:10.1146/annurev-earth-053018-060332

Miao, W., Fan, Q., Wei, H., Zhang, X., and Ma, H. (2016). Clay Mineralogical and Geochemical Constraints on Late Pleistocene Weathering Processes of the Qaidam Basin, Northern Tibetan Plateau. *J. Asian Earth Sci.* 127, 267–280. doi:10.1016/j.jseaes.2016.06.013

Milliken, R. E., Swayze, G. A., Arvidson, R. E., Bishop, J. L., Clark, R. N., Ehlmann, B. L., et al. (2008). Opaline Silica in Young Deposits on Mars. *Geol* 36 (11), 847–850. doi:10.1130/G24967A.1

Murad, E. (1996). Magnetic Properties of Microcrystalline Iron (III) Oxides and Related Materials as Reflected in Their Mössbauer Spectra. *Phys. Chem. Miner.* 23 (4), 248–262. doi:10.1007/bf00207766

Pollak, H., and Stevens, J. G. (1986). Phyllosilicates: A Mössbauer Evaluation. *Hyperfine Interact.* 29 (1), 1153–1156. doi:10.1007/bf02399439

Poulet, F., Bibring, J.-P., Bibring, J.-P., Mustard, J. F., Gendrin, A., Mangold, N., et al. (2005). Phyllosilicates on Mars and Implications for Early Martian Climate. *Nature* 438, 7068623–7068627. doi:10.1038/nature04274

Rampe, E. B., Bristow, T. F., Morris, R. V., Morrison, S. M., Achilles, C. N., Ming, D. W., Vaniman, D. T., Blake, D. F., Tu, V. M., Chipera, S. J., Yen, A. S., Peretyazhko, T. S., Downs, R. T., Hazen, R. M., Treiman, A. H., Grotzinger, J. P., Castle, N., Craig, P. I., Des Marais, D. J., Thorpe, M. T., Walroth, R. C., Downs, G. W., Fraeman, A. A., Siebach, K. L., Gellert, R., Lafuente, B., McAdam, A. C., Meslin, P. Y., Sutter, B., and Salvatore, M. R. (2020). Mineralogy of Vera Rubin Ridge from the Mars Science Laboratory CheMin Instrument. *J. Geophys. Res. Planets* 125 (9), e2019JE006306. doi:10.1029/2019je006306

Rampe, E. B., Morris, R. V., Archer, P. D., Jr, Agresti, D. G., and Ming, D. W. (2016). Recognizing Sulfate and Phosphate Complexes Chemisorbed onto Nanophase

Weathering Products on Mars Using *In-Situ* and Remote Observationsk. *Am. Mineralogist* 101 (3), 678–689. doi:10.2138/am-2016-5408CCBYNCND

Ryan, P. C., and Reynolds, R. C. (1997). The Chemical Composition of Serpentine/chlorite in the Tuscaloosa Formation, United States Gulf Coast: EDX vs. XRD Determinations, Implications for Mineralogic Reactions and the Origin of Anatase. *Clays Clay Minerals* 45 (3), 339–352. doi:10.1346/ccmn.1997.0450305

Smyth, J. R., Dyar, M. D., May, H. M., Bricker, O. P., and Acker, J. G. (1997). Crystal Structure Refinement and Mössbauer Spectroscopy of an Ordered, Triclinic Clinochlore. *Clays Clay Minerals* 45 (4), 544–550. doi:10.1346/ccmn.1997.0450406

Sun, Y., Li, Y., Li, K., Li, L., and He, H. (2021). Massive Deposition of Carbonate Nodules in the Hyperarid Northwest Qaidam Basin of the Northern Tibetan Plateau. *Geochem Geophys Geosyst* 22, e2021GC009654. doi:10.1029/2021GC009654

Sun, Y., Li, Y., Li, L., and He, H. (2019). Preservation of Cyanobacterial UVR-Shielding Pigment Scytonemin in Carbonate Ooids Formed in Pleistocene Salt Lakes in the Qaidam Basin, Tibetan Plateau. *Geophys. Res. Lett.* 46 (17-18), 10375–10383. doi:10.1029/2019gl083321

Tosca, N. J., Knoll, A. H., and McLennan, S. M. (2008). Water Activity and the Challenge for Life on Early Mars. *Science* 320 (5880), 1204–1207. doi:10.1126/science.1155432

Wilson, M. J. (1999). The Origin and Formation of Clay Minerals in Soils: Past, Present and Future Perspectives. *Clay Min.* 34 (1), 7–25. doi:10.1180/000985599545957

Wordsworth, R., Knoll, A. H., Hurowitz, J., Baum, M., Ehlmann, B. L., Head, J. W., et al. (2021). A Coupled Model of Episodic Warming, Oxidation and Geochemical Transitions on Early Mars. *Nat. Geosci.* 14 (3), 127–132. doi:10.1038/s41561-021-00701-8

Xiao, L., Wang, J., Dang, Y., Cheng, Z., Huang, T., Zhao, J., et al. (2017). A New Terrestrial Analogue Site for Mars Research: the Qaidam Basin, Tibetan Plateau (NW China). *Earth-Science Rev.* 164, 84–101. doi:10.1016/j.earscirev.2016.11.003

Zolotov, M. Y., and Mironenko, M. V. (2007). Timing of Acid Weathering on Mars: A Kinetic-Thermodynamic Assessment. *J. Geophys. Res.* 112, E7. doi:10.1029/2006JE002882

Conflict of Interest: The authors declare that the research was conducted in the absence of any commercial or financial relationships that could be construed as a potential conflict of interest.

Publisher's Note: All claims expressed in this article are solely those of the authors and do not necessarily represent those of their affiliated organizations, or those of the publisher, the editors and the reviewers. Any product that may be evaluated in this article, or claim that may be made by its manufacturer, is not guaranteed or endorsed by the publisher.

frontiers | Frontiers in Microbiology

ORIGINAL RESEARCH
published: 27 June 2022
doi: 10.3389/fmicb.2022.811904

Lipid Profiles From Fresh Biofilms Along a Temperature Gradient on a Hydrothermal Stream at El Tatio (Chilean Andes), as a Proxy for the Interpretation of Past and Present Biomarkers Beyond Earth

*Valentine Megevand[1,2], Daniel Carrizo[1], María Ángeles Lezcano[1], Mercedes Moreno-Paz[1], Nathalie A. Cabrol[3], Víctor Parro[1] and Laura Sánchez-García[1]**

[1] Centro de Astrobiología (CAB), INTA-CSIC, Madrid, Spain, [2] Department of Earth Sciences, Ecole Normale Supérieure de Lyon, Université Claude Bernard Lyon, Lyon, France, [3] Carl Sagan Center for Research, The SETI Institute, Mountain View, CA, United States

OPEN ACCESS

Edited by:
David Flannery,
Queensland University of Technology, Australia

Reviewed by:
Carolina Munoz-Saez,
University of Nevada, Reno, United States
Nagendra Thakur,
Sikkim University, India

***Correspondence:**
Laura Sánchez-García
lsanchez@cab.inta-csic.es

Specialty section:
This article was submitted to Extreme Microbiology, a section of the journal Frontiers in Microbiology

Received: 09 November 2021
Accepted: 18 May 2022
Published: 27 June 2022

Citation:
Megevand V, Carrizo D, Lezcano MÁ, Moreno-Paz M, Cabrol NA, Parro V and Sánchez-García L (2022) Lipid Profiles From Fresh Biofilms Along a Temperature Gradient on a Hydrothermal Stream at El Tatio (Chilean Andes), as a Proxy for the Interpretation of Past and Present Biomarkers Beyond Earth. Front. Microbiol. 13:811904. doi: 10.3389/fmicb.2022.811904

Hydrothermal systems and their deposits are primary targets in the search for fossil evidence of life beyond Earth. However, to learn how to decode fossil biomarker records in ancient hydrothermal deposits, we must first be able to interpret unambiguously modern biosignatures, their distribution patterns, and their association with physicochemical factors. Here, we investigated the molecular and isotopic profile of microbial biomarkers along a thermal gradient (from 29 to 72°C) in a hot spring (labeled Cacao) from El Tatio, a geyser field in the Chilean Andes with abundant opaline silica deposits resembling the nodular and digitate structures discovered on Mars. As a molecular forensic approach, we focused on the analysis of lipid compounds bearing recognized resistance to degradation and the potential to reconstruct the paleobiology of an environment on a broader temporal scale than other, more labile, biomolecules. By exploiting the lipid biomarkers' potential to diagnose biological sources and carbon fixation pathways, we reconstructed the microbial community structure and its ecology along the Cacao hydrothermal transect. The taxonomic adscription of the lipid biomarkers was qualitatively corroborated with DNA sequencing analysis. The forensic capacity of the lipid biomarkers to identify biosources in fresh biofilms was validated down to the genus level for *Roseiflexus*, *Chloroflexus*, and *Fischerella*. We identified lipid biomarkers and DNA of several new cyanobacterial species in El Tatio and reported the first detection of *Fischerella* biomarkers at a temperature as high as 72°C. This, together with ecological peculiarities and the proportion of clades being characterized as unclassified, illustrates the ecological singularity of El Tatio and strengthens its astrobiological relevance. The Cacao hydrothermal ecosystem was defined by a succession of microbial communities and metabolic traits associated with

a high- (72°C) to low-(29°C) temperature gradient that resembled the inferred metabolic sequence events from the 16S rRNA gene universal phylogenetic tree from thermophilic to anoxygenic photosynthetic species and oxygenic phototrophs. The locally calibrated DNA-validated lipidic profile in the Cacao biofilms provided a modern (molecular and isotopic) end member to facilitate the recognition of past biosources and metabolisms from altered biomarkers records in ancient silica deposits at El Tatio analogous to Martian opaline silica structures.

Keywords: lipid biomarkers, El Tatio geyser field, hot springs, early life analog, silica deposits on Mars, DNA sequencing analysis, paleobiology, astrobiology

INTRODUCTION

Hydrothermal springs are terrestrial environments characterized by extreme environmental conditions, such as high water temperature, sometimes several tens of degrees above the mean air temperature, pH values ranging from acidic to alkaline, or hydrothermal fluids often concentrated in noxious elements, such as Hg, Sb, B or As (Rothschild and Mancinelli, 2001). However, despite their apparent inhospitality, terrestrial hydrothermal springs are recognized habitats for microbial life on Earth (Brock, 1978) and are of scientific interest for the study of extremophilic microbial communities that resist and adapt to the extreme environments. In addition, terrestrial hydrothermal springs are credible candidate sites for the origin of life (Deamer and Georgiou, 2015; Damer and Deamer, 2020; Van Kranendonk et al., 2021), where the abundant supply of geothermal energy and nutrients (including B, Zn, Mn, and K, in addition to C, H, N, O, P, and S), as well as the alternate of wet-dry cycles, may have favored the prebiotic synthesis of complex organic compounds (Deamer and Georgiou, 2015). Thus, the colonization of geothermal environments by microbial communities attracts the interest of biogeochemists and astrobiologists to understanding the early evolution of the biosphere on Earth and the implications for a hypothetical development of life elsewhere in the Solar System.

Furthermore, terrestrial hydrothermal systems are also strategic targets to search for signs of past life since they accumulate deposits with potential for biosignatures preservation. Due to the rapid cooling and evaporation of silica-saturated fluids, siliceous sinters precipitate rapidly as amorphous silica (i.e., opal-A), allowing the preservation of microfossils, textural biosignatures, and organic biomolecules from the microbial communities that could have inhabited the silicifying hot spring waters (e.g., Campbell et al., 2015; Teece et al., 2020; Wilmeth et al., 2021). In addition, the silica surface provides a physical shield that protects against the high-intensity UV radiation, thus, favoring the preservation of biological remnants entombed within by avoiding extensive cellular damage (Phoenix et al., 2006). Siliceous sinter occurs throughout the rock record up to 3.5 Ga and includes the earliest evidence for life in non-marine environments (Djokic et al., 2017).

Opaline sinter deposits of ∼3.8 Ga that argue for the existence of hydrothermal activity in Hesperian times are also preserved on Mars (e.g., Gusev crater or Syrtis Major), constituting targets for future investigations of sedimentology and potential astrobiological signatures (Skok et al., 2010; Ruff and Farmer, 2016; Ruff et al., 2019). Thus, since proposed by Walter and Des Marais (1993), siliceous hydrothermal spring deposits are considered key Martian astrobiological targets because of their high habitability potential and ability to capture and preserve biosignatures (Walter and Des Marais, 1993; Cady et al., 2018; Teece et al., 2020). However, while physical access to opaline silica samples from Mars is unattainable at this stage, an indirect exploration through the analysis of analogous sinter deposits on Earth appears as a good alternative (e.g., Campbell et al., 2015).

From the extensive catalog of hydrothermal systems on Earth (e.g., Krýsuvik, Hveragerdi, Hveravellir or Namafjäll in Iceland; Octopus Spring, Mushroom Spring, Chocolate Pots or Fountain Paint Pots in Yellowstone National Park in the United States; Uzon Caldera, Geysir Valley, or Pauzhetka hot springs in Kamchatka, Russia; Umukuri, Tahunaatara, Mangatete, Te Kopia or Orakei Korako in the Taupo Volcanic Zone in New Zealand; Black Water, Gaet'ale, or other unnamed springs in the Dallol region in Ethiopia, etc.), the El Tatio geyser field in the Chilean Andes represents one of the best Martian analogs (e.g., Ruff and Farmer, 2016) because of the number of features resembling the Early Mars. Such common features include the high elevation of El Tatio (4,320 masl), which makes the Andean geyser field a unique environment with harsh conditions similar to some on Mars (Cabrol et al., 2007, 2018), such as an intense surface ratio of UV radiation (Cabrol et al., 2014), a large daily thermal oscillation, or high atmospheric dryness (i.e., a precipitation rate of 100 mm per year) (Fernández-Turiel et al., 2005). Thus, the El Tatio geyser field is a unique scenario to investigate the distribution of microbial life in high-altitude extreme conditions and to learn about the preservation of biosignatures in sinter deposits that resemble opaline silica outcrops described on Mars.

However, to interpret properly the information enclosed in old sinter deposits from El Tatio, we need to first understand the modern biomarker record and its preservation over time, and, therefore, it is crucial to know what biological sources contribute to it locally. Learning to interpret in detail modern biomarker records is relevant for recognizing past biosources and metabolic features in geological samples, where the preferential degradation of more labile biomolecules (e.g., DNA or proteins; Sánchez-García et al., 2020, 2021; Lezcano et al., 2022) makes the lipid remnants one of the most suitable biomarkers as their hydrocarbon skeletons can retain information for billions of years (Brocks et al., 2005). While the microbial diversity

in the hydrothermal region of El Tatio is largely known by studies based on petrographic examinations of siliceous sinter deposits (Fernández-Turiel et al., 2005), *in situ* thermal imaging of microbial mats (Dunckel et al., 2009), electron microscopy of terrace sinter, and cyanobacterial biomass (Phoenix et al., 2006), or by microscopical analysis and DNA sequencing of partially silicified microbial communities (Barbieri et al., 2014; Wilmeth et al., 2021), little has been done by exploring highly resistant lipid biomarkers (Sánchez-García et al., 2019; Teece et al., 2020).

In active hydrothermal systems, the water temperature plays a key role in determining the composition and distribution of microbial mats or biofilms (Purcell et al., 2007) that may induce the biological precipitation of silica sinter (microbial silicification) from metabolic biochemistry (e.g., oxygenic photosynthesis or respiration) (Konhauser et al., 2004; Dupraz et al., 2009), although the exact role of microbes in the formation of siliceous sinters remains unclear (Gong et al., 2021; Jones, 2021). To interpret biological fingerprints in silicified/fossilized deposits of sinter, we need to understand well the effect of the temperature on the distribution of modern microbial communities in siliceous-rich hydrothermal springs. In this study, we investigated the molecular and isotopic composition of eight biofilms growing at different temperatures in a hot spring from El Tatio, dubbed the "Cacao" stream. By characterizing the lipid biomarkers profile from 29 to 72°C, we aimed to capture the transition of biological sources and prevailing metabolisms, with the increasing temperature to reconstruct the associated biofacies along the hydrothermal transect. We chose lipid biomarkers as a forensic tool because of the generally much higher resistance to degradation of lipids compared to other biomolecules (Sánchez-García et al., 2020, 2021; Lezcano et al., 2022), which makes them applicable to decoding fossil counterparts of silica sinter deposits within a wide time framework (Walter and Des Marais, 1993; Cady et al., 2018; Teece et al., 2020). We assessed the precision of the taxonomic assignation based on the organismic-ubiquitous lipid biomarkers by analysis of small subunit ribosomal ribonucleic acid (SSU rRNA) sequencing. The qualitatively validated forensic capacity of the lipid biomarkers to detect microbial biosources in the Cacao biofilms provided a fresh molecular and isotopic end member for interpreting fossil biomarkers in ancient silica records in El Tatio and analogous siliceous deposits on Mars.

MATERIALS AND METHODS

Description of the Study Area

El Tatio geyser field (22°20′S 68°01′W), located in the modern volcanic arc of Central Andes in the Altiplano plateau in northern Chile (**Figures 1A,B**), is the largest known geyser field in the southern hemisphere. The hydrothermal area comprises more than 80 active geysers and thermal manifestations that expand over 30 km^2 at elevations from 4,200 to 4,600 m.a.s.l. (Glennon and Pfaff, 2003; Fernández-Turiel et al., 2005). Hydrothermal fluids are mostly meteoric, with minor magmatic components. The fluids rich in silica generate local silica deposits on the surface that overlaps the geological sequence composed of ignimbrite, dacitic/andesitic lavas, and glacial and alluvial deposits (Lucchi et al., 2009). The hydrothermal area is divided into three distinct basins: upper, middle, and lower (**Figure 1C**); in all of them thermal features like geysers, fumaroles, geothermal springs, and mud volcanoes can be encountered (Muñoz-Saez et al., 2018).

The hydrothermal springs of El Tatio hold diverse microbial communities with the presence of photosynthetic thermophilic bacteria (e.g., *Chloroflexus* like), *Cyanobacteria* (e.g., *Oscillatoria*, *Nostoc*, *Phormidium, Leptolyngbya*, and *Calothrix*) and diatoms deduced from microscopic observations and thermal imaging (Fernández-Turiel et al., 2005; Phoenix et al., 2006). More recently, the presence of eukaryotic golden and green algae, as well as *Firmicutes* (*Bacillales* and *Clostridiales*), *Proteobacteria* (*Rhodobacteriales*, *Rhizobiales*, *Burkholderiales*, and *Desulfuromonadales*), *Bacteroidetes*, *Planctomycetes*, *Verrumicrobia*, or *Actinobacteria* (*Actinomycetales*) has also been reported from the use of DNA sequencing analysis on sinter deposits (Barbieri et al., 2014; Sánchez-García et al., 2019; Gong et al., 2020; Wilmeth et al., 2021).

Sample Collection

Fresh biofilms from a hydrothermal stream in the middle basin of the El Tatio geyser field were sampled in November 2018 during a field campaign funded by the NASA Astrobiology Institute (NAI) within the NAI CAN7 project (ref. 13-13NAI7_2-0018). In total, eight biofilm samples were collected along the proximal to the distal apron of the hydrothermal stream named by our team as Cacao, along a transect of 10–12 m in length, covering a temperature gradient from 72°C in the hot spring pool to 29°C further down in the cooler *terracettes* (**Figure 1D**). The water pH was measured *in situ* and observed to vary little along the relatively small transect (i.e., from 6.9 to 7.2; **Table 1**), so the temperature was considered the main variable environmental factor. Two samples were collected from the upstream hot spring pool, CE6 (72°C) and CE5 (67°C) (**Figure 1E**), and three from the channel flowing down the pool, where water temperature decreases from 56°C (CE4 and CE4gr) to 46°C (CE3) (**Figure 1F**). Both CE4 and CE4gr were collected from the same site and at the same temperature, but their different aspects suggested a somehow different microbial composition (**Figure 1D**), that is, filaments dominantly orange (CE4) or green (CE4gr). Finally, two more biofilms, CE2 (32°C) and CE1 (29°C) were collected from the downstream *terracettes* formed by the precipitation of silica sinter as the water cools down at lower locations in the distal apron (**Figure 1G**). An additional biofilm was sampled from a parallel branch of the hydrothermal stream, the so-called Cacao West, at a temperature of 30°C (i.e., CW1). We added this sample to the set because of its different aspects (i.e., black; **Figure 1H**) compared to its temperature counterpart in Cacao East (i.e., CE1). See also **Table 1**.

At each temperature, a total sample of 15-100 g was collected from different spots (n = 3–5) on the microbial mats, combined to assure a representative sampling. The biofilm samples were retrieved with ethanol-clean spatulas and spoons, wearing a clean white suit, booties, and nitrile gloves to avoid contamination. They were stored in solvent-clean polypropylene containers and kept cold (i.e., 4°C) until arrival at the *Centro de Astrobiología*

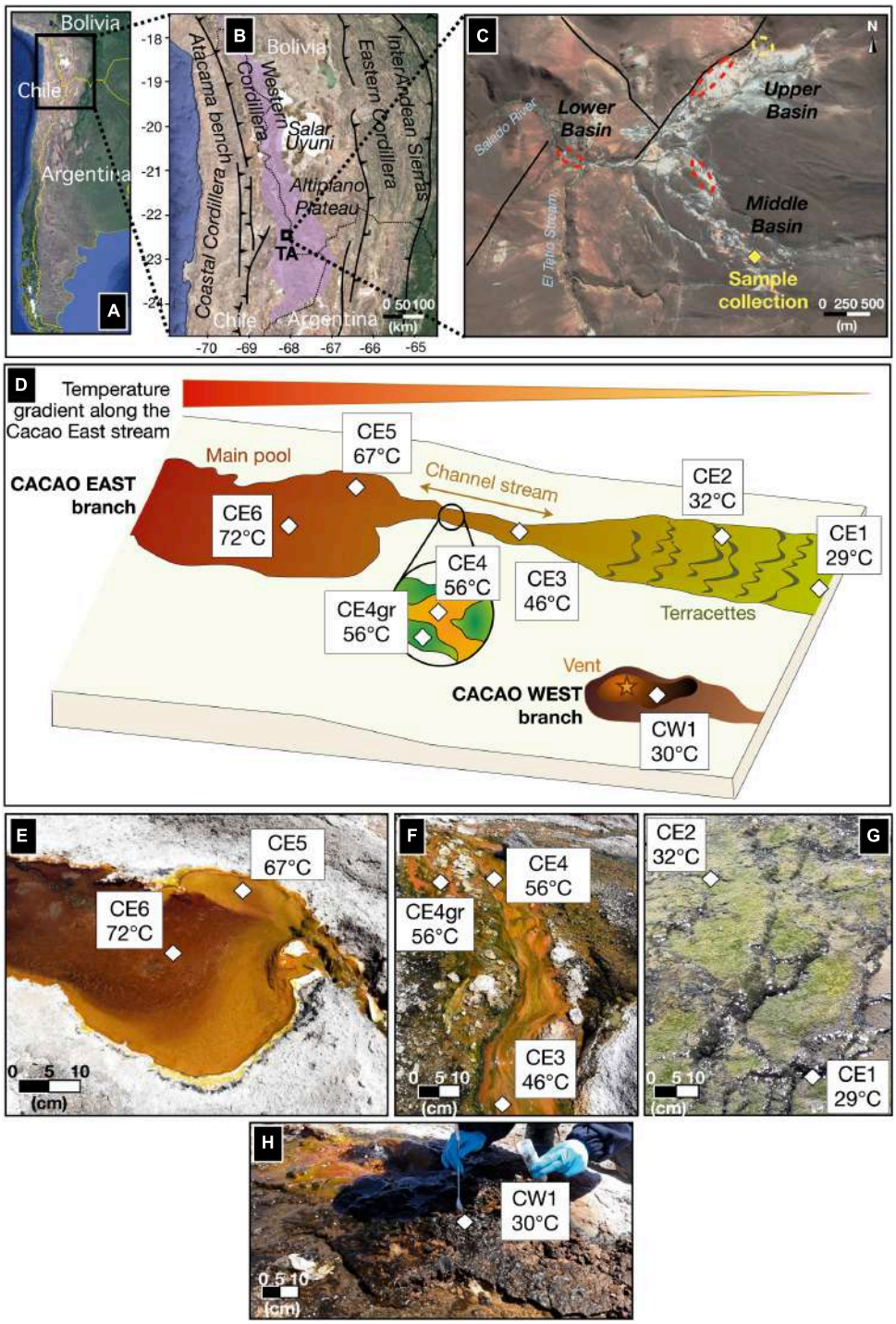

FIGURE 1 | A study site and a sampling area along the Cacao hydrothermal stream in the geothermal region of El Tatio. **(A)** Location of the El Tatio geyser field in northern Chile; **(B)** the black rectangle zooms in the Chilean Altiplano, where the Andean modern volcanic arc (a.k.a. Altiplano-Puna Volcanic Complex or APVC) is located (the purple area). The regional fault system, corresponding to sectors of contractional tectonics, makes the APVC a very highly uplifted area, explaining the high elevation of the El Tatio (TA) area (Lucchi et al., 2009). **(C)** The black square marked TA represents the inset view of El Tatio as a *Google Earth* image, showing the three basins, comprising the hydrothermal system (modified from Muñoz-Saez et al., 2018) and the location of the Cacao stream (yellow diamond), where the eight biofilm samples were collected. Local faults (black lines) allow hydrothermal circulations and explain part of the repartition of the primary areas with geysers and spouters (red dashed circles) or mud pools and volcanoes (yellow dashed circles). **(D)** A sketch of the hydrothermal transect (from 72°C to 29°C) studied along the Cacao stream, with seven biofilm samples collected from the East branch (CE) and one from the West branch (CW). **(E–H)** a close view of the seven CE biofilms along the Cacao stream; **(E)** the vent pool, **(F)** the mid-apron channel, and **(G)** distal-apron *terracetes*. **(H)** A close view of the eighth biofilm (CW1) collected from the West branch of the Cacao stream.

TABLE 1 | Location and description of the fresh biofilms studied along the Cacao hydrothermal stream, in the El Tatio middle basin.

Sample name[a]	Site latitude (S)	Site longitude (W)	Altitude (m)	Location on the stream	Sample visual description	Temperature (°C)	pH
CE6	22°21.022′	68°0.483′	4328	Upstream Cacao East, mean hot spring pool	Rusty colored biofilm with abundant mineral grains	72	6.96
CE5	22°21.022′	68°0.483′	4328	Upstream Cacao East, edge of the hot spring pool	Green borders over orange base with stream tufts	67	7.07
CE4	22°21.022′	68°0.483′	4328	Cacao East channel stream, upper half	Green-orange biomass	56	6.96
CE4gr	22°21.022′	68°0.483′	4328	Cacao East channel stream, upper half	Intense green biomass	56	6.96
CE3	22°21.020′	68°0.485	4327	Cacao East channel stream, lower half	Red-orange biomass	46	6.95
CE2	22°21.019′	68°0.486′	4327	Downstream Cacao East, on *microterracetes* surface	Bright green biomass	32	7.18
CE1	22°21.017′	68°0.485′	4326	Downstream Cacao East, furthest spot from the hot spring pool	Greenish-brown biomass	29	7.13
CW1	22°21.025′	68°0.480′	4328	Upstream Cacao West, outer layer around the vent	Blackish-brown biomass	30	7.15

[a] *The sample names are built according to a code (CE or CW) that refers to the stream branch (East or West, respectively) from which the samples were collected.*

of Madrid, where they were frozen at –20°C. Before analysis, the samples were freeze-dried, and between 0.3 and 20 g of dry mass were available for the different biogeochemical analyses.

Bulk Geochemistry Analysis

The stable carbon isotopic composition (δ^{13} C) of the biomass was measured on the bulk biofilm samples with isotope-ratio mass spectrometry (IRMS), following USGS methods (Révész et al., 2012). Briefly, subsamples of the freeze-dried biofilms (300 mg) were homogenized by grinding with a corundum mortar and pestle (except for sample CE4gr that had not enough material for all analyses). Subsequently, HCl was added to remove carbonates, and we let it equilibrate for 24 h, adjusting, then, the pH to neutral values with ultrapure water. Afterward, the residue was dried in an oven (50°C) for 72 h or until constant weight, and then it was analyzed by IRMS (MAT 253, Thermo Fisher Scientific, Waltham, MA, United States). The δ^{13}C values were reported in the standard per mil notation using three certified standards (USGS41, IAEA-600, and USGS40), with an analytical precision of 0.1‰. The content of total organic carbon (TOC%) was measured with an elemental analyzer (HT Flash, Thermo Fisher Scientific, Waltham, MA, United States) during the stable isotope measurements.

Lipid Biomarkers Extraction, Fractionation, and Analysis

Depending on the available amount of sample, between 0.5 and 2 g of freeze-dried sample were extracted with a mixture of dichloromethane and methanol (3:1, v/v) to obtain a total lipid extract (TLE) by an ultrasonic bath (further details in Sánchez-García et al., 2018). A mixture of three internal standards (tetracosane- D_{50}, myristic acid-D_{27}, and 2-hexadecanol) was added to the samples before the extraction to allow for the quantification of compounds in each lipidic fraction, namely, apolar, polar, and acidic. The TLE has concentrated to ca. 2 ml by rotary evaporation, and elemental sulfur was removed overnight with activated copper. Then, the clean extract was hydrolyzed overnight with methanolic KOH (6% MeOH) at room temperature. *n*-Hexane was added to the hydrolyzed TLE to obtain the neutral fraction through liquid-liquid extraction. The remaining lipidic extract was then acidified with HCl (37%) to remove K^+ from the solution by precipitation of KCl, allowing the recovery of the liberated carboxylic groups by liquid-liquid extraction with *n*-hexane (acidic fraction). Further separation of the neutral fraction into apolar (hydrocarbons) and polar (alcohols) was conducted by using activated alumina (Sánchez-García et al., 2019). Before analysis by gas chromatography linked to mass spectrometry (GC-MS), both acidic and polar fractions were derivatized with BF_3 in methanol (the fatty acids) and with N, *O*-bis (trimethylsilyl) trifluoroacetamide (the alcohols) to increase the volatility of their carboxyl and hydroxyl groups by transformation into fatty acid methyl esters (FAME) and trimethylsilyl derivates, respectively.

The three lipid polarity fractions (apolar, acidic, and polar) were analyzed by GC-MS using a 6850 GC system, coupled to a 5975 VL MSD, with a triple-axis detector (Agilent Technologies, Santa Clara, CA, United States), with electron ionization at 70 eV and scanning from m/z 50 to 650. For the apolar fraction, the oven temperature was programmed from 40°C to 150°C at 15°C·min^{-1} (held 2 min) to 255°C at 5°C·min^{-1} (held 20 min), and then to 300°C at 5°C·min^{-1} (held 10 min). For the polar and acidic fractions, the oven temperature was programmed from 50°C to 130°C at 20°C·min^{-1} (held 2 min) and to 300°C at 6°C·min^{-1} (held 20 min or 25 min for the acidic or polar fraction, respectively). The injector temperature was 290°C, the transfer line was 300°C and the MS source at 240°C. Compound identification was based on the comparison of mass spectra and/or reference materials using the NIST library provided by the MSD ChemStation software. For quantification, we used external calibration curves of *n*-alkanes (C_{10} to C_{40}), *n*-fatty acids as FAME (C_8 to C_{24}), and *n*-alkanols (C_{10}, C_{14}, C_{18}, and C_{22}). All chemicals and standards were supplied by Sigma Aldrich. The recovery of the internal standards averaged 70 ± 21%.

Compound-Specific Isotope Analysis

Compound-specific isotope analysis (CSIA) of the lipid biomarkers was performed on the three extracted polarity fractions to determine individual δ^{13}C values assignable to

carbon fixation pathways (**Supplementary Text 1**). The carbon isotopic composition of individual lipids was measured by coupling gas chromatography-mass spectrometry (Trace GC 1310 ultra and ISQ QD MS) to an isotope-ratio mass spectrometry system (MAT 253 IRMS, Thermo Fisher Scientific, Waltham, MA, United States). The conditions for the GC analysis were identical to those used for the molecular analysis of the polar fraction, whereas those for the IRMS analysis included an electron ionization of 100 eV, Faraday cup collectors of m/z 44, 45, and 46, and a temperature of the CuO/NiO combustion interface of 1,000°C. The samples were injected in a splitless mode, with an inlet temperature of 250°C, and helium as carrier gas at a constant flow of 1.1 ml·min^{-1}. The δ^{13}C values of the individual lipids separated by GC were calculated using CO2 spikes of known isotopic composition, introduced directly into the MS source, three times at the beginning and the end of every run. Reference mixtures from Indiana University (US) of the known isotopic composition of *n*-alkanes (A6) and FAMEs (F8) were run every four samples to check the accuracy of the isotopic ratio determined by GCMS-IRMS. The δ^{13}C data for individual carboxylic acids were calculated from the resulting FAME values by correcting them for the one carbon atom added in the methanolysis (Abrajano et al., 1994). Similarly, the values from the trimethylsilyl derivates in the polar fraction were also corrected for the 3 carbons added in the derivatization process.

DNA Extraction, PCR Amplification, and DNA Sequencing

In addition to the molecular and isotopic characterization of the lipid biomarkers, the eight biofilms were subjected to genetic analysis to determine with precision the taxonomic composition of the hydrothermal samples. This complimentary analysis aimed to test the reliability and specificity of the lipid biomarkers to infer biological sources and to attempt taxonomical affiliations.

Biofilms DNA Extraction

Genomic DNA of the freeze-dried biofilms was extracted using a DNeasy Power Biofilm Kit (QIAGEN, Hilden, Germany), following the manufacturer's instructions with several modifications. Samples from 0.1 to 0.25 g (depending on the available amount of material for each sample) were split into two subsamples to increase the DNA extraction yield. Based on previous tests, we considered that this amount of sample was sufficient for efficient DNA extraction and that it was representative of the whole biofilm as the subsamples (i.e., extraction replicates) were taken from the homogenized freeze-dried samples. Then, from ca. 550 μL to 1 ml of MBL solution was added to each biofilm material to prevent the total absorption of the liquid by the freeze-dried biofilms. Moreover, the samples were incubated two times with 100 μL of IRS solution on ice to efficiently remove the high amount of non-DNA organic and inorganic material in the biofilms. The final subsample DNA extractions were combined in the MB Spin Columns, and several additional centrifugation steps at 20,000 × *g* were carried out to remove the ethanol completely before recovering the DNA with 50 μL of sterile water. Negative control of the kit without a sample was also performed. DNA concentrations were determined using the Qubit dsDNA BR Assay kit (Invitrogen, Thermo Fisher Scientific, Waltham, MA, United States), and DNA extracts were stored at –20°C until sequencing analysis at the genomic service of *Fundación Parque Científico de Madrid* (FPCM, Spain).

PCR Amplification of Small Subunit Ribosomal Ribonucleic Acid Genes and Sequencing

The distribution of bacteria, archaea, and eukarya, as well as the specific cyanobacterial community, was analyzed by the construction of amplicon libraries and sequenced on an Illumina MiSeq sequencer (Illumina Inc., San Diego, CA, United States) at the genomic service at FPCM. The bacterial 16S rRNA V3–V4 hypervariable gene region was amplified with the primer pair Bakt_341-F/Bakt_805- R (Herlemann et al., 2011). The archaeal 16S rRNA V2–V3 hypervariable gene region was amplified with the primer pair Arch1F/Arch1R (Cruaud et al., 2014), and the eukaryotic 18S rRNA V4–V5 hypervariable gene region was amplified with the primer pair 563F/1132R (Hugerth et al., 2014). These primers have been previously used to characterize the microbial communities in sinter samples from El Tatio (Sánchez-García et al., 2019) and other geothermal environments (Lezcano et al., 2019). The 16S rRNA gene of cyanobacteria was amplified with the specific primer pairs CYA359F/CYA781Ra and CYA781Rb (Nübel et al., 1997) in separate reactions. These specific cyanobacterial primers are widely used to identify cyanobacteria in different environments (e.g., Dorador et al., 2008; Azúa-Bustos et al., 2011; Mehda et al., 2021). Further information about the PCR conditions is available in the **Supplementary Text 2**. The negative control showed absence of gene amplification and then was removed for the sequencing analysis. The PCR of the eukaryotic community showed gene amplification in CE1, CE2, and CW1 and was negative for the rest of the samples. Thus, only 18S rRNA gene amplicons from CE1, CE2, and CW1 were sequenced. Final amplicon pools were denatured before seeding on a flow cell and sequenced using the MiSeq Reagent kit v3 (Illumina, Inc., San Diego, CA, United States) in a 2 x 300 pair-end sequencing run on an Illumina MiSeq sequencer.

Raw sequences of bacteria (1,918,397), archaea (915,696), eukarya (479,652), and cyanobacteria (478,079 with primer pairs CYA359F/CYA781Ra, and 456,825 with primer pairs CYA359F/CYA781Rb) were processed in Mothur software v.1.45.3 (Schloss et al., 2009), following the MiSeq SOP pipeline (Kozich et al., 2013). Forward and reverse reads were merged and quality-filtered by removing the (i) reads below 400 bp for bacteria, 300 bp for archaea, 500 bp for eukarya, and 400 bp for cyanobacteria, (ii) ambiguous nucleotides, (iii) homopolymers longer than 8 bp and (iv) chimeras identified with VSEARCH (Rognes et al., 2016). Final sequences were clustered into OTUs at 97% similarity, and taxonomic assignments were performed against the SILVA database (v. 132; Quast et al., 2013). Singletons and sequences that were assigned to non-bacterial, non-archaeal, non-eukaryotic, and non-cyanobacterial entities in their respective gene libraries were removed to avoid misinterpretations. This final data screening resulted in the elimination of 0.62% of the sequences in the bacterial library

(0.6% were singletons), 96.4% in the archaeal library (96.1% were bacterial sequences), 9% in the eukaryotic library (all were singletons), 35% in the cyanobacterial library with the primer pairs CYA359F/CYA781Ra (34.5% were other bacteria different from *Cyanobacteria*) and 29.8% in the cyanobacterial library, with the primer pairs CYA359F/CYA781Rb (29.3% were other bacteria different from *Cyanobacteria*). Then, the resulting cyanobacterial reads were combined to get a single data set.

Shannon-Wiener, Simpson, and Fisher diversity indices were calculated with the vegan package (Oksanen et al., 2020) in R 4.1.3 as α-diversity estimators for the community composition of bacteria, cyanobacteria, archaea, and eukaryotes in the El Tatio biofilms.

RESULTS

Bulk Geochemical Characterization of the Eight Biofilms Collected From Cacao Along a Thermal Gradient

All biofilm samples except CE4gr, which did not have sufficient material for bulk characterization, showed a biomass content (measured as TOC) from 0.46 to 27% of the dry weight (DW), and values of the bulk $\delta^{13}C$ ratio, ranging from –19.5‰ to –4.7‰ (**Table 2** and **Supplementary Figure 1**). The samples from 46 to 56°C were the most biomass-rich biofilms (i.e., CE3 and CE4), and that from 72°C (CE6) were the poorest (**Supplementary Figure 1**). In the latter sample, the biomass was particularly depleted in ^{13}C (i.e., showed the most negative $\delta^{13}C$ values), whereas, in CW1, CE1, CE2, and CE5, the biomass was rather enriched (i.e., showed less negative $\delta^{13}C$ values).

Molecular Distribution of Lipid Biomarkers Along the Cacao Hydrothermal Transect

The total concentration of lipidic compounds identified in the Cacao biofilms varied within the samples from 0.088 $mg{\cdot}g^{-1}$ in CE6 (72°C) to 28.3 $mg{\cdot}g^{-1}$ in CE4gr (56°C), relative to the dry weight (**Supplementary Figure 2**). Of the three polarity fractions isolated, the acidic fraction was the most abundant in all biofilms, particularly in the CE4gr sample, where its concentration represented fivefold that of the two other fractions (**Supplementary Figure 2**). A varied distribution of compounds was detected in each lipidic fraction of the biofilms (**Supplementary Table 1** and **Supplementary Figure 3**), where those of concentration representing more than 1% of the total mass concentration are plotted in **Figure 2**. Beyond the absolute concentration of lipid compounds, what is really of interest in the lipid biomarker approach is the molecular distribution within lipid families and the relative abundance of compounds. Therefore, our analysis here will focus on the detection of molecular patterns associable with biological sources according to assignments described in the literature based on culture-based studies or molecular, isotopic, microscopic, or genetic analyses.

Apolar Lipid Fraction

The distribution of lipidic compounds from the apolar fraction varied among the eight biofilms at different temperatures (**Figure 2A**). In general, there was a relatively higher proportion of compounds of low molecular weight (LMW) ($\leq$ 18 carbons) in the biofilms at temperatures of $\leq$56°C, while of high molecular weight (HMW) in the samples at higher temperatures. In particular, the three biofilms thriving at temperatures $\leq$ 32°C (i.e., CW1, CE1, CE2) showed a relative abundance of different isomers of heptadecene (i.e., 17:1), and pentadecane (n-C_{15}), mostly in CE2 (**Figure 2A**). From 46 to 56°C (only CE4gr), the predominant compounds were heptadecane and to a minor extent, different methyheptadecanes, either mono- (Me-C_{17}) or dimethyl- (DMe-C_{17}) homologs. From CE4gr to CE4 at 56°C, the molecular distribution of apolar compounds shifted drastically from a relative abundance of LMW to HMW and polyunsaturated hydrocarbons (**Figure 2A**). A set of compounds from 29 to 33 carbons with mono-, di-, and tri-unsaturations (i.e., one, two, or three double bonds) with the dominance of hentriacontatriene (31:3) was similarly observed in CE4 and CE5. Finally, at 72°C, a mix distribution of all the above-mentioned compounds was found to compose the apolar fraction of CE6, with shared dominance of n-C_{17} and 31:3, a generalized presence of all saturated alkanes from 12 to 29 carbons, and a relatively abundant and varied distribution of Me-C_{17} and DMe-C_{17} homologs. This varied distribution of methylheptadecanes contrasted with those of the samples CE3 or CE4gr, which contained almost exclusively the 5Me-C_{17} and 6Me-C_{17} homologs. Squalene was also detected in the apolar fraction of all biofilms except CE4gr (**Figure 2A**), and the hopanoid diplotene was only found in CE1, CE2, CE3, and CE4gr (**Supplementary Table 1**).

TABLE 2 | Bulk geochemical characterization of the biofilms from the West and East branches of the Cacao hydrothermal stream (for CE4gr, there was no sufficient material for conducting the bulk geochemistry analysis).

Samples	CW1		CE1		CE2		CE3		CE4		CE5		CE6	
Temperature	30°C		29°C		32°C		46°C		56°C		69°C		72°C	
	Mean	std	Mean	std	Mean	std	Mean	std	Mean	std	Mean	std	Mean	std
$\delta^{13}C$ (‰)	–8.5	0.08	–5.4	0.16	–6.9	0.07	–10.5	0.09	–11.1	0.10	–4.6	0.03	–19.4	0.07
TOC (%)	3.7	0.07	1.5	0.13	5.4	0.20	17	0.20	27	0.24	4.2	0.02	0.5	0.01

The stable-carbon isotopic ratio ($\delta^{13}C$) of the total organic carbon (TOC) was measured on replicates (n = 4).

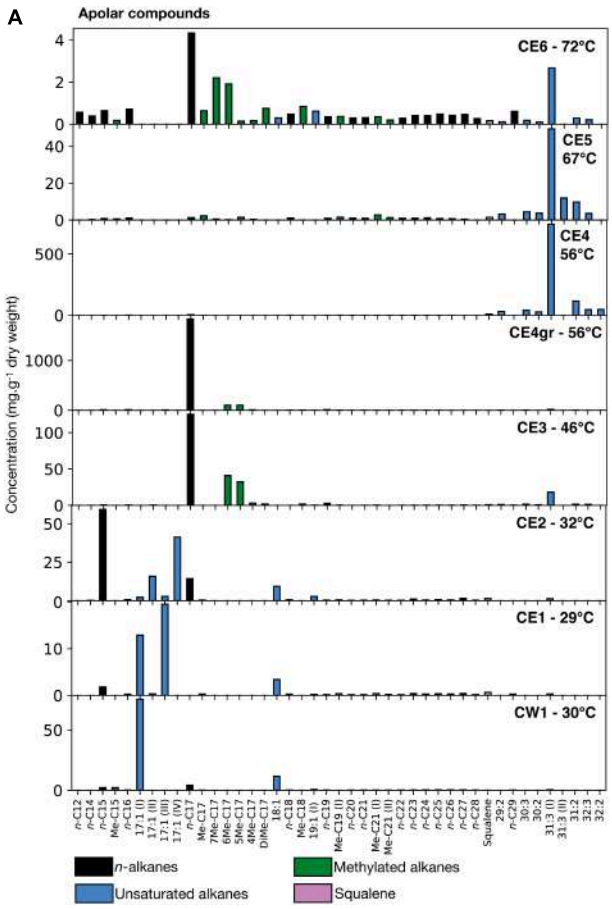

FIGURE 2 | Continued

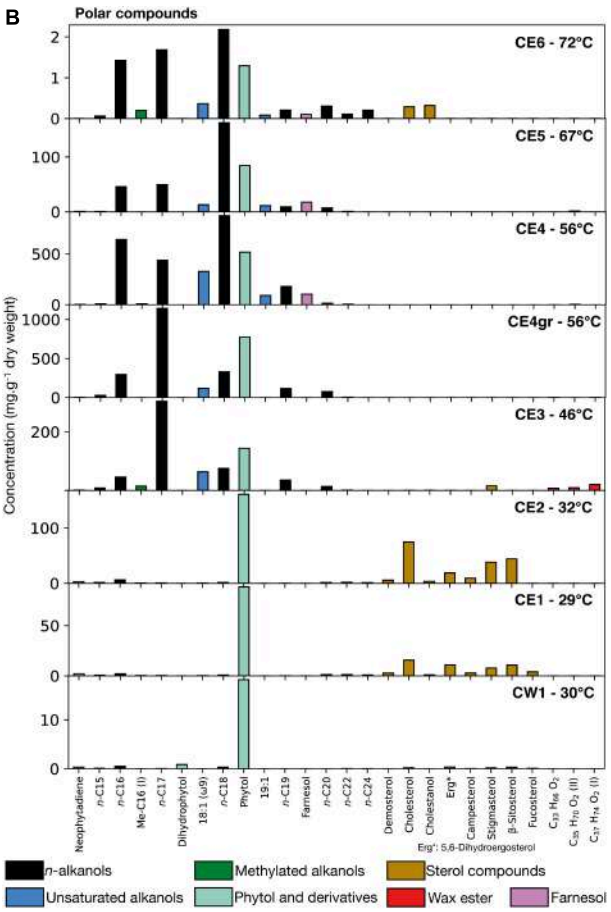

FIGURE 2 | Continued

Polar Lipid Fraction

In the polar fraction, two different distribution patterns were observed among the eight biofilms (**Figure 2B**). In samples from temperatures of ≤32°C, the molecular distribution exhibited clear dominance of phytol and, mostly, in CE1 and CE2, a relative abundance of diverse sterol compounds (mostly cholesterol, β-sitosterol, stigmasterol, campesterol, fucosterol, and 5,6-dihydro ergosterol). In contrast to phytol, the sterol compounds were no longer detected in biofilms above 46°C (except for CE6 at a very low concentration). In addition, at temperatures of ≥ 46°C, the dominant presence of phytol was accompanied by *n*-alkanols from 16 to 24 carbons and monounsaturated alkanols of 18 and 19 carbons (i.e., 18:1 and 19:1). Among the *n*-alkanols series, heptadecanoic (*n*-C_{17}) showed the highest relative abundance in CE3 and CE4gr, whereas octadecanoic (*n*-C_{18}) was the most abundant in CE4, CE5, and CE6 (**Figure 2B**). A series of wax esters with carbon chains from 33 to 38 carbons (**Supplementary Table 1** and **Supplementary Figure 4**) was also detected in the polar fraction of mostly CE3 (**Figure 2B**), as well as in CE4gr, CE4, and CE5 (**Supplementary Table 1**). Finally, the sesquiterpene farnesol was detected only at temperatures ≥ 56°C (i.e., from CE4 to CE6).

Acidic Lipid Fraction

The acidic profiles of all biofilms showed a molecular distribution dominated by the presence of LMW compounds (≤ C_{20}) (**Figure 2C**), in particular, hexadecanoic acid (*n*-C_{16}). Other saturated and unsaturated compounds are distributed differently among the eight biofilms. For instance, the monounsaturated acids 16:1 (ω5 and/or ω7) and 18:1 (ω7 or mostly ω9) were relatively more abundant at temperatures of ≤ 56°C, whereas the heptadecanoic (*n*-C_{17}) and octadecanoic (*n*-C_{18}) acids were rather more abundant at temperatures of ≥ 46°C, or the monounsaturated 19:1 (ω9) from 56°C to 67°C (**Figure 2C**). The presence of polyunsaturated acids, such as 18:4 (ω3), 18:3 (ω6), or 20:4, and 20:5 (ω3) was limited to the biofilms at lower temperatures (i.e., ≤ 32°C), whereas mid-chain cyclo-propyl acids (mostly Cy-C_{17} and Cy-C_{19}) were relatively more abundant at temperatures ≥ 56°C. In contrast, monomethylated acids with *iso* and *anteiso* configuration (i.e., chains with a methyl group in positions N-1 and N-2, respectively) distributed ubiquitously (mostly the *i*/*a*-C_{15} and *i*/*a*-C_{17} pairs), although with higher relative abundance in the biofilms at 32, 46, and 72°C (**Figure 2C**).

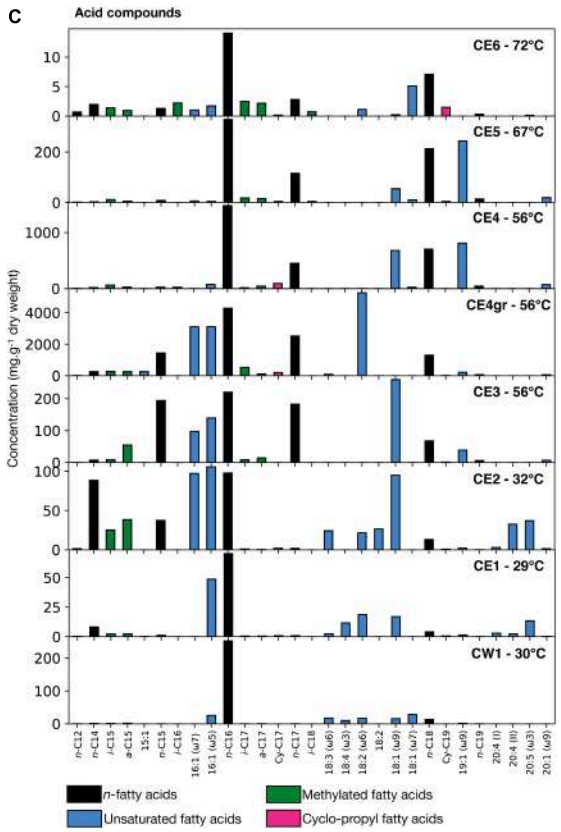

FIGURE 2 | Concentration (mg·g^{-1} of dry weight) of the different lipid compounds identified in the eight Cacao biofilms along three polarity fractions; **(A)** apolar, **(B)** polar, and **(C)** acidic. Within each fraction, only the main compounds that represent more than 1% of the total mass concentration are plotted. Note that the vertical scale is different for each biofilm as the total concentration of organic matter varied between samples, and we focus on the relative distribution of lipid compounds. Different colors are used to represent different types of molecules (linear and saturated or *normal* chains, chains with double bonds or branches, aromatics, etc.). In the three panels, "unsaturated" compounds stand for chains with double bonds represented in the N:M format, where N indicates the number of carbons composing the chain and M the number of double bonds (e.g., 18:1 is a chain of 18 carbons with one double bond). In **(B)** the "phytol and derivatives" category includes neophytadiene and dihydrophytol besides phytol. In **(C)** *iso* and *anteiso* compounds (*i*-/*a*-) are monomethylated chains with one methyl group at the N-1 or N-2 carbon, respectively. In **(C)**, the position of the double bond is defined using the omega notation, that is, the position starting from the final carbon. In **(C)** Cy-C_N corresponds to mid-chain cyclo-propyl compounds, with chains of N carbons. The raw mass chromatograms used for compound identification and building the bar plots are available in the **Supplementary Figure 3**.

Stable Carbon Isotopic Composition of Microbial Lipid Biomarkers Along the Cacao Hydrothermal Stream

The compound-specific carbon isotopic composition ($\delta^{13}C$) of all the identified lipid compounds ranged from –33.5‰ to +4.9‰ in the eight biofilms and showed different distribution patterns, depending on the temperature and the polarity fraction (**Figure 3**).

In the apolar fraction (**Figure 3A**), the values of the compound-specific $\delta^{13}C$ varied from –30.6‰ to +4.9‰ and clustered into two general groups; (i) one of the relatively ^{13}C-enriched values (i.e., $\delta^{13}C$ from ca., –12‰ to + 4.9‰) largely corresponding to HMW poly-unsaturated alkanes ($\geq$ 29 carbons), and (ii) another of relatively ^{13}C-depleted values (i.e., from ca., –30.6‰ to –12‰) that included most of the remaining apolar compounds. In particular, *normal* alkanes of middle molecular weight (i.e., from 19 to 26 carbons) showed the most depleted $\delta^{13}C$ values, mostly in CE6, CE5, and CE4 (**Figure 3A**), whereas those of LMW presented a more dispersed range of values, from as high as –8.4‰ in the *n*-C_{17} of CE2 to as low as –29.9‰ in the 5Me-C_{17} of CE5 (**Figure 4A**). Among the samples, the most ^{13}C-enriched values were measured in the HMW compounds of CE4 and CE5 (i.e., 56 and 67°C).

The stable-carbon isotopic composition was relatively more homogeneous among the compounds in the polar fraction, where the $\delta^{13}C$ values ranged only from –26.7‰ to –2.3‰ (**Figure 3B**). Similar to the apolar fraction, the samples CE4 (56°C) and CE5 (67°C) showed the most ^{13}C-enriched $\delta^{13}C$ values, whereas CE3 (46°C), CE4gr (56°C), and, mostly, CW1 (30°C) displayed the most ^{13}C-depleted signatures.

In comparison, the range of variation of $\delta^{13}C$ was broader in the acidic fraction (from –33.5‰ to +2.3‰), with values showing different distribution patterns among the eight biofilms (**Figure 3C**). The most enriched $\delta^{13}C$ values (from –5‰ to + 2.3‰) were consistently found in compounds from CE4 and CE5, whereas the most depleted values were those of compounds (mostly *i*-/*a*-C_{15}, *i*-/*a*-C_{17}, *i*-C_{16}, and *i*-C_{18}) detected in the highest-temperature CE6 (from –14.3 to –33.5‰). The range of variance of the compound-specific $\delta^{13}C$ was narrowest in the low-temperature CE1 and CE2 (from –14.6 to –8.‰), and relatively broader in CW1 (from –24.9 to –14.4‰), CE3 (from –20.7 to –9.9‰), and CE4gr (from –25.7 to –10.3‰).

Taxonomic Analysis of the Cacao Biofilms Based on DNA Sequencing Data

Taxonomic analysis of the 16S rRNA gene sequences of the eight biofilms showed that bacterial and archaeal communities were present in all the biofilms except CE3, where no *Archaea* were detected after the quality-filtering of the sequences (all were *Bacteria*) (**Supplementary Figure 5**). Despite the identification of *Archaea* in the rest of the samples, they only represent 0.3% of the total sequences in the archaeal libraries (the rest were *Bacteria*), and, therefore, interpretations must be considered with caution. In contrast to *Bacteria* and *Archaea*, the 18S rRNA gene from *Eukaryota* was amplified only in the low-temperature biofilms ($\leq$ 32°C), indicating detectable eukaryotic communities in CW1, CE1, and CE2.

In the bacterial community, the relative abundance of the phyla varied among the eight biofilms thriving at different temperatures in the hydrothermal stream (**Figure 4A**). In the low-temperature biofilms ($\leq$ 32°C), *Proteobacteria* (recently renamed as *Pseudomonadota*) were largely predominant (> 60% of the bacterial sequences), with a lesser but still relevant representation of *Cyanobacteria* (from 9.4 to 16.7%). Among

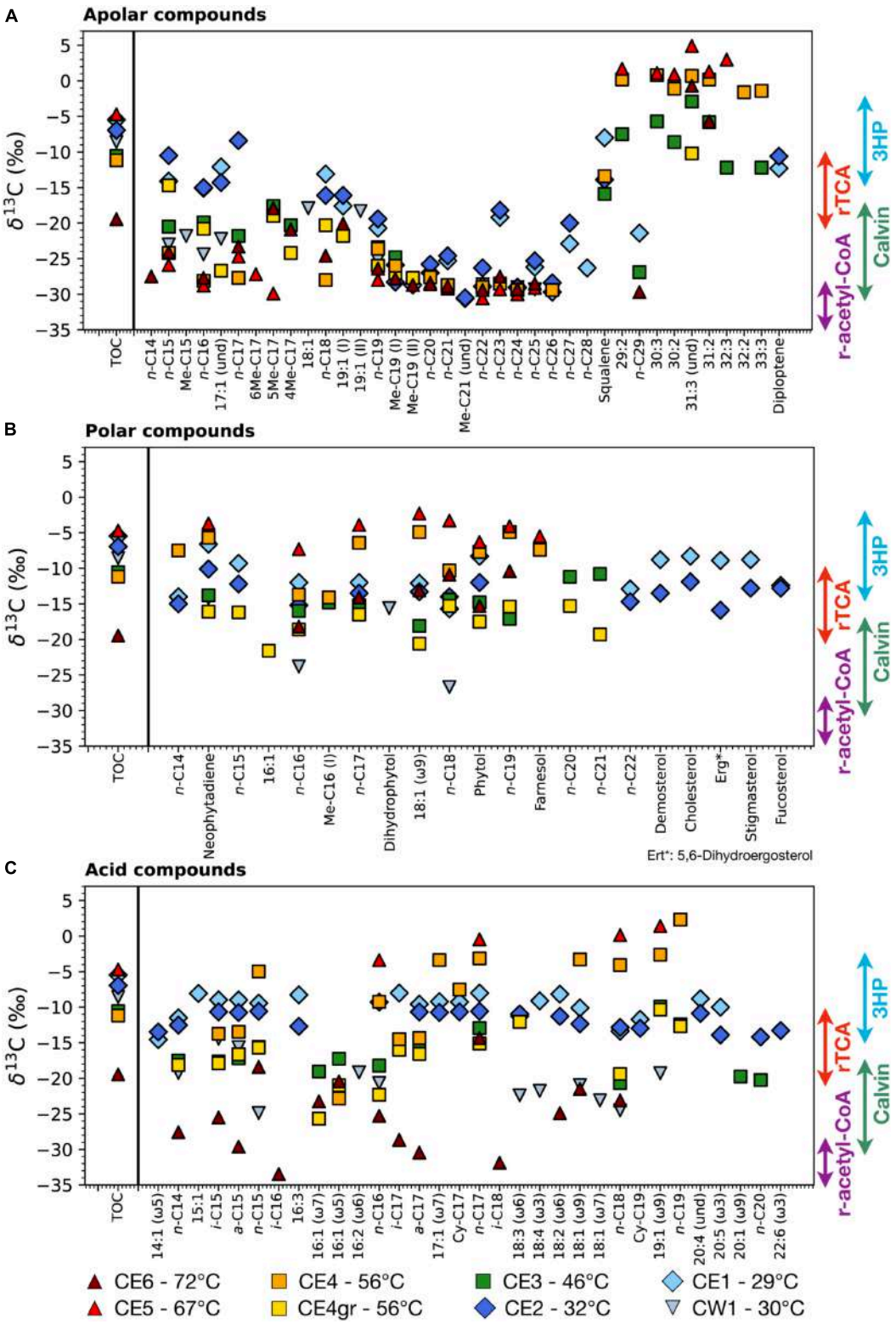

FIGURE 3 | Compound-specific isotopic composition ($\delta^{13}C$) of the lipid compounds identified in the three polarity fractions; **(A)** apolar, **(B)** polar, and **(C)** acidic. The isotopic composition of the total biomass ($\delta^{13}C_{TOC}$) is shown in each fraction for comparing the isotopic composition of the bulk cell material with that of individual lipid compounds. Colored arrows represent canonical biomass $\delta^{13}C$ values associated with the four primary carbon fixation pathways (Preuß et al., 1989; van der Meer et al., 2000; Hayes, 2001). Note that individual lipid compounds are typically lighter (i.e., more negative $\delta^{13}C$) than the bulk organic matter, except for those synthesized through the reductive tricarboxylic acid (rTCA) cycle and, sometimes, the 3-hydroxypropionate (3HP) bicycle (Meyers, 1997; Jahnke et al., 2001).

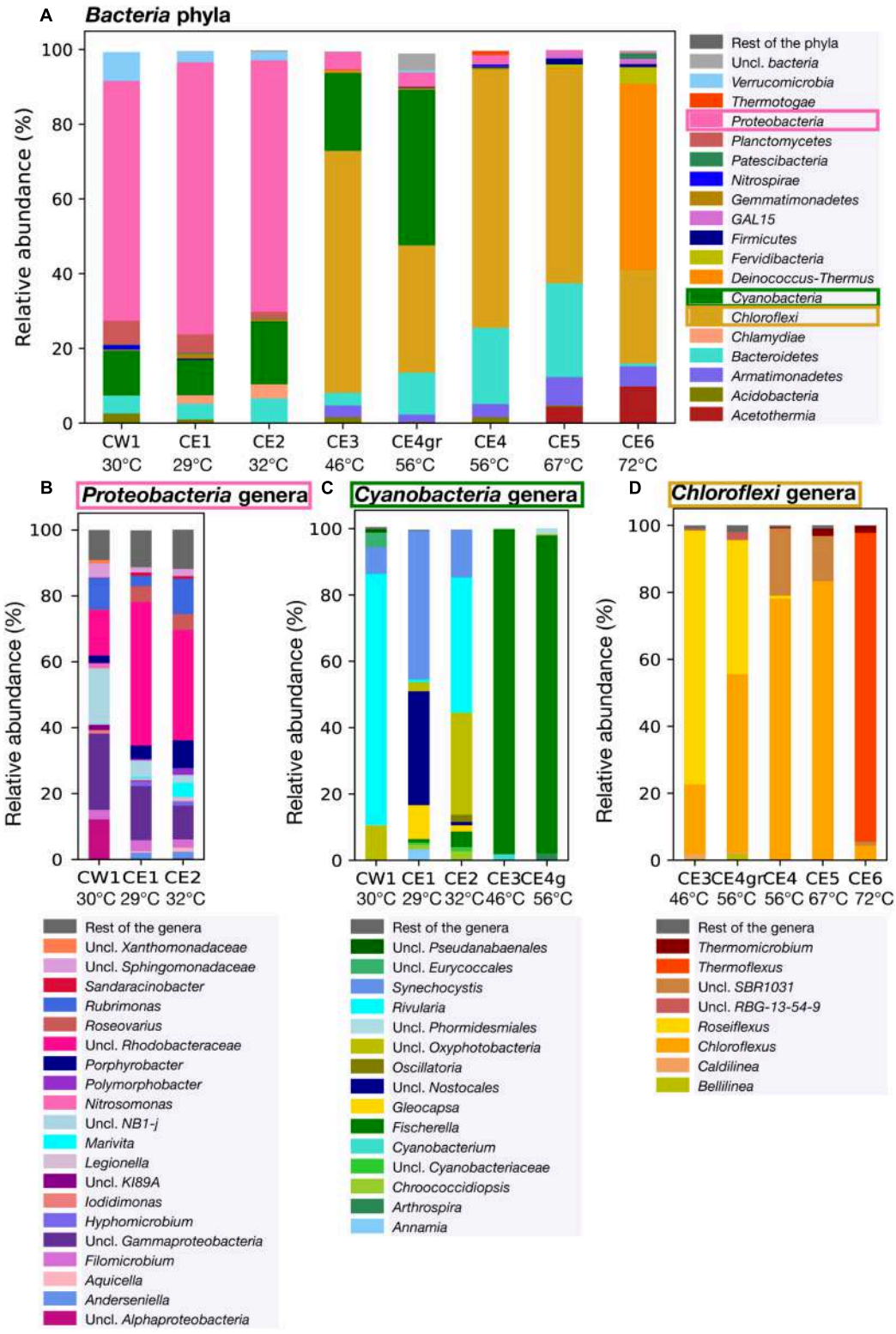

FIGURE 4 | Relative abundance of the bacterial community composition in the eight Cacao biofilms based on DNA sequencing. **(A)** Relative abundance of the bacterial phyla within the eight biofilms. **(B)** Relative abundance of *Proteobacteria* genera in the low-temperature biofilms (≤ 32°C), where the phylum was the most abundant. **(C)** Relative abundance of *Cyanobacteria* in biofilms of low and mid-temperature (from 29 to 56°C) at the genus level based on the 16S rRNA gene amplified with the specific primers for *Cyanobacteria*. Only the cyanobacterial profiles of the low temperature biofilms are shown, as this phylum was relatively more abundant in those samples. **(D)** Relative abundance of *Chloroflexi* in the mid to high-temperature biofilms (from 46 to 72°C) at the genus level. *Uncl,* unclassified.

Proteobacteria (**Figure 4B**), unclassified (uncl.) *Rhodobacteraceae* (within the *Rhodobacterales* order) were the most represented in CE1 and CE2 (44 and 34% of the *Proteobacteria* sequences, respectively), followed by uncl. *Gammaproteobacteria* (10% and 16%), and uncl. *NB1-j* (2 and 5%). In CW1, the dominance of the uncl. *Gammaproteobacteria* (23% of the *Proteobacteria* sequences) was followed by a similar representation of uncl. *NB1-j* (17%), uncl. *Rhodobacteraceae* (14%), and uncl. *Alphaproteobacteria* (12%). Among *Cyanobacteria,* the genera *Rivularia*, uncl. *Oxyphotobacteria* and *Synechocystis* dominated in CW1 and CE2, while those of *Synechocystis,* uncl. *Nostocales*, and *Gloeocapsa* dominated in CE1.

In the biofilms from 46 to 56°C, the proportion of *Cyanobacteria* increased to 21% in CE3 and 42% in CE4gr (**Figure 4A**). In contrast to the low-temperature biofilms, the qualitative distribution of *Cyanobacteria* in CE3 and CE4gr was substantially more homogeneous (**Figure 4C**) and was dominated by *Fischerella* (> 95% of the cyanobacterial sequences).

Together with *Cyanobacteria*, the phylum of *Chloroflexi* (i.e., green non-sulfur bacteria) started to be the most representative of the bacterial communities in the biofilms from temperatures ≥ 46°C (**Figure 4A**), with a maximum (69%) at 56°C (i.e., CE4). Qualitatively, the distribution of *Chloroflexi* also changed at the genus level among the biofilms at different temperatures (**Figure 4D**). *Roseiflexus* and *Chloroflexus* were the most represented genera in CE3 (76 and 21%, respectively) and CE4gr (53 and 40%, respectively). The relative abundance of *Chloroflexus* increased in biofilms at higher temperatures, from 20% in CE3 (46°C) to a maximum of 83% in CE5 (67°C), whereas the relative abundance of *Roseiflexus* dropped drastically at 56°C from 40% in CE4gr to 1% in CE4 (**Figure 4D**). In CE4 (56°C) and CE5 (67°C), *SBR1031* was the second most represented genus after *Chloroflexus*. Finally, at the highest temperature (72°C), the genus *Thermoflexus* dominated the *Chloroflexi* community (92%), with the lower representation of *Chloroflexus* (4%) and *Thermomicrobium* (2%).

Deinococcus-Thermus was a phylum almost exclusively detected in CE6, where it represented 50% of the bacterial sequences (**Figure 4A**). Other bacterial phyla represented in smaller proportions in CE6 samples were *Acetothermia* (10%), *Armatimonadetes* (5%), *Fervidibacteria, Firmicutes* (now *Bacillota*), and *Planctomycetes* (all < 5%). While *Bacteroidetes* (now *Bacteroidota*) was ubiquitous in the Cacao biofilms majorly up to 67°C, where it showed its maximum relative abundance (25%), the distribution of *Verrumicrobia* and *Planctomycetes* was mostly restricted to the biofilms at temperature ≤ 32°C, and that of *Acetothermia* to those at temperature ≥ 67°C (**Figure 4A**).

Similar to the bacterial community, the distribution of *Archaea* and *Eukaryota* also exhibited differences among the biofilms at different temperatures (**Supplementary Figure 5**). In the archaeal community, *Crenarchaeota* was the only phylum identified in the biofilms CE5 (67°C), CE6 (72°C), and CW1 (30 °C), and the most abundant in CE4 (56°C) (**Supplementary Figure 5A**). In contrast, a mix of *Thaumarchaeota, Euryarchaeota*, and *Nanoarchaeota* composed the archaeal community of CE1 (29°C), and that of CE2 (32°C) and CE4gr (46°C) was exclusively comprised by *Nanoarchaeota*. Concerning the *Eukaryota* domain, the 18S rRNA genes could only be amplified in the low-temperature biofilms CW1, CE1, and CE2 (**Supplementary Figure 5B**), with most of the sequences in CE1 and CE2 related to uncl. *Eukaryota* and those in CW1 to the *Nematoda* (55%) and *Arthropoda* (37%) phyla.

Richness (number of different OTUs) and diversity indices (Shannon-Wienner, Simpson, and Fisher) showed variations among samples, reflecting a relationship with temperature (**Table 3**). Bacteria and eukaryotes showed the highest diversity and richness at the lowest temperatures (i.e., CW1, CE1, and CE2), whereas cyanobacteria also showed similar richness up to 56°C and a variable diversity with temperature. Archaea were hardly detected in the samples, except in CE6, where 19,064 sequences and 42 different OTUs were obtained, although mainly composed of a single OTU (85% order *Desulfurococcales*, phylum *Crenarchaeota*), which explains the low Simpson's diversity value (0.26).

DISCUSSION

Biological Composition of the Fresh Biofilms Along the Cacao Hydrothermal Stream Based on Lipid Biomarkers

Lipids are cell membrane constituents with powerful diagnosis potential for several biological groups (i.e., biomarkers) that can be limitedly specific to some taxa (Summons et al., 2021). Their analysis provides identification of prevailing biological sources in an environmental sample and variable distribution patterns as a function of environmental factors. In the Cacao hydrothermal stream, we detected several lipid compounds that can be associated with diverse prokaryotic and eukaryotic biosources according to the literature (**Table 4**).

Low molecular weight compounds from 16 to 19 carbons [e.g., *n*-C_{17}, $C_{17:1}$, Me-C_{17}, and DMe-C_{17}, *n*-C_{19} alkanes; *n*-C_{17} alkanol; or 16:1 (ω5 or ω7), 18:1 (ω7 or ω9), and 18:3 (ω6) fatty acids] are often considered biomarkers, more or less, specific for cyanobacteria (see references in **Table 4**). For instance, prevailing peaks at *n*-C_{17} in molecular distributions of alkanes may be generally attributed to a cyanobacterial source in general, while the presence of heptadecane isomers or methyl heptadecanes (mono and di) may be more related to specific cyanobacterial clades (up to species), depending on the relative proportion of the isomers (Coates et al., 2014). In the present study, all the mentioned cyanobacterial biomarkers were observed to be dominant in the biofilms from temperatures ≤ 56°C (i.e., CW1, CE1, CE2, CE3, and CE4gr) (**Figure 2**), with also the presence of some of them [mostly the *n*-C_{17} and Me-C_{17} alkanes, as well as the 16:1 (ω7) fatty acid] in the highest-temperature biofilm (CE6). The latter, together with CE3 and CE4gr (and minorly CE5), showed a prevailing peak of heptadecane (*n*-C_{17}), with a relatively large proportion of mid-chain methyl heptadecanes (**Figure 2A**), which resembles the hydrocarbon composition described for the cyanobacterial genus *Fischerella* (Coates et al., 2014; Teece et al., 2020). The presence of such

TABLE 3 | Number of filtered sequences (Seqs), richness (number of different OTUs), and diversity indices (Shannon-Wiener or H′, Simpson, and Fisher) in the biofilm samples from the high-throughput sequencing of the 16S rRNA gene of bacteria, cyanobacteria, and archaea, and the 18S rRNA gene of eukaryotes.

		CW1	CE1	CE2	CE3	CE4gr	CE4	CE5	CE6
Bacteria	Seqs	144399	148819	125521	117441	169208	134093	111025	120713
	Richness	658	1268	1111	392	485	310	260	289
	H′	3.76	4.40	4.35	1.88	2.38	1.68	1.87	1.68
	Simpson	0.95	0.97	1.00	1.00	0.78	1.00	0.73	0.69
	Fisher	89.01	190.30	167.87	50.58	61.20	37.94	31.88	35.54
Cyanobacteria	Seqs	92627	87869	94367	90517	85339	19385	107	3576
	Richness	132	148	171	139	141	54	11	42
	H′	1.65	2.42	2.38	0.85	0.94	0.74	1.95	2.80
	Simpson	0.71	0.86	0.86	0.52	0.53	0.50	0.83	0.92
	Fisher	15.14	17.35	20.24	16.10	16.49	6.79	3.07	6.68
Archaea	Seqs	4	27	20	n.a.	160	91	245	19064
	Richness	3	4	2	n.a.	3	9	10	42
	H′	1.04	1.26	0.67	n.a.	0.72	1.64	1.03	0.66
	Simpson	0.63	0.69	0.48	n.a.	0.50	0.74	0.55	0.26
	Fisher	5.45	1.30	0.55	n.a.	0.52	2.48	2.10	5.11
Eukaryota	Seqs	41997	102884	47861	n.a.	n.a.	n.a.	n.a.	n.a.
	Richness	943	1787	1311	n.a.	n.a.	n.a.	n.a.	n.a.
	H′	2.16	1.86	2.63	n.a.	n.a.	n.a.	n.a.	n.a.
	Simpson	0.69	0.58	0.79	n.a.	n.a.	n.a.	n.a.	n.a.
	Fisher	171.26	307.21	249.07	n.a.	n.a.	n.a.	n.a.	n.a.

"n.a." indicates not available.

an alkane pattern mostly in CE3 and CE4gr, but also in CE6 and, to a lesser extent, in CE5 (**Figure 2A**) is compatible with cyanobacterial communities dominated by *Fischerella* from temperatures $\geq$ 46°C. In contrast, the distinct hydrocarbon pattern in CW1, CE1, and CE2 (i.e., rather dominated by isomers of the $C_{17:1}$ and/or *n*-C_{15}; **Figure 2A**) pointed to the dominance of alternative genera of cyanobacteria.

The ubiquitous detection of phytol in the polar fraction of all biofilms revealed the generalized presence of phototrophs along the Cacao hydrothermal transect (**Figure 2B**). This alcohol is a degradation product of chlorophyll and may be produced by phototrophic organisms, including (mostly) cyanobacteria, green algae, and higher plants but also green sulfur and non-sulfur bacteria (Didyk et al., 1978). The relative abundance of phytol over other free alcohols may assist in discriminating the specific biological source based on its primary photopigment. For instance, the predominance of phytol over octadecanoic (*n*-C_{18}) has been related to chlorophyll*a* and thus restricted to cyanobacteria (Shiea et al., 1991) or other oxygenic phototrophs (i.e., algae and higher plants), while the dominance of octadecanoic over phytol has been rather attributed to bacteriochlorophyll c_s, the major pigment in anoxygenic photoautotrophs, such as *Chloroflexus aurantiacus* (Ward et al., 1989). In the Cacao biofilms, the prominent presence of phytol over octadecanoic in CW1, CE1, CE2, C3, and CE4gr was argued to be most likely related to cyanobacterial sources, as well as to eukaryotic phototrophs according to the detection of phytosterols, such as campesterol, stigmasterol, or β-sitosterol (Volkman, 2003) and polyunsaturated fatty acids [18:3(ω6), 18:4(ω3), 20:4, or 20:5(ω3); Ahlgren et al., 1992; Dijkman et al., 2010] mostly in CE1 and CE2 (**Figures 2B,C**). In contrast, the inverse predominance of octadecanoic over phytol in CE4, CE5, and CE6 rather pointed to relative enrichment in *Chloroflexus*-like microorganisms in the high-temperature biofilms.

The hypothesis of relative enrichment in green non-sulfur bacteria with temperature was supported by the detection of a series of HMW polyunsaturated alkanes from 29 to 32 carbons and a maximum peak at 31:3 (i.e., hentriacontatriene) in samples of temperature $\geq$ 46°C, mostly CE4, CE5, and CE6 (**Figure 2A**). These HMW polyunsaturated alkanes are described, together with wax esters from C_{30} to C_{37}, as predominant lipidic compounds in mats of the thermophilic *Chloroflexus aurantiacus* and other phylogenetic relatives from the *Chloroflexi* phylum (van der Meer et al., 2008, 2000). In addition, wax esters from C_{38} to C_{40} have been also detected in *Chloroflexi* specimens, particularly from the species *Roseiflexus castenholzii* (van der Meer et al., 2010). In the Cacao stream, the detection of *Rosiflexus*-related wax esters was restricted to CE3 and CE4gr, whereas those associated with *Chloroflexus*-like microorganisms (from C_{33} to C_{37}) were more ubiquitous from CE3 to CE5 (**Supplementary Figure 4**).

Other microbial sources inferred from the lipid biomarkers include sulfate-reducing bacteria (SRB), green sulfur bacteria (GSB), and purple sulfur bacteria (PSB). The presence of SRB has been largely related to the detection of *i*/*a*-pairs of the C_{15} and C_{17} fatty acids (Taylor and Parkes, 1983), whereas that of GSB or PSB has been rather associated with the presence of cyclo-propyl acids of either 17(Cy-C_{17}) (Kenyon and Gray, 1974; Jungblut et al., 2009) or 19 (Cy-C_{19}) carbons (Grimalt et al., 1991; van der Meer et al., 1998), respectively. In the Cacao stream, the mentioned lipid biomarkers were generally detected in all

TABLE 4 | Potential biological sources of lipidic molecules isolated from the Cacao stream biofilms.

Compound	Potential biological source[a]	References
Hydrocarbons		
17:1	*Cyanobacteria*	Shiea et al., 1990; Grimalt et al., 1992; Coates et al., 2014
n-C_{17}	*Cyanobacteria*	Gelpi et al., 1970; Shiea et al., 1990; Coates et al., 2014
3/4/5/6/7Me-C_{17}	*Cyanobacteria*	Shiea et al., 1990; Teece et al., 2020; Coates et al., 2014
Me-C_{19}	*Cyanobacteria*	Kenig et al., 2005
Squalene	Most organisms, *Archaea* likely predominant	Grice et al., 1998
$\geq$ 29:n	*Chloroflexi*	Shiea et al., 1991; van der Meer et al., 1999, 2001
Diploptene	*Cyanobacteria*, methanotrophic bacteria	Gelpi et al., 1970; Rohmer et al., 1984; Sakata et al., 1997
Alcohols and Sterols		
n-C_{17}	*Cyanobacteria*	Bühring et al., 2009
Phytol	Phototrophs (plants, algae, *Cyanobacteria*, green sulfur and non-sulfur bacteria)	Didyk et al., 1978
Neophytadiene	Likely transformation product of phytol	Didyk et al., 1978
Dihydrophytol	Likely transformation product of phytol (from hydrogenation)	Didyk et al., 1978
Farnesol	Purple sulfur bacteria	Bühring et al., 2009
Cholesterol	Animals, microalgae, diatoms, red algae	Volkman, 2003
Demosterol	Precursor of cholesterol	Volkman, 2003
5,6-Dihydroergosterol	Possibly derived from ergosterol. Ascomycetes, basidiomycetes, unicellular green algae.	Nes and McKean, 1977; Weete et al., 2010
Stigmasterol	Higher plants (mostly) and microalgae	Volkman, 1986, 2003
Fucosterol	Microalgae, macroscopic brown algae, diatoms, detected in lacustrine *Bacillus* sp.	Patterson, 1972; Mercer et al., 1974
Stigmast-5-ene	Likely derived from stigmasterol (mostly higher plants and microalgae)	Volkman, 2003
Wax ester (C_{33} to C_{37})	*Chloroflexi* (*Chloroflexus aurantiacus* and relatives)	Shiea et al., 1991; van der Meer et al., 2000
Wax ester (C_{37} to C_{40})	*Chloroflexi* (genus *Roseiflexus*)	van der Meer et al., 2010
Fatty acids		
i/a-C_{15}, *i/a*-C_{17}	Gram-positive bacteria, sulfate-reducing bacteria	Taylor and Parkes, 1983; Lei et al., 2012
16:1 (ω5)	*Cyanobacteria*	Coates et al., 2014
16:1 (ω7)	*Cyanobacteria*	Ahlgren et al., 1992; Dijkman et al., 2010; Coates et al., 2014
Cy-C_{17}	Gram-negative bacteria, anaerobic bacteria, sulfur- and iron-oxidizing bacteria, green sulfur bacteria	Kenyon and Gray, 1974; Jungblut et al., 2009
18:1 (ω7/9)	*Cyanobacteria*	Ahlgren et al., 1992; Dijkman et al., 2010; Coates et al., 2014
18:2 (ω6)	*Cyanobacteria*	Ahlgren et al., 1992; Jungblut et al., 2009; Dijkman et al., 2010
18:3 (ω6)	Microalgae/Diatoms/*Cyanobacteria*	Ahlgren et al., 1992; Jungblut et al., 2009; Dijkman et al., 2010
18:4 (ω3)	Microalgae/Diatoms/*Cyanobacteria*	Ahlgren et al., 1992; Dijkman et al., 2010
Cy-C_{19}	Gram-negative bacteria, anaerobic bacteria, sulfur-oxidizing bacteria, purple sulfur bacteria	Grimalt et al., 1991; van der Meer et al., 1998; Jungblut et al., 2009
20:4 (ω10)	Diatoms	Ahlgren et al., 1992; Dijkman et al., 2010
20:5 (ω3)	Diatoms	Ahlgren et al., 1992; Dijkman et al., 2010

*For nomenclature details, see **Figure 2**.*
[a]*Most likely biological source, considering the compound-specific stable-carbon isotopic composition observed here (**Figure 3**).*

biofilms (**Figure 2C**), suggesting the ubiquitous presence of SRB, GSB, and PSB along the hydrothermal gradient, although with the greater relative abundance of SRB in CE2, CE3, and CE6; of GSB in CE4gr and CE4; and of PSB in CE6.

Finally, the contribution from eukaryotic sources other than green algae and higher plants was inferred from the detection of sterols, such as cholesterol and derivatives (i.e., present in animals or microalgae; Volkman, 2003), fucosterol (a biomarker of microalgae and macroscopic brown algae; Patterson, 1972; Mercer et al., 1974), and 5,6-dihydro ergosterol (likely derived from ergosterol, a biomarker of fungi; Patterson, 1972; Nes and McKean, 1977). Except for cholesterol and cholestanol, which were also detected in CE6, all other sterol compounds were almost exclusively found at temperatures $\leq$ 46°C, mostly in CE1 and CE2, which illustrates the preference of the local eukaryotic organisms (mostly those related to algae and plants) to low temperatures ($\leq$32°C).

Carbon Metabolism of Microbial Communities Along the Cacao Hydrothermal Transect

Compound-specific stable carbon isotope analysis may provide a rapid screening tool for carbon fixation pathways (**Supplementary Text 1**). Autotrophic organisms build their biomass by incorporation of inorganic carbon, primarily in the form of (mostly atmospheric) CO_2 or dissolved inorganic carbon (mostly HCO_3^-), which show different carbon isotopic compositions ($\delta^{13}C$), varying from values as low as ca. –8‰ in atmospheric CO_2 (Graven et al., 2017) to as high as from ca. –2 to 0‰ in bicarbonate (Mook et al., 1974). Because of the enzymatic preference for $^{12}CO_2$ relative to $^{13}CO_2$, carbon isotopic fractionation occurs during carbon fixation, a discrimination process against the heavy isotope that varies widely, depending on the carbon assimilation pathway (Hayes, 2001; Jahnke et al., 2001). Thus, knowing the bulk or compound-specific isotopic composition of a sample, we can infer the metabolic pathway followed by the autotrophs (**Supplementary Text 1**) and learn about the microbial community composition, as different phylogenetic lineages assimilate inorganic carbon typically, using a particular pathway (Hügler and Sievert, 2011).

In the Cacao stream, the compound-specific $\delta^{13}C$ patterns of the lipids in three polarity fractions revealed different metabolic traits along the hydrothermal transect. In the apolar fraction, the compound-specific $\delta^{13}C$ clustered into three groups of values (**Figure 3A**): (i) those highly enriched in ^{13}C (i.e., $\delta^{13}C$ from –12.3 to + 4.9‰) of the HMW compounds, (ii) those highly depleted in ^{13}C (i.e., $\delta^{13}C$ from –30.6 to –18.2‰) of the mid-molecular-weight compounds, and (iii) a much broader range of values, ranging from –29.9 to –8.4‰ of the LMW compounds. The most enriched $\delta^{13}C$ values measured in the *Chloroflexus*-related HMW polyunsaturated compounds, mostly in CE4 and CE5 (**Figure 2A**), are compatible with the use of the 3HP bicycle (van der Meer et al., 2000). The most depleted $\delta^{13}C$ values (i.e., ca. < -18‰) were detected in (linear or branched) saturated alkanes of all samples, but CE1 and CE2 (**Figure 3A**) were consistent with a Calvin-mediated carbon fixation (Hayes, 2001). Finally, the intermediate $\delta^{13}C$ values (ca. from –18 to –8‰) largely found in CE1 and CE2 were, instead, compatible with a predominance of the rTCA pathway (Preuß et al., 1989; Hayes, 2001) or mixed participation of different metabolic routes. Typical users of the rTCA cycle that were detected in CE1 and CE2 are *Chlorobiales*, *Nitrospirae*, or ε-*Proteobacteria* (Takai et al., 2005; Hügler and Sievert, 2011). Thus, the compound-specific $\delta^{13}C$ distribution in the apolar fraction reflects some fragmentation of the carbon assimilation pathways as a function of the temperature (**Figure 3A**), with a predominance of the rTCA at low temperatures, of the 3HP (mostly) from 56 to 67°C, and with the ubiquity of the Calvin cycle at all temperatures.

In the polar and acidic fractions, the distribution pattern of $\delta^{13}C$ with the biofilm temperature was relatively less defined. Still, the range of $\delta^{13}C$ values in the polar fraction (ca. from –26.7 to –2.3‰) covered fingerprints associable with the use of different carbon assimilation routes, with a general predominance of rTCA, together with 3HP in CE4 and CE5, or Calvin in CW1, CE3, and CE4gr (**Figure 3B**). In the acidic fraction, the range of $\delta^{13}C$ values was even broader (ca. from –33.5 to +2.3‰) and covered even more carbon metabolic pathways. The compound-specific isotopic signature of the fatty acids in the low-temperature samples CE1 and CE2 reflected a predominant use of the rTCA pathway, while those in CE3 and CE4gr appeared to combine rTCA with the Calvin cycle. The most enriched $\delta^{13}C$ values in CE4 and CE5 denoted instead relatively greater employment of the 3HP bicycle apart from the rTCA cycle, while the most depleted $\delta^{13}C$ values in the highest-temperature CE6 suggested the use of the r-acetyl-CoA pathway, likely together with the Calvin cycle (**Figure 3C**). Interestingly, the most negative $\delta^{13}C$ values in CE6 were detected in fatty acids of *i*/*a* configuration (*i*/*a*-C_{15}, *i*-C_{16}, *i*/*a*-C_{17}, and *i*-C_{18}) related to sulfate reduction (Taylor and Parkes, 1983; Jiang et al., 2012). SRB are metabolically versatile microorganisms that can degrade a wide variety of organic compounds heterotrophically, while some can also grow autotrophically, fixing inorganic CO_2 into central metabolic intermediates like acetyl-CoA (Widdel and Hansen, 1992). The lowest $\delta^{13}C$ values measured in CE6 could be explained by either the autotrophic assimilation of carbon through the r-acetyl-CoA pathway or the heterotrophic growth of SRB on isotopically depleted biomass (e.g., from r-acetyl-CoA or Calvin cycle users). The relevant contribution of the r-acetyl-CoA pathway in the high-temperature CE6 was reflected in the isotopic composition of the organic matter (i.e., TOC), which showed the lowest bulk $\delta^{13}C$ value (**Figure 3**).

Considering together the stable-carbon isotopic composition of the lipid biomarkers from the apolar, polar, and acidic fractions, we conclude that the microbial transition along the hydrothermal transect is accompanied by an alternate of the carbon metabolic routes, where the use of the rTCA pathway is ubiquitous along the whole temperature spectrum, whereas the Calvin cycle is relatively more relevant mostly in samples up to 56°C, the 3HP bicycle in samples from 46 to 72°C, and the r-acetyl-CoA pathway almost exclusively in CE6 (i.e., 72°C).

The DNA Sequencing Qualitatively Validated the Forensic Capacity of the Lipid Biomarkers to Identify Primary Biosources in the Cacao Hydrothermal Stream

The combination of molecular and isotopic analysis of lipid biomarkers allowed us to identify the primary biosources and autotrophic metabolism prevailing along the Cacao hydrothermal stream. Whereas a biological source assessment based on lipid biomarkers commonly entails a generalist reconstruction of the community structure, in this study, we were able to detect some relatively specific molecules (e.g., *Fischerella* related 4, 5, and 6 Me-C_{17} alkanes; *Chloroflexus*-attributed dominance of *n*-octadecanoic over phytol; or *Rosiflexus*-related C_{38} wax esters) that could be more precisely linked to particular biological sources (i.e., at the genus level). To test the validity of the identity assignation derived from using the lipid biomarkers, we first needed to learn about the phylogeny of

the hydrothermal microbial community. To that end, we used a taxonomically specific technique such as DNA sequencing. We thus compared the microbial community structure built on 16S and 18S rRNA gene sequencing data, with the compositional reconstruction based on lipid biomarkers, to qualitatively calibrate the taxonomic diagnosis precision of the latter.

The DNA sequencing returned a microbial community structure that reflected relevant compositional differences between the samples. Overall, the microbial community was richer and more diverse in the low-temperature (≤32°C) samples (i.e., CW1, CE1, and CE2) than those above 46°C (**Table 3**), where the high temperature may favor the dominance of specialized microorganisms, resulting into less diverse communities. Interestingly, despite the low microbial richness and diversity measured in CE3 and CE4, these samples showed the highest biomass concentrations measured as TOC (**Table 2**). This could be related to a relatively large proportion of exopolysaccharides (i.e., a binding agent) in these slime and jelly-like biofilms at the steepest part of the transect compared to the other samples, situated in less dynamic zones and, instead, composed of thin layers, green flocculates, or disaggregated biomass of rougher and less jelly appearance. Furthermore, it cannot be ruled out that, considering the ever-changing conditions of hydrothermal systems, the actual temperature in this part of the hydrothermal channel is likely to move between 40 s °C and 50 s °C rather than being fixed at the putative 56°C measured at the time of sampling. Such a temperature range could be favorable/tolerable for both mesophilic and thermophilic microorganisms, thus leading to a relatively higher ecological productivity (i.e., biomass).

The compositional differences were already clearly visible at the phylum level (**Figure 4A**), where the microbial composition of the lowest-temperature biofilms (≤32°C) was largely dominated by *Proteobacteria* and *Cyanobacteria*, the mid-temperature biofilms (from 46 to 56°C) by *Cloroflexi* and *Cyanobacteria*, the high-temperature biofilms (from 56 to 67°C) by *Cloroflexi* and *Bacteroidetes*, and the highest-temperature biofilm (72°C) by *Deinococcus-Thermus, Chloroflexi*, and *Acetothermia*. The taxonomic differences observed along the thermal spectrum were generally mimicked at the isotopic level by the lipid biomarkers (**Figure 3**). Thus, the isotopic composition of the lipid biomarkers reflected a combined use of the rTCA and Calvin (mostly in CW1) cycles in samples with a high representation of *Proteobacteria* and *Cyanobacteria* (CW1, CE1, and CE2); a dominant use of the Calvin cycle in those with relatively higher abundance of *Cyanobacteria* (CE3 and CE4gr); a prevailing use of the 3HP bicycle in samples with the highest relative abundance of *Chloroflexi* (CE4 and CE5); and a combination of the Calvin and r-acetyl-CoA pathway in CE6, where the most representative phyla (*Deinococcus-Thermus* or *Acetothermia*) are thermophiles reported to fix inorganic carbon through the r-acetyl-CoA pathway (Takami et al., 2012; Badhai et al., 2015).

The taxonomic composition of the microbial community in the low-temperature samples (≤32°C) was largely composed of uncl. *Rhodobacteraceae*, uncl. γ-*Proteobacteria*, *Rubrimonas*, and uncl. *NB1-j* (**Figure 4B**). In contrast to CE1 and CE2 of fairly comparable *Proteobacteria* communities at the genus level, CW1 showed more relative abundance of uncl. α-*Proteobacteria,* uncl. γ-*Proteobacteria,* and uncl. *NB1-j.* While the set of lipid compounds detected did not include biomarkers specific enough to reflect the taxonomic composition of the Cacao *Proteobacteria* community, their compound-specific carbon isotopic composition provided instead metabolic clues that explained, to some extent, the taxonomic variability observed between the three samples. Overall, lipid compounds in CW1 were generally imprinted by Calvin $\delta^{13}C$ signatures (**Figure 3**) consistent with their relative abundance of Calvin users, such as α-*Proteobacteria* and γ-*Proteobacteria* (Hügler and Sievert, 2011). In contrast, the higher $\delta^{13}C$ values in CE1 and CE2 suggested relatively greater use of the rTCA cycle, potentially conducted by some of the abundant unclassified *Proteobacteria* (**Figure 4B**).

The relevant presence of *Cyanobacteria* in CW1, CE1, CE2, CE3, and CE4gr was correctly diagnosed by the lipidic approach, where several biomarkers of the mentioned phylum (*n*-C_{15}, *n*-C_{17}, $C_{17:1}$, Me-C_{17} alkanes; and 16:1 and 18:1 fatty acids) were detected mostly ≤ 56°C (**Figures 2A,C**). Zooming in at the genus level, the DNA sequencing showed further compositional differences in the *Cyanobacteria* community, with *Rivularia* representing most of the cyanobacterial sequences in CW1; *Synechocystis* and uncl. *Nostocales* in CE1; uncl. *Oxyphotobacteria* and *Rivularia* in CE2; and *Fischerella* in CE3 and CE4gr (**Figure 4C**). The relevant presence of *Fischerella* from 46 to 56°C (>95% of the cyanobacterial sequences) was anticipated by the lipid biomarkers 5Me-C_{17} and 6Me-C_{17} (Coates et al., 2014; Teece et al., 2020), whose detection was prominent in CE3 and CE4gr (**Figure 2A**). In the biofilms from lower temperatures, the different distribution patterns of (apolar and acidic) cyanobacterial biomarkers (**Figure 4**) suggested an abundance of alternative genera. We hypothesize that the characteristic predominance of pentadecane (*n*-C_{15}), together with certain isomers of heptadecene [17:1(II) and (IV)] and nonadecene [19:1 (I)] observed in CE3 (**Figures 2A,C**) could be related with a relative abundance of the class *Oxyphotobacteria* (**Figure 4C**), whereas the prevalence of 17:1 [II] among the isomers of heptadecene in CE1 (**Figure 2A**) could be related, instead, to the order *Nostocales* (**Figure 4C**). While a precise identification of the different isomers of heptadecene was not possible [i.e., 17:1(I-IV) in **Figure 2A**], each isomer could be related to specific cyanobacteria genera according to their different relative distribution in the samples CW1, CE1, and CE2 (**Figure 4C**).

In the *Chloroflexi* phylum, the analysis at the genus level of the samples, containing more than 1% of *Chloroflexi* sequences within the bacterial community, revealed compositional differences between samples (**Figure 4D**). From 46 to 56°C, the biofilms were largely composed of *Roseiflexus* (mostly CE3) and *Chloroflexus* (mostly CE4gr). From 56 to 67°C, the proportion of *Roseiflexus* decreased drastically at the expense of mostly *Chloroflexus*, whose abundance increased progressively with temperature. At 72°C, a completely different *Chloroflexi* community consisted greatly of *Thermoflexus* and minority proportions of *Chloroflexus* and *Thermomicrobium*.

Overall, this *Chloroflexi* community structure agreed with the presence of a *Roseiflexus*-related C_{38} wax ester (van der Meer et al., 2010) only in CE3 and CE4gr (**Supplementary Figure 4**), and the ubiquitous detection of *Chloroflexus*-related biomarkers (HMW polyunsaturated alkanes and wax esters from C_{33} to C_{37} (van der Meer et al., 2000, 2008) in all samples from water temperature $\geq$ 46°C (**Figure 2A** and **Supplementary Figure 5**).

In sum, the taxonomic identification based on the DNA sequencing results confirmed, to a reasonable extent, the qualitative microbial community structure built on the lipid biomarkers. While the taxonomic specificity of the lipid biomarkers is not as high as that of the DNA due to their nature (i.e., lipids are structural components of cell membranes generally present in most phylogenetic groups), they can provide (more or less specific) both identity assignation and metabolic traits identification by combining their analysis at molecular and isotopic levels. Thus, the microbial community composition of the Cacao biofilms was defined, reaching in some cases relatively good taxonomic fidelity at phylum (e.g., *Cyanobacteria* or *Chloroflexi*) or even the genus (e.g., *Fischerella*, *Roseiflexus*, or *Chloroflexus*) level, whereas, in other cases, it responded to more general criteria, such as ecology or metabolism (e.g., thermophiles, SRB, GSB, or PSB). Therefore, using the DNA sequencing technique, we qualitatively validated the forensic capacity of the lipid biomarkers to reconstruct the microbial community in the Cacao hydrothermal stream and to trace the evolution of the biofacies with temperature.

Ecological Singularities Along the Cacao Hydrothermal Stream

The combined (molecular and isotopic) analysis of lipid biomarkers with the DNA sequencing analysis allowed us to recreate the ecological system along the Cacao hydrothermal transect, where a transition of microbial components and prevailing metabolisms was observed from the hot hydrothermal vent to the cooler waters downstream (**Figure 5**). The prevalence of thermophiles at 72°C gave way to a microbial community dominated by *Chloroflexi* from 56 to 67°C, to one of the coexisting *Cyanobacteria* (mostly *Fischerella*) and *Chloroflexi* (*Roseiflexus* and *Chloroflexus*) from 46 to 56°C, and then, to a population of abundant mesophilic *Proteobacteria* (mainly *Rhodobacterales*) and *Cyanobacteria* (**Figure 5**). This microbial succession was coupled with a metabolic gradient from generally ubiquitous rTCA and prevailing r-acetyl-CoA and 3HP r-acetyl-CoA pathways at high temperatures toward Calvin assimilation routes as the water temperature decreased (**Figure 5**). The reconstruction of this sequence has ecological significance, as trends in the composition and metabolism of the microbiota along thermal gradients (from high to low temperature) somehow mimic the sequence of evolutionary events inferred by the SSU rRNA phylogenetic tree for the global biosphere, from thermophilic species to anoxygenic and oxygenic photosynthetic species (Farmer, 2000).

The thermophilic community at 72°C was largely composed of *Deinococcus-Thermus* (mostly *Thermus*), *Chloroflexi* (mostly *Thermoflexus*), and *Acetothermia* (**Figure 4A**), as well as *Crenarchaeota* (**Supplementary Figure 5**). The relative abundance of the orangish *Thermus* at the hottest site in Cacao (i.e., the hot spring vent at 72°C) agreed with the temperature distribution reported for the thermophilic genus in other hydrothermal systems from Island, the Yellowstone National Park, or the northern Thailand, where the temperature ranged from 75 to 89°C (Purcell et al., 2007). Other thermophilic components of CE6 were *Acetothermia*, a recently proposed phylum of thermophilic and chemolithotrophic bacteria likely related to *Thermotogae* (Rinke et al., 2013), and *Thermoflexus*, a heterotrophic bacterium from the *Chloroflexi* phylum (Thomas et al., 2021).

At 67°C, a first compositional shift was observed from dominant thermophiles to that of the *Chloroflexi* community (**Figure 4D**), with a prominence of *Chloroflexus* from 67 to 56°C (CE4) or *Roseiflexus* from 56 (CE4gr) to 46°C (CE3). The relative abundance of *Roseiflexus* or *Chloroflexus* was explained by the respective optimum growth of both genera from either 45 to 55°C and from 52 to 60°C, respectively (Pierson and Castenholz, 1974; Hanada et al., 2002). Their relative distribution in the Cacao hydrothermal stream was consistent with those previously described in hydrothermal systems from the Yellowstone National Park, such as the Mushroom and Octopus hot springs (Ward et al., 2012).

The compositional shift in the *Chloroflexi* community was accompanied by changes in the biofilm color (green-orange in CE4, intense green in CE4gr, and red-orange in CE3; **Figure 1**), which may, in turn, denote metabolic shifts. Whereas the red-orange-brownish tones of CE3 were associated with the relative abundance of *Roseiflexus* in this biofilm (Hanada et al., 2002), the green color in CE4gr was instead related to specific proportions of *Fischerella* and/or *Chloroflexus*. Concerning *Chloroflexus*-rich CE4, green and orange filaments in this biofilm could denote variable availability of oxygen, as *Chloroflexus* may form microbial mats of either dull green or orange aspect depending on aerobic or anaerobic conditions, respectively (Pierson and Castenholz, 1974). Thus, the coexistence of green and orange filaments in the stream middle channel suggests a possible metabolic transition in the *Chloroflexi* community at 56°C from photoheterotrophy to photoautotrophy. Species of both *Roseiflexus* and *Chloroflexus* are capable of growing photoheterotrophically by synthesis of chlorophyll in anaerobiosis, while some *Chloroflexus* sp. strains are photoautotrophic, fixing inorganic carbon through the 3HP bicycle (Pierson and Castenholz, 1974; van der Meer et al., 2010). While lipids synthesized through the 3HP bicycle are typically enriched in ^{13}C (Hayes, 2001), those resulting from a heterotrophic growth are generally less enriched (i.e., more negative) because most of the carbon heterotrophically assimilated by the *Chloroflexaceae* derives from fermentation products and other photosynthates released by cyanobacteria (van der Meer et al., 2010) that fix carbon through the

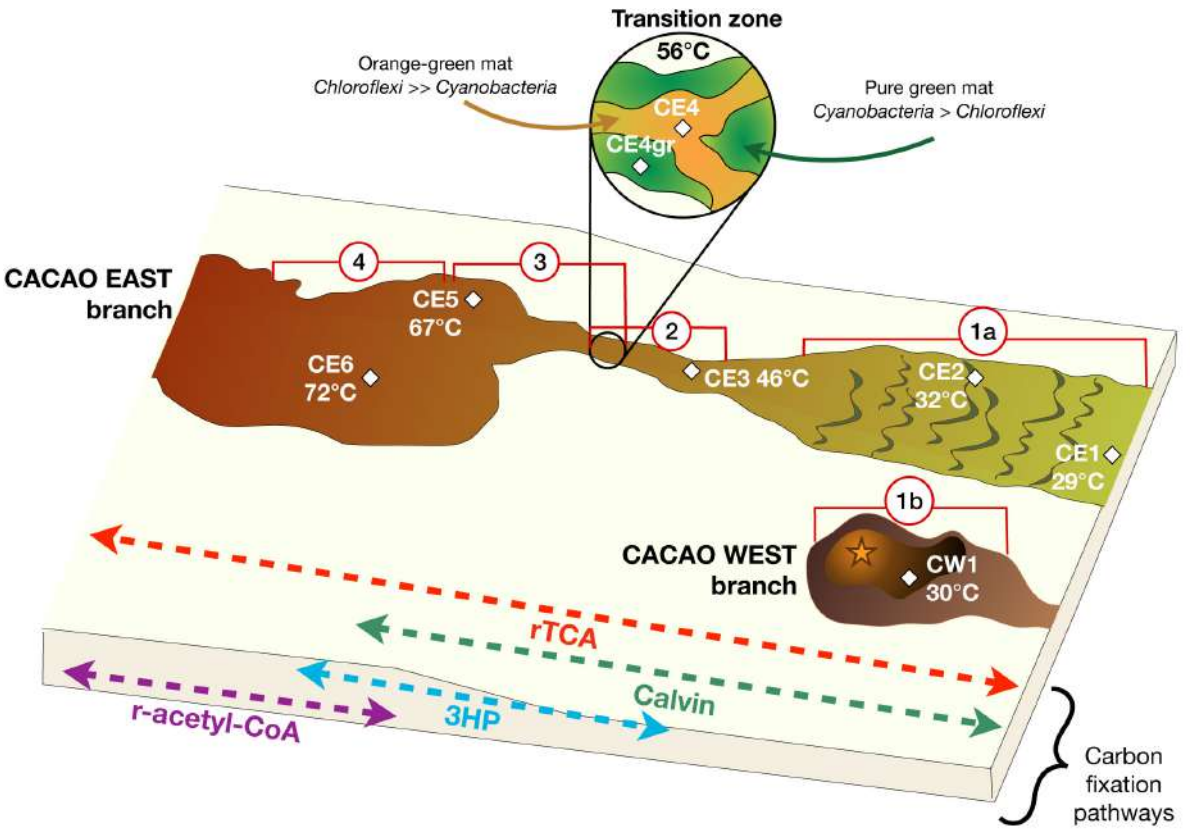

	4 HIGHEST-TEMPERATURE POOL (72°C)	3 HIGH-TEMPERATURE POOL-CHANEL (56-67°C)	2 MID-TEMPERATURE LOWER CHANNEL (46-56°C)	1 LOWEST-TEMPERATURE TERRACETTES (29-32°C)	
				1a East branch	1b West branch
Main phyla and genera	*Deinococcus-Thermus* (*Thermus*)	*Chloroflexi* (*Chloroflexus*)	*Cyanobacteria* (*Fischerella*)	*Proteobacteria* (uncl. *Rhodobacteraceae* & uncl. *Gamma-proteobacteria*)	*Proteobacteria* (uncl. *Gamma-proteobacteria* & uncl. *NB1-j*)
	Chloroflexi (*Thermoflexus*)	*Bacteroidetes* (uncl. *SM1H02* & *Rhodothermus*)	*Chloroflexi* (*Chloroflexus* & *Roseiflexus*)	*Cyanobacteria* (*Synechocystis*, uncl. *Nostocales* & *Rivularia*)	*Cyanobacteria* (*Rivularia*, uncl. *Oxyphotobacteria* & *Synechocystis*)
	Acetothermia				

FIGURE 5 | Ecological reconstruction of the microbial community distribution along the Cacao hydrothermal transect based on lipid biomarkers and DNA sequencing. The hydrothermal ecosystem was defined by a succession of microbial community structures and metabolic traits along the temperature gradient, with dominance of thermophilic species at high temperature, of anoxygenic photosynthetic species at intermediate temperatures (67–46°C), and mesophilic and oxygenic photosynthetic species at low temperature (≤32°C). In the channel, the compositional and metabolic transition at 56°C represented an ecological tipping point where aerobic and anaerobic conditions may alternate (from coexistence of *Cyanobacteria* and *Chloroflexi* to dominance of *Chloroflexi* and from a *Chloroflexi* community, largely photoheterotrophic to one mostly photoautotrophic). The abbreviation "uncl" means unclassified.

Calvin cycle (i.e., strongly depleted in ^{13}C). In the Cacao stream, the slight isotopic depletion of the *Chloroflexi*-lipid biomarkers in the red-orange CE3 and the green CE4gr relative to those in CE4 and CE5 (**Figure 3A**) was compatible with a mixotrophic growth of the *Chloroflexi* community (mostly *Roseiflexus* in CE3, and mix of *Roseiflexus* and *Chloroflexus*

in CE4gr) below 56°C, and photoautotrophic above 56°C (mostly *Chloroflexus* in CE4 and CE5). In CE3 and CE4gr, the co-occurrence of *Cyanobacteria* and *Chloroflexaceae* may explain a photoheterotrophic growth of the latter by cross-feeding on the relatively ^{13}C-depleted cyanobacterial exudates (van der Meer et al., 2008). This would have resulted in isotopic compositions, ranging between those typical of strict use of either the Calvin or the 3HP cycle. In contrast, the negligible amount of *Cyanobacteria* in CE4 and CE5 (**Figure 4A**) would have limited the growth of the *Chloroflexus*-dominated *Chloroflexi* community to an autotrophic mode. Thus, the relative proportion of *Cyanobacteria* and *Chloroflexi* as determined by DNA sequencing appears to be a key to determine the isotopic signatures of the biofilms along the hydrothermal gradient, with 56°C representing a compositional and metabolic tipping point (**Supplementary Figure 6**).

A last compositional shift was observed at 46°C for a *Cyanobacteria* community dominantly composed of *Fischerella* to one represented by a variety of genera, such as *Synechocystis, Nostocales, Rivularia,* or *Oxyphotobacteria* at $\leq$ 32°C (**Figure 4C**). The detection of *Rivularia*, *Chroococcidiopsis*, *Cyanobacterium*, or *Nostocales* was consistent with previous descriptions of El Tatio (Phoenix et al., 2006; Gong et al., 2021; Wilmeth et al., 2021), whereas other genera, such as *Phormidium, Lyngbya, Leptolyngbya*, or *Calothrix*, previously identified in regional hot springs (Fernández-Turiel et al., 2005; Phoenix et al., 2006; Wilmeth et al., 2021), were not found in the present study. To the best of our knowledge, it is the first time that some genera of *Cyanobacteria* (e.g., *Synechocystis*, *Gloeocapsa*, or *Annamia*) are reported in the geysers field of El Tatio. The predominance of the genus *Fischerella* in the cyanobacterial community of Cacao from 46 to 56°C was comparable to that observed in a similar hydrothermal system at Yellowstone National Park (*White Creek*) between 39 and 55°C (Ward et al., 2012). However, the detection of *Fischerella* biomarkers occurs up to 72°C, a temperature very close to the upper limit of chlorophyll *an* (i.e., degradation at ∼73–74°C; Miller and Castenholz, 2000). While some species of *Fischerella* are considered to be thermophilic representatives of *Cyanobacteria* (i.e., able to grow well or best above 45°C; Castenholz, 1981), the maximum temperature at which this genus had been observed so far is ∼60°C (Ward et al., 2012; Wilmeth et al., 2021). While Wilmeth et al. (2021) have described recently the presence of *Fischerella* (11% of cyanobacterial sequences) in microbial mats at 61°C in hot springs from the Middle Basin at El Tatio, this is the first time that its biomarkers are found at a temperature as high as 72°C. We consistently detected in CE6 DNA sequences of *Fischerella* (901 sequences, representing 25% of the total cyanobacterial sequences in CE6; **Supplementary Table 2**), as well as lipid biomarkers associated with this genus (i.e., the relative abundance of 5Me-C_{17} and 6Me-C_{17}; Coates et al., 2014; **Figure 2A**).

As a result, the microbial ecosystem in the Cacao hydrothermal stream was defined by a transition of microbial communities and metabolic traits along the temperature gradient, where 67, 56, and 46°C represented ecological tipping points. Understanding the principles of microbial community ecology in modern, operative thermal spring systems is paramount for learning how to interpret the paleobiology of ancient hydrothermal deposits on Earth.

Paleobiological and Astrobiological Relevance of Understanding Modern Hydrothermal Ecosystems

Highly resistant lipid biomarkers offer a powerful forensic tool for the detection of biological signals over geologically relevant periods with relevance for paleobiology and astrobiology. In contrast to DNA and other labile biomolecules, lipid compounds can be preserved in the geological records for up to billions of years (Brocks et al., 2005) through mechanisms such as mineral-organic interaction, xero preservation, or mineral entombment (e.g., in silica sinter). Lipid profiles displaying comparable transitions with temperature to those observed here have been described in silica sinter deposits from worldwide hydrothermal systems; Yellowstone National Park in the US (e.g., Parenteau et al., 2014), the Taupo Volcanic Zone in New Zealand (e.g., Pancost et al., 2006; Campbell et al., 2015), or El Tatio in the Chilean *Altiplano* (e.g., Sánchez-García et al., 2019; Teece et al., 2020). To correctly underpin the paleoecological interpretation of fossil hot spring deposits, a detailed understanding of the primary biosignatures before silicification is essential. Here, we determined the molecular and isotopic fresh end members of the local microbiota at El Tatio to provide a kind of "qualitative calibration" of the lipid biomarkers at the local scale that will be a key to interprete fossil records in this or other similar spring systems on Earth. Furthermore, by unveiling the molecular and isotopic fingerprints of life in modern silica-rich hot springs with the same analytical technique (i.e., GC-MS) currently employed (a NASA-funded MSL SAM instrument) or to be employed soon (an ESA-funded ExoMars MOMA instrument), we contribute to provide robust criteria for recognizing hypothetical biogenic features in analogous silica deposits on Mars. The close resemblance of the nodular and digitate silica deposits at El Tatio with the opaline silica structures discovered by the Spirit rover at Gusev Crater makes the hydrothermal system of El Tatio a primary study site for deciphering fossil biomarkers records in ancient silica deposits on Mars. Interpreting its modern biosignatures in fresh biofilms is a key to advancing our strategies to explore signatures of life or prebiotic chemistry on silica structures on Mars.

However, the interpretation of potential life signals beyond the Earth requires extreme caution, especially regarding the possible ambiguity of biogenicity. The Astrobiology Community agrees that the first point to elucidate when dealing with possible extraterrestrial biosignatures is to discern the actual biogenicity of the signal to avoid "false positives" (i.e., morphologies, textures, patterns, or compounds that resemble life but are abiotic). There are several ways to differentiate abiotically synthesized from biologically generated lipid compounds. One criterion for discriminating between biogenic vs abiogenic origin of organics is attending to the molecular distribution within a compound family or polarity fraction (i.e., hydrocarbons, fatty

acids, or alcohols). Abiotic hydrocarbons resulting from Fischer-Tropsch reactions show typical Schultz-Flory distributions of smooth, homogeneous decreasing abundance with increasing carbon numbers (Szatmari, 1989), absence of molecular patterns, and lack of even-over-odd or odd-over-even carbon number predominance in oxygenated (fatty acids and alcohols) or defunctionalized hydrocarbon (alkanes and alkenes) series, respectively (McCollom et al., 1999). In contrast, biogenic lipid series, instead, show irregular distributions with a preference for the even or odd carbon numbers, the presence of one or more peaks of compounds standing out from the rest (e.g., in this study, cyanobacterial heptadecane and heptadecane isomers or *Chloroflexus*-associated long-chain polyunsaturated alkenes in the apolar fraction; **Supplementary Figure 3A**), as well as of other compounds than saturated and *normal* hydrocarbons (e.g., isoprenoids, monomethyl alkanes, or hopanes). In addition, a Schultz-Flory distribution of synthetic hydrocarbon mixtures produces nearly constant ratios (below ∼0.6) of the compounds with successive carbon numbers (i.e., C_{n+1}/C_n; Szatmari, 1989), while biogenic alkane series instead generate variable and heterogeneous values of the ratio.

Another criterion often used to assess the biogenicity of a carbonaceous material is considering its stable carbon isotopic composition. Overall, ^{13}C-depleted signatures derived from a strong fractionation against the heavier carbon isotope relative to the inorganic source of carbon are typically attributed to biological sources, since no known inorganic process results in long-chain carbonaceous material being depleted in ^{13}C as living organic matter (Peters et al., 2005). However, laboratory experiments reproducing Fischer-Tropsch reactions have reported synthesized hydrocarbons with $\delta^{13}C$ values as depleted relative to CO_2 as much as 36‰ (McCollom and Seewald, 2006; McCollom et al., 2010). Still, when analyzing intramolecular carbon atoms within larger lipid compounds, a more robust biosignature can be achieved (e.g., different $\delta^{13}C$ values in alternating carbons, such as those observed in this study; **Figure 3**). Fischer-Tropsch synthesized organic compounds typically have a constant ^{13}C composition for all carbons (McCollom and Seewald, 2006), whereas fatty acids and other compounds formed by biosynthetic pathways usually have distinctive ^{13}C signatures between alternating compounds (i.e., even- versus odd-numbered carbon atoms within a series of *normal* lipids), arising from the fatty acid assembly mechanism (i.e., the addition of 2-carbon acetyl units, where the methyl and carboxyl groups differ substantially in their isotopic composition). While it may be difficult to differentiate biogenic from abiotic organic compounds based solely on the isotopic composition of bulk biomass or even individual compounds, the combination of the isotopic analysis of intramolecular carbon atoms with a rigorous analysis at a molecular level brings together the identification of not only one but several individual biomarkers may help to overcome the risk of assigning a biological origin to purely abiotic compounds. Thus, the risk of pitfalls and false positives will be minimized with the increasing complexity of the biosignature, so a co-occurrence of numerous anomalies or patterns in the overall molecular profile of extraterrestrial organic matter could still be strongly suggestive of biosynthesis (Marshall et al., 2017; McMahon and Cosmidis, 2021).

In this study, the extensive set of diverse and relatively complex lipids with variable but generally depleted carbon isotopic signatures of heterogeneous distribution within homologous lipid series, together, attest to a biogenic fingerprint. In the same geyser field of El Tatio, sinter deposits are reported to display bulk $\delta^{13}C$ values comparable to those measured here for the fresh biofilms, more similar to CE3 and CE4 in proximal slopes (40–75°C; from –9.9 to –16.9‰), or to CE6 in near vent deposits (> 75°C; from –15.9 to –25.1‰) (Muñoz-Saez et al., 2020). More specifically, individual $\delta^{13}C$ values of apolar (from –22 to –28‰), acid (from –20 to –37‰), and polar (from –25 to –30‰) lipids contained in sinter deposits from hydrothermally active and inactive geyser mounds in El Tatio (Sánchez-García et al., 2019) were also in the (lower) range of those measured here in the eight fresh biofilms. By recording the fresh biosignatures in the active hydrothermal system of Cacao, we dispense a molecular and isotopic template for the recognition of past biosignals in silicified counterparts on Earth and (if any) on Mars in analogous silica-rich hydrothermal systems. By spanning a wide gradient of temperature, we increase our chance to capture a broader variety of microorganisms and metabolisms and, so, a more comprehensive variety of lipid profiles. According to the hypothesis of possible extraterrestrial life, "as we know it" by Bartlett and Wong (2020), lipids emerge as ideal target compounds with a double astrobiological value, as potential biomarkers of universal (ubiquity in all types of organisms as components of their cell membranes) and paleo-reconstructive (high potential for preservation in the fossil record) character.

CONCLUSION

This study aimed to interpret biosignatures in modern hydrothermal systems to learn how to decipher fossil records in ancient silica deposits. Exploiting the diagnosis potential of highly resistant lipid biomarkers, we characterized the primary biological sources and prevailing carbon metabolic routes operating in the modern hydrothermal ecosystem. The taxonomic precision (at the phylum and even at the genus level sometimes) of the lipid biomarkers-diagnosis tool was validated by parallel DNA sequencing, and its forensic capacity to identify primary biosources and autotrophic metabolisms calibrated at the local scale.

Together, the molecular, isotopic, and genetic results provided a global understanding of the modern ecosystem at the Cacao site and revealed a compositional and metabolic succession along the thermal gradient, from a majority of thermophiles (*Deinococcus-Thermus*, *Chloroflexi*, and *Acetothermia*), growing mostly by assimilation of inorganic carbon through the r-acetyl-CoA pathway at 72°C; to dominance of anoxygenic photosynthetic species (mostly *Chloroflexus*), primarily using the 3HP bicycle to grow from 56 to 67°C; to coexistence of anoxygenic (*Roseiflexus* and *Chloroflexus*) and oxygenic (*Fischerella*) photosynthetic species that grow photoheterotrophically (crossfeed on cyanobacterial exudates) or photoautotrophically (the Calvin

cycle), respectively, from 56 to 46°C; and to eventual dominance of mesophilic oxygenic phototrophs from *Proteobacteria* (mostly *Rhodobacterales*) and *Cyanobacteria* (*Synechocystis, Nostocales, Rivularia,* or *Oxyphotobacteria*) that combined the use of the rTCA and Calvin cycles at temperatures of $\leq$ 32°C.

The detection of several singular ecological traits along the Cacao stream (e.g., presence of *Fischerella* up to 72°C; first identification of the cyanobacterial genera *Synechocystis* at El Tatio, *Gloeocapsa*, or *Annamia*; or the likely alternate at 56°C of aerobic and anaerobic conditions, with a transition from photoheterotrophic to photoautotrophic growth of the *Chloroflexi* community) illustrated the ecological uniqueness of the Cacao stream and highlighted the astrobiological interest of El Tatio. The hydrothermal system and its deposits provide excellent settings to advance the understanding of the limits of life and the emergence of early life on Earth. The taxonomically calibrated microbial community structure built on the lipid biomarkers provided a local (molecular and isotopic) fresh end member to recognize past biosources and metabolisms from altered biomarkers profiles in ancient silica deposits. Correlating resistant lipid biomarkers with ancestral metabolisms is critical for interpreting molecular biomarkers in analog planetary contexts.

DATA AVAILABILITY STATEMENT

Raw DNA sequence reads were deposited at the NCBI Sequence Read Archive (SRA) under the BioProject ID PRJNA777431 (https://www.ncbi.nlm.nih.gov/bioproject/PRJNA777431).

AUTHOR CONTRIBUTIONS

LS-G designed the present case study and collected the samples together with VP and NC. VM and LS-G conducted the extraction and molecular analysis of the lipid biomarkers, while DC took care of the stable-carbon isotopic analysis. VM and ML were in charge of extracting the DNA and analyzing and interpreting the sequencing data. VM and LS-G interpreted the lipid biomarkers results, integrated all the results, and wrote the manuscript, with the contribution of all co-authors. All authors contributed to the article and approved the submitted version.

FUNDING

This work was funded by the Spanish Ministry of Science and Innovation/State Agency of Research MCIN/AEI/10.13039/501100011033 and by "ERDF A way of making Europe," through grant nos. RYC2018-023943-I (LS-G), FJC2018-037246-I (ML), RTI2018-094368-B-I00 (VP), and MDM-2017-0737 (DC), Unidad de Excelencia "Mariía de Maeztu"-Centro de Astrobiología (CAB), INTA-CSIC. The field campaign to El Tatio was funded by the CAN7 project of the NASA Astrobiology Institute (ref. 13-13NAI7_2-0018).

ACKNOWLEDGMENTS

We acknowledge the *Complejo Turìstico Tatio Mallku* (Chile) for allowing access and sampling in the El Tatio geysers field. We thank the genomic service of the *Fundación Parque Cientìfico de Madrid* (Spain) for the DNA amplification and sequencing work. Finally, we also thank Paloma Martìnez-Sarmiento (Centro de Astrobiología) for stable isotopes analysis at the *Centro de Astrobiología*.

SUPPLEMENTARY MATERIAL

The Supplementary Material for this article can be found online at: https://www.frontiersin.org/articles/10.3389/fmicb.2022.811904/full#supplementary-material

REFERENCES

Abrajano, T. A., Murphy, D. E., Fang, J., Comet, P., and Brooks, J. M. (1994). $^{13}C/^{12}C$ Ratios in individual fatty acids of marine mytilids with and without bacterial symbionts. *Org. Geochem.* 21, 611–617.

Ahlgren, G., Gustafsson, I. B., and Boberg, M. (1992). Fatty acid content and chemical composition of freshwater microalgae. *J. Phycol.* 28, 37-50.

Azúa-Bustos, A., González-Silva, C., Mancilla, R. A., Salas, L., Gómez-Silva, B., McKay, C. P., et al. (2011). Hypolithic cyanobacteria supported mainly by fog in the coastal range of the Atacama Desert. *Microb. Ecol.* 61, 568–581. doi: 10.1007/s00248-010-9784-5

Badhai, J., Ghosh, T. S., and Das, S. K. (2015). Taxonomic and functional characteristics of microbial communities and their correlation with physicochemical properties of four geothermal springs in Odisha, India. *Front. Microbiol.* 6:1166. doi: 10.3389/fmicb.2015.01166

Barbieri, R., Cavalazzi, B., Stivaletta, N., and López-García, P. (2014). Silicified biota in high-altitude, geothermally influenced ignimbrites at El Tatio Geyser Fielsd, Andean Cordillera (Chile). *Geomicrobiol. J.* 31, 493-508. doi: 10.1080/01490451.2013.836691

Bartlett, S., and Wong, M. L. (2020). Defining lyfe in the universe: from three privileged functions to four pillars. *Life* 10, 1–22. doi: 10.3390/life10040042

Brock, T. D. (1978). *Thermophilic Microorganisms and Life at High Temperatures*. New York, NY: Springer-Verlag. doi: 10.1007/978-1-4612-6284-8

Brocks, J. J., Love, G. D., Summon, R. E., Knoll, A. H., Logan, G. A., and Bowden, S. A. (2005). Biomarker evidence for green and purple sulphur bacteria in a stratified Palaeoproterozoic sea. *Nature* 437, 866–870. doi: 10.1038/nature04068

Bühring, S. I., Smittenberg, R. H., Sachse, D., Lipp, J. S., Golubic, S., Sachs, J. P., et al. (2009). A Hypersaline microbial mat from the Pacific Atoll Kiritimati: insights into composition and carbon fixation using biomarker analyses and a ^{13} C-labeling approach. *Geobiology* 7, 308-323. doi: 10.1111/j.1472-4669.2009.00198.x

Cabrol, N. A., Feister, U., Häder, E. D.-P., Piazena, H., Grin, A., and Klein, A. (2014). Record solar UV irradiance in thetropical Andes. *Front. Environ. Sci.* 2:19. doi: 10.3389/fenvs.2014.00019

Cabrol, N. A., Grin, E. A., Kiss, K. T., Ács, E., Grigorszky, I., Szabò, K., et al. (2007). "Signatures of habitats and life in Earth's high-altitude lakes: clues to Noachian aqueous environments on Mars," in *The Geology of Mars, Chapter 14: Evidence from Earth-Based Analogs*, ed. M. Chapman (Cambridge: Cambridge University Press), 349–370.

Cabrol, N. A., Grin, E. A., Zippi, P., Noffke, N., and Winter, D. (2018). "Evolution of altiplanic lakes at the Pleistocene/Holocene transition: a window into early Mars declining habitability, changing habitats, and biosignatures," in *From*

Habitability to Life on Mars, eds N. A. Cabrol and E. A. Grin (Amsterdam: Elsevier), 153–179.

Cady, S. L., Skok, J. R., Gulick, V. G., Berger, J. A., and Hinman, N. W. (2018). "Siliceous hot spring deposits: why they remain key astrobiological targets," in *From Habitability to Life on Mars*, eds N. A. Cabrol and E. A. Grin (Amsterdam: Elsevier), 179-210. doi: 10.1016/B978-0-12-809935-3.00007-4

Campbell, K. A., Lynne, B. Y., Handley, K. M., Jordan, S., Farmer, J. D., Guido, D. M., et al. (2015). Tracing biosignature preservation of geothermally silicified microbial textures into the geological record. *Astrobiology* 15, 858-882. doi: 10.1089/ast.2015.1307

Castenholz, R. W. (1981). "Isolation and cultivation of thermophilic cyanobacteria," in *The Prokaryotes*, eds M. P. Starr, H. Stolp, H. G. Trüper, A. Balows, and H. G. Schlegel (Berlin: Springer-Verlag), 236–246.

Coates, R. C., Podell, S., Korobeynikov, A., Lapidus, A., Pevzner, P., Sherman, D. H., et al. (2014). Characterization of cyanobacterial hydrocarbon composition and distribution of biosynthetic pathways. *PLoS One* 9:e85140. doi: 10.1371/journal.pone.0085140

Cruaud, P., Vigneron, A., Lucchetti-Miganeh, C., Ciron, P. E., Godfroy, A., and Cambon-Bonavita, M. A. (2014). Influence of DNA extraction method, 16S RRNA targeted hypervariable regions, and sample origin on microbial diversity detected by 454 pyrosequencing in marine chemosynthetic ecosystems. *Appl. Environ. Microbiol.* 80, 4626-4639. doi: 10.1128/AEM.00592-14

Damer, B., and Deamer, D. (2020). The hot spring hypothesis for an origin of life. *Astrobiology* 20, 429-452. doi: 10.1089/ast.2019.2045

Deamer, D. W., and Georgiou, C. D. (2015). Hydrothermal conditions and the origin of cellular life. *Astrobiology* 15, 1091-1095. doi: 10.1089/ast.2015.1338

Didyk, B. M., Simoneit, B. R. T., Brassell, S. C., and Eglinton, G. (1978). Organic geochemical indicators of palaeoenvironmental conditions of sedimentation. *Nature* 272, 216-222. doi: 10.1038/272216a0

Dijkman, N. A., Boschker, H. T. S., Stal, L. J., and Kromkamp, J. C. (2010). Composition and heterogeneity of the microbial community in a coastal microbial mat as revealed by the analysis of pigments and phospholipid-derived fatty acids. *J. Sea Res.* 63, 62-70. doi: 10.1016/j.seares.2009.10.002

Djokic, T., Van Kranendonk, M. J., Campbell, K. A., Walter, M. R., and Ward, C. R. (2017). Earliest signs of life on land preserved in ca. 3.5 Ga hot spring deposits. *Nat. Commun.* 8:15263. doi: 10.1038/ncomms15263

Dorador, C., Vila, I., Imhoff, J. F., and Witzel, K.-P. (2008). Cyanobacterial diversity in Salar de Huasco, a high altitude saline wetland in northern Chile: an example of geographical dispersion? *FEMS Microbiol. Ecol.* 64, 419–432. doi: 10.1111/j.1574-6941.2008.00483.x

Dunckel, A. E., Cardenas, M. B., Sawyer, A. H., and Bennett, P. C. (2009). High-resolution in-situ thermal imaging of microbial mats at El Tatio Geyser, Chile shows coupling between community color and temperature. *Geophys. Res. Lett.* 36:L23403. doi: 10.1029/2009GL041366

Dupraz, C., Reid, R. P., Braissant, O., Decho, A. W., Norman, R. S., and Visscher, P. T. (2009). Processes of carbonate precipitation in modern microbial mats. *Earth Sci. Rev.* 96, 141–162.

Farmer, J. D. (2000). Hydrothermal systems: doorways to early biosphere evolution. *GSA Today* 10, 1–9.

Fernández-Turiel, J. L., García-Valles, M., Gimeno-Torrente, D., Saavedra-Alonso, J., and Martínez-Manent, S. (2005). The hot spring and geyser sinters of El Tatio, Northern Chile. *Sediment. Geol.* 180, 125-147. doi: 10.1016/j.sedgeo.2005.07.005

Gelpi, E., Schneider, H., Mann, J., and Oró, J. (1970). Hydrocarbons of geochemical significance in microscopic algae. *Phytochemistry* 9, 603–612. doi: 10.1016/S0031-9422(00)85700-3

Glennon, J. A., and Pfaff, R. M. (2003). The extraordinary thermal activity of El Tatio Geyser Field, Antofagasta Region, Chile. *GOSA Trans.* 8, 31–78.

Gong, J., Munoz- Saez, C., Wilmeth, D. T., Myers, K. D., Homann, M., Arp, G., et al. (2021). Morphogenesis of digitate structures in hot spring silica sinters of the El Tatio geothermal field, Chile. *Geobiology* 20, 137–155. doi: 10.1111/gbi.12471

Gong, J., Myers, K. D., Munoz- Saez, C., Homann, M., Rouillard, J., Wirth, R., et al. (2020). Formation and preservation of microbial palisade fabric in silica deposits from El Tatio, Chile. *Astrobiology* 20, 500–524. doi: 10.1089/ast.2019.2025

Graven, H., Allison, C. E., Etheridge, D. M., Hammer, S., Keeling, R. M., Levin, I., et al. (2017). Compiled records of carbon isotopes in atmospheric CO_2 for historical simulations in CMIP6. *Geosci. Model Dev.* 10, 4405–4417.

Grice, K., Schouten, S., Nissenbaum, A., Charrach, J., and Sinninghe Damsté, J. S. (1998). Isotopically heavy carbon in the C_{21} to C_{25} regular isoprenoids in halite-rich deposits from the Sdom formation, Dead Sea Basin, Israel. *Org. Geochem.* 28, 349–359.

Grimalt, J. O., de Wit, R., Teixidor, P., and Albaigés, J. (1992). Lipid biogeochemistry of *Phormidium* and *Microcoleus* mats. *Org. Geochem.* 19, 509–530. doi: 10.1016/0146-6380(92)90015-P

Grimalt, J. O., Yruela, I., Saiz-Jimenez, C., Toja, J., de Leeuw, J. W., and Albaigés, J. (1991). Sedimentary lipid biogeochemistry of an hypereutrophic alkaline lagoon. *Geochim. Cosmochim. Acta* 55, 2555-2577. doi: 10.1016/0016-7037(91)90373-D

Hanada, S., Takaichi, S., Matsuura, K., and Nakamura, K. (2002). *Roseiflexus castenholzii* gen. nov., sp. nov., a thermophilic, filamentous, photosynthetic bacterium that lacks chlorosomes. *Int. J. Syst. Evol. Microbiol.* 52, 187-193. doi: 10.1099/00207713-52-1-187

Hayes, J. M. (2001). "Fractionation of the isotopes of carbon and hydrogen in biosynthetic processes," in *Proceedings of the National Meeting of the Geological Society of America* (Boston, MA: Geological Society of America). doi: 10.1515/9781501508745-006

Herlemann, D. P. R., Labrenz, M., Jürgens, K., Bertilsson, S., Waniek, J. J., and Andersson, A. F. (2011). Transitions in bacterial communities along the 2000 Km salinity gradient of the Baltic Sea. *ISME J.* 5, 1571-1579. doi: 10.1038/ismej.2011.41

Hugerth, L. W., Muller, E. E. L., Hu, Y. O. O., Lebrun, L. A. M., Roume, H., Lundin, D., et al. (2014). Systematic design of 18S RRNA gene primers for determining eukaryotic diversity in microbial consortia. *PLoS One* 9:e95567. doi: 10.1371/journal.pone.0095567

Hügler, M., and Sievert, S. M. (2011). Beyond the Calvin cycle: autotrophic carbon fixation in the ocean. *Annu. Rev. Mar. Sci.* 3, 261-289. doi: 10.1146/annurev-marine-120709-142712

Jahnke, L. L., Eder, W., Huber, R., Hope, J. M., Hinrichs, K. U., Hayes, J. M., et al. (2001). Signature lipids and stable carbon isotope analyses of octopus spring hyperthermophilic communities compared with those of Aquificales representatives. *Appl. Environ. Microbiol.* 67, 5179-5189. doi: 10.1128/AEM.67.11.5179-5189.2001

Jiang, L., Cai, C. F., Zhang, Y. D., Mao, S. Y., Sun, Y. G., Li, K. K., et al. (2012). Lipids of sulfate-reducing bacteria and sulfur-oxidizing bacteria found in the Dongsheng uranium deposit. *Chin. Sci. Bull.* 57, 1311–1319. doi: 10.1007/s11434-011-4955-4

Jones, B. (2021). Siliceous sinters in thermal spring systems: review of their mineralogy, diagenesis, and fabrics. *Sediment. Geol.* 413:105820. doi: 10.1016/j.sedgeo.2020.105820

Jungblut, A. D., Allen, M. A., Burns, B. P., and Neilan, B. A. (2009). Lipid biomarker analysis of cyanobacteria-dominated microbial mats in meltwater ponds on the McMurdo Ice Shelf, Antarctica. *Org. Geochem.* 40, 258–269.

Kenig, F., Simons, D. J. H., Crich, D., Cowen, J. P., Ventura, G. T., and Rehbein-Khalily, T. (2005). Structure and distribution of branched aliphatic alkanes with quaternary carbon atoms in Cenomanian and Turonian black shales of Pasquia Hills (Saskatchewan, Canada). *Org. Geochem.* 36, 117-238. doi: 10.1016/j.orggeochem.2004.06.014

Kenyon, C. N., and Gray, A. M. (1974). Preliminary analysis of lipids and fatty acids of green bacteria and *Chloroflexus aurantiacus*. *J. Bacteriol.* 120, 131-138. doi: 10.1128/JB.120.1.131-138.1974

Konhauser, K. O., Jones, B., Phoenix, V. R., Ferris, G., and Renaut, R. W. (2004). The microbial role in hot spring silicification. *Ambio* 33, 552–558. doi: 10.1579/0044-7447-33.8.552

Kozich, J. J., Westcott, S. L., Baxter, N. T., Highlander, S. K., and Schloss, P. D. (2013). Development of a dual-index sequencing strategy and curation pipeline for analyzing amplicon sequence data on the MiSeq. *Appl. Environ. Microbiol.* 79, 5112–5120. doi: 10.1128/AEM.01043-13

Lei, J., Chun-Fang, C., Yong-Dong, Z., Sheng-Yi, M., Yong-Ge, S., Kai-Kai, L., et al. (2012). Lipids of sulfate-reducing bacteria and sulfur-oxidizing bacteria found in the *Dongsheng uranium* deposit. *Chin. Sci. Bull.* 11, 1311–1319.

Lezcano, M. Á., Moreno-Paz, M., Carrizo, D., Prieto-Ballesteros, O., Fernández-Martínez, M. Á., Sánchez-García, L., et al. (2019). Biomarker profiling of

microbial mats in the geothermal band of Cerro Caliente, Deception Island (Antarctica): life at the edge of heat and cold. *Astrobiology* 19, 1–15. doi: 10.1089/ast.2018.2004

Lezcano, M. Á., Sánchez-García, L., Quesada, A., Carrizo, D., Fernández-Martínez, M. Á., Cavalcante-Silva, E., et al. (2022). Comprehensive metabolic and taxonomic reconstruction of an ancient microbial mat from the McMurdo Ice Shelf (Antarctica) by integrating genetic, metaproteomic and lipid biomarker analyses. *Front. Microbiol.* 13:799360. doi: 10.3389/fmicb.2022.799360

Lucchi, F., Tranne, C. A., Rossi, P. L., and Gallardo, C. (2009). "Volcanic and tectonic history of the El Tatio area (central Andes, northern Chile): explanatory notes to the 1:50,000 scale geological map," in *Geological Constraints on the Onset and Evolution of an Extreme Environment: the Atacama Area*, ed. P. I. Rossi (GeoActa, Special Publication 2), 1–29.

Marshall, S. M., Murray, A. R. G., and Cronin, L. (2017). A probabilistic framework for identifying biosignatures using pathway complexity. *Philos. Trans. R. Soc. A Math. Phys. Eng. Sci.* 375:20160342. doi: 10.1098/rsta.2016.0342

McCollom, T. M., Lollar, B. S., Lacrampe-Couloume, G., and Seewald, J. S. (2010). The influence of carbon source on abiotic organic synthesis and carbon isotope fractionation under hydrothermal conditions. *Geochim. Cosmochim. Acta* 74, 2717–2740.

McCollom, T. M., Ritter, G., and Simoneit, R. T. (1999). Lipid synthesis under hydrothermal conditions by Fisher-Tropsch-type reactions. *Orig. Life Evol. Biosph.* 29, 153–166.

McCollom, T. M., and Seewald, J. S. (2006). Carbon isotope composition of organic compounds produced by abiotic synthesis under hydrothermal conditions. *Earth Planet. Sci. Lett.* 243, 74–84.

McMahon, S., and Cosmidis, J. (2021). False biosignatures on Mars: anticipating ambiguity. *J. Geol. Soc.* 179:jgs2021-050.

Mehda, S., Muñoz-Martín, M. Á., Oustani, M., Hamdi-Aïssa, B., Perona, E., and Mateo, P. (2021). Microenvironmental conditions drive the differential cyanobacterial community composition of biocrusts from the Sahara Desert. *Microorganisms* 9:487. doi: 10.3390/microorganisms9030487

Mercer, E. I., London, R. A., Kent, I. S. A., and Taylor, A. J. (1974). Sterols, sterol esters and fatty acids of *Botrydiumgranulatum*, *Tribonemaaequale* and *Monodussubterraneus*. *Phytochemistry* 13, 845–852.

Meyers, P. A. (1997). Organic geochemical proxies of paleoceanographic, paleolimnologic, and paleoclimatic processes. *Org. Geochem.* 27, 213–250. doi: 10.1016/S0146-6380(97)00049-1

Miller, S. R., and Castenholz, R. W. (2000). Evolution of thermotolerance in hot spring cyanobacteria of the genus *Synechococcus*. *Appl. Environ. Microbiol.* 66, 4222-4229. doi: 10.1128/AEM.66.10.4222-4229.2000

Mook, W. G., Bommerson, J. C., and Staverman, W. H. (1974). Carbon isotope fractionation between dissolved bicarbonate and gaseous carbon dioxide. *Earth Planet. Sci. Lett.* 22, 169-176. doi: 10.1016/0012-821X(74)90078-8

Muñoz-Saez, C., Manga, M., and Hurwitz, S. (2018). Hydrothermal discharge from the El Tatio Basin, Atacama, Chile. *J. Volcanol. Geotherm. Res.* 361, 25-35. doi: 10.1016/j.jvolgeores.2018.07.007

Muñoz-Saez, C., Manga, M., Hurwitz, S., Lagter, S., Churchill, D. M., Reich, M., et al. (2020). Radiocarbon dating of silica sinter and postglacial hydrothermal activity in the El Tatio geyser field. *Geophys. Res. Lett.* 47:e2020GL087908.

Nes, W. R., and McKean, M. L. (1977). *Biochemistry of Steroids and Other Isopentenoids*. Baltimore, MD: University Park Press.

Nübel, U., Garcia-Pichel, F., and Muyzer, G. (1997). PCR primers to amplify 16S RRNA genes from cyanobacteria. *Appl. Environ. Microbiol.* 63, 3327-3332. doi: 10.1128/AEM.63.8.3327-3332.1997

Oksanen, J., Blanchet, F. G., Friendly, M., Kindt, R., Legendre, P., McGlinn, D., et al. (2020). *Vegan: Community Ecology Package. R package Version 2.5-7*. Available online at: https://CRAN.R-project.org/package=vegan

Pancost, R. D., Pressley, S., Coleman, J. M., Talbot, H. M., Kelly, S. P., Farrimond, P., et al. (2006). Composition and implications of diverse lipids in New Zealand geothermal sinters. *Geobiology* 4, 71–92.

Parenteau, M. N., Jahnke, L. L., Farmer, J. D., and Cady, S. L. (2014). Production and early preservation of lipid biomarkers in iron hot springs. *Astrobiology* 14, 502–521. doi: 10.1089/ast.2013.1122

Patterson, G. W. (1972). Sterols of *Nitellaflexilis* and *Charavulgaris*. *Phytochemistry* 11, 3481–3483.

Peters, K. E., Walters, C. C., and Moldowan, J. M. (2005). *The Biomarker Guide - Part II - Biomarkers and Isotopes in Petroleum Exploration and Earth History*. New York, NY: Cambridge University Press.

Phoenix, V. R., Bennett, P. C., Engel, A. S., Tyler, S. W., and Ferris, F. G. (2006). Chilean high-altitude hot-spring sinters: a model system for UV screening mechanisms by early precambrian cyanobacteria. *Geobiology* 4, 15-28. doi: 10.1111/j.1472-4669.2006.00063.x

Pierson, B. K., and Castenholz, R. W. (1974). A phototrophic gliding filamentous bacterium of hot springs, *Chloroflexus aurantiacus*, Gen. and Sp. Nov. *Arch. Microbiol.* 100, 5-24. doi: 10.1007/BF00446302

Preuß, A., Schauder, R., Fuchs, G., and Stichler, W. (1989). Carbon isotope fractionation by autotrophic bacteria with three different CO_2 fixation pathways. *Z. Naturforsch. C* 44, 397-402. doi: 10.1515/znc-1989-5-610

Purcell, D., Sompong, U., Yim, L. C., Barraclough, T. G., Peerapornpisal, Y., and Pointing, S. B. (2007). The effects of temperature, pH and sulphide on the community structure of hyperthermophilic streamers in hot springs of Northern Thailand: hyperthermophilic diversity and abiotic variables. *FEMS Microbiol. Ecol.* 60, 456–466. doi: 10.1111/j.1574-6941.2007.00302.x

Quast, C., Pruesse, E., Yilmaz, P., Gerken, J., Schweer, T., Yarza, P., et al. (2013). The SILVA ribosomal RNA gene database project: improved data processing and web-based tools. *Nucleic Acids Res.* 41, D590–D596. doi: 10.1093/nar/gks1219

Révész, K., Qi, H., and Coplen, T. B. (2012). "Determination of the $\delta^{15}N$ and $\delta^{13}C$ of total nitrogen and carbon in solids. RSIL lab code 1832, chap. 5 of stable isotope-ratio methods," in *Methods of the Reston Stable Isotope Laboratory (Slightly Revised from Version 1.1 Released in 2007)*, eds K. Révész and T. B. Coplen (Reston, VA: U.S. Geological Survey).

Rinke, C., Schwientek, P., Sczyrba, A., Ivanova, N., Anderson, I. J., Cheng, J. F., et al. (2013). Insights into the phylogeny and coding potential of microbial dark matter. *Nature* 499, 431–437. doi: 10.1038/nature12352

Rognes, T., Flouri, T., Nichols, B., Quince, C., and Mahé, F. (2016). VSEARCH: a versatile open source tool for metagenomics. *PeerJ* 4:e2584. doi: 10.7717/peerj.2584

Rohmer, M., Bouvier-Nave, P., and Ourisson, G. (1984). Distribution of hopanoid triterpenes in prokaryotes. *Microbiology* 130, 1137–1150.

Rothschild, L. J., and Mancinelli, R. L. (2001). Life in extreme environments. *Nature* 409, 1902–1910.

Ruff, S. W., Campbell, K. A., Van Kranendonk, M. J., Rice, M. S., and Farmer, J. D. (2019). The case for ancient hot springs in Gusev crater, mars. *Astrobiology* 19, 475–499. doi: 10.1089/ast.2019.2044

Ruff, S. W., and Farmer, J. D. (2016). Silica deposits on Mars with features resembling hot spring biosignatures at El Tatio in Chile. *Nat. Commun.* 7:13554. doi: 10.1038/ncomms13554

Ruff, S. W., Farmer, J. D., Calvin, W. M., Herkenhoff, K. E., Johnson, J. R., Morris, R. V., et al. (2011). Characteristics, distribution, origin, and significance of opaline silica observed by the Spirit rover in Gusev Crater. *J. Geophys. Res.* 116:E00F23. doi: 10.1029/2010JE003767

Sakata, S., Hayes, J. M., McTaggart, A. R., Evans, R. A., Leckrone, K. J., and Togasaki, R. K. (1997). Carbon isotopic fractionation associated with lipid biosynthesis by a cyanobacterium: relevance for interpretation of biomarker records. *Geochim. Cosmochim. Acta* 61, 5379–5389. doi: 10.1016/S0016-7037(97)00314-1

Sánchez-García, L., Aeppli, C., Parro, V., Fernández-Remolar, D., García-Villadangos, M., Chong-Diaz, G., et al. (2018). Molecular biomarkers in the subsurface of the Salar Grande (Atacama, Chile) evaporitic deposits. *Biogeochemistry* 140, 31–52. doi: 10.1007/s10533-018-0477-3

Sánchez-García, L., Carrizo, D., Lezcano, M. A., Moreno-Paz, M., Aeppli, C., García-Villadangos, M., et al. (2021). Time-integrative multi-biomarker detection in Triassic-Jurassic rocks from the Atacama Desert: relevance for searching basic life beyond the Earth. *Astrobiology* 21, 1421–1437. doi: 10.1089/ast.2020.2339

Sánchez-García, L., Fernández-Martínez, M. A., García-Villadangos, M., Blanco, Y., Cady, S. L., Hinman, N., et al. (2019). Microbial biomarker transition in high-altitude sinter mounds from El Tatio (Chile) through different stages of hydrothermal activity. *Front. Microbiol.* 9:3350. doi: 10.3389/fmicb.2018.03350

Sánchez-García, L., Fernández-Martínez, M. A., Moreno-Paz, M., Carrizo, D., García-Villadangos, M., Manchado, J. M., et al. (2020). Simulating Mars drilling mission for searching for life: ground-truthing lipids and other complex

microbial biomarkers in the iron-sulfur rich Río Tinto analog. *Astrobiology* 20, 1029-1047. doi: 10.1089/ast.2019.2101

Schloss, P. D., Westcott, S. L., Ryabin, T., Hall, J. R., Hartmann, M., Hollister, E. B., et al. (2009). Introducing mothur: open-source, platform-independent, community-supported software for describing and comparing microbial communities. *Appl. Environ. Microbiol.* 75, 7537–7541. doi: 10.1128/AEM.01541-09

Shiea, J., Brassel, S. C., and Ward, D. M. (1990). Mid-chain branched mono- and dimethyl alkanes in hot spring cyanobacterial mats: a direct biogenic source for branched alkanes in ancient sediments? *Organ. Geochem.* 15, 223-231. doi: 10.1016/0146-6380(90)90001-G

Shiea, J., Brassel, S. C., and Ward, D. M. (1991). Comparative analysis of extractable lipids in hot spring microbial mats and their component photosynthetic bacteria. *Organ. Geochem.* 17, 309-319. doi: 10.1016/0146-6380(91)90094-Z

Skok, J. R., Mustard, J. F., Ehlmann, B. L., Milliken, R. E., and Murchie, S. L. (2010). Silica deposits in the Nili Patera caldera on the Syrtis Major volcanic complex on Mars. *Nat. Geosci.* 3, 838-841. doi: 10.1038/ngeo990

Summons, R. E., Welander, P. V., and Gold, D. A. (2021). Lipid biomarkers: molecular tools for illuminating the history of microbial life. *Nat. Rev. Microbiol.* 20, 174–185. doi: 10.1038/s41579-021-00636-2

Szatmari, P. (1989). Petroleum formation by Fischer-Tropsch synthesis in plate tectonics. *Am. Assoc. Pet. Geol. Bull.* 73, 989–998.

Takai, K., Campbell, B. J., Cary, S. C., Suzuki, M., Oida, H., Nunoura, T., et al. (2005). Enzymatic and genetic characterization of carbon and energy metabolisms by deep-sea hydrothermal chemolithoautotrophic isolates of *Epsilonproteobacteria*. *Appl. Environ. Microbiol.* 71, 7310-7320. doi: 10.1128/AEM.71.11.7310-7320.2005

Takami, H., Noguchi, H., Takaki, Y., Uchiyama, I., Toyoda, A., Nishi, S., et al. (2012). A deeply branching thermophilic bacterium with an ancient Acetyl-CoA pathway dominates a subsurface ecosystem. *PLoS One* 7:e30559. doi: 10.1371/journal.pone.0030559

Taylor, J., and Parkes, R. J. (1983). The cellular fatty acids of the sulphate-reducing bacteria, *Desulfobacter* sp., *Desulfobulbus* sp., and *Desulfovibrio desulfuricans*. *J. Gen. Microbiol.* 129, 3303–3309.

Teece, B. L., George, S. C., Djokic, T., Campbell, K. A., Ruff, S. W., and Van Kranendonk, M. J. (2020). Biomolecules from fossilized hot spring sinters: implications for the search for life on Mars. *Astrobiology* 20, 537–551. doi: 10.1089/ast.2018.2018

Thomas, S. C., Payne, D., Tamadonfar, K. O., Seymour, C. O., Jiao, J. Y., and Murugapiran, S. K. (2021). Genomics, exometabolomics, and metabolic probing reveal conserved proteolytic metabolism of *Thermoflexus hugenholtzii* and three candidate species from China and Japan. *Front. Microbiol.* 12:632731. doi: 10.3389/fmicb.2021.632731

van der Meer, M. T. J., Klatt, C. G., Wood, J., Bryant, D. A., Bateson, M. M., Lammerts, L., et al. (2010). Cultivation and genomic, nutritional, and lipid biomarker characterization of *Roseiflexus* strains closely related to predominant in situ populations inhabiting Yellowstone hot spring microbial mats. *J. Bacteriol.* 192, 3033-3042. doi: 10.1128/JB.01610-09

van der Meer, M. T. J., Lammerts, L., Skirnisdottir, S., Sinninghe Damsté, J. S., and Schouten, S. (2008). Distribution and isotopic composition of bacterial lipid biomarkers in microbial mats from a sulfidic Icelandic hot spring. *Organ. Geochem.* 39, 1015–1019. doi: 10.1016/j.orggeochem.2008.04.002

van der Meer, M. T. J., Schouten, S., de Leeuw, J. W., and Ward, D. M. (2000). Autotrophy of green non-sulphur bacteria in hot spring microbial mats: biological explanations for isotopically heavy organic carbon in the geological record. *Environ. Microbiol.* 2, 428-435. doi: 10.1046/j.1462-2920.2000.00124.x

van der Meer, M. T. J., Schouten, S., and Sinninghe Damsté, J. S. (1998). The effect of the reversed tricarboxylic acid cycle on the ^{13}C contents of bacterial lipids. *Organ. Geochem.* 28, 527–533.

van der Meer, M. T. J., Schouten, S., van Dongen, B. E., Rijpstra, W. I. C., Fuchs, G., Sinninghe Damsté, J. S., et al. (2001). Biosynthetic controls on the 13C-contents of organic components in the photoautotrophic bacterium *Chloroflexus aurantiacus*. *J. Biol. Chem.* 276, 10971–10976.

van der Meer, M. T. J., Schouten, S., Ward, D. M., Geenevasen, J. A. J., and Sinninghe Damsté, J. S. (1999). All-cis hentriaconta-9,15,22-triene in microbial mats formed by the phototrophic prokaryote *Chloroflexus*. *Organ. Geochem.* 30, 1585–1587. doi: 10.1016/s0146-6380(99)00141-2

Van Kranendonk, M. J., Baumgartner, R., Djokic, T., Ota, T., Steller, L., Garbe, U., et al. (2021). Elements for the origin of life on land: a deep-time perspective from the Pilbara Craton of Western Australia. *Astrobiology* 21, 39–59. doi: 10.1089/ast.2019.2107

Volkman, J. K. (1986). A review of sterol markers for marine and terrigenous organic matter. *Organ. Geochem.* 9, 83–99.

Volkman, J. K. (2003). Sterols in microorganisms. *Appl. Microbiol. Biotechnol.* 60, 495-506.

Walter, M. R., and Des Marais, D. J. (1993). Preservation of biological information in thermal spring deposits: developing a strategy for the search for fossil life on Mars. *Icarus* 101, 129–143. doi: 10.1006/icar.1993.1011

Ward, D. M., Castenholz, R. W., and Miller, S. R. (2012). "Cyanobacteria in geothermal habitats," in *Ecology of Cyanobacteria II*, ed. B. A. Whitton (Dordrecht: Springer Netherlands), 39-63. doi: 10.1007/978-94-007-3855-3_3

Ward, D. M., Shiea, J., Zeng, B., Dobson, G., Brassell, S., and Eglinton, G. (1989). "Lipid biochemical markers and the composition of microbial mats," in *Microbial Mats: Physiological Ecology of Benthic Microbial Communities*, eds Y. Cohen and E. Rosenberg (Washington, DC: Am. Soc. Microbiol.), 439–454.

Weete, J. D., Abril, M., and Blackwell, M. (2010). Phylogenetic distribution of fungal sterols. *PLoS One* 5:e10899. doi: 10.1371/journal.pone.0010899

Widdel, F., and Hansen, T. A. (1992). "The dissimilatory sulfate- and sulfur-reducing bacteria," in *The Prokaryotes*, 2nd Edn. eds A. Balows, H. G. Truper, M. Dworkin, W. Harder, and K.-H. Schleifer (New York, NY: Springer-Verlag), 583–624.

Wilmeth, D. T., Myers, K. D., Lalonde, S. V., Mänd, K., Konhauser, K. O., Grandin, P., et al. (2021). Evaporative silicification in floating microbial mats: patterns of oxygen production and preservation potential in silica-undersaturated streams, El Tatio, Chile. *Geobiology* 20, 310–330. doi: 10.1111/gbi.12476

Conflict of Interest: The authors declare that the research was conducted in the absence of any commercial or financial relationships that could be construed as a potential conflict of interest.

Publisher's Note: All claims expressed in this article are solely those of the authors and do not necessarily represent those of their affiliated organizations, or those of the publisher, the editors and the reviewers. Any product that may be evaluated in this article, or claim that may be made by its manufacturer, is not guaranteed or endorsed by the publisher.

Frontiers in
Astronomy and Space Sciences

Explores planetary science and extragalactic astronomy in all wavelengths

Advances the understanding of our universe - from planetary science to extragalactic astronomy, to high-energy and astroparticle physics.

Discover the latest Research Topics

See more →

Frontiers

Avenue du Tribunal-Fédéral 34
1005 Lausanne, Switzerland
frontiersin.org

Contact us

+41 (0)21 510 17 00
frontiersin.org/about/contact